Durham E-Theses

Pyrite oxidation in coal bearing strata:: controls on in-situ oxidation as a precursor of acid mine drainage formation

Roy, Samita

How to cite:

Roy, Samita (2002) *Pyrite oxidation in coal bearing strata:: controls on in-situ oxidation as a precursor of acid mine drainage formation*, Durham theses, Durham University. Available at Durham E-Theses Online: http://etheses.dur.ac.uk/3753/

Use policy

Frontispiece – Spherical pyrite framboid made up of individual pyrite crystals, imaged by scanning electron microscope. From the Beaumont Coal - Westphalian Lower Coal measures, Northumberland Coalfield, UK.

Pyrite Oxidation in coal-bearing strata: Controls on *in-situ* oxidation as a precursor of Acid Mine Drainage formation.

Samita Roy

Thesis submitted to University of Durham in fulfilment of the degree of Doctor of Philosophy.

Department of Geological Sciences, 2002

ii

Pyrite oxidation in coal-bearing strata: Controls on *in-situ* oxidation as a precursor of acid mine drainage formation.

Samita Roy

Abstract

Pyrite oxidation in coal-bearing strata is recognised as the main precursor to Acidic Mine Drainage (AMD) generation. Predicting AMD quality and quantity for remediation, or proposed extraction, requires assessment of interactions between oxidising fluids and pyrite, and between oxidation products and groundwater. Current predictive methods and models rarely account for individual mineral weathering rates, or their distribution within rock. Better constraints on the importance of such variables in controlling rock leachate are required to provide more reliable predictions of AMD quality.

In this study assumptions made during modelling of AMD generation were tested including; homogeneity of rock chemical and physical characteristics, controls on the rate of embedded pyrite oxidation and oxidation front ingress.

The main conclusions of this work are:

- The ingress of a pyrite oxidation front into coal-bearing strata depends on dominant oxidant transport mechanism, pyrite morphology and rock pore-size distribution.

- Although pyrite oxidation rates predicted from rate laws and derived from experimental weathering of coal-bearing strata agree, uncertainty in surface area of framboids produces at least an order of magnitude error in predicted rates.

- Pyrite oxidation products in partly unsaturated rock are removed to solution via a cycle of dissolution and precipitation at the water-rock interface. Dissolution mainly occurs along rock cleavage planes, as does diffusion of dissolved oxidant.

- Significant variance of whole seam S and pyrite wt % existed over a 30 m exposure of an analysed coal seam. Assuming a seam mean pyrite wt % to predict net acid producing potential for coal and shale seams may be unsuitable, at this scale at least.

- Seasonal variation in AMD discharge chemistry indicates that base-flow is not necessarily representative of extreme poor quality leachate. Summer and winter storms, following relatively dry periods, tended to release the greatest volume of pyrite oxidation products.

Acknowledgements

Table of Contents

List of Tables

replicates for the initial and final part of an hour long flushing period, as described in Case 1.

List of Figures

Table of abbreviations commonly used in the text

ABA	Acid base accounting
ALD	Anoxic limestone drain
AMD / ARD	Acid Mine / Rock Drainage
ANOVA	Analysis of variance – a statistical test used to identify significant differences between means within a sampled population.
FESEM	Field emission scanning electron microscope
FT-IR	Fourier transform diffuse reflectance infrared spectroscopy.
ICP-OES	Inductively coupled plasma – optical emission spectroscopy
LOI	Loss on ignition
Milli-Q	Ultra-pure water
Milli-RO	Water purified by reverse osmosis
MPA	Maximum potential acidity
NAPP	Net acid producing potential
PCA	Principle component analysis – mathematical analysis of data producing several non-correlating groups of correlated measured characteristics for pattern recognition.
pzc	Point of zero charge – pH at which a mineral surface has a neutral charge
SCM	Shrinking core model – mathematical model describing the weathering of a particle as a shrinking core of un-affected material.
SEM-EDAX	Scanning electron microscope – energy dispersive x-ray spectrometry
SEM-SE	Scanning electron microscope - secondary electron imaging
SEM-BSE	Scanning electron microscope – back scattered electron imaging
XPS	X-ray Photoelectron Spectroscopy
XRD	X-ray diffraction
XRF	X-ray fluorescence
σ	Standard deviation of the mean
n	Population size used to calculate the mean value

Declaration

The content of this thesis is the original work of the author alone. Other peoples work, where included, is acknowledged by reference. This work has not been previously submitted for a degree at this or any other university.

Samita Roy

Durham 2002

Chapter 1

Pyrite oxidation in coal-bearing strata as a precursor to AMD formation

1.1. Typical consequences of Acid Mine Drainage formation

Currently, the formation of highly toxic Acid Mine or Rock drainage (AMD/ARD) affects around 1000 km of streams in England and Scotland, a large proportion of which is a consequence of coal-mine abandonment (Younger and Adams, 1999). Pollution of a receiving watercourse by AMD typically leads to the easily recognisable bright orange ochre deposits blanketing stream beds. Loss of visual quality coincides with loss of bio-diversity within the water column, halting the use of a water source for agricultural, industrial and public supply use (Earle & Callaghan 1999, Jarvis and Younger 1997). Degradation of a river by AMD requires treatment if that source is used for industrial or domestic purposes. Where a polluted watercourse is proximal to cement structures, acidic or metal-laden waters may weaken building foundations. The mining industry in the US alone spends over $1 million per day in the treatment of AMD (Evangelou and Zhang, 1995). Consequences of mine abandonment are obviously far-reaching, with wide ranging ecologic and economic effects.

In the following sections current thinking with regard to AMD formation is described. A brief review of current treatment practises, a rationale of work presented in the main body of the thesis and a synopsis of chapters is also presented. Chapter 2 comprises a review of subjects pertinent to the study.

1.2. Generation of AMD

Pyrite oxidation in coal-bearing strata during mining operations is recognised as the principal precursor to Acidic Mine or Rock drainage (AMD/ARD) formation (Evangelou, 1998, Bierens de Han, 1991). Naturally produced acidic sulphate water is also common, however this work focuses on the anthropogenically derived discharges. Weathering of pyrite and other sulphide minerals occurs on exposure of the host rock to an oxidising environment. The unsaturated nature of spoil material allows the rapid influx of oxidant and removal of polluted leachate. Where the water-table has been depressed to allow extraction of rock, remaining strata and workings above the level of depression are exposed to an oxidising atmosphere. Secondary minerals such as the ubiquitous Fe-hydroxides e.g. goethite and ferrihydrite, and Fe-hydroxy-sulphates e.g. melanterite and schwertmannite, form as a result (Nordstrom, 1982). Depending on rock saturation, these salts are either removed concurrently or stored and dissolved

during the next rainfall or flooding event. The resultant solution may contain high concentrations of Fe, SO_4^{2-}, Mn and Al, plus trace metals such as As, Cu, Ni, and Zn (Rose & Cravotta 1999). Low pH of the solution is provided by the high metal and hydrogen ion content, although the latter may be lost to buffering by carbonate and alumino-silicate weathering. Neutral AMD discharges are a common occurrence, however potentially high concentrations of dissolved salts, metals, metalloids and radionuclides are still of concern in such discharges (Deissmann and Bolduc, 2000). Aeration and / or neutralisation of acidic solutions leads to precipitation of dissolved metals in amorphous forms of the salts mentioned above. Subsequent decomposition and re-precipitation leads to the formation of stable crystalline mineral deposits, which act as repositories for acidity and dissolved metals over long periods of time (Bigham et al., 1996, Blowes and Jambor, 1991, Macklin et al., 1997 and 1999). Adsorption of dissolved metal species such as Pb, As, Al, Cu and Zn by iron-hydroxides has also been reported (Herbert, 1996, Leblanc et al., 1996). Changes in pH of the local system, e.g. during storm events, initiate erosion of stream-bed sediment and can lead to a deleterious release of these contaminants.

1.3. Current remediation strategies

Pollution by AMD may be arrested at three main stages in its production (Connely et al., 1994):

1. **Source control** - Initial pyrite oxidation and leaching of products is prevented.

Current treatments involve minimising the oxygen supply to the pyrite by compaction of spoil heaps, submersion of waste in mine lakes, covering heaps with a humic substrate to encourage reducing conditions, and air-sealing mine adits.

Geochemical studies show that restricting oxygen transport to relatively slow diffusion, by compaction or submersion of tailings is effective in minimising AMD production (Schüring et al., 1997). Physically blocking the pathway of atmospheric oxygen does not account for dissolved oxygen and Fe^{3+} in the form of Fe-hydroxide, both of which may continue oxidizing free Fe^{2+} iron within the submersed tailings (Webb and Sasowsky, 1994).

2. **Migration control** - Effluent is trapped as it migrates from source.

Examples of this are; covering or grouting of spoil heaps with concrete, using physical barriers to divert ground water flow from the most contaminated pathway, settling ponds which isolate effluent from local ground-water.

As cement is weathered to ettringite under low pH conditions, the trapping of potentially acidic products is not a long-term solution (Wiggering, 1993). Similarly the use of physical barriers and diversion ditches rely on consistent groundwater flow and do not cover the eventuality of a change in flow direction or flooding of the system.

3. **Release control** - Effluent is collected and treated.

Remediation of low pH, high conductivity effluent includes chemical treatment to neutralize acidity and precipitate metals using chemicals such as lime and barium chloride combined with aeration. The resultant sludge is often itself classed as hazardous waste (Stefanoff and Kim, 1994). Alternatively, limestone rock, coal fly ash and phosphate rock, have been mixed into spoil heap waste to neutralize acidity, or prevent pyrite oxidation by the precipitation of Fe^{3+}, in insoluble Fe-phosphates (Stiller et al., 1989, Spotts and Dollhopf, 1992, Stewart et al., 1997, Doolittle and Hossner, 1997). Unfortunately, the limestone and phosphate rock usually becomes coated with Fe-hydroxide or Fe-phosphate inhibiting their effectiveness (Evangelou and Zhang, 1995).

Passive treatments include the use of constructed wetlands where acidity and dissolved metals are removed by passing the AMD through various substrates. Common substrates consist of limestone gravel to neutralise acidity, and organic rich layers where sulphate reducing bacteria thrive and precipitate metal-sulphides. However, inhibition of neutralisation by Fe-hydroxide precipitation on limestone surfaces can render passive treatments ineffective. This is avoided by passing AMD through an Anoxic Limestone Drain (ALD) which allows neutralisation and but stops the precipitation of Fe-hydroxide. The AMD still contains high concentrations soluble metals including Fe^{3+} which will hydrolyse when the water comes into contact with the atmosphere producing further acidity (Webb and Sasowsky, 1994). Combining an ALD with a wetland increases the removal capability for both acidity and dissolved metals. Wetlands and ALDs tend to be designed for a specific pH and total dissolved concentration of the drainage at the time of design. However, spoil heap weathering involves several chemical buffering systems provided by the breakdown of carbonates, alumino-sillicates, clays and sulphides (Kerth and Wiggering, 1998). AMD quality may remain constant over a period of time, then rapidly change when the mineral weathering to buffer solution pH is consumed. Such fluctuations in properties of the

treated effluent suggest that passive treatments require monitoring for the lifetime of the pollution source.

Given the potential problems associated with passively and actively treating AMD, an understanding of discharge longevity and possible changes in quality is required in order to design a cost effective remediation scheme.

1.4. Predicting AMD quality and quantity for design of treatment

Pre-mining requirements in most developed countries now involve a study into the polluting potential of mining activity at a site. Where large-scale coal extraction has been terminated, local water table depression may still continue until a costed prediction of pollutant treatment and longevity is decided, and financially responsibility allocated (Jarvis and Younger, 1997).

Several methods are available to the investigator for site specific projections of discharge quality.

Static and kinetic tests

In general testing of overburden polluting potential is carried out using kinetic and static tests. Kinetic testing involves monitoring columns of material through time, under laboratory or field conditions, in order to mimic the weathering of a larger mass of similar material. Static testing involves monitoring the net pollutant production of a rock type using humidity cells and Acid-Base Accounting (ABA) (Hornberger and Brady, 2000). Estimates of pollutant quality may also be made on the basis of pyrite content, and on the environment of rock seam deposition (Younger, 2000).

Numerical modeling

Simulation of AMD forming processes, using numerical modelling, provides a more sophisticated method of predicting AMD quality (Wunderly et al, 1996, Destouni et al., 1998).

Given the critical role of pyrite oxidation in the formation of AMD, the reaction rate is an important constituent of any simulation or prediction of waste rock weathering. Experimentally derived rate laws for the oxidation of pyrite by O_2 and Fe^{3+} indicate a fractional to first-order reaction dependence on oxidant concentration (Mckibben and Barnes, 1986, Evans et al., 2001). However, the rate of embedded pyrite oxidation is dependent on oxidant transport to the mineral surface. The time taken for resultant dissolved material to reach the rock particle surface also depends on the dominant transport mechanism in the rock matrix. Both factors affect the rate at which dissolved

material is incorporated into final leachate. Where the transport of mineral weathering product at the waste rock particle surface is rapid, leachate formation rate may be limited by the advective transport of soluble matter from this surface. However, if the rate of dissolved pyrite oxidation product diffusion to the water-rock interface is relatively slow, AMD formation will be limited by diffusive transport. Some simulations assume the former case and directly relate pyrite oxidation rate to AMD leachate quality. Seasonal variations in the rate of flushing of waste material may lead to a combination of transport and oxidation rate control of AMD generation.

Strömberg, (1997) accounted for diffusive transport in rock particles, and incorporated elements of the Shrinking Core Model (SCM) (Levenspiel, 1979) in a numerical simulation of AMD production from sulphidic waste rock. Wunderly et al. (1996) also applied the SCM to sulphidic mine tailings oxidation with good agreement with actual discharge quality. Sedimentary rock, particularly coal-bearing strata, has a very different pore structure to the igneous and metamorphic rock commonly associated with sulphide ore deposits. Commonly, processed mine tailings consist of finely ground particles, often mono-mineralic, with a small particle size distribution. Particles in waste rock from coal mining usually range in size from microscopic to macroscopic.

Typical assumptions made by modeling

Key assumptions made about pyrite oxidation, during AMD formation include:

- Homogeneity of pyrite morphology and its distribution in weathered material
- Uniform diffusion of oxidant into, and consequent diffusion of pyrite oxidation product out of, the rock matrix.
- Homogeneity of pyrite oxidation rate independent of pyrite morphology
- Control of oxidant diffusion depth by supply and uptake in oxidation
- The removal of pyrite oxidation products from the spoil material or rock strata by uniform percolation of meteoric water.

Although these assumptions are made in order to simplify models, and to actually allow some assessment of AMD formation, the size of error in prediction is unknown. Problems of scaling between small-scale laboratory experiments, and the natural environment, contribute to the fact that there is currently no standard method of predicting AMD quality (Malstrom et al., 2000). Some of the problems associated with scaling between numerical and laboratory simulations and the natural environment, may relate to key assumptions made during predictive modelling.

Possible errors in making assumptions

- Pyrite distribution can vary on several scales, depending on diagenetic processes forming the sulphide phase and the final manner of disposal of waste rock material (Evangelou and Zhang, 1995).

- Rock characteristics such as porosity and permeability are rarely accounted for in the use of ABA, one of the most commonly used AMD prediction methods.

- Most detailed models of pyrite oxidation exist for mine tailings where pyrite commonly forms as a separate fine-grained phase, yet in coal-bearing strata pyrite is usually embedded.

- Stromberg, (1997) goes the furthest towards modelling oxidation of embedded pyrite in waste rock, incorporating permeability and reactive transport. However, such an application may not be appropriate for sediment hosted pyrite where cleavage may preferentially direct fluid flow, in the rock.

- In the final stages of AMD formation the mixing between percolating meteoric water and pyrite oxidation products dissolved in spoil pore water is assumed to be continuous and homogeneous. Seasonal changes in hydrological flow-paths, and their effect on AMD quality is poorly constrained (McGiness and Johnson, 1993).

1.5. Rationale

It is not the intention of this study to criticise current working methods of predicting AMD quality and quantity, or to provide alternative methods of prediction. Rather an investigation of some of key assumptions made during pollutant prediction is made, with an aim towards contributing to improvements in current practice.

The objectives of this study are to:

- Follow the ingress of an abiotic pyrite oxidation front in coal-bearing strata using tracers

- Compare *in-situ* abiotic pyrite oxidation rates with those predicted from pyrite alone

- Analyse the homogeneity of pyrite distribution and other rock characteristics in coal-bearing strata at a small scale.

- Investigate seasonal changes in chemistry of an AMD discharge and the controls on discharge chemistry

In this study experimental work focuses on waste particle scale processes. Monitoring of this scale is usually thought of as un-important in the prediction of AMD quality (Wunderly et al., 1996, Bain et al., 2000). Processes of pyrite oxidation and acidic weathering within these particles control the final AMD discharge chemistry. Therefore small-scale processes require characterisation in order to infer controlling processes at larger scales.

A combination of leachate chemical analysis, scanning electron microscope (SEM) observations and rock characterisation methods are used to investigate the controls on rock weathering, at this scale. Monitoring of an AMD discharge is also performed to investigate the manner in which final discharge formation occurs. Statistical methods and experimental design are used in the analysis of chemical data where appropriate. Combining direct observations, the findings of previous investigations and the identification of statistically significant processes, will lead to a more robust interpretation of the collected data. Although bacterial mediation of the pyrite oxidation reaction is a very important factor in AMD generation, the monitoring of this factor is beyond the bounds of this work.

1.6. Synopsis

The work presented in this thesis is divided into 7 sections, with a detailed introduction to the work described given at the start of each chapter:

Chapter 1 introduces the work and key hypotheses tested with a review of current methods used to quantify and predict AMD generation due to pyrite oxidation.

Chapter 2 contains an overview of the pyrite oxidation reaction, mechanisms and rate controlling factors. It is the aim of this chapter to provide the reader with preliminary information on the main theme of the project, i.e. pyrite oxidation as a precursor to AMD formation.

Chapter 3 describes the investigation into pyrite encapsulation as a form of AMD prevention. The study involves several factorial designed experiments used to rapidly identify the optimal combination of phosphate and hydrogen peroxide solution for pyrite coating and prevention of oxidation.

Chapter 4 presents the analysis of variance (ANOVA) of coal-bearing strata physical and chemical characteristics. This study specifically investigates variation in pyrite content between and within coal and shale seams to test the assumption of homogenous distribution in acid-base accounting (ABA). As ABA is currently one of

the most commonly used tests for overburden AMD formation potential, the investigation should shed some light on the suitability of this test at a small scale.

Chapter 5 details an investigation into *in-situ* pyrite oxidation rates within coal-bearing strata. Here, the controls on pyrite oxidation are identified and the ingress of a pyrite oxidation front monitored and compared to currently used models. In-situ pyrite oxidation rates are compared to those predicted from rate laws originally derived from oxidation of pyrite alone.

Chapter 6 describes a sub-set experiment to that in chapter 5, where pyrite oxidation in coal-bearing strata undergoing flushing with purified and mineralised water is studied. Flow-path weathering is described and differences between water-rock regimes analysed both by direct observation and by ANOVA.

Chapter 7 presents the separation of pore water sources contributing to an AMD discharge, using classical chemical hydrograph separation and principal component analysis (PCA). In analysing the chemical and physical data from the monitored discharge over a period of seasonal change, the contribution and potential composition of spoil pore water can be spatially and temporally defined. Identification of the typical characteristics of spoil pore water in water-rock regimes similar to those mimicked is compared to the findings of experiment leaching in the final discussion.

Chapter 8 summarises the results of chapters 3 to 7 whilst testing experimental results from chapters 5 and 6, using ANOVA to show significant differences between water-rock regimes. The findings of this analysis, and experimental work in chapters 5 and 6, are compared with monitoring of the AMD discharge in chapter 7 to confirm the findings of small-scale experiments. Finally the implications for the survey of AMD and predictive methods are presented.

Chapter 2

Pyrite oxidation rate – identified controlling factors

2.1 Introduction

In the previous chapter a rationale for the investigation of key assumptions made in the prediction of AMD quality and formation was presented. Here, important factors in the study of pyrite oxidation in relation to AMD formation are presented to complement a review of the investigated subject at the start of each chapter. The manner of pyrite oxidation including; reactions, surface oxidation mechanisms, experimentally derived rates and rate controlling factors, are reviewed.

2.2 Pyrite Oxidation

Pyrite (FeS_2) is considered to be the most prolific producer of acidity in AMD as oxidation of one mole will produce 4 moles of protons (Webb and Sasowsky, 1994), (reaction 2.4). Controls on pyrite oxidation rate include; pH, pO_2, specific surface area, morphology, the presence of bacteria and clay minerals, and hydrological conditions (Evangelou and Zhang, 1995). The chemical reactions most commonly presented when describing the process of pyrite oxidation cover a series of steps, represented in the following equations:

$$FeS_{2(s)} + 7/2O_2 + H_2O = Fe^{2+} + 2SO_4^{2-} + 2H^+ \qquad (2.1)$$

$$Fe^{2+} + 1/4O_2 + H^+ = Fe^{3+} + 1/2H_2O \qquad (2.2)$$

$$Fe^{3+} + 3H_2O = Fe(OH)_{3(s)} + 3H^+ \qquad (2.3)$$
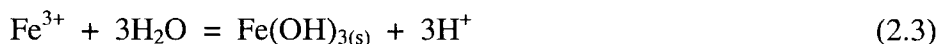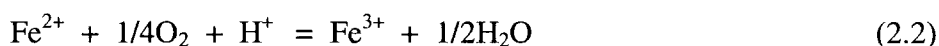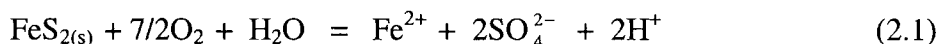
Reactions 2.1-2.3 can be summarised by:

$$FeS_{2(s)} + 15/4\,O_2 + 7/2H_2O = Fe(OH)_{3(s)} + 2SO_4^{2-} + 4H^+ \qquad (2.4)$$

$$FeS_2\,(s) + 14Fe^{3+} + 8H_2O = 15\,Fe^{2+} + 2SO_4^{2-} + 16H^+ \qquad (2.5)$$
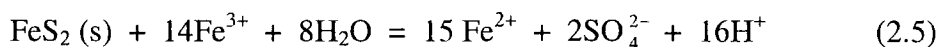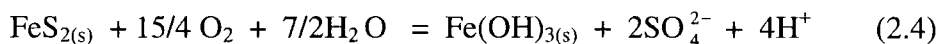
In this classical interpretation of the pyrite oxidation process the initial rate of reactions 2.1 and 2.2 are slow, making the oxidation of Fe^{2+} the rate-controlling step (Moses and Herman, 1991, Evangelou and Zhang, 1995, Bonissel-Gissenger et al.,

1998). The effect of pH on the overall oxidation reaction is caused by the decreasing solubility of Fe-hydroxides at increased pH, and the reported increase in pyrite oxidation by Fe^{3+} at low pH. With decreasing pH the oxidation reaction may be represented by:

$$FeS_2 + 14Fe^{3+} + 8H_2O = 15Fe^{2+} + 2SO_4^{2-} + 16H^+ \qquad (2.6)$$
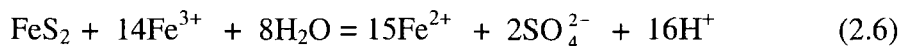
2.2.1 Pyrite surface oxidation mechanisms

Such descriptive reactions do not represent rate reactions, and typically stoichiometrically summarise processes occurring during oxidation (Evangelou and Zhang, 1995). Investigation of pyrite oxidation reactions under varying pH (Moses et al., 1987, Moses and Herman, 1991, Bonnissel-Gissenger et al., 1998) and consideration of molecular interactions (Evangelou and Zhang, 1995) have shown that Fe^{3+} is the dominant oxidant of pyrite at low and high pH. Previously the oxidation of pyrite by O_2 was thought to be dominant at high to neutral pH, as Fe^{3+} was removed from solution by Fe-hydroxide precipitation. However, the role of O_2 is more likely one of Fe^{2+} oxidation to Fe^{3+}, rather than any direct interaction with the pyrite surface. The oxygen atoms associated with sulphate produced by pyrite oxidation, are derived from water molecules, indicating that only dissolved O_2 plays an active role in oxidation (Moses et al., 1987). Oxidation at pyrite surfaces is thought to occur via the formation of an 'aquo-complex' by Fe^{3+} with 6 waters of hydration (Moses and Herman, 1991). The complex molecule attaches to the pyrite surface by exchange of electrons with one S of the pyrite molecule. Pyrite S has two unpaired electrons in its outer orbital, allowing species such as metal cations, halogens and hydrogen peroxide to bond to the pyrite surface in a Lewis acid-base style. The high positive charge of Fe^{3+} makes this species more likely to accept these unpaired electrons (Moses et al., 1987). A *per sulfido* bridge is formed where the S is shared by the pyrite Fe^{2+} and hydrated Fe^{3+}. Electron transfer occurs from the S to Fe^{3+} aquo complex up to six times, leading to the formation of Fe-thiosulphate, which then becomes detached from the pyrite surface. When Fe^{3+} is present in excess the oxidation of thiosulphate to sulphate is rapid. Where Fe^{3+} is depleted due to precipitation at high pH, thiosulphate will tend to dominate the S species, as its oxidation by O_2 is relatively slow (Evangelou and Zhang, 1995). The increase in thiosulphate concentration at the pyrite surface, during oxidation, has been confirmed by Bonnissel-Gissenger et al. (1998). At low pH little trace of thiosulphate

species is found in both field and experimental cases (Moses et al., 1987, Evangelou and Zhang, 1995).

Consideration of surface mechanisms of pyrite oxidation suggests that Fe^{3+} is the dominant oxidant with dissolved O_2 only oxidizing Fe^{2+}. Due to its role as a supplier of Fe^{3+}, the depletion of O_2 will retard the pyrite oxidation reaction overall.

2.2.2 Measured rates of oxidation and controlling factors

Experimental derivation of pyrite oxidation rate indicates a first to fractional order rate dependence on oxidant concentration (typically Fe^{3+} and O_2), and at low pH, a square root dependence on H^+ concentration (McKibben and Barnes, 1986, Destouni et al 1998, Nicholson et al., 1988). Rates of mineral dissolution are usually calculated using the volumetric dissolution rate (McKibben and Barnes, 1986, Lasaga, 1984)

$$R_{vol} = -k\frac{A}{V}\prod(M_i^{ni}) \qquad (2.7)$$

where R_{vol} depends on the rate constant k, total mineral surface A, volume of solution V, molarity of species i, M_i affecting the rate with n orders of dependence on M. When A, V, M_i , n and R_{vol} are known, k can be calculated and a R_{vol} converted in to a specific rate R_{sp} :

$$R_{sp} = -K[M]^n \qquad (2.8)$$

(McKibben and Barnes, 1986). The selection of rate constants and measured rates shown in Table 2.1 indicate the wide variety in orders of dependence and units of reporting.

Oxidant and reaction conditions	Order of dependence on oxidant	Rate constant, k	Actual rate	Investigators
O_2 at pH 2 to 4	0.5	$10^{-6.77}$ mole FeS_2 cm^{-2} min^{-1}		McKibben and Barnes (1986)
O_2 pH 6.7 to 8.5		3.07×10^{-6} m h^{-1} $\pm 46\%$ (surface rate constant)		Nicholson et al. (1990)
O_2, Field survey			$5.9 \pm 2.1 \times 10^{-10}$ mole FeS_2 m^{-2} s^{-1}	Elberling et al, (1994).
O_2 Rock waste columns	0.5 to 0.8			Strömberg, (1997)

Table 2.1. Reported rates of pyrite oxidation, rate constants, and orders of dependence on oxidant concentration.

2.2.3 Retardation by precipitation of oxidation products

Nicholson et al. (1988) suggest that the wide range of reported oxidation rate values is due to the control of measured rate dependence by oxidation product breakdown. They report the good fit of pyrite oxidation data at variable O_2 concentrations, and pH > 6.7 with Langmuir adsorption relationship where rate of oxidation can be described by:

$$R = \frac{R_m KC}{(1 + KC)} \qquad (2.9)$$

where the rate of oxidation R depends on R_m, the rate based on maximum saturation of available surface sites, K is the adsorption equilibrium constant for O_2 on pyrite and C is the O_2 concentration (Nicholson et al., 1988). Moses et al., (1987) suggest that the good fit of the model proposed by Nicholson et al. (1988) is due to the blocking of available oxidation sites by Fe^{2+}, rather than pyrite oxidation products. At pH greater than 2 i.e. the point of zero charge for pyrite (pH_{pzc}, Widler and Seward, 2002), the surface of the mineral will be negatively charged, and below the pH_{pzc} the surface has a positive charge. Therefore at high pH the pyrite surface will selectively attract cations with a high positive charge. Moses and Herman, (1991) suggest that ferrous Fe exists mainly as Fe^{2+} at pH > 6, yet Fe^{3+} exists as $Fe(OH)_2^+$ and $Fe(OH)_3^0$. Thus the higher positive charge on the Fe^{2+} species at high pH should lead to a greater electrostatic attraction compared to Fe^{3+} species. X-ray Photoelectron Spectroscopy (XPS) investigation of aqueous pyrite oxidation at low pH (2-4) confirms the presence of Fe^{3+}, $FeOH^{2+}$ and $Fe(OH)_2^+$. Thus at low pH Fe^{3+} is available and should be preferentially adsorbed to the pyrite surface relative to Fe^{2+}.

Similar investigation of surface oxidation also suggests that the only forms of O_2 present are molecular water, hydroxide and oxide groups. No evidence of direct adsorption of gaseous O_2 to the pyrite surface was found (Bonnissel-Gissenger et al., 1998). At high pH, Fe^{3+} hydroxides coat the pyrite surface, yet over short periods of time (close to a month) pyrite oxidation is not slowed by precipitation (Bonnissel-Gissenger et al., 1998, Moses and Herman, 1991). Both Bonnissel-Gissenger et al. (1998) and Moses and Herman (1991) report that at short time-scales, the precipitation of Fe-hydroxides is not homogenous, typically occurring at points of high surface energy such as edges, pits and fractures. Similarly SEM investigation of oxidised pyrite by McKibben and Barnes (1986) showed oxidation at regions of high surface energy,

i.e. pits, edges and fractures. Over a period of several months to a year, precipitation of Fe-hydroxide probably becomes cohesive enough to retard oxidation, due to the oxidant having to diffuse through this layer (Nicholson et al., 1990).

2.2.4 Bacterial mediation of pyrite oxidation

Direct and indirect catalysis of the pyrite oxidation reaction by bacterial activity increases the reaction rate substantially over abiotic oxidation. *Thiobacillus Ferrooxidans* and *Thiobacillus Thioxidans* have been identified as the predominant aciderophilic bacteria in mine spoil material (Evangelou and Zhang, 1995). Both species can oxidise S^0 and metal sulphide to H_2SO_4, however only *Ferroxidans* oxidises Fe^{2+}, increasing the rate of pyrite oxidation by a factor of up to 10^6. Controls on the increase in pyrite oxidation caused by the presence of bacteria include temperature, O_2 supply and pH. Optimal conditions for the bacterial mediation of the oxidation reaction are > 0.01 mole O_2, pH 3.2 and temperatures above 5°C (Evangelou and Zhang, 1995, Stromberg, 1997). At higher pH the precipitation of Fe-hydroxide removes Fe^{3+} from solution, and at pH below 1.5 bacteria perform poorly due to physiological effects. Thus peak bacterial mediation of the pyrite oxidation reaction occurs at pH lower than 5 and higher than 2.

Although bacterial oxidation of pyrite is obviously an important component in the overall rate of AMD formation and quality, its investigation is beyond the bounds of this study. All laboratory experiments were carried out under abiotic conditions, although the prior presence of bacteria from rock samples cannot be disproved. Prior heating of samples used in main experiments to 105°C, to remove pore water in an attempt to halt further oxidation, may have removed any bacteria present.

2.2.5 Morphology of pyrite in coal-bearing strata

In Equation 2.1 and Table 2.1 the rate of pyrite oxidation and rate constants are given in moles of pyrite per unit surface area of mineral. Obviously mineral surface area plays an important role in the overall measured rate of reaction. McKibben and Barnes (1986) report that the oxidation of pyrite tends to be concentrated at regions of high surface energy of the pyrite grains, i.e. edges, pits and fractures. Typical pyrite morphology and therefore abundance of such features will affect the overall measured rate of pyrite oxidation.

Pyrite morphology depends on the manner of formation. In coal-bearing strata pyrite may form within peat, during peat burial diagenesis or during post burial lithification

(Spears, 1987). Typically pyrite forms as individual crystals, infills veins or replaces soft organic matter. The formation of this sulphide obviously depends on the availability of Fe and S, typically supplied from Fe bearing detrital minerals and the reduction of sea-water sulphate. Extensive investigation of the manner of formation of the pyrite morphology, particularly framboidal pyrite has been carried out. However, the manner in which varying pyrite morphology affects oxidation rate is of more interest in this study.

Pyrite in coal- bearing strata exists as euhedral, massive pyrite, framboidal pyrite and anhedral infilling material (Kotenski, and Kostova, 1995, Wilkin et al., 1996). Framboidal pyrite is has the greatest surface area per accumulated mass of pyrite, and therefore will oxidise most rapidly. Framboids of pyrite are generally spherical, densely packed aggregates of pyrite crystals. The typical individual crystal diameter is 0.2 to 2 µm although framboid diameter can be between 1-50 µm (Wilkin et al, 1996, Butler and Rickard, 2000). Calculation of the individual crystal content per framboid suggests that between 10^2 and 10^5 discrete micro-crystals exist in each framboid (Wilkin et al., 1996). Therefore, unless an estimate of actual surface area is made, calculations of pyrite oxidation rate based on surface area calculated framboid diameter will grossly underestimate actual oxidation rates.

Chapter 3

Development of a pyrite phosphate coating using statistical methods.

3.1 Introduction

One of original propositions of this study was to refine a method of halting pyrite oxidation by encapsulation, as suggested by previous authors (Evangelou 1995, Nyavor et al., 1995, Vandiviere and Evangelou, 1998). The method could then be used in the prevention of AMD generation or to measure *in-situ* pyrite oxidation rates. Halting of oxidative pyrite weathering has previously been achieved using micro-encapsulation or coating techniques, effectively blocking the access of oxidants to the mineral surface. Surface reaction of pyrite with various aqueous solutions including phosphate, precipitates an insoluble coating, thus preventing further access to pyrite by the oxidant. As phosphate is usually present as a discrete mineral phase rather than associated with coal-hosted pyrite, the coating may also be used as a chemical tracer of *in-situ* oxidation. The aqueous nature of the coating treatment means that it may be used to trace the pyrite oxidation front formed during the ingress of an oxidising fluid into a rock particle. Currently attempts to trace oxidation fronts in rock particles initiated by reaction with water and dissolved oxygen may be confused by the presence of prior oxidation products. Using the phosphate coating solution as a tracer of oxidation reaction should eliminate this problem. This chapter describes the development of a phosphate coating technology and its testing on isolated mineral pyrite, in preparation for use on coal hosted *in-situ* pyrite for the uses described above.

Coating Technology

Coating technologies rely on the halting of pyrite oxidation by blocking the path of oxidants with an insoluble, relatively impenetrable, layer. The layer is produced by sacrificial oxidation to release Fe^{3+} at the mineral surface. The dissolved Fe^{3+} is rapidly precipitated with solution reactants to form the coating. Development of coating technologies has included the use of acetyl acetone, humic acid, lignin, sodium silicates, phosphate, hydroxide and silica as solution reactants, to various degrees of success (Wiggering, 1987, Nyavor et al., 1995, Evangelou 1995, Belzile et al., 1997). It has been shown that a coating of Fe-phosphate can be produced on pyrite grain surfaces using a weak oxidising solution of H_2O_2 followed by a phosphate solution to react with releasedFe^{3+}, (Figure 3.1, Evangelou, 1995). However, the increase in solubility of a Fe-phosphate coating with decreasing pH have led Vandiviere and Evangelou, (1998)

to conclude that silica coatings would be more stable under fluctuating pH. Natural buffering systems of clay and carbonate weathering, present in actual waste rock, would potentially hold pore water pH at the levels required for Fe-phosphate coating stability. After successful coating formation the lack of pyrite oxidation would also hold the rock pH at stable levels.

$$
\begin{array}{c}
\underline{\mathbf{A}} \\[2pt]
\mathrm{-Fe(II)-S_2(I)} \\
\mathrm{-S_2(I)-Fe(II)} \\
\mathrm{-Fe(II)-S_2(I)} \\
\mathrm{-S_2(I)-Fe(II)}
\end{array}
\quad + \; H_2O_2 \; + \; KH_2PO_4 \quad \longrightarrow \quad
\begin{array}{c}
\underline{\mathbf{B}} \\[2pt]
\mathrm{-Fe(II)\cdots PO_4} \\
\mathrm{-S_2(I)\cdots Fe(III)} \\
\mathrm{-Fe(II)\cdots PO_4} \\
\mathrm{-S_2(I)\cdots Fe(III)}
\end{array}
\quad + \; K_2SO_4
$$
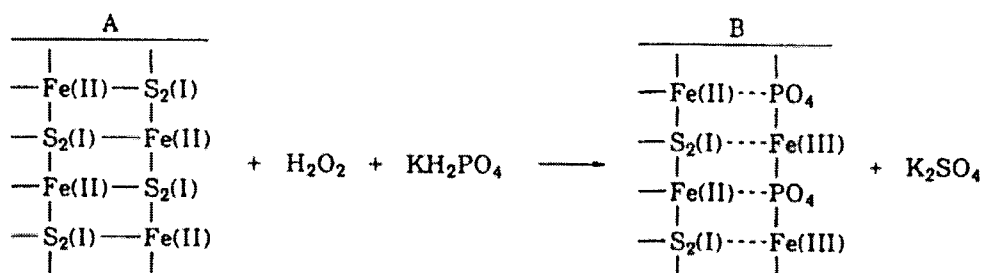
Figure 3.1. Schematic representation of H_2O_2 inducing phosphate coating on FeS_2, from Evangelou (1995).

During previous experimental development the coating technique has been tested on isolated pyrite grains and also on pyritic rock waste. Treatment solution composition and experimental set up varies between authors. However, the basic method involves the reaction of pyrite, usually derived from mine waste, with a flowing treatment solution in a column or reactor vessel. In some cases a buffer is added to the solution to keep pH at an optimum level. The pyrite may be initially mixed with quartz sand or glass beads to improve hydraulic flow and to separate grains. Pyrite is typically packed into the reactor vessel with treatment solution pumped through the material, supplying fresh coating solution to the pyrite grains. Evangelou (1995) used a treatment solution containing 0.088 $molL^{-1}$ (0.3%) H_2O_2, 10^{-4} $molL^{-1}$ (13.6mgL^{-1}) KH_2PO_4 and 0.2 $molL^{-1}$ NaCl as a background electrolyte. The solution was applied to a mixture of 50 mg pyrite and 500 mg quartz sand at 0.5 mL min^{-1} over 1000 minutes. Constant monitoring of the leachate conditions allowed the adjustment of solution pH to 4 using either NaOH or HCl. Nyavor and Egiebor (1995) treated 50 g pyrite mixed with glass beads in a sealed reactor vessel with 200 mL of coating solution (0.1 $molL^{-1}$ (13.6 mgL^{-1}) KH_2PO_4 and 1-2% H_2O_2) for 1 hour. Both Evangelou (1995) and Nyavor and Egiebor (1995) found that coating at 40–80 °C provided a thicker layer of Fe-phosphate than at ambient

temperatures. This did not improve the inhibition of pyrite oxidation significantly as the thick layer began to fracture.

Several techniques have been used to test the success of the coating procedure. Evangelou (1995) incorporated changing leachate chemistry with the theoretical kinetics of the treatment reaction to predict whether ferric-phosphate formed as a discrete phase or a coating on the pyrite. Pyrite was also examined using field emission scanning electron microscope (FESEM) and diffuse reflectance infrared spectroscopy (FT-IR) to confirm the presence of a coating. Nyavor and Egiebor (1995) confirmed the presence of a coating using scanning electron microscopy (SEM) and energy dispersive x-ray spectrometry (EDS). Direct testing of the coating's ability to inhibit pyrite oxidation involved the use of accelerated weathering columns and pressure oxidation techniques (Nyavor and Egiebor, 1995, Evangelou, 1995). Accelerated weathering of the treated pyrite consisted of exposing treated pyrite to fresh distilled water and compressed air every 3-7 days, over a total period of 81 days. Pressure oxidation was performed by heating the pyrite to 25-60°C at pressures of 100-1000 psi whilst administering 99.9% pure oxygen for 600 minutes. Leachate chemistry for the treated pyrite showed a 75% reduction in the oxidation rate of pyrite compared to untreated pyrite (Nyavor and Egiebor, 1995).

The use of phosphate coating techniques to retard pyrite oxidation in waste rock has been tested by Evangelou (1995) using columns of 500 mg of pulverised pyritic shale (6.5% pyrite) and sand. Treatment was with an aqueous solution containing 10^{-4} molL^{-1} (13.6 mgL^{-1}) KH$_2$PO$_4$ (i.e. 3.1 mgL^{-1}P), and 0.053 molL^{-1} (0.18%) H$_2$O$_2$. This was applied at a flow rate of 0.5 mLmin^{-1} and constant temperature of 40 °C. The treatment process consumed 10% of the pyrite. During 13 hours of testing oxidation inhibition with 0.088 molL^{-1} (0.3%) H$_2$O$_2$, only 20% of the sample's pyrite was oxidised, compared to over 80% from a column of untreated pyritic shale.

Vandiviere and Evangelou (1998) investigated the leaching of outdoor columns of spoil material, comparing conventional methods of mixing spoil material with limestone or rock phosphate with micro-encapsulation treatments i.e. phosphate or silicate coatings. Treatment solutions contained either 300 or 3000 mgL^{-1}of P with calcium hypo-chlorite (Ca(OCl)$_2$) as an oxidant. During the span of the experiment (615 days), material treated with 3000 mgL^{-1} P released less sulphate - S than the untreated column, suggesting that a portion of the pyrite had been encapsulated successfully. After four months of exposure outdoors, some of the treated columns were inoculated with the *Thiobacillus ferooxidans* bacteria, in order to assess the coating's resistance to

bacterially mediated oxidation. The pH of leachate fell from around 7 to 2 for all the inoculated columns apart from those pre-treated with 3000 mgL^{-1} P and 150 mgL^{-1} Si. The leachate pH for these dropped to 5, where it remained for the duration of the experiment. The use of a 3000 mgL^{-1} P solution to treat pyritic rock waste material retarded chemical and bacterial oxidation of pyrite.

Using the pyrite encapsulation treatment requires a sacrificial portion of pyrite, increasing initial acidity and releasing excess phosphate to the environment. As phosphate is a pollutant in excessive amounts, its release to local catchment would be deleterious. The use of a buffer solution is required to counteract this effect, however in the natural environment the amount of buffer required would be difficult to regulate. The buffering system provided by the weathering of clay and carbonate minerals may provide the pH required in the phosphate treatment of pyritic waste rock.

Factorial Designed Simplex Optimisation Experiment.

In this chapter the use of statistical methods to optimise the initial treatment solution without a buffer is described. In the following experiments the aim was to minimise Fe and SO_4^{2-} release yet maximise phosphate uptake, whilst forming an insoluble coating on individual pyrite grains. In order to obtain a leachate with minimal Fe, S and greatest uptake of P, within a short period of time a simplex optimisation experiment (Miller and Miller, 1993) incorporating a complete factorial design was performed. The factorial designed experiment groups several different concentrations of both oxidant and phosphate solution in all possible combinations. The combinations are then used to treat a unit mass of the cleaned pyrite. By doing so the effect of varying two factors i.e. phosphate concentration and H_2O_2 concentration can be investigated in terms of leachate P, Fe and SO_4^{2-} in one experiment. At the end of each factorial design stage, the best response, in terms of these factors, is used to define the region of phosphate and H_2O_2 combination to focus on. A new factorial design experiment using concentrations within this newly defined range is performed to find the best response within the smaller range of concentrations. By repeating this process the optimal concentrations of phosphate and H_2O_2 for coating should be found more quickly than by varying only one factor whilst all others are constant. The number of combinations plus replicate samples was large making the use of complex apparatus such as columns and reactor vessels time consuming. Therefore acid washed glass flasks were used as reactor vessels.

During investigation the reaction kinetics and order of solution addition were thought to have an effect on the reported results. These factors were subsequently studied along with reproducibility of results. Once a satisfactory combination of oxidant and phosphate was found, the solution was tested on actual coal samples. Treatment of coal samples with phosphate solution is described in Chapter 5.

3.2   Method and Materials

Two samples of pyrite were treated in the following experiments. The first was a sample of museum standard pyrite from the Pennine Orefield, UK, and the second was massive coal hosted pyrite collected from the Tilley Seam, Pegswood Opencast, Morpeth UK (NZ205880). Nicholson et al., (1988) report little difference in oxidation rates found using pyrite of different geological origin, citing surface area as the main cause of variation. Therefore the use of two different pyrite sources should not affect the results of experimental treatments.

All pyrite was washed in high purity de-ionised water (Milli-Q water) in an ultrasonic bath to remove fine surficial particles and sulphate phases. Sulphide was dried at 105°C and then crushed and sieved through a 150 μm mesh. The <150 μm portion of pyrite was re-washed in 10% HCl then in Milli-Q water, then acetone before being dried in air at 105°C, then stored under argon prior to treatment. Phosphate solutions were made up using Milli-Q water and KH_2PO_4 (Analar grade) with P concentrations given in mgL^{-1}.

3.2.1   1st Optimisation.

In the 1st Optimisation the prepared pyrite was immersed in all possible combinations of the following solutions; 1240 mgL^{-1}, 124 mgL^{-1}, 12.4 mgL^{-1} P or Milli-Q water and, 0.03%, 0.01% H_2O_2 or Milli-Q water. This range of concentrations was chosen for its proximity to the solution composition used by Evangelou, (1995).

Twelve acid washed, conical glass flasks containing 0.1 g of the cleaned < 150 μm pyrite, were filled with 10 mL of a H_2O_2 solution followed by 10 mL of a KH_2PO_4 solution. Duplicates of each mixture were prepared, and another flask per combination was prepared without pyrite, as a blank. The flasks were agitated for 10 minutes to thoroughly mix the solutions and pyrite, then covered and left overnight.

At the end of treatment sample leachate was vacuum filtered through a 0.45 μm cellulose nitrate membrane filter. Residue and filter paper rinsed in Milli-Q water, air dried at 40°C, weighed and retained in sealed plastic bags. The filtrate was analysed by ICP-OES for total Fe, S and P content (Appendix I Methods).

H_2O_2 %	P (mgL^{-1})
0.03	1240
0.01	124
0.00	12.4
	0.00

Table 3.1. Solution content and label for first optimisation experiment.

To test the extent of coating, a portion of the residual pyrite from each treatment was weighed then placed in a glass conical flask containing 25 mL of 1.2% H_2O_2 solution, and left overnight. A flask containing no pyrite was also prepared as a blank to monitor degradation of H_2O_2. Tested samples were vacuum filtered as described above, and 25 mL of Milli-Q water was used to rinse the residue. Half of the now diluted filtrate was acidified with H_2SO_4, then titrated against 0.1 molL^{-1} KMnO$_4$ to calculate the proportion of H_2O_2 remaining in the test solution. The remaining half of the filtrate was analysed by ICP-OES for total Fe, S and P. To compare the results of testing treated pyrite with the oxidation of untreated pyrite, 0.1g of clean untreated pyrite was leached overnight with 20 mL of 0.001, 0.01, 0.1 and 1% solutions of H_2O_2. Untreated pyrite was filtered as described above and the leachate analysed for dissolved total Fe and S by ICP-OES.

3.2.2 1st Optimisation - Results

1st Optimisation treatment leachate chemistry.

Blank corrected Fe and S filtrate concentrations were further corrected for the mass of pyrite treated, producing a concentration per gram of original material – mgL^{-1}g^{-1} pyrite (Table 3.A - Appendix II Results). Dissolved Fe varied between 0.02 ± 0.01 and 64 ± 4 mgL^{-1}g^{-1} and dissolved S between 10 ± 4 and 139 ± 6 mgL^{-1}g^{-1}. The uptake of P from solution is not informative. Variation in initial solution concentrations between replicates masks any precipitation of dissolved phosphate. Analysis of variance (ANOVA) indicates that changes in P concentration fell within measurement error (at 95 %), therefore no change in concentration may be concluded from dissolved P uptake. ANOVA of S and Fe fell outside the measurement error, indicating that variations in the concentrations of these analytes can be used in determining interactions within treatments.

The proportions of dissolved Fe and S can be used to determine the relative extent of oxidation during treatment. Rapid formation of a stable coating will lead to a fall in the concentration of Fe and S release relative to a treatment where coating formation is poor.

Comparison of the treatment leachate Fe and S shows three distinct groups (Figure 3.2); a cluster of low S and Fe (trend A), a line of high S and low Fe, (trend B) and a line where S is always close to twice the concentration of Fe, (trend C).

Trend A is made up of samples treated with high concentrations of phosphate (1240-124 mgL^{-1}) and all levels of H_2O_2. This group contains leachate with low Fe concentrations and relatively low S, having an upper limit of 0.07 ± 0.07 mgL^{-1}g^{-1} Fe and 35 ± 4 mgL^{-1}g^{-1} S, and a lower limit of 0.02 ± 0.01 Fe and 10 ± 4 mgL^{-1}g^{-1} S.

Trend B is made up of pyrite treated with the lowest P concentration (12.4 mgL^{-1}) and increasing H_2O_2. Samples in this trend contain low Fe and high S with 3 ± 3 mgL^{-1}g^{-1} of Fe and 133 ± 5 mgL^{-1}g^{-1} of S at the peak and at the lower end 1.0 ± 0.3 mgL^{-1}g^{-1} of Fe and 29 ± 7 mgL^{-1}g^{-1} of S.

Trend C is made up of samples treated with increasing concentrations of H_2O_2 alone. The peak of this trend is at 64 ± 4 mgL^{-1}g^{-1} of Fe and 139 ± 6 mgL^{-1}g^{-1} of S, and was treated with the highest initial H_2O_2 at 0.03%. The leachate from pyrite originally treated with Milli-Q water alone is at the lower end of this trend with 11 ± 9 mgL^{-1}g^{-1} Fe and 30 ± 14 mgL^{-1}g^{-1} S.
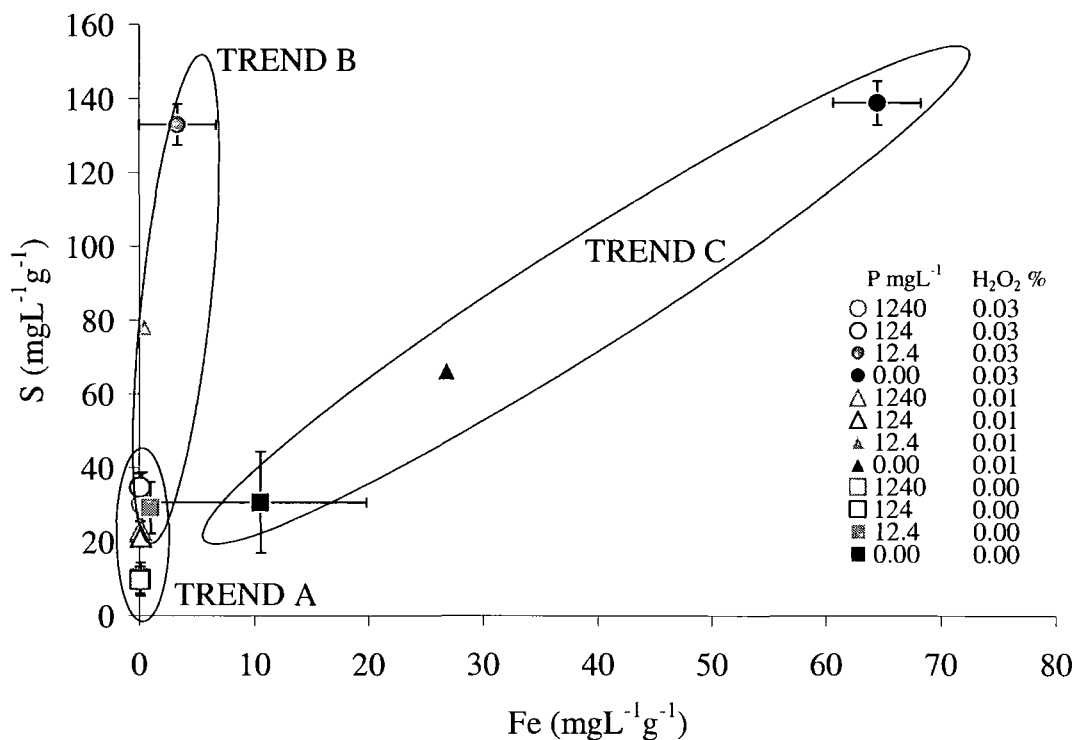
Figure 3.2. Mean S concentration against mean Fe concentration, errors are 1σ, n=3. Key refers to treatment solution content.

In summary, treatment leachate chemistry suggests that pyrite pre-treated with 1240 to 124 mgL^{-1} P and 0 to 0.01% H_2O_2 should provide a phosphate coating, whilst minimising Fe and S release to solution.

Testing the treated pyrite for inhibition of oxidation

Test leachate S, Fe and P behaved similarly with changing treatment solution combination (Figure 3.3, Table 3A, Appendix II Results). In general, high treatment P provided increased S and Fe during testing for each level of treatment H_2O_2. Decreasing the treatment oxidant level led to less change in the range of S, Fe and P released during testing. Here, the variation in dissolved content of solution, removed after testing treated pyrite, is described for changes in the original treatment combination of phosphate and H_2O_2.

For samples treated with 0.03% H_2O_2, dissolved S during treatment increased from 1469 $\pm$ 173 mgL^{-1}g^{-1} to 1630 $\pm$ 364 mgL^{-1}g^{-1} when treatment P was lowered from 1240 mgL^{-1}g^{-1} to 124 mgL^{-1}g^{-1}. Decreasing the treatment P further from 12.4 to 0 mgL^{-1}g^{-1} resulted in a decrease in test leachate S of 1500 $\pm$ 80 mgL^{-1}g^{-1} and 1450 $\pm$ 201 mgL^{-1}g^{-1}. Similarly for treatment H_2O_2 of 0.01%, the test leachate S concentrations fell from 1894 $\pm$ 506 mgL^{-1}g^{-1} through 1576 $\pm$ 321 mgL^{-1}g^{-1} to 1412 $\pm$ 117 mgL^{-1}g^{-1} as the treatment P concentration decreased from 1240 to 0 mgL^{-1}. Test leachate S, from pyrite treated with 0.01% H_2O_2 alone, reached a maximum of 1785 $\pm$ 568 mgL^{-1}g^{-1}. Pyrite treated with the highest P level (1240 mgL^{-1}) alone produced 1511 $\pm$ 13 mgL^{-1}g^{-1} S during testing of 1st Optimisation pyrite. Pyrite treated with 124 mgL^{-1} of P released 1597 $\pm$ 282 mgL^{-1}g^{-1} of S on testing. For pyrite treated with 12.4 to 0 mgL^{-1} P, later testing pyrite with H_2O_2 released S concentrations of 1286 $\pm$ 216 mgL^{-1}g^{-1} and 1207 $\pm$ 101 mgL^{-1}g^{-1} respectively.

Test leachate Fe concentration behaved in a similar manner to dissolved S during testing (Figure 3.3). For samples treated with 0.03% H_2O_2 and high P (1240 mgL^{-1} or 124 mgL^{-1}), Fe concentration increased from 706 $\pm$ 50 mgL^{-1}g^{-1} to 899 $\pm$ 234 mgL^{-1}g^{-1}. Decreasing treatment P from 12.4 to 0 mgL^{-1} led to a decrease in Fe concentration removed during testing, from 728 $\pm$ 101 mgL^{-1}g^{-1} to 686 $\pm$ 144 mgL^{-1}g^{-1}. For pyrite treated with 0.01% H_2O_2, test leachate Fe fell from 991 $\pm$ 247 mgL^{-1}g^{-1} to 478 $\pm$ 282 mgL^{-1}g^{-1}, as treatment P concentration decreased from 1240 to 0 mgL^{-1}. When pyrite was treated with phosphate solution alone the sample treated with the high P concentration of 1240 mgL^{-1} released the greatest amount of Fe of 791 $\pm$ 160 mgL^{-1}g^{-1} during testing. Pyrite samples treated with 124, 12.4 and 0 mgL^{-1} P alone, released
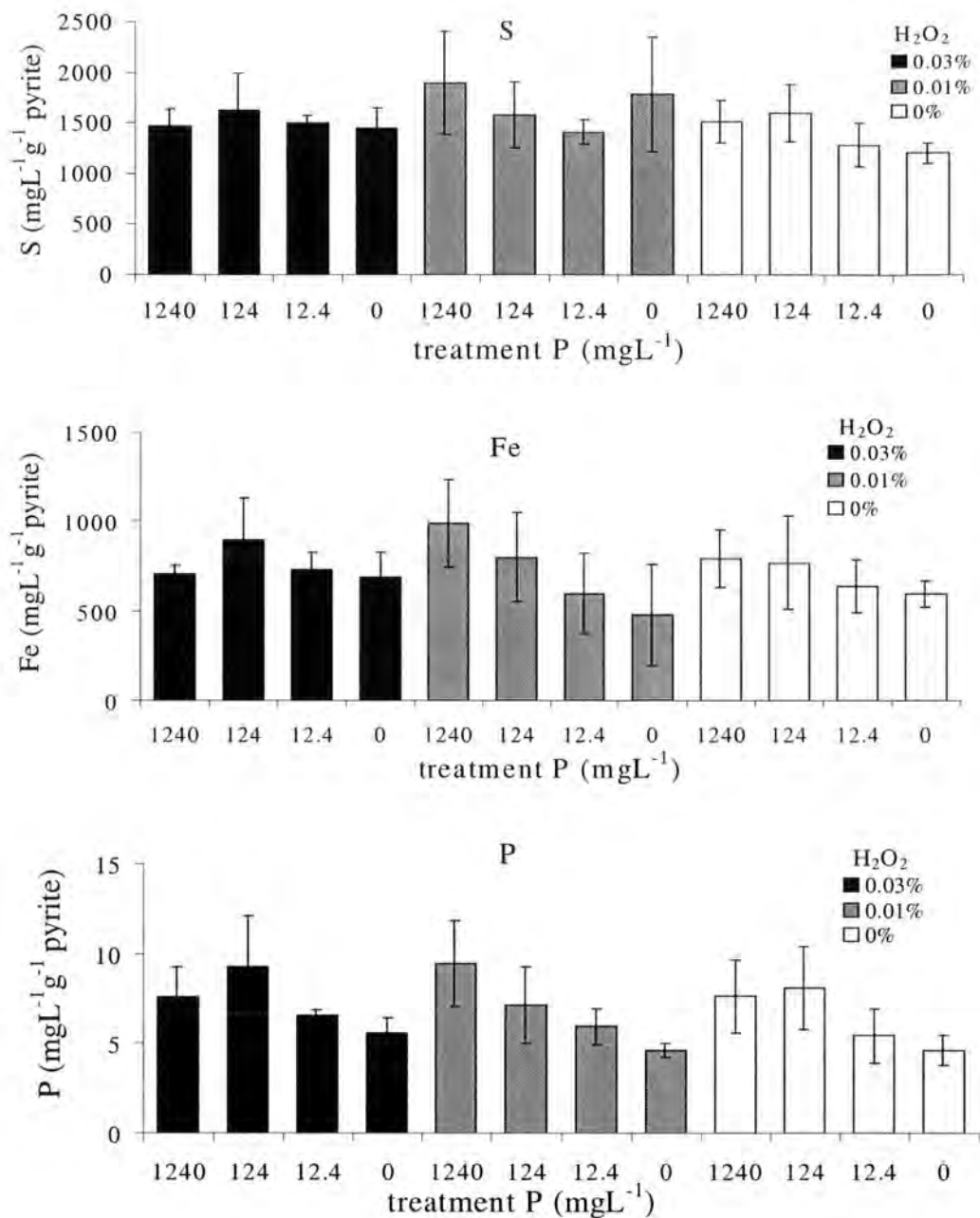
Figure 3.3. Histograms of mean S (upper), Fe (middle) and P (lower) concentration produced per g of 1st Optimisation treated pyrite during oxidation with 1.2% H$_2$O$_2$. Sample labels refer to treatments described in Table .3.1. Errors are 1 σ, n=2.

decreasing test leachate Fe concentrations of 770 ± 260 mgL^{-1}g^{-1}, 641 ± 147 mgL^{-1}g^{-1} and 596 ± 72 mgL^{-1}g^{-1} respectively.

Any release of P to solution during testing of treated pyrite should be derived from the dissolution of phosphate retained as a solid during treatment. However, P was present in the test leachate of pyrite not previously treated with phosphate solution (Table 3.A. Appendix II Results). Cross-contamination during filtering, despite thorough washing of equipment between samples with high purity water, would account for the presence of dissolved P. A filter blank of Milli-Q water was run at the beginning and end of filtering and provided an initial value 1.79 mgL^{-1} P and a final value of 0.08 mgL^{-1}. The P concentration in test leachates for pyrite treated with 0.03%, 0.01% and 0% H$_2$O$_2$ alone, remained at 5.6 ± 5 mgL^{-1}g^{-1}, 4.6 ± 0.4 mgL^{-1}g^{-1} and 4.6 ± 0.4 mgL^{-1}g^{-1} respectively. Phosphate treated pyrite released higher levels of P during testing than samples originally not treated with phosphate. The pattern of P release correlated with the increase in prior treatment P (Figure 3.3). It is therefore assumed that phosphate treated samples were releasing P retained from previous treatment.

In general, pyrite treated with high concentrations of phosphate released the most dissolved P, on testing for each treatment level of H$_2$O$_2$. Pyrite treated with the highest concentrations of P and H$_2$O$_2$ on testing released P concentrations which were slightly lower (8 ± 2 mgL^{-1}g^{-1}) than released from pyrite treated with 124 mgL^{-1} and 0.03% H$_2$O$_2$ (9 ± 3 mgL^{-1}g^{-1}). At the 12.4 to 0 mgL^{-1} P concentration treatment level, subsequent pyrite testing released 6.5 ± 0.4 mgL^{-1}g^{-1}. At the lower treatment H$_2$O$_2$ level of 0.01%, P released during testing decreased from 10 ± 2 mgL^{-1}g^{-1} to 6.0 ± 0.9 mgL^{-1}g^{-1} as treatment P decreased. Pyrite treated with 1240 mgL^{-1} phosphate solution alone released 7 ± 2 mgL^{-1}g^{-1} P to solution during testing. As the treatment P concentration decreased with no oxidant present, test oxidation P increased to 8 ± 2 mgL^{-1}g^{-1} for 124 mgL^{-1} of P, then decreased to 5 ± 2 mgL^{-1}g^{-1} for the 12.4 mgL^{-1} sample.

In summary, there is a strong relationship between increasing treatment P level and test leachate Fe and P content. The release of S during test oxidation was less controlled by treatment P concentration. Any correlation was more prominent when H$_2$O$_2$ is included in the treatment solution. Without this oxidant, there was less change in test leachate content with increasing treatment P. The results of test oxidation of 1st Optimisation treated pyrite suggest that treatment with low H$_2$O$_2$ (0.01%) and 124 to 1240 mgL^{-1} P provides better protection against oxidative attack.

Treatment H$_2$O$_2$ (%)	Treatment P (mgL^{-1})	Final Test Leachate H$_2$O$_2$ content (mM)	
		Replicate 1	Replicate 2
Pyrite free blank		5.9	5.9
0.03	1240	0.55	0
0.03	124	0	0
0.03	12.4	0.35	0
0.03	0	0	0.25
0.01	1240	0	0.15
0.01	124	0.25	0
0.01	12.4	0	0.25
0.01	0	0	2.9
0.0	1240	0	0
0.0	124	2.85	0.025
0.0	12.4	0.25	0
0.0	0	0	0

Table 3.2. Remaining H$_2$O$_2$ in test leachate after oxidising treated pyrite with 1.2% H$_2$O$_2$ for 24 hours. Both replicates are shown for each initial treatment.

Titration of remaining H$_2$O$_2$ in test leachate.

Results of the titration of test leachate H$_2$O$_2$ show that replicates of similarly treated samples differ by an order of magnitude, indicating that individual samples reacted to the phosphate treatment with differing levels of success (Table 3.2). Leachates from two replicates treated with initial solutions of 0% H$_2$O$_2$ and 124 mgL^{-1} P and 0.01% H$_2$O$_2$ and 0 mgL^{-1} P, both have the largest remaining concentration of H$_2$O$_2$ of with a difference of 3 mmol H$_2$O$_2$ from the blank value of 5.9 mmol. All other leachates differed from the blank value by 5 to 6 mmol H$_2$O$_2$, suggesting that a negligible volume of peroxide remained in the test leachate. As the results of this style of testing did not compare well with the chemical analysis of leachate, this method was not subsequently used.

3.2.3   Discussion of 1st Optimisation Treatment and Testing

Minimising P, Fe and S release to solution during treatment.

The change in control of pyrite oxidation by varying P and H$_2$O$_2$ concentrations in the treatment solution can be clearly seen from Figure 3.2. For samples pre-treated with no phosphate, increasing H$_2$O$_2$ concentration wholly controlled the extent of reaction. Similarly, in the samples treated with 12.4 mgL^{-1} P, oxidation was controlled by H$_2$O$_2$, but most of the Fe produced was removed from solution by precipitation with the phosphate. As the S level remained similar for samples in trend B as for those reacted with H$_2$O$_2$ alone (trend A), it may be concluded oxidation continued to the same extent.

Any Fe-phosphate produced was therefore not precipitated as a coating on pyrite grains, but as a discrete phase. For the highest initial phosphate treatments at 1240 and 124 mgL^{-1}, oxidation still occurred as demonstrated by an increase in leachate S. However, the lower than expected S content shows that the extent of oxidation was depressed compared to samples with lower phosphate. Such depression was probably due to the production of a phosphate coating, reducing the oxidation of pyrite during treatment compared to other treatment combinations.

Evangelou (1995) introduced a concept of requiring super-saturation of the surface of pyrite grains with respect to $FePO_4$ (or a hydrated Fe-phosphate) in order to form an insoluble coating. The results from the performed treatment experiment suggest that 124 to 1240 mgL^{-1} P solutions provide super-saturation of the pyrite surface. The chemistry of the treatment leachates for 1240 mgL^{-1} and 124 mgL^{-1} samples are similar. If phosphate use is to be minimised then the preferred treatment P concentration will be closer to the lower 124 mgL^{-1} P value.

Testing 1st optimisation treated pyrite – leachate chemical content and titration.

The testing of treated pyrite with 1.2% H_2O_2 led to unexpected results, given the interpretation of the optimisation treatment leachate chemistry above. Contrary to the findings of treatment leachate chemistry, the lower P concentrations seem to be more successful at providing post-treatment protection against oxidation.

Titration of the test solution to determine remaining H_2O_2 showed that for all treatments, except two replicates of different treatments, the oxidant had been consumed. The two exceptions were a replicate treated with 0.01% H_2O_2 alone and another replicate treated with 124 mgL^{-1} P alone.

Comparing testing of phosphate treated pyrite with untreated pyrite

When log values of Fe from the untreated pyrite are plotted as a function of log S from the same source, an exponential curve may be fitted to the points (Figure 3.5). The curve may be calibrated for increasing values of Fe and S produced by increasing treatment H_2O_2 strength. Treated pyrite samples have slightly higher S concentrations and cluster in a region corresponding to oxidation with approximately 0.1 - 0.4 % H_2O_2. The elevated S concentration can be attributed to the dissolution of soluble oxidation products formed during prior phosphate treatment. The Fe released during the treatment was potentially precipitated with phosphate during drying of the samples.
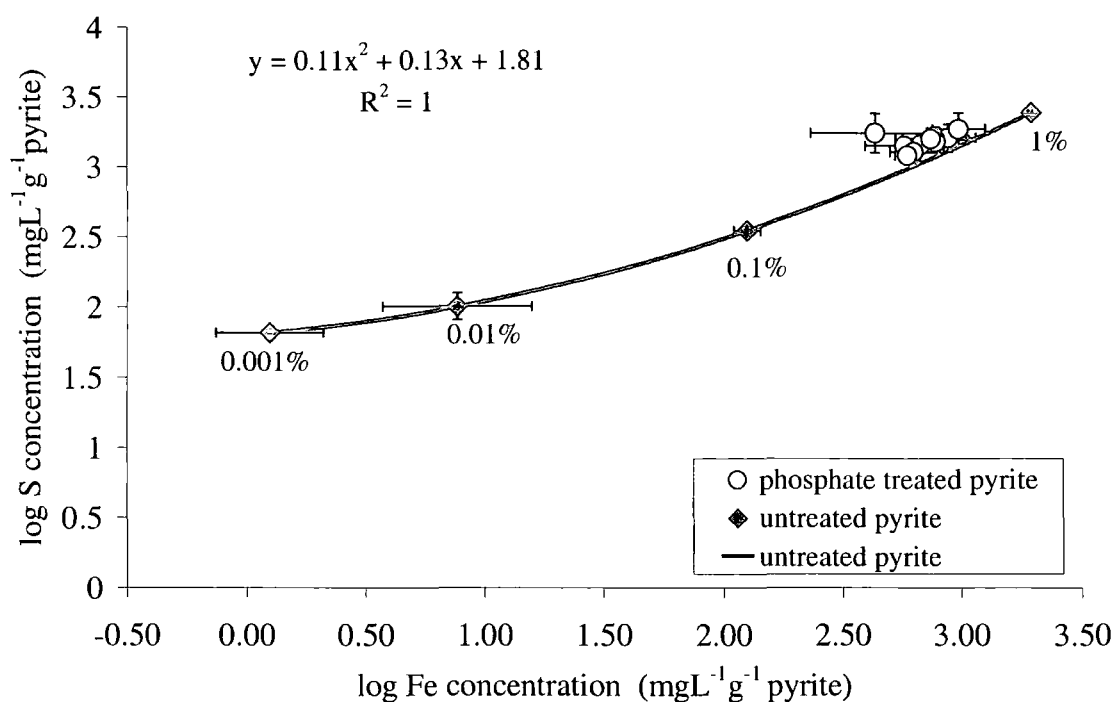
Figure 3.4. Log-log plot of Fe and S concentration in test leachate of pre-treated pyrite and untreated pyrite. The trendline represents leachate from 0.1g of untreated pyrite oxidized with increasing strengths of H_2O_2 as labelled on the diagram.

Comparing phosphate treated pyrite with H_2O_2 treated pyrite from the same group

The clustering of phosphate treated samples in a region corresponding to lower H_2O_2 than used suggests that the surface area of pyrite exposed to the oxidant is less than that of the untreated pyrite (Figure 3.4). Reduced treated pyrite surface area was caused either by precipitation of an oxidation inhibiting coating, or pyrite consumption during prior treatment. The distribution of Fe and S released during testing of treated pyrite samples is such that pyrite treated with low to zero phosphate have lower test S and Fe (Figure 3.5). Therefore, either the low phosphate samples have more protection against oxidation, or are consumed to a point where the change in particle size significantly affects subsequent oxidation rates. Such a change would also lead to less oxidant uptake during testing, resulting in a high level of H_2O_2 remaining for titration.

Dissolved concentrations from samples treated with H_2O_2 alone can be used to estimate the proportion of the sample consumed during treatment. The calculated loss of mass ranges from 0.63 to 0.11% for 0.1g of pyrite oxidised with 20mL of 0.03%, 0.01% and 0% H_2O_2 respectively (Table 3.3). The change in mass is low in comparison to the total mass of the sample. The non-phosphate treated samples were unprotected over the whole of the treatment period, unlike some of the phosphate samples discussed above. Therefore more of the non-phosphate treated pyrite would have been consumed,

leading to a lower surface area, and the lower Fe and S release seen during testing. The uncertainty in the post treatment surface area of the pyrite and its effects on subsequent oxidation rates brings the comparison with untreated pyrite and increasing H_2O_2 levels (previous section) into question. However, the argument for formation of a protective coating during treatment within phosphate and an oxidant is not weakened.
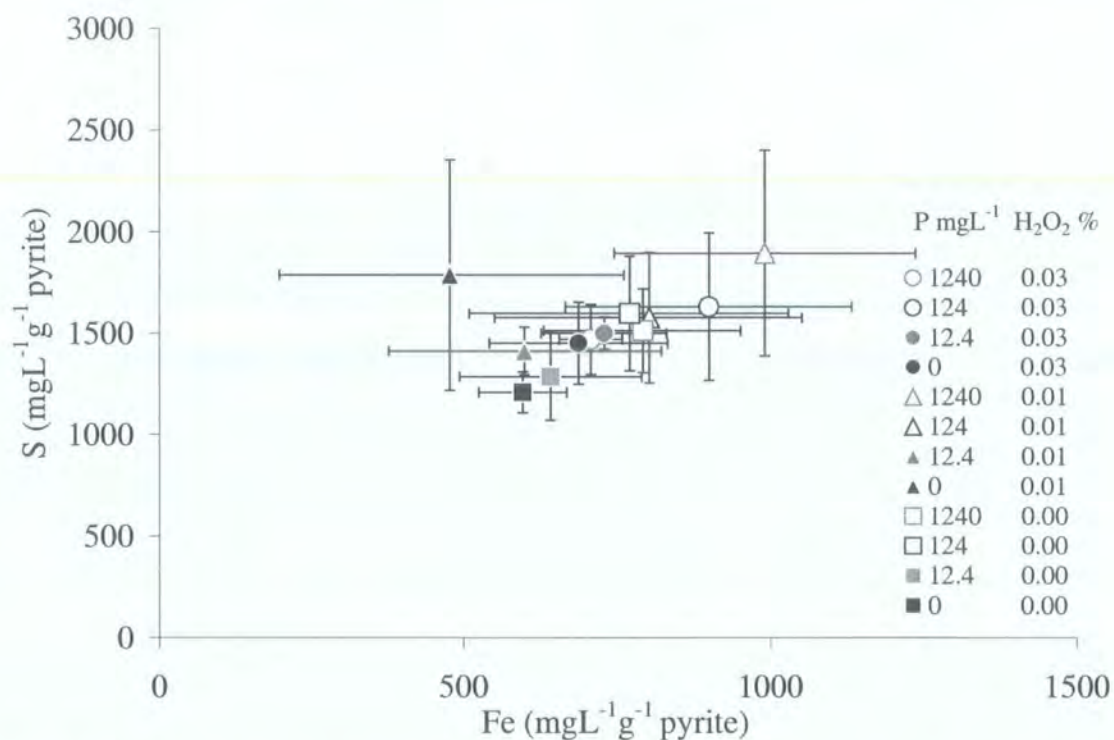
Figure 3.5. Concentration of S and Fe in test leachate of 1st Optimisation treated pyrite. Errors are 1σ (n = 2). Legend shows treatment solution composition.

Treatment H_2O_2 (%)	Fe (mgL^{-1})	Pyrite consumed (%)	Mass remaining (g)
0.03	6.4 ± 0.4	0.63	0.0994
0.01	2.68 ± 0.01	0.26	0.0997
0.00	1.1 ± 0.9	0.11	0.0999

Table 3.3. Calculated change in the mass of 0.1g pyrite during treatment oxidation.

The oxidation of pyrite during prior treatment may have produced a surface precipitation of Fe-hydroxide on drying. Thorough rinsing of samples prior to drying may have led to further oxidation of any un-coated pyrite. The high titration H_2O_2 value and inconsistent values of S and Fe in the test leachate of a sample treated with 0.01% H_2O_2 alone supports this. However, the release of P during testing suggests that pyrite treated at high P concentrations formed Fe-phosphate during treatment. Test

leachate chemistry shows that all 1st Optimisation treated pyrite suffered subsequent oxidation, yet to a lower extent than predicted from untreated pyrite (Figure 3.4). Thus pyrite treated with 124 - 1240 mgL^{-1} P and either 0.01% - 0.03% H_2O_2 formed a protective coating of insoluble phosphate. The coating retarded oxidation during treatment and testing when compared to untreated pyrite samples. Investigation of pyrite oxidised with H_2O_2 has shown that surface pits, scratches and edges require lower activation energies for oxidation and therefore may act as focus points for reaction (Lasaga 1984, McKibben and Barnes, 1986). As the coating reaction requires the oxidation of pyrite to take place it will be focused on the high-energy areas of grains and form an uneven or partial coating. The phosphate coating should form in the same manner, providing only a partial coating of pyrite. A more complete coating of pyrite may form over a longer period of treatment. The incompleteness of the coating leads to oxidation during testing and a drop in pH. If solution pH falls below 4 dissolution of Fe-phosphate will occur (Stumm and Morgan, 1996). This explains the presence of P in the test solution of pyrite treated with high P solutions.

3.2.4 Summary of 1st Optimisation Experiment

Treatment of pyrite with 1st Optimisation treatment solutions shows evidence of inhibition of oxidation, and the precipitation of Fe in a solid phase assumed to be Fe-phosphate. Treatment solutions containing 1240 – 124 mgL^{-1} P and 0.03 to 0.01% H_2O_2 provide this protection against oxidation. During subsequent oxidation of the treated pyrite with 1.2% H_2O_2 all samples produced lower amounts of Fe and S than predicted from oxidation of untreated pyrite. The formation of a partial coating would allow continued oxidation. Pyrite treated with low P solutions released the least amount of Fe and S on testing, contrary to treatment predictions, possibly as a result of Fe-hydroxide precipitation, which also retards subsequent oxidation (Nicholson et al., 1990). However, Fe-hydroxide precipitation may not retard pyrite oxidation during short-term reactions (Moses et al., 1990, Bonnisel-Gissenger et al., 1998). To focus in on the combination providing the least S and Fe during treatment and requiring the lowest treatment P, the region of 1240 to 124 mgL^{-1} P and 0.01 - 0.0% H_2O_2 should be investigated.

3.3   2nd Optimisation

From the previous experiment it was concluded that the best region to focus down on, to optimise the Fe-phosphate coating of pyrite, would be between 800 mgL^{-1} and 80 mgL^{-1} with peroxide at lower concentrations of 0.01, 0.005, and 0.0% H_2O_2. These concentrations were chosen as they were thought to provide the minimum concentrations of P and H_2O_2 required to form a coating, and to minimise initial S and Fe release to solution.

3.3.1   2nd Optimisation - Method

The technique a previously described in section 3.4 was used to clean and prepare pyrite for treatment with 2nd Optimisation solutions. In this experiment coal-hosted pyrite from the Pegswood Opencast, UK (NZ 205880) was used. Also reaction vessels were disposable sterilin tubes in place of previously used the glass conical flasks. 20 mL of treatment solution, in all possible combinations of concentrations in Table 3.4, were mixed in the sterilin tubes and 0.1 g of freshly cleaned pyrite was added to each.

H_2O_2 %	P mgL^{-1}
0.01	800
0.005	550
0.00	300
	80

Table 3.4. Concentrations of P and H_2O_2 for combination in 2nd Optimisation treatment solutions.

Three replicates of each treatment were made up plus a blank containing no pyrite. The tubes were sealed and shaken for 10 minutes to mix the solution and pyrite, then left for 24 hours. The method of removal of treated sample and their testing was the same as used in the previous experiment (section 3.2). Here 0.07g of treated pyrite was dried at 105°C, then tested with 20 mL of 1.2% H_2O_2 for 24 hours, in a clean sterilin tube. Again filtrates were analysed by ICP-OES for dissolved Fe, S and P (Appendix I Methods). The pH of the filtrate was also measured using a Whatman bench pH meter calibrated with pH 4 and 7 buffer solutions prior to use.

3.3.2 Results of 2nd Optimisation treatments

Coating Treatment

Overall dissolved concentrations of Fe varied between 2 ± 2 mgL^{-1}g^{-1} and $85 \pm$ 20 mgL^{-1}g^{-1} and S from 8 ± 1 mgL^{-1}g^{-1} to 433.6 ± 0.9 mgL^{-1}g^{-1} during treatment with 2nd Optimisation solutions (Table 3.B., Appendix II Results). The effect of increasing H$_2$O$_2$ concentration in treatment solution is clear (Figure 3.6). Leachate from samples treated with 0.01% H$_2$O$_2$ contained between 420 ± 57 mgL^{-1}g^{-1} and 433.8 ± 0.9 mgL^{-1}g^{-1} of S, whereas treatment with 0.005% H$_2$O$_2$ released 184 ± 12 mgL^{-1}g^{-1} to 270 ± 24 mgL^{-1}g^{-1} of S. Samples treated with P alone produced a leachate S concentration of 7.4 ± 1 mgL^{-1}g^{-1} to 9.0 ± 0.4 mgL^{-1}g^{-1}. Changes in treatment concentration of dissolved P had less control over the final treatment solution dissolved S. For each treatment H$_2$O$_2$ level, the S content remained constant with changing P concentration (Figure 3.6).
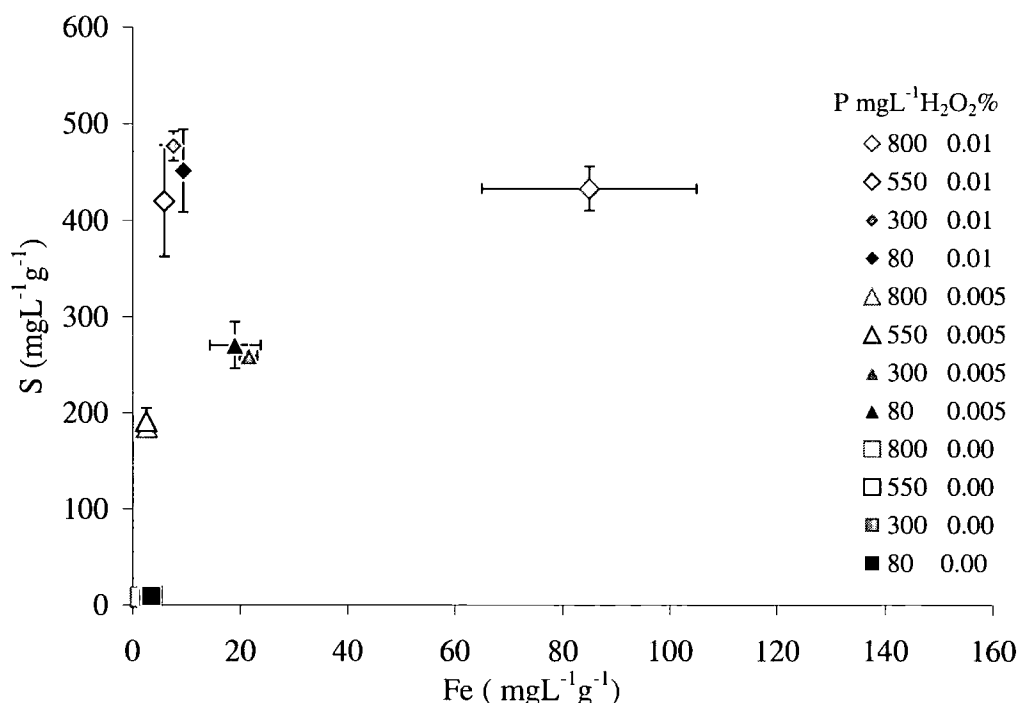
Figure 3.6. Mean concentration of Fe plotted against S, in the 2nd optimisation treatment leachate, n=3. Errors shown are 1σ (n=3). Key refers to pre-treatments.

Fe concentration showed a greater response to the treatment P level than S. When combined with H$_2$O$_2$, samples treated with 550-800 mgL^{-1} of P released less Fe than those treated with 80-330 mgL^{-1} of P. Pyrite treated with 0.005% H$_2$O$_2$ and high

concentrations of P produced 2.6 ± 0.4 $mgL^{-1}g^{-1}$ to 2.5 ± 0.1 $mgL^{-1}g^{-1}$ of dissolved Fe during treatment. When the treatment P is lowered to 80-330 mgL^{-1} pyrite produces almost 10 times as much Fe, at 19 ± 8 $mgL^{-1}g^{-1}$ to 22 ± 3 $mgL^{-1}g^{-1}$ respectively. Increasing treatment H_2O_2 to 0.01% led to a smaller difference in Fe release for high and low treatment P concentrations. The 550 mgL^{-1} treatment P sample contained $5.8 \pm$ 0.8 $mgL^{-1}g^{-1}$ of Fe, and the 80-300 mgL^{-1} treatment P sample contained 9.3 ± 0.7 $mgL^{-1}g^{-1}$ and 7.4 ± 0 $mgL^{-1}g^{-1}$ of Fe respectively. Pyrite treated with the highest P and H_2O_2 concentrations did not the pattern of lowered Fe release with high treatment P, releasing 85 ± 20 $mgL^{-1}g^{-1}$ of Fe. Considering the high P content of the treatment solution for this sample, the relatively high Fe release is unexpected.

Treatment leachate Fe and S content derived from pyrite treated with 0.005% to 0.01% H_2O_2 and 550 to 800 mgL^{-1} P, were lower than from pyrite treated with P of 80 to 300 mgL^{-1}. Higher concentration of P in treatment solutions, when combined with a low concentration of oxidant, retards oxidation during treatment more effectively than lower P concentrations. The exception to this is treatment with 800 mgL^{-1} P and 0.01% H_2O_2, where Fe content was high relative to treatments with comparative H_2O_2, yet there was no correspondingly high S release.

Testing 2nd Optimisation treated pyrite.

The pattern of behaviour of S and Fe for pyrite treated with the same P concentration wass similar (Figure 3.7, Table 3.B., Appendix II Results). Both S and Fe increased in the test solution as treatment H_2O_2 was increased. Test oxidation released the lowest P from pyrite treated with phosphate alone. For the whole 2nd Optimisation group of treated pyrite, test leachate Fe varied between 69 ± 19 $mgL^{-1}g^{-1}$ to 32 ± 5 $mgL^{-1}g^{-1}$, with S from 146 ± 24 $mgL^{-1}g^{-1}$ to 90 ± 17 $mgL^{-1}g^{-1}$ and P from 2.6 ± 0.6 $mgL^{-1}g^{-1}$ to 1.5 ± 0.1 $mgL^{-1}g^{-1}$.

For pyrite treated with 0.01% H_2O_2 there is a clear boundary between pyrite treated with 800 to 550 mgL^{-1} and 300 to 80 mgL^{-1} of P (Figure 3.8). Testing of the pyrite originally treated with high concentrations of P, released 37 ± 8 to 32 ± 5 $mgL^{-1}g^{-1}$ of Fe and 95 ± 17 to 90 ± 17 $mgL^{-1}g^{-1}$ of S. Lower concentrations of treatment P produced pyrite which on testing released higher concentrations of Fe from 47 ± 20 to 45 ± 2 $mgL^{-1}g^{-1}$, and S of 121 ± 37 to 116 ± 2 $mgL^{-1}g^{-1}$. The release of P to solution from pyrite originally treated with 0.01% H_2O_2 was between 2.2 ± 0.5 and 2.6 ± 0.6 $mgL^{-1}g^{-1}$.

Decreasing treatment H_2O_2 to 0.005% led to increases in both Fe and S released to solution during test oxidation, with decreasing treatment P (Figure 3.7). In this group,
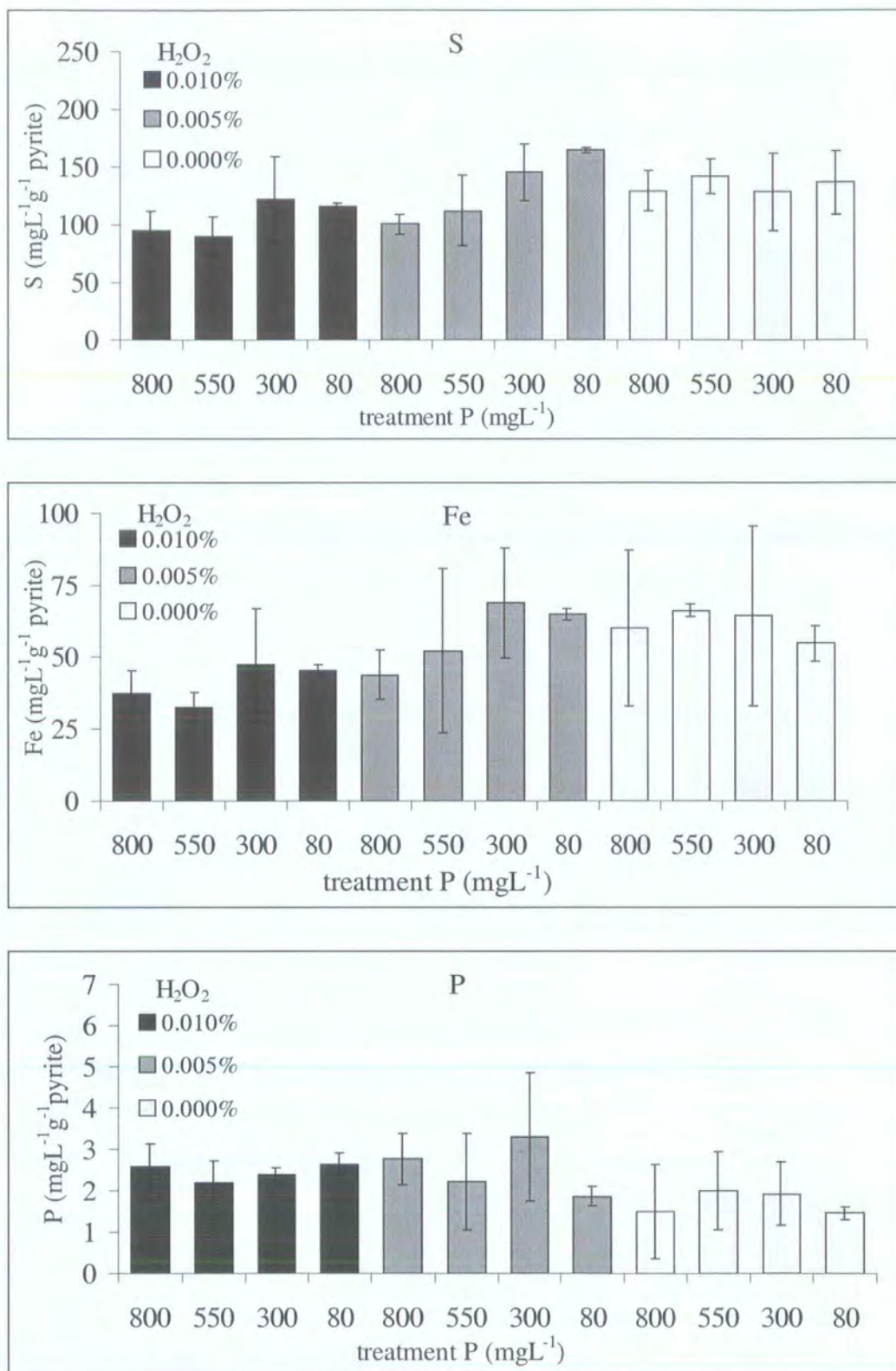
Figure 3.7. Histograms of Fe, S and P concentration in the 2nd optimisation test leachate. Errors shown are the 1σ, n=3.

Fe increased from 44 ± 9 to 69 ± 19 mgL^{-1}g^{-1} for an increase in treatment P of 800 to 300 mgL^{-1}. For pyrite treated with 80 mgL^{-1} of P, test leachate Fe departed from this trend, falling to 65 ± 2 mgL^{-1}g^{-1}. The S content of the test leachate solution increased for samples treated with 800 to 80 mgL^{-1} P and 0.005% H_2O_2 from 101 ± 8 to 165 ± 3 mgL^{-1}g^{-1}. Dissolved P released during testing of the pyrite samples treated with 800 to 80 mgL^{-1} P and 0.005% H_2O_2, was higher than from pyrite treated with 0.01% H_2O_2. Typical dissolved concentrations ranged from 3 ± 2 to 1.9 ± 0.2 mgL^{-1}g^{-1} of P.

The oxidation of pyrite treated with phosphate solution alone produces the highest S values of whole 2nd Optimisation group (Figure 3.7). As treatment P concentration was lowered from 800 to 80 mgL^{-1}, the S released to solution during testing fluctuated between 129 ± 33 mgL^{-1}g^{-1} and 142 ± 15 mgL^{-1}g^{-1}. At the same time Fe increased from 60 ± 27 mgL^{-1}g^{-1} to 66 ± 2 mgL^{-1}g^{-1} as treatment P decreased from 800 to 550 mgL^{-1}. For the lower P treatments, Fe release decreased to 64 ± 31 then 54 ± 6 mgL^{-1}g^{-1} during test oxidation. For this group of treated pyrite, testing produces dissolved P which decreases from 2 ± 1 mgL^{-1}g^{-1} to 1.5 ± 0.1 mgL^{-1}g^{-1} as original treatment P decreases. Dissolution of P from pyrite treated with 0.005% H_2O_2 or phosphate alone was controlled by the initial treatment P concentration.

Initial treatment concentrations		Treatment solution pH	Treatment leachate pH	Test leachate pH
H_2O_2 %	P mgL^{-1}g^{-1}			
0.01	800	4.61	3.01 ± 0.03	3.34 ± 0.05
0.01	550	4.64	2.86 ± 0.07	3.36 ± 0.08
0.01	300	4.64	2.69 ± 0.02	3.27 ± 0.03
0.01	80	4.86	2.57 ± 0.03	3.07 ± 0.08
0.005	800	4.45	2.87 ± 0.46	3.34 ± 0.06
0.005	550	4.64	3.19 ± 0.03	3.28 ± 0.1
0.005	300	4.73	2.99 ± 0.04	3.10 ± 0.03
0.005	80	4.86	2.79 ± 0.05	2.95 ± 0.13
0.00	800	4.63	4.48 ± 0.06	3.20 ± 0.09
0.00	550	4.64	4.50 ± 0.01	3.11 ± 0.05
0.00	300	4.73	4.49 ± 0.04	3.13 ± 0.0
0.00	80	5.00	4.50 ± 0.02	3.09 ± 0.02

Table 3.5. 2nd Optimisation treatment solution pH before and after leaching of pyrite, and test leachate pH after reaction for 24 hours.

The test leachate pH decreased with increased treatment P concentration (Table 3.5). Samples treated with the highest H_2O_2 concentration had pH ranging from 3.36 to 3.20,

whereas pyrite treated with 0.005% H_2O_2 had a test solution pH range of 3.10 to 3.28. Pyrite treated with phosphate had the lowest range of test leachate pH from 2.95 to 3.13, the upper limit being from pyrite treated with 800 mgL^{-1} P.

The Fe and S concentration and solution pH produced during testing of treated pyrite suggest that pyrite treated with 0.01% H_2O_2 and 800-500 mgL^{-1} P undergo the least amount of oxidation. The pattern of P release to solution suggests that treatment oxidant is necessary to retain phosphate in the solid phase.

3.3.3 Discussion of 2nd Optimisation treatments

Compared to 1st Optimisation treatment and test leachate, 2nd Optimisation treatment of pyrite produced approximately an order of magnitude higher Fe and S, whilst testing produced an order of magnitude lower Fe and S. Production of greater amounts of Fe and S from the pyrite used in the 2nd Optimisation may be attributed to oxidation prior to treatment. Pyrite was not stored under argon as treatment was carried out within 24 hours of cleaning with HCl and acetone. The release of more Fe and S during testing of the 1st Optimisation again is probably due to the storage of treated pyrite prior to testing. In 2nd Optimisation experiment, the drying of pyrite and testing took place on the same day as treatment. For the 1st Optimisation experiment, pyrite was dried and stored for at least a day prior to testing. However, the distribution of Fe and S in treatment leachates may still be used to identify possible coating.

Coating treatment leachate chemistry

The treatment of pyrite with combinations of phosphate and H_2O_2 used in this 2nd Optimisation stage demonstrates the control of the oxidant strength on leachate S and, to a lesser extent, Fe. The concentration of P used to treat the pyrite, when in combination with H_2O_2, affected the Fe released to solution during treatment.

As with the interpretation of the 1st Optimisation, the suppression of S during treatment can be used here to indicate the presence of an oxidation inhibiting coating. Pyrite treated with phosphate alone releases low concentrations of Fe and S, and solution pH remains above 4. Under these conditions a reaction should take place. However, the lack of strong oxidant means that the production of Fe^{3+} is slow. Without this important reactant, the formation of substantial amounts of Fe-phosphate will not occur over the period of treatment.

Pyrite treated with 0.005% H_2O_2 shows a definite difference in reduction of S release by approximately 80 mgL^{-1} between the high and low P treatments. At treatment P

levels of 800-550 mgL^{-1} rather than 300–80 mgL^{-1}, there is sufficient P present to super-saturate the surface of the pyrite, precipitating a coating to suppress oxidation. Thus in the process of forming a Fe-phosphate precipitate, the super-saturation of the pyrite surface is futile unless Fe^{3+} is present and vice versa.

Treatment leachate from pyrite treated with 0.01% H_2O_2 and 550 mgL^{-1} of P contains slightly less S and Fe than treatments with 330-80 mgL^{-1} of P. Compared to the lower treatment level of 0.005% H_2O_2, the removal of Fe from solution is much better for low P treatments. Considering that the oxidation of this group of samples should be greater with the lower 0.005% H_2O_2, the removal of Fe^{3+} from solution is good for both high and low P treatments. The suppression of S release, and hence oxidation is not as marked as from the 0.005% level of treatment H_2O_2.

Solution pH

Solution pH controls precipitation even when super-saturation is reached. The high oxidant treatments have the lowest range of pH from 3 to 2.57 compared to the original solution pH of 4.61 to 4.86 (Table 3.5). As treatment solutions were not stirred throughout the reaction a diffusion gradient away from the pyrite surface of oxidation products probably formed (Lasaga, 1984). Therefore a gradient of pH should exist away from the pyrite surface, into the main body of the treatment solution. The upper and lower limits of this gradient will change with time. At the start of the treatment experiment leachate pH will be greater than 4, Fe^{3+} concentration will be close to zero and phosphate at the treatment concentration. The final treatment solution pH is a combination of this gradient's lowest and highest limits. Thus the final pH of less than 3 is lower and higher than actual pH, respectively closer to and further away from the pyrite surface. The lower pH range will ensure that both Fe^{3+} and P stay in solution close to pyrite. However, within the main body of the solution Fe^{3+} will be able to precipitate a discrete Fe-phosphate phase. The size of this diffusion gradient will depend upon the treatment oxidant strength and P concentration. A balance between of oxidant and phosphate is required which keeps pH high enough, yet produces sufficient Fe^{3+} and surface saturation with respect to P, in order to precipitate surface Fe-phosphate.

The anomalous high Fe concentration released during the treatment of pyrite with 800 mgL^{-1} P and 0.01% H_2O_2 could have been caused either by continued oxidation or by the dissolution of precipitated Fe-phosphate or Fe-oxide with decreasing pH. Continued oxidation would be accompanied by a concurrent increase in S. However, S released from this sample during treatment was similar to that from other treatments

with 0.01% H_2O_2 i.e. between 420 and 476 $mgL^{-1}g^{-1}$. The pH of all treatments using H_2O_2 was between 2.57 and 3.19, just below the stability field of Fe-phosphate and most Fe-oxides (Stumm and Morgan, 1999). The high reactant concentrations of the treatment of this sample could have produced a discrete Fe-phosphate phase in the manner described above. With continued oxidation of un-coated pyrite and lowering of pH this phase would begin to break down, releasing Fe and P. The pyrite for this sample was taken from the upper part of the storage bottle. Oxidation of pyrite during storage under inert conditions has been reported by many authors (Evangelou, 1995, Nicholson et al., 1988). It is possible that the inconsistent Fe concentration, produced during this treatment, was due to a combination of prior oxidation and the break down of initially precipitated Fe-phosphate.

Comparison of test oxidation chemistry of treated pyrite with untreated pyrite

There is good agreement between the predictions made from 2nd Optimisation treatment chemistry for the final test leachate Fe and S distributions. Both suggest that treatment with high P concentration, in the presence of an oxidant, provided some protection against further oxidation both during treatment and during testing (Figures 3.6 and 3.7). This supports the interpretation of the treatment reaction that coating formation requires sufficient treatment oxidant and P to super-saturate the pyrite surface with P and Fe^{3+} at a suitable pH. The removal of P to solution during testing was higher for pyrite treated with an oxidant than without (Figure 3.7). This either shows that the presence of a treatment oxidant precipitates a solid phosphate phase, or that lack of a treatment oxidant provides a more stable coating. The pattern of Fe and S removal to solution during testing suggests that the former situation was the case (Figure 3.8).

Comparing test oxidation Fe and S log values to those from untreated pyrite, the 2nd Optimisation group plots in the region of oxidation with 0.01 – 0.1% H_2O_2, i.e. lower than the 1st Optimisation samples (Figure 3.9). As the 2nd Optimisation treatment used slightly lower volume of H_2O_2, i.e. 20 mL rather than 25 mL 1.2% H_2O_2, this is as expected. However, the release of Fe and S from 2nd Optimisation testing of treated pyrite is 10 to 100 times lower than from 1st Optimisation testing. During treatment, Fe and S release was 10 times more than from 1st Optimisation samples. Possibly a reduction in surface area was significant in affecting the test oxidation products compared to the untreated pyrite. The proportion of pyrite consumed during treatment can be estimated by using the S release to solution. The S value is used as all treatment solutions contain P, and precipitation of Fe from solution would lead to underestimation of pyrite consumption if Fe concentration were used. Up to 3.8% of pyrite is consumed
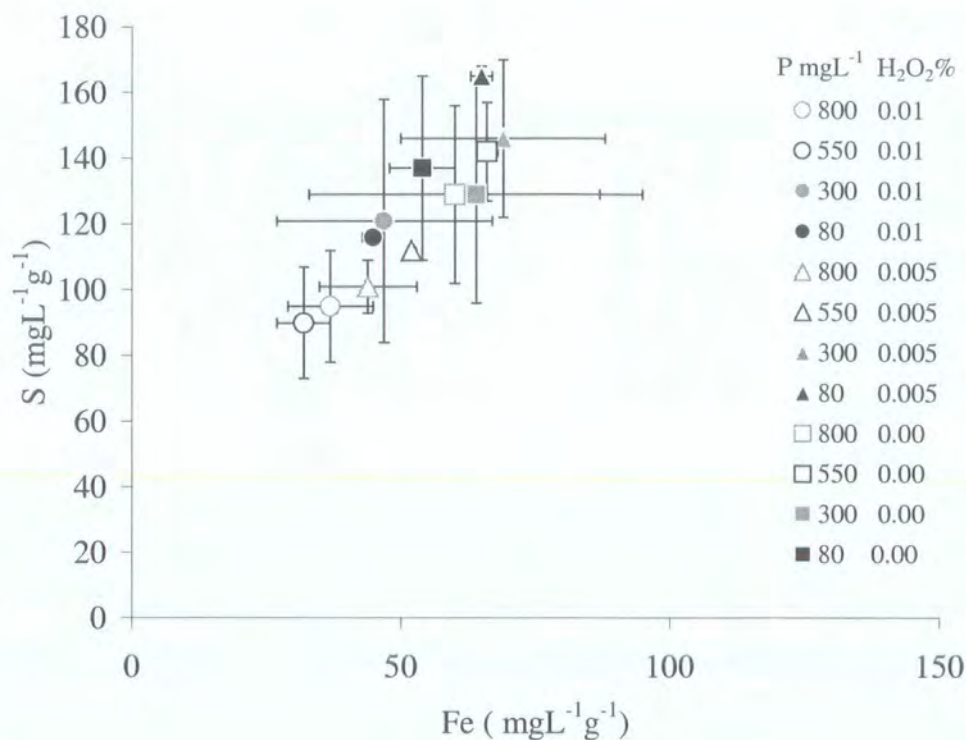
Figure 3.8. Mean concentration of Fe plotted against S, in the 2nd optimisation test
leachate. Errors shown are 1σ, n=3. Key refers to pre-treatments.
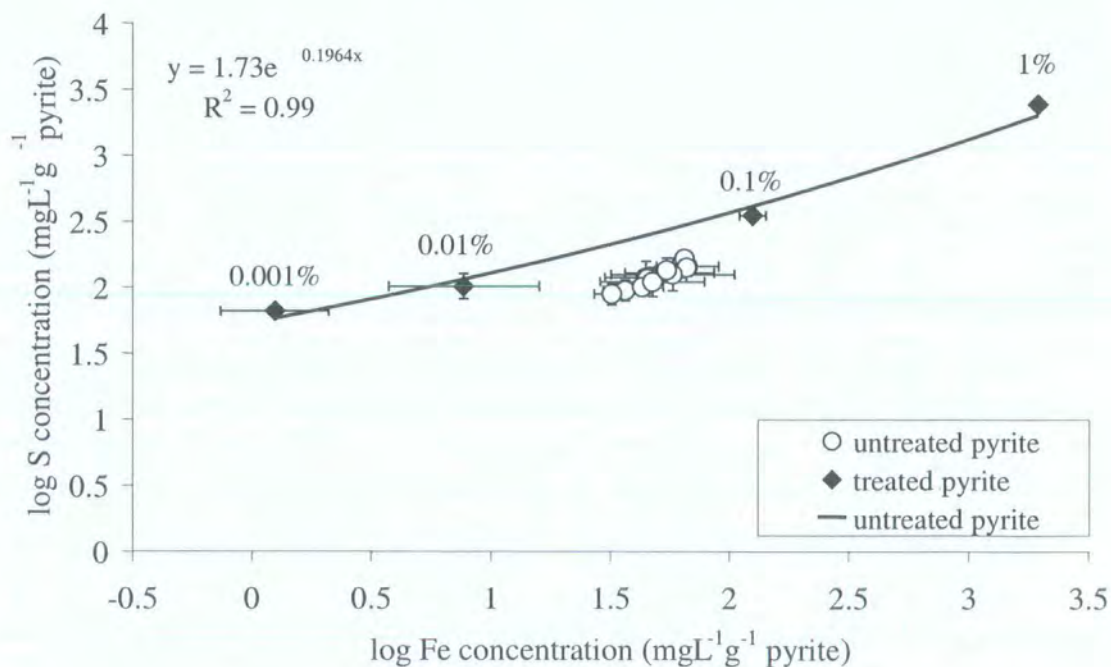
Figure 3.9. Log-log plot of Fe and S concentration produced during testing of 2nd
Optimisation treated pyrite with 1.2% H_2O_2. Untreated pyrite tested with
increasing strengths of H_2O_2 as labelled on trendline is also shown for
comparison. Errors shown are 1 σ (n=3).

during the treatment process (Table 3.6). Whether this decrease in sample volume is significant in reducing oxidation rate compared to that of untreated pyrite is uncertain. However, Nicholson et al., 1988 report a linear correlation of oxidation rate with decreasing surface area.

The test group Fe and S also lies below the untreated pyrite oxidation line suggesting that either S is too low or Fe is too high in comparison. Such a difference would be expected if the original treatment removed S from the pyrite whilst retaining Fe in a solid phosphate phase. The Fe-phosphate would break down due to the lowering of solution pH during oxidation of un-coated pyrite during testing.

Treatment H_2O_2 (%)	Mean S (mgL^{-1})	Pyrite consumed (%)	Mass remaining (g)
0.01	2.2 ± 0.1	3.8 ± 0.2	0.0962 ± 0.0002
0.005	1.1 ± 0.2	1.9 ± 0.4	0.0981 ± 0.0004
0.00	0.04 ± 0.003	0.071 ± 0.006	$0.0999 \pm 6 \times 10\text{-}6$

Table 3.6. Calculated mass of pyrite remaining after 2nd Optimisation treatments. S is used to calculate a mean value (n=4, σ=1) for groups of pyrite treated with the same H_2O_2 level, as it is not removed from solution by phosphate, unlike Fe.

Test leachate pH and partial coatings

The pH of test leachates suggests that although dissolution of Fe-phosphate should have taken place, retardation of pyrite oxidation was greatest in samples treated with highest P. Treatment of pyrite with phosphate alone produced a solution pH closest to the blank value, indicating that these samples may have formed a coating. However, the test leachate chemistry indicates that they have as much protection against oxidation as other pyrite treated with an oxidant. As previously discussed the partial coating of pyrite is due to the manner in which pyrite is oxidised by H_2O_2. Formation of a coating at areas of high excess surface energy would lead to an incomplete covering of the pyrite surface. During testing probable oxidation of this exposed pyrite led to the lowering of pH and consequently the breakdown of previously formed Fe-phosphate. The initial solution pH was above that required for a coating to form. The time for the decrease in treatment pH may allow for the precipitation of Fe-phosphate at the start of the experiment, with dissolution occurring towards the end of leaching.

3.3.4 2nd Optimisation - Summary of Findings

Samples treated with 800 and 550 mgL^{-1} P with 0.01% or 0.005% H_2O_2 seem to have the most protection against oxidative attack with 1.2% H_2O_2. Samples treated with phosphate alone have less protection against subsequent oxidation. The presence of H_2O_2 is required to form the Fe-phosphate coating which is most successful at retarding oxidation. Compared to untreated pyrite, the 2nd Optimisation treated pyrite produced Fe and S representative of oxidation with 0.01 to 0.1 % H_2O_2 rather than 1.2%, lower than the range found for 1st Optimisation samples. However, there is some uncertainty in comparing 2nd Optimisation treated with untreated pyrite testing, due to the un-quantified effect of decreasing sample surface area. The pH of the treatment and test solutions at the end of leaching suggests that any produced Fe-phosphate should be unstable. However, the formation of a gradient of pH and dissolved Fe^{3+} extending from the pyrite surface, would allow for variable solution pH and the precipitation of Fe-phosphate in apparently unsuitable conditions. The correct balance between surface Fe^{3+} and P is required to form a coating, and is therefore strongly dependent upon treatment combination at the time-scales investigated. Continued oxidation of pyrite after treatment is indicative of the formation of a partial coating on the pyrite surface. The manner of oxidation of pyrite by H_2O_2, at points of excess surface energy will also dictate the locality of a Fe-phosphate coating. It is possible that longer exposure to treatment solution may aid the formation of a more extensive coating.

3.4 Summary of Optimisation Experiments

Comparison of Fe and S, released during treatment and testing of pyrite with varying reactant strengths, was made difficult by uncertainty about prior atmospheric oxidation. The effect of decreased sample surface area due to prior oxidation also hampered the comparison of treated and untreated pyrite oxidation products. However, the pattern of Fe, S and P release during treatment and testing allowed interpretation of the effects of experimental oxidation, within each experiment. Despite the problems caused by uncontrolled atmospheric oxidation, the first two stages of optimisation have shown that so far the best combination of H_2O_2 and P concentrations are 550mgL^{-1} and 0.01% H_2O_2. This mixture produced the lowest amount of Fe and S at low treatment P, whilst suppressing oxidation during treatment. Testing of pyrite treated with this combination also produced relatively low Fe and S within its group. Both the test and treatment leachates for each optimisation stage have shown that the production of Fe^{3+} requires the presence of a strong oxidant, at these experimental time-scales. The formation of a

gradient of oxidation product concentration away from the pyrite surface allowed the precipitation of Fe-phosphate under seemingly unsuitable whole solution pH conditions. The chemical conditions within the fluid surrounding the pyrite particles will depend upon the treatment solution and the time over which the diffusion gradient may form. However, treatment over the period of a day forms a partial coating, probably at regions of excess surface energy such as edges and pits, in the manner of pyrite oxidation by H_2O_2 (McKibben and Barnes, 1986).

3.5 Reaction Kinetics Experiment

During the optimisation reactions some of the kinetics of the treatment reaction were brought into question. In order to understand the process of reaction more fully as a function of time the coating treatment was carried out over 48 hours with pH and treatment leachate chemistry monitored throughout.

3.5.1 Method - Kinetic Experiment

The cleaned pyrite used in the 1st Optimisation (section 3.4.1) was used for this experiment. A solution containing 60 mgL^{-1} P and 0.005% H_2O_2 was prepared in 48 conical flasks and 0.1g of previously cleaned pyrite was added to each flask with 12 of the flasks left without pyrite, to act as blanks. The flasks were grouped into fours, three flasks with pyrite and one without as a blank flask. Each group represented a time stage at which the treatment of pyrite inside the flasks would be halted. The halting times were 5, 10, 20, 35, 45, 60, 120, 480, 600, 1440 and 2880 minutes. The reaction was halted by vacuum filtering samples through a 0.45 μm pore cellulose nitrate membrane filter, with the residue retained, dried at 40 °C then stored a sealed glass bottle. The filtrate was analysed for Fe, S and P by ICP-OES. The pH of each replicate was recorded as the reaction was halted.

To test the presence and stability of any coating formed 0.07g of the dried treated pyrite was leached overnight with 0.01% H_2O_2 with the leachate analysed for Fe, S and P by ICP-OES. During removal of pyrite from dried filter papers at least one replicate was partially lost per treatment. Therefore for all but the 10 and 20 minute samples only one replicate was tested.

3.5.2 Results of Kinetic Experiment

Treatment leachate chemistry

ICP-OES analyses of Fe, S and P concentrations in the treatment leachate at each consecutive time stage are presented in Table 3.C (Appendix II Results), and also plotted as a function of time in Figures 3.10 to 3.12. Leachate concentrations are given as values of solute concentration per gram of original pyrite.
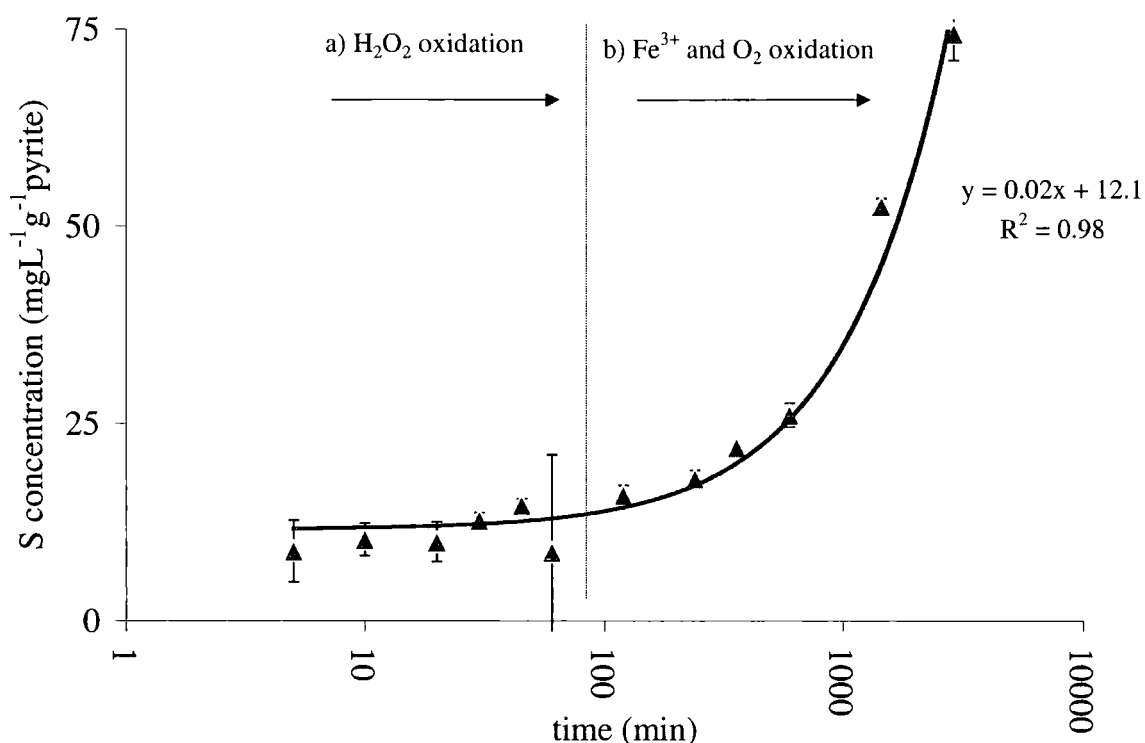
Figure 3.10. Concentration of S in treatment leachate as a function of time, for 0.1g pyrite treated with 60 mgL^{-1} P and 0.005 % H_2O_2 over a period of 48 hours. At least two rates of oxidation are observed a) pyrite oxidation with H_2O_2 which shows a transport control b) oxidation with oxygen and Fe^{3+}which shows a mixture of transport and surface control.

The release of S to solution during treatment increases with time, although the rate of release slows due to changes in dominant oxidant (Figure 3.10). The initial leachate S content increased from 9 ± 4 to 14.6 ± 0.8 $mgL^{-1}g^{-1}$, through the first 45 minutes, falling to 9 ± 12 $mgL^{-1}g^{-1}$ at 60 minutes. After the drop in concentration at 60 minutes the rate of S release increased from 0.138 $mgL^{-1}g^{-1}min^{-1}$, through 16 ± 1 to 26 ± 2 $mgL^{-1}g^{-1}$ at 600 minutes, giving an increased rate of release of 0.0217 $mgL^{-1}g^{-1}min^{-1}$. For the final period of leaching S content in solution increased to 75 ± 3 $mgL^{-1}g^{-1}$ at 2880 minutes,
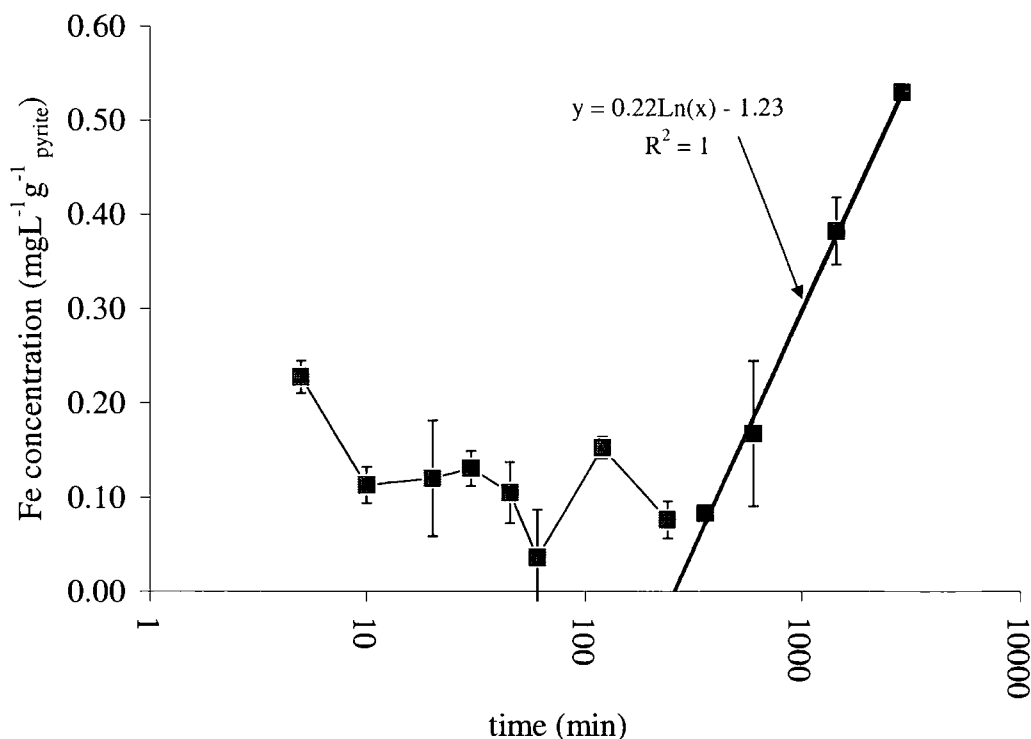
Figure 3.11. Fe concentration in leachate of 0.1g pyrite treated with 60 mgL^{-1} P and 0.005 % H_2O_2. After 300 minutes the dissolution rate exhibits a logarithmic curve (equation on graph) suggesting transport-controlled dissolution.
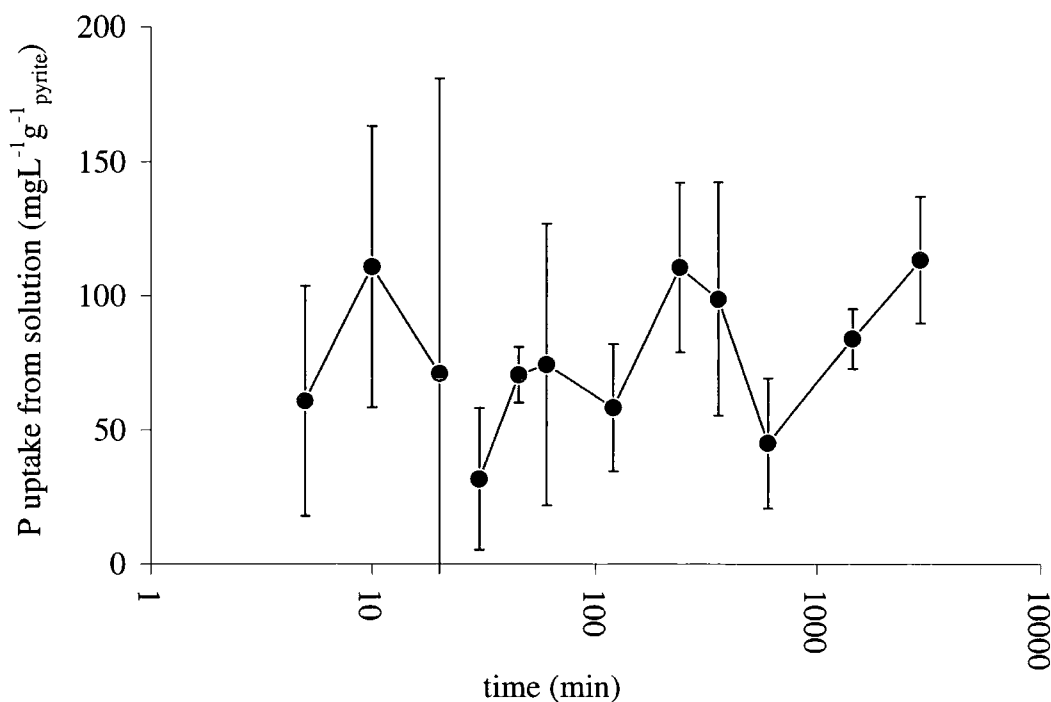
Figure 3.12. Calculated uptake of P from treatment solution of 0.1g pyrite treated with 60 mgL^{-1} P and 0.005% H_2O_2, as a function of time. Initially uptake is controlled by the release of Fe^{3+}, then decreases, eventually becoming very slow. Errors shown are 1σ, n= 3.

giving a final rate of 0.0153 $mgL^{-1}g^{-1}min^{-1}$. The release of S to solution is linearly proportional to time, indicating a surface controlled rate of dissolution, (Lasaga, 1984, Stumm and Morgan 1999).

Fe concentration for the period of treatment varied between 0.04 ± 0.05 and 0.53 ± 0.01 $mgL^{-1}g^{-1}$. During the first 360 minutes Fe concentration fluctuated between 0.22 ± 0.02 and 0.04 ± 0.05 $mgL^{-1}g^{-1}$ (Figure 3.11). For the remainder of the treatment period Fe release to solution increased to a final concentration of 0.53 ± 0.01 $mgL^{-1}g^{-1}$, showing a logarithmic relationship with the square root of time. Such a relationship indicates that the release of Fe to solution was diffusion controlled after 360 minutes.

The P uptake concentration values are calculated by taking the solution from the blank value and converting to a concentration per gram of pyrite by dividing through by 0.1g (Figure 3.12, Table 3.C., Appendix II Results). Thus the projected treatment P for 1 g of pyrite would be 600 mgL^{-1} P. Uptake of P varies between 111 ± 32 and 32 ± 26 $mgL^{-1}g^{-1}$. Within the first 120 minutes the amount of P taken up by pyrite fluctuates between 32 ± 26 and 110 ± 52 $mgL^{-1}g^{-1}$ (Figure 3.12). The large errors shown for P uptake at this time indicate the variation between individual pyrite samples, suggesting that during this period P uptake may be controlled by physical characteristics of samples. At 240 minutes P uptake from solution peaks at 111 ± 32 $mgL^{-1}g^{-1}$, then decreases to 45 ± 24 $mgL^{-1}g^{-1}$ at 600 minutes. After this trough in uptake, P removal from solution begins to increase to a final value of 113 ± 24 $mgL^{-1}g^{-1}$ at 2880 minutes. Mean pH values (n=3) vary between 4.3 and 5.6 throughout the period of the experiment (Table 3.C. Appendix II Results, Figure 3.13). The starting pH of 5.12 was slightly lower than that of the blank value of 5.3. However leachate pH rises to a peak of 5.62 at 240 minutes, then falls to 4.3 by the end of the treatment period.

Leaching treated samples

The Fe and S concentrations released during testing of treated pyrite follow similar patterns (Figure 3.14, Table 3.D Appendix-Results), although the amount of Fe released is much lower than S. The S concentration varies between 41.4 and 96.3 $mgL^{-1}g^{-1}$, Fe between 2.6 and 19.5 $mgL^{-1}g^{-1}$ and P from 0.02 to 2.6 $mgL^{-1}g^{-1}$. In general the concentrations released to solution are higher for pyrite treated for less than 120 minutes. Treatment after this period seems to provide more protection against oxidation. The release of P from treated pyrite increases with time of treatment over the initial 20 minutes. After 60 minutes of treatment a peak P value of 2.6 $mgL^{-1}g^{-1}$ coincided with a drop in Fe and a rise in released S. For samples treated for longer than
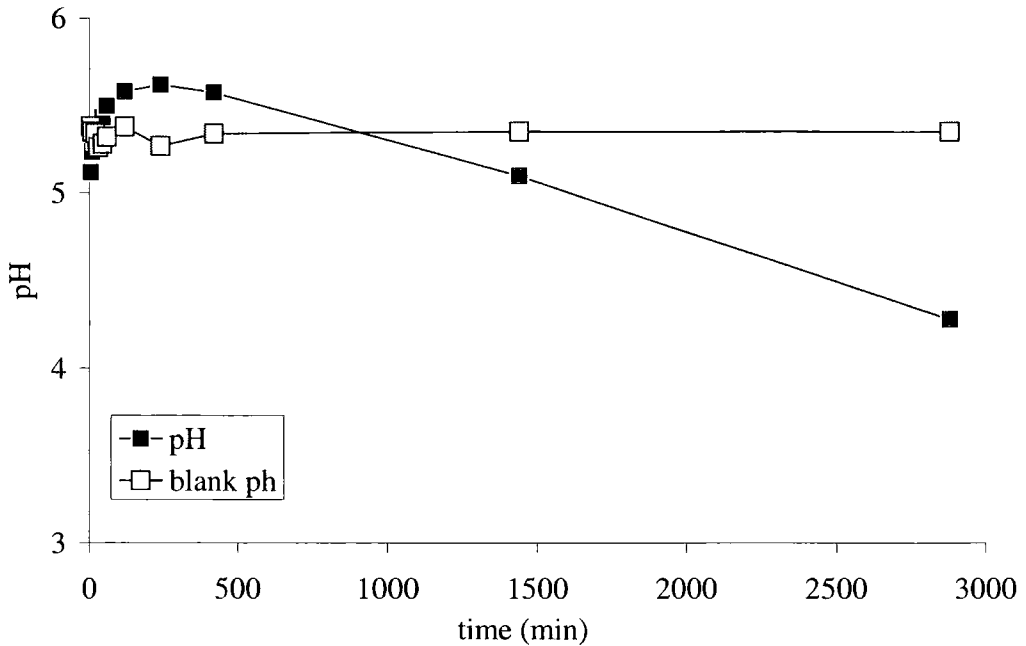
Figure 3.13. Leachate pH during treatment of pyrite as a function of time, compared to a pyrite free treatment solution.
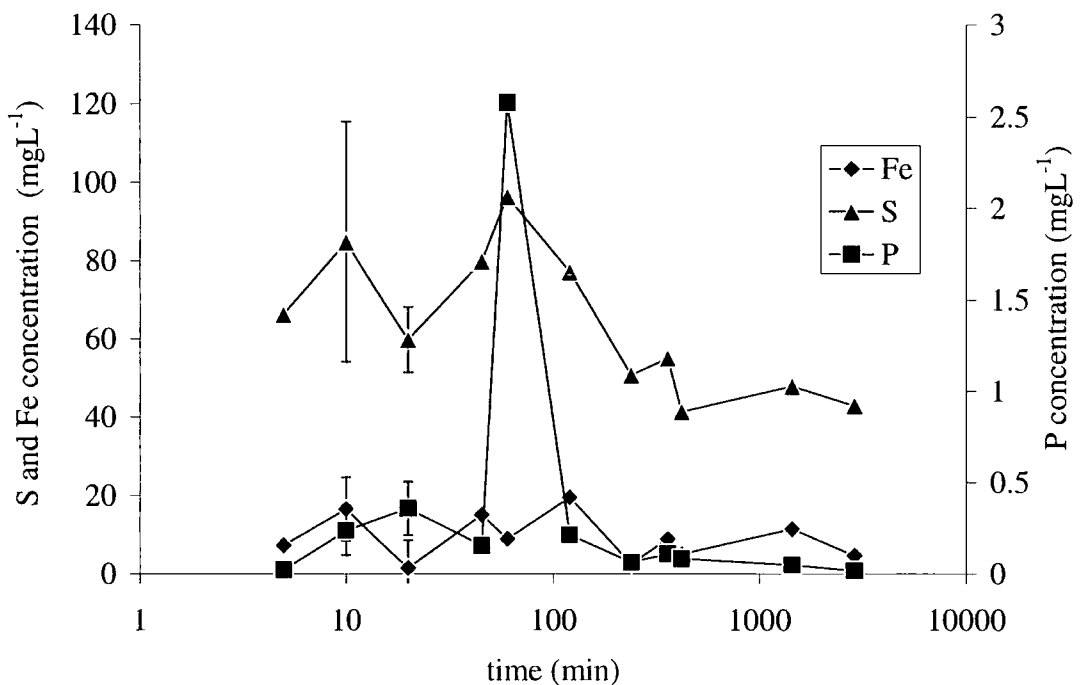
Figure 3.14. Concentration of P, S and Fe produced during testing of pyrite treated for increasing amounts of time. A log plot is used to show detail for pyrite treated for shorter periods of time. Samples treated for the longest period of time show least reaction. Errors shown are 1σ, n=2.

60 minutes, the released P concentration released during testing falls and remains close to 0.1 mgL^{-1}. After 60 minutes the precipitation of P during treatment seems to drop. The cause of the drop in expected Fe may be the precipitation of Fe-phosphate during testing. The pH of test solutions were not recorded, yet it seems unlikely, considering other test solutions (Table 3.5), that pH would be high enough for Fe-phosphate precipitation. However, if as previously discussed, there is a gradient of increasing pH in solution away from the pyrite surface, it may have been possible for a small amount of discrete phase Fe-phosphate to form. The better protection of samples treated over a period of 100 to 2880 minutes may be due to a formed coating of Fe-phosphate or hydroxide, or a combination of both.

3.5.3   Kinetics of treatment reaction – Discussion

Treatment reaction

The linear relationship of S release with time suggests that oxidation has a surface controlled rate with respect to this analyte. There is a sharp decrease in the rate of release of S after 60 minutes. McKibben and Barnes (1986) note the accelerated destruction of H_2O_2 by Fe^{3+}. The change in rate of S release may therefore be attributed to the complete consumption of H_2O_2, and the continued oxidation of pyrite with Fe^{3+} and dissolved oxygen.

Fluctuations in the Fe and P concentrations over the first 240 minutes of treatment are related to the precipitation of Fe^{3+} and P in Fe-phosphate. The variability in Fe and P release and uptake from solution during this period can be attributed to individual pyrite sample characteristics. As grain size varies below 150 μm any finer particles would rapidly produce dissolved Fe on reaction, leading to a rapid uptake of P from solution. Any gradient in Fe concentration away from the pyrite surface would also be affected by the pyrite grains morphology. Thus, the saturation of the grain's surface with dissolved Fe and P would vary with time until equilibrium was reached, leading to the observed fluctuations in these reactants. After this period Fe was released to solution by diffusion, suggesting that dissolution at the surface was fast compared to transport away from the pyrite surface. As the pH at this point was beginning to fall, the oxidation of pyrite was probably beginning to dominate the leachate chemistry.

Testing of the treated samples

Pyrite treated for at least 240 minutes appeared to have more resistance to oxidative attack, although the sample treated for 20 minutes also performed relatively well in

terms of Fe and S release. The sample treated for 60 minutes released the most Fe, S and P to solution, suggesting little protection against oxidative attack, despite this presence of a phosphate phase. The P released from this sample was probably the result of precipitation of a discrete phosphate phase during treatment. As the pH of the treatment solution remained above 5 for all apart from the longest treated samples, the precipitation of a coating of either Fe-phosphate or hydroxide would be possible. Pyrite samples treated for more than 120 minutes seem to have benefited from this extended treatment.

3.5.4   Conclusions –Kinetics of treatment reaction

The coating reactions of pyrite occurred mainly within the initial 240 minutes of treatment, in agreement with results from Nyavor and Egiebor (1995). Slowing in S release after 1 hour was caused by the total consumption of treatment H_2O_2 and the continued, albeit slower, oxidation of pyrite with Fe^{3+}. The steadily increasing leachate pH indicates the suppression of oxidation at this point by reaction of Fe^{3+} with phosphate. Dissolved P did not increase in solution over the last 44 hours of the experiment, indicating that Fe-phosphates did not undergo extensive degradation caused by falling pH. The continued production of S can be attributed to oxidation of the un-coated portion of the sample, which dominated the leachate chemistry after 240 minutes. .

3.6   Ordering Experiment

3.6.1   Method – Order of additions

To determine the effect of the order in which the H_2O_2 and phosphate solutions are added to pyrite in the 1st Optimisation, three 0.1g portions of pyrite were treated with 10 mLs of 60 mgL[-1] P solution plus 0.005% H_2O_2. The treatment solutions were added in alternate order to two samples, and simultaneously in the third case. Each treatment was prepared in duplicate and with a blank sample. The samples were left overnight, and then vacuum filtered and the leachate prepared for ICP-OES analysis for Fe, S and P as described above.

3.6.2   Results - Order of Additions

The concentrations of analyses are presented in mgL[-1] and are not corrected for mass of original pyrite. Fe concentrations were either 0.04 mgL[-1] or 0.05 mgL[-1] with this variation occurring between replicates of the same samples. Similarly S varied between

6.88 mgL^{-1} to 7.21 mgL^{-1} for the addition of peroxide first, 6.84 mgL^{-1} to 7.81 mgL^{-1} for the addition of P first and 6.50 mgL^{-1} -6.98 mgL^{-1} for the addition of the solutions together. Again variation was between the different replicates and there was no significant variation between samples due to order of solution addition.

P uptake is between 5.76 mgL^{-1} and 1.66 mgL^{-1} with larger differences between replicates than occur for Fe and S. This could be caused by differences in pyrite surface area between samples or by potential contamination of the H_2O_2 source as the blank for the sample where this is H has higher P than the other samples.

	Order of solution addition	Rep 1	Rep 2	Mean	1 σ	Variance	Within sample variance	Between sample variance	F-test
Fe	H_2O_2 first	0.05	0.05	0.05	0.00	6.60×10^{-6}	5.61×10^{-5}	1.47×10^{-6}	0.03
	P first	0.05	0.04	0.05	0.01	8.57×10^{-5}			
	Together	0.04	0.05	0.05	0.01	7.60×10^{-5}			
S	H_2O_2 first	6.88	7.21	7.04	0.23	0.05	0.21	0.26	1.21
	P first	7.81	6.84	7.33	0.69	0.47			
	Together	6.50	6.98	6.74	0.34	0.12			
P	H_2O_2 first	-2.67	-6.74	-4.70	2.88	8.27	3.79	1.78	0.47
	P first	-4.46	-2.00	-3.23	1.74	3.04			
	Together	-4.18	-4.53	-4.36	0.25	0.06			

Table 3.7. Results of ANOVA of order of addition of solutions experiment. Concentration of Fe, S and P in leachate derived from treatment of 0.1 g pyrite with 60 mgL^{-1} P and 0.005% H_2O_2. Separate P and H_2O_2 solutions were added to pyrite in different orders and then together, as labelled in the second column.

One way ANOVA as described by Miller and Miller (1993) was carried out on the results of this experiment to test whether there was a significant variation in Fe, S and P measurements within samples and between samples. The results of this are shown in Table 3.7, and show that to the 95% confidence interval there is no significant difference between the mean values of Fe, S and P in all three methods of applying the coating solution. However, the time between additions in this experiment, due to the smaller population of samples, is less that for larger experiments. Therefore to eliminate any doubt, it may be best to mix the H_2O_2 and phosphate solutions prior to addition to pyrite.

3.6.3 Conclusions – Order of Additions

The order in which solutions making up the coating treatment are added to pyrite has been shown to make no significant difference in treatment leachate, however the length of time between additions is shorter than in larger experiments possibly effecting the comparison of this test to large scale experiments.

3.7 Reproducibility of optimisation results.

To test the reproducibility of the low Fe and S concentration found from the 1st optimisation treatment leachate the 124 mgL^{-1} P and 0 or 0.01% H$_2$O$_2$ combinations were repeated at the same concentrations and also at 10 mgL^{-1} below and above 124 mgL^{-1} P.

3.7.1 Method – Reproducibility of optimisation coatings

The pyrite used in this experiment was prepared as described for the 1st optimisation experiment. Solutions containing 124 mgL^{-1}, 114 mgL^{-1} or 134 mgL^{-1} P and 0.01% H$_2$O$_2$ were made up. 100 mL of each phosphate solution was placed in 6 conical glass flasks, with 0.1g of the prepared pyrite, and then the H$_2$O$_2$, if used, was added. The reverse procedure to that used in the 1st Optimisation was used here as the prior addition of H$_2$O$_2$ was thought to be adverse to the coating formation reaction. For each treatment a pyrite free blank was also prepared. Samples were left to react overnight and then the reaction was halted by vacuum filtering the leachate through a 45 μm pore cellulose nitrate membrane. The filtrate was analysed for Fe and S by ICP-OES.

3.7.2 Results - Reproducibility of optimisation coatings

The mean leachate Fe, S and P values for samples treated in this experiment are compared to those treated with 124 mgL^{-1} P and 0 or 0.01% H$_2$O$_2$ in the 1st Optimisation experiment in Table 3.8.

The leachates for pyrite replicates treated with 0.01% H$_2$O$_2$ and 115, 120 or 125 mgL^{-1} showed a trend of increasing Fe and S with increasing treatment P concentration, at 1.1 to 1.6 mgL^{-1}g^{-1} for Fe and 550 to 780 mgL^{-1}g^{-1} for S (Figure 3.15). The opposite was true of pyrite treated with phosphate solution alone. The leachate concentrations from these samples varied between 2.8 to 0.33 mgL^{-1}g^{-1} for Fe and 580 to 2.1 mgL^{-1}g^{-1} S.

Initial treatment concentrations		Treatment leachate concentrations	
H_2O_2 (%)	P (mgL^{-1})	Fe mgL^{-1}g^{-1} (n=6)	S mgL^{-1}g^{-1} (n=6)
0.01	115	1.1 ± 0.1	550 ±70
0.01	120	1.3 ± 0.1	630 ± 40
0.01	125	1.6 ± 0.2	780 ± 98
0.00	115	2.8 ± 0.2	121 ± 9
0.00	120	4.7 ± 0.1	58 ± 4
0.00	125	0.33 ± 0.04	75 ± 4
0.01	*124*	*0.11 ± 0.03*	*21 ± 2*
0.00	*124*	*0.02 ± 0.01*	*10 ± 4*

Table 3.8. Concentration of Fe, S and P in treatment leachate for samples treated with 115 – 120 mgL^{-1} P and 0.01% or 0.0% H_2O_2, to test the reproducibility of the original 1st optimisation results. Values in italics are the original 1st Optimisation samples treated with 124 mgL^{-1} P and 0.0-0.01% H_2O_2 where n=3. All errors shown are 1σ.

3.7.3 Discussion - Reproducibility of optimisation coatings

The oxidation of pyrite by H_2O_2 was evident from the difference between Fe and S dissolved during treatment with oxidant, to that from pyrite treated with phosphate alone. Increasing the concentration of treatment P caused slight increases in the extent of oxidation, although the low Fe compared to S indicates that Fe-phosphate was being precipitated. The control of Fe release to solution is shown by pyrite treated with phosphate alone. The sample treated with the highest P and H_2O_2 concentrations released the most Fe.

Compared to Fe and S concentrations produced by 1st Optimisation pyrite during treatment with the same reactants, these samples dissolved a greater amount of both Fe and S (Figure 3.16). Although the pyrite source for this experiment and the 1st Optimisation treatments was the same, in this experiment pyrite was stored under argon for a longer period after cleaning. Uncontrolled oxidation during this period is a therefore the probable source of the high Fe and S values. Despite this, the pattern of Fe and S value distribution can still be interpreted in the manner of former treatment experiments. The extent of prior weathering may be minimised but not controlled, leading to unexpected differences in the observed oxidation product between experiments.
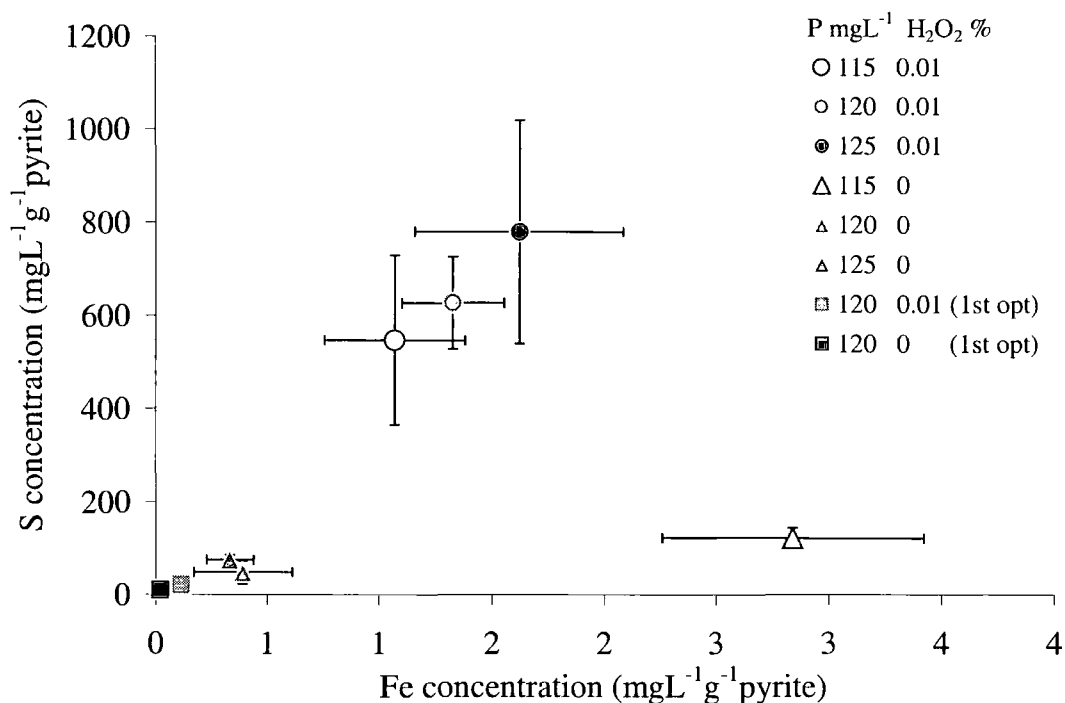
Figure 3.15. S as function of Fe concentration ($mgL^{-1}g^{-1}$) from treatment leachate of investigation of reproducibility of the coating treatment chemistry. Key refers to pre-treatments.

3.7.4   Conclusions - Reproducibility of optimisation coatings

The reproducibility of results of treating pyrite with phosphate coating solution is good within one experiment. Between experiments, systematic errors caused by the use of slightly oxidised pyrite have led to the increase in release of analyte to solution compared to original experiments.

3.8   Summary of Experimental Findings for Phosphate Coating development.

To form a coating of insoluble Fe-phosphate on the surface of pyrite, an oxidant and phosphate solution must be combined in the correct concentrations to provide super-saturation of the pyrite surface with respect the phosphate ion and Fe^{3+}. Initially precipitation of a coating will partially cover the pyrite grains, depositing in areas of preferred oxidation i.e. grain edges and pits. Investigation of the rate of the reaction shows that oxidation with H_2O_2 ends within a few hours, after which pyrite oxidation occurs at a faster rate than precipitation of Fe-phosphate. Although comparative testing of coating has been made problematic by the uncertainty in the extent of atmospheric oxidation during storage, the inhibition of oxidation has been shown to occur. The optimal coating found within these experiments for pyrite alone, was 500 mgL^{-1} P and

0.005 to 0.01% H_2O_2. However, for treatment of waste rock samples, especially those with high organic content, the conditions required for coating may not be present. The partial coating of pyrite in waste material is evident from published results of testing where oxidation is not wholly suppressed (Evangelou, 1995, Nyavor and Egiebor, 1994). Continued oxidation will decrease solution pH eventually, even with addition of a buffer solution leading to degradation of the Fe-phosphate coating. Therefore the use of phosphate to prevent pyrite oxidation would eventually fail. However, the technique could be used as a tracer of a pyrite oxidation front, through a rock host. A method for using phosphate solution as a tracer of pyrite oxidation is developed further in Chapter 5.

Chapter 4

Characterisation of coal-bearing strata – scale dependant variance

4.1 Introduction

At the present time there is no standard methodology for the prediction of an AMD severity or longevity. Existing technologies, in common with those developed over the past twenty years, focus on the geochemistry of rock strata from the proposed mining region. The most widely used method, acid base accounting (ABA), was originally developed by Sobek et al. in 1978, as a soil analysis technique. Advances in geochemical testing have been made with the introduction of kinetic testing which provides a measure of the time-scale of discharge evolution (Hornberger and Brady, 2000). Prediction of future discharge quality forms the basis of any contemporary application for mining extraction with details of a remediation scheme if deleterious Usually the body applying for mining permission is required to provide discharge is predicted. Therefore the ability to estimate future water quality and quantity is crucial from an industrial as well as scientific point of view.

Novel methods of assessing the risk of AMD generation such as geochemical core logging analysis and mathematical modelling have led to advances in predictive techniques. Core logging using geophysical tools allows rapid calculation of the net acid producing potential (NAPP) of whole rock columns speeding up geochemical analysis (OSMRE, 2002). The development of predictive modelling has greatly enhanced our capability of identifying the factors controlling discharge chemistry. Numeric modelling uses the chemical and physical processes governing AMD generation to predict discharge quality and longevity at a specific site. Calibration with site data allows modelling of future water quality (Malstrom et al., 2000).

Regardless of these advances in developing predictive technologies, scaling test results to the field situation is a consistent problem (Malmstrom et al., 2000). Probably as a result of this inability to mimic field conditions, even after 45 years of kinetic test development alone, a single predictive methodology has not been adopted (Hornberger and Brady, 2000).

Characteristics controlling variability in rock strata

Some of the difficulty encountered in replicating field scale situations can be attributed to variation in the natural environment compared with controlled laboratory testing. Malstrom et al (2000) identified temperature, pH, mineral content, hydrological flow and particle size distribution as physicochemical factors that should be accounted

for in any laboratory to field-scale projection. Most factors depend to some extent on local climate and the style of spoil processing and deposition or the structure of rock strata. However, mineral content, especially of in-situ strata, is the result of depositional environment and subsequent diagenesis. Indeed the paleo-environment of coal formation has previously been used as an indicator of acid generating potential (Williams and Keith, 1963, Younger, 2000). However, geographically, one site of extraction is usually much smaller than the total extent of the seam being removed. Therefore the resolution of any variability in seam-scale mineral content will not be good enough to speculate on variation at the mine scale (Watson et al., 2001).

The physical characteristics of rock are also known to control the style of pollutant release (Şenel et al. 2001, OSMRE, 2002). Release rate of acidity from pyrite hosting sandstone have been found to be faster than those of argillaceous shale (Ziemkiewicz, 1991 from OSMRE, 2000). Examination of the laws governing reactive transport within porous media demonstrates the effect of pore void characteristics on dissolved species transport and thus leachate formation. For advective transport within a porous media Darcy's law states that:

$$V = -\frac{K\partial P}{l\mu}$$
(4.1)

where V is the velocity of a fluid with viscosity μ, K is permeability of the rock, and l is the distance over which the change in pressure ∂P is measured. For diffusive transport within porous media Fick's first law states that:

$$J = -\phi.D_e.\frac{\partial C}{\partial Z}$$
(4.2)

where the dissolved flux J depends upon ϕ the effective porosity, D_e the effective diffusion coefficient, and the change in concentration C over a distance Z (Schuring et al., 1997).

Diffusive and advective solute transport both depend on parameters describing pore void space (i.e. total porosity) both volumetrically and spatially. As permeability of a rock type describes the interconnectivity of the pore space void it governs the advection of fluid or gases. Void space shape controls the tortuosity of a diffusing particle pathway and effects electrical conductivity in the pore solution. The control of

diffusive transport by void space shape suggests pore size distribution influences the rate of poor quality leachate formation as suggested by Ziemkiewicz, (1991).

The reactive surface area of a rock-type is the area available for interaction with a fluid or gas phase. Due to the bias of coal internal surface area towards micro-pores, this characteristic is usually measured by a combination of methods including of N_2, He and low pressure CO_2 gas adsorption. Previous investigations have shown that although coal macro and meso-porosity decreases with increasing rank, micro-porosity (< 2 nm) tends to increase at higher ranks (Bustin, 1999, Şenel et al, 2000, Gűrdal and Yalçin, 2001). Gűrdal and Yalçin, (2001) have attributed rank association with micro-porosity to bitumen formation in micro-pores with increasing temperature and therefore coal rank. When the bitumen cracking temperature is reached during burial diagenesis micro-pore space is increased.

Whether the micro-porosity of the coal matrix is important in the transport of dissolved species at the time-scales of AMD formation is questionable. Modelling of gas transport within pore space of coal has shown that most movement occurs within the meso and macro-porosity (Clarkson and Bustin., 1999). Obviously the rate of fluid transport within micro-pores will be far lower than within the macro and meso-porosity of fracture and cleat.

The reactive surface area of the mineral phase of coal and coal-bearing strata is more relevant to the rate of pollutant formation. The reactive surface area of coal with respect to mineral weathering can be taken as the inorganic phase surface area. We can speculate on this value for minerals such as pyrite by using typical grain diameter from SEM investigation and wt % content calculated from Fe and S. Given the variability in pyrite morphology and distribution between samples, this would probably lead to an under-estimation of reactive pyrite surface area.

Statistical Analysis

Variability in rock strata characteristics within the boundaries of one mine is also controlled by local depositional paleo-environment. It is possible that weathering becomes an important factor in the mineral budget of a seam at this scale. The significance of deviation from mean values of rock characteristics can be quantified statistically and applied to pollution generation predictions.

In the past 20 years the use of statistical methods to analyse coal-bearing strata geochemistry has emerged. Usually studies have involved the use of very large datasets collated over equally large geographical areas. A good example of this is the recent use

of geostatistical methods to predict the S content of the Pittsburgh Coal bed by Watson et al., (2001). Here the authors use 738 records (from a total of 3377) of S content analyses from core, outcrop and mine samples in a region spanning 100 square miles. The analysis performed by Watson et al., (2000) was based on the analysis of core S content alone. Obviously the overall geochemistry and mineralogy of a seam will affect its pollutant producing potential. Dulong and Blaine (2000) used a geostatistical approach to investigate variability in spatial (regional) and stratigraphic geochemistry of the northern and central Pennsylvanian coal-bearing strata. They suggest that high variability in rock geochemistry will lead to difficulty in predicting waste rock leachate quality. Regional scale interpretations performed in these investigations do not facilitate resolution to mine scale predictions of leachate quality (Watson et al., 2001).

Analysis of Variance and Experimental Design

The use of analysis of variance (ANOVA) in the characterisation of materials has been well-documented (Miller and Miller, 1993). Here this statistical test was used to identify significant differences in the chemical and physical properties of collected coal-bearing strata from the 30 m exposure of the Main Seam of the Durham Coalfield.

The experiment was designed to address the following:

1. Do wt % S and pyrite, the two predictors of maximum potential acidity (MPA), vary significantly within seams?

2. What are the main controls on rock characteristic variability and at what scale does their effect become variable, leading to significant heterogeneity?

3. What implications for ABA and laboratory to field scaling does rock heterogeneity have?

Sample collection was designed for investigation of variance within seams and between seams. Sampling was carried out at three points along the length of the 30 m exposure of four rock types. Three sub-samples of each sample were analysed for the suite of characteristics described in section 4.2.4.

By studying the patterns of chemical and physical property distribution we can comment upon the scale of processes controlling their existence in the rock. Investigating the scale at which controls over final rock composition operate provides useful information when scaling between laboratory and field scenarios.

More importantly the use of mean values from a small sample area as representative of a larger scale distribution will be tested. Classical sampling methods assume that the

mean of several sampling points along the exposure is representative of that length of seam. Triplicate sampling of each seam and subsequent sub-sampling in triplicate will allow testing of significant differences within seams and between seams. Between seams significant difference at the 95 % confidence interval, indicate that as expected each seam is different from the others. Within seam variance will be caused by significant differences between individual sample values in one seam. Significant within seam variance suggests that classical sampling does not provide representative mean values over the area of interest and should be used with caution. Between sub-sample variance indicates that one sample contains significantly different sub-samples.

A nested two-way ANOVA experiment was used to investigate variance in coal-bearing strata characteristics. Such a model allows the testing of the significance of variance at two levels, namely between seams and within seam variance. As the variance in rock characteristics within a seam does not affect differences between that and another seam the levels of analysis were nested. The nested hierarchy was as follows; 'between sub-sample' variance nested in 'within seam' variance, nested in 'between seam' variance of chemical and physical characteristics (Table 4.1). A *post-hoc* Tukey test (Howell, 1997) and main effects plots were also used to identify correlation of seam characteristics.

Level	Comparison	Tested
1	Between seam variance	Between 4 seams
2	Within Seam Variance	Between 3 sampling points
3	Between sub-sample	Between 3 sub-samples

Table 4.1. Nested hierarchy and statistical test used to compare variance between samples and between sub-samples.

Summary and objectives

Chemical, mineralogical and physical properties of coal-bearing strata all affect the formation rate and quality of leachate discharge. External controls on leachate formation from spoil waste include temperature, hydrological flow, pH and particle size distribution (Malstrom et al., 2000). Variance for these controls strongly depends on localised factors such as climate and is therefore site-specific. Conversely, the rock-forming process does control the variance of rock characteristics, which in turn controls leachate formation. Knowing the scale at which significant differences in rock properties occur will aid scaling from laboratory to field experiments. Inter and intra-

seam behaviour of a rock characteristic that does not vary significantly should be easier to scale to field behaviour, compared to a significantly variable characteristic.

ABA uses seam whole S and pyrite content to predict the maximum potential acidity (MPA) and subsequent leachate quality. Given the possible significant variance of seam characteristics, the assumption of whole seam representation by the mean value may be flawed.

Here the investigation of variance in chemical and physical properties at a smaller scale than in the studies of Watson et al., (2000) and Dulong and Baine (2002) is described. Both problems of scaling and variance of characteristics within rock seams are addressed using statistical methods.

4.2   Methods and Materials

4.2.1   Site and Geological description.

Coal-bearing strata were sampled at the now closed Northwood opencast, Brandon, County Durham (NZ 208402, Figure 4.1). At this locality exposed seams are from the Westphalian B (Middle) Coal Measures of the Durham Coalfield. The Westphalian coal measures of the Durham Basin were deposited within a deltaic coastal plain environment with little topographic relief. During the period of peat formation, this locality was possibly part of a channel belt which may have been migrating or contained islands of non-channel sediment (Fielding, 1982).

The seams exposed by extraction at the time of sampling were the Main to Five-Quarter seams of the Durham Coalfield. The sequence of coals sampled were included in those analysed by Worrall and Pearson (2001) (Figure 4.2). At the time of sampling only the Main Seam was accessible. The seam had been extracted throughout the 19th century using the 'pillar and board' method where pillars of material are left intact as roof supports. The opencast mining operation was extracting the remaining pillar material. At the place of sampling the Main Seam consisted of an upper and lower leaf of vitrinitic coal, with a shale parting separating the two. The shale consisted of very organic rich shale variably interspersed with thin (2 mm) coal bands along its length. Beneath the bottom leaf a fire clay or seat-earth graded sharply into the coal. This strata has been reported to be extensively contaminated with iron from the old workings above (Banks Ltd. Site Report, 1995-6).

To the north-east of the opencast site (NZ 212402) a small spring, supplied by a perched aquifer, runs with a pH of 3.1. Worrall and Pearson (2001) compared REE
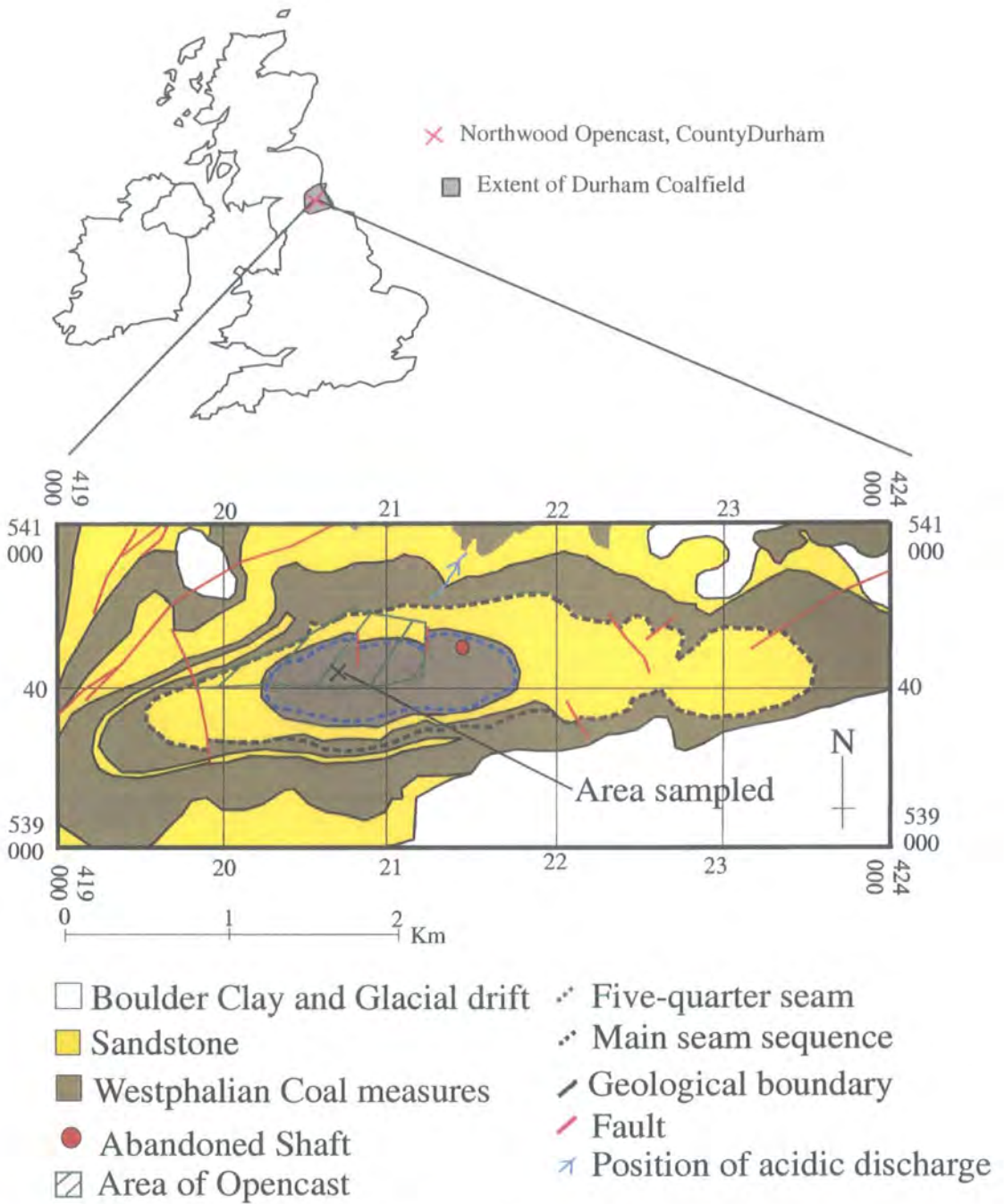
Figure 4.1. Locality in UK and summary of geological features of region surrounding the Northwood Opencast taken from BGS Wolsingham Sheet 261:50000 series, drift edition and Banks Group Ltd site report.
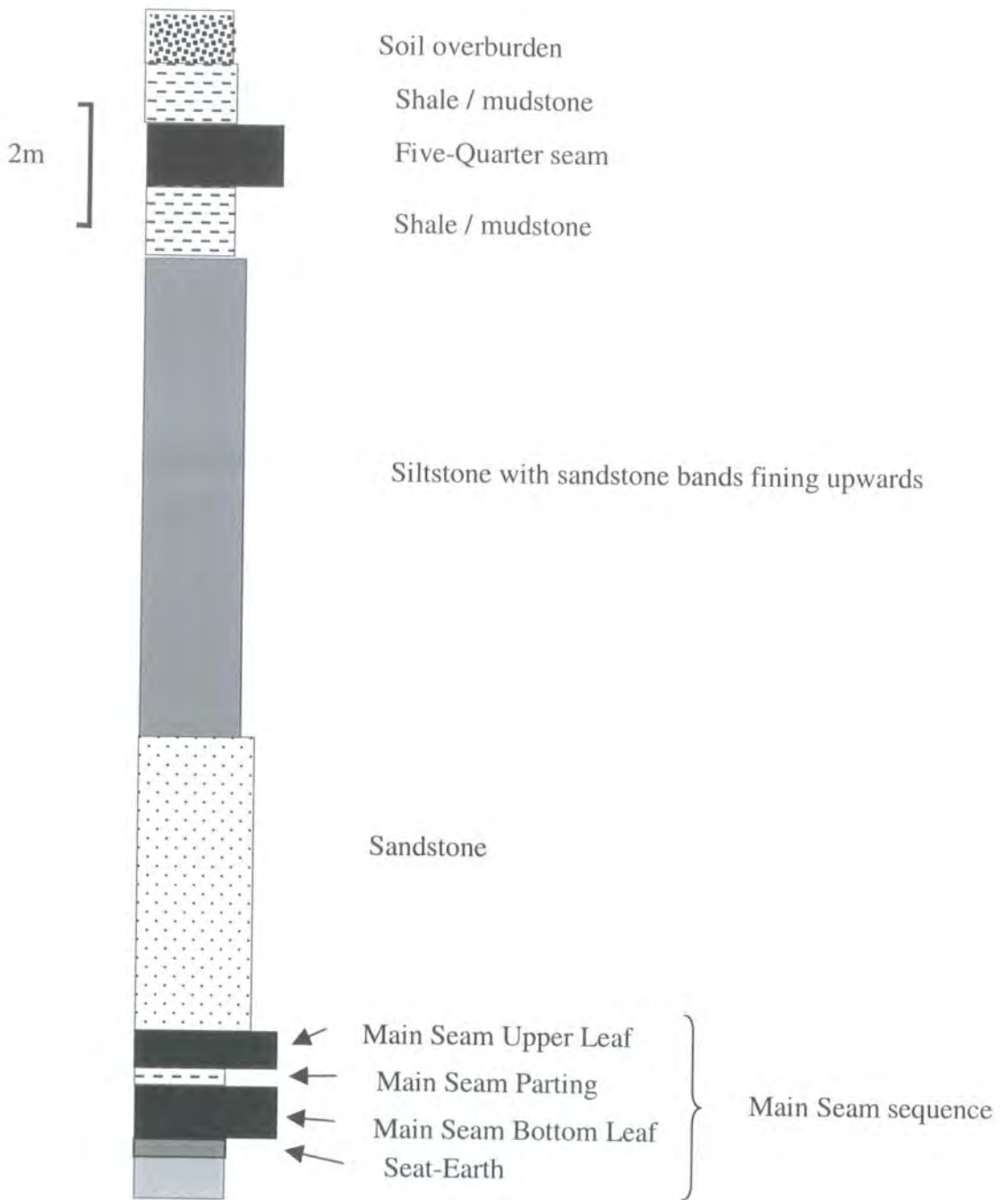
Figure 4.2. Sedimentary succesion of Northwood exposure sampled for seam characterisation (after Worrall and Pearson, 2000)

distributions in samples of spring water and selective extracts of coal-bearing strata from the site in an attempt to fingerprint the contaminant source. Their study showed that the carbonate and silicate buffering capacity of interacting rock strata had already been used up. Pyrite oxidation in the upper layers of the Main Seam, at the time of sampling, was the main buffering reaction of water chemistry for the Northwood spring. Worrall and Pearson (2001) identified a mid-REE enrichment pattern in the sampled Northwood discharge. Johannesson et al., (1996) attributed such enrichments in naturally acidic terrestrial waters to the dissolution of mid-REE enriched sulphate complexes, secondary mineral growths, Fe-Mn surface coatings and/or suspended particulate matter. Throughout the rest of this chapter the coal leafs sampled are referred to as MSUL for the Main seam upper leaf and MSBL for the Main seam bottom leaf. In tables and figures the shale parting is shortened to MSP and the seat-earth to MSSE. References in the text are to the parting and the seat-earth as this provides easier identification of the rock-types.

4.2.2 Sampling Strategy and Preparation

The upper and lower leafs of the Main Seam, the parting and the seat earth were all sampled three times along their length. The regions of sampling were roughly equally spaced over a 30 m length of the exposed seam. At each sampling point, 1 kg of each rock type was sampled in triplicate. On return to the laboratory each 1 kg sample was sampled in triplicate again with around 100 g of rock removed for each sub-sample. The sub-samples of each rock type were crushed in a mechanical jaw crusher and half the sample was powdered by Tema disc mill. The remaining crushed portion was used for Hg intrusion porosimetry and surface area studies. The powdered fraction was analysed for oxidizable sulphur, XRD and XRF analysis.

4.2.3 Rock analysis methods

Chemical and physical characterisation of the selected samples of the coal-bearing strata collected involved several techniques. Mineralogy and whole rock chemistry of whole rock powders (< 30 micron particle diameter) were analysed using XRF and XRD. Rock fragments of the MSUL coal were split perpendicular to the cleat direction and the exposed surface examined by SEM.

4.2.3.1 Chemical and mineralogical analysis

4.2.3.1.1 XRD

As XRD was used as a qualitative tool, only one split from each collected sub-sample was analysed. Powder was analysed by a Hilton-Brooks D2G x-ray generator equipped with a Phillips Goniometer to measure 2θ of $5°$ to $80°$, at a scan speed of $0.02°s^{-1}$, and step size of $0.04°$.

4.2.3.1.2 XRF

Powder briquettes of raw coal samples were used for XRF analysis of all samples. These were analysed for wt % major element oxides and S by a Phillips PW 1400 automatic XRF spectrometer with chromium $k\alpha$ radiation as a primary source. International coal standard SARM18 and sediment standards were run throughout for calibration.

4.2.3.1.3 Pyrite content

A method for pyritic sulphur extraction developed by Sobek et al. (1978) was used to quantify this phase. This method involves the removal acid leachable phases using dilute HCl, then successive heating with excess H_2O_2 to remove oxidizable sulphur. The resultant leachate is then titrated against NaOH to calculate H_2SO_4 formed during oxidation and hence the original S content (Appendix I Methods).

4.2.3.2 Physical Characterisation

Physical characterisation of rock samples included analysis of porosity by Hg intrusion, and effective porosity.

4.2.3.2.1 Hg Porosimetry

Rock preparation for intrusion porosimetry involved drying rock samples and crushing to approximately 0.5 cm diameter. Weighed samples were intruded with Hg at increasing pressure steps using an Autopore II 9220 Micrometrics porosimeter, capable of intrusion up to 39000 psi. The pressure of intrusion (p) is related to pore throat size by the Washburn equation (Katsube et al., 1991) -

$$d = -2\gamma \cos(\theta) / p \qquad (4.5)$$

Here the pore diameter (d) is twice the product of Hg surface tension (γ Nm^{-1}) and the cosine of $\theta°$ the contact angle of Hg and the rock surface divided by intrusion pressure p (psi).

4.2.3.2.2 Effective porosity

Effective porosity was measured using the immersion technique described by Katsube et al., (1991). Oven dried (105°C) samples were saturated in distilled water under vacuum for 48 hours and the difference in dry and wet mass used to calculate connected porosity.

4.3 Coal characterisation – Results and Interpretation

The following section includes a brief description of the chemical and physical characteristics of the sampled coal-bearing strata. Mean values for each seam are presented $\pm$ 1σ calculated from all sub-samples of that seam. The characteristics of each seam are reviewed and summarised. Following this summary the results of the performance of nested ANOVA on the seam characteristics is described.

4.3.1 Chemical Characterisation of Coal

4.3.1.1 SEM examination of MSUL coal

A prominent pyrite phase was found in the split sections of MSUL coal examined by SEM. Pyrite tended to be framboidal and formed in large rounded clusters, along cleavage planes and also as discrete isolated framboids throughout the coal matrix. Further description of SEM examination and images of MSUL coal is presented in section 5.23, Chapter 5.

4.3.1.2 Oxidizable Sulphur – Pyrite content

Pyrite content of samples was calculated from the oxidizable S phase. Sub-sample pyrite content varied between 11.7 wt % to 0.2 wt % for all rock types (Table 4.A. Appendix II-Results). Mean pyrite content for each seam was calculated from all sub-samples rather than the means of each sub-sample group (Table 4.2). The parting had the highest mean pyrite content at 5 $\pm$ 4 wt %. One of the sub-samples of the parting seam could not be analysed. After three attempts at extraction, reaction with H_2O_2 was so rapid that each time part of the sample was lost. However XRF of the same sub-sample provided a value of 24.4 wt % S suggesting a pyrite content of 45.7 wt %. This

Seam	Sample	Sample mean	Seam mean
MSUL	2	1.1 ± 0.6	3 ± 2
	3	5 ± 4	
	4	3 ± 1	
MSBL	1	1.2 ± 0.2	1.4 ± 0.5
	2	1.8 ± 0.5	
	3	1.2 ± 0.4	
MSP	1	6 ± 3	5 ± 4
	2	2.1 ± 0.6	
	3	8 ± 5	
MSSE	1	0.25 ± 0.09	0.4 ± 0.1
	2	0.36 ± 0.06	
	3	0.5 ± 0.2	

Table 4.2. Sample and seam mean pyrite content wt % derived from oxidizable S extract of all rock-types. Errors shown are 1σ, n=3 except MSP3 where n=2.

	Quartz	Calcite	Kaolinite	Illite	Albite	Dolomite	Siderite	Gypsum	Pyrite
MSUL2	✔		✔						✔
MSUL3	✔		✔	✔	✔	✔			
MSUL4	✔	✔	✔			✔			✔
MSBL1	✔		✔	✔			✔	✔	
MSBL2			✔						✔
MSP1	✔		✔						
MSP2	✔		✔	✔		✔	✔		
MSP3	✔		✔	✔		✔	✔		✔
MBSE1	✔	✔	✔		✔				
MBSE2	✔		✔					✔	
MSBE3	✔		✔		✔			✔	

Table 4.3. Mineralogy of coal-bearing strata rock types from XRD analysis of three samples from each seam. For 2θ vs cps plots see Figures 4.A-K Appendix II Results.

very high value was possibly the result of selecting a sub-sample with a large amount of massive pyrite. However this is indicative of the possible variation in S content at the hand specimen scale.

Upper and Lower Coal seam samples (MSUL and MSBL) contained 3 ± 2 wt % and 1.4 ± 0.5 wt % pyrite respectively. Previously, S content of the Main Seam coal within the Durham Basin was found to be between 0.88-1.62 wt % S (Fielding, 1982).

The seat-earth had the lowest sulphide content at 0.4 ± 0.1. Whether this was pyrite or remnants of sulphate not totally dissolved during acid leaching are uncertain, as no pyrite was identified during XRD analysis (see below).

4.3.1.3 XRD

As XRD was used as a qualitative rather than quantitative tool only one sub-sample from each sample was analysed (Table 4.3). All rock-types contained kaolinite and quartz. Pyrite, dolomite and illite were the next greatest abundant minerals, none of which were identified in the seat-earth (Figures 4.B-L, Appendix II Results). Albite, siderite and gypsum were each found in at least three of the samples analysed. Siderite and gypsum were both present in the MSBL coal. The parting also contained siderite, and the seat-earth gypsum. Albite was identified in two seat-earth samples and also in the MSUL coal. The presence of albite in the coal indicates a relatively high detrital input. Indeed, one sample of MSUL coal also contains illite and dolomite. Calcite is the least commonly identified mineral being found only in a MSUL coal and a seat-earth sample. The dominance of dolomite over calcite as the main Ca bearing mineral in the MSUL coal and the parting suggests that a pervasive dolomitic cement may exist in the sampled seams.

4.3.1.4 XRF

Both the parting and the seat-earth had a large mineral phase compared to the coals (Table 4.4, Table 4.A, Appendix II Results). The Si and Al contents of both sedimentary rock types were relatively high. As expected the coals both had low Al and Si contents. Sphene or Ti-oxide usually occurs as detrital material in sedimentary rocks. Accordingly Ti-oxide was present in the greatest proportion in the sediment-rich parting and seat-earth at 0.62 ± 0.27 and 1.02 ± 0.03 wt % respectively. Similarly the distribution of clay associated elements Na and K was also be biased towards sediment-rich rock types. There was even some difference between the coals, with MSUL having slightly higher Na and K wt% compared to the MSBL. The higher Al, Si, Na and K and

Ti wt % of the MSUL relative to the MSBL implies a greater inorganic content of the upper leaf compared to the lower leaf in sampled area.

Typical carbonate minerals within the rock types are calcite, dolomite and siderite. The presence of these minerals may partially be identified by the distribution of Ca, Mg and Fe. Both Ca and Mg were present in greater amounts in the sedimentary rocks compared to the coals (Table 4.4). Higher Ca and Mg content in the MSUL coal samples again points to a larger inorganic mineral phase compared to the MSBL coal. In general Mg and Ca content of all rock types was low, suggesting that the carbonate phase may have largely been removed during previous acid weathering.

	SiO_2	Al_2O_3	Fe_2O_3	MgO	CaO	Na_2O	K_2O	TiO_2	S	Total
MSUL	3 ± 2	2 ± 1	1 ± 1	0.02 ± 0.02	0.02 ± 0.02	0.01 ± 0.01	0.2 ± 0.3	0.11 ± 0.09	1.67 ± 0.09	8 ± 4
MSBL	0.8 ± 0.5	0.6 ± 0.3	2 ± 3	0.01 ± 0.01	0.01 ± 0.01	0.00 ± 0.00	0.01 ± 0.01	0.06 ± 0.05	2 ± 2	5 ± 5
MSP	30 ± 11	19 ± 7	7 ± 11	0.5 ± 0.3	0.1 ± 0.2	0.11 ± 0.06	2 ± 1	0.6 ± 0.3	5 ± 10	64 ± 13
MSSE	49 ± 5	28 ± 3	1.3 ± 0.3	0.57 ± 0.07	0.01 ± 0.01	0.15 ± 0.01	1.6 ± 0.2	1.02 ± 0.03	0.01 ± 0.01	82 ± 2

Table 4.4. Mean oxide wt % from XRF analyses of all rock samples. Errors shown are 1σ, n=9.

The parting had the highest Fe content at 7 ± 11 wt %. Distinction between coal and sediment rocks for Fe was less clear as coals and seat-earth contained similar amounts. Considering the high pyrite content of the parting sample (5 ± 4 wt %) the large Fe value is not surprising. The relatively small pyrite content of the seat-earth suggests that this rock type probably contained siderite or Fe-hydroxide.

Coal-bearing strata S content can divided between organic, sulphate and sulphide S fractions (Casagrande, 1987). Given this, the coals and parting would be expected to have the greatest S wt % due to their previously discussed pyrite and high organic content. In keeping with the high pyrite content of the parting, this rock type had the greatest S content of 5 ± 10 wt % (Table 4.4). Coal seam S contents were close to each other at around 2 wt %. The MSUL pyrite wt % of 3 ± 2 wt % provides 1.74 wt % of the coals total S budget, slightly higher than XRF total S of 1.67 wt%. Similarly the seat-earth with an XRF S value of 0.01 ± 0.01 wt% had a mean oxidizable S content of 0.23 wt %. Overestimation of pyritic S wt % for the coals and seat-earth is possibly due

partial oxidation of organic S. Kania (2000) reports that difficulties in measuring actual pyritic S content often leads to problems with ABA which is the reason why whole S often provides a more reliable leachate quality prediction. Fielding (1982) reports the total Main Seam coal S content within the Durham Basin to be 0.88-1.62 wt % S, slightly lower than the range at the Northwood section of the Main seam. Such a difference questions the use of the mean S wt % for the formulation of the acid producing potential of a seam.

4.3.2 Physical Characterisation of Coal

The physical properties of a porous material govern the accessibility of its internal portions to fluid and gas phases, and therefore the rate of reactive transport (Şenel et al, 2000). Quantification of these properties is consequently crucial before any attempt at modelling reactive transport during weathering of rock-strata can be made.

4.3.2.1 Porosity (Hg-intrusion) and pore-size distribution

Coal pore size diameter have been sub-divided into three groups, micropores (< 2 nm), mesopores (2-50 nm) and macropores (> 50 nm) by IUPAC (Şenel et al, 2000, Gürdal and Yalçin, 2001). Here pore size distributions are grouped into macro and meso-porosity to describe the proportion of the 'total' porosity represented in each rock-type.

Both coal leafs had large total porosity with mean values of 50.8 ± 0.6 % for the MSUL and 53 ± 3 % for the MSBL (Table 4.5). Total porosity for the parting was 24 ± 8 % and the seat-earth 6 ± 1 %.

Mean pore size distributions for all rock types displayed a large bias towards micro-porosity i.e. diameter < 2 nm (Table 4.B, Appendix II Results).

For the two coals 95% of porosity was in the form of micro-porosity, with meso-porosity of 4 ± 1% in the MSUL and 3.5 ± 0.9% in the MSBL (Figure 4.3, Table 4.B, Appendix II Results). Macro porosity (>50 nm) only accounted for 1.4 ± 0.8% and 1.0 ± 0.3% of the MSUL and MSBL coals respectively. Both parting and especially seat-earth had less biased pore size distributions with 77 ± 31% and 55 ± 24 % micro-porosity respectively. The meso-porosity of the parting was closer to that of the coals at 7 ± 5 % compared to the 46 ± 25 % of the seat-earth. However both parting and seat-earth had relatively high macro-porosity.

Seam	Sample	Sample mean	Seam mean
MSUL	2	50.5 ± 0.8	50.8 ± 0.6
	3	50 ± 2	
	4	51.5 ± 0.2	
MSBL	1	51.2 ± 0.9	53 ± 3
	2	50.9 ± 0.4	
	3	55 ± 7	
MSP	1	30.7 ± 0.9	24 ± 8
	2	16 ± 3	
	3	27 ± 8	
MSSE	1	4.2 ± 0.6	6 ± 1
	2	7 ± 2	
	3	6 ± 3	

Table 4.4. Results of Hg intrusion porosimetry (%) for all seams. Values given are means of sample groups and mean values for each seam $\pm$ 1σ, n=3.

Seam	Sample	Sample mean effective porosity (%)	Seam mean effective porosity (%)
MSUL	2	4 ± 1[*]	4 ± 1[$]
	3	4.5 ± 0.7	
	4	3 ± 2	
MSBL	1	3.6 ± 0.3	4 ± 1
	2	5.6 ± 0.9	
	3	2.9 ± 0.2	
MSP	1	11 ± 6	16 ± 16[$]
	2	25 ± 25	
	3	8.9 ± 0.7	

Table 4.5. Mean effective porosity for each sample (n=3, [*] n=2), and each seam (n=9, [$] n=8).
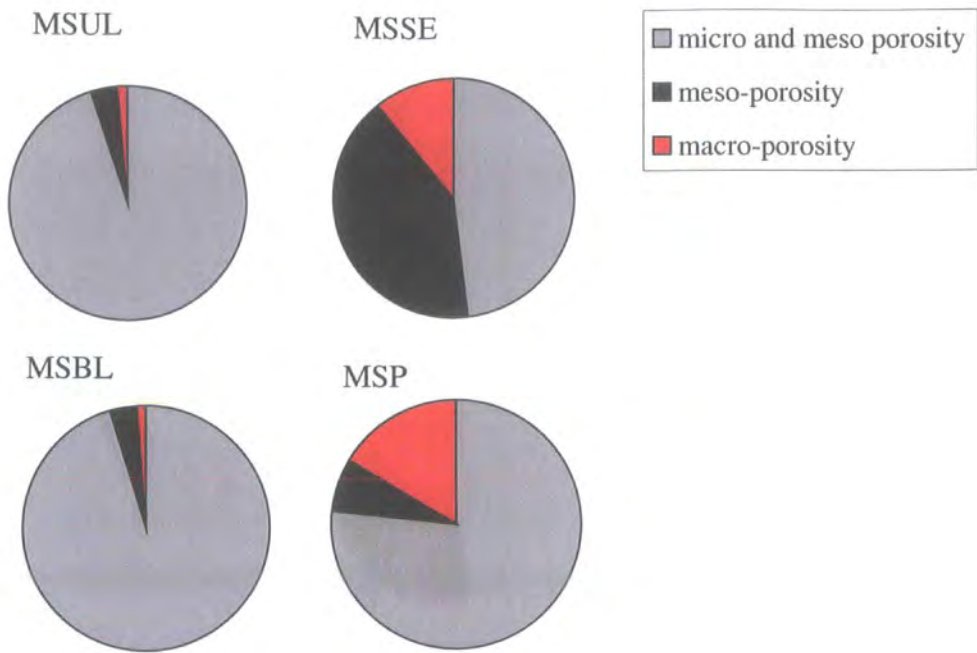
Figure 4.3. Pore size distributions for all rock-types, with divisions of > 50 nm –
macro-porosity, 2-50 nm – meso-porosity and < 2 nm micro-porosity.
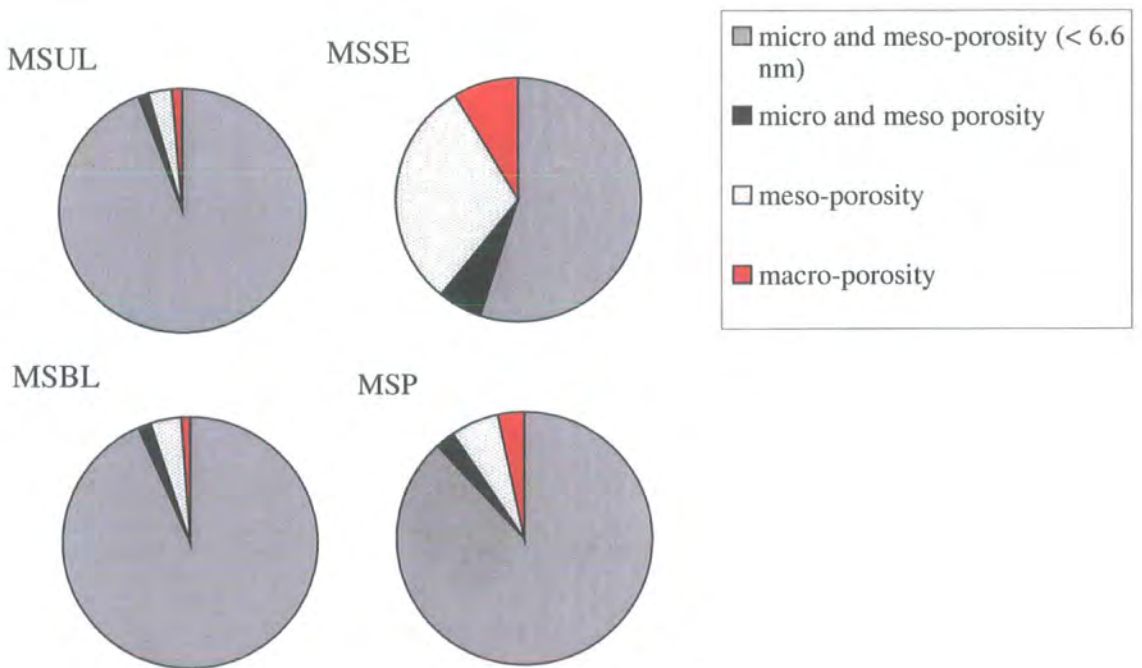
Figure 4.4. Pore size distributions for all rock-types with radii measured down to 6.6
nm. Divisions are as for Figure 4.5.

Pore volume for a small group of samples was measured below 9nm down to 6 nm, with only a small volume measured over this 3 nm decrease in pore-throat diameter. Between 3-9 nm the greatest pore space was measured for the seat-earth (Figure 4.4). Most of the porosity of the rock-types measured was, as suggested by Gűrdal and Yalçin, (2001), micro-porosity and therefore outside the limits of Hg-intrusion.

4.3.2.2 Effective Porosity

Effective porosity measurements were hampered due to disintegration due to slaking of the parting and seat-earth samples. However, coal samples and some parting samples remained sufficiently intact that a good estimate or overestimate of effective porosity could be derived from the difference in dry sample and water-saturated mass. Sample volumes were calculated using dry mass and density derived from Hg-intrusion (Table 4.B Appendix II Results).

The two coals have similar mean effective porosity of 4 ± 1 %, whereas 16 ± 16 % of the parting is made up of connected void space (Table 4.5). The parting value probably over-estimates the actual value, which is probably closer to the MSP3 sample value of 8.9 ± 0.7 %. Given the pore size distribution of macro and meso-porosity from Figures 4.3 and 4.4, it is likely that most connected porosity is made up of these fractions. Investigations of gas transport in the coal matrix have shown that macro and meso-porosity surrounds clusters of micro-porosity (Clarkson and Bustin, 1999). Separate micro-porosity clusters are connected to the remaining rock via of meso and macro-porosity, with gas transport occurring mainly in these areas

4.3.2.3 Summary of seam characteristics

The sediment content of each rock-type and therefore paleo-environment of deposition defines the divide between rock types in terms of mineralogy and chemistry. The parting and seat-earth had high Si, Al and Ti compared to the coals and the parting had the greatest pyrite content. The distribution of carbonate hosted elements such as Ca, Mg and Fe generally followed that of clay minerals. However Fe distribution was also associated with pyrite content.

The sequence of deposition of the seams also controls rock composition (Figure 4.2). The MSBL underlain by the soil horizon of the seat-earth, is organic macerel rich and has relatively high pyrite content. The overlying parting has an unclear contact with the coal and probably formed during an influx of brackish water into the peat, perhaps as a result of channel migration. Regression of this water body left a substrate available for

deposition of the MSUL forming plant matter. Reworking of the shale and continued sediment flux contributed to the elevated sediment content of the overlying coal. Elevated pyrite content of the MSUL may also be as a result of reworked pyrite or the prior presence of brackish water.

Physical properties of coal are directly related to the processes undergone by peat during burial diagenesis. Similarly the physical properties of organic rich shale and seat-earths are also related to lithification processes. Post-diagenetic mineralisation of coal-bearing strata rock usually includes the precipitation of sulphides when conditions are appropriate (Spears, 1987). Therefore the position of mineralisation with respect to micro and macro porosity is important when assessing the pollutant potential of a rock-type. In this study pore size distribution indicates that porosity for both coals is almost all micro-porosity. The similarity of the coal meso and macro-porosity proportion of rock volume to effective porosity suggests that larger pores are made up of connected pore space. Parting porosity was more evenly distributed between macro and micro-porosity. Seat-earth pore size distribution tended even more towards a normal radii distribution (Figures 4.3 and 4.4). This is consistent with the positive correlation between increased permeability and kaolinite content of shales found by Katsube et al., (1991). The combination of elevated permeability and high pyrite content of the parting suggests that pollutant production from this rock type would be relatively fast.

4.3.3 Statistical Analysis

Statistical analysis has been used to investigate and quantify the variability of seam characteristics. As mean seam whole S and pyrite content are usually used to quantify the MPA of a rock type any significant variance of either S or pyrite wt %, the use of the mean seam value to predict MPA will lead to inaccurate estimations.

Mineralogical and physical characteristics of coal-bearing strata may be attributed to the style of rock formation. Peat formation, peat diagenesis and post-diagenetic processes such as cleat formation and secondary mineralisation from pore fluids, all play important roles in mineral distribution (Spears, 1987). In order to use mean values to describe rock strata the assumption is made that these processes operate relatively consistently over a seam. To make the assumption of consistent mean values the scale at which intra and inter-seam differences become insignificant is required. By comparing the mean intra and inter-seam values, two scales of variance – 30 m of seam exposure and 0.5 m of seam sampling point has been examined. Comparison of

variance plus distribution of main effects make ANOVA a powerful tool in the identification of patterns not obvious from the raw data.

4.3.3.1   Interpretation of nested ANOVA

Of all the characteristics analysed for variance only whole S was not significantly different between seams at the 95% confidence level (Table 4.6). This lack of significant variation in S distribution is testament to the ubiquity of this element in coal-bearing strata. Despite the apparent large range in within seam whole S content the mean values for each seam are still not significantly different from each other. This suggests that mean S cannot be used to discriminate between seams at this locality. As the whole S values of each seam do not differ significantly, mean whole S is not statistically useful as a seam marker. Whole S sources includes organic material, sulphides and gypsum possibly derived from the weathering of sulphides. Source distribution between seams is pre-determined to a certain extent by organic material content and association with sulphate enriched brackish or marine waters. Organic and early diagenetic sulphide S is relatively static compared to dissolved sulphate S from marine water or sulphide weathering. It is probable that sulphide and sulphate S re-distribution, during burial and post-diagnetic processes, has led to the lack of difference between the seams' whole S. Gayer et al., (1998a and 1999) suggested that a hydrothermal system re-distributed pyritic S within the Amman Rider seam of the South Wales Variscan foreland basin. However, this phenomena was confined to one seam, whereas in this study there is no significant difference between whole S means of four seams. For the Northwood strata it is more likely that periodic marine flooding and the presence of saline groundwater led to distribution of sulphate (Gayer et al., 1999). Sulphate distribution therefore controls between seam whole S variation and is in turn controlled by syn-diagenetic saline water intrusion. Watson el at., (2001) showed regional trends in whole S content of the Pittsburgh coal bed over an area of 160 km^2. A general east - west increase in whole S over160 km with smaller scale variations over 3-7 km was identified. This suggests differences in between seam whole S means become significant at a far larger scale than investigated here.

What is of greater interest to this study is the within seam variation of whole S as this is used to predict MPA in ABA. Mean whole S in the three samples taken from each seam was found to differ significantly. Thus whole S does vary significantly over the 30 m sampled exposure of each seam. As discussed above, between seam whole S variation is controlled by the distribution of sulphate from saline waters, over a larger

scale than sampled at. Within seam whole S content variation is therefore controlled by organic and sulphide S distribution. Organic S has been shown to be derived from plant and microbial cell amino acids, H_2S formed from sulphate in pore water and elemental S (Casagrande, 1987). The ubiquity of potential organic S sources in peat suggests that within seam whole S variation is probably not controlled by this S fraction. Only sulphide distribution remains as the potential control of whole S within seam variation. Thus whole S variation is representative of within seam pyrite variation, and may be used to speculate on seam pyrite content at this locality.

Characteristic	Significantly different (P = 0.05)	
	Between seams	Within seams
Total porosity	✔	✔
Micro-porosity	✔	✘
Meso-porosity	✔	✘
Macro-porosity	✔	✘
Effective Porosity (Coals and parting only)	✔	✘
Wt % pyrite	✔	✔
Si	✔	✔
Al	✔	✔
Fe	✔	✔
Mg	✔	✘
Ca	✔	✔
Na	✔	✘
K	✔	✔
Ti	✔	✔
S	✘	✔

Table 4.6. Probability of rock type characteristic significant variance at the 95% confidence interval. Results are derived from one-way nested ANOVA of inter and intra-seam means.

Pyrite content variance is significant between and within seams, suggesting that neither mean pyrite or whole S values should be used as the sole basis of MPA prediction. Between seam significant difference in pyrite content indicates that individual seam formation conditions control this mineral's distribution. Kortenski and Kostova (1995) pyrite distribution to peat bog conditions (including Eh and pH, bacterial and groundwater activity), the Fe and S content of adjacent rocks and tectonic processes during lithification. Peat formation conditions alone are the most likely cause of within seam pyrite variation, although localised post-diagenetic tectonic processes may affect distribution. Gayer et al. (1999) attributed vertical trends in pyrite distribution within seams to the interaction of lower and upper sections of peat with saline water. This type of trend would contribute to between seam variance in pyrite

content rather than within seam differences. However, the manner of sampling in this study was based on point sampling rather than cross-sections of seams. Therefore vertical trends may have been randomly sampled, potentially leading to the apparent within seam variation.

With the exception of Na, Mg, effective porosity, specific surface area and pore size distribution, all seam characteristics differed significantly between samples. The difference between seam and sample means for rock physical characteristics indicates which factors control these characteristics. Physical characteristics depend upon sediment content, coal rank and post-diagenetic processes such as cementation, cleat formation and mineralisation. The effect of these processes only varies significantly within each seam, over the exposed 30 m. Each seam has its own different physical characteristics that do not vary significantly along the sampled seam length. The Na and Mg wt % distribution follows the same trend, suggesting relatively even dispersal throughout the sampled seam lengths. The Na content of coals has been attributed to pore water derived from groundwater at time of deposition and may also be associated with the organic phase of low rank coals (Glick and Davis, 1987, Crowley et al., 1993). Katsube et al., (1991) found a positive correlation between connected porosity and kaolinite content and negative correlation with calcite and dolomite content in shales. Ion exchange with kaolinite may be a possible reason for Na and Mg correlation with physical characteristics. However the Mg^{2+} ion would be enriched in the clay phase compared to the Na^+ ion. Main effect plots, described in the following section, show that Mg and Na between and within seam content trends are similar. Given the even distribution of the Na content, and the vitrinitic nature of the coals connate pore water is the most likely source of this element. Dolomitic precipitation is usually associated with marine transgressions, suggesting that Mg is also derived from saline waters (Mackowsky, 1968). The lack of significant variation in Na and Mg distribution within seams is probably due to their presence in pore and groundwater associated with the original peat. The provenance of these elements in pore water may also account for their association with the physical characteristics of each seam. As discussed above the distribution of sulphate is also controlled by pore and groundwater salinity. However, Na, Mg and whole S show different distributions at inter and intra-seam scales. Clay minerals containing Na and Mg will provide the significant difference in between seam variance shown. Sedimentary input to coal-bearing strata will remain *in-situ* compared to relatively easily soluble sulphate. At the intra-seam scale the distribution of pore-

associated Mg and Na is more important than clay minerals. Similarly, within seams, whole S content differs due to the variation in sulphide distribution.

4.3.3.2   Main effects – Identifying processes controlling rock characteristics

The previously interpreted analysis of seam characteristic variance only identifies the presence of differences. Main effect plots show the patterns of characteristic mean value distribution for each seam, sample and sub-sample (Figures 4.5-4.6). In these figures the mean values for each factor are plotted within the groupings of the ANOVA model. Thus in each plot the 'Between Seams' category contains a plot of the mean of all effective porosity values for each seam. The 'Within Seams' category plot is of mean effective porosity at sampling points 1 to 3 regardless of seam.

Four patterns can be found from main effect plots for between seam variation. One pattern is made up of high means for physical characteristic values in the parting and seat-earth, including meso and macro-porosity and effective porosity (Figure 4.5). The Ti-oxide main effect plot also follows this trend suggesting some correlation between this and the physical characteristics (Figure 4.6). Given that the presence of Ti-oxide is usually indicative of detrital matter, and that the presence of relatively large sediment grains increases macro and meso-porosity, this is not surprising. However, Ti-oxide may also represent the presence of secondary magnetite.
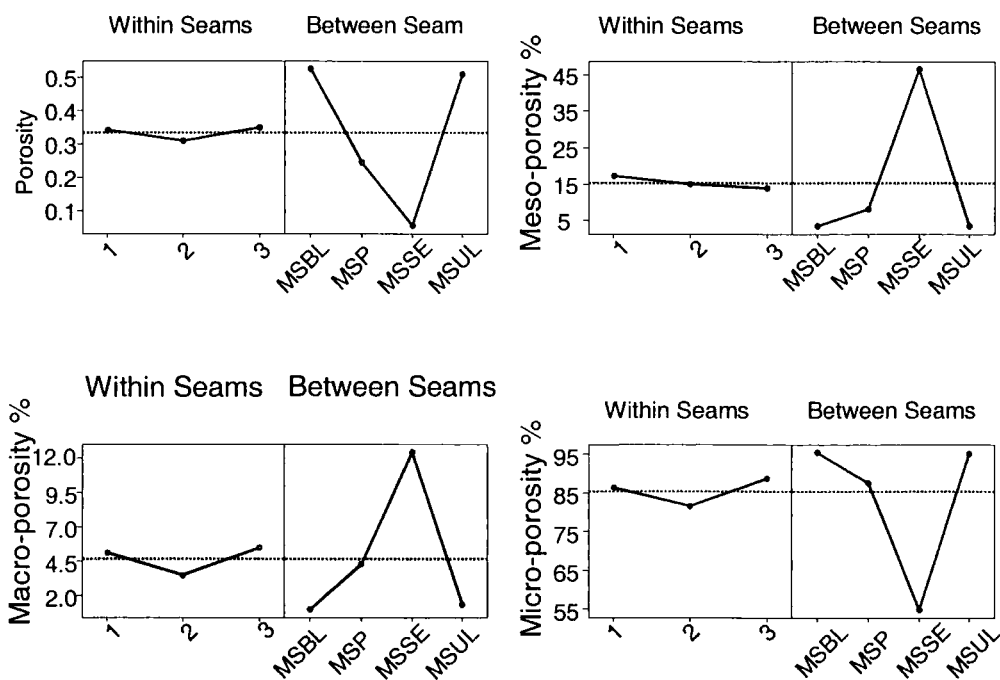
Figure 4.5. Main effect plots for physical characteristics.
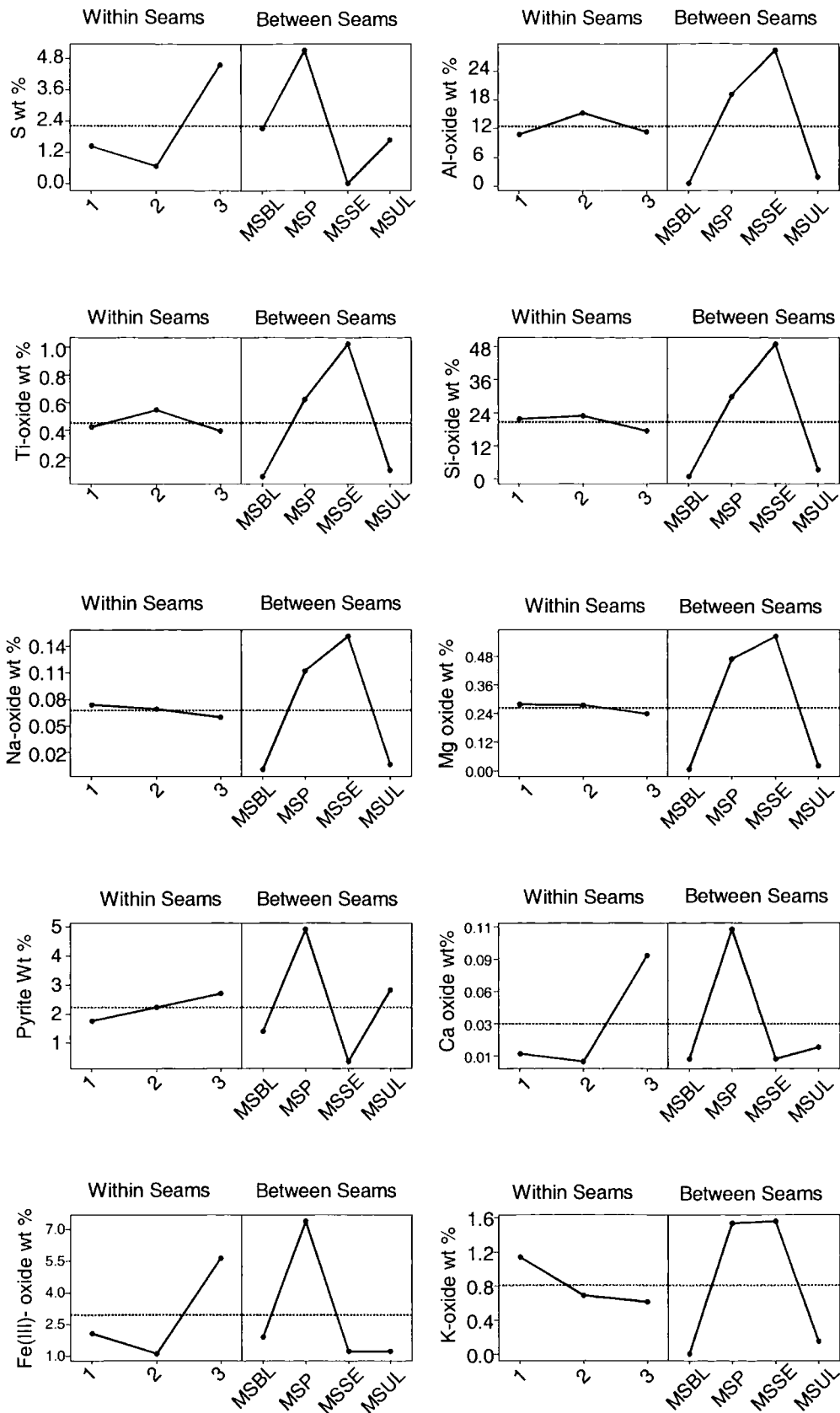
Figure 4.6. Main effect plots for oxide, total S and pyrite wt %, between and within seams.

The second pattern is the reverse of the first, and is shown by total porosity and micro-porosity (Figure 4.5). The concentration of a high proportion of coal porosity in the micro-pore phase agrees with this trend. The opposing patterns of the parting and coals suggests something about the manner in which these rock types will release dissolved matter. As previously mentioned it has been shown that sandstone will release acidic leachate at a faster rate than argillaceous shale (OSMRE, 2002). In this case the parting rate of leachate release would be faster than the coals as fluid transport through micro-porosity is very slow.

The third group divides seams into low means for coals and high means for seat-earth and the parting or rather seams are divided by high or low sediment content (Figure 4.5). The Al, Si, K, Mg, and Na wt % contents follow this trend indicating control by an alumino-silicate or sediment content related factor. The lack of significant variation of Na and Mg can be observed in the intra-seam and inter-sample main effects plot (Figure 4.6). Even at the sub-sample level Na and Mg do not vary significantly, showing the relatively even distribution of these elements at the cm scale. This is more evidence for the association of these elements with an evenly distributed late stage pore water phase. At the between seam scale however these elements are highest in the sediment-rich rocks indicating that Na and Mg may be sediment (i.e. clay) and pore water associated. However as mentioned above, sediment content is also connected to pore size distribution. The proportions of Na and Mg derived from the sediment and pore water sources is therefore unclear.

High mean values for Ca, Fe, pyrite and S wt % from the parting make up the fourth group (Figure 4.6). Obviously mineralogy plays an important role in this trend. The minerals siderite, gypsum and pyrite can all account for the presence of this high trend. The pyrite content accounts for Fe and S, although the presence of Ca also suggests that gypsum is present. The presence of siderite was identified in the parting and in the MSBL coal (Table 4.3). The whole S mean values for the coal seams are higher than expected compared to other elemental main effect plots. Organic S content is the most likely source of this elevation.

Within-seam main effect plots are not very informative in that they are fixed to sampling points. However the relative magnitude of variance at this level compared to the inter-seam level can be observed. As discussed above, in the case of Mg and Na, this provides some evidence for the processes controlling the distribution of these elements. It also suggests that Na and Mg mean seam content may be used as an identifying characteristic of a seam.

4.3.3.3   Post-Hoc Tukey test – Identifying the sources of difference

Nested ANOVA identified significant differences in seam and sample mean values within each level of testing (at 95%). Main effect plots displayed the patterns of mean value distribution for characteristics at inter-seam, intra-seam and inter sub-sample levels. *Post-hoc* testing is used here to show which seam means are significantly different from each other. The ability to analyse to this level is useful in assessing the magnitude of variance. For example one seam or one particular sample maybe the cause of the significant difference shown by ANOVA. Seams causing variance at the 95% confidence interval were identified by a *post-hoc* Tukey test with pair-wise comparisons of mean values (Table 4.7).

In general the *post-hoc* test shows similar results to the main effect plots. Micro-porosity varied significantly between the coals and the parting and seat-earth (Table 4.7). Porosity, macro and meso-porosity and effective porosity all vary significantly between the seat-earth and the rest of the seams. Elements associated with clay and silicate phases (Na, K, Mg, Si, Al) all show a significant difference between coals and the parting plus seat-earth groups. The Al and Si distribution also shows the decline in sediment content progressively up sequence.

Apparent correlation between pyrite content and Ti in main effect plots is due to elevated pyrite content and increased Ti from higher detrital input in the parting. Significant difference between the overlying MSUL and parting and the seat-earth is attributed to low pyrite and high Ti in the seat-earth. Unexpectedly, Fe differs significantly between the MSUL and the parting, and the seat-earth and the parting. The presence of siderite in the MSBL and parting may lower the difference in Fe content between these seams. Siderite precipitation occurs at reduced sulphur species activities, when competition for Fe is reduced. Such conditions would be available in a fresh-water environment or below the depth of sulphate diffusion (Spears, 1987). Considering the association of the parting with a brackish water incursion, siderite formation at depths below sulphate diffusion is the most likely reason for its coexistence with pyrite.

Significantly high Ca content of the parting is derived from dolomite (Table 4.3). As Ca mineral distribution is usually associated with syn or post-diagenetic pore fluid circulation, Ca distribution should follow the pattern of Na and Mg. Elevated Ca content (and therefore dolomite) in the parting may be due to the association with brackish water.

Grouped characteristics	Seam differences	Controlling Factor
Total porosity, macro-porosity, meso-porosity, effective porosity	Coals & Parting ≠ Seat-earth	Sediment vs organic content, affecting lithification process
Micro-porosity, specific surface area	Parting & Seat-earth ≠ Coals	Coal micro-porosity and seat-earth clay content
TiO_2, pyrite content	Coals ≠ Parting MSUL & Parting ≠ Seat-earth	Sediment vs organic content Pyrite in MSUL coal and parting – opposed to sediment content of MSBL coal and seat-earth
MgO, K_2O, Na_2O	Coals ≠ Parting & Seat-earth	Sediment vs organic content Clay associated elements
Al_2O_3, SiO_2	Coals ≠ Parting & Seat-earth Parting ≠ Seat-earth	Sediment vs organic content Progressive upwards decline in silicate input
MnO, P_2O_5	Coals ≠ Parting MSUL ≠ Seat-earth	Organic or siderite content Difference in organic content
Fe_2O_3	MSUL ≠ Parting Parting ≠ Seat-earth	Parting contains high Fe compared to Seat-earth and MSUL. MSBL coal also has Fe mean indifferent from other seams.
CaO	Coals ≠ Parting Parting ≠ Seat-earth	Parting has low Ca mineral content
S	No significant difference between seams.	Large range of S distribution leads to low differences between seam means.

Table 4.8. Analysis of *post-hoc* test results (Tukey) for significant difference between seam mean characteristic values. Characteristics are grouped according to matching patterns of significant difference, (≠ - significantly different to) with a suggested controlling factor given.

4.3.3.4 Summary of statistical analysis

Overall the most important finding was of within seam significant variation of whole S and pyrite, suggesting that over 30 m mean values would not provide accurate MPA predictions. However, whilst the sources of whole S are threefold, the within seam variation of this element is closely associated with that of pyrite content. Sulphate distribution controls between seam whole S variation, whilst within each seam the sulphide content lead to differences in sample mean values.

Detrital sediment input controlled the between seam variance of Al, K, Ca, Mg and Na. Correlation of the within seam Na and Mg distribution with porosity, pore size distribution and effective porosity suggests that these elements were associated with pervasive pore fluids. Porosity is related to compression, cementation and dissolution of the rock matrix. Obviously, plant material will be more compressible on burial than sediment, suggesting that higher sediment content may provide larger pore sizes. Sediment phases are more likely to undergo dissolution, increasing pore size, although rank increases and bituminization of coal have been shown to affect porosity (Gürdal and Yalçin, 2001). The relatively even distribution of porosity and pore sizes implies that the 30 m exposure experienced consistent pore space defining processes.

Rutile and sphene ($CaTiO_3$) are common detrital sedimentary mineral phases in coals. The variation of Ti content strongly correlates with that of effective porosity and meso and macro-porosity supporting the connection between sediment content and porosity. Correlation of Ti with pyrite distribution may be a good indicator of coal-bearing strata with elevated porosity and pyrite content, and therefore pollutant potential. However, the presence of secondary magnetite may also provide such as correlation.

ANOVA suggests that controls of chemical and physical non-variation are pore-water S, Na and Mg content and the burial processes inherent to each seam respectively. Control on variation of rock chemistry is due to the relatively immobile mineral phase. Post-diagenetic cleat mineralisation would lead to less variation as the same burial fracturing controls the distribution of cleat as is experienced by the whole seam. Examination of the sampled strata showed no obvious cleat mineralisation, although yellow staining ran parallel to bedding planes in the parting. SEM inspection of MSUL samples showed framboidal mineralisation along bedding planes suggesting syn-diagenetic formation. Chemical variation is controlled by *in-situ* mineralogy present during peat burial diagenesis. Although pyrite content was found to vary within seams,

point sampling may have been biased and possibly missed vertical trends in pyrite distribution.

The Ca content of the parting is high and dolomite found in the XRD analysis of this rock suggests an extensive cement precipitation, requiring the presence of saline water. Potential weathering of the pyrite of the parting and the superior MSBL seam may have mobilised sulphate leading to gypsum precipitation. The association of Ca with pore water diffusion suggests a relatively pervasive trend similar to Na and Mg. Similar vertical trends as in pyrite content may also present for Ca, leading to apparent variation from random sampling. The insignificant variance of Na and Mg compared to other pore-water associated elements suggests an origin in peat pore-water and retention within micro-porosity. Horizontally little chemical variation may occur over vertical depths of a few centimetres.

4.3.4   Discussion

4.3.4.1   Controls on variability – Scaling from Laboratory to field

The distribution of minerals within coal-bearing strata is highly dependent on the processes that placed them within the rock. For instance coal whole S primary distribution is dependant on plant material and peat pore fluid composition which are controlled by depositional environment (Chou, 2001). Burial diagenesis also affects the final distribution of coal whole S. The scales at which depositional environment and burial processes act will influence the variance in final coal S content. Peat pore water sulphate is controlled by seawater diffusion, and would therefore be pervasive on a regional basis. Plant-based organic S may be more static and therefore prone to smaller seam-scale variation. Sulphide S is present during peat formation, during burial diagenesis and late stage fracture mineralisation from pore fluids. The latter process will provide more evenly distributed S than the former *in-situ* processes. Similarly, elements associated with silicate input would be expected to be relatively static compared to mobile pore water phases, although the presence of dissolved Al and Si has been shown from kaolinite in-filled voids (Spears, 1987). Control of one process over the variance of a characteristic's distribution does not necessarily relate to a quantitative measure of that element. In the coals the organic and sulphate S may make up the bulk of whole S. However if these phases are evenly distributed and only sulphidic S varies significantly, sulphide-producing processes control the overall variation in whole S.

Processes controlling chemical and physical distribution within coal-bearing strata can be shown to act at least at two different scales of within seams i.e. spatially to between seams i.e. regionally (Dulong and Blaine, 2000). If the scale at which a characteristic begins to vary significantly is known, then prediction extrapolation should be possible within that scale.

The Northwood strata

Only Na, Mg and the physical characteristics did not vary significantly within each seam and sample. This suggests that seam mean values for these characteristics can be used to predict their effect on leachate quality, at least for the 30 m exposure of the Northwood strata. Similarly, in laboratory experiments used to predict leachate quality, these characteristics would be most easily scaled from laboratory to field.

No between-seam variation was found for total S because larger scale regional variations in sulphate may swamp variance in total S distribution between seams. The large range of seam whole S values is due to the low and high mean values of the seat-earth and parting respectively. High whole S values within one parting sample (MSP3) may have also skewed the analysis. It is probable that this sample was from a zone enriched by secondary sulphide precipitation relative to the rest of the parting. At the 30 m scale whole S variation between seams is low. However at the 10 m scale, within each seam whole S and pyrite contents do vary significantly, probably due to sampling of vertical trends. Pyrite and whole S means will not be representative of randomly sampled values along seam at the 95 % confidence interval. Insignificant between seams variance in whole S suggests sulphate distribution was influenced by groundwater flow. The lack of significant Na and Mg variance within seams was associated within connate pore-water.

All remaining analysed elements varied within and between seams, however the two main processes controlling their distribution are pore-water composition and sediment input. Silicate phase elements included Al, Si, K, Ti, Mg and Na. Although pore water composition controlled Na and Mg distribution within seams, regional variations were controlled by sediment input. Detrital sediment input to coals is water or air-borne, with both styles introducing minerals either in separate partings or distributed within the coal matrix itself (Spears, 1987). This style of mineral distribution will introduce vertical fluctuations in mineral content within each seam.

Pore-water composition controlled the variation in Fe and Ca distribution between and within seams. Precipitation of Fe bearing siderite during burial diagenesis, below

sulphate diffusion, was responsible for its co-existence with pyrite. Input of Fe to peat is controlled by detrital clay composition (Spears, 1987). Pore-water composition with respect to sulphate, carbonate, pH and Eh, controls the manner in which dissolved, clay-derived Fe will precipitate. Considering the requirement for a Fe source in the relatively static clay phase, Fe-bearing secondary mineral distribution may remain relatively close to source.

High concentrations of Ca within the parting may be a result of dolomitic cement identified by XRD, or gypsum precipitation.

The processes of pore water movement and precipitation and detrital sediment input control identified variation in most coal element distributions. Pore water diffusion would be expected to be more pervasive and evenly distributed than static sediment minerals. However, reaction with coal as a fluid diffuses through the matrix and the need for point sources of elements for precipitation, i.e. Fe may cause the variations identified here. Gayer et al., (2001) identified within seam vertical layering in coal sulphate composition caused by the association of the upper and lower parts of the coals with sea-water. Holz et al., (2001) also found evidence for vertical variation due to changing coal depositional environments of Early Permian Brazilian coals. Random sampling across vertical trends within each seam was probably responsible for apparent significant variation within seams of the mineral phase derived from pore-water and detrital material.

Implications for scaling

Within seam variation is problematic not only when testing for rock MPA, but also in scaling laboratory experiments to field scenarios. Malstrom et al., (2000) identified pH, temperature, mineral content and hydrological conditions as factors influencing the ability to scale from laboratory to field conditions. Out of these factors we have analysed mineral content variation, and have shown it to be a significant problem at the 30 m scale. Small-scale column leaching experiments will provide information on weathering processes occurring within cells of coal overburden material the same size as the column. Extrapolating to the field-scale has become the main task of numerical modelling. However, if each modelled cell of material does not show the variation in characteristics of the actual material then some error in leachate quality prediction will be introduced. The use of statistical analysis to characterise sampled materials in relation to in-situ field material, prior to experimental work, may address this problem. Within one seam, sub-stratification due to pore fluid infiltration and sedimentation will

act across different vertical depths. In order to experiment on representative rock from a seam, the whole seam thickness should be characterised at different points along seam. Depending on the use of the seam mean, i.e. for predictions of spoil waste or *in-situ* strata leachate quality this characterisation will have varying implications (see section 4.3.4.3 below). An important point to note is that exploratory bore-hole coverage of potential extractable coal strata, may miss variation in environmentally hazardous elements such as Al and Mn.

4.3.4.2 Variability of S and pyrite – implications for acidic discharge prediction

One of the main objectives of this analysis was to investigate within seam variance of whole S and pyrite wt %. As wt % S is typically used to calculate the MPA of a rock-type the assumption that mean seam values are representative of the actual content was tested. In acid base accounting (ABA) the difference between calculated negative MPA and positive neutralizing potential (NP) is used to predict leachate quality from a site. If the difference is positive, alkaline water should be produced, if it is negative leachate will be acidic (Sobek et al., 1978, Kania, 2000, Skousen et al., 2002). MPA is based on the maximum amount of sulphuric acid produced from a rock type on weathering. This value is calculated stoichiometrically from whole S content of the rock type in an equation describing sulphide oxidation and neutralization reactions:
describing sulphide oxidation and neutralization reactions:

$$FeS_2 + 2CaCO_3 + 3.75O_2 + 1.5H_2O \Rightarrow Fe(OH)_3 + 2SO_4^{2-} + Ca^{2+} + CO_{2(g)} \quad (4.7)$$
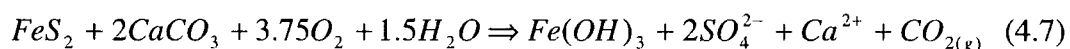
Therefore 2 moles or 200g of $CaCO_3$ will neutralize 1 mole of pyrite, containing 64 g of S and 1000 tons of rock containing 1wt% pyrite will be neutralised by 31.25 tons of $CaCO_3$ (Kania, 2000, Skousen et al., 2002). In a closed system such as open-cast backfill, CO_2 should react with water to produce carbonic acid (Cravotta, 1991 in Skousen et al., 2002):

$$FeS_2 + 4CaCO_3 + 3.75O_2 + 3.5H_2O \Rightarrow Fe(OH)_3 + 2SO_4^{2-} + 4Ca^{2+} + 4HCO_3^- \quad (4.8)$$
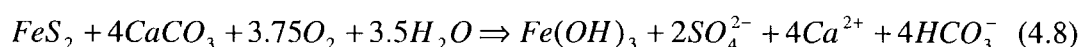
with 62.5 tons of $CaCO_3$ required to neutralise 1 wt % pyrite in 1 ton of overburden (Kania, 2000, Skousen et al., 2002). The MPA of a rock type will provide some idea of whether poor quality leachate is produced. However the ratio of NP/MPA and the net

neutralizing potential (NNP=NP-MPA) have been found to provide a far better prediction of the final acidity of any discharge (Skousen et al., 2002). The NP of a rock-type is calculated from the extent of reaction with HCl. We have not carried out this procedure here as our aim is to identify error in the measurement of rock characteristics rather than test the validity of the overall ABA calculation.

Statistical analysis demonstrated significant variation (at 95 %) in whole S and pyrite wt%, over a 30 m exposure of four seams. Using seam values to calculate MPA will therefore lead to incorrect evaluation for the whole seam. The magnitude of this error depends upon the differences between the sample means within each seam.

Required CaCO₃ for MPA neutralisation has been calculated for the coals and parting for sample and seam whole S means in order to show the effect of variation (Table 4.8). Considering most ABA is performed on samples of exploration bore-holes of coal-bearing strata an assumption of insignificant variance in surrounding strata must be made. Carbonate requirement calculated from the MSUL coal mean MPA compared favourably with those calculated from MSUL individual sample MPAs (Table 4.8).

Seam	sample	Sample S mean	Seam S mean	Carbonate required		Carbonate required when backfilled	
		(wt %)	(wt %)	(tons)		(tons)	
MSUL	2	1.7 ± 0.3	1.8	55	53	110	105
	3	1.2 ± 0.3	±		38		75
	4	2 ± 3	0.9		66		132
MSBL	1	3 ± 3	2	70	105	139	210
	2	1.4 ± 0.1	±		42		84
	3	1.6 ± 0.2	2		51		102
MSP	1	0.7 ± 0.2	6	179	21	358	42
	2	0.14 ± 0.04	±		4		9
	3	15 ± 14	10		454		908

Table 4.8. Calculation of carbonate required to neutralise maximum acidity produced by seam whole S wt%. Tonnage of CaCO₃ is calculated for seam means and within seam sample means to show the effect of variation. MSUL – Main seam upper leaf, MSBL – Main seam bottom leaf, MSP- Mains seam parting.

However MSBL coal and parting sample means require a wider range of carbonate amounts for neutralisation compared to the whole seam means. The differences of 450 and 63 tons $CaCO_3$ between the upper and lower sample means of the parting and MSBL respectively suggest that large errors may be made in ABA. In the course of ABA the calculated NP of the rock may decrease differences in the MPA figure to some extent. However, NP is also based upon a characteristic, i.e. Ca content, which has been shown to vary significantly both between and within seams. Dulong and Blaine (2000) suggest coal-bearing strata with significantly variable NP and total S, will be the most difficult strata to predict mine drainage quality for.

The incorrect prediction of potential leachate quality is of concern because a negative ABA result is a pre-requisite of site evaluation for permitting surface mining in the USA and many other countries (Skousen et al., 2002). Bore-hole data should be used with caution when estimating the behaviour of seam characteristics over the typical scale of extraction.

4.3.4.3 Application of findings to spoil material and in-situ strata

Spoil material is composed of coal overburden and high pyrite coal, usually elevated by extraction processes, making it difficult to characterise from seam analysis alone. Analysis of spoil material can be carried out using the same statistical methods, however findings may be quite different from analysis of the *in-situ* seam material.

Intact coal-bearing strata geochemistry is typically used in the prediction of mine water quality for proposed extraction sites and for the cessation of pumping on mine abandonment (Younger, 1995). As previously discussed, numerical modelling based on the results of column leach tests, must assume material homogeneity in order to make predictions for larger volumes of material. Regional trends in rock geochemistry can be identified by analysis of bore-hole and mine sample data (Dulong and Blaine, 2001, Watson et al., 2001). However resolution to the actual site of extraction has not been previously attempted. Here the scale of significant variance for most elements has been shown to exist spatially at the 10 m scale within each seam and stratigraphically. Physical properties and elements associated with connate brines such as Na and Mg only vary stratigraphically, between seams. Horizontal trends in the distribution of acid producing and neutralising minerals were not found. Vertical trends within each seam probably lead to the identified variance in distribution. In order to identify such trends whole seam thicknesses should be analysed.

4.3.5 Summary of investigation into seam and sample scale variance

Significant variance in whole S and pyrite content occurs over a 30 m exposure of the Main Seam of the Durham Coalfield. Mean seam characteristic values should be used with caution when used to predict and model leachate quality.

Correlation of variance in other chemical and physical properties of the sampled coal-bearing strata provides information about the controlling processes in their distribution. Physical properties and Na and Mg do not vary within seams suggesting that the two elements are associated with connate brines. The lack of significant variance for pore space characteristics along seam is indicative of pore space dependence on seam material compressibility and solubility. The scaling of the effects of these characteristics on leachate water quality will be relatively simple due to their insignificant variance within each seam. Ti content also showed strong correlation with effective, meso and macro-porosity suggesting that detrital sediment was associated with larger pore spaces. Positive correlation of pyrite and Ti content may be a primary indicator of a highly polluting rock type, although further investigation of the source of Ti is required. Larger connected pore spaces will lead to faster and more invasive transport of oxidant and dissolved metals.

For other elements the sedimentary input and pore-water composition both control the pattern of distribution, leading to significant variance within and between seams. Identified variation may be due to the random sampling of vertical trends in sediment and fluid diffusion. To identify such trends the whole thickness of a seam would need to be analysed at various points. The effect of this scale of resolution on the ability to successfully scale from laboratory to field scenarios is questionable for ABA. However numerical models may benefit from the identification of sub-seam vertical and lateral trends.

Chapter 5

Oxidation rates of coal-hosted pyrite – in-situ leaching using static methods

5.1 Introduction

It has long been accepted that pyrite oxidation and the subsequent acidic weathering of associated minerals is the driving force behind the generation of AMD (Evangelou, 1998, Bierens de Han, 1991). However, this reaction is one of a series of chemical and physical interactions controlling the discharge characteristics. For each pyrite grain embedded within a waste rock particle, the weathering process can be broken down into three stages:

1. **Influx of oxidant into the rock host.** Oxygenated water in macro-pores, *in-situ* fluid in micro-pores or pore fluid in contact with mineral surfaces acts as a essential pathway for the introduction of oxidant to the mineral surface (Moses et al., 1987).

2. **Actual oxidation of sulphides.** Oxidation occurs initially with dissolved oxygen, and is subsequently oxidised by Fe^{3+} produced during the initial reaction. Oxidation only occurs in the presence of water (Moses and Herman, 1991).

3. **The removal of the oxidation product.** Sulphide oxidation leads to the production of metal laden, pH altered pore water. Neutralisation of the acidic product by weathering reactions with carbonate and alumino-silicate minerals may affect the produced leachate. Oxidation product is either removed from the mineral surface or precipitates secondary minerals. Again water is essential to leachate formation as a solvent and transport medium.

Predicting AMD using numerical modelling

Of the several methods currently available for prediction of site specific discharge quality the most sophisticated is numerical modelling. Field data describing waste rock mineralogy, porosity, pore space oxygen content and climate is used for boundary conditions in modelling current processes. Results are compared to field or laboratory measurements of discharge chemistry (Drever, 1997), with the success of the model as an interpretation of field processes gauged accordingly. Typical models are used to project mass transport (e.g. MINTRAN, Wunderly et al, 1996), chemical equilibrium (e.g. RATAP, Destouni et al., 1998) and to describe elements of mass transport, chemical dissolution reactions and the decreasing pyrite content (e.g. MINTOX, Wunderly et al., 1996). A Shrinking Core Model (SCM, Figure 5.1) has previously been used to mathematically describe describe the dissolution of a solid particle. As the

Outer oxidized material

Partially oxidized material

Un-oxidized material

Spherical shrinking core model
(no cleavage or cleat)

Shrinking core in coal bearing
strata with cleavage
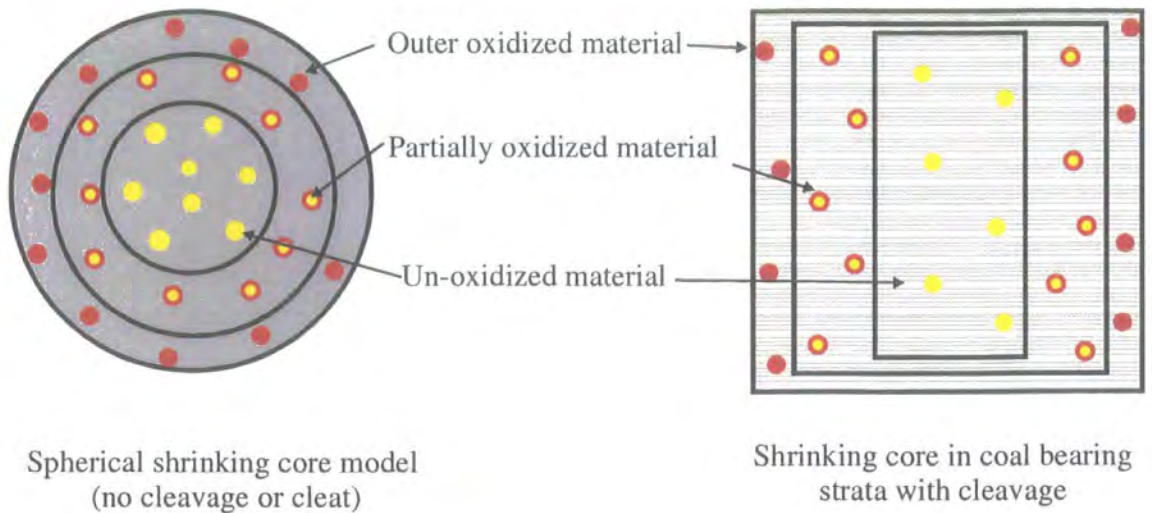
Figure 5.1. Shrinking core model in spherical with homogenous porosity and cuboid
waste particles with cleavage.

Totally oxidized particle

Meteoric precipitation

Partially oxidized particle

O_2

Waste rock
particle

O_2

Vadose zone

Water table

O_2

Capillary fringe

O_2

Phreatic zone

O_2

Un-oxidized particle

Acidic plume

Ground water flow

Neutralization
reactions
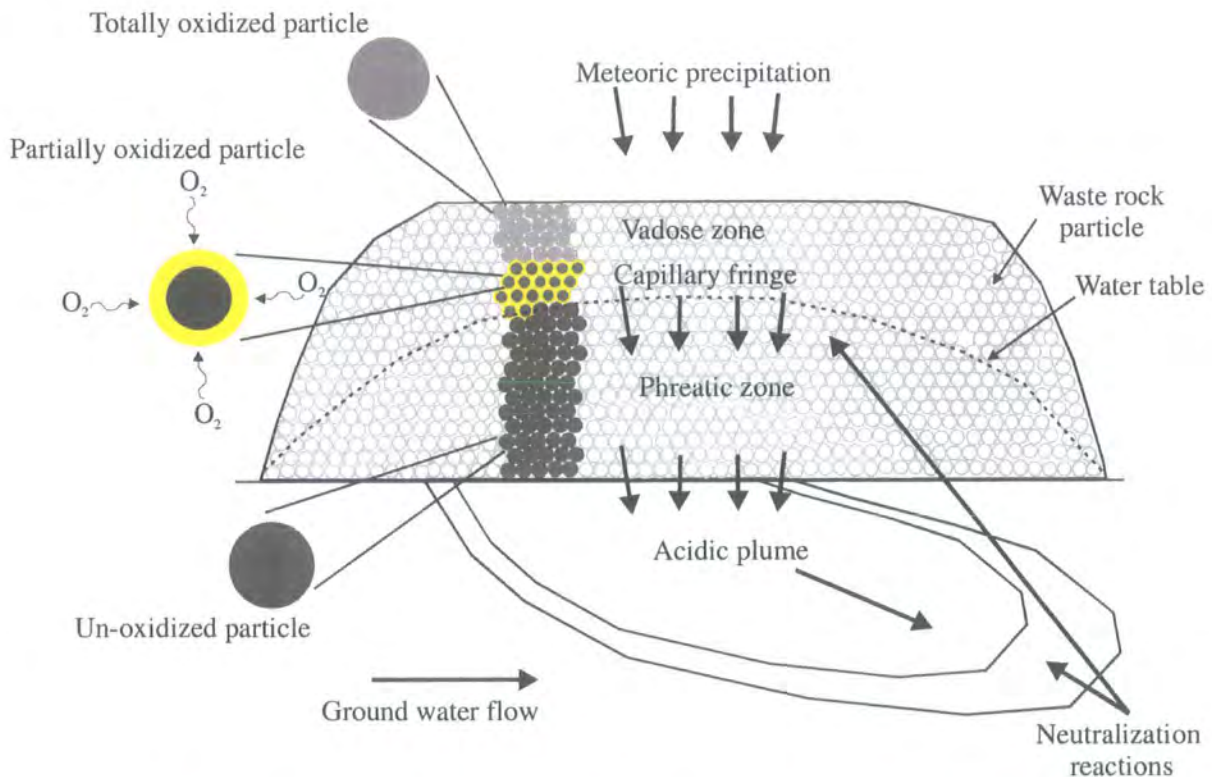
Figure 5.2. Summary of processes occurring during spoil heap material weathering.
Shrinking core model is shown on the left-hand side with the active
oxidation zone within the vadose zone of the spoil material. The production
of an acid plume in ground water is also shown as a consequence of
infiltration of meteoric water through the weathered zones of spoil material.
After Blowes and Jambor (1990) and Wunderly et al. (1996).

reaction progresses the radius of the particle shrinks and its surface area decreases leading to a decrease in reaction rate (Schafer et al., 1979, Levenspiel, 1999). The shrinking core of un-oxidised material within each particle of waste material is modelled either as consisting wholly of pyrite or as having a homogenous pyrite distribution. The rate of weathering is assumed to be uniform within a steadily encroaching weathering front (Figure 5.1, Nicholson et al. 1990, Wunderly et al., 1996, Strömberg, 1997, Bain et al., 2000). In the case of processed mine tailings, with a high or total pyrite content for each particle, this is a good approximation. For embedded pyrite within a rock matrix, the SCM may over-estimate the weathering output. In sedimentary rock the presence of a cleavage plane of potentially higher porosity gives rise to the concept of different rates of oxidation front motion for different faces (Figure 5.2). Coal spoil, due to its sedimentary origin, tends to form oblate pieces rather than spherical, therefore the use of an ovoid-shrinking core may be more suitable.

In order to model the oxidation of pyrite within waste rock particles the distribution and morphology of pyrite must be assumed to be homogenous. Although the presence of pyrite is dependent on the environment of deposition (Casagrande, 1986, Younger, 1995a), its morphology depends on syn and post-diagenetic processes. Framboidal pyrite predominates in sedimentary rock (Evangelou, 1995), with massive pyrite surrounding framboidal structures (Strauss and Schieber, 1989). Hydrothermal pyrite may also mineralise fractures during burial diagensis (Spears, 1986).

Pyrite oxidation rates

The prominent role of pyrite oxidation in AMD generation makes the rate of this reaction a key factor in waste rock weathering simulation. Experimental measurements of pyrite oxidation by O_2 and Fe^{3+} indicate oxidant concentration dependence, controlled by fractional to first order kinetics (Table 2.1). The use of pyrite oxidation rate as the rate-limiting step in AMD generation for embedded pyrite assumes relatively rapid leachate transport through the rock pore space. Given the complex nature of an organic macerel rich, rock matrix, leachate transport may be the rate-limiting step in AMD generation at the waste particle scale.

Zones of water-rock interaction

Another important aspect in the modelling of rock waste weathering is the variability in rock saturation with respect to water. Vertical profiles of waste rock heaps consist of an active oxidising layer in the vadose zone, bounded by an overlying oxidised layer
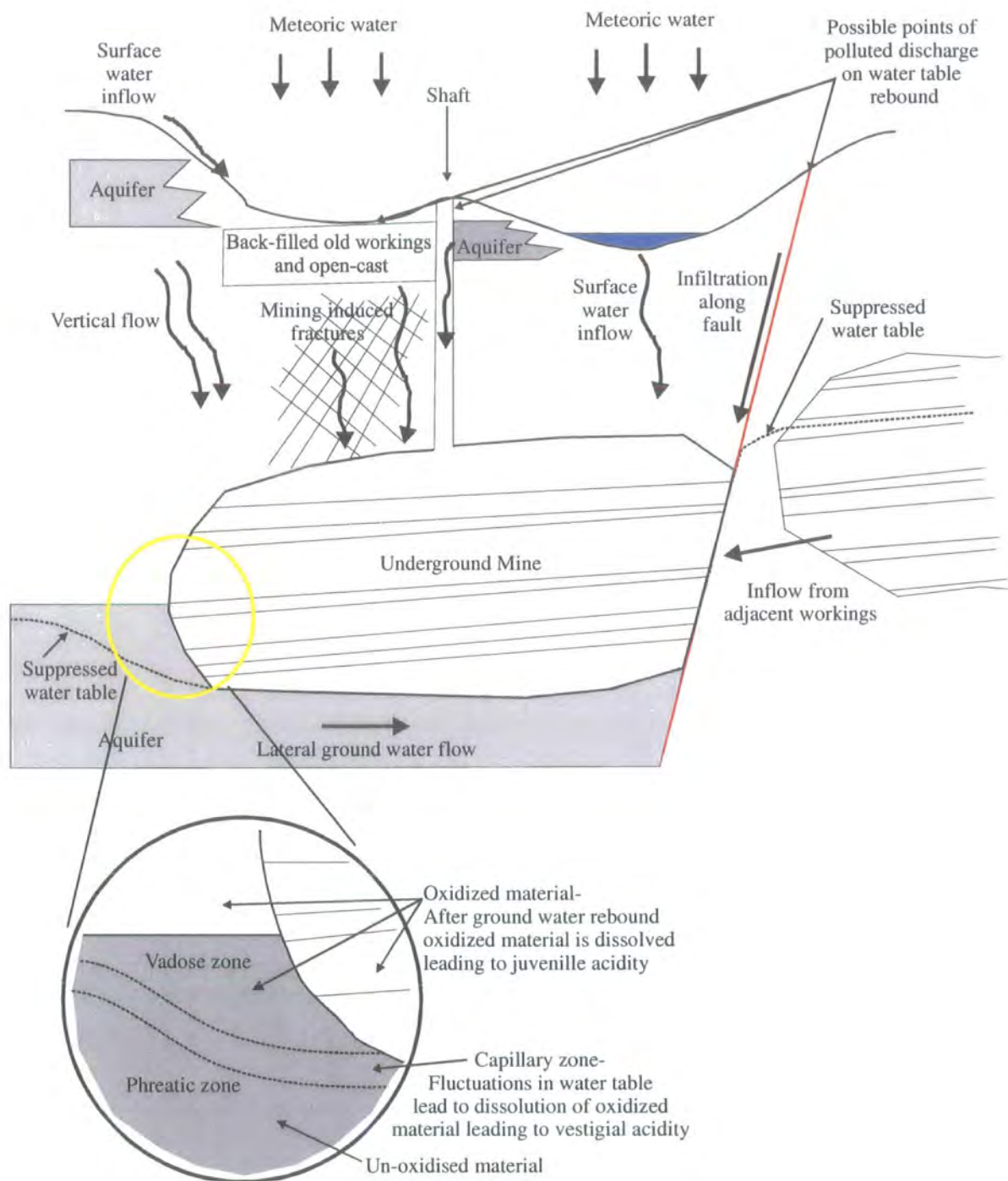
Figure 5.3. Typical pathways of water infiltration to mined workings and possible points of discharge on pumping cessation. Inset shows the areas of oxidised and un-oxidised material from which vestigial and juvenille acidity is produced (Younger, 1995). After Sadler (1999).

and the underlying water table (phreatic zone) (Figure 5.2, Blowes and Jambor, 1990, Elberling et al., 1994, Elberling and Nicholson, 1996, Wunderly et al., 1996). Similarly in intact rock strata the position of the water table dictates the region of oxidation. Younger (1995a) suggests that seasonal fluctuations in suppressed water table level lead to the formation of oxidation products and their removal as vestigial acidity (Figure 5.3). During ground water rebound, at the end of suppression, a far larger volume of oxidation products are sampled leading to the production of juvenile acidity.

Water-rock conditions in each zone have been simulated in column leaching experiments by various authors to investigate waste rock weathering (Strömberg, 1997, Elberling and Damgaard, 2001). Interpretation of mineral behaviour within each zone from leachate chemistry is made difficult by the large uncertainty in describing processes such as mineral precipitation and dissolution without direct observation (Vandiviere and Evangelou, 1998).

Objectives

In this chapter, results of leaching experiments designed to investigate coal and shale-hosted pyrite reaction in simulated saturated and capillary zone conditions is reported. *In-situ* pyrite oxidation in coal-bearing strata is investigated to test the suitability of isolated pyrite oxidation rates and the SCM in predicting coal-rock waste polluting potential. To assess pyrite oxidation front monitoring methods, small-scale experiments were performed using SEM to monitor Milli-RO water and phosphate solution induced reaction. The final large-scale leaching experiments were performed over a year under stagnant and cyclic wetting conditions. The following points were addressed:

- Does the rate of *in-situ* pyrite oxidation differ from values predicted from the oxidation of pyrite alone?
- Is the movement of the pyrite oxidation front into rock particles represented well by the shrinking core and other models? How does oxidant influx and dissolved product exit from the rock host affect pyrite oxidation and the rate of leachate generation?
- To what extent does pyrite content and morphology affect weathering potential?

In Chapter 6 a similar experiment involving the leaching of rock under flowing water is described, with a comparison made between all simulated water-rock regimes.

5.2   Developing a method for static leaching of coal-bearing strata

Phosphate tracers

Following the movement of the pyrite oxidation front, induced by the passage of oxygen through a coal or rock matrix, may be problematic where prior oxidation products are present. In order to trace the initiated oxidation of pyrite, the phosphate coating technology investigated in Chapter 3 can be used. There the coating of pyrite grains by using H_2O_2 to oxidise pyrite then phosphate solution to form a coating with ferric Fe at the grain surface. SEM-EDAX may be used to identify precipitated phases formed during rock leaching with the H_2O_2 - phosphate solution and therefore trace an *in-situ* pyrite oxidation front. In order to monitor the kinetics of the pyrite oxidation front movement with phosphate solution samples examined were leached for different time intervals. These samples then provide 'snap-shots' of the extent of oxidation at the time of removal. As well as monitoring an oxidation front, this method may also be used to investigate the mechanisms controlling leachate transport within the rock matrix.

Observing the oxidation front and associated chemical response

Another objective of the investigation was to study the dependence of leachate chemistry on the physical and chemical characteristics of the rock-type. Cleavage planes by definition have a greater effective porosity compared to bedding face planes. An investigation of the difference in chemical output from these two different surfaces of coal is described, along with an SEM study of some controls on the ingress of a H_2O_2 induced oxidation front.

In the following section phosphate tracers of pyrite oxidation and the chemical behaviour of coal cleavage and bedding face planes are investigated. Subsequently the findings of these experiments are used in the design of a large-scale static leaching experiment described in the final part of this chapter.

5.2.1   Comparison of chemical output from coal cleavage and bedding faces.

5.2.1.1   Method and materials

Coal samples from the bottom leaf of the County Durham Coalfield Main Seam were collected from the Northwood Open-cast, Brandon, County Durham (NZ 401200) (Figure 4.1). A complete chemical and physical analysis of this rock type is described

in Chapter 4 with a discussion on causes of variation within the Main Seam Coal characteristics. Physical and chemical characteristics are summarised in Table 5.1.

Major Element wt %	Al	Si	Fe (II)	Mg	Ca	Na	K	P	S
	0.05 ± 0.05	0.16 ± 0.16	0.18 ± 0.13	0.001 ± 0.002	0.0010 ± 0.0003	0.0004 ± 0.0003	0.02 ± 0.007	0.001 ± 0.001	0.15 ± 0.06

Pyrite Content	3 ± 2 wt %
Mineral content	Quartz, Calcite, Gypsum, Kaolinite, Albite, Dolomite, Pyrite
Total Porosity	50.8 ± 0.5 %
Effective Porosity	4 ± 1 %
Pore size distribution	Macro-porosity – 1.4 ± 0.7 %, Micro-porosity - 95 ± 1 %, Meso-porosity - 4 ± 1 %
Specific surface area	29 ± 9 m^2

Table 5.1. Summary of characteristics of Main Seam Coal discussed in Chapter 4.

Accelerated weathering of the coal was carried out using 1 % H_2O_2 solution. Samples of the original intact coal were cut into 4 blocks measuring 2.75 cm × 2.75 cm × 1.3 cm deep. Two of the coal samples were cut with the cleavage parallel to the exposed surface and the remaining two were cut with the cleavage perpendicular to this surface. All blocks were embedded in epoxy-resin to allow the fluid access to only one surface.

Each sample was placed in an acid washed 1L Pyrex beaker and then immersed in 1000 mL of 1% H_2O_2 solution. A large volume of solution was added to keep the H_2O_2 solution in excess with respect to the sample throughout the experiment.

Background reaction samples (hereafter referred to as blanks) were prepared by leaching the remaining orientated coal blocks 1L of Milli-Q water. Although Milli-Q water is relatively aggressive due to its low ionic content the difference between in its oxidising properties and those of H_2O_2 are sufficient for blank experiments to provide essential base-line information on the water-rock interaction.

Reaction vessels were covered with PVC film and left at room temperature and conditions for the whole of the experiment. Aliquots of 10 ml of solution adjacent to the coal surface were taken at 5 and then 10 minute intervals over the first hour, every 2 to 4 hours, and finally every day after the first 24 hours for the remaining 6 days. The aliquots of solution were acidified with concentrated HNO_3, vacuum filtered and the

filtrate analysed by ICP-OES for major element concentrations (Appendix I Methods). At the end of the experiment coal samples treated in H_2O_2 were allowed to dry, then were split perpendicular to the exposed surface. The cut face was set in resin, polished and carbon coated for examination by SEM.

Zygarlicke and Steadman (1990) used SEM-BSE (Back-Scattered Electron) imaging to rapidly identify mineral phases in coal. BSE imaging was also used to rapidly identify high atomic mass inorganic phases from the organic matrix and speed up investigation of mineral weathering. As SEM-EDAX is semi-quantitative, collected x-ray spectra may be compared to identify potential sites of oxidation. Typical 'un-oxidised' pyrite spectra usually have a $K^{\alpha}Fe$ peak half to a third the size of the S K^{α} peak (Figure 5.4). When oxidised the Fe and S K^{α} may remain relatively proportional, however the K^{α} O peak rises (Figure 5.5). High Fe, S or O K^{α} peaks over those collected from un-oxidised pyrite may also be used to identify oxidation.

5.2.1.2 Results and interpretation of rock leaching.

As Fe and S leachate concentrations reflect the oxidation of pyrite, the main focus of investigation, their dissolution with time is discussed here.

5.2.1.2.1 Chemical behavior of cleavage parallel and cleavage perpendicular mineral leaching.

Leachate Fe and S concentrations from cleavage parallel and perpendicular exposed intact coal samples show a general increase with time (Figures 5.6 and 5.7, Tables 5A-5B, Appendix II Results).

Coal blocks with both orientations of cleavage leached with Milli-Q water released Fe at concentrations close to zero throughout the period of the experiment (Figure 5.6). In the same leachate, S concentration was also low. The cleavage parallel leachate concentration varied between 0.75 mgL^{-1} and 1.52 mgL^{-1} S, and the cleavage perpendicular leachate between 0.59mgL^{-1} to 1.36 mgL^{-1} (Figure 5.7).

Treatment with 1% H_2O_2 solution produced dissolved Fe between 0 and 0.84 mgL^{-1} from the cleavage-perpendicular orientated coal sample faces. Under the same treatment cleavage parallel coal face released 0 to 0.07 mgL^{-1} (Figures. 5.6 and 5.7). The cleavage perpendicular leachate contained a peak concentration of S almost twice that of the cleavage parallel sample. Values ranged from 0.65 to 2.73 mgL^{-1} of S in the cleavage perpendicular leachate and 0.79 mgL^{-1} to 1.32 mgL^{-1} of S in cleavage parallel leachate.
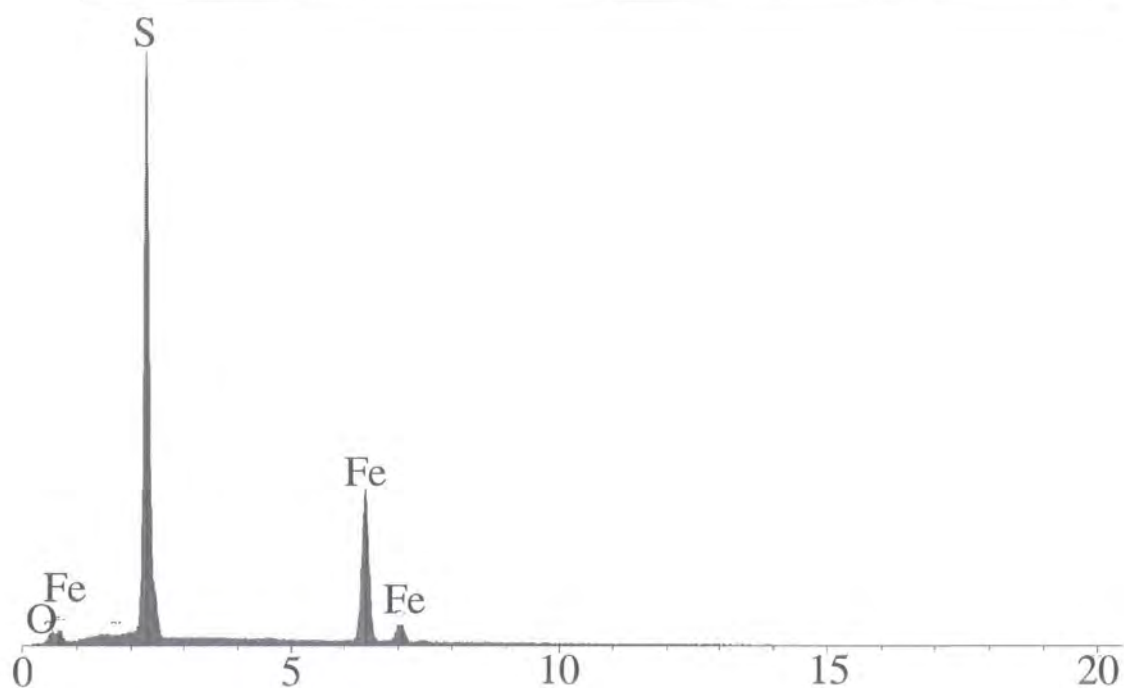
Figure 5.4. Typical collected spectra from un-oxidised pyrite. Full scale cps 25000.
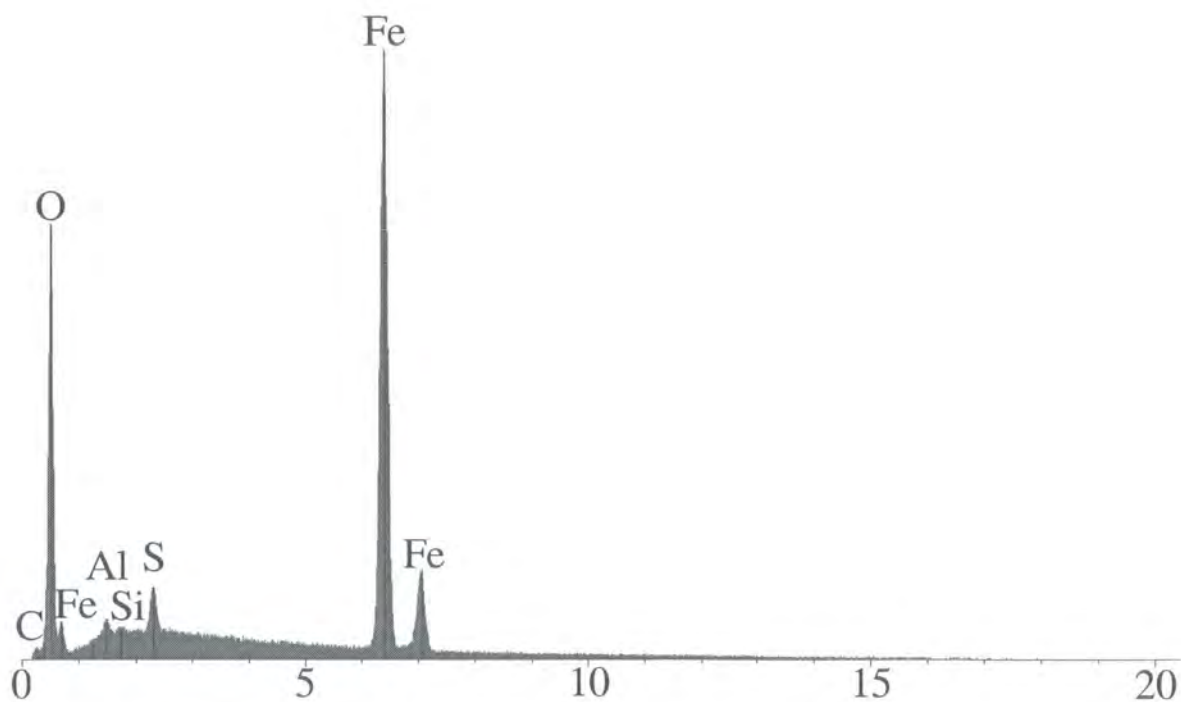
Figure 5.5. Collected spectra by SEM-EDAX from the oxidised edge of a pyrite grain. Full scale cps 9080.
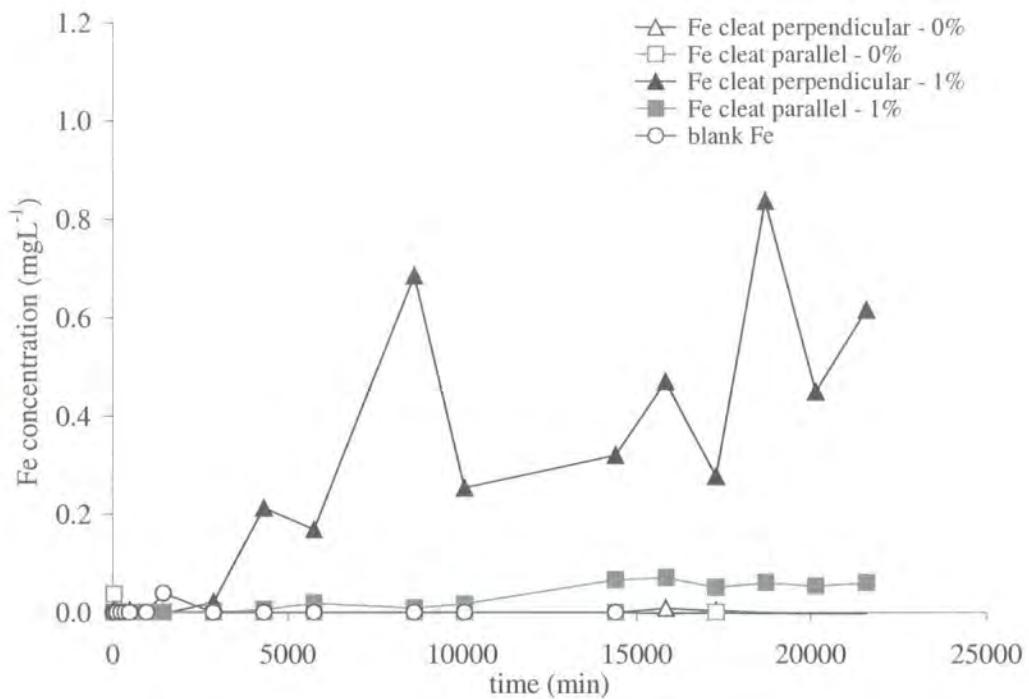
Figure 5.6. Leachate Fe concentration for coal with cleat perpendicular and parallel to leaching solution. Percentages represent treatment H_2O_2 concentration.
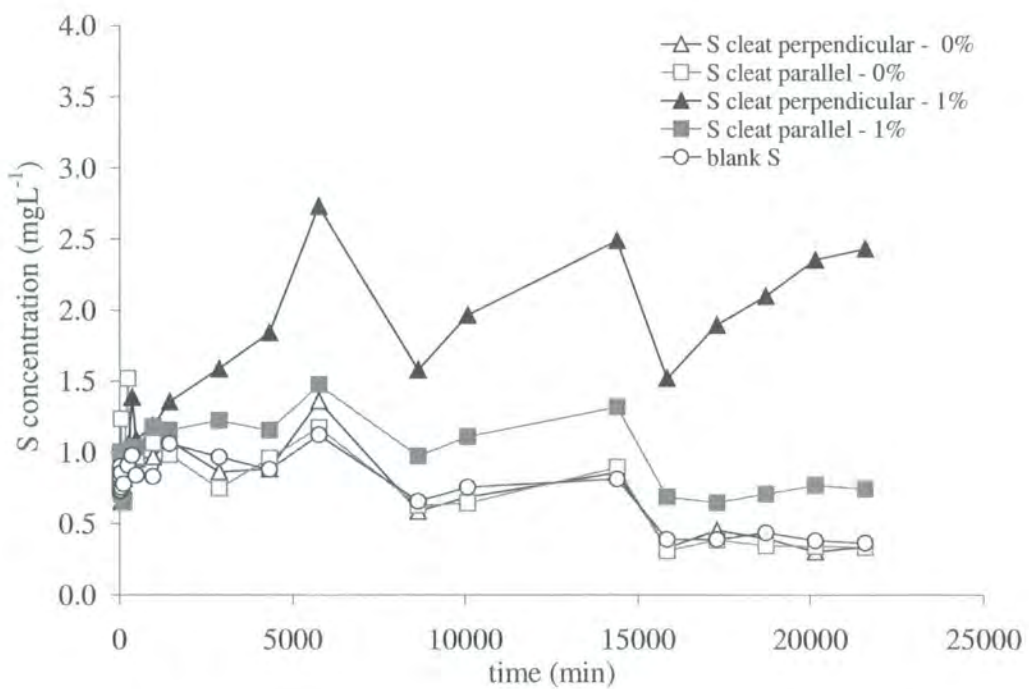
Figure 5.7. Leachate S concentration for coal with cleat perpendicular and parallel to leaching solution. Percentages represent treatment H_2O_2 concentration.

Exposure of the cleavage perpendicular face of coal samples imparted more Fe and S to solution than the cleavage parallel face. It was therefore assumed that cleavage plane minerals are more vulnerable to the influx of fluid, leading to greater leaching and potentially oxidation. Dissolution of the cleavage perpendicular face of coal was assumed to represent the maximum release from coal matrix weathering of that surface area and restricted volume. Released element concentrations from the cleavage perpendicular coal samples are therefore compared with the briquette leachate chemistry.

5.2.1.2.2   SEM examination of oxidized coals.

Examination of the leached coal by SEM and SEM-EDAX was used to visually identify the pyrite oxidation front. Despite the difficulty in interpreting 3-D processes from observations of 2-D images, the relevance of matrix structure to fluid diffusion through coal is still emphasised. The coal was not pre-examined to estimate the extent of weathering. This made it difficult to clearly distinguish between initiated and pre-treatment oxidation. However, as a strong oxidant was used in leaching it was assumed that pyrite weathering had taken place. As only one face of samples was exposed to the leaching fluid, the weathering front was presumed to have moved into the rock from this face.

The intact coal had a very prominent pyrite phase, formed of spherical clusters of framboids along cleavage planes and also as discrete isolated framboids (Figure 5.8). Isolated pyrite framboids seemed to be the least oxidised, whereas closely grouped crystals were oxidised and the central portions removed, presumably during polishing. Interconnectivity of pyrite crystals was obviously an important factor in easing oxidant diffusion and increasing the rate of mineral oxidation. Some larger interconnected pyrite framboids away from the exposed surface of the treated coal seem to be protected from oxidation. Joints and fractures surrounding these clusters may have provided protection against oxidation by diverting fluid away from the less fractured areas.

5.2.1.3   Summary of coal cleavage and bedding plane face weathering

The experiments described above have shown that it is possible to use SEM and SEM-EDAX to follow a pyrite oxidation front in coal. Coal cleavage is more permeable compared to the perpendicular face, suggesting that a core of un-oxidized pyrite may shrink at different rates along and across cleavage.

Exposed edge

Remnants of individual pyrite framboids, at the edges of a larger original cluster. Smaller massive pyrite grains in the surrounding coal remain intact.
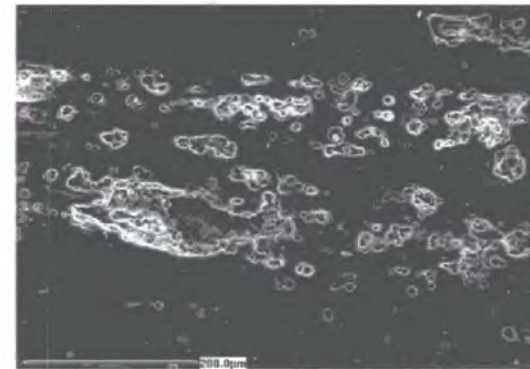
Bedding plane pyrite mineralisation in coal sample. Interconnected pyrite is most affected by oxidation. Isolated grains close to the weathered areas remain intact

Cleavage plane mineralisation furthest from exposed edge. Unaffected pyrite is at the same depth as a highly weathered area. This suggests possible protection of certain areas by jointing.

Figure 5.8. SEM –SE images of coal treated with 1% H_2O_2 over a period of 15 days. Exposed surface, marked by white line, is to the right of the large image. Enlargements of circled areas are described in adjacent text.

5.2.2 Leaching of coal with H_2O_2 and phosphate solutions; an SEM –EDAX investigation

In the experiment described above, assumptions were made about the movement of the pyrite oxidation front away from the exposed surface of the samples. Previously in Chapter 3 the development of a phosphate coating on pyrite to retard oxidation was described. The treatment was found to be unsuccessful in preventing further oxidation of crystals due to the formation of partial coatings. However, the reaction of coal hosted *in-situ* pyrite with mixture of phosphate and H_2O_2 solutions could still be used as tracer of oxidation. Main Seam Coal treatment, with phosphate alone or different combinations of phosphate and H_2O_2 solution, was performed over 5 days and 3 weeks. Here, SEM-EDAX is used to monitor the extent of reaction with phosphate with time and depth into the examined sample sections.

5.2.2.1 Methods and Materials

Blocks of Main Seam coal weighing 10g were dried at 40°C, then placed in 200mL of either 1M or 0.1M (31000 or 3100 mgL^{-1}) P solution, with duplicates prepared. No H_2O_2 was used in these treatments as the oxidant was thought to produce low pH under which Fe-phosphate would not form (Stumm and Morgan, 1990). After 5 days of reaction the coal blocks were removed and dried under air at 40°C. Dry coal blocks were split perpendicular to the cleavage plane and the exposed surface set in resin then polished and carbon coated in preparation for SEM examination.

P mgL^{-1}	H_2O_2 %
100	1
100	0.1
10	1
10	0.1

Table 5.2. Concentrations of P in phosphate solutions (mgL^{-1}) and H_2O_2 (%) solutions used in all possible combinations for treatment of coal.

A longer 3 week treatment period of coal with the phosphate and H_2O_2 solution was also carried out. Four blocks of coal weighing approximately 10 g of Main Seam coal were selected and dried in a 40°C oven. The dry coal blocks were each placed in an acid washed 1L glass beaker containing 100 mL of a phosphate solution and 100 mL of

a H_2O_2 solution. All possible combinations of 10 mgL^{-1} and 100 mgL^{-1} phosphate solution and 1% and 0.1% H_2O_2 solution were used (Table 5.2).

After three weeks of treatment coal samples were removed from the beakers and air-dried in a 40°C oven. Dried coal was split perpendicular to the cleavage plane and the exposed surface prepared for observation by SEM.

5.2.2.2   SEM investigation of phosphate treated coals - Results and Interpretation

5.2.2.2.1   Samples treated for 5 days

Coal blocks treated with differing concentrations of phosphate and hydrogen peroxide all showed varying degrees of reaction. In the samples treated with phosphate alone, any reaction is restricted to pyrite in the outer 400 μm of the sample. SEM-EDAX showed that post-oxidation mineralisation of pyrite framboid cavities was comprised of alumino-silicate, jarosite and epsomite. The alumino-silicate may have been a remnant of the clay material originally supporting the pyrite crystals within each framboid. Coals also showed reaction with phosphate in the form of the precipitation of P, Fe and K containing sulphates along fractures close to exposed edges. Main sites of pore water and ambient fluid leaching would have been macro and meso-porosity and the water-rock interface i.e. the edge of the sample. The void spaces included in these pore sizes and the outer edge of the samples were the areas in which a large volume of leaching solution was present. It is probable that the precipitation of phosphate containing salts occurred during the drying of the sample, and drainage of pore-water into macro-porosity at the base of the sample.

5.2.2.2.2   Samples treated for 3 weeks

Coal samples treated with a combination of phosphate and H_2O_2 solutions for 3 weeks showed a more advanced stage of reaction compared with coal treated for 5 days. A combination of accelerated weathering by H_2O_2 and extended treatment time led to a defined zone of pyrite removal (Figure 5.9). In samples treated with a 1% H_2O_2 solution the stripped zone extended from 3 to 10 mm into the sample with greater depths of reaction achieved for pyrite situated in cleavage. During treatment with 0.1% H_2O_2 pyrite was removed at up to 4 mm into the sample. Removal in both cases was probably a combination of dissolution and abrasive removal during polishing of the examined section. Pyrite framboids within the main body of the coal were relatively intact. However, loosening of the central portion of pyrite framboids from their clay

matrix by oxidation reactions occurred, leaving void spaces within the sample's weathered zone. Within this weathered outer zone two rims existed, one of complete pyrite removal and one of partial pyrite removal (Figure 5.9).

Treatment with 10 mgL^{-1} P solution and 1 or 0.1% H_2O_2 produced minimal reaction in the coal. Cavities remaining after pyrite removal were lined with illite, kaolinite, Fe-hydroxide and perhaps epsomite as suggested by the presence of Mg. The elemental composition, high atomic number identified by BSE imaging, and amorphous habit suggest that the lining was composed of the clay matrix which originally supported the pyrite framboid structure (Bierens de Haan, 1990). Low pH of pore water produced by pyrite oxidation in the coal kept halted the precipitation of Fe-phosphate. On removal from the leaching fluid and drying out, evaporation forced the precipitation of these minerals in areas of macro-porosity.

Treatment with a combination of 100 mgL^{-1} P and 0.1 % H_2O_2 solution provided sufficient phosphate to precipitate Fe-phosphate in association with, or as a weathering product after pyrite (Figures 5.10 and 5.11). When this concentration of P was combined with 1 % H_2O_2 solution there was little evidence of Fe-phosphate precipitation in association with pyrite. However fractures close to the sample edge contained Fe-phosphate precipitation, which as previously suggested shows where leachate typically exits from the coal matrix.
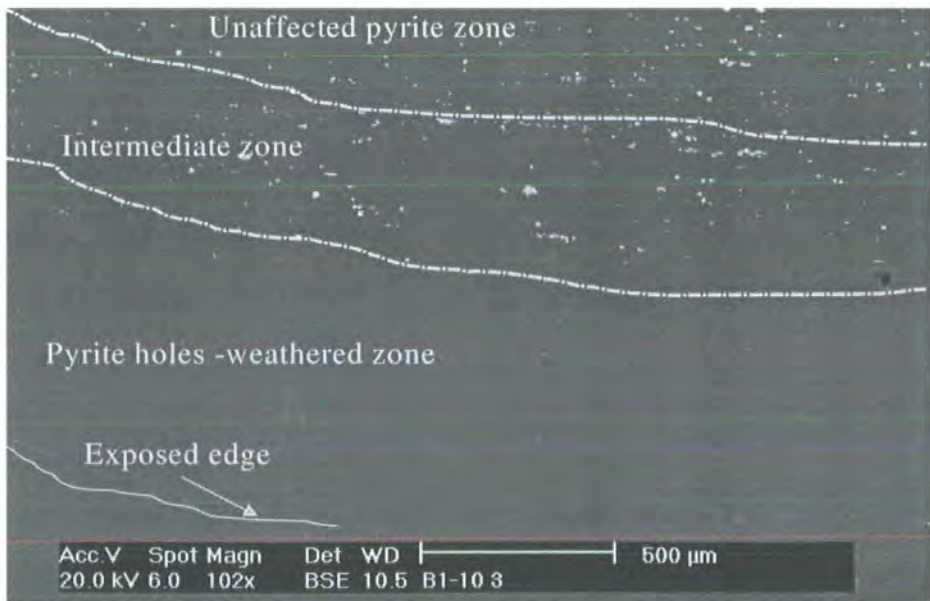
Figure 5.9. Zonation of pyrite stripping in coal treated for 3 weeks with 1% H_2O_2 and 10 mgL^{-1} P.
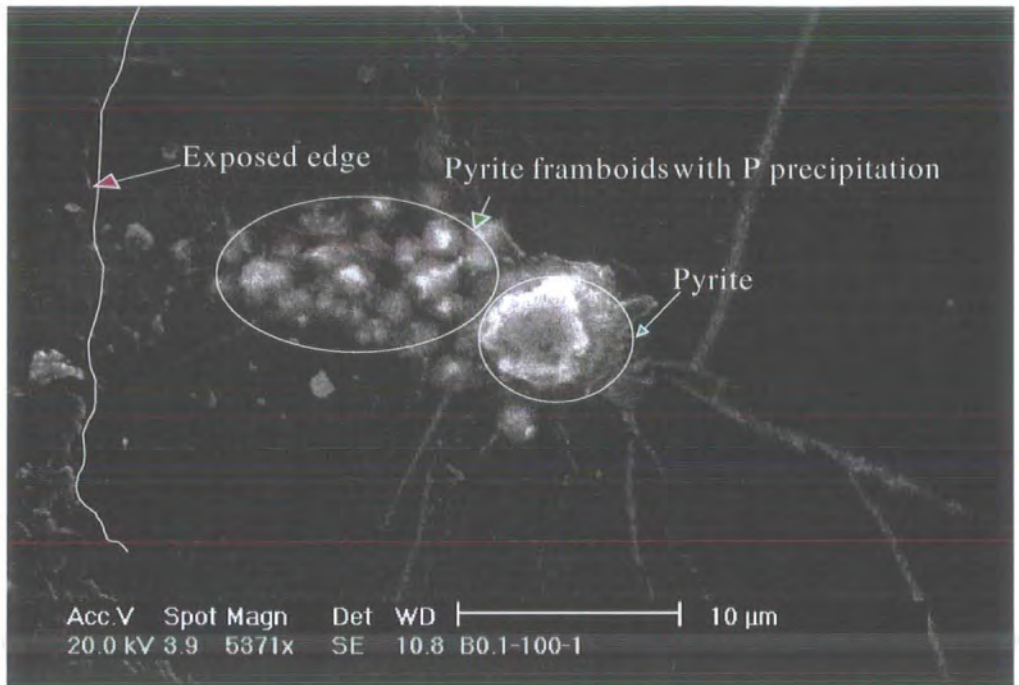
Figure 5.10. Precipitation of phosphate on pyrite framboids close to exposed edge of coal treated for 3 weeks with 0.1% H_2O_2 and 100 mgL^{-1}P.
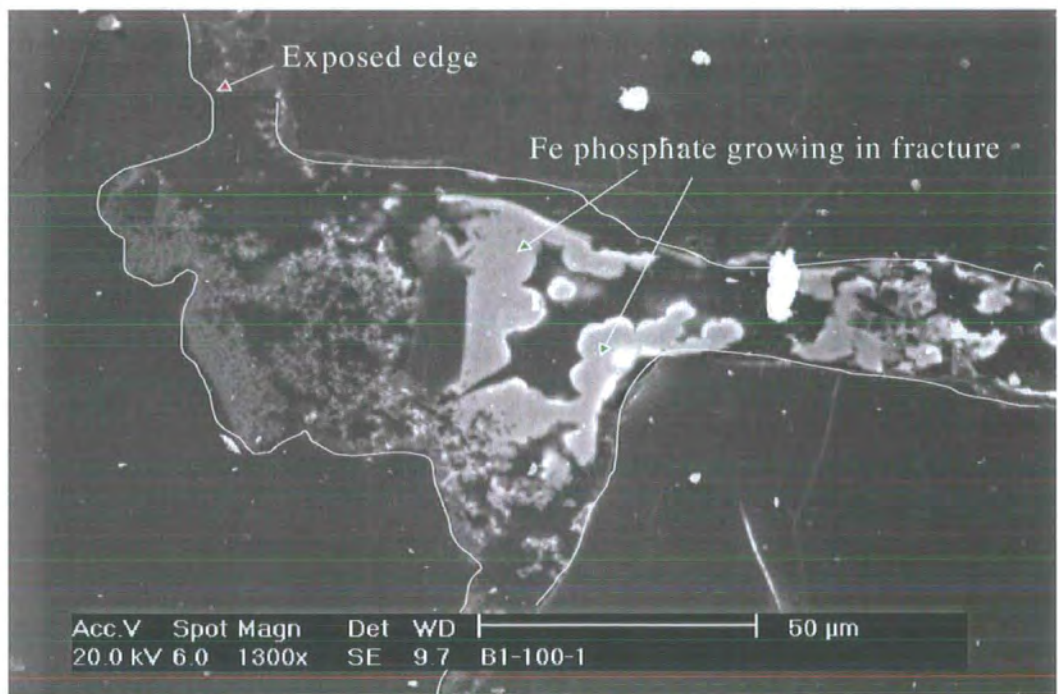
Figure 5.11. Fe-phosphate precipitation in a fracture at the exposed edge of a coal treated with 0.1% H_2O_2 and 100 mgL^{-1} P.

Increasing the period of treatment with high concentration phosphate solution, from 5 days to 3 weeks lead to a reaction with pyrite. Precipitated acidic sulphate salts, formed by coal weathering, have been shown to either surround weathered pyrite or be removed from the rock matrix through macro-porosity. Local pore water pH plays an important role in the eventual position of any precipitation.

5.2.2.3 Leaching of coal with phosphate and H_2O_2 solution - Conclusions

Investigation of the influx of a solution containing 0.1% H_2O_2 and 100 mgL^{-1} P into coal and its reaction with the *in-situ* pyrite phase provided the most informative results. Here the treated coal showed evidence of phosphate reaction with framboidal pyrite and the removal pathways of mineralised fluids through fractures. In samples where a higher H_2O_2 concentration was used reaction with pyrite was fast and lowered pH too much to precipitate Fe-phosphate. Where a relatively low 10 mgL^{-1} P solution was used, saturation with respect to phosphate was too low at the pyrite surface to promote Fe-phosphate precipitation.

5.2.3 Summary of preliminary coal leaching experiments

Comparative testing of different phosphate and H_2O_2 combinations revealed coal matrix characteristics that may limit the rate of oxidation and production of a leachate. Easier removal of products from coal cleavage and pyrite framboid clay cements both affected leachate production rates. Pyrite morphology was also an important control over oxidation rate and ultimately leachate quality. Aggressive H_2O_2 oxidation led to stripping out of the pyrite phase from the edge inwards. Long-term oxidation may follow the shrinking core model with a fringed pyrite oxidation front. Testing of the phosphate and H_2O_2 solution on coal samples demonstrated process by which pyrite framboids are oxidised from the edge of the sample inwards. Storage of secondary minerals as precipitates on the pyrite framboids or within fractures or macro-porosity close to the sample edge was also observed.

The faster rate of H_2O_2 oxidation is difficult to scale to the natural system behaviour of O_2 oxidation. Acceleration of pyrite oxidation changes the kinetics of other reactions in the coal matrix with carbonate and clay weathering, which would normally buffer the fluid chemistry, possibly being overwhelmed during H_2O_2 oxidation.

5.3   Large Scale leaching of coal waste material.

The objectives described in the introduction to this chapter were to investigate the following at the waste particle scale:

o   *In-situ* pyrite weathering and the movement of a pyrite oxidation front

©   Transport mechanisms for dissolved oxidant and pollutant at the waste particle scale

o   Weathering of coals and overburden rock-types

o   Effect on pyrite oxidation of different water-rock regimes.

To investigate *in-situ* pyrite oxidation and the movement of a pyrite oxidation front in coal and overburden rock types, for cyclic and stagnant water-rock regimes, a large scale leaching experiment was designed. Small pieces of coal and overburden rock were leached in Milli-RO water or phosphate solution. Individual pieces of rock were used rather than columns of material as this allowed more control over particle position and the retrieval of leachate. Considering the large amount of published data already available from column leaching the results of individual particle leaching may be compared to this data.

Two water-rock regimes were simulated; the first leaching with a stagnant solution and the second with cyclic wetting and drying over a weekly period. Stagnant and cyclic leaching were designed to mimic conditions in vadose and phreatic zones of rock strata. Instead of using an equilibrium speciation model, comparison of leachate chemistry with SEM-EDAX investigation was used to confirm rather than infer mineral precipitation (Blowes and Jambor, 1990).

To follow the movement of the pyrite oxidation front, samples were allocated for removal from reaction every two months over a total period 382 days of leaching. SEM-EDAX was used to identify the deepest points of pyrite oxidation relative to the edges of sections from stagnant and cyclic leached samples.

In this experiment, four coal and shale rock-types at two stages of weathering were used. Previously oxidised waste rock should provide a very different leachate composition to un-oxidised rock due to the different acidic buffering systems in each rock-type (Kerth and Wiggering, 1998). Of the four sampled seams one coals and one shale were exposed at outcrop for a year and the other coal and shale for two weeks. Unfortunately the un-weathered coal and shale had significantly less pyrite than the weathered rock-types, hampering the monitoring of any oxidation front. Therefore weathered coal and shale leachate composition was used to calculate *in-situ* pyrite oxidation and also examined by SEM.

5.3.1 Methods and materials.

5.3.1.1 Site geology and sample collection

Coal seams from the Westphalian A of the lower Northumbrian coal measures were used in large-scale static leaching experiments. Samples were collected from the Pegswood Opencast coalmine (Figure 5.12, NZ 205880) with seams chosen on the basis of time of exposure at outcrop. At the time of sampling extraction had exposed the Tilley coal and overlying Bottom Yard Parting at outcrop for a week. A further 20 m up sequence the Beaumont coal and overlying shale had been exposed at outcrop for one year (Figure 5.13).

Both coals and overlying shale partings occur at the top of the Westphalian A stage. At the point of sampling the Tilley coal was up to 60 cm thick and was overlain by a thin shale parting of up to 10 cm thickness. Massive sulphide and silicate mineralisation occurred in jointing of the Tilley coal indicating diagenetic mineralisation (Spears, 1986). Hand specimens of the Tilley coal displayed well-defined glassy vitrinite bands interspersed with duller bands on the mm scale. Previous measurements of Tilley seam total S content in the south of the Durham Basin give values between 0.69-3.37 % (Fielding, 1982).

The overlying Bottom Yard parting has a similar appearance to kaolinitic claystone bands of the Middle Tilley coals in the Durham Basin, identified by Fielding (1982). At the point of sampling the parting stood proud of the rock face and was extremely hard to break, a quality that Fielding (1982) attributed to induration with ankerite (Ca (Mg Fe)(CO_3)$_2$). In hand specimen the parting contain lenses of beige coloured clay material surrounded by a darker brown fine-grained matrix.

The Beaumont coal locally underlies the Harvey marine band, the 'marine' transgression boundary between Westphalian A and B stages by up to 25 m (Lawrence and Jackson, 1990). Lawrence and Jackson (1990) report the S content of clean Beaumont coal to be less than 3%, with a mineral content of 10%. Fielding (1982) suggests that the Harvey marine incursion was partially caused by lack of sediment supply during the end of the Westphalian. Successive drowning of land surfaces prior to the marine incursion would have increased pore water sulphate, and therefore potential sulphide content of the Beaumont seams. At outcrop Beaumont Seam pyrite weathering was evident from orange staining of rock surfaces and pooling of ochreous water. At the point of sampling the whole Beaumont coal and shale thickness was up to 1m. However the true thickness was obscured by debris from the overlying soils.
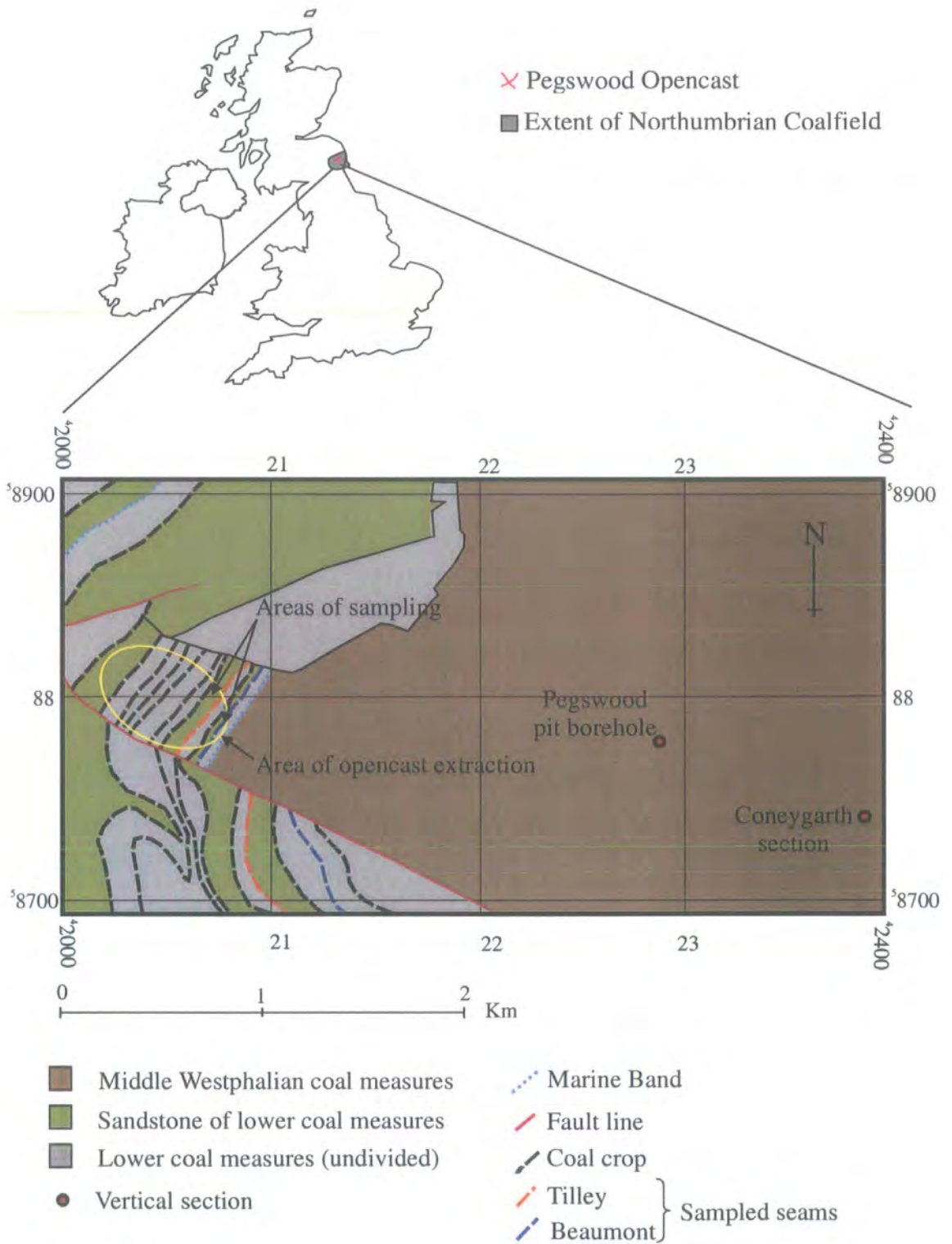
Figure 5.12. Summary of geology surrounding Pegswood Opencast, showing position of vertical sections in Figure 5.19.
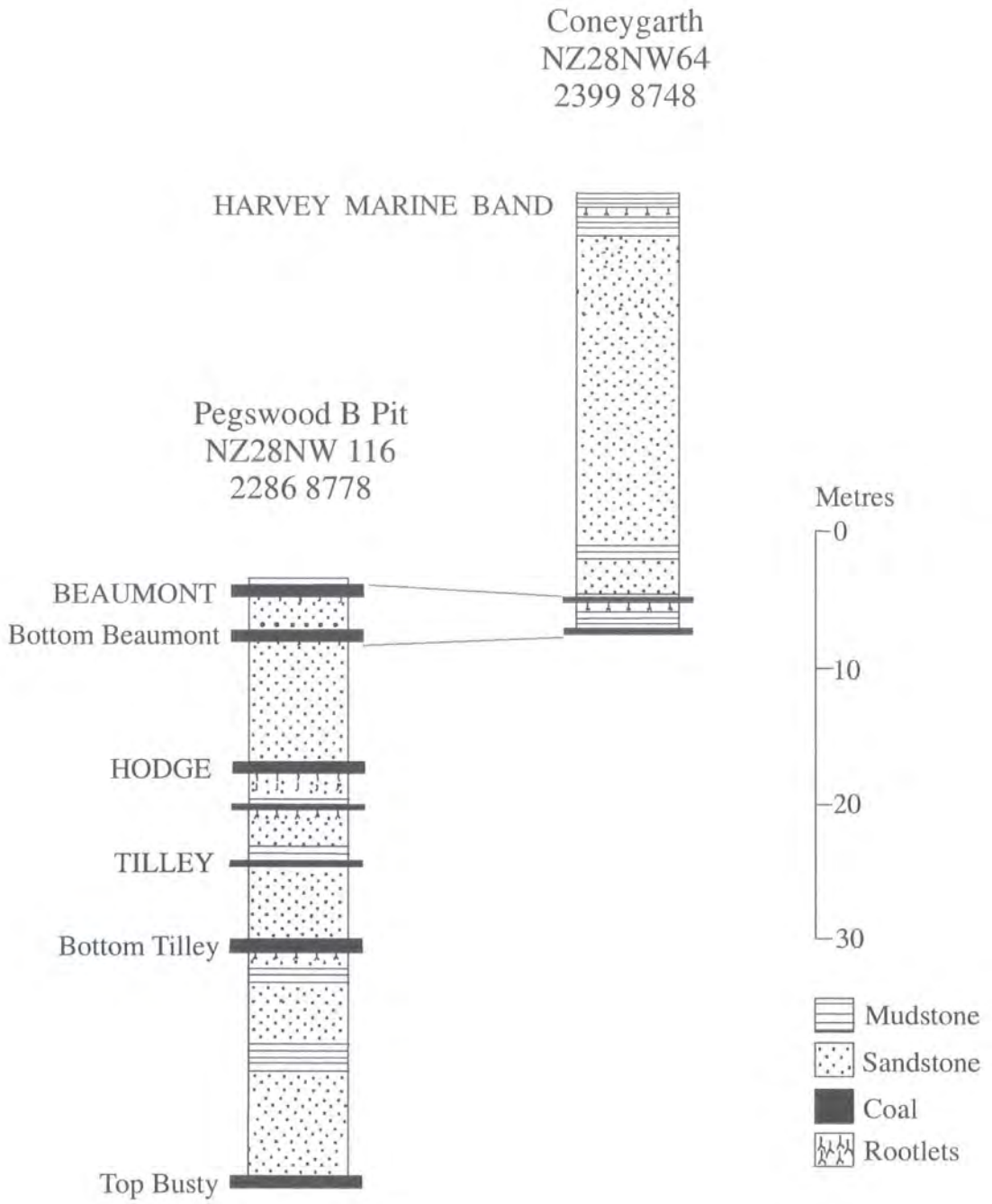
Figure 5.13. Vertical section of coal-bearing strata in the region adjacent to the Pegswood Opencast. See previous Figure for section localities. After BGS technical reportWA/90/19, Lawrence and Jackson (1990).

To avoid lengthy descriptions the Tilley coal and Bottom Yard parting are hereafter referred to as un-weathered coal or shale (UWC or UWS) and the Beaumont coal and shale as the weathered coal or shale (WC or WS).

5.3.1.2 Mineralogical and chemical analysis.

On return to the laboratory, the rock samples were washed in tap water to remove surficial mud, and dried in an oven at 105°C to remove pore water in an attempt to halt further oxidation reactions during sample preparation.

A sample of each rock type was crushed and powdered for X-Ray Diffraction (XRD) analysis. A Hilton-Brooks D2G x-ray generator equipped with a Phillips Goniometer was used to measure 2θ of 5-80°, at a scan speed of 0.02° s^{-1} and a step size of 0.04°. Three sub-samples of each rock type sample were ashed at 900°C to remove the organic phase in preparation for X-Ray Fluorescence (XRF) analysis. Loss on ignition (LOI) was recorded and used to assess mineral content. The resultant ash was fused with a barium silicate flux to form a glass disc. The glass was analysed by an XRF Automated Philips PW2404 spectrometer with a lowest detection limit of 1ppm, for major element abundance.

A method modified after Sobek (1978) was used to analyse the chemistry of the acid leachable and oxidizable extracts of each rock-type (Appendix I Methods). Where possible the same samples analysed by XRF were used for extraction. Both acid leached and oxidizable phase filtrates were analysed for major element content by ICP-OES (Appendix I Methods). Three samples of each rock type were set in polished resin blocks and examined by SEM to determine matrix pattern and general mineral phase distribution.

5.3.1.3 Experimental Design

Collected rock was cut into blocks approximately 3 x 2 x 2 cm using a Junior Clipper masonry saw with water coolant. Once cut, the blocks were rinsed in tap water and dried at 105°C. The blocks mass and dimensions were recorded for later calculation of relative leaching rates between samples.

Four treatments were carried out on each rock type: static leaching in Milli-RO water; alternate weekly cyclic leaching in Milli-RO water and air drying; static leaching in a low concentration (100 mgL^{-1}) phosphate solution; alternate weekly leaching in a low concentration (100 mgL^{-1}) phosphate solution and air drying. Whole rock and rock partially set in epoxy-resin, with the exposed surface perpendicular to the sample

cleavage, was leached. Coated samples were used to decrease edge effects that may obscure the pyrite oxidation front. The leachate chemistry from these 'cleavage edge' samples is also compared to similarly prepared samples, leached with flowing water (Chapter 6).

	Sample type			
Leachate	**Whole sample**		**Cleavage Edge**	
Milli-RO water	Cyclic leaching	Stagnant leaching	Cyclic leaching	Stagnant leaching
Phosphate Solution	Cyclic leaching	Stagnant leaching	Cyclic leaching	Stagnant leaching

Table 5.3. Experimental design for large-scale leaching. 18 samples of each rock type were treated in each combination i.e. cyclic leaching with phosphate solution of the sample cleavage edge as shown by the shaded text.

18 blocks of each rock type underwent each treatment described in Table 5.3. The blocks were placed in polypropylene beakers were covered with 70mL Milli-RO water or 100 mgL^{-1} P solution and the beaker covered with clear PVC film and aluminium foil to minimise contamination and light. At 2, 4, 6, 8, 10 and 12 months (or 2 and 4 months for P treatment) three samples from each treatment were removed from solution. Remaining leachate was acidified with concentrated HNO_3, then analysed for major element chemistry by ICP-OES (Appendix I Methods). A Hanna portable meter was used to measure pH and temperature of the solution prior to acidification. Both meters were calibrated before use using commercially available buffer solutions at pH 4 and 7. Any pH value measured outside of these limits may be in error.

One of the three removed replicates was chosen for examination using SEM. Chosen samples were allowed to dry in air, coated in epoxy-resin, split through the centre and the cut surface polished and carbon coated for SEM examination.

For all Milli-RO water stagnantly-leached samples, evaporation after the third sampling at 205 days led to some samples becoming semi-submerged. Therefore 60 mL of Milli-RO water was added to all remaining beakers. The addition of extra Milli-RO water is considered in the description and discussion of stagnant sample leachate evolution and weathering profile.

5.3.2   Analytical Results and Interpretation

Analysis of physical and chemical characteristic for all rock-types is described in the following sub-sections. A summary of the characteristics for each rock-type is also provided in Table 5.7. at the end of this section, for quick reference.

5.3.2.1   Mineralogy

The organic phase in the powdered samples was not removed for XRD analysis as it represented a large proportion of all rock types. Consequently a large 'hump' present between $2°$ to $30°$ of 2θ was assumed to contain diffraction peaks from organic macerels (Figures 5.A. – 5.D., Appendix II Results).

All rock types analysed by XRD contained kaolinite, illite, quartz and pyrite (Table 5.4, Figures 5.A. to 5.D., Appendix II Results). Only the un-weathered rock-types contained albite, apatite and siderite whereas only the weathered rock types contained goethite, Ti-oxide, barite and alunite. Jarosite was identified in the UWC, WS and WC. However the WS had the most varied secondary weathering mineral phase with lepidocrocite, melanterite, rozenite and goethite all identified by XRD. The WC also contained a wide range of prior pyrite oxidation products including alunite, goethite and coquimbite. Both coals contained calcite and gypsum, whilst the UWS and WC contained dolomite.

5.3.2.1.1   Mineral Content

Inorganic mineral wt % was calculated from LOI data (Table 5.5). As the mineral fraction looses some mass during ashing due to volatile species such as H_2O, S and CO_2 the mineral wt % slightly under-estimates the actual content. UWS had the highest mineral content at 77.8 wt % $\pm$ 0.1, the WS contained 4.9 wt % $\pm$ 0.3. The WC and UWC had inorganic mineral contents of 3.8 wt % $\pm$ 0.4 and 3.5 wt % $\pm$ 0.4 respectively.

Two-way nested ANOVA was performed on the inorganic mineral contents of all rock types. Differences between rock type mineral content explained most of the variance. However a significant proportion of variance in mineral content between all samples was explained by within rock-type mineral variance. Consequently, within sample mineral content variance will cause relatively small deviations from the mean in the bulk chemistry of replicate samples. However this should not obscure differences between weathering of the rock types.

5.3.2.1.2 SEM investigation of rock-types

In order to monitor experimental weathering of coal-bearing strata each of rock type was assessed by transmitted light microscope (UWS), SEM and SEM-EDAX.

Un-weathered shale - UWS (Bottom Yard Parting)

The un-weathered shale contained pale buff coloured angular to rounded clasts of kaolinite associated with Ti and Fe. Clast layers are inter-layered in places with darker silt material containing Fe-sulphate. A fine-grained dark brown matrix was made up of kaolinite and organic matter and supported clasts up to 0.3 mm in diameter. In isolated areas the rock became clast supported. Small amounts of framboidal pyrite existed within darker organic material with typical diameter < 10 μm. Apatite was also found within the organic areas. Fielding (1982) identified the presence of this phosphate mineral in the kaolinitic claystones of the Tilley coal seam within the Durham Basin. However unlike the Durham kaolinitic claystones no evidence of ankerite formation was observed.

Un-weathered coal - UWC (Tilley coal)

In hand specimen the un-weathered coal showed extensive sulphide and silicate cleat mineralisation probably formed during late burial diagensis (Spears, 1987). Layers of featureless vitrinitic material and semi-fusinite or fusinite formed defined bands in the coal. Microscopic fractures are filled with crystalline alumino-silicate and sulphate and in places original pyrite framboid features are replaced by gypsum. Elsewhere kaolinite, Fe-sulphate and possibly ankerite fill framboid 'holes'. Replacement by gypsum and Fe-sulphate of the pyrite framboid phase which formed prior to peat diagenesis suggests that oxidation of this phase has already occurred. Oxidation of the original peat may have occurred during periods of low water table i.e. during dry seasons (Spears, 1987). The replacement of pyrite framboids with gypsum and Fe-sulphate therefore probably occurred during pre-burial processes. Later compaction removed Fe and sulphate rich pore water, which precipitated within the cleat jointing during burial diagenesis.

Weathered shale - WS (Beaumont shale)

The weathered shale consisted of fusinite and semi-fusinite layers interbedded with 100 μm thick clays containing angular quartz, suggesting periodic sediment input to the original peat. Flayser bedding and slumping in the clay layers indicates a low energy

environment. Macerel structures were locally replaced with alumino-silicate and in places, pyrite infilled void spaces.

Usually pyrite was mainly associated with kaolinite, illite and quartz rich bands which ran parallel to cleavage direction (Figure 5.14 and 5.15). Framboidal pyrite was generally close to 30 μm in diameter and typically isolated (Figure 5.16). A more consolidated form of pyrite also occurred, with earlier framboid forms visible within these structures (Figure 5.17). Kortenski and Kostova (1996) report similar overgrowths of pyrite on former framboids suggesting stages in inorganic pyrite formation within pre-cursor peat. Late stage diagenetic massive pyrite was also present in-filling veins and rootlets (Figure 5.18). Pyrite oxidation was evident with voids in clay material formed by prior oxidation containing quartz, sulphate and more rarely alunite and gypsum. Alunite replaced some areas of clay suggesting that silicate buffering of the pyrite oxidation reaction had previously occurred. Accessory minerals include apatite and Ti-oxide both associated with quartz rich sediment bands. The presence of Ti-oxide is indicative of detrital sediment input to the precursor peat of the weathered shale.

Weathered coal WC (Beaumont coal)

The weathered coal was similar to the overlying weathered shale described above in that fusinite and semi-fusinite layers made up the organic fraction of the rock. Pyrite was associated with clay and quartz bands although the proportion of inorganic minerals in the coal was lower than in the shale. Up to 5% of sediment bands were associated with of pyrite framboids, suggesting detrital Fe within clays was a primary source for pyrite formation. Crystalline pyrite was also found in a WC sample (Figure 5.19). Little weathering of massive and consolidated framboidal pyrite was evident although isolated framboidal pyrite was weathered in parts.

5.3.2.2 Bulk Chemistry

5.3.2.2.1 XRF

Comparison of element wt % derived from combined sequential extracts and from XRF analysis indicates the lower value for most elements from XRF totals (Table 5.D., Appendix II Results). However, most differences can be accommodated within the error margin given of 1σ.

During ashing of samples at 900°C the volatilisation of H_2O from clays, CO_2 from calcite and S from sulphides and sulphate were expected. Therefore, over-estimation of the LOI value for each sample resulted from volatile loss during ashing. Calculation of the elemental wt % of a rock type from the oxide wt % provided by XRF analysis of ash will therefore be less than the actual value. A correction for this effect can be made using the Parr Formula (WVGES, 2001), where

$$\text{Mass of mineral matter} = 1.08\ A + 0.55\ S \qquad (5.1)$$

with A the wt % ash and S the total wt % S. However total S analysis was not performed during sample analysis and so this correction was not carried out. However, it is obvious that an increase in a calculated ash wt % would occur if the Parr Formula was applied.

Detection limits for the analytical techniques used (1ppm for XRF, 1ppb for ICP-OES) are higher than the elemental wt % of Mn, Na and Mg calculated from oxide wt % (Table 5.D., Appendix II Results). Apparent differences in XRF and ICP-OES acid leachable and organic phase elemental wt % values can be explained by LOI inaccuracy and elemental concentrations lower than detection limits of the analytical method.

The measurement of Al, Fe and Si by ICP-OES and XRF usually agreed well (Figures 5.20). However, both WC and WS had higher total Fe of 5 ± 7 wt % and 6 ± 4 wt % in combined sequential extracts. The large volume of WS required to provide sufficient ash for analysis meant that a different sample was used for sequential extracts. Given the significant variance in mineral content shown in section 5.3.2.1.1, this would have led to differences in mineral content between samples used for XRF and sequential extracts. The oxidizable extract provided most of the WS and WC Fe, indicating that variation in pyrite content probably accounted for most of the difference in total Fe content (Table 5.6).

5.3.2.2.2 Sequential Extracts

The major element content of sequential acid and oxidizable extracts is summarised in Table 5.E (Appendix III Results). The UWS released high concentrations of Al and Si on acid and oxidation leaching, probably from kaolinite dissolution (Figure5.21). The weathered rock types released high S and Fe during oxidation leaching. The UWS and WS relatively high release of S can be attributed to gypsum dissolution and pyrite
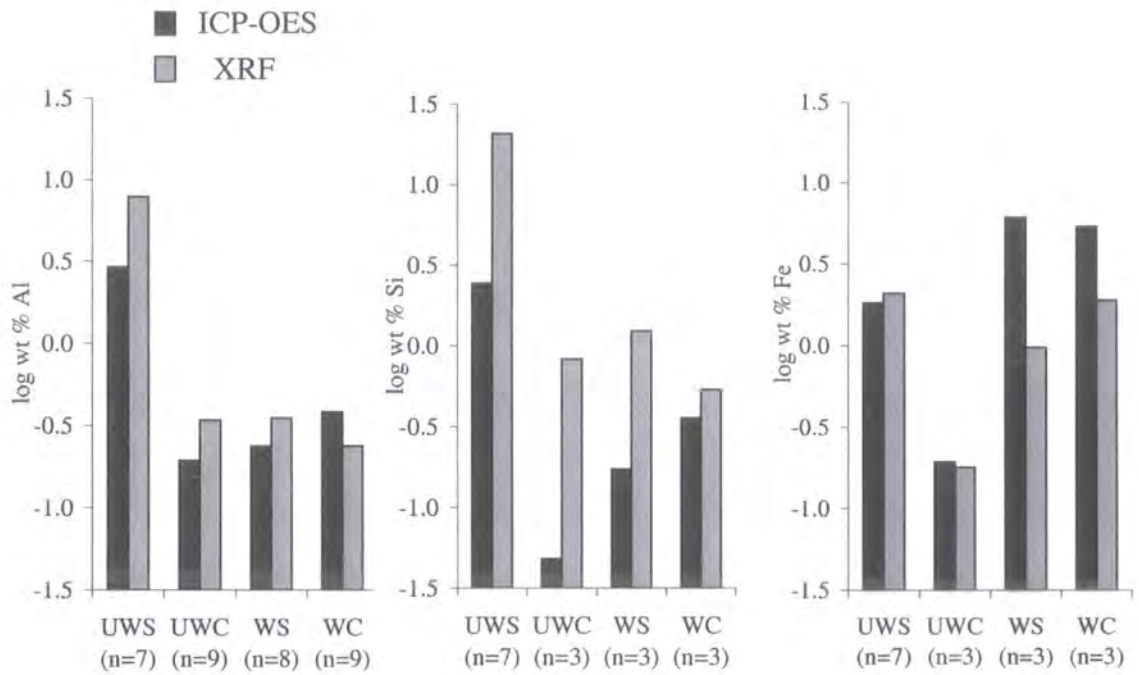
Figure 5.20. Histogram of log cumulative wt % Al, Si and Fe from acid leachable and oxidizable phase extracts analysed by ICP-OES and total wt 5 from XRF. Errors shown are 1 σ, n is shown with rock type.
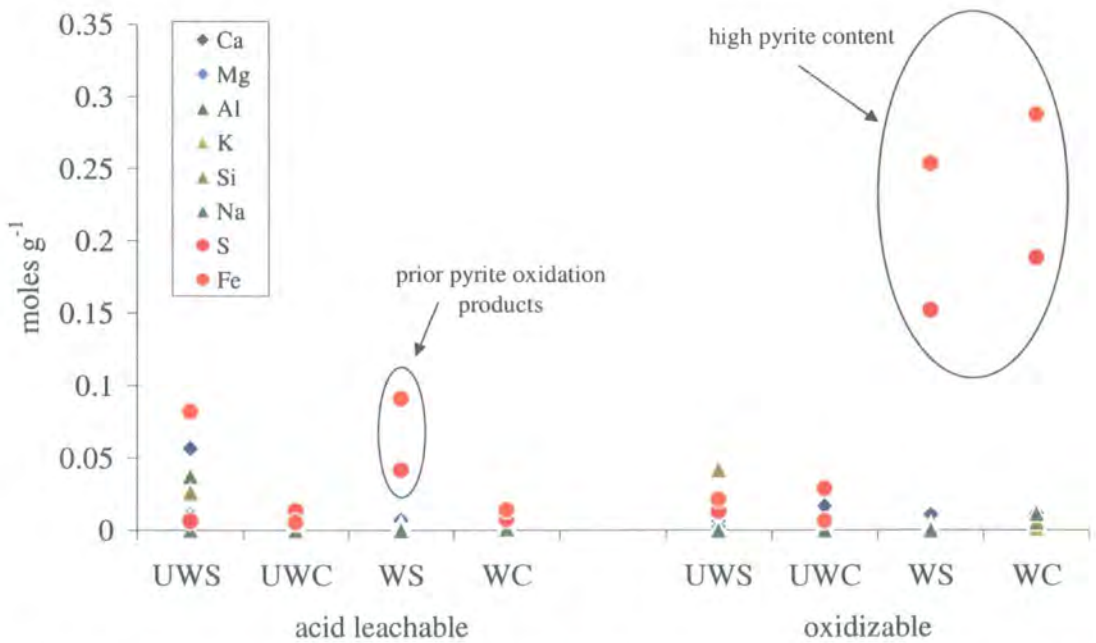
Figure 5.21. Summary graph of acid and oxidizable extracts chemistry, given in moles per g of original sample. High Fe and S in the acid leachable and oxidizable phases represents high pyrite content and prior pyrite oxidation products in the WS and WC.

weathering respectively. High release of carbonate related elements Mg and Ca was evident in acid leaching of the UWS.

Extraction of the oxidizable phase of coal and associated overburden was primarily performed to estimate the pyrite content of each rock types. Sulphate content of the oxidizable phase was assumed derived from pyrite oxidation and used to stoichiometrically calculate the original pyrite wt % (Table 5.6). Oxidation of the rock powder may have also reacted with some of the S bearing organic phase of the rock, leading to overestimates of actual pyrite content. However calculated values are similar to estimates made during SEM examination of samples.

	UWS	**UWC**	**WS**	**WC**
Pyrite wt %	0.7 ± 0.2	1.7 ± 0.6	9 ± 5	11 ± 10

Table 5.6. Pyrite wt % calculated from S content of oxidizable extract, errors shown are 1σ, n = 4.

5.3.2.3 Summary of rock-type characteristics

Physical and chemical characteristics of the four collected rock types as described in Chapters 4 and 5 are tabulated below (Table 5.7).

UWS

Mineralogy	Kaolinite, Quartz, Gypsum, Anhydrite, Albite, Calcite, Apatite, Pyrite, Illite, Siderite, Dolomite
Acid leachable phase	Mostly Al, Ca, Fe and Si
Oxidizable phase	Mostly Al and Si
SEM-investigation	Rounded kaolinite clasts surrounded by finer kaolinite / Fe-sulphate matrix with pyrite and apatite.
Physical characteristics	High porosity, with PSD evenly distributed between macro, meso and micro-porosity.

UWC

Mineralogy	Kaolinite, Gypsum, Albite, Jarosite, Calcite, Apatite, Pyrite, Dolomite.
Acid leachable phase	Mostly Al, Ca, and P
Oxidizable phase	P, S, Fe, Ca and Al
SEM-investigation	Pyrite phase is rare, most framboids are replaced by gypsum, with vein mineralisation the main pyrite morphology.
Physical characteristics	High porosity, with high proportion of micro-porosity

WS

Mineralogy	Kaolinite, Illite, Quartz, Goethite, Melanterite, Lepidocrocite, Jarosite, Gypsum, Alunite, Rozenite, Barites, Ti-oxide, Fe-Mn-oxide, Mg-sulphate.
Acid Leachable phase	>1 wt % Fe and S, <1 wt % Al and Ca
Oxidizable phase	>1 wt % Fe and S, <1 wt % Ca, Al, P and Si.
SEM investigation	Massive, framboidal and consolidated pyrite are all represented, however small framboids were oxidised and replaced by gypsum or alunite.
Physical characteristics	High porosity with a large proportion of micro-porosity, yet more meso and macro-porosity than in coals

WC

Mineralogy	Kaolinite, Illite, Gypsum, Albite, Calcite, Barite, Apatite Pyrite, Ti-oxide, Goethite, Coquimbite, Jarosite and Alunite
Acid Leachable phase	Less than 1 wt % of Fe, Al, Ca, S and Si
Oxidizable phase	High Fe, S and P, lower Al, Ca, Na, Zn and Si
SEM investigation	Pyrite morphology and content similar to WS (above), and was mainly associated with sedimentary mineral bands. Pyrite framboids were oxidised, however consolidated framboids were not obviously affected.
Physical characteristics	High porosity, with high proportion of micro-porosity

Table 5.7. (continued) Summaries of rock characteristics as described in the previous section. Assumed physical characteristics are based on porosimetry of varied rock-types in Chapter 4.

5.3.3 Experimental Results and Interpretation

The following section is divided into two parts; the first describes the changing leachate chemistry of cyclically and stagnantly leached samples, and the second with the chronological SEM investigation of the same samples. A discussion of the results of both chemical leachate and SEM investigations follows.

5.3.3.1 Leachate Chemistry

Analysed major element leachate chemistry was blank corrected and corrected for original sample mass to give a molar concentration per unit mass of sample ($molL^{-1}g^{-1}$). Mean leachate content from cyclically (n=4) and stagnantly (n=3) leached samples is summarised here for sulphide and carbonate constituents Fe, S and Ca. These analytes

120

were most commonly released at relatively high concentrations. A more detailed description of leachate major element chemistry is presented in Appendix II Results (Tables 5.F-5.U).

5.3.3.2   Summary of chemical evolution produced by cyclic leaching

In general cyclic leaching released maximum elemental concentrations within the initial 58 days (Figure 5.22). After 100 days of cyclic leaching the release of dissolved matter either fell below detection or continued at a much slower rate. Of the major elements analysed for, Fe, S and Ca were released in the greatest magnitude. For the UWS and UWC, high Ca and S release was attributed to gypsum, calcite and dolomite dissolution. In the WS and WC the concurrent release of Fe suggested that pyrite oxidation products were being dissolved. Some evidence of jarosite formation in the later stages of leaching was suggested by elevated Na and K release from the WS and WC (Chapter 5 Results, Appendix II).

Leachate pH

Weathered rock-type leachate tended to have pH between 3 and 4, which decreased between days 183 and 205 to below 2 (Figure 5.23). Rapid pyrite oxidation by Fe^{3+} and the precipitation of jarosite during dry periods lead to the rapid fall in Milli-RO water pH (typically 5.7) on contact with the weathered rock types. Un-weathered rock type pH remained above 5 throughout leaching, although both showed a decreasing trend with time. Leachate pH ranges suggest buffering by the clay and pyrite phases in the weathered rock types. Acidity produced by pyrite oxidation in the un-weathered rock types was buffered by the dissolution of dolomite and calcite. The lack of dissolved Fe leached from UWS and UWC was caused by precipitation of Fe-hydroxides at the range of pH for un-weathered rock type leachate.

Cleavage edge leaching

In the cyclic leachate of rock sample cleavage edge, the same pattern of chemical evolution for un-weathered and weathered rock types was observed. However, the effects of pore size distribution in coals and shale, and restriction of fluid circulation to one plane in cleavage samples, caused the differences between total fluxes (Figure 5.24). Cyclic increases and decreases in pyrite oxidation product dissolution and pH were observed in both whole and cleavage edge samples. Such pulses were more common in the cleavage edge samples of weathered rock types where little buffering capacity, in the form of carbonate minerals, existed. The time lag between the release
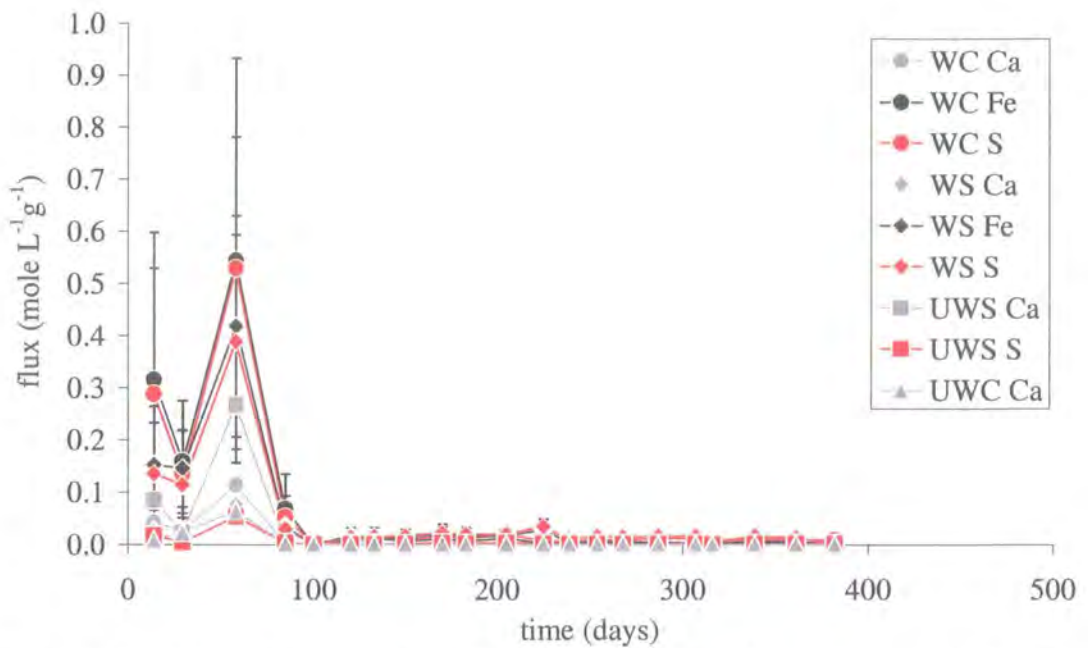
Figure 5.22. Summary graph of cyclic leachate S, Fe and Ca molar concentration, per
L of solution, per g of sample, over the period of leaching. Ca, Fe and S
concentrations were the highest dissolved species for all rock-types.
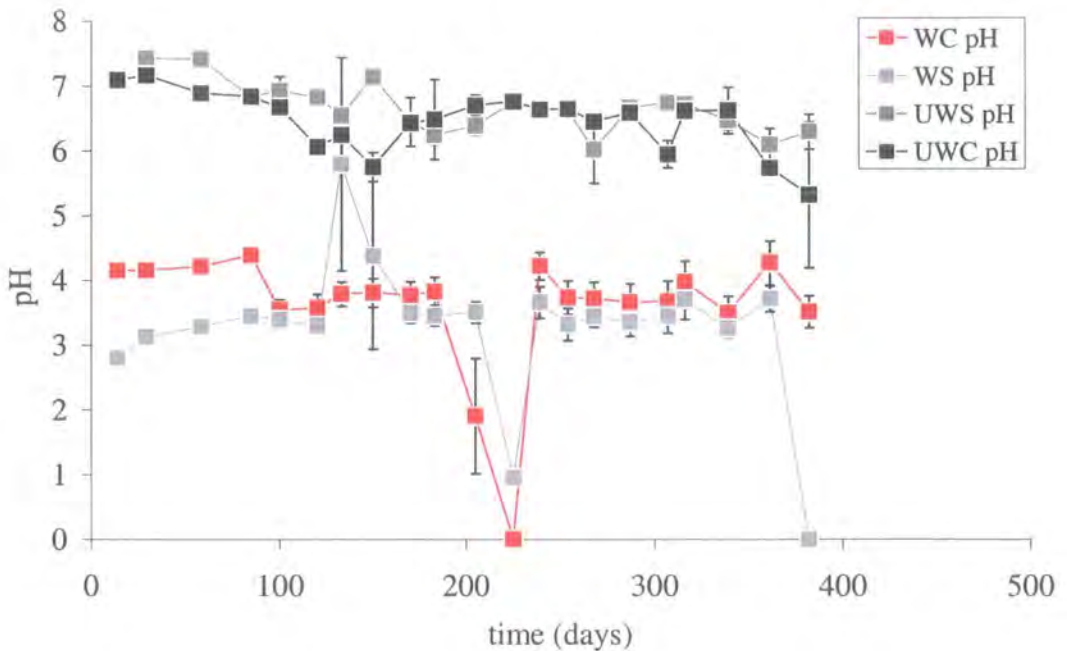
Figure 5.23. Leachate pH for whole rock-type samples over the period of cyclic
leaching. Errors shown are 1σ, n=4.

of acid product from pyrite oxidation and subsequent buffering reactions was thought to cause this pattern of chemical output.

5.3.3.3   Stagnant leaching of coal-bearing strata

It was expected that during stagnant leaching, leachate content would initially increase, reaching a plateau once the solution and rock were at equilibrium with respect to dissolution. Evaporation necessitated the topping up with Milli-RO water, between days 200 to 300, of leachate solutions leading to dilution and pH increase.

Although the UWS and UWC leachate chemistry reached the expected plateau, topping up with Milli-RO water appeared to increase pyrite oxidation due to fresh dissolved O_2, whilst encouraging precipitation due to pH changes (Figure 5.25). Both rock-types released Ca and S suggesting the dissolution of gypsum or a carbonate phase initiated by pyrite oxidation.

The weathered rock-types released high levels of Fe and S suggesting that pyrite oxidation products were being dissolved (Figure 5.26). Alunite and jarosite dissolution from the stagnantly leached WC was suggested by the release of Al and Na (Tables 5R to 5U, Appendix II Results). Contrary to the un-weathered rock-types, addition of fresh Milli-RO water to counteract evaporation led to dilution of Fe and S rather than an increase.

Leachate pH

For the different buffering systems present during leaching of weathered and un-weathered rock types, the influx of dilute, neutral pH, leaching solution changes leachate chemistry in a different manner. Where pH values for pore-water and Milli-RO water were similar introducing fresh Milli-RO water generally increased dissolved O_2 concentration, previously depleted by pyrite oxidation (Figure 5.27). In weathered rock types pore water pH was very low in comparison to Milli-RO water and the dominant oxidant was Fe^{3+}. The addition of Milli-RO water of higher pH probably led to a large amount of precipitation of pore water dissolved content, mainly within the outer pore space of the sample. Dilution and precipitation of dissolved Fe^{3+} also reduced the rate of pyrite oxidation substantially. Oxidation by dissolved O_2 from Milli-RO water probably increased. Dissolution of minerals such as jarosite, precipitated during evaporation of leachate, led to the sharp decrease in pH by the release of Fe^{3+} and H^+ on addition of Milli-RO water.
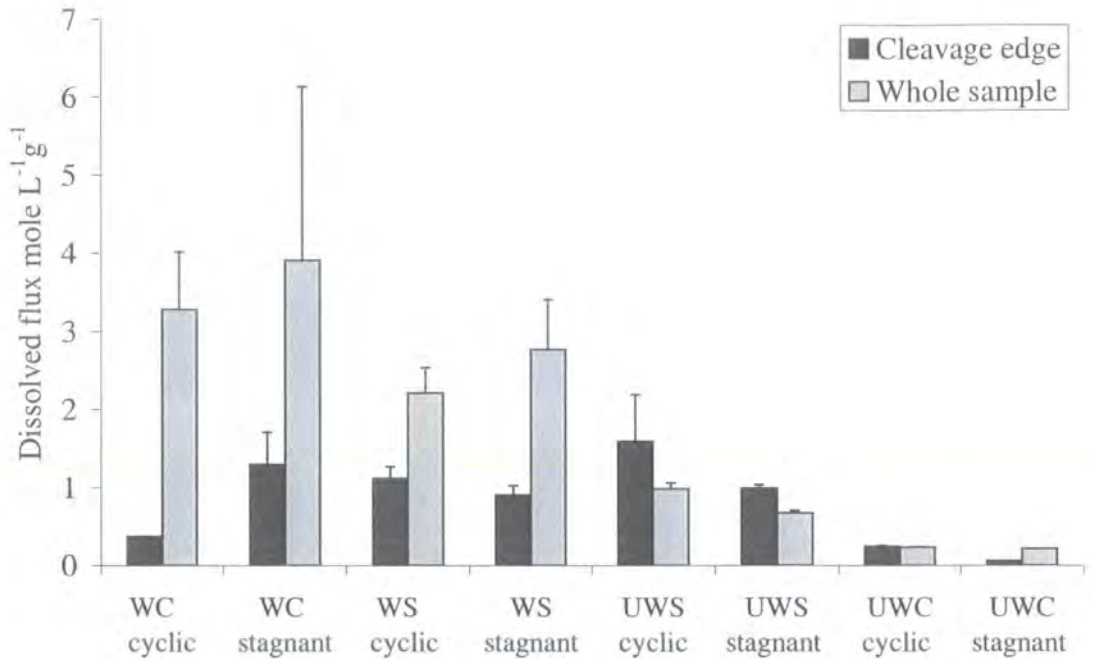
Figure 5.24. Total and peak dissolved flux (mole $L^{-1}g^{-1}$) for each rock-type under cyclic and stagnant leaching respectively of whole and cleavage edge samples. Values shown are the cumulative total or peak flux of all elements analysed for. Errors shown are propagated from the original individual measurement errors.
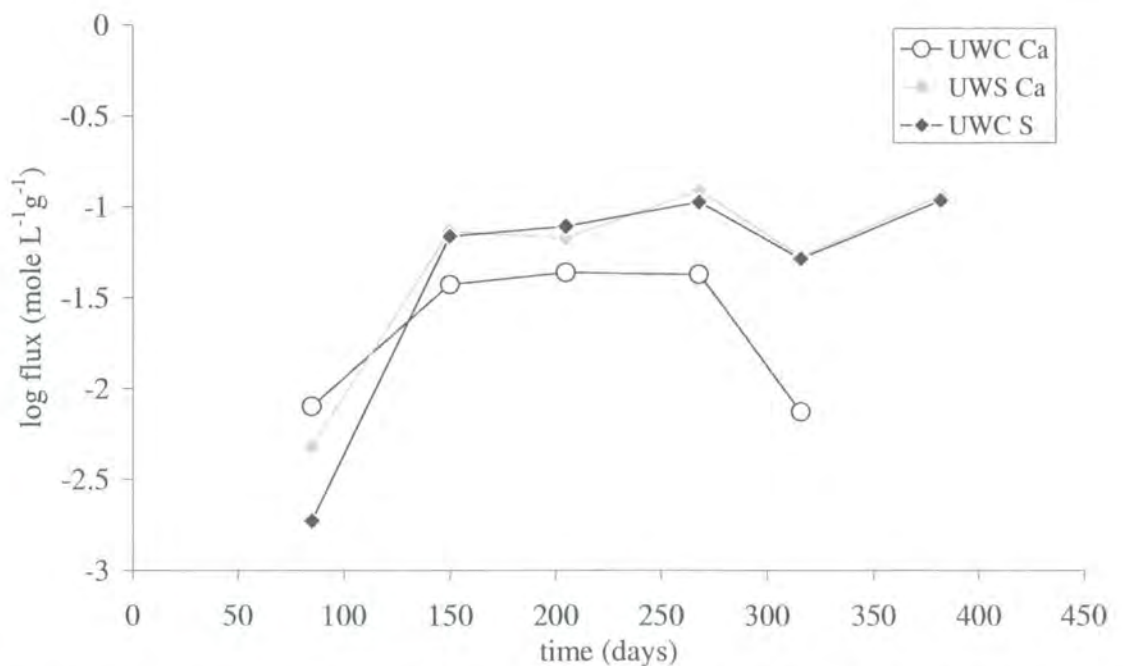
Figure 5.25. Log stagnant leachate concentrations of Ca and S from the whole unweathered rock-type samples, showing expected plateau in concentration. Correlation of Ca and S flux from the UWS suggests that gypsum dissolution dominated the leachate chemistry.
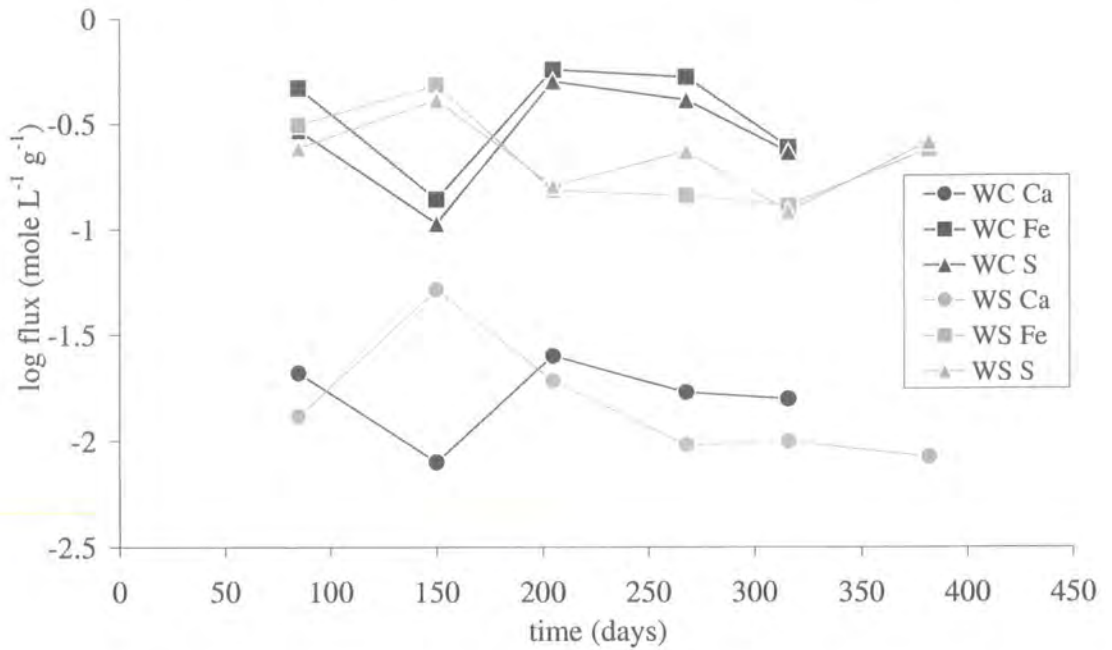
Figure 5.26. Log stagnant leachate molar concentration of Ca, Fe and S from whole weathered rock-type samples over the period of leaching. The flux of the analytes was the greatest of all major elements analysed for. Correlation of Fe, S and Ca flux suggests that the dissolution of pyrite oxidation of pyrite oxidation products dominated leachate chemistry.
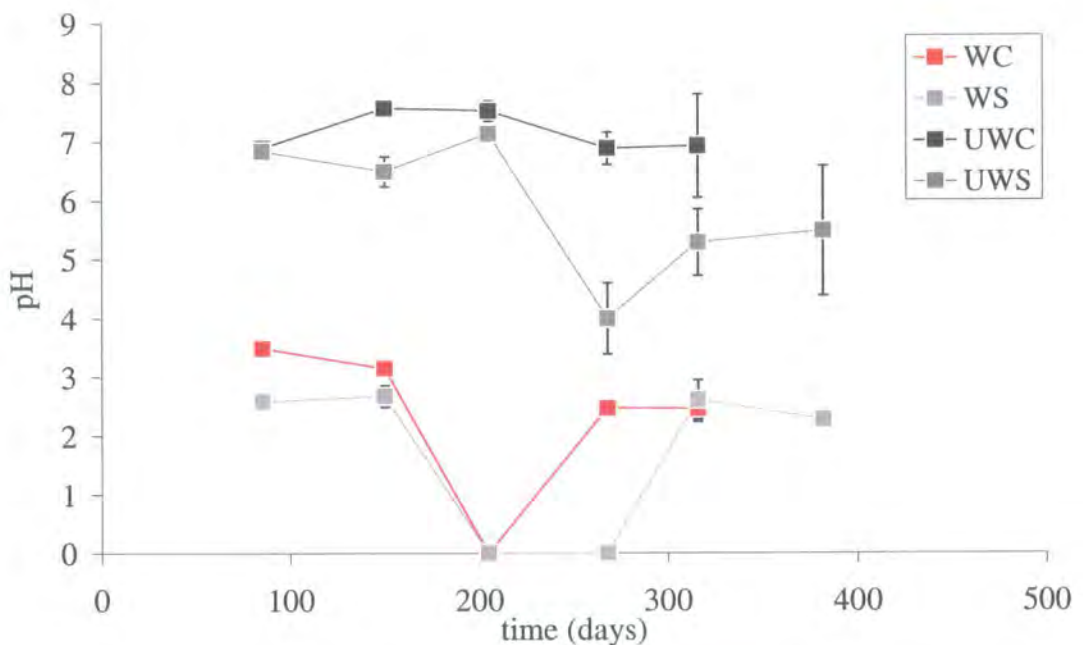
Figure 5.27. Leachate pH after stagnant leaching of whole rock-type samples. Errors shown are 1σ, n=3.

Leaching the cleavage edge

Cleavage edge leaching of the UWS and UWC produced leachate that behaved as expected, increasing to a plateau then decreasing on addition of Milli-RO water to counteract evaporation. For the UWC subsequent increased pyrite oxidation led to a rise in dissolved S, Ca and Mg towards the end of leaching. For cleavage edge leaching of both the WS and WC, a similar plateau of concentration, not observed in leaching of whole samples, were followed by lowered solution content (Appendix II Results). Dilution by addition of Milli-RO water in the later stages of leaching and precipitation of minerals on increased pH both contributed to the pattern of leachate evolution.

Lower total dissolved flux was expected from the cleavage edge samples compared to whole samples, due to the smaller exposed surface area of the former. For the UWC, WS and WC where pyrite oxidation was thought to be the main source of dissolved material, total flux was lower from cleavage edge leaching. However, the UWS total flux, where gypsum dissolution was assumed to be the main source of dissolved material, was close for both types of samples (Figure 5.24). This suggests that the cleavage plane supplies most of the dissolved material, whilst restriction of oxidant influx to one cleavage plane reduces the rate of pyrite oxidation.

5.3.4 SEM-EDAX Investigation of the pyrite oxidation front

WS and WC samples removed from cyclic and stagnant leaching with Milli-RO water and 100 mgL^{-1} phosphate solution at consecutive 2-month stages is described here. The WS and WC were examined as both had an easily identifiable pyrite phase. As some examined sections did not contain enough pyrite to determine weathering front position the extent of particle weathering is described where possible.

5.3.4.1 SEM Investigation of leached WS samples

5.3.4.1.1 Cyclic Leaching of whole samples with Milli-RO water

Cyclical leaching of the WS for 85 days produced little difference from the original sections (section 5.3.2.1.2), with most reaction restricted to outer 100 μm of samples. Fe-oxide filled fractures and coating pyrite within this zone (Figure 5.28), yet where pyrite was associated with kaolinite no oxidation was observed.

After 150 days pyrite framboids were oxidised at 2 mm into the sample, with significantly less oxidation of consolidated framboids. Small framboids (< 10 μm) were
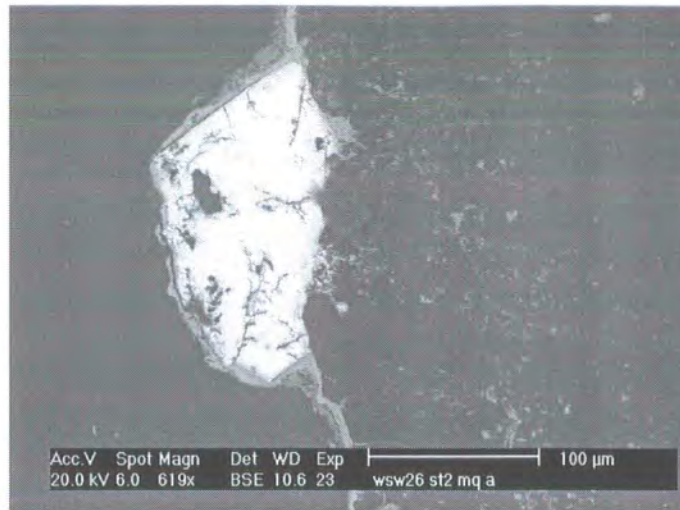
Figure 5.28. Fe-hydroxide coating on massive pyrite at edge of WS, after 85 days of stagnant leaching.
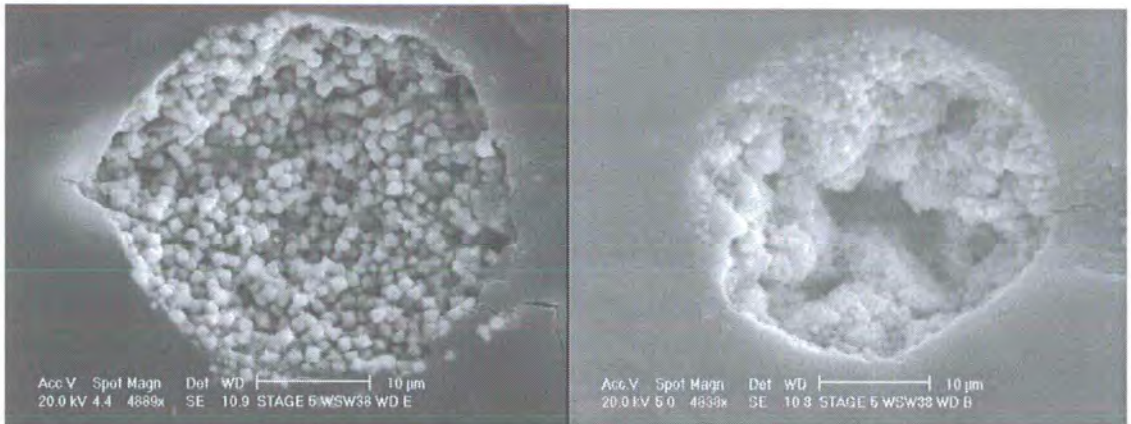
Figure 5.29. Pyrite framboids in a cyclically leached WS samples after 316 days. Framboid on right was situated at 500 µm from the exposed edge and was covered in amorphous Fe-sulphate, with alumino-silicate still present. The framboid on the left was situated at 7 mm into the sample and collected spectra show slight elevation of the O K$^\alpha$ peak.
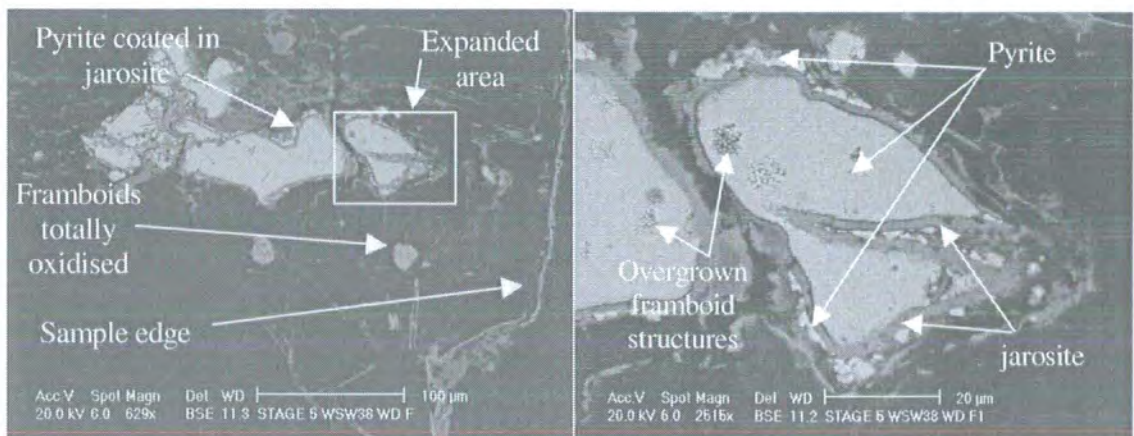
Figure 5.30. Jarosite rim surrounds massive pyrite grains at the 'base' of the same sample shown in previous Figure 5.45 (WS cyclically leached). Growth of the secondary mineral almost fractures the massive pyrite and breaks edges of the particle. Close to lower corner of sample jarosite fills porosity. Original alumino-silicate material in the matrix is covered in jarosite.

oxidised throughout whilst larger framboids (> 40μm) were oxidised at the edges alone. Leachate pH in this experiment dropped from day 133 to 170, possibly due to jarosite precipitation. A large (>50 μm) kaolinite surrounded framboid had a rim of jarosite, suggesting some reaction between pyrite and the local clay matrix.

At 205 days of cyclic leaching, solution pH was < 1, with high concentrations of Fe and S. Complete oxidation of framboids at 1 to 4 mm from the section edge and oxidation of the edge of large (>40 μm) framboids was observed. The ingress of the pyrite oxidation front in the WS agrees well with the drop in solution pH at this time. Low leachate pH and jarosite precipitation indicates the presence of Fe^{3+} in sample pore water.

Precipitation of oxidation products on pyrite was rarely observed in the WS after 268 and 316 days of cyclic leaching. At 3mm from the exposed edge variable oxidation was identified, but not at 2 mm or 8 mm from the edge (Figure 5.29). Jarosite was present throughout the sample, in fractures, as rims on massive pyrite and at the base of some samples (Figure 5.30).

Given the low pH of leachate (3-4) compared to Milli-RO water (5-6) introduced at each cycle, pore water pH must have been less than 3 during later leaching stages. A pH gradient probably existed, with low pH at the sample edge within a zone of oxidation increased towards the centre of the sample. Depletion of O_2 and Fe^{3+} by oxidation at in the outer regions of samples probably retarded oxidation in the centre of samples. Jarosite is stable at pH < 3 suggesting that pore water reaction with clays released K^+, (Bigham et al., 1996). The lack of *in-situ* jarosite precipitation in the outer regions of the samples was due to the higher ionic product of $[K^+]$, $[Fe^{3+}]$ and $[SO_4^{2-}]$ in macro-pores compared to micro-pores.

5.3.4.1.2   Cyclic Leaching of cleavage exposed samples with Milli-RO water

After 85 days of cyclic leaching, consolidated pyrite framboids situated along the WS cleavage plane were weathered to Alunite and Fe-sulphate at up to 1 mm into the sample. Up to 100 μm along the exposed face from this high concentration of cleavage pyrite, framboids showed much less oxidation.

Rare oxidation product was found on pyrite grains close to the exposed surface after 150 days of cyclic leaching (Figure 5.31). S had sorbed to kaolinite associated with consolidated pyrite at 2mm from the exposed edge, whilst at 5 mm into the sample *in-situ* pyrite oxidation products were observed. Buffering of leachate pH at 100 days of cyclic leaching increased pH from 5 ± 1 to 5.9 ± 0.5. At low pH anion exchange on the

positively charged hydrated surfaces of Al and Fe-oxides leads to the uptake of divalent anions such as SO_4^{2-}, and releases monovalent anions i.e. OH^-, increasing pH (Drever, 1997, Morgan and Stumm, 1999). The presence of S sorbed to kaolinite implies that anion exchange led to increased pH.

Isolated framboids were totally oxidised at 5mm and consolidated framboids had rims of Fe-sulphate at 15 mm along cleavage after 205 days of WS cyclic leaching. Rare oxidation was noted close to the sample's exposed edge (Figure 5.32). Leachate pH for this sample of 5 ± 1 suggests some dilution of acidity produced by pyrite oxidation, although Fe and S concentrations reach a peak at 205 days. Rare precipitation of oxidation products at the exposed edge suggests that dissolution at the water-rock interface was greater than precipitation.

Pore water pooling at the WS unexposed edge after 268 days of cyclic leaching led to incision of consolidated pyrite framboids by the growth of oxidation products. During dry periods the percolation of Fe^{3+} rich pore water into the sample accelerated oxidation and precipitation at the sample base. A 20 μm diameter void space containing dolomite was observed associated with gypsum produced during reaction with acidic pore water. On the dolomite side of the sample pyrite oxidation was less advanced. Although alkalinity released by this mineral retarded oxidation, the heterogeneous dolomite distribution, compared with acid producing pyrite, limited it's effect on pore water pH.

Rare *in-situ* pyrite oxidation product was observed in the WS sample leached for 316 days, especially in the area adjacent to the exposed edge. Although most consolidated framboids associated with clays had little *in-situ* oxidation product, sulphate sorption to clays was observed at the exposed surface. Weathering of isolated framboids within 1 mm of the un-exposed surface suggested pooling of Fe^{3+} rich pore water.

5.3.4.1.3 Cyclic Leaching of WS samples with phosphate solution

Cyclic leaching with phosphate solution was performed to identify experimentally initiated pyrite oxidation. Precipitation of Fe-phosphate was observed on rare framboids at up to 300 μm from the cleavage edge after 111 days of leaching. Although clay swelling fractured pyrite grains, most framboids within 500 μm of the sample edge appeared un-oxidised after 177 days of leaching. Surface precipitation of Fe-phosphate was the only manifestation of leaching with phosphate solution. Similarly, little evidence of oxidation was found at the centre of Milli-RO water leached WS samples over a similar period, with oxidation products mainly filling fractures. Such similarities
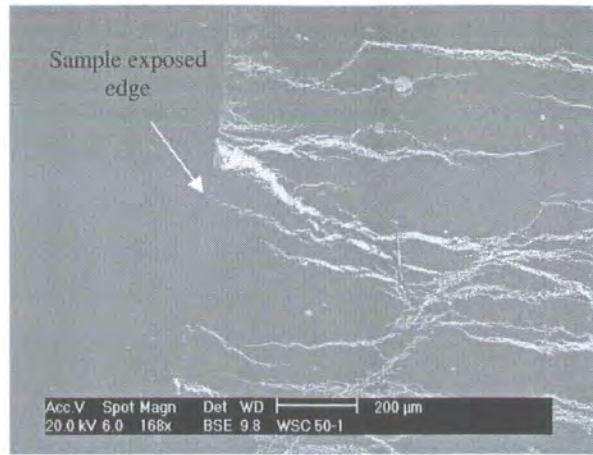
Figure 5.31. WSC after 150 days of leaching. Veined pyrite oxidised at exposed edge has a coating of Fe-sulphate. Opposite unexposed edge was highly oxidised.
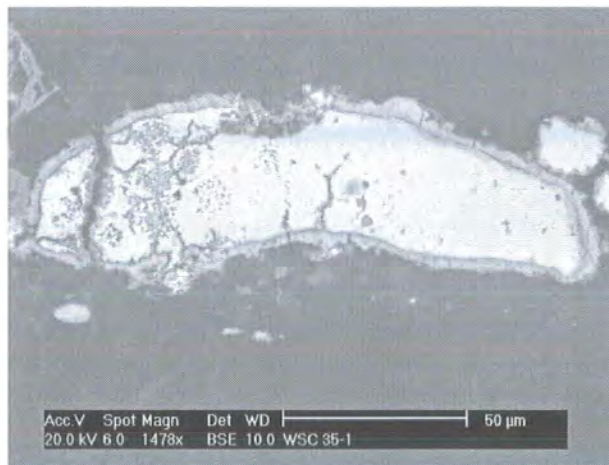
Figure 5.32. Rim of jarosite around consolidated pyrite framboid after 205 days of cyclic leaching of the cleavage edge. Some fracturing appears at the left side of the pyrite original where framboid features are more prominent.

Figure 5.33. Stagnantly leached WS after 316 days. At 200µm from sample edge framboids are removed and remaining matrix is made up of alunite and jarosite.

between leaching with phosphate solution and Milli-RO water suggest that experimental leaching did initiate the observed pyrite oxidation.

5.3.4.1.4 Stagnant Leaching of whole WS samples with Milli-RO water

Stagnantly leached samples were immobile compared to cyclically leached samples during treatment, leading to rapid pooling of highly concentrated pore water at their base. Initially static leaching of the WS led to greater weathering of framboidal compared to more consolidated pyrite. Fe-sulphate precipitated at the edge of consolidated pyrite at 500 μm in to the sample and some framboid voids contained gypsum. Stagnant leaching for 85 days produced more *in-situ* oxidation product found in cyclically leached samples.

Pyrite oxidation front ingress to 4 mm into the stagnantly leached WS, after 150 days, was marked by total framboid oxidation, peak leachate Fe and S and low pH (2.5). Jarosite and alunite were typical oxidation products at this stage, yet at 6 mm into the sample only pyrite framboid edges were oxidised.

Pyrite throughout the examined WS sample leached for 205 appeared slightly oxidised with alunite as a common oxidation product. Leachate pH at this time was below detection and dissolved content had fallen, consistent with the precipitation of minerals such as alunite and jarosite (Figure 5.27 and 5.33). Massive pyrite vein mineralisation in this sample probably also provided a source of low pH on oxidation.

Crusts of Fe-sulphate, containing Ti, up to 4 μm thick were produced at the section edges during stagnant leaching of the WS for 250 days. Framboidal pyrite was totally oxidised at 8mm into the section, yet only edge weathering of consolidated pyrite occurred at up to 4 mm. Variable oxidation of framboids occurred within central portions of examined sections.

Framboidal pyrite was oxidised in the centre of the WS stagnantly leached for 316 days. Elevated S K^{α} peaks collected from the edge of these central framboids suggests that dominant Fe^{3+} oxidation led to the lack of O K^{α} peak change. Low leachate pH (~2) is consistent with Fe^{3+} being the dominant oxidant. Consolidated pyrite had rare oxidation product at the edges. At the assumed lower edge of the sample alunite precipitation within cleavage planes occurred due to pooling of mineralised pore water in the lower part of the sample, possibly during drying prior to.

Along cleavage consolidated pyrite oxidation reached 5 mm into the WS after 382 days of stagnant leaching, whilst across cleavage oxidation halted at 3 mm. Local

perturbations in this oxidation front occurred where clay swelling and fracturing altered porosity.

5.3.4.1.5 Stagnant leaching of WS cleavage edge with Milli-RO water

After 85 days of stagnant leaching different extents of pyrite oxidation were shown throughout the WS sample. At the exposed edge precipitation was rarely apparent although at 400 μm into the sample pyrite had a rim of Fe-sulphate and gypsum. Oxidation of isolated framboids was common at 7 mm into the sample, whilst pyrite next to the un-exposed face was most oxidised, probably due to pooling of Fe^{3+} rich pore water.

A 3-4 mm long vein of pyrite mineralisation, in the sample examined after 205 days of stagnant leaching, was most heavily altered to Fe-sulphate at the exposed edge. Pyrite framboids close to the vein were also totally oxidised to Fe-sulphate. A 100 μm strip parallel to the exposed edge was fractured in parts, with angular rock fragments held within a Fe-hydroxide matrix. Secondary mineral precipitation appeared to promote fracturing of the exposed surface then support the resultant fragments. Clay at 3 mm from the un-exposed face had sorbed Fe-sulphate, yet adjacent pyrite framboids showed rare oxidation.

During the remainder of stagnant leaching framboid oxidation within 1 mm of the exposed edge was typically associated with Fe-oxide precipitated on clays. Further into samples pyrite associated with clay was rarely oxidized. Clays surrounding pyrite further into the WS appeared to retard oxidation, yet acidic products of pyrite oxidation should react with these clays first.

The lack of oxidation product in the centre of samples, removed in the later leaching stages, suggests a depletion of oxidant concentrations within a zone of active oxidation, close to the exposed edge. Identification of the percolation of acidic metal saturated water through samples implies that pore water in the centre of samples may have had low pH, retaining oxidation products in solution. Precipitation of jarosite and alunite at low pH, at the edge of samples, suggests that either the central portion of rock was not oxidised, or that saturation indices were not reached in micro-pores dominating this region of samples. Given the increase in macro-porosity closer to the surface of the sample it is also probable that higher ionic products in the larger void spaces allowed most precipitation at the sample edge.

5.3.4.1.6 Stagnant Leaching of cleavage exposed samples with phosphate solution

Leaching the WS cleavage edge for 177 days with phosphate solution led to: pyrite oxidation, Fe-phosphate precipitation and very rare precipitation of Fe-phosphate on framboids at the exposed and unexposed edges. No precipitation of phosphate was observed on consolidated framboids and massive pyrite. Fe-phosphate precipitated at the unexposed edge of the sample provides evidence of pore-water pooling.

5.3.4.2 SEM Investigation of WC static and cyclic leaching

5.3.4.2.1 Cyclic Leaching of whole samples WC with Milli-RO water

At both 85 and 150 days of cyclically leaching whole WC samples pyrite oxidation occurred further into the sample along the cleavage plane than across it. Pyrite framboids were variably oxidised at up to 400 μm across cleavage and 1 mm along cleavage.

Within 400 μm of the sample edge consolidated pyrite was associated with jarosite, whilst less consolidated framboids were totally oxidised after 205 days of leaching. Framboidal pyrite was variably and rarely oxidised at 4 mm and 7 mm respectively into the sample. Jarosite precipitation and the consequent H^+ release may explain the very low pH of the subsequent sample and the drop in leachate Fe and S content (Figures 5.26 and 5.27).

Leaching the WC for 268 days produced pyrite weathering at depths of 1.5 mm into the sample. Isolated framboids were less affected than those clustered in sedimentary bands. In the coal matrix higher porosity in sediment rich bands, compared to organic macerels, makes sediment-hosted pyrite more vulnerable to oxidation. Clay particles with sorbed Fe were observed in the outer part of the examined section. Interaction between acidic pore water and the alumino-silicate fraction led to an increase in solution pH and the decrease in leachate concentrations prior to the removal of this sample (Figure 5.34).

Complete oxidation of pyrite framboids at 2 mm along cleavage and rims of oxidation on consolidated pyrite occurred after 316 days of cyclic leaching. Across cleavage oxidation occurred up to 500 μm into the sample.

Leaching for 382 days completely oxidised smaller framboids to Fe-sulphate. Fracturing of sample corners by clay expansion and precipitation of jarosite also occurred, with clays commonly replaced by jarosite and natro-jarosite. Jarosite precipitation subsequent to oxidation by Fe^{3+} would explain low leachate pH and the
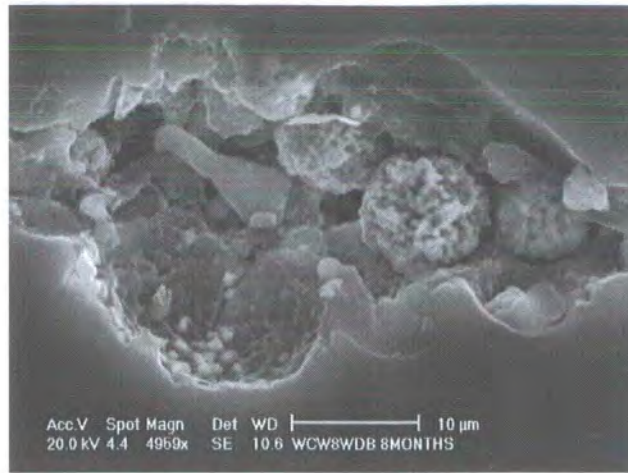
Figure 5.34. Pyrite framboids weathered in the WC after 268 days of
cyclic leaching. Amorphous Fe-hydroxide coats framboid
structures.
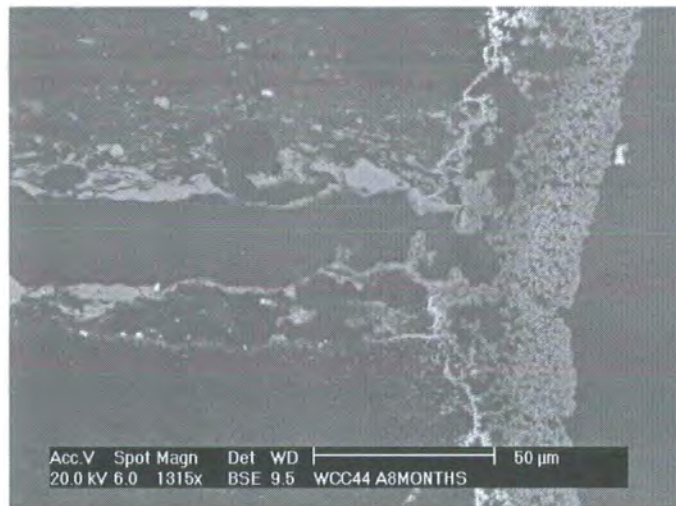
Figure 5.35. Pyrite framboids weathered in the WC after 268 days of cyclic
leaching. Amorphous Fe-hydroxide coats framboid structures.
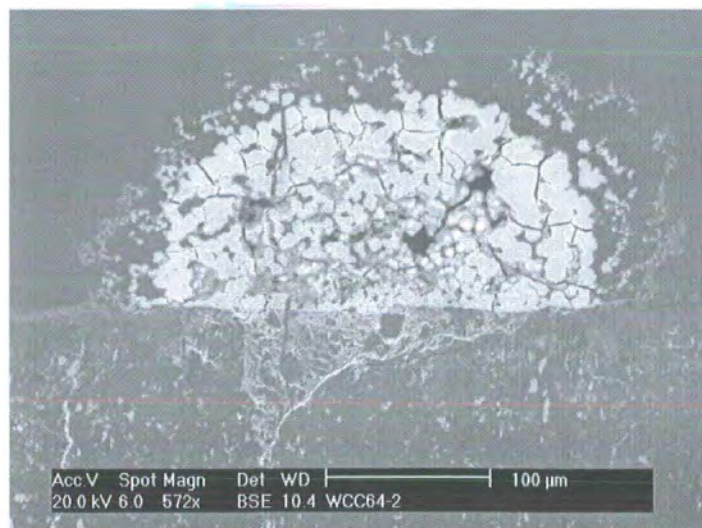
Figure 5.36. Colloform precipitation of Fe-phosphate at the end of a fracture in
the WC. Surface below formation is fractured and filled with
jarosite.

drop in oxidation due to precipitation of Fe^{3+}. Consistent leachate pH of close to 3.5 suggests that pore water pH is slightly lower. The presence of Fe^{3+} minerals precipitation in fractures appears to increase within the final three cycles as jarosite is dissolved and re-precipitated, leading to a decrease in leachate pH.

5.3.4.2.2 Cyclic Leaching of cleavage exposed WC samples with Milli-RO water

Pyrite framboids were completely and variably oxidised at 1 and 4 mm into the sample respectively after 85 days of cyclic leaching. Jarosite, alunite and gypsum filled fractures and replacing small framboids, consistent with decreasing leachate pH prior to this point.

Extensive precipitation of jarosite and gypsum at the sample's exposed edge and rare *in-situ* oxidation products at 4 mm were observed in WC leached for 150 and 250 days. At the un-exposed edge *in-situ* pyrite product was rare. Dissolution of jarosite during wetting periods was suggested by the release of K to solution. The low proportion of Fe to S implies that Fe uptake, either through precipitation or further pyrite oxidation, had occurred (Chapter 5 Results in Appendix II Results).

Variable oxidation of both framboids and consolidate framboids occurred at up to 2 mm from the exposed WC sample edge, after 316 days of cyclic leaching. Weathering of framboids at 1 mm from the unexposed edge suggests that pooling of Fe^{3+} rich pore water took place in the lower part of the sample. Dissolution of jarosite during wetting cylces would have provided the Fe^{3+}, with the pore fluid filling pore space around pyrite and clays adjacent to the un-exposed edge. Leachate chemistry evolution of increasing pH and S after a previous drop at day 307 suggests a combination of increased clay weathering and pyrite oxidation in the lower part of the sample.

WC leaching for 382 days led to high oxidation at the un-exposed edge of the sample again due to continued pooling of acidic Fe^{3+} enriched pore water. Clays at the base of the sample had sorbed Fe. Within 50 μm of the exposed surface pyrite framboids were totally oxidised, the surface was fractured with the Fe-sulphate matrix supporting angular fragmented clasts (Figure 5.35). By this point dissolved S concentrations were increasing and pH was falling suggesting that renewed pyrite oxidation was occurring.

5.3.4.2.3 Cyclic leaching of WC with phosphate solution

Over the total 177 days of cyclic leaching with phosphate solution, no WC section showed any direct reaction between Fe and P. Only fractures contained any Fe-

phosphate, suggesting that Fe released from oxidation was only precipitated within macro-porosity where solution pH was probably higher (Figure 5.36).

5.3.4.2.4 Stagnant Leaching of whole WC samples with Milli-RO water

Low pyrite content of examined stagnantly leached WC samples up to 150 days, made assessment of weathering difficult. Only samples leached for over 205 days are described.

Solution pH after 205 days of stagnant leaching was below detection. Sample examination revealed extensive sorption of S to the edges of clays, jarosite precipitation on the sample edge and as 3 μm thick rims on consolidated framboids at the sample edge. In places a subsequent rim of alunite surrounded original consolidated pyrite framboid rims of Fe-sulphate, providing some protection to the framboid centres. Peak concentrations of dissolved S and Fe were reached after 205 days of stagnant leaching. Jarosite precipitation would have released acidity contributing to low very leachate pH.

Stagnant leaching over 268 days produced jarosite and alunite within a fracture in the rock (Figure 5.37). Dolomite associated with clay minerals in one part of the sample was altered to gypsum at the edges (Figure 5.38). Locally, pyrite framboids were also altered to gypsum. Along cleavage oxidation extended up to 1.5 mm from the exposed edge, whereas across cleavage oxidation rarely reached up to 500 μm. Pooling of pore water was demonstrated by a 200 μm thick band of sub-horizontal Fe-sulphate, forming 2 mm above the assumed sample base and a similarly orientated band of clay (Figure 5.39). The impermeable layer formed by the clay allowed the pooling of dissolved Fe and S rich pore fluids, forming the observed Fe-sulphate.

Alunite and jarosite precipitated on the assumed base of WC stagnantly leached for 316 days. Rapid Fe^{3+} oxidation may have caused the extensive framboidal oxidation adjacent to this lower edge. Relative to the previous sample, less *in-situ* oxidation product was observed at 3 to 5 mm into the sample across and along cleavage respectively. Dissolution due to low pore water pH may be the reason for the lack of in Fe-sulphates and oxides.

After 382 days of stagnant leaching extensive reaction coincided with clays with precipitation of jarosite and Fe-sulphate in fractures. *In-situ* pyrite oxidation was only found within the outer 500 μm of the sample. Low oxidation product precipitation within the central area of samples suggests that low pore water pH retained dissolved products in solution.
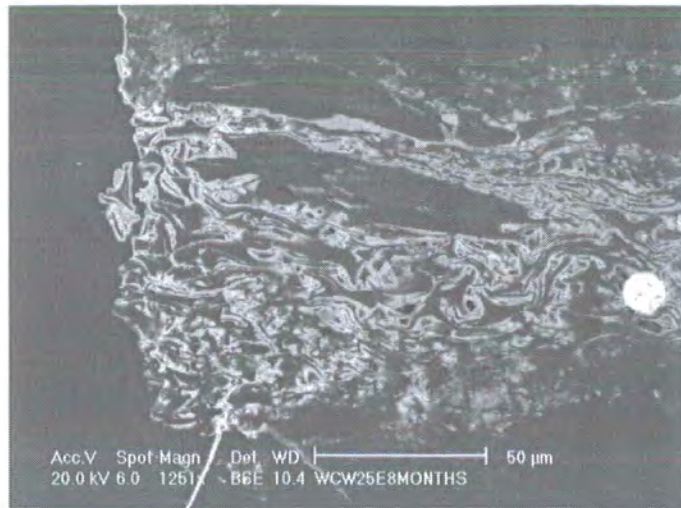
Figure 5.37. Alunite precipitation within the matrix of the WC after 268 days of leaching.
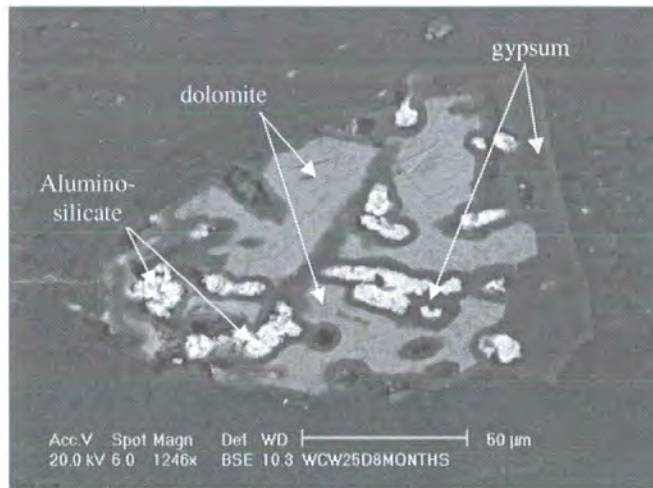
Figure 5.38. Dolomite heavily altered to gyspsum, bright areas are inclusions of alumino-silicate.
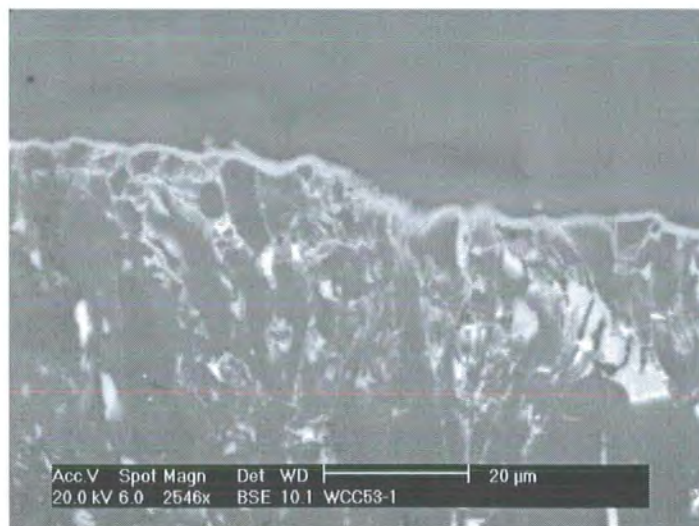
Figure 5.40. Fracturing of the exposed edge of WC after 382 days of stagnant leaching. Fragments are held in place by a matrix of Fe-sulphate and alunogen.

137
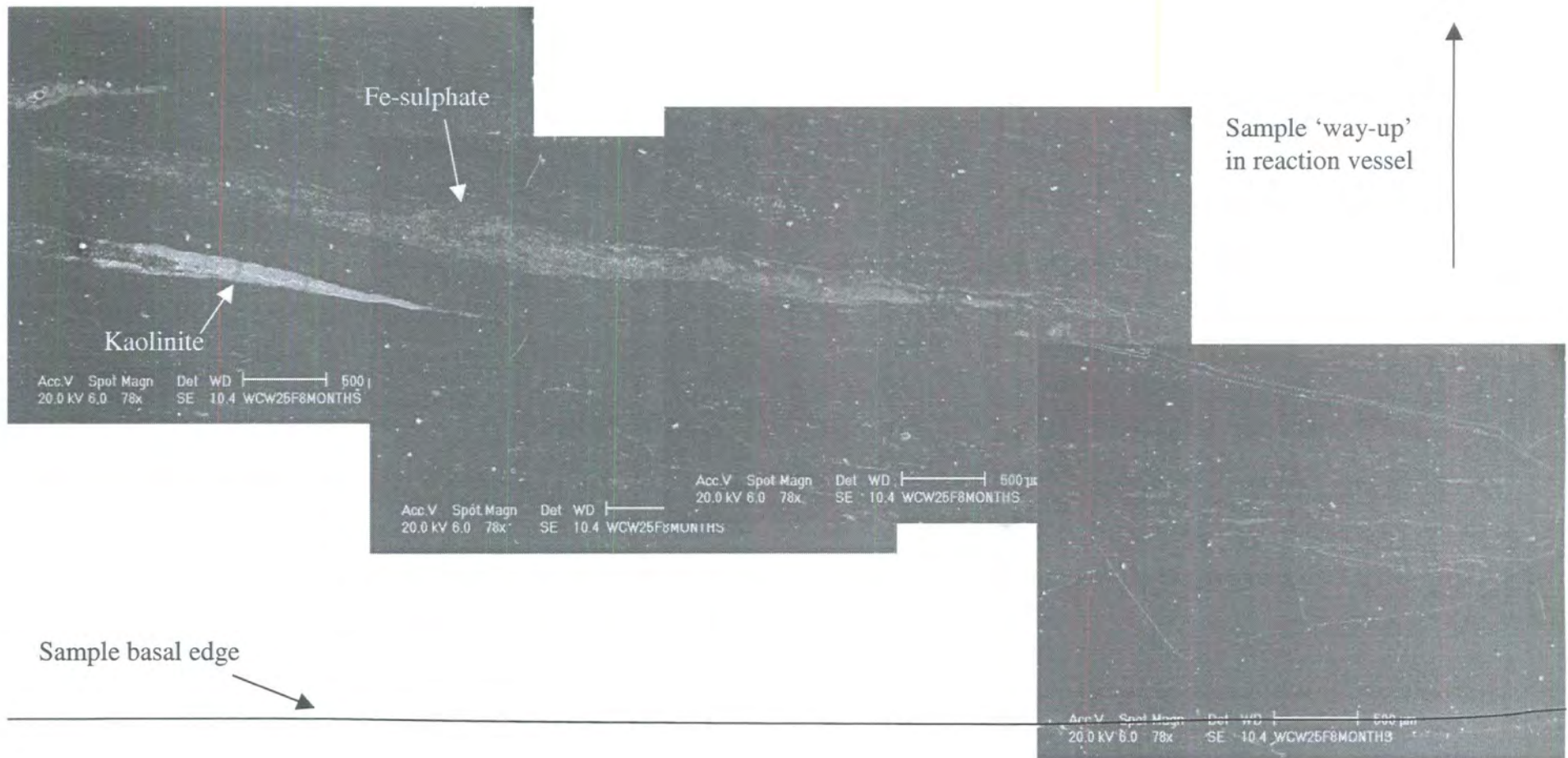
Figure 5.39. Fe-sulphate formation above an impermeable alumino-silicate band in the WC after 268 days of stagnant leaching. Proximity to the sample base suggests pooling of metal enriched pore-water either during drying or leaching or both.

5.3.4.2.5 Stagnant Leaching of WC cleavage edge with Milli-RO water

After 85 days of stagnant leaching of the WC cleavage edge, jarosite was identified at the exposed edge and framboids were oxidised at 1 mm into the sample. Most framboids in the 150 day WC sample were oxidised, with the extent of weathering decreasing away from the sample edge and precipitation of Fe-sulphate on framboids at up to 4 mm.

A pH drop of 6 to 4 occurred in leachate between 150 and 205 days, accompanied by increased dissolved S and Fe. After 205 days of leaching, pyrite framboids were totally oxidised at up to 6 mm away from the exposed edge, with alunite precipitation at the sample surface, possibly contributing to falling pH. Lower pore water pH and subsequent dissolution of precipitated Fe-sulphate probably caused the increase in dissolved Fe and S.

Pooling of pore water occurred at the un-exposed edge of WC leached stagnantly for 268 days. Pyrite oxidation occurred at up to 5 mm into the sample, with most extensive oxidation occurring within 500 μm of the exposed edge. At 268 days of leaching dissolved content dropped and pH rose above 5 due to the addition of Milli-RO water to samples at 205 days leading to precipitation from solution.

Swelling of clays encouraged sample fracturing after 382 days of stagnant leaching. The exposed surface was fractured by Fe-sulphate precipitation and angular fragments were held in a matrix of the oxidation product (Figure 5.40). Little evidence of *in-situ* pyrite oxidation remained in the examined section. Although solution pH was > 5, internal pore-water pH was probably slightly lower. Pore-water dilution and prior oxidation product dissolution by fresh Milli-RO water added to prevent evaporation may have led to the lack of oxidation product in later stages. Rapid fracture inducing precipitation at the water-rock interface was probably produced by the addition of dilute Milli-RO water causing a sharp pH gradient in this area.

5.3.4.2.6 Stagnant Leaching of WC samples with phosphate solution

Leaching samples of WC in phosphate solution for 63 days only produced Fe-phosphate in fractures. Further leaching for 177 days led to phosphate reaction with framboids at 500 μm into the sample. Jarosite and Fe-phosphate precipitated at the base of cleavage leached samples. Precipitation of Fe-phosphate on pyrite after 177 days was probably retarded by a solution pH of 3, with extensive jarosite precipitation encouraged by excess dissolved K.

WS	85 days	150 days	205 days	268 days	316 days	382 days
whole sample cyclic leaching	Framboids oxidised at 100 μm, relatively low oxidation, Fe-hydroxide is main oxidation product	Isolated framboids oxidised at 2-3 mm into sample Jarosite associated with clays and pyrite	Complete oxidation of framboids at 1-4 mm depth, consolidated pyrite oxidised at edge	Framboids with oxidation product 3 mm, yet not at 2 and 8 mm depth. Fe-sulphate in fractures	n/a	n/a
whole sample stagnant leaching	Oxidation at 500 μm, gypsum and Fe-sulphate fill framboid voids	Complete oxidation of framboids at 4 mm	All framboids oxidised, alunite present	Fe-Ti-sulphate crust at surface. Complete pyrite framboid oxidation 8 mm, consolidated pyrite at 4mm	Complete oxidation of framboids to centre of sample alunite present	Oxidation product on consolidated framboids at 5 mm along and 3mm across cleavage
cleavage edge cyclic leaching	Framboid oxidation at 1mm into sample, aluinte present	Oxidation at 5mm into sample.	Oxidation product identified at 15 and 5 mm into sample	Complete oxidation at 4mm in, evidence of fluid pooling at base	Little in-situ evidence, 1mm oxidation from upper and basal surfaces	
cleavage edge stagnant leaching	Oxidation at 400 μm, Fe sulphate and gypsum also present	Oxidation at 1mm in. Fracturing of surface with Fe-sulphate and hydroxide	1 mm oxidation and precipitation at exposed surface	Little evidence of pyrite oxidation, clays may be protecting pyrite		

Table 5.8. Summary of SEM investigation of pyrite oxidation front in the cyclical and stagnant leached whole and cleavage edge leached WS.

WC	85 days	150 days	205 days	268 days	316 days	382 days
whole sample cyclic leaching	Framboid oxidation at 200-400 μm across cleavage and 1mm along cleavage	As previous	Jarosite on pyrite at 400 μm in. Framboid oxidation at 4 mm	1.5 mm oxidation at corners, with alunite and jarosite precipitation on cleavage planes	Oxidation at 2 mm along cleavage, 500 μm across cleavage	Complete oxidation of framboids, jarosite and natro-jarosite present
whole sample stagnant leaching	n/a	n/a	Jarosite up to 3 μm thick on framboids at sample edge	Jarosite and alunite on bedding plane, oxidation at 1.5 mm along cleavage and 500 μm across cleavage	Alunite and jarosite present. Framboids oxidised at 3-5 mm along cleavage, rare *in-situ* oxidation product	Jarosite and Fe-sulphate in fractures. Oxidation front at 500 μm, otherwise little evidence.
cleavage edge cyclic leaching	1 mm complete framboid oxid, 4 mm varied oxidation, jarosite and alunite in fractures	Jarosite and gypsum present. Oxidation at 4 mm into sample	As previous	n/a	Oxidation at 2 mm from the exposed edge and 1mm from the un-exposed edge	Framboid total oxidation at 50 μm from exposed edge. Sample surface is fractured and contains Fe-sulphate
cleavage edge stagnant leaching	Jarosite at the sample edge and framboid oxidation at 1 mm	Oxidation at 4 mm into sample with Fe-sulphate precipitation	Alunite at sample edge, complete framboid oxidation at 6 mm into sample	Oxidation at 5mm into sample, extensive framboid oxidation at 500 μm	n/a	Fracturing of sample surface with Fe-sulphate precipitate. Little in-situ oxidation product.

Table. 5.8 (continued). Summary of SEM investigation of pyrite oxidation front in the cyclical and stagnant leached whole and cleavage edge leached WC.

5.3.5   Discussion of stagnant and cyclic leaching experiments

Leaching of individual particles of coal-bearing strata, under different water-rock conditions, was performed to investigate the following:

- *In-situ* pyrite weathering and the movement of a pyrite oxidation front
- Transport mechanisms for dissolved oxidant and pollutant at the waste particle scale
- Weathering of different coals and overburden rock-types
- Effect on pyrite oxidation of different water-rock regimes.

In the following sections these points are discussed in relation to the interpretation of waste rock particle-scale weathering processes described previously.

5.3.5.1   Pyrite oxidation – rates, fronts and controls.

Various investigations of pyrite oxidation rate report a rate reaction order of between 0 and 1 in the form

$$R_{sp} = -K[M]^n \tag{5.2}$$

where specific rate R_{sp} depends on concentration of reactant M and is n the order of dependence of rate on the reactant species (Nordstrom, 1982, McKibben and Barnes, 1986, Moses et al., 1987, Strömberg, 1996, Evans et al., 2001).

Nicholson et al. (1988) suggest that the variety of rate reaction orders reported is due to the rate dependence on oxidation product decomposition, leading to a Langmuir adsorption isotherm relationship :-

$$R = \frac{R_m KC}{(1 + KC)} \tag{5.3}$$

where the rate of oxidation R depends on R_m the rate based on maximum saturation of available surface sites, K is the adsorption equilibrium constant for O_2 on pyrite and C is the O_2 concentration (Nicholson et al., 1988). Although pyrite oxidation at variable O_2 concentrations for pH > 6.7 fits this relationship well, Moses and Herman (1990) suggest that the good fit is caused by blocking of oxidation sites by Fe^{2+} at pH > point of zero charge (pH$_{pzc}$ = 2.5). Surface X-ray Photoelectron Spectroscopy (XPS) studies of aqueous pyrite oxidation show that the pyrite surface is mainly associated with Fe^{2+}

rather than Fe^{3+} at low pH (Bonnissel-Gissenger et al., 1998). Moses and Herman (1991) report that although coating of pyrite surfaces by Fe^{3+} hydroxides coat at high pH, oxidation is not retarded in the short term. Over longer periods of experiment, surface oxidation product decomposition is expected to be a controlling factor of the measured rate.

Despite advances in pyrite oxidation monitoring under various conditions and oxidants, calculations usually provide a rate order of 0 to 1. Therefore this value is used in the following comparisons of *in-situ* and predicted oxidation rates.

5.3.5.1.1 Pyrite oxidation rate dependence on pyrite surface area and mass

The dependence of pyrite oxidation rate on sample surface area has previously been supported and refuted by various authors. McKibben and Barnes' (1986) SEM investigation of isolated pyrite, oxidised at low pH, suggested that reactive surface area was less than actual sample surface area with reaction taking place along edges and pits, i.e. areas of high surface energy. Other authors report that oxidation over the longer period of a year provides evidence of rate dependence on surface area (Nicholson et al., 1988, 1990, Moses and Herman, 1991).

Heterogeneity in pyrite morphology leads to difficulties in applying this surface area dependence to *in-situ* pyrite. Organic and inorganic framboidal pyrite, consolidated pyrite framboids and massive vein mineralising pyrite were all identified in the WC and WS. Inorganic and consolidated framboids made up 80 % of the pyrite population with 50 % of this consisting of less consolidated framboid material. A rough calculation of the error margin produced by using framboid diameter to estimate surface area can be made. The cross section of a 15 μm diameter WS framboid containing 120 individual 1 μm diameter crystals, assuming equal spacing, provides around 540 individual crystals in the framboid sphere of surface area 3.1×10^{-12} m^2. The total pyrite surface area of the framboid is 1.7×10^{-9} m^2, an order of magnitude larger than the surface area of a 15 μm diameter solid sphere (7.1×10^{-10} m^2). The large difference in surface areas agrees with fast oxidation of framboidal pyrite as noted in SEM examination of WS and WC samples.

In order to provide some comparison with previous authors' calculated, surface area dependant isolated pyrite oxidation rates, a relationship between surface area (S), mineral mass (M), density (ρ) and diameter (d) used by Nicholson et al. (1988) is used here.

$$S = 6M/(\rho_s d) \qquad (5.4)$$

Assuming grain diameter of 50 μm, surface areas of 2.64 m^2 for the WC, 2.16 m^2 for the WS and 0.02 m^2 for the UWC are used. Any under-estimation in surface area will decrease the calculated rate of pyrite oxidation, compared to the actual value.

5.3.5.1.2 Prior oxidation products and other sources of dissolved S

A comparison of total elemental flux from leaching of all lithologies with their total acid leachable extract indicates prior weathering products were dissolved throughout leaching (Table 5.9). Although the simultaneous removal of prior and contemporary oxidation products leads to overestimation of pyrite oxidation rates, a relatively large volume of soluble products was removed during initial flushing. It is therefore assumed the bulk of prior oxidation product dissolution occurred during the initial 120 day peak cyclic leachate dissolved content, allowing an estimate of *in-situ* oxidation rate from leachate S content after this point. Prior oxidation products remain with the products of current oxidation in stagnant leachate solution, making calculation of oxidation rates difficult. Gypsum dissolution from the UWS also masks the actual S derived from pyrite oxidation. Therefore only leachate S collected after 120 days of cyclic leaching of the UWC, WS and WC are used to calculate pyrite oxidation rates.

	Acid leachable phase (mgg^{-1})	Cyclic leaching cumulative flux (mgg^{-1})	Stagnant leaching peak flux (mgg^{-1})
UWS	63 ± 3	1.8 ± 0.2	0.6 ± 0.2
UWC	12 ± 4	0.44 ± 0.06	0.2 ± 0.1
WS	34 ± 10	3.8 ± 0.6	1.6 ± 0.9
WC	13 ± 2	6 ± 1	2.3 ± 0.7

Table 5.9. Total element content in mg per g of sample of the acid leachable phase, cumulative total flux dissolved during cyclical leaching and the peak flux from stagnant leaching.

5.3.5.1.3 Calculating an oxidation rate using dissolved S

Despite the possibility of intermediate thiosulphate and sulphite changing oxidation reaction stoichiometry, dissolved SO_4^{2-} content has been used to calculate pyrite oxidation rates (McKibben and Barnes, 1986, Nicholson et al., 1988, Moses et al., 1987, Evans et al., 2001). Bonnissel-Gissenger et al., (1998) reported an increase in the range of dissolved S species at pH > 6, with SO_4^{2-} alone identified at pH < 6, after 36 hours of reaction. Moses and Herman (1991) also report the lack of intermediate sulphate phases during pyrite oxidation at circumneutral pH. Given the low pH of WS and WC

leachates measured in the experiment described here, it is assumed that SO_4^{2-} was the main S species present. Dissolved leachate S was used as a proxy for sulphate and converted to a pyrite dissolution rate using the stoichiometry of the following equations, depending on leachate pH.

$$FeS_2 + \tfrac{7}{2}O_2 + H_2O \Rightarrow Fe^{2+} + 2SO_4^{2-} + 2H^+ \qquad pH < 4 \qquad (5.5)$$

$$FeS_2 + \tfrac{15}{4}O_2 + \tfrac{7}{2}H_2O \Rightarrow Fe(OH)_3 + 2SO_4^{2-} + 4H^+ \qquad pH > 6 \qquad (5.6)$$
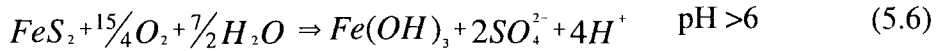
Published oxidation rates have reported as mol pyrite g^{-1} h^{-1} (Nicholson et al., 1988), mol pyrite $cm^{-2}min^{-1}$ (McKibben and Barnes, 1986) and mol pyrite m^{-2} s^{-1} (Elberling et al., 1994). Given the possible error of an order of magnitude in calculating pyrite surface area discussed previously, calculated rates are presented both in moles of pyrite, oxidised per original g of pyrite or per original m^2, per second ($mol_{py}^{-1} g_{pyO}^{-1} s^{-1}$ or $mol_{py}^{-1} m_{pyO}^{-2} s^{-1}$ (Table 5.10)).

Rock type	Original wt% pyrite	Estimated surface area (m^2g^{-1})	Pyrite oxidation rate	
			$mol_{py}^{-1} g_{pyO}^{-1} s^{-1}$	$mol_{py}^{-1} m_{pyO}^{-2} s^{-1}$
WS	9 ± 5	0.0022	$3 \pm 2 \times 10^{-13}$	$1.3 \pm 0.7 \times 10^{-11}$
WC	11 ± 10	0.0026	$1.7 \pm 0.9 \times 10^{-13}$	$7 \pm 4 \times 10^{-12}$
UWC	1.7 ± 0.6	0.0004	$3 \pm 5 \times 10^{-14}$	$2 \pm 4 \times 10^{-13}$

Table 5.10. Pyrite oxidation rates calculated from dissolved S in UWC, WS and WC cyclic leachate after 120 days. Values are presented in as rate dependant on original mass and surface area of pyrite, errors shown are 1σ, n=16. Surface area per g of original sample is estimated using typical pyrite consolidated framboid diameter of 50 μm.

5.3.5.1.4 Controls over the evolution of oxidation rate

A drop in the oxidation rate of pyrite for UWC, WC and WS at days 225 to 239 coincided with a steep drop in pH over days 205 to 225 for the weathered rock types (Figures 5.41 and 5.42). For all three rock-types oxidation rate suffered a drop of an order of magnitude, after which point pH recovered, but oxidation rate did not. The change in pyrite oxidation rates and prior drop in pH for the WS and WC leachate was mirrored by an apparent regression of pyrite oxidation front. *In-situ* oxidation products on further cyclic leaching appeared to be removed by dissolution, particularly in the outer 2 mm of examined sections. Little oxidation front ingress after cyclic leaching for 205 days suggests that available oxidant was depleted in the outer region of samples.

Increased precipitation of jarosite, natro-jarosite and alunite in macro-porosity implies reaction with alumino-silicates took place after 205 days. Buffering by the clay phase may have retarded pyrite oxidation rates and contributed to leachate pH increase after day 239 for both WC and WS.

Changes in dominant oxidant, oxidant depletion or reactive surface area reduction may have led to the decreased oxidation rate. Both Moses and Herman (1991) and Bonnissel-Gisenger (1998) report that at a pH 4 - 10, pyrite oxidation by O_2 and Fe^{3+} is limited by the adsorbtion of Fe^{2+} to the pyrite surface. Bonnissel-Gisenger (1998) also suggests that although a build up of Fe^{3+} hydroxides occurs at the pyrite surface in this pH range, further oxidation is not prevented. These experiments were relatively short term at 24 to 36 hours, compared to Nicholson et al.'s (1990) year-long oxidation of pyirte at high pH (>4) which led to Fe-hydroxide build-up retarding oxidation rates. Although cyclic leaching of the UWC, WC and WS was performed over a similar time-span as Nicholson et al.'s experiment, pH conditions reported here were lower. Refreshing of leachate with dilute Milli-RO water in cyclic leaching may have also dissolved oxidation products in the outer rim of samples.

Association of a fall after a rise in oxidation rate with a drop and rise in pH suggests that a change in, or depletion of oxidant was the more likely cause of the drop in rate, than blocking of the pyrite surface. Prior to days 205 or 225 the falling pH would have accelerated oxidation rate by increasing Fe^{3+} availability. Depletion of this oxidant either by rapid consumption or by dilution during cyclic leaching would lead to an overall drop in oxidation rate.

The sharp rise in oxidation rate can be attributed to drop in pH below the point of zero charge of pyrite (2.4 - Moses and Herman, 1991, Wilder and Seward, 2002). At pH 2-4, dissolved Fe^{3+} exists as $Fe(OH)_2^+$ and $Fe(OH)^{2+}$ species which would be preferentially adsorbed to the pyrite surface at pH < 2.4, compared to Fe^{2+} (Bonnissel-Gissenger et al., 1998). Similarly an Fe^{3+} 'aquo' complex, i.e. Fe^{3+} associated with 2 -6 water molecules $(Fe(H_2O)_6^{3+}$, Singer and Stumm, 1970, Moses et al., 1987) would also be preferentially adsorbed to a positively charged pyrite surface below pH 2.4. Unless the depletion of Fe^{3+} during pyrite oxidation is compensated by Fe^{2+} oxidation by O_2 the oxidation rate will decrease. During cyclic leaching dissolved O_2 was replaced, however, removal of leachate containing Fe^{3+} during a drying cycle would have halted oxidation, leading to the observed precipitation of jarosite.

5.3.5.1.5 Comparison with predicted rates

Modelling pyrite oxidation using rates from isolated mineral leaching assumes that these rates also represent *in-situ* oxidation. Experimental pyrite oxidation is performed in excess leachate under sterile conditions, whilst embedded pyrite oxidation is affected by; rock matrix porosity, pore water chemistry, adjacent mineral composition, morphology and bacterial action. Direct use of experimentally derived pyrite oxidation rates in modelling AMD formation without recognition of such factors will also result in inaccurate predictions. In an attempt to gauge the affect of these factors, pyrite oxidation rates reported in Table 5.10 are compared to predicted rates using pyrite wt% and published rate constants.

The specific rates derived for pyrite oxidation at low pH (1-4) by McKibben and Barnes (1986) provided the following initial rates equations for the oxidants O_2 and Fe^{3+}:

$$R_{sp,Fe^{3+}} = -10^{-9.74} M_{Fe^{3+}}^{0.5} M_{H^+}^{-0.5} \qquad \text{pH 1-2 (5.7)}$$

$$R_{sp,O_2} = -10^{-6.77} M_{O_2}^{0.5} \qquad \text{pH 2-4 (5.8)}$$

During cyclic leaching the main oxidant was assumed to be dissolved O_2 after 225 days, with some contribution from Fe^{3+}. Average WC and WS pyrite oxidation rates were $7 \pm 4 \times 10^{-12}$ and $1.3 \pm 0.7 \times 10^{-11}$ $mol_{py} m_{py_o}^{-1} s^{-1}$ respectively, for leachate pH < 4.

Using Henry's Law the dissolved O_2 content of 70 mL of purified water at 25°C is 0.018 moles, ($K_{O_2} = 1.26 \times 10^{-3}$ at 25 °C, Stumm and Morgan, 1996). Typical pO_2 in equilibrium with embedded pyrite fluctuated between 0.21 atm during drying and leaching fluid dissolved O_2 concentration, although only dissolved O_2 reacts with the pyrite surface (Moses and Herman, 1991, Bonnissel-Gissenger et al., 1998). As dissolved O_2 decreases with increasing solution temperature, ionic content and by uptake in sulphide oxidation, concentration decreased during each wetting cycle and also generally from winter to summer (19 to 24°C) (Stumm and Morgan, 1996).

Estimated pyrite oxidation rate using McKibben and Barnes' (1986) rate constant for oxidation with O_2 at low pH is 2.3×10^{-8} $mol_{py} cm_{py}^{-2} min^{-1}$ or 2.3×10^{-12} $mol_{py} m_{py}^{-2} s^{-1}$. Calculated rates of pyrite oxidation measured from dissolved S in the WS and WC leachates are within the same range or an order of magnitude faster. Given the error in pyrite surface area estimation of at least an order of magnitude and the concurrent release of prior oxidation products, the small difference is surprising.

Correction of leachate concentrations for original sample mass corrects for the effect of leaching from a rock matrix. To try to gauge this effect leachate S released after 120 days from WS and WC samples prior to correction for mass can be compared with predicted S release (Table 5.11). Actual rates of S dissolution from WS and WC samples are up to two orders of magnitude higher than predicted. Under-estimation of surface area by at least an order of magnitude less than the actual value would increase predicted S content. Leaching of prior oxidation products also raises measured leachate S over predicted concentrations.

Comparison of predicted and actual dissolved S shows that pyrite oxidation is (serendipitously or otherwise) well constrained by the rate reaction. However, errors in pyrite characterisation and additional S from prior oxidation products may subsequently lead to divergence of model and actual systems. Monitoring by SEM of the pyrite oxidation front at different stages of leaching suggest that most oxidation was focused on a zone at around 3-4 mm, limited by dissolved O_2 diffusion. Given the lack of oxidation further into samples this would suggest that the close range of predicted and actual dissolved S might indeed be largely coincidental. In the following section the movement of an oxidation front is examined in further detail.

S (mg)	WC				WS			
Original sample mass (g)	14.4	13.6	13.4	13.4	13.2	16.1	17.4	20.3
Mean predicted S (per cycle)	0.008 ± 0.003	0.008 ± 0.003	0.007 ± 0.003	0.007 ± 0.003	0.006 ± 0.002	0.008 ± 0.002	0.008 ± 0.002	0.010 ± 0.002
Mean actual S (per cycle)	0.5 ± 0.2	0.3± 0.2	0.3 ± 0.2	0.14 ± 0.09	0.4± 0.2	0.9 ± 0.4	0.6 ± 0.4	0.4 ± 0.2
Predicted S (total after 120 days)	0.11	0.11	0.11	0.11	0.09	0.11	0.12	0.14
Actual S (total after 120 days)	7.23	4.01	5.34	2.22	5.37	12.92	8.47	5.48

Table 5.11. Predicted and actual dissolved S (mg) derived from cyclic leaching of WS and WC whole samples over 120 to 361 or 382 days of leaching. Predicted values are calculated using McKibben and Barnes' (1986) rate reaction for pyrite oxidation at low pH by dissolved O_2. Actual mean values per cycle are from dissolved S leachate content removed after a week of reaction, errors shown are 1 σ, n= 13.

5.3.5.2 Monitoring the pyrite oxidation front

A pyrite oxidation front was successfully followed by SEM investigation of both WC and WS cyclically and stagnantly leached samples. Water-rock regimes affected the style of influx, with stagnant leaching producing *in-situ* pyrite oxidation products at greater depth in samples compared to cyclic leaching. In general cyclic leaching led to oxidation of pyrite framboids at up to 1 mm in the initial 85 days of experiment, and up to 6 mm after 205 days of leaching. Subsequently *in-situ* pyrite oxidation products were usually only found at 3-4 mm into samples. Oxidation at depth was retarded due to depletion of oxidant at the sample edge. Dilution of pore water and the formation of a pH gradient at the sample edge led to the removal of pyrite oxidation products and precipitation within macro-porosity and at the sample edge. The concentration of oxidation at the 3-4 mm region of the sample led to an increase in dissolved Fe^{3+} content. Catalysis of pyrite oxidation by Fe^{3+} was halted by depletion of this species, caused by the slower rate of dissolved O_2 supply and oxidation of Fe^{2+}. Raising of pore water pH by clay weathering probably also contributed to the slowing of Fe^{3+} pyrite oxidation. Remaining Fe^{3+} was precipitated on dilution with fresh Milli-RO water of subsequent wetting cycles, typically within macro-porosity. Consequently oxidation of pyrite continued at a lower rate in the cyclically leached samples.

In stagnant leaching, a diffusion gradient between the water-atmosphere and water-rock interfaces remained intact over the period of experiment. The precipitation of *in-situ* pyrite oxidation products occurred further into the sample and material was generally not removed from outer regions of the samples. However the higher porosity of the WS led to greater oxidation of pyrite compared to the WC. Pooling of pore water also affected the position of oxidation front by providing a source of dissolved Fe^{3+} for oxidation in the lower region of samples.

Various authors have reported the inhibition of pyrite oxidation and poor quality leachate formation by the flooding of tailings (Simms et al, 2000). Here, stagnant leaching of rock rapidly produced low quality leachate and *in-situ* oxidation products throughout samples. These oxidation products were not rapidly removed as the lack of leaching solution and pore water mixing allowed equilibrium between precipitation and dissolution at the water-rock interface. In cyclic leaching such equilibrium is not allowed to develop, due to influx of fresh leaching solution.

Various numerical models based upon the shrinking core model (SCM) have been used to simulate pyrite weathering in waste rock (Levenspiel, 1970, Nicholson et al 1988, Wunderly et al., 1996, Strömberg, 1997, Bain et al., 2000). Most use the SCM to

define mineral reaction with pyrite particles, coupled with a reactive transport code to predict leachate quality, assuming that pyrite weathers homogeneously with each time step (Figure 5.1, Wunderly et al., 1996, Strömberg, 1997, Bain et al., 2000). Examination of both WS and WC samples indicated that in coal-bearing strata, oxidation front ingress is heterogeneous, depending on pyrite morphology and larger interconnected pore space. In the following sections the factors affecting the style of pyrite oxidation identified in stagnant and cyclic leaching experiments are discussed and comparison made with the SCM.

5.3.5.2.1   Effect of cleavage plane weathering

Comparison of total element flux from cleavage edge and whole samples in Figure 5.24 suggested that soluble material was rapidly removed from the cleavage plane. The formation of cleavage plane is a result of aligning of proto-lith minerals during burial diagenesis with original sediment bedding plane. Coal (and shale) cleat forms as a result of further metamorphic pressures leading to jointing in the vertical plane (Spears, 1980). As coal and shale tends to fragment along cleat planes rather than cleavage, cleavage probably has more control over permeability at the waste particle size. Alignment of rock minerals can channel fluid flow in the direction of cleavage, leading to directionally dependant permeability (Katsube et al., 1991).

Studies of coal porosity suggest that dual-porosity exists in the rock matrix with fluid flowing by advective and diffusive transport in macro and meso interconnected porosity (Clarkson and Bustin, 1999). Micro-pores have a diameter of > 3 nm (30 Å) whilst the diameter of a water molecule is 2.5 Å. Thus micro-pores water will be relatively stagnant with transport controlled by molecular diffusion. Pyrite associated with fractures or cleavage planes in a rock matrix will therefore contribute to leachate more rapidly than pyrite isolated within coal micro-porosity.

SEM examination of WC and WS showed that stagnant leaching of the WS cleavage edge lead to greater ingress of the pyrite oxidation front. Faster ingress of the pyrite oxidation front into the stagnantly leached WS was allowed by the greater influx of oxidant and higher permeability. Although dissolution rate tended to be similar from cleavage and whole sample leaching, the extent of pyrite oxidation was reduced in cleavage edge samples. Here the volume of dissolved oxidant was limited by diffusion over a smaller surface area and uptake by pyrite oxidation close to the exposed surface.

Dissolved O_2 can generally be expected to diffuse more rapidly along cleavage than across, a point supported by SEM observation of the pyrite oxidation front. In the WS

where cleavage permeability was higher than the WC and dissolved O_2 flux was faster, the pyrite oxidation front moved at a faster rate.

5.3.5.2.2 The effect of pyrite morphology on oxidation front

The effect of surface area on the predicted rate of pyrite oxidation has previously been discussed. Where several transitional stages in pyrite morphology, from organic framboids to more consolidated inorganic framboids exist (Kotenski and Kostova, 1995) the volume of oxidation product formed is difficult to estimate. However, greater surface area and structural porosity make framboidal pyrite more susceptible to oxidation. The position of pyrite i.e. isolated or clustered along cleavage planes has already been shown to affect its oxidation potential (section 5.2.1.2.2).

SEM investigation of pyrite oxidation revealed two fronts of pyrite oxidation, depending on morphology. In general the ingress of framboidal pyrite oxidation was more rapid and complete than that of consolidated pyrite framboids. Where the isolated framboids was totally oxidised within 316 days of stagnant leaching of the WS, consolidated framboids usually only showed oxidation at the edges. Both consolidated framboids and massive vein pyrite tended to form thick layers of Fe-sulphate or Fe-oxide. The presence of the clay and quartz matrix supporting the finer pyrite framboids lead to reaction and the formation of minerals such as alunogen and alunite. Finer pyrite crystals in framboids and the higher porosity of these structures led to their rapid oxidation to Fe-sulphate. Where larger consolidated framboids were associated with clay minerals in WS whole samples, the clay seemed to provide some protection against oxidation. In cleavage edge samples increased porosity of clays in the WC allowed further oxidation front ingress. The difference in clay phase protection of pyrite minerals is associated with the porosity of the rock matrix itself. Low porosity of the organic matrix in the WC compared to sediment rich areas encourage oxidant influx to pyrite associated sediment phase minerals. During burial diagenesis of the WS, clay minerals were more likely to seal pore spaces compared to minerals such as quartz under pressure. Associated sulphides may therefore be more protected than isolated sulphide minerals.

5.3.5.3   Dissolved oxidant and oxidation product transport and storage

5.3.5.3.1   Oxidant diffusion

Predicted Flux

Diffusion of dissolved O_2 has already been discussed in terms of the effect of rock cleavage on the pyrite oxidation front. Here the effects of diffusion and uptake of oxidant over the period of leaching are discussed. In the dry rock samples, advection in the reaction vessel on addition of leachate and capillary action controlled initial fluid-flow in the matrix. The rate of fluid entry into pore space depends on rock permeability, fluid viscosity and the pressures applied to the fluid. Submersion under vacuum did not lead to measurement of micro-pore space, in either coal or shale (Chapter 4). Rock saturation and the reactive surface area in contact with fluid, both potentially restricted to meso and macro-porosity, will limit pyrite oxidation. The exchange of oxidant and oxidation product from micro-porosity can be assumed to be infinitely slow.

Using the previously described Fick's first law it is possible to describe the influx of dissolved O_2 to a rock matrix. The effect of tortuosity and porosity on the diffusion coefficient of a rock matrix can be described by

$$D_{i(rock)} = D_{i(p)} \frac{\phi}{\tau_e^2} \qquad (5.9)$$

As tortuosity is difficult to measure, the formation factor (F), or electrical resistivity of a pure solution compared with the same solution associated with a rock matrix, is used instead, giving the relationship:

$$D_{i(rock)} = \frac{D_{i(p)}}{F} \qquad (5.10)$$

and the relation ship between F and ϕ_E is described by the Archie equation:

$$F = \frac{1}{\phi_E^m} \qquad (5.11)$$

where m is the cementation exponent, relating to the rock type (Katsube et al., 1991, Okelers, 1996). Typical F values for shales measured by Katsube et al., (1991) for effective porosity (ϕ_E) close to the coal and organic rich shale are given in Table 5.20.

Formation factor of a shale of similar ϕ_E is used instead of that of a coal, as no measurement of a coal F value has been made to the authors knowledge. Using a value of 2 x 10^{-9} m^2s^{-1} for the dispersivity of dissolved O_2 (Strömberg, 1996, Simms et al., 2000), leads to diffusion coefficients of 8.3 x 10^{-12} m^2s^{-1} for coal and 3.7 x 10^{-12} m^2s^{-1} for shale. Obviously this calculation assumes that the F values measured by Katsube et al (1991) are similar to the F values of the WS and WC.

Assuming that only the meso and macro-porosity of samples is saturated with Milli-RO water, the rock surface area will be exposed to 2.5 x 10^{-5} moles cm^{-3} of dissolved O_2. For coal and shale the effective porosity measured in Chapter 4 was attributed to meso and macro- porosity. As the F values are given for an effective porosity, the diffusion of O_2 is calculated for these pore sizes alone.

During pyrite oxidation the O_2 concentration will decrease due to uptake and a change in concentration will occur. Dissolved O_2 flux as a conservative tracer can be predicted using Fick's first law when depletion of pore water O_2 occurs, due to pyrite oxidation uptake (Schüring et al., 1997). The uptake of O_2 can be calculated over a period of time using the derived diffusion coefficients and O_2 uptake by pyrite oxidation using McKibben and Barnes (1986) rate reaction (Figure 5.43). Similarly the change in flux with distance from the water rock interface can also be calculated over time for saturation of macro-porosity (Figure 5.44). Uptake of dissolved O_2 decreases with time due to the depletion of oxidant and subsequent retardation of oxidation rate. As the diffusive flux of dissolved O_2 decreases exponentially with distance from the water-rock interface, central portions of rock should be the first regions deprived of dissolved O_2.

Over the time span of a year the total uptake of dissolved O_2 in pyrite oxidation is up to two orders of magnitude smaller than the starting concentration (Table 5.12). Significant dissolved O_2 depletion will occur due to pyrite oxidation over of tens of years. The time for depletion will probably be shorter due to underestimation of pyrite surface area and oxidation of the organic fraction of coal (Chang and Berner, 1999). Recharge of dissolved O_2 is far slower at ~10^{-14} mole cm^{-2} day^{-1} suggesting that under saturated conditions i.e. flooded tailings, pyrite oxidation will be limited after a period of time. Limitation of pyrite oxidation by dissolved O_2 uptake is in agreement with findings of column and field investigations (Blowes et al., 1991, Schüring et al., 1997).

In waste rock tailings and spoil heaps, water saturated rock will remove dissolved oxidant at a greater rate than predicted here. As the ratio of water to rock of spoil material is relatively lower than the ratio used in experiments here, O_2 depletion will be even faster in field or column scenarios.

Control by the rock matrix

A divergence occurs between calculated O_2 flux for WS and WC using macro-porosity or total porosity. When total porosity is used, the WC appears to have a greater flux, whereas using macro-porosity suggests that WS will have the greater recharge (Figures 5.44 and 5.45). As pyrite oxidation continues WC should be less weathered at depth, and generally less oxidised compared to the WS.

Effective Porosity (%) (analysed in Chapter 4)	Effective Porosity (%) (for shale Katsube et al., 1991)	Formation factor F (for shale Katsube et al., 1991)	Diffusion coefficient dissolved O_2 (m^2s^{-1}) $\left(\dfrac{D_{i(p)}}{F}\right)$
Coal - 4 ± 1	Shale - 3.78	541	3.7×10^{-12}
	Shale - 4.64	268	7.4×10^{-12}
Shale - 8.9 ± 0.7	Shale - 9.24	241	8.3×10^{-12}

Table 5.12. Effective porosity of WC and WS compared to effective porosity and formation factor (F) in shale measured by by Katsube et al., (1991). Diffusion coefficient of dissolved O_2 is calculated for each F value.
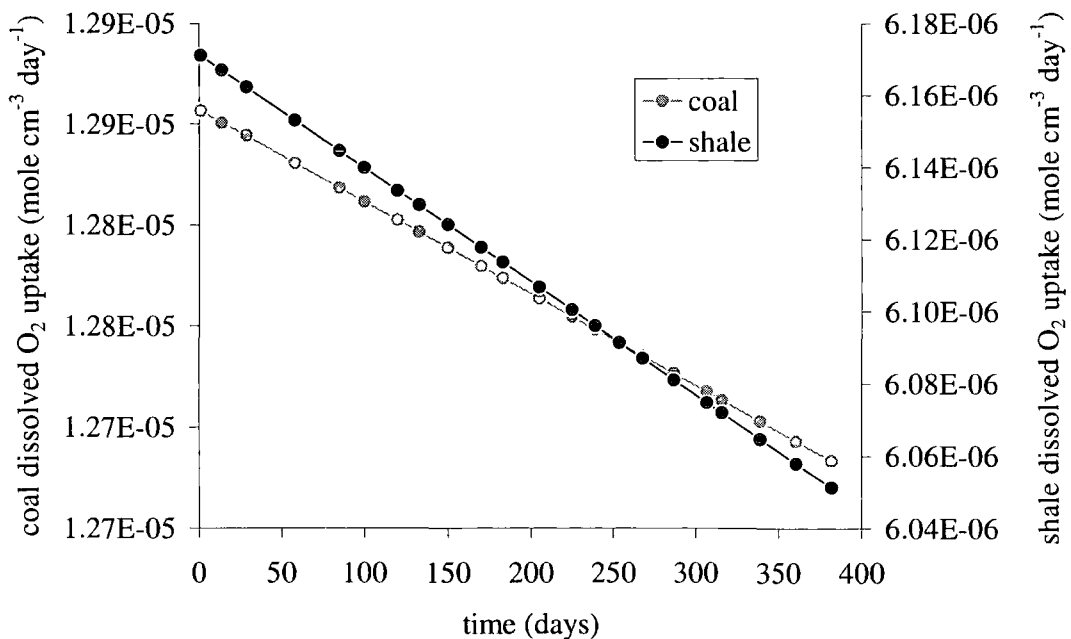
Figure 5.43. Calculated uptake per day of dissolved O_2 due to pyrite oxidation with no replenishment of O_2 concentration.

Rock type	O_2 (moles cm^{-3})	
	Starting concentration	Total uptake by pyrite oxidation over 382 days
WS	2×10^{-6}	6×10^{-8}
WC	3×10^{-7}	2×10^{-8}

Table 5.13. Calculated total O_2 uptake due to pyrite oxidation over 382 days.

The use of macro-porosity to calculate dissolved O_2 flux is supported by the higher oxidation rate of the WS compared to the WC with the higher pyrite content (Table 5.6).

Previously, it was suggested that depletion of oxidant in the outer regions and the low flux of dissolved O_2 may have limited pyrite oxidation at the centre of rock particles. Lack of dissolved O_2 influx was also blamed for the change in oxidation rate in the cyclically leached samples after 205 days. Total uptake of dissolved O_2 over the period of year was calculated for pyrite oxidation associated with 1 cm^3 of WC and WS macro and total porosity (Table 5.13). The loss of dissolved O_2 due to pyrite oxidation is significantly lower than starting concentrations, indicating that retardation of reaction rate can not be wholly due to oxidant depletion. As previously discussed, the blocking of surface sites by Fe^{2+} above pH_{pzc} (Moses and Herman, 1991) would explain the increase in Fe^{3+} oxidation below this pH.

Lack of oxidant in the centre of rock particles may instead be caused by the lack of macro-porosity further into the coal and shale samples. If only meso and macro-porosity were exposed to dissolved O_2 then initially pyrite associated with up to 8 % of the WS and 0.5 % of the WC was vulnerable to oxidation. The larger pores should be associated with fracturing, cleavage and cleat planes, mainly in the outer region of the rock. It possible therefore that the ingress of the pyrite oxidation front depends on the diffusion or interaction of influent leachate with micro-pores. As the typical micro-pore diameter is up to 30 Å and a water molecule diameter is 2.5 Å, interaction of micro-pores with leaching fluid will be very slow, being controlled by molecular diffusion. Swelling of clay phase minerals and the precipitation of oxidation product in the exterior region of rock samples would increase macro-porosity by fracturing. Therefore, the volume of rock exposed to dissolved O_2 will increase by sample physical weathering. Further ingress of oxidation front during stagnant leaching was probably allowed by combined micro-pore diffusion and macro-pore expansion. The lack of a sharp reaction front may be attributed to porosity differences in the rock matrix.

5.3.5.3.2 Oxidation product transport and storage

Despite the similar diffusivity and therefore flux behaviour of strong electrolytes such as SO_4^{2-} to dissolved O_2 (Strömberg, 1996), the release of these species depends on source i.e. mineral distribution. A high concentration of SO_4^{2-} will be present at each S containing mineral boundary. The concentration of such dissolved species will be highest at the water-rock interface due toe slower rates of to and from diffusion from sample centres, and the gradient between pore water and leachate concentration. Outer regions of samples are expected to contain high volumes of precipitation and low pH pore water. If leachate remains in contact with the rock, i.e. in stagnant leaching, and assuming conservative behaviour with no precipitation, such a gradient will eventually flatten. However in cyclic leaching, where dilute Milli-RO water mixes with concentrated pore water, the gradient remains intact, with continued pyrite oxidation and secondary mineral precipitation lowering pH (Table 5.14). Low leachate pH of WS and WC cyclic samples suggests that the H^+ concentration gradient was flattened in a week.

Saturation of a dissolved species should lead to it's precipitation. At equilibrium the solubility product (K_{so}) of a compound Me_aX_b is defined by;

$$K_{so} = \{Me^{b+}\}^a \{X^{a-}\}^b \qquad (5.12)$$

(Lumsdon and Evans, 1995). Comparison of the actual ionic activity product (IAP) gives the saturation index Q, which determines a solution's saturation or under-saturation with respect to a mineral phase (Stumm and Morgan, 1999).

$$Q = \log(IAP / K_{so}) \qquad (5.13)$$

Positive Q indicates a supersaturated solution, and a negative value reflects under-saturation with respect to the dissolved species of the original solid mineral phase. Saturation indices are more likely to be reached within the macro and meso-pore spaces (Lumsdon and Evans, 1995). Fracturing, by clay expansion during wetting and reaction with acidic pore water, increased sample macro-porosity and space available for observed precipitation in fractures. Portions of rock in direct contact with leachate were most susceptible to porosity increasing fractures. Flattening of the pH gradient over a week allowed precipitation of material within the sample. During dry periods remaining pore water would have also precipitated products by evaporation.

Dissolution of such soluble material and acidity produced by pyrite oxidation in the rock matrix lead to precipitation and further dissolution of material. Blowes and Jambor (1990) reported the control of tailings pore water chemistry by the precipitation, dissolution and re-crystallisation of Fe^{3+} mineral phases. Precipitation of amorphous Fe-hydroxides and sulphates e.g. schwertmannite releases acidity, as does subsequent dissolution and re-precipitation of more stable goethite or ferrihydrite (Bigham et al., 1996). Further dissolution and combination with alumino-silicate weathering products produces jarosite and natro-jarosite and further acidity. Simms et al. (2000) suggest that consecutive re-precipitation lowers water cover pH of flooded tailings. Cyclical formation and destabilisation of jarosite by fluctuating pH leads to long term storage of Fe^{3+} and sulphate at pH < 2.8 and Fe^{3+} release with goethite and ferrihydrite precipitation at pH > 2.8 (Bigham et al., 1996, Göttilicher and Gasharova, 2000). Such leachate pH buffering by jarosite dissolution and re-precipitation probably played a part in keeping leachate pH relatively low for the WS and WC (Göttilicher and Gasharova, 2000). Typically Fe-sulphate and Fe-hydroxides, coating pyrite close to sample edges or fractures during the initial 200 days of WC cyclic. Higher availability of K and Al from clay minerals in the WS led to earlier alunite and jarosite precipitation. After 205 days of cyclic leaching jarosite and alunite were the most common precipitants in both rock-types, usually forming at sample edges, around consolidated pyrite framboids and within fractures. Precipitation of jarosite and alunite releases twice the amount of H^+ compared to ferrihydrite and goethite, contributing to low leachate pH (Table 5.14).

Precipitation of Fe-sulphate on oxidised pyrite framboids was not removed as rapidly in stagnant leaching as in cyclic leaching. Stagnant leachate pH was usually 2-3 for WS and WC whole samples, suggesting that dilution by Milli-RO water was the main cause of dissolution of *in-situ* oxidation products. The decrease of *in-situ* oxidation product precipitation in cyclically leached samples was most likely caused by dissolution in dilute Milli-RO water.

Cleavage leaching of samples lead to precipitation of Fe-sulphate and jarosite precipitation at the exposed edge. Fracturing of the rock matrix at the water-rock interface suggests that precipitation was either very fast or that the volume of precipitation led to expansion.

Lower solubility and Fe^{3+} release during wetting for jarosite compared to ferrihydrite and goethite supports the association of retarded Fe^{3+} pyrite oxidation with jarosite precipitation, after 225 or 239 days WS and WC cyclic leaching (Table 5.14). It is probable that during this period the actual rate of oxidation was much lower than

calculated, with leachate content derived from the dissolution of secondary minerals. Jarosite precipitation, requiring a 3:2 ratio of Fe:S compared to the 1:2 release from pyrite oxidation, may account for the WC leachate Fe content change from nearly half the S concentration before to less than a third, after 205 days.

Mineral	Reaction	Log K_s
Goethite	$FeOOH + 3H^+ = Fe^{3+} + 2H_2O$	-1.0
Ferryhydrite	$Fe(OH)_3 + 3H^+ = Fe^{3+} + 2H_2O$	3.0 to 5.0[*]
Calcite	$CaCO_3 = Ca^{2+} + CO_3^{2-}$	-8.480
Dolomite (ordered)	$CaMg(CO_3)_2 = Ca^{2+} + Mg^{2+} + 2CO_3^{2-}$	-17.0
Siderite (crystalline)	$FeCO_3 = Fe^{2+} + CO_3^{2-}$	-10.89
Kaolinite	$Al_2Si_2O_5(OH)_4 + 6H^+ = 2Al^{3+} + 2Si(OH)_4^0 + H_2O$	7.435[*]
Gypsum	$CaSO_4.2H_2O = Ca^{2+} + SO_4^{2-} = 2H_2O$	-4.58
Barite	$BaSO_4 = Ba^{2+} + SO_4^{2-}$	-9.97
Melanterite	$FeSO_4.7H_2O = Fe^{2+} + SO_4^{2-} + 7H_2O$	-2.209
Alunite	$KAl_3(SO_4)_2(OH)_6 + 6H^+ = K^+ + 3Al^{3+} + 2SO_4^{2-} + 6H_2O$	-1.4[*]
Quartz	$SiO_2 + 2H_2O = Si(OH)_4^0$	-3.98
Jarosite	$KFe_3(SO_4)_2(OH)_6 + 6H^+ = K^+ + 3Fe^{3+} + 2SO_4^{2-} + 6H_2O$	-11.0[*][*]

Table 5.14. Log values of Ks for various minerals identified by XRD in the Pegswood coal-bearing strata, in Stumm and Morgan (1996), [*]Baron and Palmer (1996), [*] reaction with protons.

Pooling of acidic pore water in cleavage and stagnant samples led to an apparent increased oxidation in the lower region of samples. Flushing of surface material towards the sample base by the influx of fresh Milli-RO water increased precipitation and potential Fe^{3+} oxidation. Diffusion of O_2 through the epoxy-resin coating possibly also led to oxidation at the sample base. In stagnant leaching of cleavage edge samples evidence of pooling of metal enriched pore water was also observed, with oxidation of pyrite close to the sample base. Such movement of pyrite oxidation products is not accounted for by the SCM. In stagnantly leached rock the general flow direction is downwards, especially when along cleavage planes. Similar downward flow of

mineralised fluid is observed in tailings pore water and column leaching of spoil material (Blowes and Jambor, 1990, Simms et al., 2000).

5.3.5.4 Weathering reaction of other minerals.

Both clay and carbonate phase minerals were identified in the SEM examination of the WS and WC. Dolomite was usually found with a reaction rim of gypsum. The presence of dolomite appeared to increase local pore water pH, with reduced pyrite oxidation in the area surrounding 'pockets' of the carbonate. Clay minerals usually sorbed Fe in the early stages of leaching, possibly by the exchange of Fe^{2+} for Na^+. Later in leaching experiments, especially where leachate pH was below 4, sulphate exchange with positively charged clay surfaces occurred. Jarosite and alunite replaced or sorbed to clays, especially at the water-rock interface. Where clay was intimately associated with pyrite framboids reaction usually occurred.

Isolation of neutralising minerals such as dolomite and alumino-silicates led to a localised effect on pore water chemistry. The main buffering system, indicated by leachate pH, was the alumino-silicate phase. As pyrite oxidation in a carbonate-rich rock type was not examined it is difficult to speculate on the style of mineral leaching. From what was observed the result of localised neutralisation by dolomite was far more obvious than neutralisation by clay minerals. If jarosite and alunite are the products of clay neutralisation reactions then the lack of homogenous distribution also supports localised neutralisation. The faster rate of carbonate dissolution and the probable existence of calcite as cement, rather than a discrete phase may have lead to more uniform reaction throughout the sample.

5.3.5.5 Rock weathering under different water-rock regimes

Previous investigation of weathering of spoil and mine tailing material suggests that the vadose zone is split into three sub-horizontal zones with respect to pyrite oxidation (Figure 5.2). Cyclic and stagnant leaching of waste rock particles was performed to simulate water-rock regimes within each zone of spoil material. Cyclic leaching represented the style of water-rock interaction within the region of active oxidation in the vadose zone of spoil and intact rock (Blowes and Jambor, 1990). At the capillary fringe of the water table wetting and drying of rock fluctuates depending on the level of the water table. Kerth and Wiggering (1990) compared wetting and drying cycles of waste rock material to freeze thaw cycles in rock weathering. Both physical and

chemical weathering would therefore be expected to be important during cyclic leaching.

Stagnant leaching mimicked rock weathering beneath the water table, in saturated conditions and in flooded tailings. Flooding of tailings has been used extensively in the mining industry as preventative measure against AMD formation. Flooding waste rock has been shown, both column and field examples, to reduce pyrite oxidation compared to untreated sites (Schüring et al., 1997, Simms et al., 2000). AMD formation in flooded tailings is limited by the low diffusivity of dissolved O_2. Depletion of dissolved O_2 also retards the replacement of Fe^{3+} by further Fe^{2+} oxidation (Moses and Herman, 1991). As secondary mineral dissolution and precipitation in flooded spoil material and tailings usually controls cover water chemistry, the manner of pyrite oxidation may eventually be irrelevant.

In cyclic leaching pyrite oxidation fronts in the WS and WC remained close to the water-rock interface suggesting a limiting factor. The decrease in macro-porosity towards the centre of the rock samples would have retarded the influx of leaching fluid, and therefore the influx of dissolved O_2. Oxidation by Fe^{3+} was apparent, though limited by depletion due to uptake in the oxidation reaction and jarosite precipitation after clay weathering. Oxidation product dissolution also occurred by pore-water dilution in the outer part of samples. Cyclically leached samples contained more fractures towards the end of leaching, caused by the expansive precipitation of Fe-sulphate and hydroxides in macro-porosity.

Contrarily, stagnant leached samples appeared more chemically weathered, retaining *in-situ* oxidation products until Milli-RO water was added to prevent evaporation. Leachate pH produced by stagnant leaching of WS and WC was lower than produced during cyclic leaching. Jarosite formed during stagnant leaching suggesting that low pH was buffered by the precipitation of this and other Fe^{3+} minerals. Observation of the pyrite oxidation front at up to 8-10 mm into stagnant samples suggests that water-rock interaction period was sufficient for leachate diffusion into micro-porosity. Physical weathering by clay swelling was not as obvious in these samples, although surface jarosite and alunite precipitation caused localised fracturing.

Although the leaching of individual waste particles may not have reproduced natural conditions as well as a column of material, similar controls over leachate chemistry were present. In the active oxidation zone pyrite oxidation is limited by the influx of leaching solution. Physical weathering by swelling of clays and precipitation of oxidation products is important, increasing surface area available for reaction. Lack of

removal of *in-situ* oxidation products led to the greater weathered appearance of stagnantly leached samples. Once the active oxidation zone moves further into spoil material, perhaps on lowering of the water table during dry periods, a large volume of *in-situ* oxidation material may be available for removal.

Stagnant and cyclic leaching of all rock types is compared to flow-leaching of the same materials in Chapter 6. Processes controlling leachate chemistry in spoil heap and rock strata are discussed there.

5.4   Conclusions

Comparison of in-situ pyrite oxidation with predicted oxidation rates for pyrite alone

After accounting for under-estimation of surface area and prior oxidation product, *in-situ* pyrite oxidation rates were within range of predicted rates from pyrite oxidation alone. Secondary minerals such as jarosite and gypsum controlled leachate chemistry, as well as direct dissolution of pyrite oxidation products. Similar control has been shown in field and column experiments suggesting that Fe^{3+} pyrite oxidation in flooded tailings is probably not significant (Blowes and Jambor, 1990, Simms et al., 2000).

Shrinking core model of pyrite oxidation relative to the actual ingress

Although the observation of a pyrite oxidation front in WS and WC samples, agrees well with the SCM, a greater flux of material is removed along compared to across cleavage planes. Similarly the influx of dissolved oxidant (and oxidation front) is faster along cleavage. Previous predictions of the exponential slowing of the pyrite oxidation front in spoil material are also true at the particle scale (Schüring et al., 1997). Dissolved oxidant influx is initially limited by restricted movement into micro-pores rather than by the depletion of O_2 by pyrite oxidation.

The effect of pyrite content and morphology on weathering

Pyrite morphology also affected oxidation front ingress, with framboidal pyrite being more susceptible to rapid surface oxidation. Consolidated and massive pyrite usually formed layers of Fe-sulphate precipitation, which were initially only partial coatings. McKibben and Barnes (1986) have previously noted concentration of reaction at pyrite surface regions of high energy.

Although high pyrite content generally increased Fe and S release, differences in rock matrix porosity, introduced by clays in coal and shale, led to lower WC oxidation

rate. Lower porosity of the organic rich coal matrix retarded fluid transport and therefore oxidation rate, even when pyrite content was highest in the WC.

Oxidant influx and dissolved product transport controls over pyrite oxidation and leachate generation.

In coal-bearing strata rapid transport within macro and meso-porosity and slow diffusive transport within micro-porosity effectively control the oxidant flux. The rate of diffusion of oxidant will not limit the rate of pyrite oxidation during the period of a year, especially under water-rock regimes where there is an influx of dilute leachate.

Precipitation of oxidation products usually occurs *in-situ* unless pore water pH is low enough to retain dissolved salts in solution. Where dissolved oxidation products are transported to the sample surface, the sharp pH gradient between the ambient leachate and rock pore-water encourages precipitation. The proximity of these secondary minerals to the ambient leachate suggests that their dissolution will contribute to leachate chemistry. Goethite and ferrihydrite precipitation may dissolve and re-precipitate as jarosite, releasing further acidity. Jarosite dissolution due to increasing pH will lead to the precipitation of ferrihydrite. It is probable that changes in leachate chemistry are controlled by the output of pyrite oxidation, especially in the early stages, and then by the precipitation of secondary Fe^{3+} hydroxides.

Variations of rock type and water-rock regime

Weathering of varied coal-bearing strata demonstrated the dependence of leachate chemistry on mineral solubility, pore water chemistry and pore size distribution. Neutralisation of acidity produced during pyrite oxidation depended upon the manner of distribution of clay and carbonate phases.

Stagnant and cyclic leaching of rock samples lead to different extents of physical and chemical weathering. Cyclic leaching removed a higher magnitude of soluble material although the pyrite oxidation fronts did not ingress as far as in stagnant samples. Dissolution of *in-situ* oxidation products by dilute leaching solution was most prominent in cyclically leached samples. High removal rates in vadose zones of spoil and rock strata are attributed to the greater influx of O_2 to the un-saturated rock. At the particle scale, physical weathering, rapid oxidation product removal and a constant dissolved O_2 supply increased apparent rates of oxidation. Oxidation product build-up during stagnant leaching suggests that seasonal fluctuations of the water table will lead to their cyclic removal and precipitation. Similarly, weekly fluctuations in water table due to meteoric precipitation will lead to a shorter cycle of leachate concentrations.

Chapter 6

Experimental leaching of coal-bearing strata using flowing water.

6.1 Introduction

Although oxygen concentration has been identified as the main control on sulphide weathering in waste rock, water is an essential transport mechanism for oxidants and pollutants (Moses et al. 1991, Elberling et al., 1994, Noël and Ritchie, 1999). The supply of water and therefore oxidant strongly depends on the water-rock regime. By identifying different water-rock regimes associated with various parts of a column of *in-situ* rock or rock waste, factors controlling AMD formation can be investigated.

Water-rock regimes in rock strata and spoil material are customarily divided into sub-horizontal zones dependent upon water saturation (Figure 5.2). Fluid within the upper unsaturated zone is most likely to be meteoric, unless perched aquifers or pooled surface water exist. Flow is usually assumed to involve the effective porosity of the waste rock. In reality, the volume and uniformity of flow events also control the manner of water percolation. Dual porosity of material becomes important during transient flow, with fractures and large pore spaces receiving most of the flux (Noël and Ritchie, 1999). Preferential flow-paths caused by fractures, vegetation and heterogeneous layering in the spoil may also lead to deviations from the modelled situation. The non-uniformity of the natural environment is often a problem in scaling from experimental lab to field conditions (Malstrom et al., 2000).

Field and model investigations of sulphide weathering both suggest that most oxidation occurs within the unsaturated vadose zone of spoil heaps and mine tailings (Blowes and Jambor, 1990, Elberling et al., 1994). Meteoric water and groundwater provide the transport mechanism for metals and sulphate derived from easily soluble salts formed during oxidation. Percolating water travels downwards, pushing a plume of acidic water forward which is buffered by mineral weathering in the lower reaches of spoil (Blowes et and Jambor, 1990, Bain et al., 2000). During plume progression soluble products from the reaction zone are flushed through towards the capillary fringe. In the capillary zone water a thin film of water is retained around the rock particles and pore spaces. Increasing the volume of water decreases capillary potential will decrease, leading to flushing of pore fluids into the saturated rock pore water body. Temporal fluctuations in the water table height lead to wetting and drying cycles in this zone. In the underlying saturated material, flow is controlled by the hydraulic gradient.

The final leachate may form a plume of pollutant within groundwater or is discharged into the local water catchment (Blowes and Jambor, 1990). Fluctuations in water table position can also initiate dissolution of secondary weathering minerals, leading to contamination of groundwater (Figure 5.3, Younger, 1998).

Chemical reactions along the flow-path of percolating fluids can be modelled using various reactive transport software packages such as MINTRAN and RATAP (Wunderly et al., 1996, Destouni et al., 1998, Bain et al., 2000). However the style of particle weathering, i.e. secondary mineral location, pyrite oxidation front movement and physical weathering effects are rarely extensively investigated. Factors such as drying period, water volume and time and style of exposure to water are known to affect the chemical evolution of AMD (Morin and Hutt, 1994). The effect of these factors has been investigated by numerous authors in column experiments of varying proportions, (e.g. Strömberg, 1997, Hornberger and Brady, 2000 [review], Elberling and Damgaard, 2001, Simms et al., 2001). Column experiments and field studies tend to investigate large chemical reactions leading to AMD formation without addressing particle scale processes which form the basis of these reactions. Similarly in the numerical prediction of AMD quality, waste particle scale processes are usually ignored or generalised in order to simplify models (Wunderly et al., 1996).

In Chapter 5 *in-situ* pyrite oxidation in coal-bearing strata under semi-static to static water-rock regimes was used to monitor diffusive transport in saturated and capillary zone conditions. In this chapter a series of experiments, designed to explore the effect of advective transport on *in-situ* pyrite weathering, are described. Morin and Hutt (1994) identified elapsed drying period, flush volume along and geochemical production rates as controlling factors in waste-rock pile seepage chemistry. To simulate mineral weathering in the flow path of an oxidizing fluid an experiment was designed where a block of coal was exposed to a constant flow of Milli-Q water for a period of 6 weeks. The experiment was then expanded to cover a variety of rock types and different regimes. The importance of varying dry periods, flushing volume and flushing media in flow-path reactive transport is investigated here. Analysis of water-rock regime control over leachate chemistry is carried out using ANOVA to identify significant effects. The findings of direct observation and ANOVA are combined to provide a robust interpretation of data.

In Chapter 8, a comparison of the total and elemental flux from all water-rock regimes, including static and cyclic-leaching, is made with a final comparison with varying leachate quality from an AMD site (Chapter 7).

6.2   Flow-leaching experiment

6.2.1   Introduction

The objectives of this investigation were to:

o   Monitor pyrite oxidation front ingress under flow-leaching conditions

o   Compare embedded pyrite oxidation rates with those predicted from experimentally derived rate constants on pyrite alone

o   Investigate the controls on rock weathering along flow paths under varied conditions including intermittent flow, varied flushing media and rock type.

o   Compare the findings of the investigation with phenomena observed in the natural environment.

The rock-types described in section 5.5 were used. Each rock type was exposed to flowing water either once a day or once a week. Blocks of rock were arranged such that outflow from an upper sample ran over the exposed surface of a lower sample. Leaching was carried out over a period of 163 days (5 months), equivalent nearly to half the time of the static leaching experiments. The results of this experiment are described in the following sections. The rate of removal of weathering products and the oxidation rate of pyrite in flow-leached samples is compared to that of statically leached rock. The flow of water over the surface of the rock samples makes this experiment comparable to conditions in the upper portion of the un-saturated vadose zone.

6.2.2   Methods and Materials.

Rock samples from the same group of four types used in static leaching were used in this experiment. The rock type descriptors in this chapter are WC – weathered coal, WS - weathered shale, UWC - un-weathered coal, UWS - un-weathered shale. The methods and results of chemical and mineralogical analyses can therefore be found in sections 5.5.1 and 5.5.3. The preparation of samples was the same as described in section 5.5.1. After cutting to a uniform block shape, the mass and dimensions of each rock sample was measured and recorded. Each sample was then set in epoxy resin with one cleavage perpendicular surface remaining exposed. The sample was then set inside a 4 x 2.5 x 1.5 cm PVC mould using more epoxy resin as adhesive. The sample was arranged so that the exposed surface of the rock was flush with the edges of the mould. The mounted samples were then slotted into a perspex grid, designed to hold one sample above another (Figure 6.1). The arrangement directed the flow of mineralised
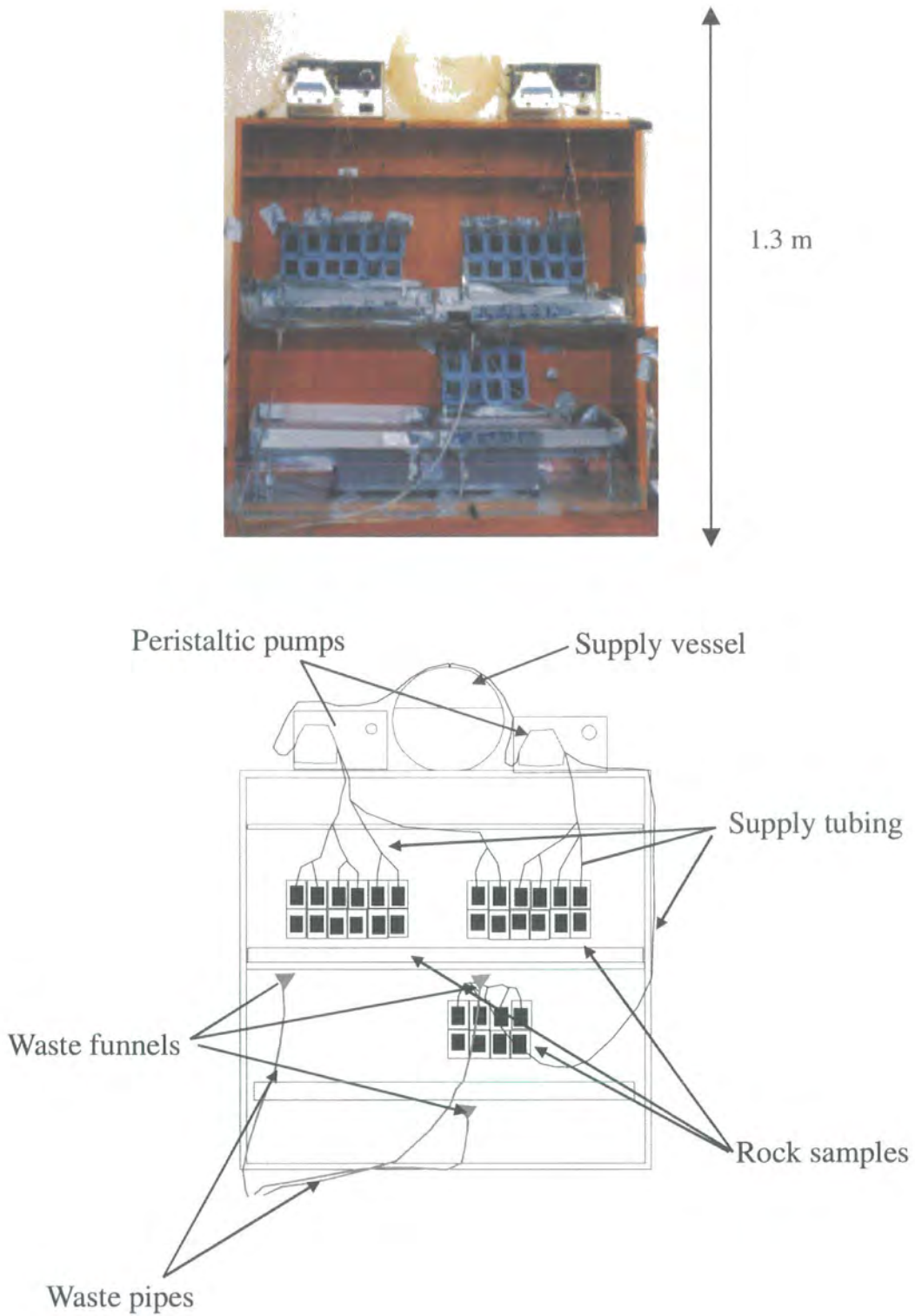
Figure 6.1. Experimental set up for flow leaching experiment for four different rock-
types.

water from the upper sample onto the sample below allowing investigation of weathering of a rock by mineralised waters. Each perspex grid panel held six samples, allowing duplicate samples from three rock types per panel. A teflon tube (0.8 mm i.d.) was secured to the to the upper edge of the top sample. The other end of the tubing was placed in the supply vessel filled with Milli-RO water, via a peristaltic pump head. The flow between tubing differed due to tubing length, peristaltic pump head cartridge arrangement and difficulty in calibrating speeds for two separate pumps. Therefore flow rates varied between 1mL min^{-1} and 0.01mL min^{-1}. However as this difference in flow rate usually varied depending on the set up of tubing and pump cartridge, most samples underwent fast and slow flow rates. In order to bring some uniformity to the experiment, the first 25 mL of outflow water was collected, whatever the flow rate. This meant that in theory each rock sample was exposed to a similar volume of water, albeit for a different period of time. Thus upper samples would be exposed to 50mL water and lower samples to 25mL water at each sampling point. Sampling of outflow usually took place once a week for both flow regimes. Otherwise daily flushed rock samples were leached with flowing purified water for at most 30 minutes each day.

Part of the collected leachate was acidified with concentrated HNO_3 and analysed for major element chemistry by ICP-OES. The pH of the un-acidified portion of the sample was measured and recorded using a Whatman bench pH meter, calibrated with buffer solutions at 4 and 7 prior to use. After 163 days of leaching, the samples that showed most reaction were allowed to dry and then cut perpendicular to the exposed surface. The cut surface was then prepared for SEM examination.

One of the objectives of the experiment was to examine the effect of flushing rock with mineralised water. Chemical characterisation of the flushing media was necessary to provide a starting point from which final leachate chemistry could be subtracted. To characterise inflow chemistry to the lower samples, outflow of upper and lower sample of UWS were collected at the start and end of an hour of flushing with Milli-RO water. This process was also carried out for lower samples of all rock types, which were flushed daily and weekly, in two consecutive weeks.

6.2.3   Results and Interpretation

Blank corrected mean values of major element leachate concentration and pH from the period of flow-leaching are presented in Tables 6Ci-iv for UWS, 6Di-iv for UWC, 6Ei-iv for WC, 6Fi-iv for WS (Appendix II - Results). Reported concentrations are corrected for sample mass and given in mgL^{-1}g^{-1}, i.e. concentration per gram of rock

sample. A detailed description of leachate evolution is given in Appendix II Results along with plots of chemical evolution, and a description of the difference between upper and lower sample outputs. Here a summary of leachate evolution is given in terms of the behaviour of Fe, S and Ca.

6.2.3.1 Separating inputs to the lower outflow

Before a description of the major element patterns displayed by rock leachate can be made, the actual contribution of the lower sample to leachate concentration should be quantified. To quantify the input of dissolved material from the lower samples to the total outflow leachate the chemical evolution of the upper outflow with time was investigated. On three separate occasions during leaching, 25 mL of upper and lower, or just lower outflow was sampled at either end of an hour of flushing at 0.01-1 mL min^{-1}. Leachate was sampled over the leaching period for: -

- **_Case 1_** - Upper and lower outflows from the UWS replicates on the first day of flushing

- **_Case 2_** - Lower out-flow from daily samples after 5 and 14 days of leaching

- **_Case 3_** - Lower out-flow from weekly flushed samples after 14 days of leaching.

Case 1 - Upper and lower outflows from the UWS replicates on the first day of flushing

Initial UWS upper and lower leachates contained Ca, Fe, Mg, Na, S and Si either at the start or end of leaching (Table 6.1). Lower outflow dissolved content was greater than upper sample outflow content at the start and end of flushing. Major element concentrations in the upper outflow varied between 0 and 0.09 mgL^{-1}, whereas lower outflow content ranged between 0 and 0.5 mgL^{-1}. Variation in mineral content of the upper and lower UWS replicate samples could have led to greater output from the lower sample. However, the cumulative dissolved content of upper and lower sample outflows should be greater than upper outflow content alone, assuming no precipitation from the upper outflow occurs.

The upper sample's leachate had relatively little solute at the end of the hour long leaching period chemistry (Table 6.1). The lower leachate still contained soluble species after an hour. Therefore, in this preliminary case, lower sample output was directly related to lower leachate content at the end of the leaching period. The exception to this was Na, whose increase in the final upper leachate may be attributed to

170

cation exchange. The lower sample outflow contained little Na over the whole period of leaching.

UWS	Ca	Fe	Mg	Na	S	Si
Initial upper	0.09	0.00	0.00	0.00	0.02	0.00
Final upper	0.00	0.00	0.00	0.09	0.00	0.00
initial lower	0.50	0.09	0.09	0.00	0.47	0.01
final lower	0.16	0.00	0.03	0.00	0.12	0.01

Table 6.1. Major element concentrations (mgL^{-1}) of outflow from one pair of UWS replicates for the initial and final part of an hour long flushing period, as described in Case 1.

Case 2 - Comparing lower leachate evolution in the first and second weeks of daily flushing.

Lower outflow dissolved content decreased during daily flushing in the first two weeks of flow-leaching. The largest drop in major element concentrations occurred in the first week (Figures 6.2 to 6.5, Table 6.Bi, Appendix II Results). A maximum drop of 0.09 $mgL^{-1}g^{-1}$ in K was recorded over the hour of leaching of the daily flushed WC (Figure 6.2). Similar decreases in concentration were shown by Ca and S from the UWS, WS and UWC (Figures 6.3-6.5). In the second week of daily flushing outflow chemistry showed little change in element concentration over the period of wetting (Table 6B, Appendix II Results). Overall concentrations were much lower in the second week than those of the first week of daily flushing. The greatest decrease was from 0.02 $mgL^{-1}g^{-1}$ to 0.00 $mgL^{-1}g^{-1}$ of Ca from the UWC (Figure 6.5). In the first week of daily flushing a large proportion of soluble matter was dissolved during the initial flushing. Low dissolved concentrations in the lower sample outflow, during the first week of daily flushing, suggest that background levels of dissolution were taking place. In the second week of daily flushing the lower sample leachate content was greatly reduced compared to the first week (Figures 6.2 - 6.5). The fall in lower sample leachate dissolved concentration over the 1 hour period of flushing was of lower magnitude during the second week compared to the first week of daily flushing. However, for most elements dissolved concentration remained steady over the leaching period, suggesting that most of the soluble phase was removed during the first week of

daily flushing. Subsequent flushing released background levels of dissolution derived from mineral weathering and dissolution of the remaining soluble phase.

If the style of outflow chemical evolution during the second week is representative of subsequent daily flushing, outflow concentrations should only decrease with time. The difference between lower and upper outflow content will represent the minimum input of the lower sample to lower outflow.

Case 3 - Comparing weekly flushed WS and WC lower outflows.

A decrease in outflow content was observed over the hour of leaching of weekly flushed WS and WC samples, during the second week (Table 6.2). The greatest drop of 0.07 mgL^{-1}g^{-1} was in S concentration for both rock-types. Concentrations of Ca, Fe, Mg and Zn also fell over the leaching period. High concentrations relative to daily flushed samples suggest that soluble phase dissolution was occurring into the second week of weekly flushing. As the outflow concentration did not increase over the hour long leaching period, the evolution of leachate chemistry is similar to that of daily flushed samples. The difference between upper and lower outflow chemistry will give the minimum lower sample dissolution for weekly flushed samples. Outflow pH, in all cases presented here, increased over the period of leaching. This pH rise indicates that dilution during flushing of soluble matter was important in outflow chemical evolution.

	Ca	Fe	Mg	Na	S	Zn	pH
WS start	0.02 ± 0.01	0.03 ± 0.01	0.01 ± 0.00	0.00 ± 0.01	0.09 ± 0.05	0.01 ± 0.00	5.40 ± 0.72
WS end	0.00 ± 0.00	0.01 ± 0.00	0.00 ± 0.00	0.00 ± 0.00	0.02 ± 0.01	0.00 ± 0.00	6.47 ± 0.18
WC start	0.02 ± 0.02	0.03 ± 0.04	0.01 ± 0.01	0.00 ± 0.01	0.08 ± 0.10	0.01 ± 0.02	5.49 ± 0.76
WC end	0.01 ± 0.00	0.00 ± 0.00	0.00 ± 0.00	0.00 ± 0.00	0.01 ± 0.01	0.00 ± 0.00	6.50 ± 0.12

Table 6.2. Initial and final lower outflow solute concentrations (mgL^{-1}g^{-1} $\pm$ 1σ, n=2) for all weekly flushed samples, in the second week of flushing, as described in Case 3.

The chemical evolution of upper and lower flushed coal-bearing strata leachates is summarised in the following sections. A more detailed description is provided in Section 6 of Appendix II Results, with the minimum lower sample input also described there.

6.2.3.1.1 Summary and Interpretation of UWS flushing

Outflow chemistry of both upper and lower samples was dominated by the dissolution of Ca and S from gypsum and dolomite (Figure 6.6). Mineral phases dissolved from the UWS samples were gypsum and dolomite, with possible cation exchange releasing Na and K to solution. The upper outflow chemistry affected the final lower leachate, with the combined inputs evolving more smoothly than the reaction between Milli-RO and UWS alone. However, the lower sample also imparted a chemical signature to the lower leachate. Correlation between dissolved content and low pH was identified for both outflows. Upper outflow chemistry sometimes lead to conflicting lower outflow pH and dissolved content (Figure 6.6). Such conflicts may occur in large-scale flow systems where high dissolved content and high pH actually relate to different zones of the same system. In such a situation the dissolved content of a leachate would relate to the time available for precipitation on raising of pH.

For all UWS water-rock regimes the greatest volume of material was dissolved during the initial 80 days of flushing. During this period isolated peaks broke up relatively smooth background concentrations. Volumetric expansion of the high clay content in the UWS, initiated by wetting, led to the eventual failure and fracturing of the rock. Slaking with rapid exposure of a larger surface area to flushing explains isolated peaks in concentration. Most UWS replicates developed single deep fractures or numerous shallow cracks. As replicates were treated similarly the slaking rate between UWS samples would have been similar, with fracturing probably occurring early in the flushing process.

In the second half of the flushing experiment dissolution from all UWS regimes fell, except from the weekly flushed lower UWS which continued to release Ca and S. Continued release from the weekly flushed lower sample was probably due to slower and gentler flushing leading to less physical weathering.

6.2.3.1.2 Summary and Interpretation UWC

Removal rates of solute from the UWC by flow-leaching were very low (Figure 6.7). Although Ca and S were most consistently present in solution the trends of release followed by these analytes did not correlate. Combined mineral sources of Ca and S were weathered in order to produce differing trends in behaviour. Calcite and pyrite are the most likely mineral sources for Ca and S. However, the overlap in output from these minerals would make any calculation of pyrite oxidation rate difficult. Any Fe

produced in this reaction would have been precipitated as Fe-hydroxide at the typical solution pH observed in these experiments (Figure 6.7).

6.2.3.1.3 Summary and Interpretation of WS flow-leaching

Intermittent flushing of the WS sample with Milli-RO water and upper sample outflow consistently produced dissolved Fe, S and Ca. During the first 70 days of daily and weekly flushing it was noticed that the output of Fe, S and Ca was concurrent (Figure 6.8, Table 6E and F, Appendix II Results). After this point peaks in dissolution Fe and S tended to precede that of Ca (Table 6E and F Appendix II Results). This pattern of element output suggested that during the first half of the experiment the wash-out of prior weathering products was dominant. However, leachate evolution in the second half of the experiment was dominated by weathering products of experimental pyrite oxidation.

The lower weekly flushed outflow contained the greatest concentration of elements, with the presence of Al and Si in late stage leachate indicative of clay weathering (Table 6F, Appendix II Results). Jarosite and natro-jarosite dissolution was also identified after the first intensive sampling period of the upper samples. As intensive sampling involved certain daily flushing, oxidation products formed during previous drier periods were being leached. Although K, Na, Fe and S were also present in lower sample outflow, their presence may have been a remnant of upper outflow chemistry. Other peaks in upper leachate chemistry were identified in lower outflow. However upper and lower WS samples usually released a similar volume of dissolved matter (Figure 6.8).

Mineral phases contributing to solution chemistry were pyrite, gypsum, calcite and dolomite. It is likely that intermediary secondary weathering minerals such as jarosite and natro-jarosite formed during weekly drying-out periods of the WS

6.2.3.1.4 Summary and Interpretation of WC flow-leaching

Upper and lower daily flushed and lower weekly flushed WC outflow contained low concentrations of all analytes, although Fe, Ca and S were most consistently present (Figure 6.9, Tables 6G and 6H, Appendix II Results). Flushing of soluble matter in the first 20 days of the experiment caused any initial peaks in Fe, Ca and S. The start of intensive sampling usually coincided with increased concentrations for the upper daily flushed WC. This can be attributed to the greater flow of water during these supervised flushing periods. Changes in lower outflow pH and chemistry were closely related to

upper outflow fluctuations (Figure 6.9). Lower outflow chemical evolution reflected the additive nature of consecutive upper and lower sample leaching. Orange staining of the lower WC samples and supporting PVC mould also suggest that precipitation of secondary minerals was occurring.

6.2.3.2 Analysis of WS and WC sample weathering using SEM-EDAX

Although interpretation of leachate chemical evolution led to identification of weathering processes such as precipitation, visual inspection should provide confirmation.

After drying out, one replicate of each treatment of WC and WS samples was selected for investigation using various SEM techniques. Rock samples were split perpendicular to the exposed face, in the direction of flow. The cut face was set in a resin block, highly polished then carbon coated prior to examination (Appendix I Methods). Here, the same method of oxidation identification described in Chapter 5 (section 5.3.4) is used. In order to identify weathering caused by the flow of water at one surface of the examined samples, sections were divided into three portions parallel to flow direction. Each section was scanned in the direction of flow to find the extent of the oxidation front. Other phenomena looked for were the styles of pyrite weathering and the manner of storage and transport of oxidation products.

6.2.3.2.1 Daily Flushed WS

Upper WS – flushed daily with Milli-RO

The examined section of daily Milli-RO flushed WS had an estimated pyrite content of up to 10% (Figure 6.10). At the top of the exposed surface the extent of framboidal and massive pyrite oxidation decreased away from the point of oxidant influx. In the upper part of the examined section, massive pyrite had rims with elevated Fe and O K^{α} at least 200 μm away from the exposed surface. Oxidation was only identified on the exposed edge side of framboids at 500 μm into the sample. Locally fractures were filled with Fe-sulphate. At 1 mm into the sample, collected spectra from pyrite framboid rims had elevated O K^{α} and no elevated Fe peak. Pyrite within a clay band 2 mm into the sample showed little oxidation, however the kaolinite matrix had sorbed Fe. Along the same band, at 8 mm into the sample, oxidation was identified on the edges of pyrite grains furthest from the sample's exposed face. This suggests that transport of oxidant to these grains came from the direction of the sample's upper corner, opposite to the actual point
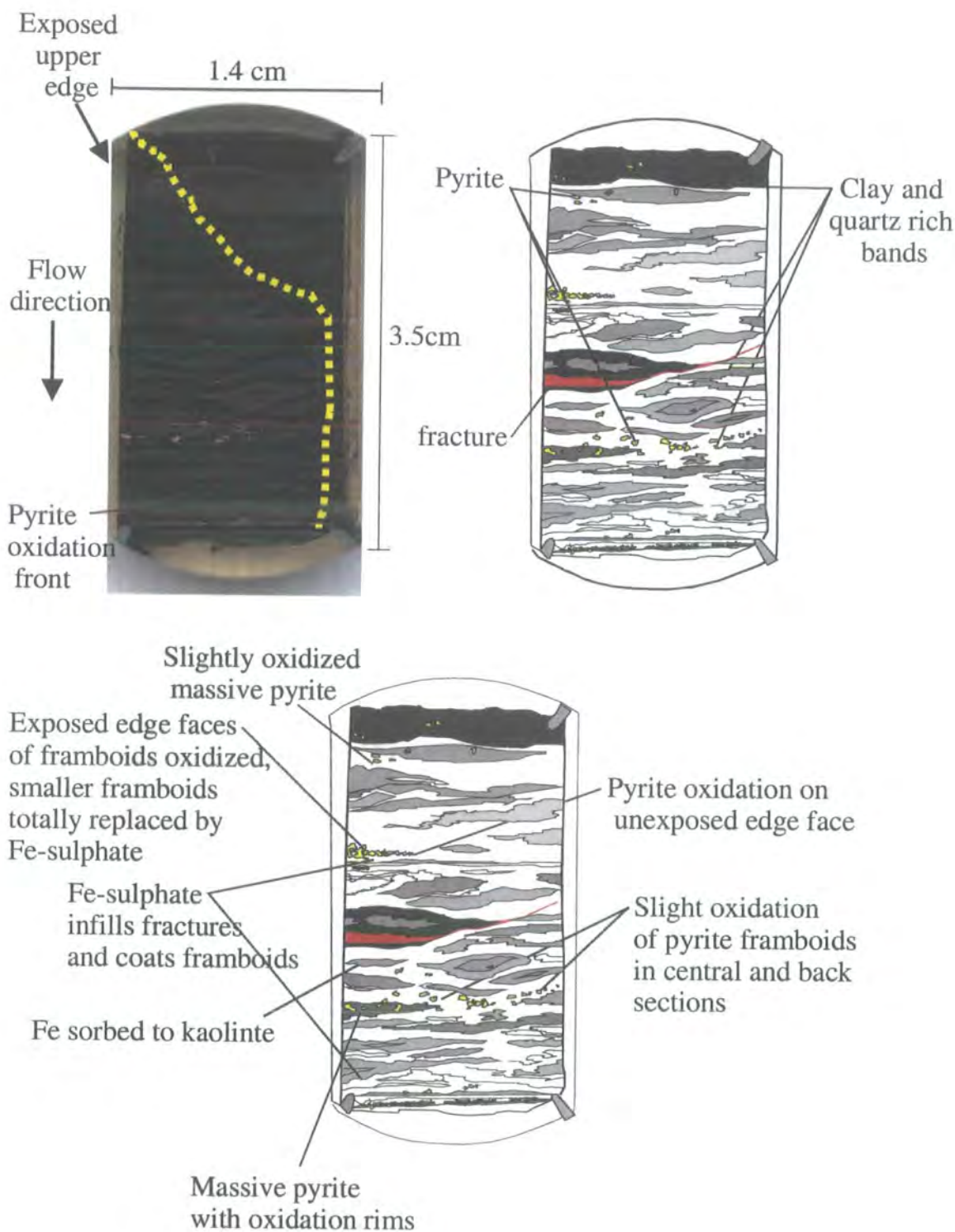
Figure 6.10.　Cross section of upper daily flushed WS sample showing scanned examined section with dimensions and estimated pyrite oxidation front (top left), lithological description (top right) and description of weathering extent (bottom).
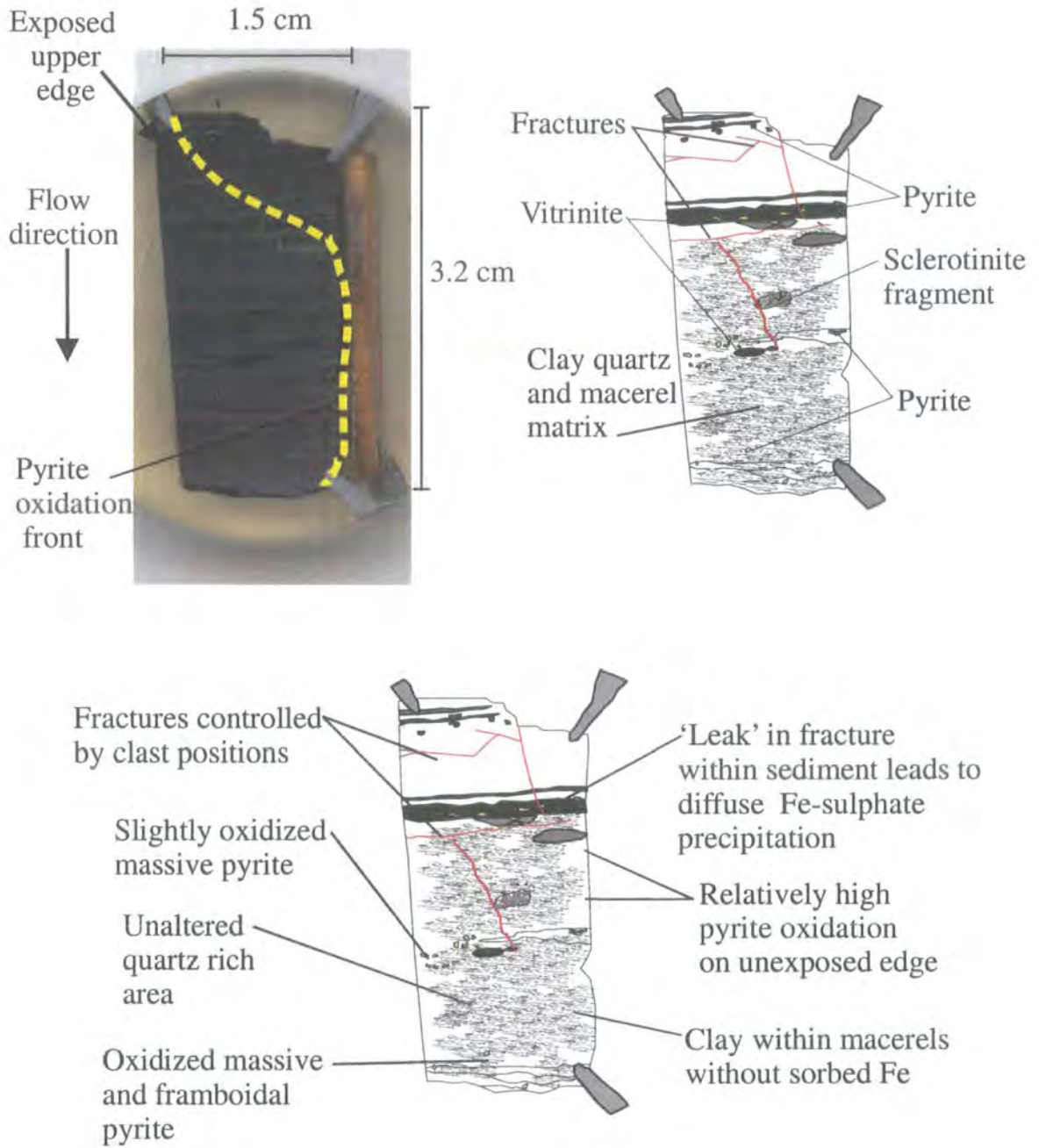
Figure 6.11. Cross section of lower daily flushed WS sample showing scanned examined section with dimensions and estimated pyrite oxidation front (top left), lithological description (top right) and description of weathering extent (bottom).

of water influx. However, within this upper corner, at the back of the sample pyrite was not oxidised. Examined sections only show part of 3 dimensional processes within the whole sample. It is therefore probable that lateral oxidation caused the apparent influx of oxidant from the un-exposed edge of the sample.

At 13 mm down the exposed face massive pyrite grain edges were slightly oxidised and 200 μm into the sample Fe-sulphate filled fractures and precipitated on framboids. At the bottom of the exposed face pyrite oxidation was comparatively low with isolated framboids being most affected. In the back and central portions of the examined section, 24 mm from the upper surface, pyrite framboids were only slightly oxidised. This suggests that only middle and lower parts of the sample closest to the exposed face were greatly affected by oxidation.

Lower daily flushed WS

Fracturing played an important role in oxidant and dissolved oxidation product transport within the examined section of daily flushed WS (Figure 6.11). A 100 μm wide sub-horizontal fracture traversed the sample in the upper zone of the exposed edge almost bisecting the rock. Before reaching the opposite side the feature joins a perpendicular fracture and continues into the centre of the sample. The perpendicular fracture probably propagated from a small area of kaolinite and pyrite situated close to the back edge of the sample. Swelling of the clay may have lead to fracturing parallel to the exposed face of the sample. Where the fracture went through the clay and pyrite zone, Fe-sulphate was deposited within the surrounding pore space and onto clay minerals. The exposed face of the sample face shows little precipitation of oxidation products. Affected pyrite had oxidation product deposited on the side of the un-exposed sample face. Pyrite oxidation was comparatively high at the un-exposed sample face with Fe-sulphate precipitation at the edge. From this un-exposed face pyrite oxidation extended at least 5 mm back into the sample. The described fracture directed oxidizing fluids into the centre and back of the rock. Oxidation from the exposed face of the sample was side stepped with oxidation possibly by Fe^{3+} occurring at the un-exposed face of the sample. In fractured samples exposed surface area is enlarged providing a greater reactive surface and potentially higher leachate loading.

Upper exposed edge

1.6 cm

Flow direction

3.9 cm

Pyrite oxidation front

Pyrite

Sporinite

Clay, quartz and macerel matrix

Illite lens on exposed edge replaced byFe-sulphate

Framboids oxidized, yet massive pyrite enclosed in unaltered illite shows no oxidation

Edge pore space and fractures filled with Fe-sulphate

No apparent pyrite oxidation, pore space filled with Fe sulphate

Oxidation at exposed edge

Crust of jarosite and barite on unexposed edge Pyrite oxidation only occurs close to unexposed edge

Variably oxidized pyrite framboids in central section

Figure 6.12. Cross section of upper weekly flushed WS sample showing scanned examined section with dimensions and estimated pyrite oxidation front (top left), lithological description (top right) and description of weathering extent (bottom).

6.2.3.2.2 Weekly Flushed WS

Upper WS – flushed weekly with Milli-RO

In the upper portion of the weekly Milli-RO flushed WS, an illite lens was completely replaced by Fe-sulphate at the exposed edge of the section examined (Figure 6.12). Original structures within the clay were retained. A further 670 μm into the sample, the original illite with sorbed Fe exists. At the same height, 1-3 mm into the section, pyrite framboids were variably oxidised whilst massive pyrite associated with a Fe-free illite showed no oxidation.

At 20 mm down the exposed surface, pore spaces were filled with Fe-sulphate, yet massive pyrite had no oxidation product at its grain boundary. This suggests that pore water pH was too low to allow precipitation until evaporation forced deposition. Alternatively little *in-situ* pyrite oxidation may have occurred. Instead precipitation of Fe-sulphate from flushed pore water may have replaced the clays surrounding the massive pyrite. The exposed surface sides of pyrite grains at 500 μm into the sample at the same height were oxidised indicating the occurrence of pyrite surface oxidation. Combined evaporation and precipitation at the exposed surface probably lead to the Fe-sulphate matrix surrounding pyrite at the exposed surface.

A further 10 to 15 mm down the surface exposed to flowing water Fe-sulphate was precipitated. However, 200 μm into the sample, even pyrite framboids show no sign of oxidation. A massive pyrite band closer to the exposed edge also shows no oxidation, with only isolated framboids being affected. Precipitation of Fe-sulphate at the exposed surface appears to have protected interior pyrite grains against oxidation. At 2 mm from the base of the exposed face massive pyrite was oxidised at the exposed edge. This suggests that at up to 100 μm into the sample pyrite oxidation occurred, beyond this oxidant infiltration was retarded by Fe-sulphate precipitation. At the top of the central portion of the sample a large, 2 mm wide lens of massive pyrite was surrounded by kaolinite with very little sorbed Fe or oxidation present. The middle and base of the central portion of the examined section contained variably oxidised pyrite framboids. Centrally positioned pyrite was not totally protected against oxidation by the exposed surface Fe-sulphate precipitation.

Jarosite and barite were precipitated from the upper to lower regions of the unexposed edge of the section furthest from the influx of oxidant. The layer of oxidation product on the unexposed edge does not extend into the sample as is typical at

Upper exposed edge

1.7 cm

Flow direction

Pyrite oxidation front

Sub-vertical cleavage in Clay, quartz and macerel matrix

3.7 cm

Clay

Pyrite

Fractures

Lithic clast surrounded by vitrinite

Massive pyrite with rims of oxidation

Framboids oxidised on exposed side edge

Pyrite surrounding fracture has oxidised rims

Fe-sulphate sorbed to clays

Framboids surrounded by clay are less weathered

Fracture filled with Fe-suphate

Oxidation products sorbed to clays within 3 mm of unexposed edge

Framboids oxidized throughout

Framboids oxidized on exposed edge side

Figure 6.13. Cross section of lower weekly flushed WS sample showing scanned examined section with dimensions and estimated pyrite oxidation front (top left), lithological description (top right) and description of weathering extent (bottom).

the exposed edge. Physical weathering at the exposed surface formed fractures and increased pore space allowing precipitation inside the rock matrix. At the unexposed edge of the section no physical weathering would have been possible. Weathering at the back of the sample suggests that pore fluids were channelled into the upper part of the sample. This fluid then percolated down into the sample leading to low oxidation in the central regions of the rock.

Lower WS – flushed weekly with rock leachate

The cleavage direction in the weekly leachate flushed lower WS sample was sub-vertical with bands of pyrite running parallel (Figure 6.13). At the top of the sample, 50 μm from the exposed edge, massive pyrite grains within a band had rims with elevated Fe and O K^α peaks. Nearby pyrite framboids were also oxidised at the rim only. At 2 mm into the sample from this point, oxidation products were identified the on exposed edge side of framboids.

At 10 mm down the flow-path of leachate, massive pyrite was oxidised on the side adjacent to the exposed edge. Below this point pyrite had rims of oxidation product at up to 50 μm from a fracture that was sub-horizontally traversing the sample. Framboids within 200 μm of the fracture were oxidised. On the unexposed face of the sample, and the other end of the fracture, oxidation products were sorbed to clays. At the unexposed lower corner of the sample, framboids were oxidised on their exposed edge side. Above this corner, pyrite framboids were oxidised throughout. In the upper unexposed corner, pyrite framboids within clay with sorbed Fe and Mg were less oxidised. For these pyrite grains only elevated O K^α indicated the presence of weathering.

6.2.3.2.3 Daily flushed WC

Upper WC – flushed daily with Milli-RO.

Examination of a cross-section of the daily Milli-RO flushed WC replicate revealed relatively low pyrite content (>1%) within an organic macerel rich matrix (Figure 6.14). Pyrite was usually framboidal with typical framboid diameter less than 50μm. Other minerals present were quartz, kaolinite, illite and Ti-oxide.

Pyrite within 5mm of the exposed face was oxidised or had been completely removed, possibly during polishing. Where framboids remained, their O K^α peak was elevated over that collected from 'un-oxidized' pyrite. Within the central portion of the examined section smaller, isolated framboids were the most oxidised pyrite phase. In

Upper exposed edge

1.8 cm

Flow direction

3.5 cm

Vitrinite

Sporinite macerels

Clay

Pyrite oxidized 5mm from exposed edge

Fracture contains Fe-sulphate sorbed clays

Unexposed section framboidal pyrite slightly oxidised

Small pyrite framboids within central section are most oxidised

Jarosite precipitation on exposed edge
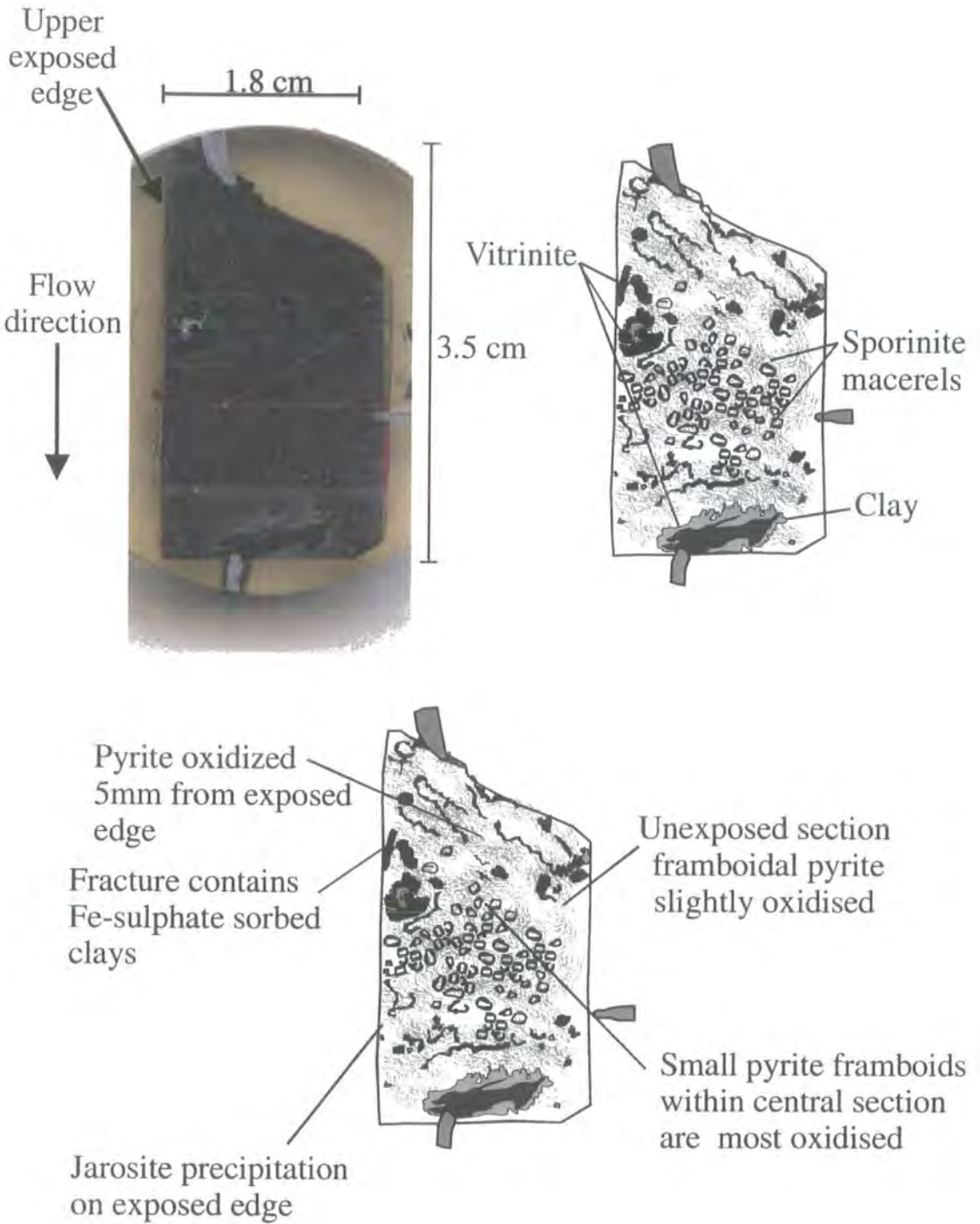
Figure 6.14. Cross section of upper daily flushed WC sample showing scanned examined section with dimensions (top left), lithological description (top right) and description of weathering extent (bottom).
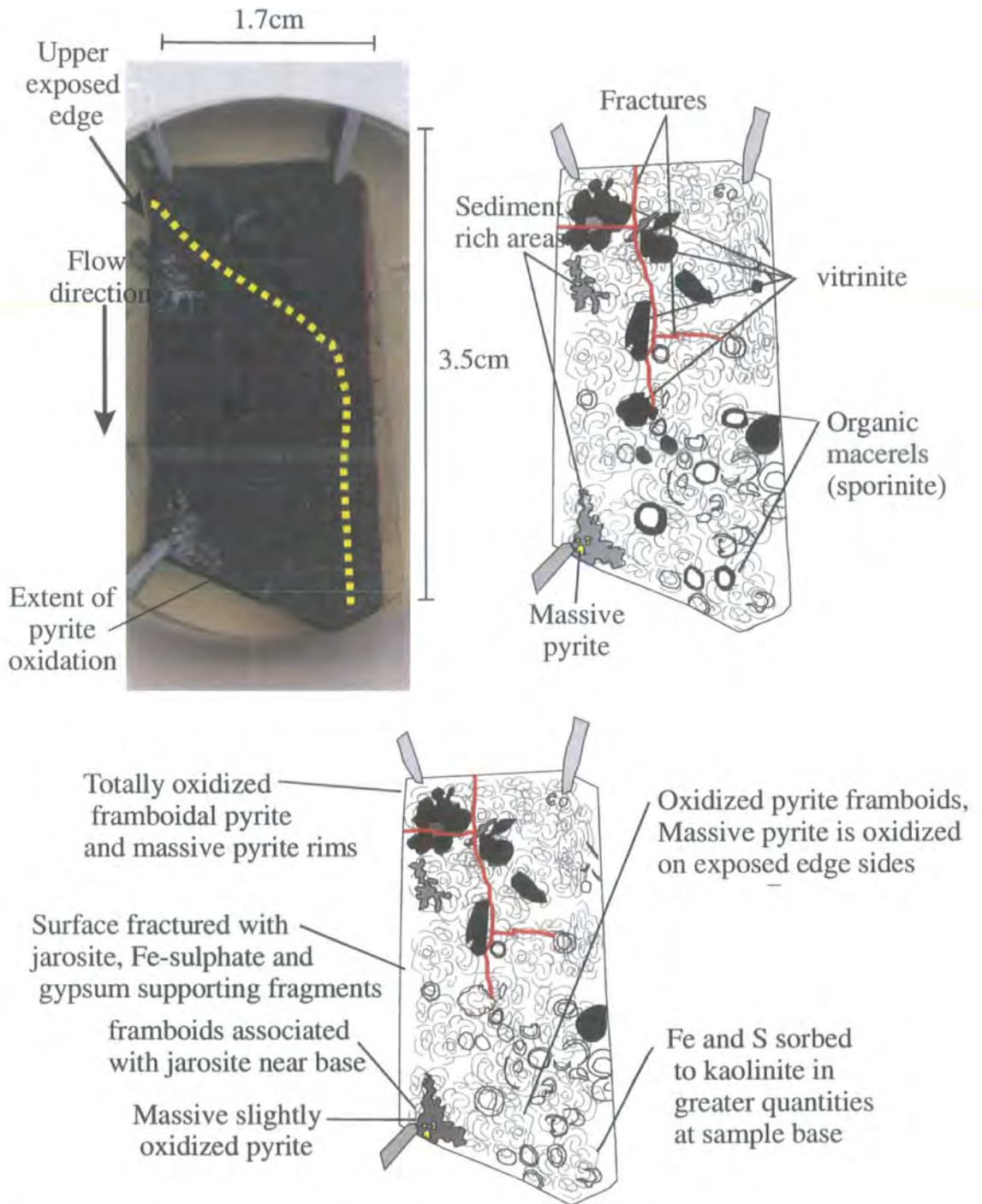
Figure 6.15. Cross-section of lower daily flushed WC sample showing scanned examined section with dimensions and estimated pyrite oxidation front (top left), lithological description (top right) and description of weathering extent (bottom).

the un-exposed section of the sample, furthest from flowing water, framboidal pyrite was slightly oxidised.

Precipitation of jarosite $(KFe_3(SO_4)_2(OH)_6)$ and alunite $((KAl_3(SO_4)_2 (OH)_6)$ were suggested by the presence of Fe, S, Al, K, O and Si (Figure 6.14). Alternatively surficial illite may have sorbed dissolved Fe and SO_4^{2-} from pore fluids containing these species. A fracture close to the upper part of the sample contained S, Fe, Al and Si. Untreated samples of the coal-bearing strata often contained fractures filled with kaolinite or illite (Chapter 5). Silicates precipitated during burial diagenesis of the rock probably weathered to form these clay phases. Sorption of Fe and S to clays suggests that pore fluids enriched with dissolved elements were channelled through connected macro-porosity such as fractures. Diffusive transport of Fe and S from areas of high to low concentration at the exposed surface was enhanced by advection caused by flowing water. Close to neutral pH Milli-RO water probably encouraged precipitation at the exposed edge of the rock. Scarcity of pyrite and heterogeneity of its distribution in this sample made it difficult to define the position of any oxidation front.

Lower WC – flushed daily with rock leachate.

In the WC replicate flushed daily with upper sample leachate, framboidal pyrite was totally oxidised within 100 μm of the exposed surface (Figure 6.15). Massive pyrite in the same zone was associated with relatively high O K^α peaks. Towards the base of the exposed surface and the adjacent 100 μm of sample, framboids were associated with jarosite. The exposed surface was fractured and mineral grains were supported in a matrix surrounded by jarosite, Fe-sulphate and gypsum. Also in this region of the sample a 1-2 mm area of massive pyrite surrounded by clay and quartz showed oxidation in parts. The central portion of the sample (6 mm from the exposed edge) contained partially oxidised pyrite framboids. The portion of sample adjacent to the un-exposed face contained illite and kaolinite with sorbed Fe and S. However in the upper part of this portion the clay phase displayed lower Fe and S K^α peaks. This indicates that less Fe and S was available for sorption in the upper part of the sample. Evidence for pyrite oxidation in the upper part of the sample occurred at 12 mm below the upper edge and up to 2 mm from the back edge.

Upper exposed edge

1.7 cm

Flow direction

3.8 cm

Pyrite oxidation front

Clay and quartz in matrix

Clay and quartz

Sporinite

Vitrinite

Kaolinite not associated with Fe

Clay in upper central and back sections unaltered

Massive pyrite oxidized on exposed edge side

Framboids variably oxidized within upper 20 mm of central section

Below 20 mm of central section massive pyrite oxidized on exposed egde side and Fe sorbed to clays

Fe sorbed to illite

Figure 6.16. Cross section of upper weekly flushed WC sample showing scanned examined section with dimensions and estimated pyrite oxidation front (top left), lithological description (top right) and description of weathering extent (bottom).

6.2.3.2.4 Weekly flushed WC

Upper WC – flushed weekly with Milli-RO

Within 400μm of the exposed edge of the Milli-RO flushed WC sample, pyrite weathering lead to parts of grain edges having elevated Fe K^α (Figure 6.16). The upper portion of the examined section contained up to 30% quartz and kaolinite, the latter of which was not associated with Fe. At the bottom of the sample's exposed edge, illite had sorbed Fe. Massive pyrite grains were also oxidised on their exposed edge side. Collected spectra from the oxidised pyrite showed elevated Fe K^α peaks. Framboids began to show elevated O K^α at 3 mm into the section. Similar variable oxidation of framboids was identified at 15mm down the un-exposed edge of the sample. At 20 mm down the sample, i.e. two-thirds of its length, massive pyrite was oxidised on the exposed surface side. Clay minerals at the top of the central and back portions contained no Fe, yet 20 mm further down the sample Fe was sorbed to illite. Oxidation and sorption patterns in the examined section suggest that oxidant transport within the rock were controlled by water flux. The greatest oxidation occurred within the middle to lower regions of the sample. The upper corner of the sample furthest from water flow-path was least affected by oxidation.

Lower WC – flushed weekly with rock leachate

The examined section of the WC sample flushed weekly with upper sample outflow had a greater pyrite content than the upper sample (Figure 6.17). Pyrite was oxidised through the sample, especially at both exposed and un-exposed faces. The exposed face exhibited a fracturing to 100 μm into the sample. The resultant angular grains were supported in a Fe-sulphate rich matrix in a similar manner to the weekly flushed lower WC sample. Here again physical weathering of the sample's exposed face lead to increased porosity.
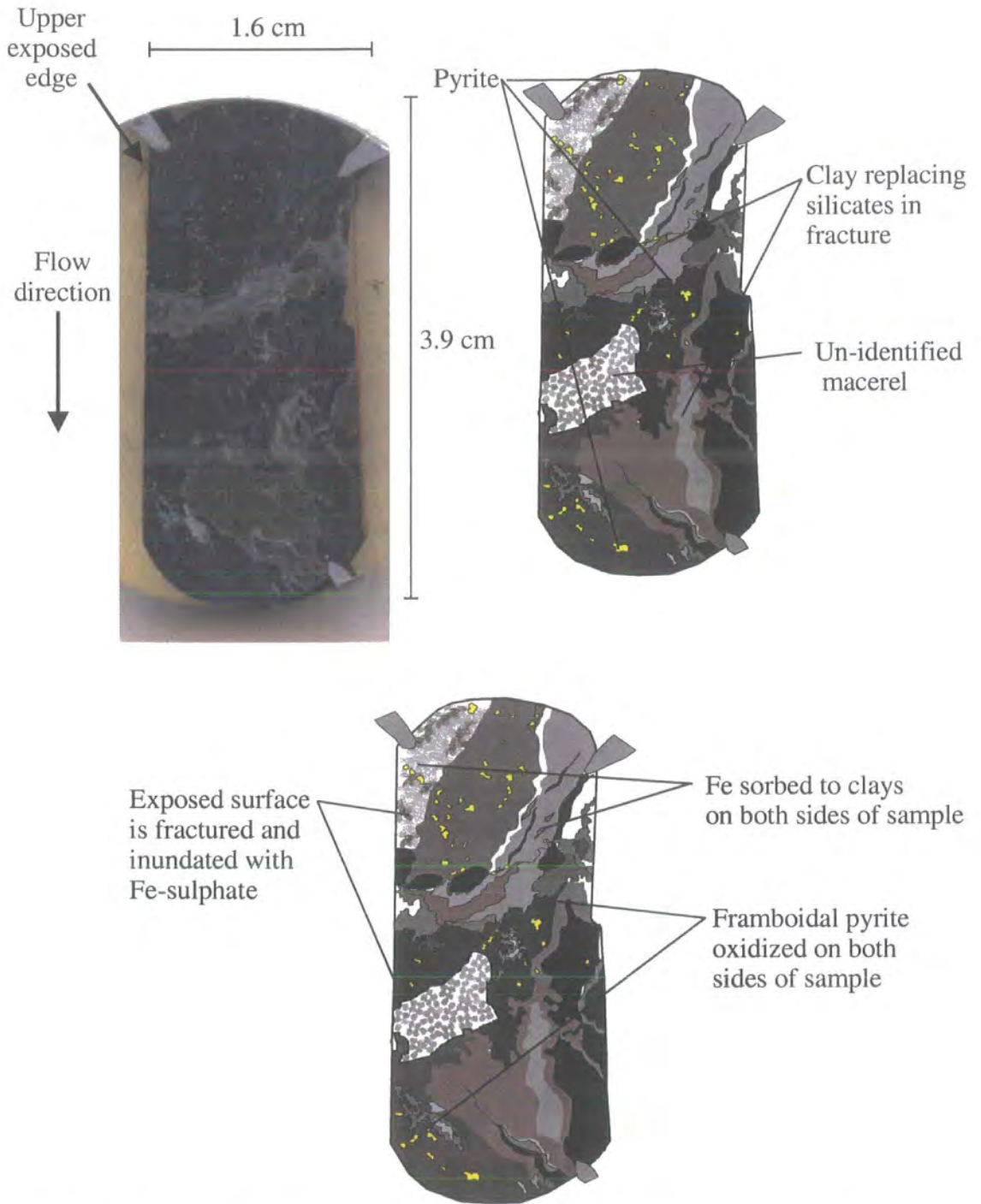
Figure 6.17. Cross section of lower weekly flushed WC sample showing scanned examined section with dimensions (top left), lithological description (top right) and description of weathering extent (bottom).

6.2.4 Discussion of Flow-leaching Experiments

Primary objectives of this study were to test model and predicted pyrite oxidation rates and oxidation front ingress, whilst investigating the effects of pyrite morphology and dissolved product transport mechanisms. In addition to these potential controls over leachate quality, the importance of dry period, flush volume and flush media were also examined.

Discussion of the controls over flow leachate chemical evolution is divided into two main parts. Initially the chemical processes controlling leachate chemical evolution are interpreted. In this section the extent of reaction with flowing water and the importance of ion exchange, dissolution, sorption and finally pyrite oxidation are considered. Pyrite oxidation rates and oxidation front ingress are treated in the same manner as in Chapter 5.

Further analysis of the control of leachate chemistry by water-rock regime is carried out using ANOVA. The factorial design of the flow-leaching experiment suggests that a two-way model can be used to compare the effect of pairs of variables on each element concentration. Combined statistical testing and direct interpretation of data should provide a more robust overall interpretation than either method alone.

6.2.4.1 Processes occurring during surface flushing

Flushing experiments were performed primarily to investigate individual waste rock particle scale *in-situ* pyrite oxidation with a continual flux of water. However, chemical processes such as ion exchange, dissolution, precipitation, sorption and physical weathering are also important factors in rock leachate evolution. Analysis of these processes was not possible in Chapter 5 as leachate was allowed to reach a pseudo-steady state with respect to mineral dissolution and precipitation. During leaching with a constant flow of dilute Milli-RO water, ion exchange and dissolution become more significant. During flushing the rock pore water is not allowed to reach an equilibrium position with respect to dissolution and precipitation by the leaching solution. As the influent Milli-RO water and upper sample leachate composition is well characterised, any deviation from this composition after leaching can be interpreted as a source or a sink process. Identifying and quantifying the dissolved contribution of processes such as ion exchange, dissolution and sorption should allow the quantification of potential experimental pyrite oxidation.

6.2.4.1.1   The extent of water-rock reaction

SEM investigation of WS and WC samples showed that most reaction occurred adjacent to the exposed edge. In all cases the corner opposite to the leachate in-flux point was least affected, supporting predicted partial sample reaction. The reporting of sample dissolution in units of concentration per g of original sample should be affected by partial sample reaction. Reported leachate concentrations in $mgL^{-1}g^{-1}$ will be lower than actual values, due to the correction made for whole sample mass when only 90% of that mass actually interacts with leachate. Although original sample mass was around 20 g, SEM examination suggests that at most 15-18 g was involved in reaction, making reported values at least 75% of actual values. As reported leachate dissolved concentrations are low, any difference caused by the correction for mass should not be significant. As partial reaction should have been of a similar magnitude for the UWC, WC and WS, chemical evolution should remain the same.

Total flux comparison

Total dissolved flux values were corrected for partial collection of the daily leachate and for volume of water passing over the surface of upper and lower samples (Table 6.3). Deviation from the actual mass of material removed during flow-leaching will involve under-estimation of water volume used in leaching and over-estimation of number of samples uncollected. The daily flushed total fluxes should therefore be the most inaccurate values.

	Daily leaching total corrected flux (mgg^{-1})	Weekly leaching total corrected flux (mgg^{-1})
UWS upper	0.44 ± 0.05	0.06 ± 0.01
UWS lower	0.29 ± 0.05	0.03 ± 0.00
UWC upper	0.27 ± 0.02	0.02 ± 0.00
UWC lower	0.15 ± 0.01	0.01 ± 0.00
WS upper	0.69 ± 0.08	0.05 ± 0.01
WS lower	0.52 ± 0.09	0.06 ± 0.01
WC upper	0.36 ± 0.02	0.03 ± 0.01
WC lower	0.28 ± 0.03	0.06 ± 0.01

Table 6.3. Total element content in mg per g of sample of the acid leachable phase, cumulative total mass (mgg^{-1}) dissolved during weekly and daily flow-leaching. Daily cumulative values are estimated using actual output recorded for 23 samples to cover the output over 163 days. Both upper and lower values are corrected for the volume of water passing over the surface of the rock i.e. 50 mL for upper samples and 25 mL for lower samples.

For the different water-rock regimes and rock type, several patterns can be observed (Table 6.3). Daily flushing produces a larger difference in total flux from the un-weathered rock types upper and lower samples than from the weathered rock types. Weekly flushing produces greater mass of dissolved material from the lower samples of weathered rock type compared to the upper sample. Un-weathered rock types still release less dissolved matter from lower samples during weekly flushing. Possible causes of this difference between rock type lower samples dissolution may be an original higher soluble phase or pyrite oxidation. In the UWS gypsum is the main soluble phase whereas secondary minerals will supply the soluble content of the WS and WC. Dissolution of these phases should follow the same pattern of gypsum dissolution in the UWS. If pyrite oxidation were producing soluble material in the lower sample at a higher rate than in the upper sample, this would account for the greater total flux of material from the WS and especially the WC. The increase in total flux only applies to weekly flushed rock, suggesting that precipitation in the lower sample must also occur and contribute to the greater output from this sample.

6.2.4.1.2 Non-sulphide chemical sources and sinks along flow-path

Lower outflow contained matter from upper and lower samples and should therefore have the greater content. Any dissolved species with a higher concentration in the upper outflow either has a lower leachate sink or a source the upper sample (Figure 6.18). Ion exchange, dissolution, pyrite oxidation product precipitation and sorption may have all affected upper and lower sample dissolved flux of Fe, S, Ca, K, Na, Mg and Si.

Ion exchange

Flow leached rock types typically contained kaolinite, illite, albite, quartz, gypsum, pyrite, dolomite, calcite and siderite (Table 5.4, Chapter 5). Milli-RO water blank samples usually contained up to 1 mgL^{-1} of all analytes, especially K, Na, Ca and Si, providing ions which would exchange with Ca^{2+} and Mg^{2+} (Stumm and Morgan, 1996).

Cumulative dissolved Na from daily and weekly flushed UWC, UWS and daily flushed WC was greater in the upper leachate than the lower leachate (Figure 6.18). Ion exchange may explain the loss of Na. All rock-types contained kaolinite and illite, both of which have low cation exchange capacities (CEC, Stumm and Morgan, 1996). Masking of Ca exchange by gypsum dissolution would have been especially true of the UWS leachate, where Ca and S dominated the solution chemistry, yet Na expulsion

197
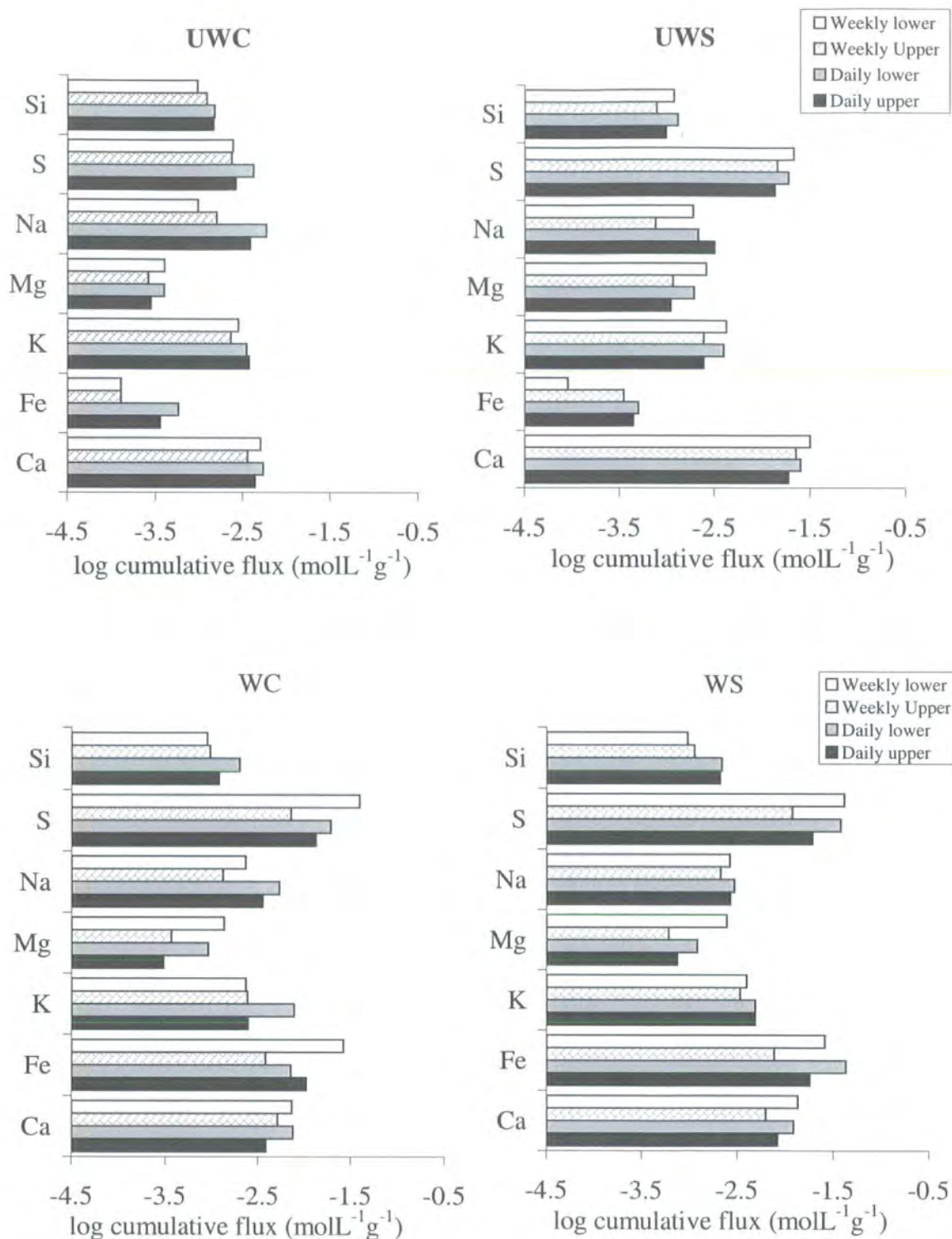
Figure 6.18. Log cumulative flux of major elements (molL-1g-1) over the period of
             daily and weekly flushing of all rock-types with Milli-RO water (upper)
             and mineralised water (lower).

would not be masked. Albite, (Na, K [Al Si_3O_8]), detected by XRD in the UWS and UWC, may have potentially exchanged Ca^{2+} for Na^+. The combined CEC of albite, kaolinite and illite would increase Na^+ expulsion compared to ion exchange with the clay minerals alone.

Dilution of the reacting solution increases ion exchange selectivity in clays and their affinity for bivalent over monovalent ions (Stumm and Morgan, 1996). Thus flushing with dilute Milli-RO water, compared to sample leachate, would lead to greater ion exchange of dissolved Na^+ and K^+. Separation of lower sample input to total leachate indicates that Na output from upper samples decreased in the second week of flushing. Lowering of Na output due to ion exchange maybe caused by reaching of the upper limit sample of exchange capacity available during flow-leaching.

Sorption

Sorption of Fe and SO_4^{2-} to clays was apparent from SEM examination of WS and WC sections. The most common clay mineral in the WC and WS was kaolinite although illite was also present. The CEC of kaolinite is the lowest of all clays, implying that Fe had probably been absorbed or adsorbed to the clay surfaces. The presence of Fe at the centre of clay particles suggests the former. Lack of sorption on clay in areas unaffected by oxidant influx and within organic macerels suggests that this process was initiated during experimental flushing. Changes in pH caused by SO_4^{2-} sorption were probably swamped by dilution and acidity from sulphide oxidation.

6.2.4.1.3 Pyrite oxidation

Pyrite oxidation rates

In Chapter 5 the rate of pyrite oxidation was calculated using the dissolved S concentration as a proxy for sulphate from the WS, WC and UWC. Treating flow leachate concentrations in the same manner produced the mean rates for the period of daily and weekly leaching shown in Table 6.4. A value is not calculated for the UWC as gypsum dissolution was thought to influence dissolved sulphate more than in the WS and WC during flow-leaching. Overall secondary mineral leaching will lead to error in calculated rates of pyrite oxidation, yet these figures are useful as a comparison with predicted rates of oxidation. Oxidation rates calculated per g or m^2 of original pyrite from flow leachate S concentrations were between ~$1 \times 10^{-13 \cdot 12}$ and $1 \times 10^{-11 \cdot 12}$ respectively (Table 6.4). Lower calculated oxidation rates for weekly flushing were

caused by the long dry period between flushing, over which continuous oxidation was assumed to occur. In reality oxidation rate probably decreases exponentially as pore water evaporates, making the actual weekly flushed sample oxidation rate of the same order as that of the daily flushed samples. The range of pyrite oxidation rates for flow-leaching are for some water-rock regimes up to an order of magnitude higher than static leaching of the same rock type (Table 5.18).

The higher rate of oxidation calculated for the flow-leached samples was probably a result of greater removal of dissolved sulphate. Prediction of pyrite oxidation rates at low pH, using McKibben and Barnes (1989) rate reaction led to a value of 2.3×10^{-12} $mol_{py} m_{py}^{-2} s^{-1}$ (Chapter 5). As leachate pH remained high, between 5 and 6, the rate constant used may be inappropriate. As minerals such as jarosite were identified by SEM-EDAX, actual pore water pH must have been far lower than the actual leachate pH (~3, Bigham et al., 1996). The order of magnitude difference between the predicted pyrite oxidation rate at low pH and calculated values can be explained by error of the same size of underestimation of pyrite surface area (Section 5.3.5.1.1). Agreement of the calculated and predicted values suggests that at this time scale, using rate constants from experimentation on pyrite alone is a good proxy for embedded pyrite oxidation rates.

	Oxidation rate – mass dependant ($mol_{py}^{-1} g_{pyO}^{-1} s^{-1}$)			
Rock type	Upper daily	Lower daily	Upper weekly	Lower weekly
WS	$3 \pm 2 \times 10^{-12}$	$3 \pm 2 \times 10^{-12}$	$4 \pm 5 \times 10^{-13}$	$6 \pm 7 \times 10^{-13}$
WC	$2 \pm 1 \times 10^{-12}$	$1.2 \pm 0.7 \times 10^{-12}$	$2 \pm 1 \times 10^{-13}$	$4 \pm 3 \times 10^{-13}$
	Oxidation rate – surface area dependant ($mol_{py}^{-1} m_{pyO}^{-2} s^{-1}$)			
Rock type	Upper daily	Lower daily	Upper weekly	Lower weekly
WS	$2 \pm 3 \times 10^{-11}$	$2 \pm 4 \times 10^{-11}$	$2 \pm 2 \times 10^{-11}$	$2 \pm 3 \times 10^{-11}$
WC	$6 \pm 6 \times 10^{-11}$	$5 \pm 3 \times 10^{-11}$	$1 \pm 2 \times 10^{-11}$	$2 \pm 2 \times 10^{-11}$

Table 6.4. Pyrite oxidation rates calculated from dissolved S in UWC, WS and WC daily and weekly flushed upper and lower leachates, from flow-leaching. Values are presented in as rate dependant on original mass and surface area of pyrite, errors shown are 1σ, n=23 (daily) or 15 (weekly). Surface area per g of original sample is estimated using typical pyrite consolidated framboid diameter of 50 μm. NB typical pyrite diameter in UWC was probably lower than 50 μm.

Changing oxidation rate with time.

As the rate of pyrite oxidation is calculated using dissolved S as a proxy for sulphate, the pattern in rate change will follow that of dissolved S, described previously. The influence of upper sample leachate on lower outflow chemistry is obvious although some changes between the two do occur. In both weekly and daily flushed leachate the difference between WS and WC is lower S from the lower sample. Dissolution of material precipitated from upper leachate in the lower sample explains the apparent source within lower samples. In general oxidation rates in the WC are lower than in the WS. As the WC contains up to 2 wt % more pyrite than the WS, this suggests that matrix effects limit pyrite weathering in the coal. A similar proposal was put forward for limiting of O_2 diffusion in Chapter 5.

Although the change in oxidation rate is higher for the WS, the WC rate appears to follow the same pattern during weekly and daily flushing. Fluctuations in flow velocity between each sampling point probably lead to the similarity in oxidation rate trend for both rock types. The control of calculated oxidation rate by flow rate may either be linked to increased physical weathering, or changes in the volume of water passing over the rock surface. As the change in WS and WC oxidation rate is relatively uniform, variable water volume for each sampling point is the most likely cause.

Both WC and WS leachate pH correlate with increases in pyrite oxidation, at least for upper sample leachate. The influence of upper sample leachate on lower sample leachate appears to alter the pH of leachate out of step with apparent increases or decreases in pyrite oxidation.

SEM investigation showed precipitation of oxidation products at the point of water influx and further down the rock face, providing easily soluble material in both WC and WS. Jarosite precipitation indicates that pore water pH was less than 3 during either wet or dry periods. It is probable that secondary mineral precipitation and dissolution controlled leachate chemistry, as suggested by the change in 'oxidation rate' with flushing volume. Pyrite oxidation supplied leachate content via the precipitation and dissolution of secondary minerals at the water-rock interface. The sharp pH gradient between the pore water and leachate would have encouraged precipitation at this interface. Such cyclic dissolution and precipitation of oxidation products suggests that deriving the pyrite oxidation rate from dissolved SO_4^{2-} either over or underestimates the actual rate. Where a combination of the two mechanisms of dissolved SO_4^{2-} production exists, calculated pyrite oxidation rates will be larger than actual rates.

Ingress of an oxidation front – oxidant transport and precipitation-dissolution mechanisms.

Although only the end points of WS and WC flow-leaching were examined, SEM investigation revealed some key mechanisms of oxidation front ingress and transport and storage of oxidation products (Figure 6.19).

In upper samples the remnant of a 'hotspot' of oxidation was usually apparent, marking the point where Milli-RO water first entered the sample. Where fracturing occurred the macro-porosity directed fluid away from the exposed surface, leading to oxidation close to these structures and further into samples. Where water was allowed to diffuse into smaller pore spaces, sample cleavage plane with clay bands were preferred pathways compared to the organic-rich matrix. In both WS and WC samples water travelled into and down the sample, leaving the opposite top corner unaffected by oxidation. The lack of extensive oxidation in the top corner of samples indicates the involvement of water in rapid pyrite oxidation and as the main method of oxidant transport.

Metal enriched low pH pore water pooled at the base of samples, coming into contact with higher pH Milli-RO water. Contact between the two bodies of water led to extensive precipitation, akin to hard pan formation in spoil heap material. Blowes et al. (1991) report hard-pan formation by Fe^{3+} minerals and Fe^{2+} minerals at and below the depth of active oxidation in spoil material. Diffusivity of the hardpan was lower than in the un-cemented tailings and restricted pore water movement. In the sample where surface precipitation was observed, the layer of Fe-sulphate appeared to protect the pyrite framboids situated behind it. However, pyrite further into the sample was oxidised. Where metal enriched pore water pooled at the base of samples, the potential for oxidation by Fe^{3+} increased as pH lowered. Indeed the precipitation of jarosite and alunite in lower samples indicated the presence of this oxidant. The source of the Fe^{3+} was probably the oxidation of dissolved Fe^{2+}, derived from the upper sample and the upper part of the lower sample.

In comparison to the shrinking core model, waste rock particles situated on preferential flow paths appear to be oxidised from the side of fluid influx. Steep gradients between pore water and influent leachate lead to precipitation of secondary minerals at exposed surfaces. Dissolution of secondary minerals combined with pyrite in the lower regions of samples led to the observed output of dissolved Fe and S. Further along the flow path the influence of physical and chemical weathering
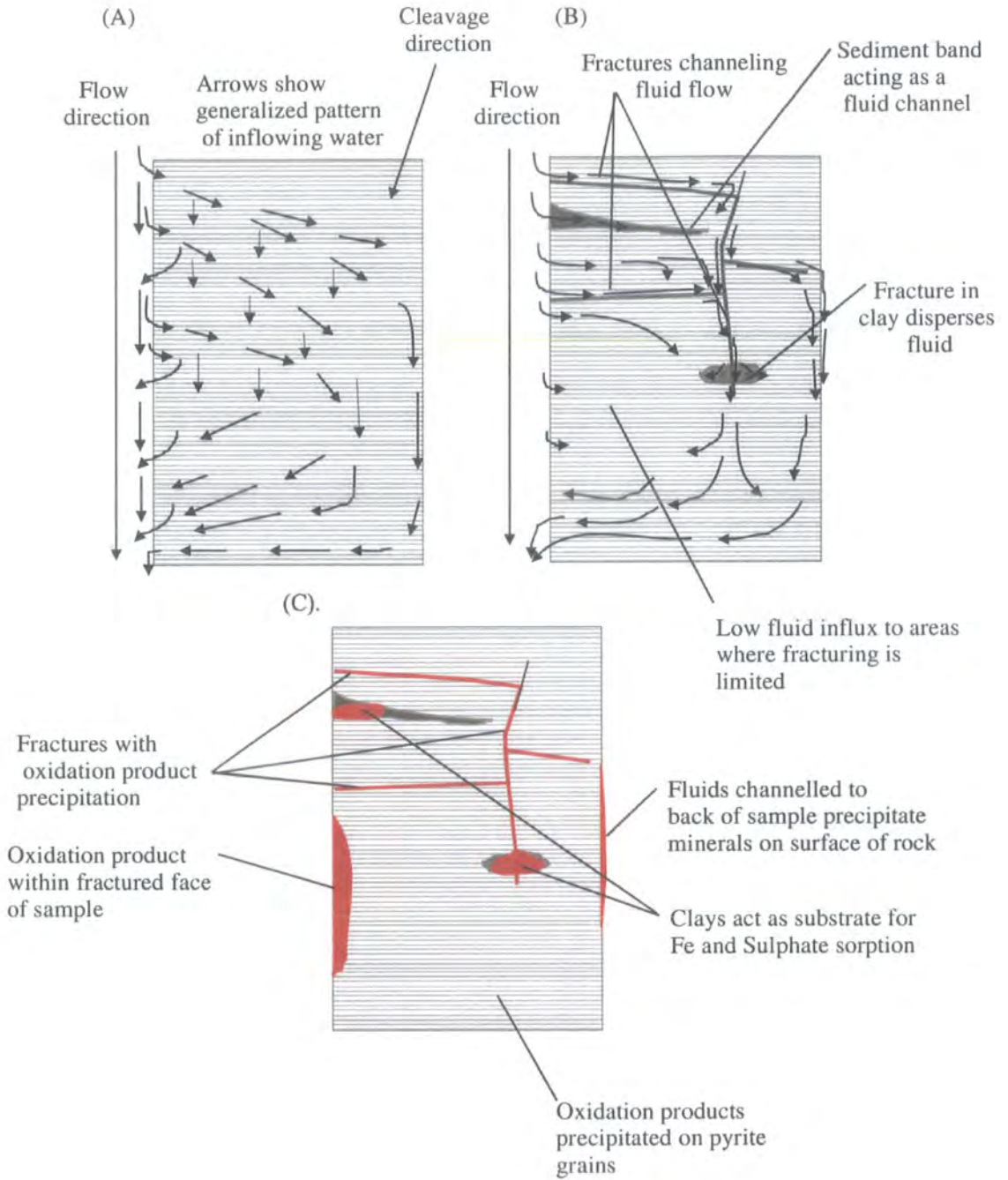
Figure 6.19. Generalised diagrams showing fluid flow direction in un-fractured (A) and fractured (B) flow-leached rock. Typical areas of pyrite oxidation product precipitation are also shown (C).

increases, leading to increased surface area and pyrite weathering. In general waste rock at the start of a flow path will be relatively clean and release Fe and S due to pyrite oxidation. Along the flow path waste particles will become more physically and chemically weathered. Waste rock will release higher concentrations of material due to the precipitation from previous influent water, of readily soluble secondary minerals.

6.2.4.2   Statistical analysis of leachate elemental flux

Experimental flow-leaching was performed to identify the control of factors such as lithology, drying out period and flushing media over leachate chemical evolution. Here, the previous discussion of these factors is enhanced by the use of analysis of variance (ANOVA).

In the flushing experiment three independent factors – lithology, flushing media and drying-out period may have affected the final outcome i.e. leachate chemistry. Within the factor of lithology there were four rock-types. Flushing substance and drying out period factors both contained two treatments – Milli-RO or mineralised water and daily or weekly flushing. The factorial design (Section 3.3) of the experiment allows investigation of the effect of all possible treatment and factor combinations without the bulk of a classically designed experiment. Total element flux per mass of original sample, per day was calculated for each replicate of all water rock regimes ($mgg^{-1}day^{-1}$ Tables 6.G and 6.H, Appendix II Results). Where daily leachate was lost due to weekly collection the intermediate loss in leachate concentration was estimated from the gap in days and the analysed leachate concentration. Although this brings error into the total element flux value for daily leaching only random error is produced and ANOVA is still applicable.

Once ANOVA has identified any significant differences in elemental concentration caused by the independent factors, the magnitude of effects can also be calculated to show their relative importance. Main effect plots are used to illustrate factor control over element flux. Where similar distribution occurs between treatments of a factor for a group of elements, one process may control element fluxes within that group. While ANOVA indicates whether a significant difference occurs between treatments in the data set, the *post-hoc* Tukey test indicates which treatments differ significantly from each other (Howell, 1997). Interpretation of these tests will show the extent of influence by each different combination of variables on dissolved elemental flux.

Previous examination of leachate flux identified the sink and source processes of ion exchange, pyrite oxidation product precipitation, dissolution and sorption. When

204

combined with statistical examination the data set a more robust interpretation can be made than by either method alone. Identification of the mechanisms controlling run-off chemistry during coal flow-leaching can then be compared to the role of these processes in the natural environment. Any differences in factors controlling leachate formation under laboratory and field conditions will contribute to difficulties in scaling behaviour between the two. In the description of leachate chemical evolution Mn was not included due to the low concentration of this element. However, Mn is included in the statistical analysis to investigate any correlation between Mn release and siderite dissolution.

6.2.4.2.1 Results of three-way ANOVA for elemental flux

As the defined variables of lithology, flushing substance and drying-out period were independent of each other the model used for analysis was a three-way ANOVA (Howell, 1997). The test identifies any interaction between variables and the relative significance of the effect of each variable on total elemental flux per day (Table 6.G. Appendix II Results).

Control over element flux by independent factors

Four combinations of the independent factors controlled leachate element content (Table 6.5). All factors affected Si, Mn and Mg fluxes, whereas only lithology and drying period controlled Al, Fe, K, Na and Zn. Lithology and flush media controlled Ca flux, whilst only lithology significantly affected the S flux.

The group of elements controlled by lithology and drying period was generally derived from alumino-silicate minerals (Al, K and Na) or from sulphides (Fe and Zn). Simms et al., (2000) note the co-precipitation or adsorption of Zn onto Fe^{3+} hydroxides in columns of mine tailings during flushing at pH>4. Such co-existence of Zn and Fe may explain the grouped control of their fluxes by drying period and lithology. The oxidation of sphalerite and pyrite would also lead to the concurrent flux of Fe and Zn.

Significant influence of Si, Mn and Mg flux by all variables suggests that different controlling mechanisms can be ascribed. Starting chemistry and mineralogy, secondary mineral dissolution and interaction of the rock with a high volume of Milli-RO water all partially controlled the flux of these elements.

The lack of control of S by any factor other than lithology is due to the presence of both sulphate and sulphide minerals in coal-bearing strata. As both groups of minerals release dissolved S due to variations in drying period and flush media, it is possible that

any significant control by individual factors is lost in the bulk release of dissolved S. Only the original wt % of S, controlled by lithology, appears to affect the final S flux from all flushing regimes. Control by lithology and flush media suggests that gypsum and carbonate dissolution and precipitation strongly influenced the flux of Ca. Drying period and therefore extent of forced evaporative precipitation did not significantly control either Ca or S total flux. Control of both Ca and S flux by gypsum, formed during pyrite oxidation product neutralisation, would lead to rapid dissolution of both elements. As evaporation and the build up of a larger volume of material for leaching had no significant effect on the total flux of Ca and S it is also probable that the same flow-path was used at each flushing event.

	Lithology	Flush media	Drying period	Lithology v Flush media	Lithology v Drying Period	Flush media v Drying period	Lithology v Flush media v Drying period
Al	✔	✗	✔	✗	✔	✔	✗
Ca	✔	✔	✗	✗	✔	✗	✗
Fe	✔	✗	✔	✗	✔	✗	✗
K	✔	✗	✔	✔	✔	✔	✔
Mg	✔	✔	✔	✔	✔	✔	✔
Mn	✔	✔	✔	✗	✔	✔	✗
Na	✔	✗	✔	✔	✔	✔	✔
S	✔	✗	✗	✗	✔	✗	✗
Zn	✔	✗	✔	✔	✗	✗	✗
Si	✔	✔	✔	✗	✔	✔	✗

Table 6.5. Significance of main factors and interaction between factors of flushing experiment in total flux: ✔ = significant at 95% confidence interval; ✗ = not significant at the 95 % confidence interval.

Similar conclusions to those drawn previously by direct interpretation of leachate chemical evolution can be made from ANOVA of the total elemental flux per day. Lithology and consequently mineralogy primarily control chemical constituents of the final leachate. Apparent lack of control over dissolved S flux by either drying period or flushing media was due to relatively high release of this element for all variations of

coal and shale leaching. Drying period significantly affected alumino-silicate and sulphide phase mineral leaching, indicating precipitation of secondary minerals as an important factor for the flux of Fe, Zn, Al, K and Na.

Interaction of variables

Significant interaction was found between lithology and dry period for all element fluxes and between flush media and dry period for all elements apart from Ca, Fe and S at the 95% level (Table 6.5). Interaction between lithology and flush media and also between all variables, was only significant for the K, Mg, Na and Zn flux.

When no significant interaction for elemental flux exists this indicates that differences caused by one factor combined with the different treatments within another variables will be the same. For example, the difference between the Ca flux from treatment with Milli-RO water and mineralised leachate changes by the same amount between daily and weekly dry periods i.e. there is no significant interaction (Figure 6.20). However, significant interaction of lithology and dry period for Ca shows that differences in flux from each rock-type during weekly and daily flushing are not the same (Figure 6.21). Lack of significant interaction between lithology and flushing media suggests that Ca flux will change proportionally with changes in variables. Such proportionality of element flux is useful in predicting changes in individual dissolved element output under changing water-rock regimes. Significant interaction between lithology and drying period was mainly caused by the release of higher elemental flux from the UWS during weekly flushing compared to daily flushing. All other rock types released higher elemental flux during daily flushing (Figure 6.22). Only Zn and Fe have P values above 0.000 (although Fe is less than 0.05) suggesting that the same process releases these elements (Figure 6.23). The difference between Fe and Zn flux from daily and weekly flushed UWS is relatively small due to the low concentration of sulphides, especially sphalerite in this lithology. Significant interaction between lithology and flushing media and also between all variables for Mg, K and Na was also a result of high flux from the lower leachate flushed UWS. The flux of Zn showed interaction between lithology and flushing media for the same reason. Flux of Mg and K from the WC were also higher from leachate flushed samples. Potential sources of these elements would be dolomite and jarosite dissolution, both of which were identified, in lower samples of the WC. Significant interaction of lithology and flushing media for the Mn flux stems from the high output of both lower and upper samples of
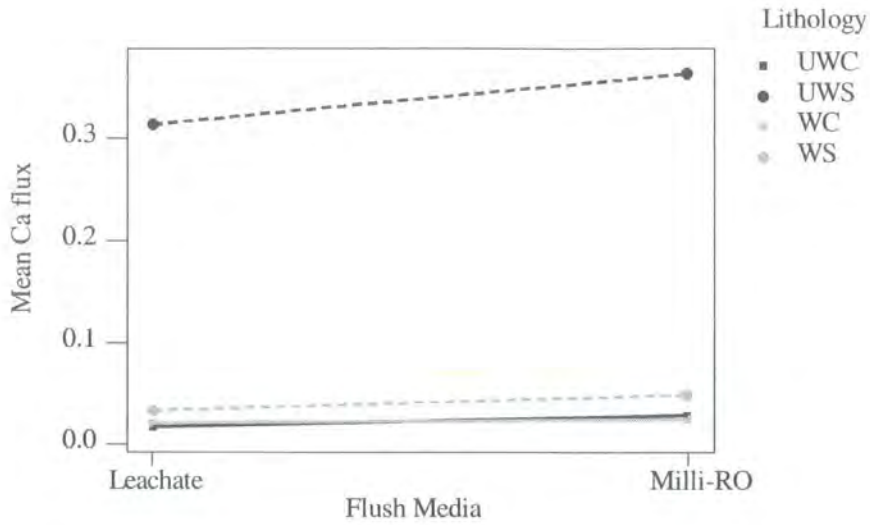
Figure 6.20. Mean Ca total flux (mgg^{-1}day^{-1}) for each lithology treated with different flush media. No significant interaction occurs between lithology and flush media, as suggested by the parallelism of the plots, implying that at higher initial leachate concentration the dissolution of Ca will decrease for all lithologies.
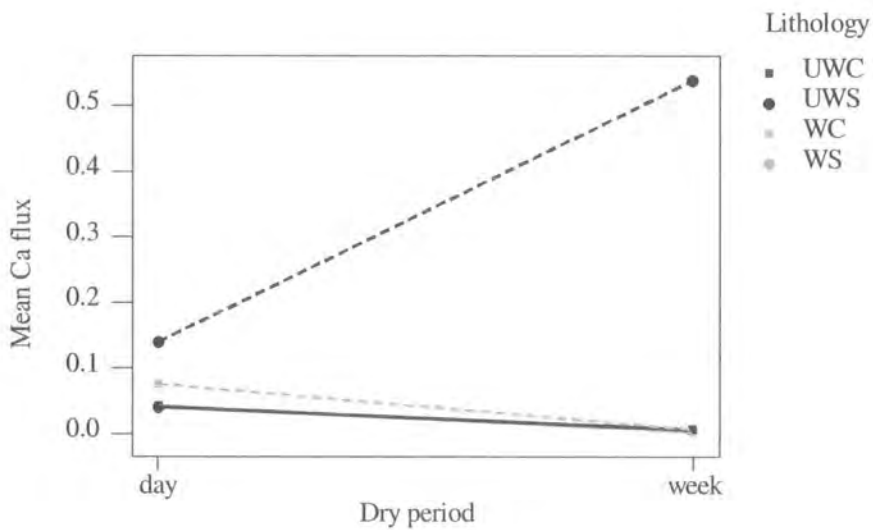
Figure 6.21. Significant interaction of dry period and lithology for Ca flux (mgg^{-1}day^{-1}). The UWC, WS and WC may release a higher flux over shorter dry periods, however the UWS release higher flux after longer periods. No prediction of Ca flux can be made for all rock types due to interaction of variables.
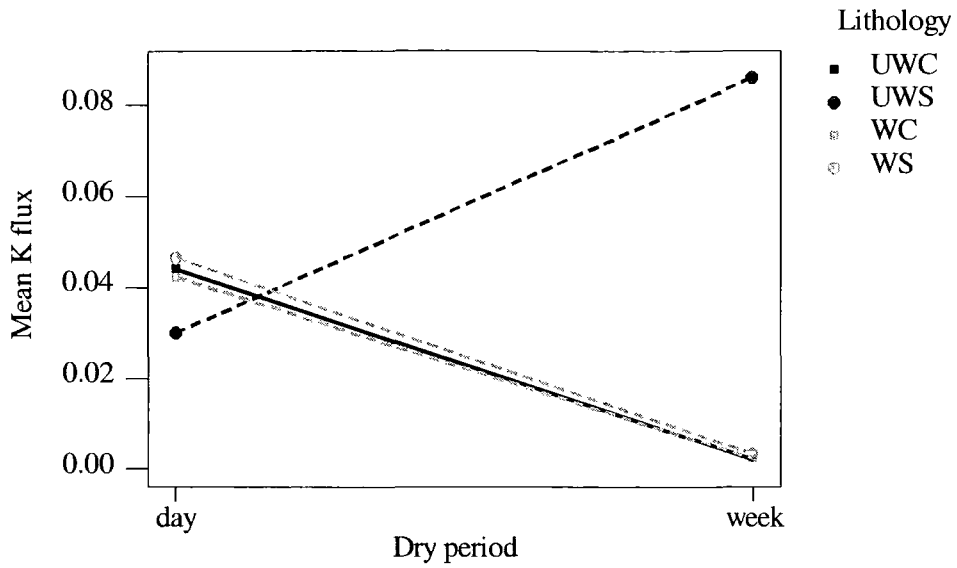
Figure 6.22. Higher element flux from weekly flushing of the UWS leads to interaction between lithology and dry period. Mean total K flux $(mgg^{-1}day^{-1})$ is shown as an example.
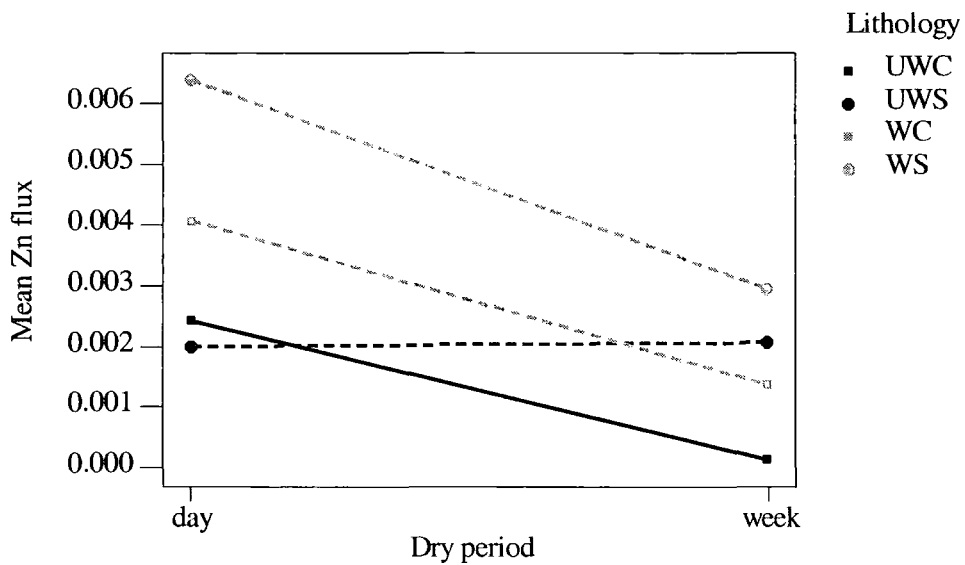
Figure 6.23. Lower flux of Zn $(mgg^{-1}day^{-1})$ from the UWS leads to a lower P value for interaction between lithology and dry period.

WS. Fe-Mn–oxide was identified by XRD in the WS, providing a source for Mn under low pH and high pe conditions prevalent in lower samples (Drever, 1997).

Significant interaction of variables can usually be attributed to the large difference in mineralogy of organic poor shale and organic rich coals. Changes in drying period and flushing media tend to affect flux in the same manner for each rock type, yet interaction due to host mineralogy makes the prediction of flux behaviour difficult. As interaction is usually caused by the UWS some prediction can be made about flux behaviour with changing treatment of the other rock types.

6.2.4.2.2 Magnitude of effects – extent of control by lithology, dry period and flushing media

Although the significance of a variable in the control of element flux during flushing has been shown, the relative importance of each effect can also be calculated using:

$$\omega^2_{effect} = \frac{\sigma^2_{effect}}{\sigma^2_{total}}$$

where the magnitude of effect ω^2_{effect} is the ratio of σ^2_{effect} the variance of the factor being examined to σ^2_{total} the total variance of all factors being analysed (Howell, 1997). Equations for ω^2_{effect} described by Howell (1997) were used to calculate the magnitude of effects for a three-way ANOVA. Proportions of effects indicate the extent of control a variable has over the response calculated for, i.e. total element flux (Table 6.6). Magnitude of effect calculated as zero represented factors found not to be significant by ANOVA.

Lithology, drying period and the interaction between these two variables had the greatest control of elemental flux (Table 6.6). Only Al, Na and Zn flux were relatively equally influenced by the both factors, with Fe also having a relatively high ω^2_{effect} value for drying period. Other element fluxes mainly controlled by lithology included Ca, Mg and S, yet excluded Si and Mn fluxes, which were controlled by drying period.

The equal control of Fe, Zn, Al and Na suggests that weathering reactions, encouraged by dry periods, aided the flux of these elements. Dry period also relates to the volume of water used to flush samples, with a higher volume used for daily flushing. Greater flushing volume and time of exposure to leachate may have led to

sampling of connate brine within pore fluids (Spears and Martinez-Tarazona, 1992). Increased flushing, leading to dilution of pore fluids, may have also encouraged ion exchange and therefore removal of Na from the rock (Stumm and Morgan, 1999).

	Lithology	Drying period	Flushing media	Lithology v Drying period	Lithology v Flushing media	Flushing media v Drying period	Lithology v Flushing media v Drying period	Error
Al	0.20	0.21	0.00	0.32	0.00	0.05	0.01	0.22
Ca	0.62	0.04	0.00	0.32	0.00	0.00	0.00	0.01
Fe	0.26	0.11	0.00	0.20	0.00	0.00	0.00	0.43
K	0.24	0.08	0.00	0.48	0.03	0.04	0.04	0.10
Mg	0.54	0.03	0.01	0.33	0.03	0.02	0.03	0.01
Mn	0.09	0.33	0.05	0.39	0.009	0.05	0.00	0.09
Na	0.12	0.16	0.00	0.40	0.04	0.12	0.07	0.09
S	0.47	0.00	0.00	0.45	0.00	0.00	0.00	0.09
Zn	0.36	0.26	0.00	0.08	0.00	0.00	0.00	0.30
Si	0.04	0.38	0.07	0.34	0.01	0.09	0.00	0.07

Table 6.6. Magnitude of effect (ω^2_{effect}) of lithology, flushing period and flushing media and interactions on the measurement error. Where factors were found insignificant by ANOVA the variable interaction terms, ω^2_{effect} were calculated as zero.

The large influence of lithology on Mg, S and Ca is most likely related to the high dissolution of gypsum and dolomite from the UWS. For Si and Mn where all variables influenced the removal of these elements the calculation of magnitude of effect is most enlightening. Calculation of ω^2_{effect} for both element fluxes indicates large effect caused by dry period and drying period and lithology interaction. Dry period is associated with either weekly of daily flushing, i.e. a longer period for precipitation or larger volume of water used for flushing. Both would affect water-rock interaction by either increasing the soluble mineral phase, acidic weathering and in daily samples increasing interaction with pore water. Siderite or simply Mn-oxide dissolution may have controlled the flux of Mn along with precipitation within secondary minerals. The flux of Mn is usually associated with removal of Fe-Mn coatings on particles and the dissolution of $MnCO_3$ within siderite (Dulong et al., 2001). The greatest Mn flux was from the WS, in which Fe-Mn –oxides were identified (Figure 5.D Appendix II Results). Instability of MnO_2

coatings at low pH and positive p*e* suggest that lowered pore water pH within the WS rock types lead to the observed Mn flux (Drever, 1997). In the UWS siderite was not dissolved due to the neutral to alkaline pH of the leachate solution. Where lithologies are mixed i.e. under field or column experiment conditions, siderite dissolution by acidic pore water will become an important process in discharge chemical evolution

6.2.4.2.3 Main effects plots

The plots of least squared mean element flux value for each rock type show different distributions depending the control of lithology each element (Figure 6.25). Such plots allow confirmation of patterns in flux control, suggested previously.

Lithology

Elemental flux distribution between the four lithologies suggests the influence of the inorganic versus organic content, porosity and the secondary mineral phase content (Figure 6.25). The flux of Al, Si, Mn, S, Ca, Mg, K and Na tended to be higher from the shale lithologies relative to coal output. However, three different elemental flux distributions were caused by original mineralogy. The flux of Si and Mn was relatively equal from UWS and WS, whereas the difference in Al flux from coal and shale was larger and generally higher in the weathered rock types. High alumino-silicate content, the presence of siderite and Fe-Mn oxides and the presence of alunite all contributed to the observed differences in element flux from the four lithologies. A similar distribution is shown for the S, Na, Mg and Ca flux, with high flux from the UWS was caused by gypsum dissolution and ion exchange.

A different distribution of element flux shown by Fe and Zn was caused by high dissolution of these elements from secondary mineral phases of weathered rock types. Again, the co-existence of these elements suggests some kind of precipitation-dissolution relationship (Simms et al., 2000). At pH > 4 present at the rock surface, co-precipitation of Zn in Fe^{3+} hydroxides would have occurred. However, low pH is required within the rock matrix to allow leaching of Fe-Mn oxides in the WS and dissolution of siderite Mn coatings from the UWS. As co-precipitation of Fe and Zn probably only occurred close to the exposed flushed surface where pH was relatively high, this phase was readily available for dissolution by acidic pore water flushed from the rock matrix. Such a mechanism suggests that there was a time lag between Fe and Zn precipitation at the sample surface and the flushing of acidic pore water from within
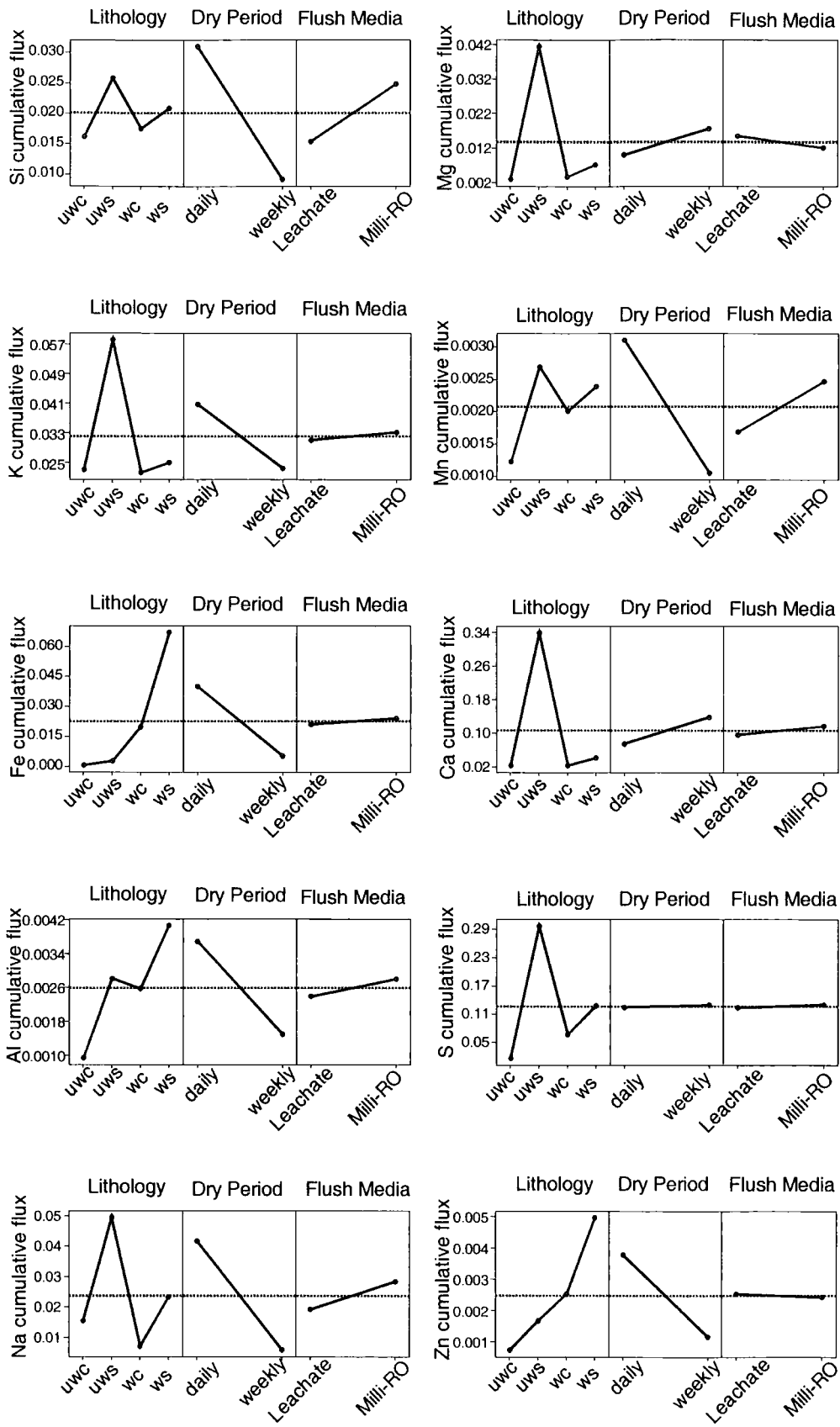
Figure 6.24. Main effect plots for major element cumulative flux (mgg^{-1}day^{-1}), calculated for factors of lithology, drying period and flushing media.

the rock. As percolation within rock porosity would take longer than flow along the sample surface, a time lag between surface and deep pore flushing is probable.

Drying period

Three distributions of element flux existed between daily and weekly drying periods. High flux from daily flushing and low flux from weekly flushing for Al, Si, Na, K, Zn and Fe can be attributed to weathering of alumino-silicates, ion exchange and increased co-precipitation and dissolution. High volumes of leaching solution used during daily flushing lead to low solution concentration and interaction with a larger volume of rock. Dilution of a solution increases its ion exchange capacity (Stumm and Morgan, 1999). Greater interaction with pore water may have formed silicate-weathering, organic acids, which may have been a source of significantly higher Si and Al (Drever, 1997). Alternatively alunite identified by SEM in the WS and WC probably contributed to the high daily flux of Al. Kaolinite dissolution at low pH would have also provided a flux of Si and Al.

Both carbonate phase constituents, Ca and Mg and to a lesser extent S had larger fluxes from weekly flushing. Precipitation of gypsum and sulphate minerals would have occurred during continued pyrite oxidation in the dry week between flushing. The lack of daily flushing led to a larger volume of sulphate minerals available for dissolution at the next flushing.

Flushing Media

Most element fluxes tended to be higher for flushing with Milli-RO water rather than mineralised leachate. Milli-RO water actually used to leach samples contained up to 1 mgL^{-1} of K, Na and Si providing exchangeable ions. The dilute nature of this leaching solution increased dissolution and ion exchange contributing to the high element flux of Na, Si and Mn calculated from blank corrected dissolved concentrations. Similarly, ion exchange would increase the flux of K and dissolution of kaolinite and secondary minerals would increase the output of Fe, S, Ca, K and Al. The lower difference between flushing with leachate and Milli-RO water can be explained by the precipitation and subsequent dissolution of secondary minerals from leachate. The higher volume of soluble material available would particularly include S, Fe, (jarosite), Ca (gypsum) and Al (alunite), skewing the observed distribution towards a higher leachate flushed flux. Both Zn and Mg flux were higher from flushing with leachate

suggesting strong influence from secondary mineral precipitation and leaching with low pH solutions.

6.2.4.2.4 *Post-hoc* Tukey test

Given the described significant differences and response behaviour for different variable combinations, identification of significant causes of difference is useful. A *post-hoc* Tukey test (section 4.3.3.3) was performed to compare element flux from each treatment or lithology within each factor and identify reasons for significant differences.

Lithology

Significant differences between UWC total flux of Al, Mn, S and Mg and all other rock types, especially shale, were due to a combination of factors (Table 6.7). Low initial soluble mineral content and greater pyrite oxidation with consequent acidic attack of carbonate minerals in the WS and WC, all contributed to the observed difference. A high proportion of Fe-hydroxides co-precipitated with Zn, after sphalerite oxidation produced high fluxes of Fe and Zn from the WS. Similarly, high clay and gypsum content of the UWS provided a substrate for ion exchange, releasing Na and K and a readily soluble source of S, Mg and Ca.

Responses	Significant differences	Controlling Process
Al, Mn	UWC ≠ all other rock types	UWC has low concentrations of soluble minerals containing either element
S	UWC ≠ WS	High pyrite content WS
Mg	UWC ≠ shales WC ≠ WS	High gypsum/dolomite content of shales and greater acidic weathering. Lower dolomite weathering in WC
Zn, Fe	WS ≠ all others	High Fe(III) hydroxide mineral content co-precipitated with Zn
Ca, K, Na, Mg, S	UWS ≠ all others	Ion exchange and gypsum dissolution high in the UWS
Na, Si, Al, K, Zn, Fe, Mn, Mg, S.	Weekly flushing ≠ daily flushed	Larger water volume leads to higher total flux for daily flushed leachate
Mg, Mn, Si	Milli-RO flush ≠ Leachate flushed	High pyrite oxidation by Milli-RO water increased clay and Mn-oxide dissolution. Greater reaction with dolomite by flushing with low pH leachate leads to high Mg flux.

Table 6.7. Summary of Tukey *post-hoc* test results; ≠ indicates significant difference.

Drying period

The influence of drying period or water volume was identified for Na, K, Si, Al, Fe and Zn flux via ion exchange, acidic weathering and Fe^{3+} hydroxide dissolution. *Post-hoc* testing also supports the significant differences controlled by varying dry period and demonstrates that Mn, Mg and S fluxes also differed due to this variable. Dissolution of Fe-Mn hydroxides increases under daily flushing (Figure 6.25). However, S and Mg dissolution was significantly higher from weekly flushing, due to precipitation of gypsum and other secondary sulphate minerals.

Flushing Media

Again Mn, Mg and Si flux was shown to significantly differ between flushing with mineralised leachate and Milli-RO water. Main effects plots for each elemental flux show the high output of Si and Mn from Milli-RO flushing, compared to the high Mg flux from leachate flushing. The greater interaction of a higher volume of water with shale material would have increased slaking and therefore exposed sample surface. Similar least squared means from UWS and WS of Mn and Si suggest that slaking increased exposed surface area of kaolinite, siderite and Fe-Mn-oxides (Figure 6.25). Such an increase would led to greater dissolution of Mn, Fe and Si. However, fracturing of samples flushed with leachate was most common. Given that Mn –oxide dissolution requires low pH and kaolinite dissolution occurs in the presence of H^+ (Table 5.9), it is most likely that low pH produced the high Si and Mn fluxes. As most pyrite oxidation appeared to occur in upper samples, pooled pore water would have relatively low pH, providing a mechanism for acidic attack on clay and Mn-oxides. Pyrite was identified in the UWS, suggesting that a similar mechanism for producing high Mn and Si flux from siderite and kaolinite was possible. A lack of significant difference in Fe flux due to change in flush media is attributed to pyrite oxidation in the WS and WC producing a significantly high Fe flux.

6.2.4.2.5 Summary of statistical analysis

Statistical analysis of total flux from flushing experiments drew similar conclusions to those of the previous section. Mineralogy, ion exchange and the dissolution of pyrite oxidation product minerals all significantly controlled element flux (Table 6.8). Lack of significant interaction of lithology and flush media, and flushing media and dry period suggests that higher Fe, Ca and S is released after long dry periods and by high volumes of dilute flush media. Upper regions of the vadose zone are usually extensively leached

during spoil leaching (Blowes and Jambor, 1990, Paktunc and Davé, 2000). Here, statistical analysis of small-scale leaching shows the control of high flush rates and long drying periods on the flux of three important AMD species.

Variable	Variable influenced processes controlling element dissolution	Elements dissolved in processes		
		Primary	Secondary	Tertiary
Lithology	Prior oxidation products	Zn, Fe, S	Mn	
	Carbonate phase	Ca, Mg		
	Clay dissolution			Si
	Ion exchange	K	Na	
Drying period	Daily flushing – high volume, low ionic strength Milli-RO water → greater dissolution.	Mn, Si	Zn, Fe, K	
	Daily flushing – ion exchange	Na		
	Weekly flushing – flow-path precipitation and higher pyrite oxidation		Ca, Mg	
Flushing media	Low pH leachate reaction with dolomite			Mg
	Acid leaching of Mn-oxides, siderite and kaolinite in upper samples		Si	Mn

Table 6.9. Summary of statistical analysis of flow-leach experiment showing the identified processes controlled by the three factors of lithology, dry period and flushing media. Elements removed by these processes are grouped by the factors magnitude of control (Table 6.7).

Ion exchange, secondary mineral dissolution and acidic weathering also controlled element flux. Long dry periods only significantly affected S, Mg and Ca, all of which are derived from pyrite oxidation products. Daily flushing with a high flush volume led to increased kaolinite and Fe-hydroxide dissolution, whilst encouraging ion exchange. Precipitation from of jarosite, alunite, Fe-sulphate and gypsum along flow-path significantly increased K, Fe, S, Ca and Al flux during subsequent flushing, in effect controlling the composition of percolating water.

6.2.4.3 Summary and conclusions of flow-leaching experiments

Pyrite oxidation front ingress under flow-leaching conditions

As in static leaching, the ingress of a pyrite oxidation front in flow-leached coal-bearing strata was controlled by rock pore size distribution and pyrite morphology. Compared to a shrinking core model the ingress of oxidation was biased towards the surface exposed to influent leachate. Pooling of acidic pore water at the base of samples leads to precipitation of secondary minerals the water-rock interface as a type of micro-scale hard pan, which protects adjacent pyrite. Fractures were important in the transport of fluid away from the exposed surface, into the centre of samples, suggesting that rock micro-porosity was connected by macro-porosity. Two fronts of oxidation were apparently dependent on the oxidation of framboidal and consolidated framboidal pyrite, with the former phase being oxidised most rapidly.

Embedded pyrite oxidation rates during flow-leaching

Predicted pyrite oxidation rates using McKibben and Barnes (1989) rate reaction for low pH oxidation were one order of magnitude lower than calculated rates from dissolved S. The difference may be accounted for in the order of magnitude error in estimating pyrite surface area.

SEM investigation suggests secondary mineral dissolution at the water-rock interface may control leachate chemistry to a greater extent than pyrite oxidation. Monitoring of flow leachate chemical evolution indicated that the dissolution of secondary minerals contributed to the flux of dissolved material. Exchange of both metal and SO_4^{2-} ions occurred especially in samples flushed with Milli-RO water.

Dissolved Fe (and Zn) flux control by drying period and lithology also suggests that dissolution of secondary minerals may affect leachate chemistry to a greater extent than pyrite oxidation itself. If pyrite oxidation rate controlled leachate chemistry then increased pyrite content (lithology) and dissolved oxidant influx (regularity of flushing) would increase the rate of Fe and Zn dissolution. However, weekly flushing increases Fe and Zn release to a greater extent than daily flushing. Dissolution of the highly soluble secondary minerals precipitated during prolonged evaporation exceeds the direct contribution of Fe and Zn from pyrite oxidation. Similar control of AMD chemistry by secondary mineral precipitation was reported in mine tailings by Blowes and Jambor, (1990) and Bigham et al., (1996).

218

Controls on flow path rock weathering under varied water-rock regimes

Statistical analysis of elemental flux confirmed the interpretation of leachate chemical evolution. Along flow-path the greatest quantity of material is removed at the start when leaching solution is dilute. High volumes of leaching solution also lead to ion exchange and acidic dissolution of Fe Mn-oxides and kaolinite. Pyrite oxidation is assumed to be the source of acidity. Greater interaction with the organic phase of the rock when flushed with a large volume of dilute solution may have lead to organic acid attack on the alumino-silicate phase (Drever, 1997, Bou-Raad et al., 2000)..

Further along the flow path the precipitation of secondary minerals controls the output of dissolved material to solution. Although pyrite oxidation still occurs within samples, diffusive transport of dissolved products to leachate probably goes through a series of precipitation-dissolution reactions as flushing stops and starts. Such a reaction would be the precipitation of goethite and subsequent re-precipitation as ferrhydrite or jarosite depending on solution pH (Göttilicher and Gasharova, 2000).

In general longer periods of drying and high flush volumes tend to produce a high flux of dissolved elements. Evans et al. (2001) found that major element concentration from coal spoil column leachate was independent of flow-rate, except at very high rates. Within a column of spoil material flow may be restricted to preferential flow paths and only high flow rates will lead to interaction with a larger volume of un-reacted material. Along preferential flow paths the oxidation of pyrite will move away from the flushed surfaces and on input of a high volume of water, the unexposed surfaces will also be leached. At normal flow rates, i.e. season dependant, micro-scale hard pans may form along flow-paths at the active oxidation surface controlling the output of material to the influent fluid. Fluctuations water volume will lead to consumption or precipitation of such mineral phases depending on pH-pe conditions.

Chapter 7

Pore water contributions at an un-controlled AMD discharge.

7.1 Introduction

AMD formation occurs as the result of pyrite oxidation product dissolution and subsequent collation and transport to a receiving water-course. Final discharge quality is therefore controlled to a large extent by mixing of rock leachate with percolating meteoric water. In previous chapters the processes controlling leachate quality produced by pyrite oxidation within coal-bearing strata were assessed. In this chapter the processes involved in the final stage of AMD formation are investigated in terms of hydrological and seasonal controls at an actual discharge.

Percolation of meteoric water into rock waste leads to the dissolution and transport of soluble salts from the oxidised vadose zone into the underlying un-oxidised saturated zones (Blowes and Jambor, 1990, Figure 7.1). Precipitation along flow path may be significant where changes in local redox conditions occur, providing a potential sink for dissolved species. Similarly dissolution of previously precipitated material along flow path may balance this sink process. The following mass balance relationship describes the overall process of AMD chemical formation:

AMD =   Rock leachate   + Meteoric water $\pm$ Solid phase precipitation / dissolution

Meteoric water (or ground water where applicable) is an essential component of AMD formation, and any variability in this factor will affect AMD quality. Seasonal changes in precipitation will not only affect the discharge quality, but also its quantity. Such a mass balance ignores the presence of chemical kinetics, simplifying the water-rock system into potential source and sink terms to provide a general description of AMD chemical quality. As final discharge and meteoric water composition can be characterised it should be possible to estimate the composition of pore water contributing to the final discharge quality. Identification of contribution or precipitation from percolating solutions would be possible using a package such as NETPATH (Soulsby et al., 1998). However, in the absence of such software, these sink or source terms can be assumed to be one of the 'sources' contributing to the final AMD chemistry.
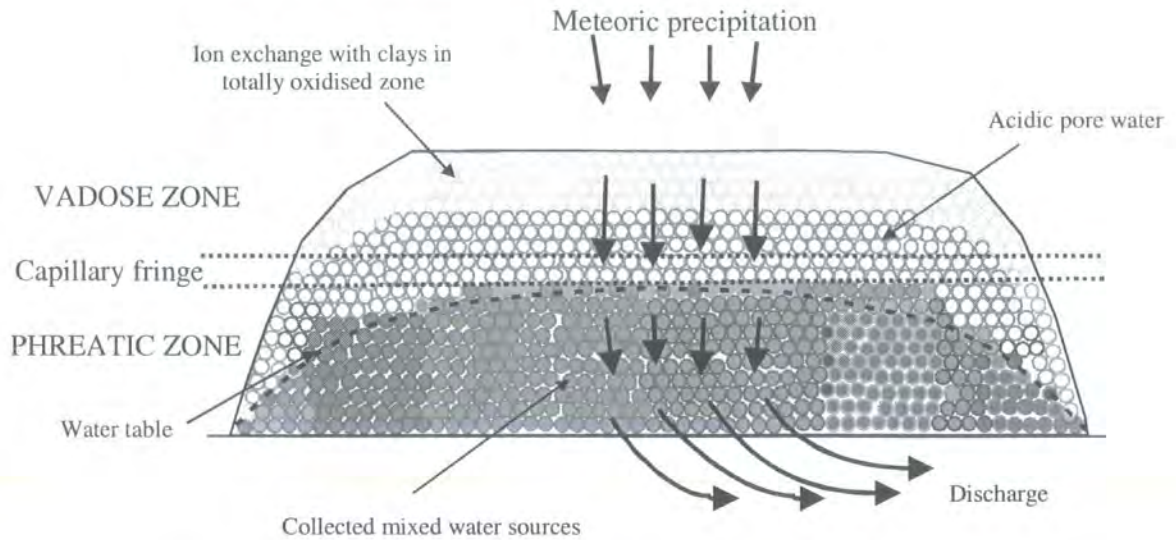
Figure 7.1. Spoil heap leaching showing sources of pore water contribution to percolating meteoric water.

Chemical hydrograph separation

A similar mass balance relationship has been used extensively in the separation of water source contribution to stream catchments (Pinder and Jones, 1969, O'Brien and Hendershot, 1993, Eshleman et al., 1994, Al and Blowes, 1996, Soulsby et al., 1998). Chemical hydrograph separation of stream discharge is based on the assumption that supply to the channel bed is from distinct (end-member) water bodies, whose chemistry is relatively constant (Pinder and Jones, 1969). Usually the contributing water bodies are ground-water or base flow (slow flow) and subsurface flow (quick flow) (Ward and Robinson, 1990). Mixing of end-member chemistry from each water body forms the final chemistry of the supplied stream discharge. Contribution of the sources of water is described by the following mass balance equation:

$$Q_s C_s = Q_o C_o + Q_n C_n \qquad (7.1)$$

where the flux of material in the total run-off (s) as the product of flow rate Q and concentration C is the sum of material flux in base-flow or old water (o), and the flux from subsurface or quick flow (n) (Pinder and Jones, 1969). The equation above can be re-arranged for the original groundwater contribution Q_o:

$$Q_o = \left(\frac{C_s - C_n}{C_o - C_n} \right) \div Q_s \tag{7.2}$$

removing the need for prior knowledge of the flux of subsurface or quick flow.

Chemical hydrograph separation has previously been used to interpret the processes controlling pore water is transport to the point of discharge (Al and Blowes, 1996, Soulsby et al., 1998). Determination of pore water composition and contribution to discharge on a seasonal basis will lead to better characterisation and prediction of future seasonal behaviour. Currently AMD discharge characterisation tends to concentrate on the worst case scenario of high, base flow dissolved concentrations during base flow. However, diluted high volumes of discharge may be as deleterious as low volumes of highly concentrated material, especially when metal colloids form (Pfiffer et al., 1996). Both types of outflow will be treated by the same remediation scheme, making characterisation of seasonal pore water composition and contribution to discharge necessary. Where the chemical treatment is used adjustments can be made relatively easily. Passive treatment schemes i.e. constructed wetlands will be more difficult to adapt to large-scale variations in discharge chemistry. Therefore, where possible, extensive characterisation of discharge chemistry, over a range of influent water volumes, is required prior to implementation of remediation.

Principal component analysis

Interpretation of discharge chemistry and hydrograph provide a method of monitoring hydrological pathways within the system of interest (Al and Blowes, 1996). However, a two component end-member mixing model for chemical hydrograph separation may be too simplistic. Although equation 7.1 can be expanded for further end-members (O'Brien and Hendershot, 1993) detailed *a-priori* knowledge about possible water sources in a water-rock system are required to do so. Where this information is available (i.e. bore-hole and well data) the accuracy of water source separation will increase. However, without information on the potential end-members mixing to produce stream chemistry, errors in the interpretation of data are highly likely.

Pattern recognition within a large multi-dimensional data set is possible using multivariate analysis (Einax et al., 1997). Principal Component Analysis (PCA) of such data sets produces several non-correlating groups of correlated measured characteristics (e.g. pH, concentration etc.). Such reduction of a large data set to a set of principal

components allows recognition of correlated characteristics. PCA involves mathematical transformation of the data matrix X, with m measured characteristics and n measurements, into component parts of factor loadings (A) and factor scores (F):

$$X = A \circledast F \qquad (7.3)$$

Factor loadings are the weights of the original characteristics within the newly produced un-correlated components. When factor loadings are low, the corresponding characteristic has little influence on the principal component. High positive or negative factor loadings indicate that the corresponding characteristic is a defining feature of the principal component (Einax et al., 1997). Eigenvalues produced during the matrix solution for factor loadings provide a measure of the variance attributable to a component when extracted from the total data set variance. To compare the produced principal components, factor scores (F) calculated from multiple regression between the original data and the factors are used. Graphical comparison of principal components is used to identify common influences on components.

PCA has been extensively used in the identification of end-members mixing to provide stream water data (Christopherson and Hooper, 1990). Variation in stream water chemistry is used to identify non-correlating components or potential end-members. Each principal component is assumed to represent a process involved in end-member mixing, but not the actual end-members. Where hydrograph separation requires end-member compositions, PCA uses correlation in the data set to identify processes leading to the mixing of different chemical sources. However, unless direct measurements are included in the analysed data set, end-member composition must lie outside the data cloud in order to mix to provide the observed patterns. Christophersen and Hooper (1990) outline End-member Mixing Model Analysis (EMMA) as a method of estimating the actual input of each end-member to the stream chemistry. Although EMMA is not used here the recommended approach to stream water analysis is followed in interpreting collected data. Conservative solutes are identified using a scatter matrix plot. PCA is then performed on all tracer data with orthogonal projections of potential end-members used to identify which best bounds the discharge data cloud. These projections are used to identify which processes dominate discharge chemistry.

The goals of the work described in this chapter are to:

o   Interpret uncontrolled AMD discharge end-members using chemical hydrograph separation, mixing plots and PCA.

o   Form a model of seasonal pore water contribution to discharge chemistry

o   Identify the effects of varying conditions on passive remediation design

Data collected from an uncontrolled discharge in the County Durham Coalfield over a period of 7 months (including winter, spring and summer) are interpreted. The final model of AMD formation is compared to the findings of experimental leaching in Chapter 8.

7.2 Methods

7.2.1. Site History

Bowden Close Colliery, Co. Durham (NZ 182360, Figure 7.2) operated for a period of 85 years from 1845 to 1930 (Durham Mining Museum). During this period the mine exploited the Top Main, Yard, Five Quarter, Harvey, Hutton, Bottom Yard and Main seams. Throughout the majority of its period of operation, coking and fireclay production and the manufacture of white and firebricks were performed on-site. The waste materials from these activites and the rock waste produced during mining would be deposited in the site heap (Figures 7.2 and 7.3).

In 1970 site reclamation was carried out over several months with 18.21 hectares of spoil landscaped. An additional 4.05 hectares of agricultural land was included in this scheme, to be returned to its original use on completion of the project. The neighbouring golf course acquired an extension formed on 9.71 hectares of spoil material and 8.50 hectares was planted with woodland (Durham County Council records). Demolition of mine buildings and emplacement of top-soil was performed with surface drainage designed in sympathy with the new landform. Few measures were taken to minimise subsurface flow through the spoil and made ground. Subsequently subsurface hydrological pathways have developed, establishing the discharge of acidic sulphate rich waters from land drains and seeping mobile tar (Younger 2001). Currently Durham City Council (DCC) are involved in a scheme to remediate the site using a Reducing and Alkalinity Producing System (RAPS) treatment scheme and anaerobic reed beds. The sampled discharge referred to in this work as Bowden Close, has previously been called Crook (Younger, 1995b) and Helmington Row (Jarvis and Younger, 1997).

7.2.2. Site Geology

Exploited seams at the Bowden Close colliery formed part of the Upper Carboniferous Westphalian A and B lower and middle coal measures. The extracted sequence represents a marine incursion followed by the development of a shallow lacustrian setting, with incipient shallowing due to sedimentation (Fielding, 1982). At the base of the sequence, the Harvey Marine band (*Vanderbeckei*) overlies the Harvey coal (typical S 1.1-3.15 %). The next overlying worked seam is the Hutton coal (typical S 0.9-5 % and high ash) representing a return to non-marine lacustriane setting (Fielding, 1982). Further up sequence exploited coals include the Durham Main seam and Five-Quarter seam described in chapter 4. Given the relatively high S content of coals and possible extraction of material from the Harvey Marine band, the sulphide content of waste rock from the Bowden Close colliery was probably large. As spoil material removed from the extracted rock would have included unusable shales and pyritic rich coal material the sulphide content would be increased further.

By-products of fire-clay bricks and coke production were co-disposed in the spoil heap. Recently, seeping tar-pit material, disposed after the coking process, was removed by DCC (Figure 7.3). By-products of both processes would have added a proportion of tar and refractory ash to the pyritic overburden material, although tar was mainly disposed of in one locality. Co-diposal of spoil and ash may have neutralised a large proportion of acidity produced by pyrite oxidation (Stewart et al., 1997), whilst possibly contributing to the high Al content of the monitored discharge. On reclamation of the site, construction material from abandoned buildings was incorporated into the spoil heap with re-shaping of the heap to lie flush with the hillside. Comparison of land surface contours, prior to and after reclamation, demonstrates the extent of spoil material spreading (Figure 7.4). Spreading of spoil would have led to little mixing, and exposure of relatively un-oxidised material from the centre of the original heap (Figure 7.5). Modelling of the effect of spoil mixing on oxidation front position indicates smearing of the oxidation front position and increased variation in underlying buffering zone chemistry (Gerke et al., 1998).
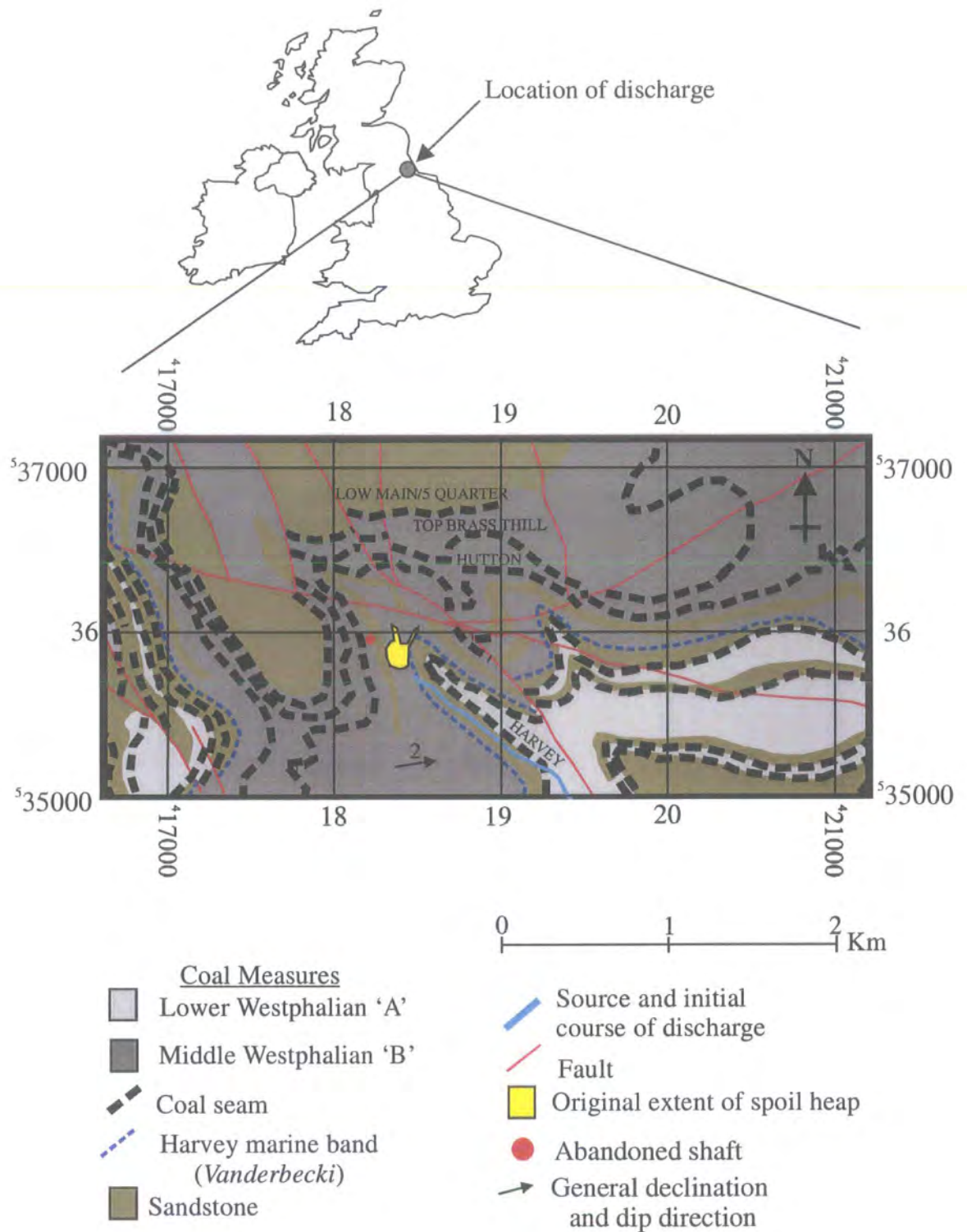
Figure 7.2. Location of sampled discharge of background of local geology and seams
extracted by Bowden Close colliery. (after Woodland et al., 1977, BGS
sheet 26 Solid edition)
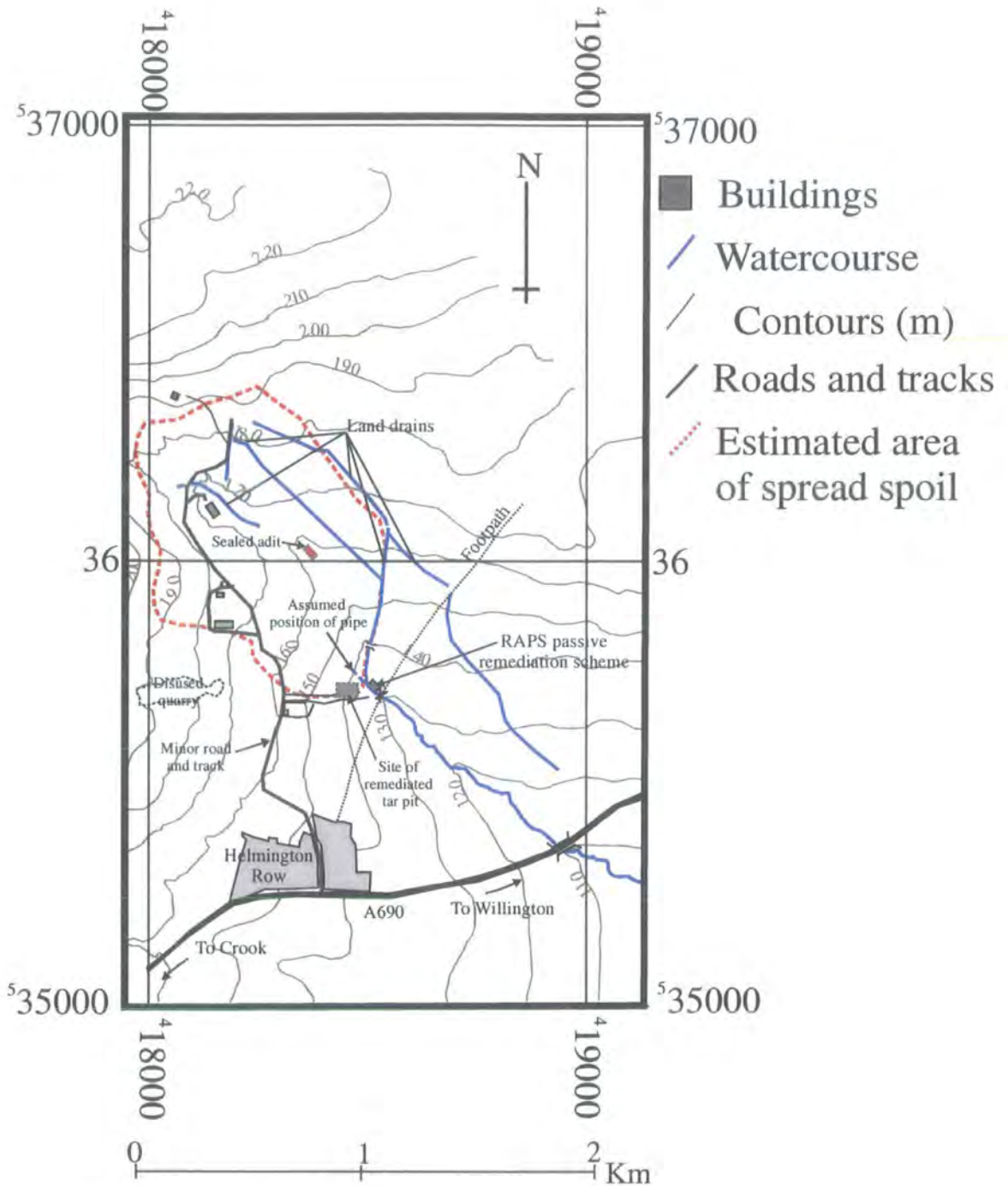
Figure 7.3. Locality of discharge in relation to surrounding topography, hydrology and estimated area of spoil spreading (Figure 7.4). Contours are taken from OS sheet map NZ 13 NE (1983) and are marked in metres.
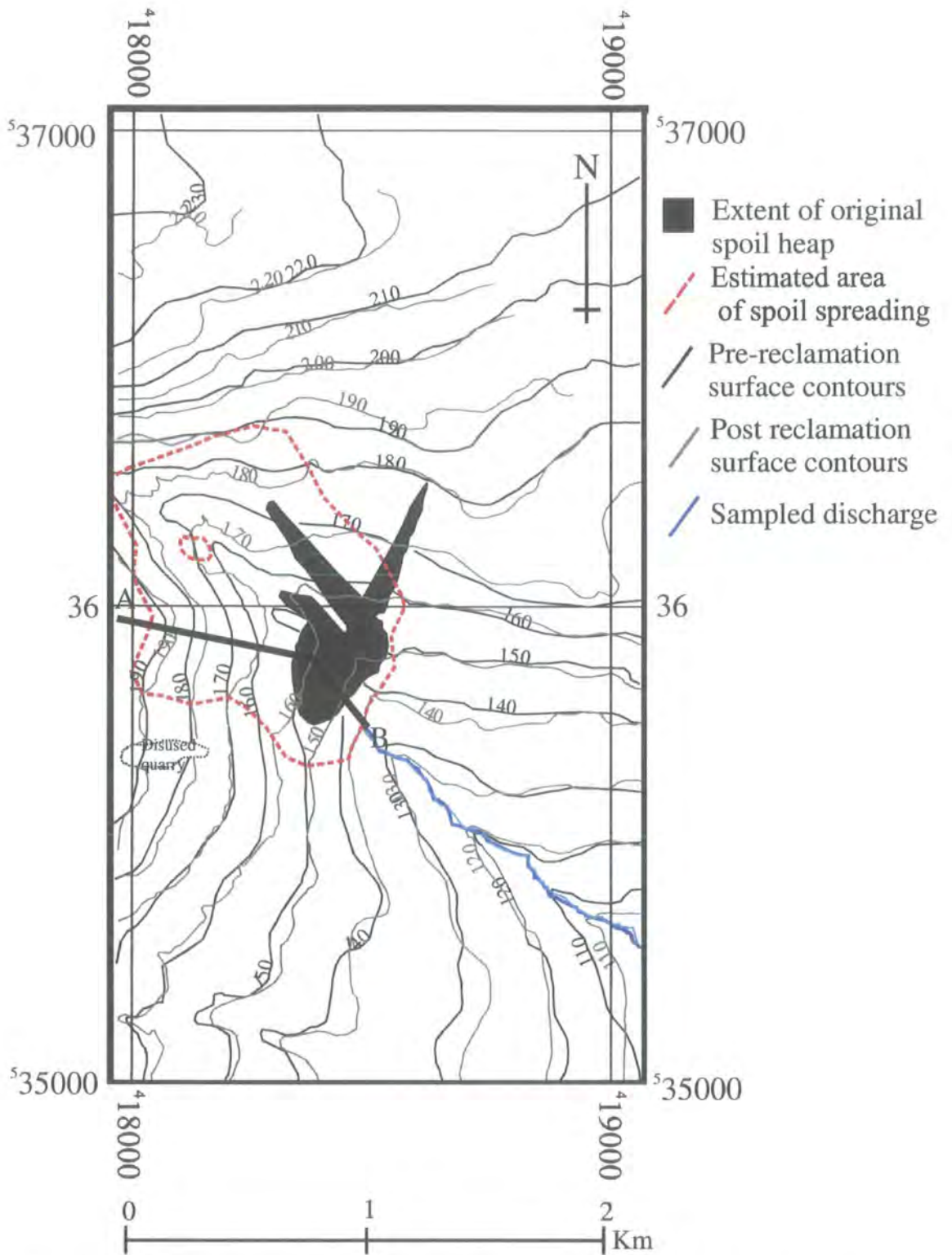
Figure 7.4. Land surface contours before and after reclamation of the Bowden Close colliery spoil heap. Contours are redrawn after OS sheet maps NZ 13 NE (1983) and NZ 13 (1957 – contours are redrawn in m from original heights marked in feet). Cross section of line AB is shown in Figure 7.5.
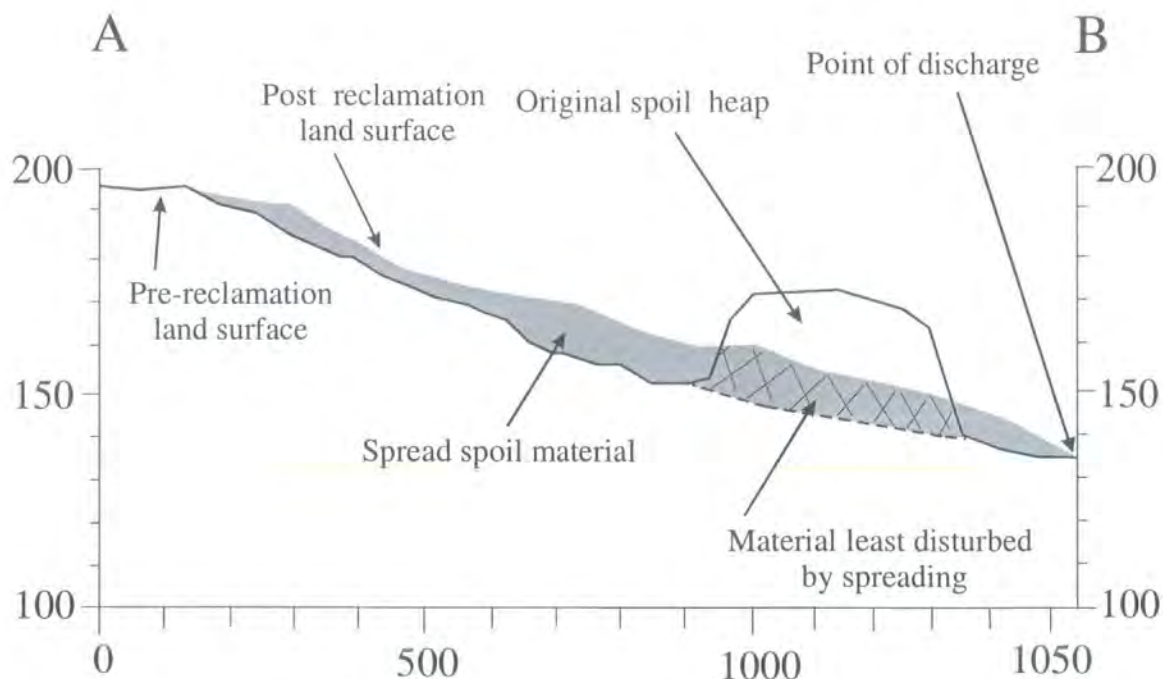
Figure 7.5. Cross section of land surface from line A to B marked on Figure 7.4.,
vertical exaggeration x 3. Original spoil heap height from a pre-reclamation
survey map from DCC records.

7.2.3. Site Hydrology

Most of the currently marked watercourses in the area of interest were artificially
built during reclamation (Figure 7.3). A natural spring probably fed by the perched
aquifer of the sandstone at the head of the valley (Figure 7.2) enters a drain prior to the
original position of the spoil heap. It is possible that this stream is the original source of
the receiving watercourse at Bowden Close, although artificial land drains also
contribute large volumes to the stream. Given the sizeable change in flow rate noted in
the spring between wet and dry seasons, the supplying aquifer capacity must be small.
The receiving watercourse flows in a south-easterly direction, and is culverted under the
town of Willington before discharging into the River Wear a further 2 km downstream.
Changes in stream bed position have been made at the site of the sampled discharge to
accommodate the pilot scheme RAPS wetland.

In comparison the sampled discharge flow rate remained relatively constant
throughout monitoring. The aquifer supplying the discharge i.e. pore water from the
spoil material has a high capacity and specific yield. At the point of sampling the
discharge emanates from a buried pipe which is assumed to be a remnant of two pre-
reclamation toe drains originally positioned at the south-east corner of the heap. It is

assumed that during reclamation the southern toe drain was buried and the continued flow (originally marked as a major watercourse) piped into the receiving burn. Given the estimated spread of spoil material (Figure 7.4) the discharge probably only receives water from the south-west side of the valley. A cross-section of the south-west side of the valley shows that most of the spoil material was spread to a thickness 15 m across in this area. Further up-slope spoil thickness decreases to around 5 m. The underlying hillside probably acts as an aquitard, with collected pore water running along this surface. Where the original land-surface was relatively flat, pooling of acidic pore water is probably common.

During remediation of tar pits approximately 20-30 m higher than the discharge site and along the direction of the sampled discharge pipe, no water table was discovered at a depth of 10 m (Figure 7.3, pers comm. R.Wood (DCC)). Remediation carried out during the summer suggested that locally the water table is deeper than 10m, as is the pipe draining the discharge.

7.2.4. Previous investigation of the Bowden Close AMD discharge

Younger (2001) reports the main AMD discharge at Bowden Close (sampled during this investigation) as having a flow rate of 200 Lmin^{-1}, high dissolved concentrations of Fe (80 mgL^{-1}) and Al (50 mgL^{-1}), and a typical pH of 4.5. Younger (1995b) classifies the discharge as derived from colliery spoil rather than a deep mine water source due to its low Cl concentration. There was also a change in typical ochre precipitation in the bed of the receiving watercourse from orange to yellow during periods of high surface run-off and dry periods. The change in ochre colour is attributed to the precipitation of gibbsite, aluminite and jarosite during dry periods and the precipitation of ferrihydrite (FeOOH) during wet higher alkalinity periods. Jarvis and Younger (1997) have shown that a sharp decrease in benthic fauna magnitude and diversity downstream of this outflow is due to the blanketing of the stream-bed in ochre.

The actual position of the other end of the pipe from which the discharge emanates has not been determined. CCTV investigation up to 30 m along the pipe was halted by debris cemented by precipitated minerals (pers.comm. R.Wood (DCC)). Extensive precipitation along the interior of the pipe's length suggests that the chemistry of the water at the end of the pipe may be different to that within the spoil. The convection of air along the pipe although retarded by such constrictions will lead to extensive precipitation of Fe-hydroxides. During periods of high flow pieces of spoil are brought down the pipe suggesting that at the other end loose spoil material is present.

7.3 Methods

7.3.1. Sampling strategy

Samples of the lower polluted discharge were collected regularly over a period of 6 months. A gap in sampling over March 2000 due to the Foot and Mouth outbreak led to sampling period of December 2000 to February 2001, and April – August 2001. During this period samples of base-flow and storm flow were sampled in winter and summer seasons. At least once a month a week long period of daily sampling was carried out to monitor daily variation in discharge chemistry. Such a strategy was implemented to monitor seasonal as well as diurnal changes in leachate chemistry.

Local precipitation was measured by rain gauge located close to the discharge site. Data from the rain gauge was supplemented by precipitation data from the Esh Winning Village weather station, 7 km to the north of the site (NZ180420, Meterological Office data supplied by British Atmospheric Data Centre). A two-day sampling strategy was also implemented to allow collection of overnight rainfall.

At each sampling two acid washed 100 mL sample bottles were filled at the point of discharge emergence from the concrete pipe. Care was taken not to disturb the stream bed sediment or ochres. One sample was acidified with concentrated HNO_3 in preparation for major element analysis. The second sample was used for measuring alkalinity by titration on return to the laboratory. The acidified sample was vacuum filtered through a 0.45μm cellulose nitrate filter paper, and the filtrate analysed for major element chemistry by ICP-OES (Appendix I Methods). If not analysed immediately samples were stored at 5°C prior to analysis, which was usually within a week of collection. Non-acidified samples were titrated against HCl for alkalinity using methyl orange as an indicator. Very low to zero alkalinity, was in keeping with Younger (1995b, 2000) and Jarvis and Younger's (1997) reports of zero alkalinity and net acidity of the Bowden Close discharge. Calculated alkalinity values are therefore not reported here.

Discharge pH, Eh (mV), pe (μs), total dissolved solids (TDS, mgL^{-1}) and temperature (°C) were measured using portable Hanna meters and probes. Each meter was calibrated prior to use with commercial buffer solutions. A total of five readings for each characteristic were taken at each sampling point, and the mean value reported.

Younger (2000) commented on the difficulty in measuring the flux of the Bowden Close discharge due to the direct discharge into the receiving burn. Such difficulty required the use of two methods of measuring discharge flux depending on the volume

of flow. During winter months when flow was high from both discharge and receiving burn, water velocity was estimated by eye. Velocity was combined with the cross section of flow, calculated from depth of water in the cylindrical concrete pipe (d = 40 cm), to give an estimate of flux. Later in April 2001, a hand held flow meter became available and was used to measure water velocity, which was again combined with water depth to give flux. In the summer when the velocity of discharge was lower than the limits of detection of the hand held meter, the flux of discharge was measured by volume difference. As the flux of the receiving burn had decreased to 5 mLmin^{-1} it was possible to measure the total combined flux of burn and discharge then use difference to give discharge flux. The summer method was used during July and August 2001. Overlap in use of the two methods allowed for calibration.

Surface flow of the discharge was faster than bottom flow, within the cylindrical pipe, especially during low flow. A large build up in debris and precipitation at about 2 m from the pipe end had led to the formation of a 20-30 cm high ledge which directed water to the left of the pipe (Figure 7.6). Calculation of discharge flux at low flow, prior to measurement by volume, therefore had to account for this difference in flow.

Using the hand held flow-meter an estimate of depth of rapid flow was made. Pooled water was assumed to be stagnant and the cross section of rapid flow used with velocity to calculate a flux value. During high flow rates pooling of stagnant water was assumed to be less significant as removal due to upper surface water drag would have increased as would turbulent mixing. Water samples were always taken from the region of high flowing surface water, as this was assumed to be less affected by precipitation in the stagnated area.

7.4 Results and Interpretation

7.4.1. Hydrology

7.1.4.1.Precipitation

Rainfall data extracted from Meteorological Office records for the Esh Village indicated maximum and minimum precipitation of 43 and 0 mm, (mean 3 ± 5 mm) for the period of sampling (January to July 2001). Rain gauge measurements for on-site precipitation were similar, with maximum and minimum values of 47 and 0 mm respectively (Table 7.1). Due to the manner of on-site rainfall collection i.e. cumulative measurement between sampling points, differences between daily precipitation and less

White alunite

Orange ferrihydrite
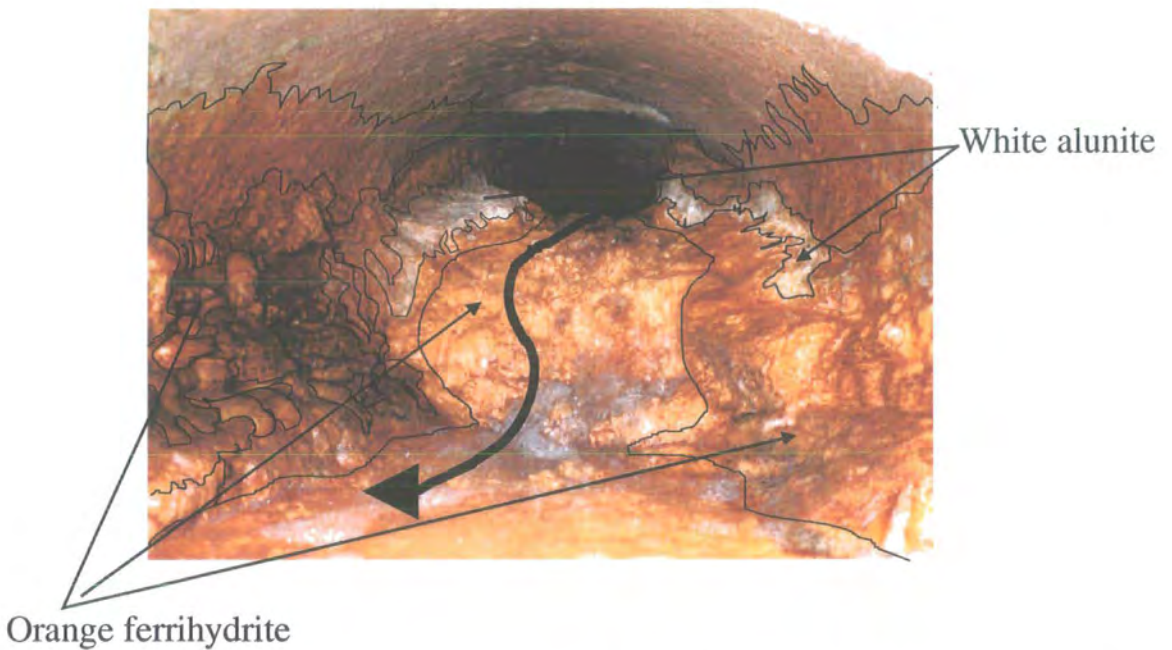
Figure 7.6. Ochre deposited inside entrance of pipe, debris cemented by precipitated
            mineral forms a ledge that directs water flow (thick arrow) to the left of the
            figure. Note precipitation of orange red mineral overlies that of paler
            minerals. Pipe diameter is 40 cm, image taken during June 2001.

frequent measurements probably occurred. Measured on-site rainfall and Meteorological Office data sets agree well for periods of heavy and light rainfall.

7.1.4.2.Discharge flow rate response

Interpretation of the hydrologic controls on water flow within a discharge catchment is made possible by monitoring of discharge response to precipitation (Ward and Robinson, 1990). In the case of Bowden Close the relationship between precipitation and discharge response is simplified by collation of water in the buried pipe before being discharged into the receiving burn. Quick-flow via shallow subsurface paths and direct precipitation contributions to the discharge will be relatively restricted. Phenomena such as ground water ridging and saturated overland flow will not contribute to the source of a buried pipe opening. Instead slow infiltrating subsurface or base-flow will probably form most of the discharged volume.

The hydrograph for the Bowden Close discharge over the 6 months of sampling indicates a general decrease in flow rate from the wet winter to dry summer period (Figure 7.7). Mean flow rate from January to April was over 1000 mLs^{-1}, compared to the average 340 mLs^{-1} during the period from April to July. The sharp drop in flow rate was probably also affected by the change in flow measurement methods at the start of April, yet a definite drop in flow rate was observed for this period. During the very dry period from June to July flow rate was relatively low with storm events causing a rapid increase then decrease in flow-rate. From January to April a slower response of the decreasing hydrograph limb was observed. Greater winter saturation of spoil material probably retarded the flow of infiltrating water compared to summer months when most of the spoil was un-saturated.

7.4.2. Chemical characteristics of Bowden Close discharge

The sampled discharge contained average dissolved Al, Ca, Fe, Mg and S of between 10 and 300 mgL^{-1} and less than 10 mgL^{-1} of Si, Zn, Na, Mn and K (Table 7.1, Table 7.A and 7.B. Appendix II Results). Maximum concentrations were usually collected at low flow rates, and are in good agreement with values reported by Younger (2000) for samples collected during periods of similar flow rate.

In general total dissolved concentrations (TDS) tended to increase with time and decreasing flow-rate (Figure 7.8). The flux of dissolved material (mgs^{-1}) in the discharge decreased from a maximum during winter, through spring, to reach a plateau in the summer dry period.
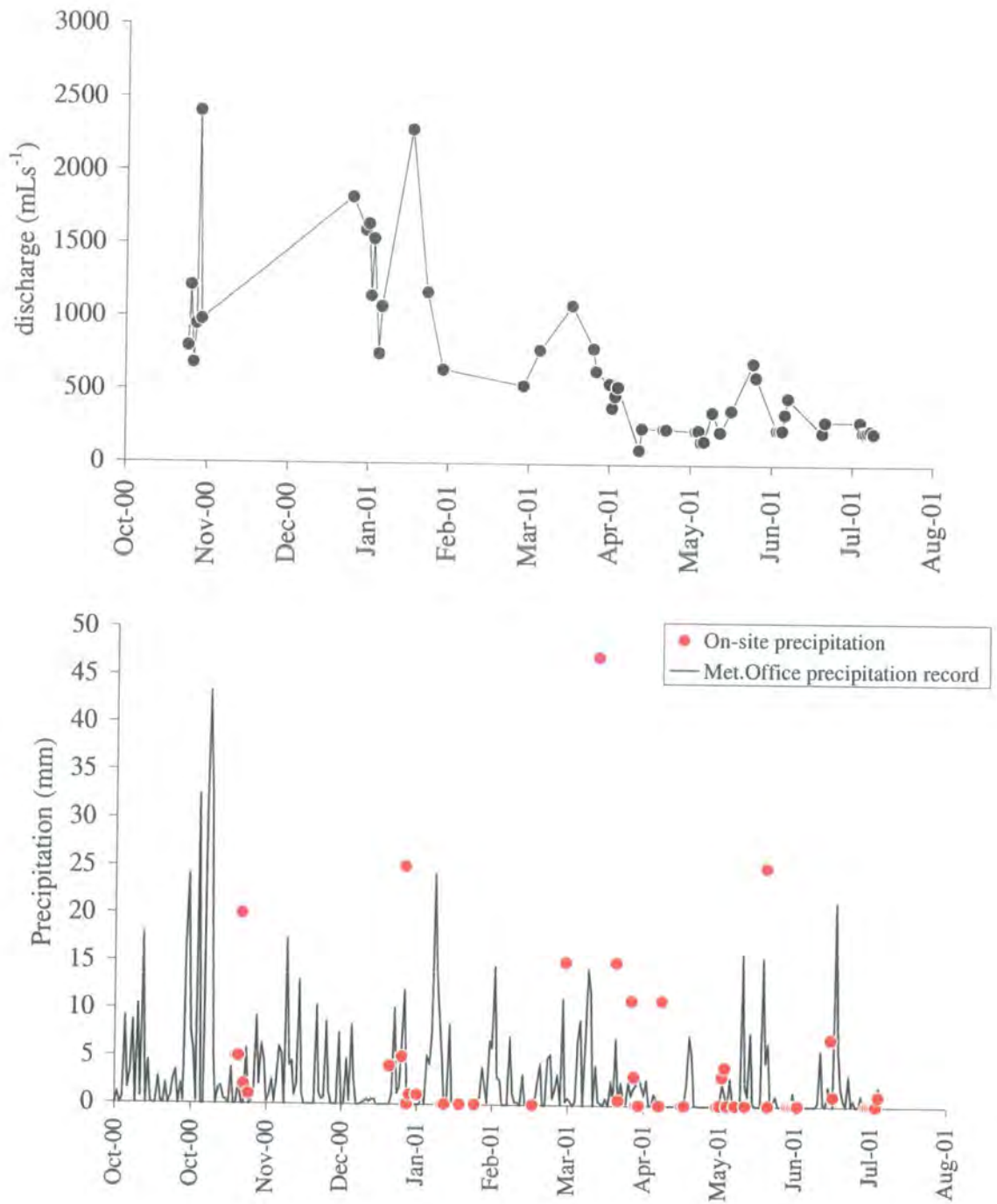
Figure 7.7.　Upper graph shows hydrograph of Bowden Close discharge over the period of sampling. Lower graph shows Met.Office precipitation data compared to onsite collected data points.
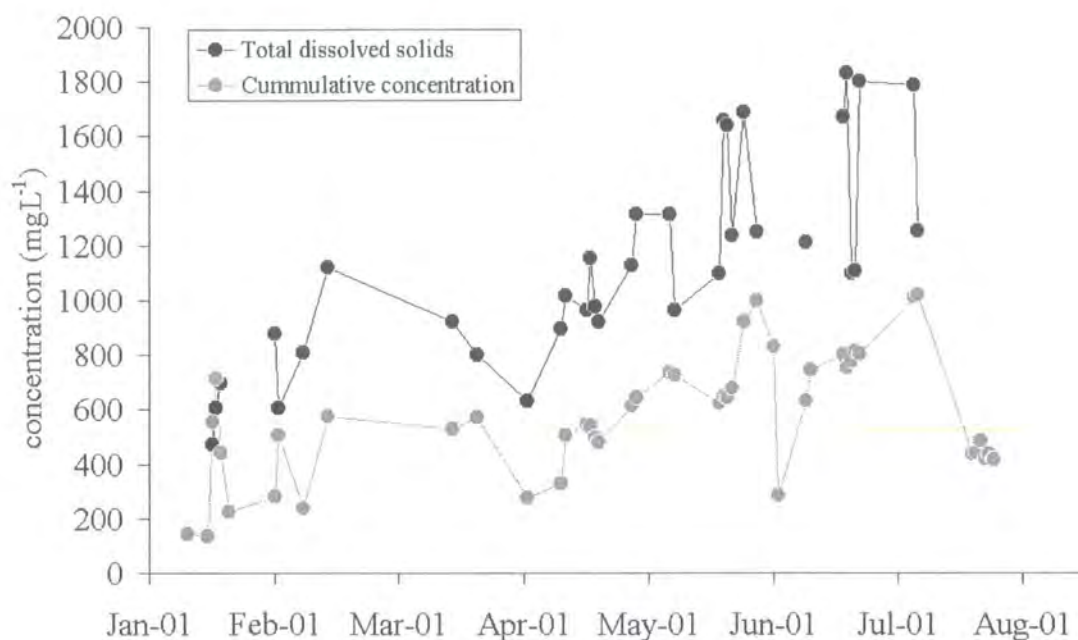
Figure 7.8. TDS and cumulative analysed concentrations (including H^{+}) measured for the Bowden Close discharge versus time.
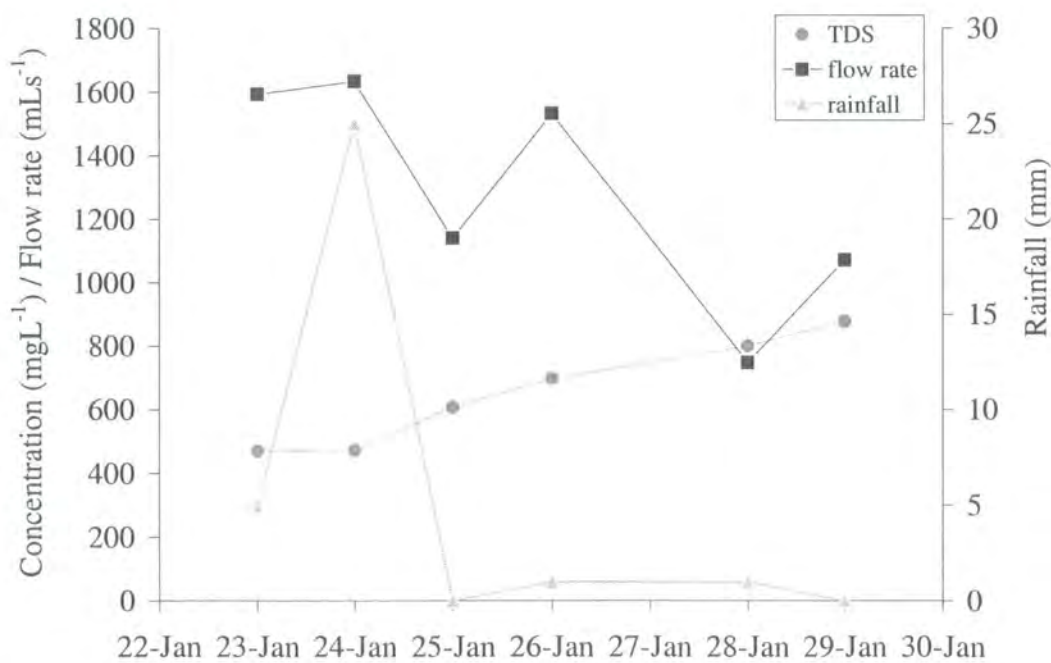
Figure 7.9. Hydrograph, rainfall and TDS during and after a winter storm event.

Daily sampling over periods of a week to four days during winter and summer suggest that after precipitation events flow rate tends to increase, as does TDS. However, in winter and spring flow rate increased after a day, whilst in the summer flow rate increased immediately (Figures 7.9 to 7.11). TDS also tended to increase the day after recorded winter and summer precipitation. In spring TDS increased after two days after the recorded precipitation event (Figure 7.10). Differences in magnitude of precipitation event (winter - 25 mm, spring - 11 mm, summer - 1 mm) may have led to the observed seasonal change in behaviour. As noted above, outside of daily sampling flow-rate response to precipitation was observed to be rapid during the summer and slow in winter / spring.

Factor	Mean $\pm$ 1σ	Range	Younger (1995b)	Younger (2000)
pH	4.8 $\pm$ 0.4	4.2-6.2	4.8	4.5
Conductivity (μs)	1734 $\pm$ 676	678-2850		
Temperature (°C)	9 $\pm$ 1	6.6-10.5		
Total dissolved solids (mgL^{-1})	1134 $\pm$ 371	473-1830		
Flow rate (mLs^{-1})	598 $\pm$ 508	157-2280		
Rainfall (mLday^{-1})	4 $\pm$ 9	0-48		50
Al (mgL^{-1})	25 $\pm$ 12	1-49	4.2	
Ca (mgL^{-1})	138 $\pm$ 44	47-222	185	
Cu (mgL^{-1})	0.1 $\pm$ 0.1	0.00-0.36	0.23	
Fe (mgL^{-1})	56 $\pm$ 25	3-102	79.8	80
K (mgL^{-1})	6 $\pm$ 1	4-8	6.8	
Mg (mgL^{-1})	62 $\pm$ 25	0-114	93	
Mn (mgL^{-1})	6 $\pm$ 3	1-12	6.9	7
Na (mgL^{-1})	9 $\pm$ 5	2-20	21.5	
P (mgL^{-1})	0.2 $\pm$ 0.2	0.0-0.7		
S (mgL^{-1})	271 $\pm$ 109	52-515	270	
Zn (mgL^{-1})	2 $\pm$ 1	0-4	0.045	3
Si (mgL^{-1})	13 $\pm$ 3	6-19		

Table 7.1. Mean chemical and physical characteristics of Bowden Close AMD discharge over a period of 7 months (winter to summer) compared to data from Younger (1995b and 2000) (spring and summer).

TDS only follows this pattern for the spring and summer precipitation events, increasing immediately after the winter precipitation event. Precipitation over January 2001was relatively low, allowing for a build up of weathering products in the spoil material. The start of heavy precipitation during February led to flushing of a high flux of dissolved material during precipitation events. Continual flushing during March and April decreased the spoil leachate concentration, however, the subsequent dry period
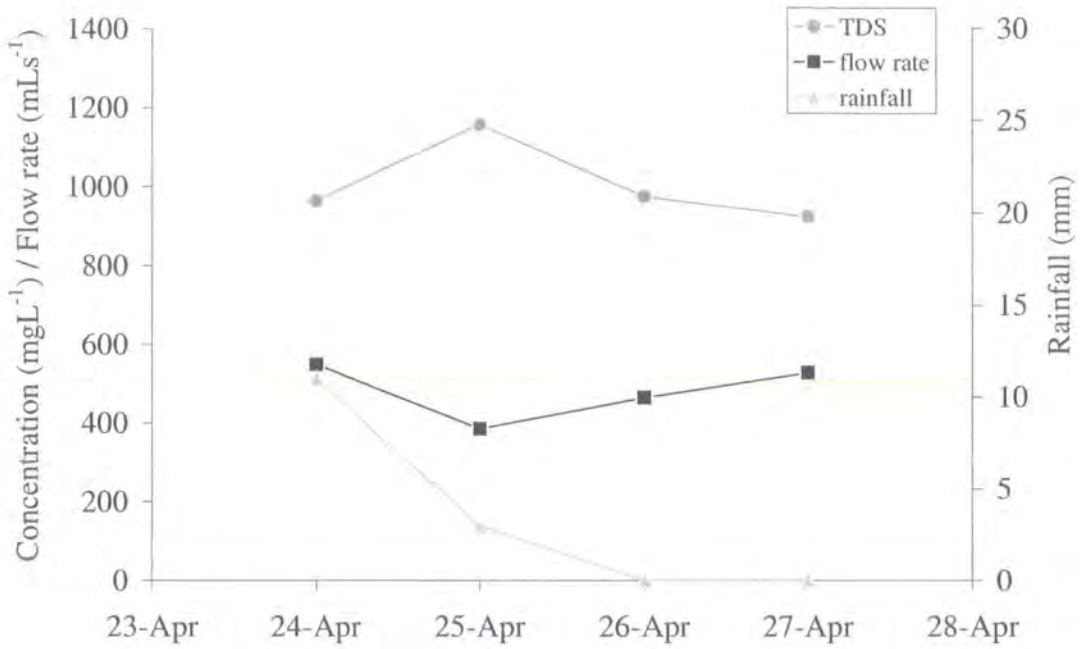
Figure 7.10. Hydrograph, rainfall and TDS during and after a spring storm event.
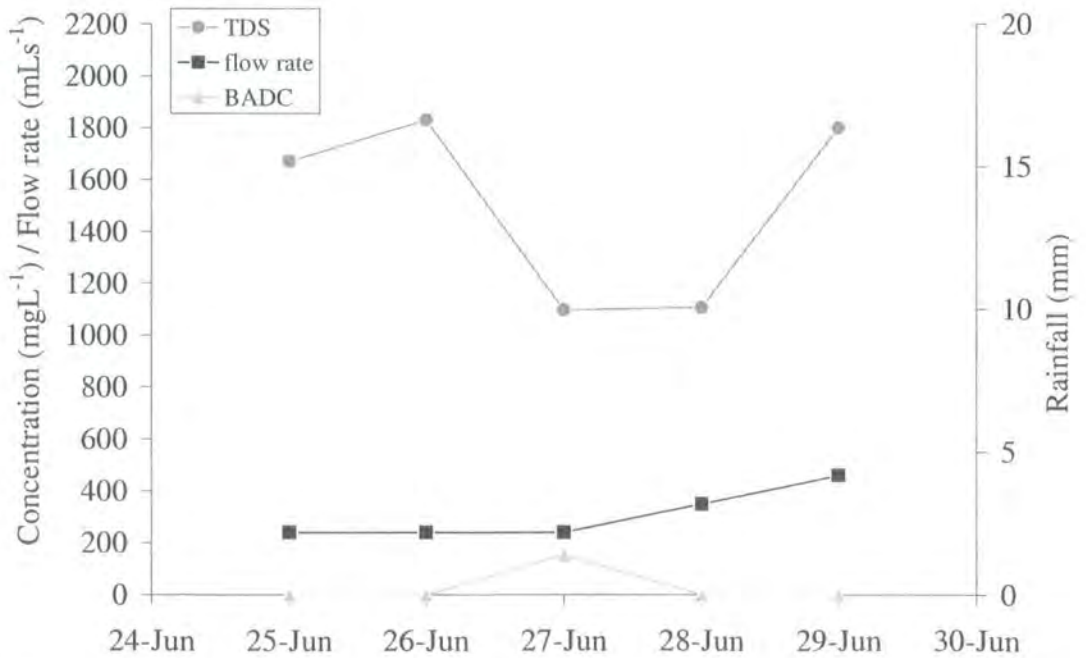
Figure 7.11. Hydrograph, rainfall and TDS during and after a summer precipitation event.

from April to June led to a build up in weathering products. Summer base-flow was composed of the remnants spring period precipitation with inputs of high concentration from precipitation events, which flushed newly formed weathering products.
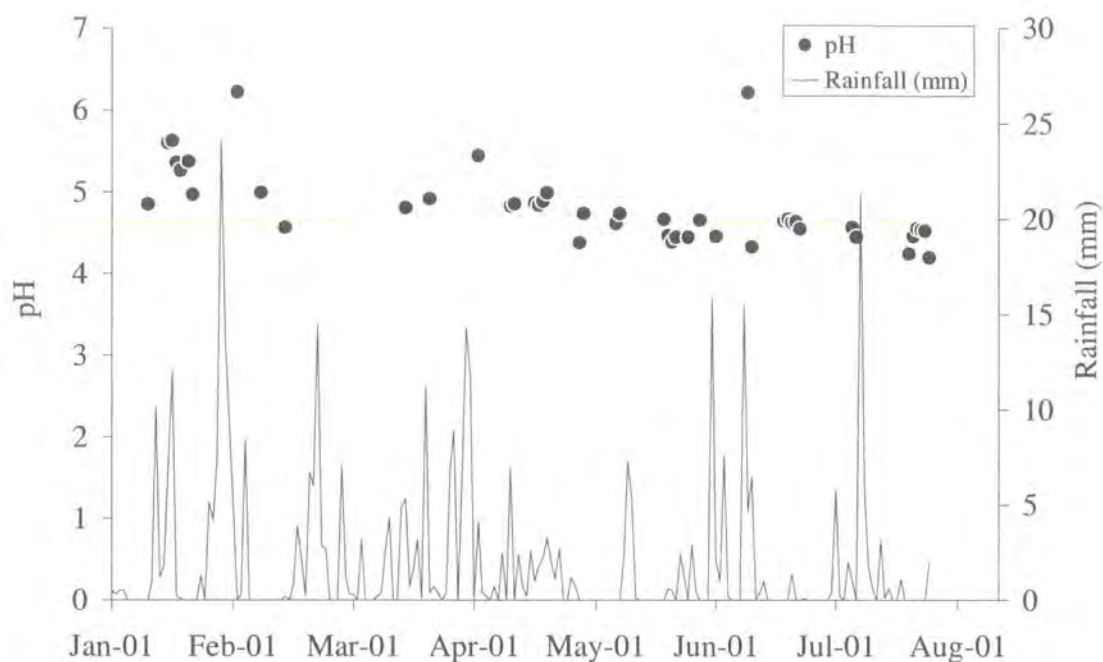
Figure 7.12. Meteorological Office rainfall data and measured discharge pH.

A comparison of measured Total dissolved solids (TDS) and total analysed ion concentration (including H^+) shows a similar increasing trend towards the summer (Figure 7.8). The almost constant difference between measured TDS and cumulative ion concentration is due to the presence of carbonate, bicarbonate, nitrate and organic ions. During and after storm events the difference between measured and cumulative TDS decreases, suggesting that the un-measured dissolved ion source was diluted. It is possible that the 2°C difference in winter-summer temperature increases biological activity within the spoil heap, leading to an increase in dissolved bicarbonate ions. Generally pH decreased over the sampling period, remaining within a narrow range of values below 5.7. However, increases in pH also coincided with or followed high precipitation, indicating dilution of the low pH water source within the spoil (Figure 7.12). Such dilution of pore water characteristics indicates meteoric water and rock leachate mixing.

Dilution of TDS and pH by heavy rainfall during winter and increase in TDS and pH during summer, both support a seasonal change in hydrological flow paths. During winter apparent increased dilution is due to the volume of rainfall flushing oxidation and weathering products from the spoil porosity. In summer, the lack of constant flushing and higher temperature led to an increase in pyrite oxidation and acidic weathering. Summer precipitation therefore leads to high concentrations and a rapid response to rainfall events. In winter and especially spring low concentrations of rock leachate and a slow response to precipitation suggests that flow collected by the pipe is retarded by the saturation of spoil material.

7.2.4.1. Ochreous deposits

During the 7 months of sampling a change in predominant ochre colour, precipitated on the receiving stream- bed and discharge pipe wall, was observed. From the previous November (2000) to February 2001 the dominant ochre on the streambed was pale yellow (Figure 7.13). From March to July 2001, the ochre blanketing the receiving watercourse was dark orange-brown (Figure 7.13). It was assumed that the change in colour was caused by precipitation of Al-hydroxide minerals in wet weather conditions and Fe (III) hydroxides during drier periods. Layering of the orange on yellow ochre in summer and yellow on orange ochre in winter is present (Figure 7.13). Younger (1995b) reports a contradictory colour change. Jarosite and gibbsite precipitation during dry periods is suggested as the source of yellow ochre, with orange ochre produced by FeOOH precipitation after surface runoff. A similar colour scheme has been reported during sampling 2 years prior to this study (Worrall, F., pers. comm.). The geochemical speciation package MINTEQ2A was used to calculate equilibrium saturation indices for monthly water chemistry. As only total concentrations in the discharge samples were analysed, all Fe was assumed to be Fe^{3+} as oxidising conditions prevailed along the length of the pipe. From January to February a decrease in the SI values of alunite, gibbsite and $Al_4(OH)10SO_4$ lead to a drop in precipitation of these typically pale yellow minerals (Figure 7.14, Nordstrom, 1982). A simultaneous drop in haematite, goethite and lepidocrocite SI value, was not sufficient to prevent precipitation of these minerals (Figure 7.15). Discharge saturation with respect to K, Na and hydrated jarosite all increased from January to June leading to increased precipitation of the yellow minerals. Although the discharge became saturated with respect Al-hydroxides after February, saturation of Fe^{3+} hydroxide minerals was greater. A comparison of typical discharge chemistry reported by Younger in 1995(b), with
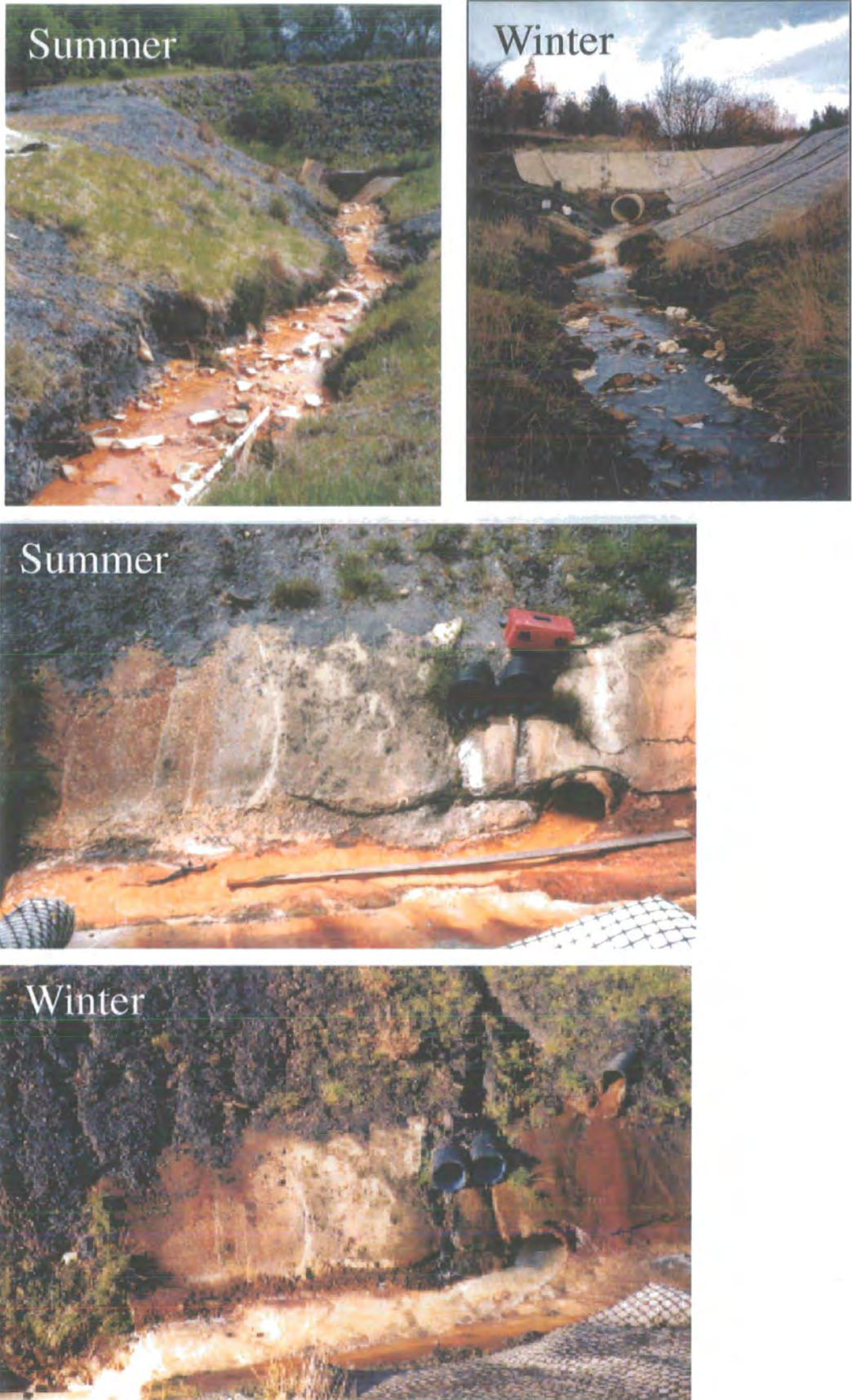
Figure 7.13. Colour change of precipitate ochre during from pale yellow-white in winter to dark orange in summer. Change in typical receiving watercourse is most marked going from Al 'foam' to blanketing Fe-hydroxide.
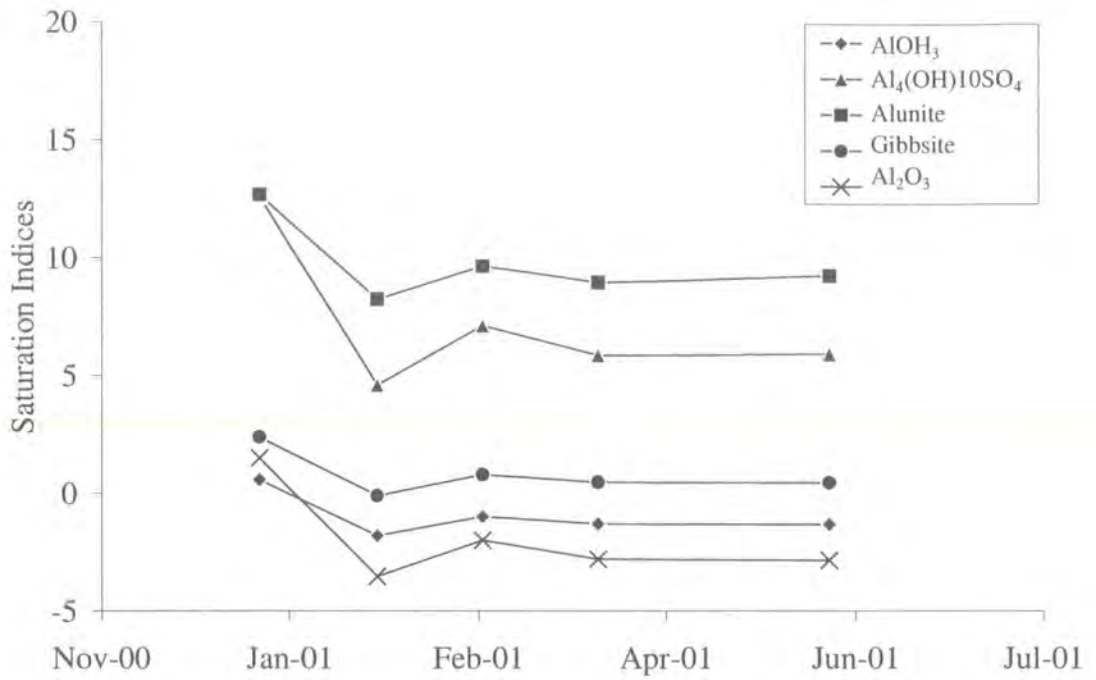
Figure 7.14. Saturation indices for Al hydroxides, calculated from discharge data from winter to summer using MINTEQ2A.
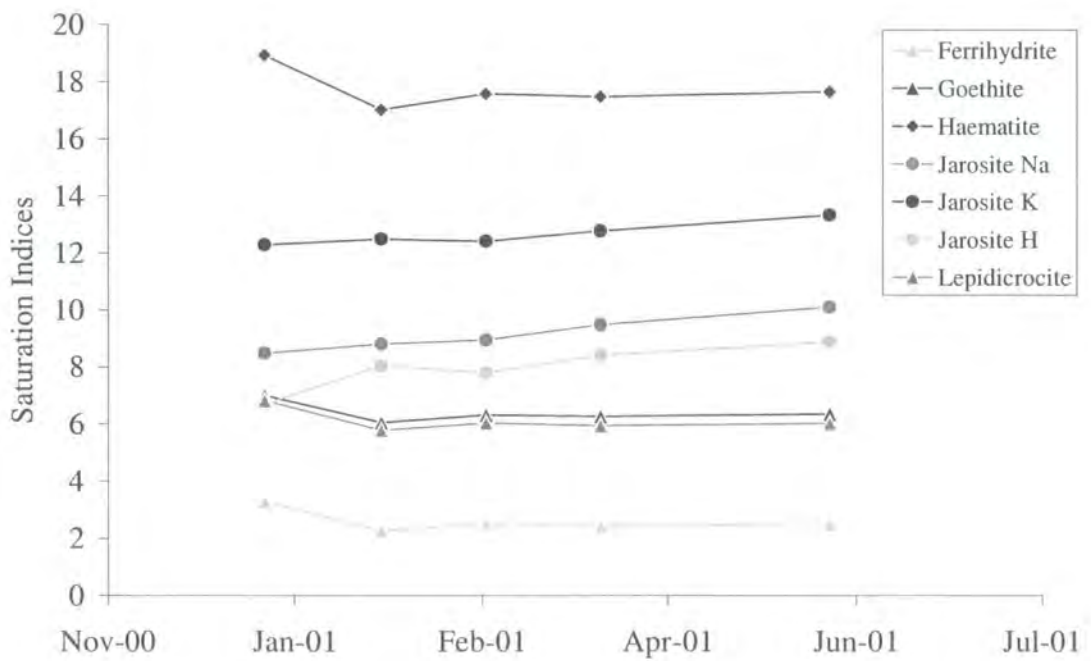
Figure 7.15. Saturation indices for Fe-hydroxides, calculated from discharge data from winter to summer using MINTEQ2A.

mean values collected in 2001 indicate an increase in dissolved Al and Zn. Mean dissolved Al, Ca, Fe, Mg and Na concentrations collected during 2001 represented a range including values reported by Younger in 1995(b). The range of dissolved Zn measured in this study, and most of the Al concentrations (Table 7.B, Appendix II Results), were greater than dissolved concentrations for the discharge reported by Younger (1995b). The equilibrium SI of gibbsite increases with decreasing pH from the solubility minimum of pH 6.2 (Drever, 1997). Assuming relatively constant dissolved Al concentration throughout the year, lowered pH during summer months would lead to an increase in gibbsite SI and a decrease in precipitation. In the winter months, increased discharge pH would have led to a drop in gibbsite SI and an increase in precipitation. Such a mechanism would explain the seasonal ochre colour change and the higher concentration of Al in solution rather than in the solid phase.

Increased dissolved Zn concentrations may have been produced by dissolution of Fe hydroxides precipitated on the pipe and watercourse bed. The co-precipitation and adsorption of Al and Zn with Fe hydroxides and oxides has widely been reported (Simms et al., 2001, Fuge et al., 1994, Herbert, 1996). Lowered discharge pH in spring and summer would increase dissolution of these Fe hydroxides, increasing dissolved Al and Zn. However, this mechanism would be in place during previous years of sampling. The suggested mechanisms for increasing dissolved Al and Zn compared to concentrations reported in previous years require a significant change between winter and summer pH. Heavy precipitation over the previous winter (2000) would have lead to flushing of a greater volume of soluble material increasing discharge pH over spring as well as winter. Re-grassing of the land overlying most of the pipe's watershed during spring 2001 would have also exposed the spoil to greater infiltration of meteoric water. Flushing of a high proportion of material during the previous year may have left the spoil material relatively 'clean' with respect to acidic soluble salts. Increased infiltrating flow allowed by a change in surface vegetation would have contributed to the flushing of soluble material. Prior extensive flushing of heap material and resultant increased winter and spring discharge pH led to decreased summer discharge dissolved Al and controlled the observed ochre colour change.

7.5 Discussion

7.5.1. Chemical hydrograph separation.

The relative contributions of pore water to the AMD discharge over the period of sampling were calculated using the storm hydrograph. Pinder and Jones (1969) described stream water chemistry in terms of conservative tracer mixing between two chemically distinct sources with respect to the tracer (equation 7.1). Chemical interaction between groundwater (base-flow) and direct run-off, and changes in source chemistry through time are assumed not to occur.

In this study the highest and lowest concentrations of Si and Na, as measured during sampling, were assumed to represent base-flow and direct run-off chemistry. Separation was performed using Na and Si as these dissolved ions have been used previously for an AMD discharge (Al and Blowes, 1996). Comparison of the pore water contribution with the total discharge composition suggests that at times of event flow, base-flow contribution was up to 50 % (Figures 7.16 and 7.17). However, during relatively steady flow the pore water contribution is low, below 10-5%. The storm hydrograph contribution is in agreement with previous studies of mine tailings (Al and Blowes, 1996). The difference between Na and Si chemical hydrograph suggests that Na does not act conservatively relative to dissolved Si behaviour (Figures 7.16 and 7.17).

7.1.5.1.Conservative mixing and potential end-members

A matrix scatter plot of all major element concentrations shows two end-member mixing lines from high to low concentration for most comparisons (Figure 7.18). The two end members represent peak flow during winter, i.e. high dilution and peak flow during summer, i.e. post precipitation flushing of high concentrations into base-flow (Figure 7.19). However, comparison of K, Si and Na with other element concentrations suggests the presence of three end-members. Closer examination indicates that the different hydrological sources are produced by seasonal changes in precipitation and spoil heap saturation (Figure7.20). In the case of K versus Fe, the three end-members represent; winter peak flow, summer base flow and summer peak flow. Low concentrations removed during summer base flow imply that the precipitation of jarosite may have affected the K concentration. During high flow in summer and increased pH, jarosite would have dissolved releasing K. Smearing of the data towards the centre of the mixing line suggests that during spring such a release mechanism was
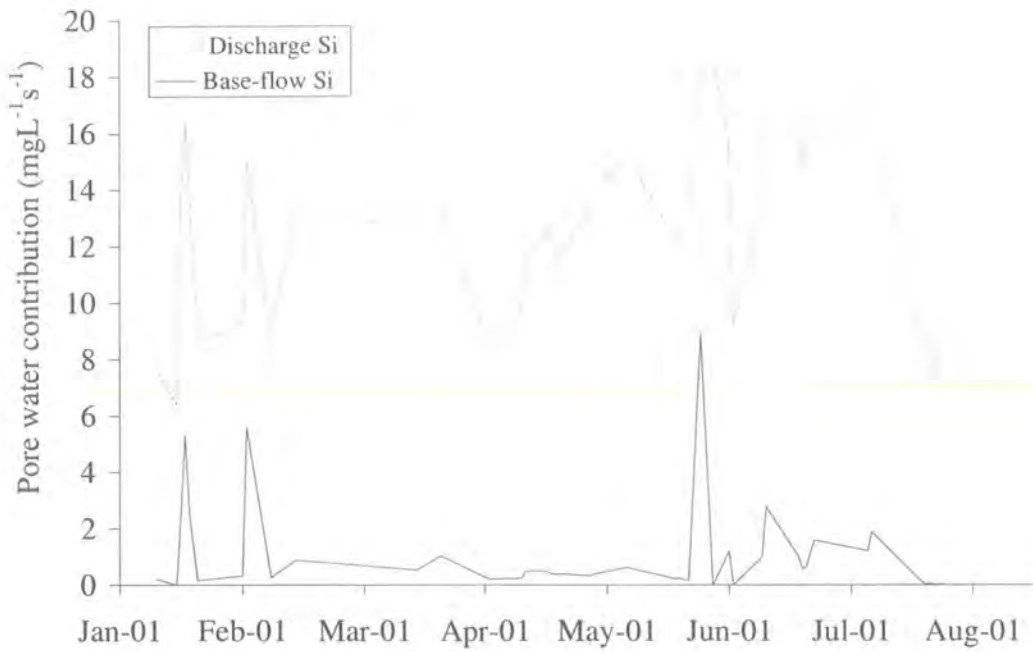
Figure 7.16. Chemical hydrograph separation over the period of sampling using Si
concentration in base-flow and peak-flow and the method described by
Pinder and Jones, (1969).
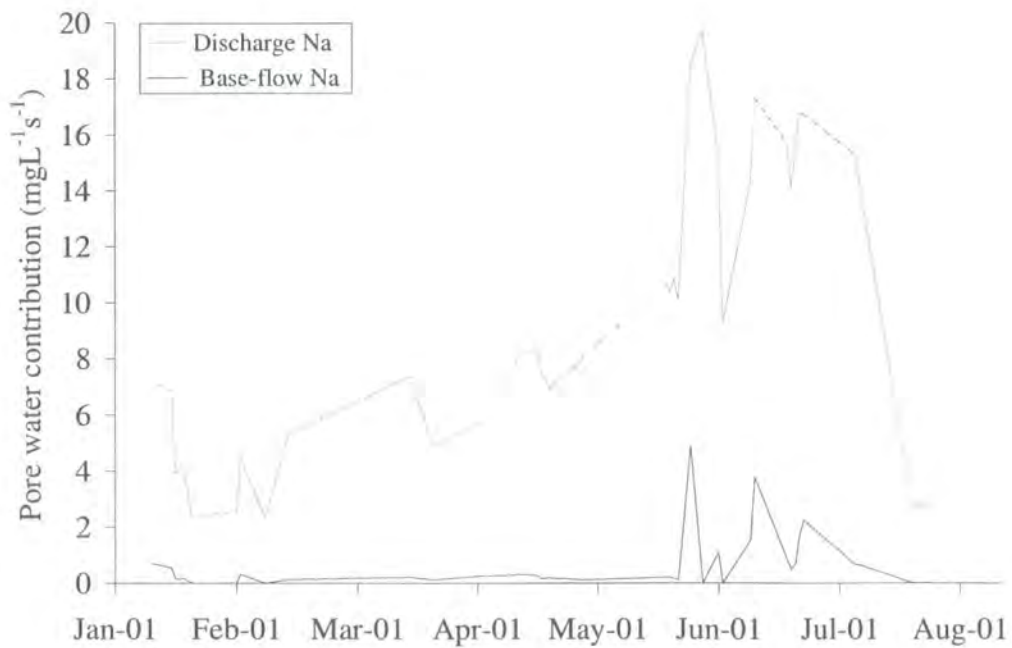
Figure 7.17. Chemical hydrograph separation over the period of sampling using Na
concentration in base-flow and peak-flow and the method described by
Pinder and Jones, (1969).

partially in place. High flow in winter would have increased cation exchange leading to higher dissolved K. The trend of high K during winter and spring flow can be attributed to greater cation exchange within the clay phase of the spoil material. In summer, hydrological flow paths are short and lead to interaction with base-flow, which probably originates in the oxidised zone of the spoil.

Such comparison of the chemical characteristics of the discharge and the discharge chemical hydrograph suggests that in the summer a lower volume of material is interacted with in terms of flow-path, apart from during storm events when a large amount of material is dissolved. A high volume of material interacts with water when the water table is high. Continued flushing of the spoil material in spring leads to the removal of low concentrations of dissolved salts. Responses to event rainfall in terms of chemical dilution may be low suggesting that pore water was already diluted within spoil due to the high water table. During the summer response is sharp with high dilution and rapid recovery after rainfall. Dry summer periods allowed the precipitation of soluble salts that were rapidly dissolved during relatively low volume storm events. Thus although the relative flow volume is lower than in the winter and spring, the flux of dissolved salts is of a similar if not higher magnitude in the summer. The dry and cold period over the winter months prior to sampling led to high concentrations during the initial storm events of the year. Although summer base-flow is assumed to represent the maximum concentration of dissolved salts, a winter high is also possible.

7.5.2. Principal component analysis

PCA was performed on solute concentrations for Al, Ca, Fe, K, Mg, Na, S, Zn, and Si, then for these solutes plus pH and flow-rate. Data was standardised by taking the mean from the actual value and dividing by the standard deviation. Such a transformation allows direct comparison of small and large values and of measurements in different units. A correlation matrix is used to scale the data by their variance.

7.2.5.1. Major element chemistry, pH and flow-rate PCA

PCA of discharge Al, Ca, K, Fe, Mg, Mn, Na, S, Zn and Si concentration produced four components which described up to 97% of the variation in data (Table 7.2).

The first component explained 76 % of variation with positive loadings for all elements and negative loadings values for pH and flow-rate. The second component explained up to 15 % of variation with positive loading on Al, Fe, S, Zn and Mn and high negative loading on Ca, K, Mg, Na, Si, pH and flow-rate. Such groupings suggests an ion exchange / clay reaction versus sulphide oxidation / acidic weathering
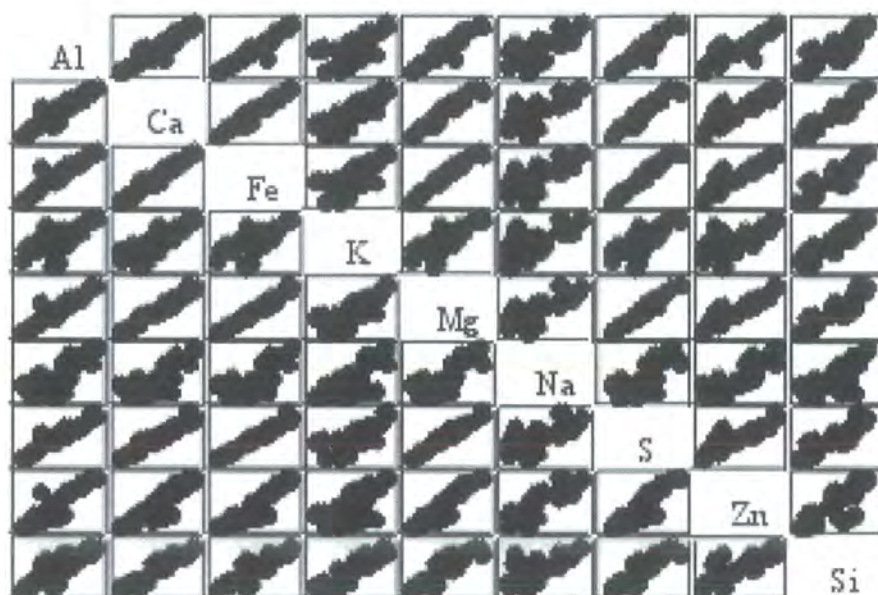
Figure 7.18. Matrix scatter plot, comparing all major element dissolved concentrations which each other over the period of discharge sampling.
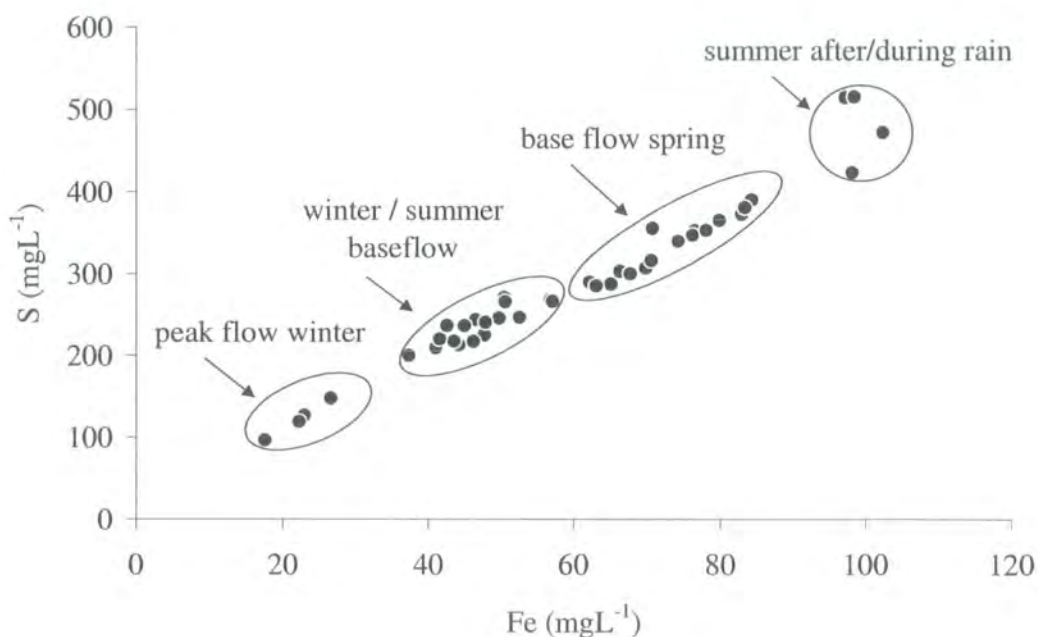
Figure 7.19. Plot of discharge dissolved S versus Fe concentration over the period of sampling. Water sources are marked on graph showing 2 potential end-members of peak winter and summer flow.
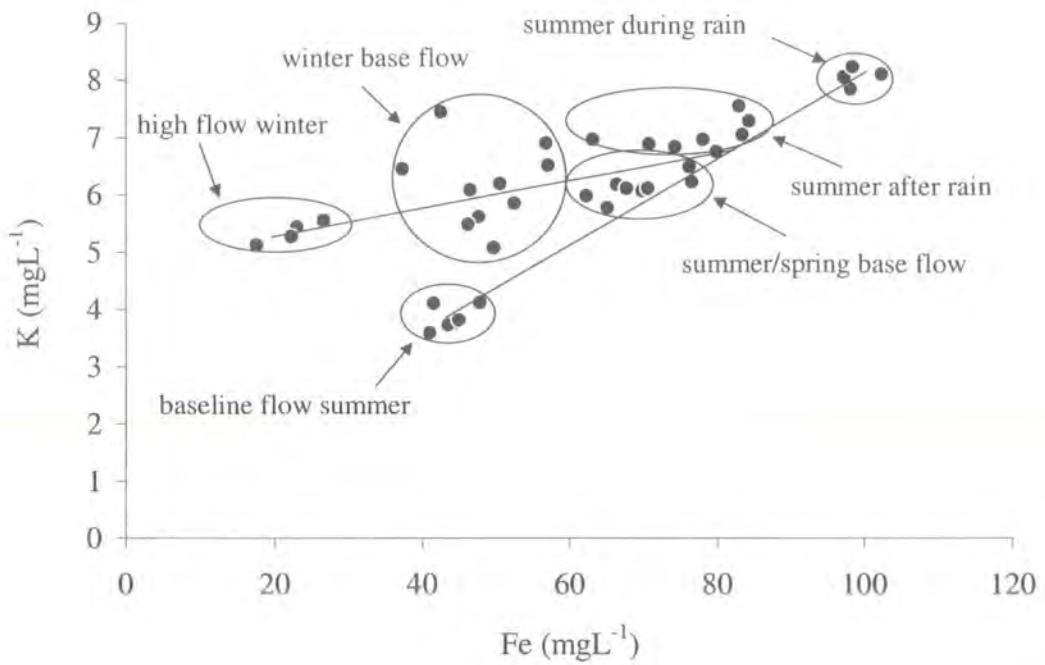
Figure 7.20. Plot of discharge dissolved K versus Fe concentration over the period of sampling. Water sources are marked on graph showing 3 potential end-members of peak winter and summer flow and summer base flow.
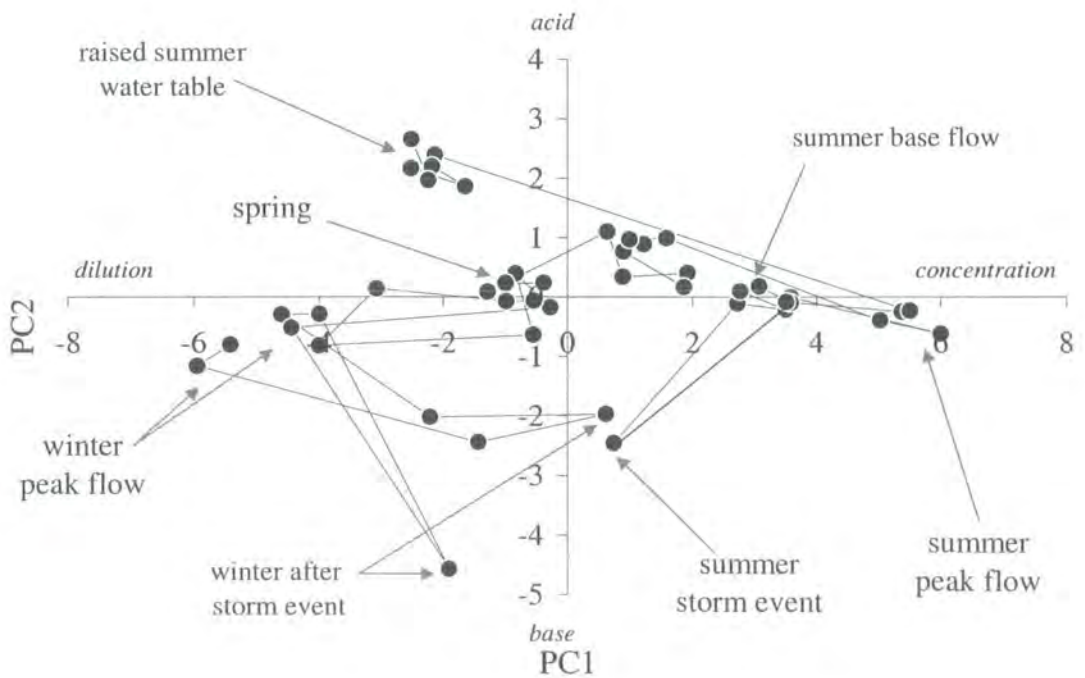
Figure 7.21. Comparison of factor scores for first and second principal components derived from PCA on discharge major element concentration, pH and flow rate. Characteristics of each component are marked in italics on each axis. Line shows chronological order of samples.

component. It is probable that this component represents the flushing of pyrite oxidation products from the heap after dry periods and the input of ion exchange and clay dissolution after continual heap flushing.

Characteristic	PC1	PC2	PC3	PC4
Al	0.316	0.071	0.195	0.132
Ca	0.322	-0.105	0.180	-0.061
Fe	0.327	0.032	0.190	0.056
K	0.254	-0.422	-0.112	-0.331
Mg	0.317	-0.079	0.022	0.071
Mn	0.321	0.085	0.134	0.118
Na	0.282	-0.095	-0.795	0.035
S	0.323	0.002	0.281	0.026
Zn	0.314	0.099	-0.341	0.203
Si	0.295	-0.282	0.170	-0.240
PH	-0.131	-0.609	0.073	0.769
Flow-rate	-0.185	-0.567	0.014	-0.393
% variance	76	15	3	2

Table 7.2. Calculated principal component characteristic loadings for Bowden Close discharge chemistry and flow-rate over January to July 2001.

A third component with high negative Na, Zn and K was identified, explaining up to 3 % of the data variation. Positive factor loadings on pH and flow-rate are low for this component, but still identify with a general summer to winter pH and flow-rate positive correlation. As Na and K are products of ion exchange, the third principal component represents a certain amount of chemical reaction. Positive Zn and negative pH factor loading suggests leaching of Zn originally adsorbed or co-precipitated with Fe-hydroxides (Simms et al., 2000). Such leaching also supports prolonged reaction of meteoric water with spoil material. Potentially the third principal component represents the extent of chemical evolution of the discharge, i.e. the contribution from rapid subsurface flow paths and slowly infiltrating flow paths i.e. base-flow.

The fourth identified component explains 2 % of data variation and describes high positive pH versus negative flow-rate, Si, K and Ca. Negative correlation of pH and flow-rate for this component suggests mixing between summer peak flow and summer

base-flow. In scatter plots K and Si showed the different input to summer base flow and other mixed compositions far better than any other element concentration. Low concentrations of these elements in the summer base flow is due to the lack of input of ion-exchanged and clay weathering products. The lack of Ca also suggests that products of carbonates and gypsum dissolution are not identified in the discharge until rainfall occurs. Summer base-flow therefore originates in the lower levels of spoil material where the products of oxidation are removed.

7.2.5.2. Identifying potential end-member sources.

Comparison of the scores for each principal component should allow identification of the relative positioning of end-member compositions mixing to provide discharge chemistry. Orthogonal projection of the first three identified components (PC1, 2 and 3) reveals mixing between four chemically distinct sources or end-members, each of which depend on the extent of spoil flushing and previous drying (Figures 7.21 to 7.23). Comparison with the fourth component of summer base-flow - summer peak flow is inconclusive. Only two sample points make up the variation described by component four when plotted against other component scores. As neutralisation in the upper levels of spoil material was identified by this component, suggesting that the neutralisation capacity of carbonate phase minerals in the spoil is low. Processes described by this component are therefore relatively unimportant to the data set as a whole. It is possible that year round sampling may have led to an increase in samples affected by this fourth principle component.

Concentration versus acid-base / flow rate characteristics

Mixing between high and low concentration pore water strongly controls discharge chemistry, whilst pH and flow-rate produce an orthogonal departure from this main trend (Figure 7.21). The composition of summer and winter peak flow differ most in terms of dissolved concentration. Obviously high rainfall during winter months leads to greater dilution of base-flow. Despite the differences in dissolved content caused by summer storm events flushing the unsaturated spoil, the acid-base character of this flow is close to that of winter peak flow. During flushing of the un-saturated zone the some neutralisation of flushed acid pyrite oxidation products must have taken place. Summer rainfall removes pyrite oxidation products from the un-saturated zone increasing concentration relative to summer base-flow. Summer base-flow contributes to both summer peak flow caused by rainfall and summer storm events, although in the later case dilution is also important. A group of summer samples plot in the region of
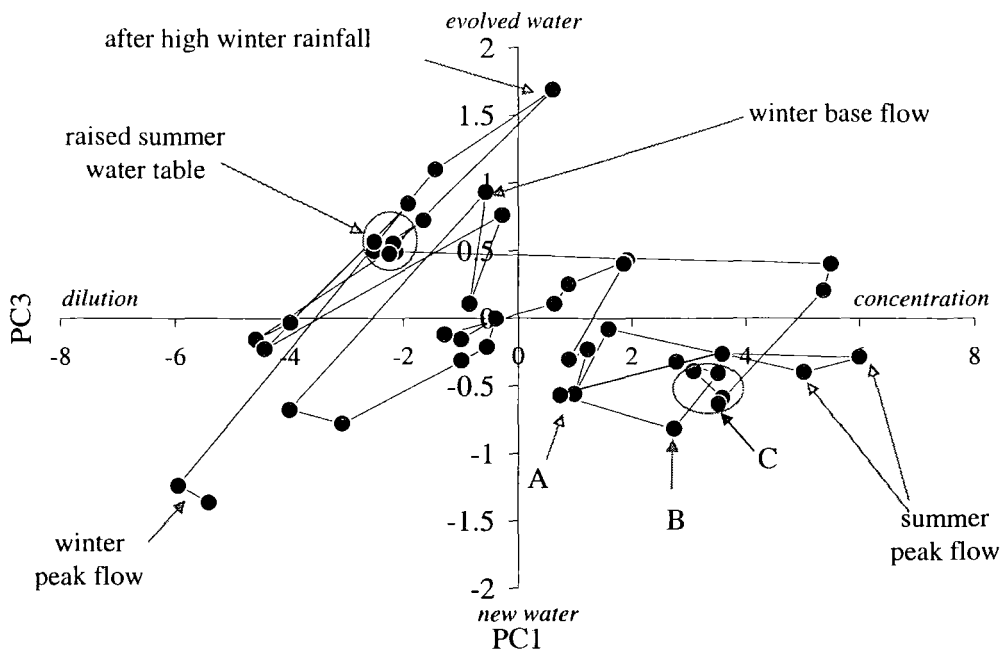
Figure 7.22. Comparison of factor scores for first and third principal components derived from PCA on discharge major element concentration, pH and flow rate. Characteristics of each component are marked in italics on each axis. Labels A-C are described in the text. Line shows chronological order of samples.
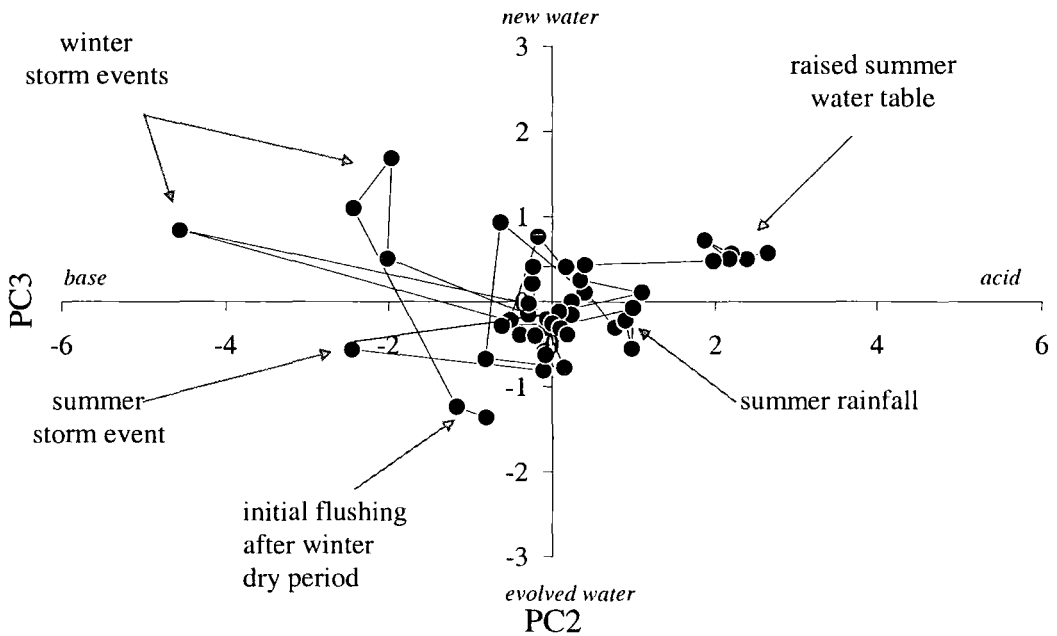
Figure 7.23. Comparison of factor scores for third and second principal components derived from PCA on discharge major element concentration, pH and flow rate. Characteristics of each component are marked in italics on each axis. Line shows chronological order of samples.

251

increased dilution and acidity (Figure 7.21). The samples were collected after 14 days of continual rainfall following a storm event that increased the height of spoil saturation. Elevation of the water table would have forced infiltrating rainfall to flow rapidly, through recently oxidised material.

Mixing rainfall composition and spoil pore water, i.e. high pH plus ion exchange and clay weathering products, produces winter discharge chemistry. More dilute compositions represent water that has travelled through the spoil material along rapid flow-paths, i.e. quick-flow. The more 'reacted' water, with a greater basic character, has travelled more slowly through saturated spoil to the point of discharge. During spring (February-April) composition and flow-rate remain relatively constant as rainfall decreases and the evolved remnants of winter base-flow are released. Storm events during this period lead to dilution of base-flow. Summer peak discharge chemistry results from flushing of pyrite oxidation products in unsaturated spoil along rapid subsurface flow-paths. Summer base flow results from the remnants of peak discharge, and is made up of water which infiltrated the spoil material along slow flow paths, probably travelling through the saturated zone. When the summer water table rises due to prolonged rainfall, discharge chemistry becomes more dilute, yet the acid character of the discharge increases due to flushing of pyrite oxidation products.

Concentration component versus old water / new water component

Comparison of concentration and old / new water components demonstrates mixing between dilute rainfall and an evolved or reacted water source (Figure 7.22). In general variation in mixing between meteoric water and the spoil pore water decreases towards the summer due to the lack of rainfall. Summer samples collected during increased saturation of the spoil show a similar extent of dilution as caused by winter rainfall.

Winter peak and base flow differ due to the input of rainfall, leading to high flow rates, high pH and decreased concentration. Although winter base-flow composition has high concentrations of ion exchange and pyrite oxidation products, discharge after winter peak flow has even higher TDS. During winter and summer storm events TDS only appears to increase after peak rainfall (Figures 7.9 to 7.11). Chemical hydrograph separation suggests that the contribution of base-flow to discharge during winter storms can be up to 50%. Piston flow, produced by displacement of spoil pore water into the discharge during high rainfall, would provide such a large volume of chemically evolved base-flow (Ward and Robinson, 1990).

During the transition from winter to summer, lower rainfall leads to lower variation in contributions from old and new water. As previously mentioned the storm hydrograph for summer and winter months suggests that contribution from a high concentration water source is delayed until after peak rainfall. Comparison of the evolved nature of a water source and the discharge concentration indicates that during a summer storm (Figure 7.22 point A), discharge composition was diluted. Directly after the storm event discharge concentration increased (Figure 7.22 point B), and subsequently the discharge composition contained a greater proportion of evolved water (Figure 7.22 point C). Interpretation of such a sequence suggests that initially subsurface rapid flow of rainwater contributed to the discharge. A day after the storm event, discharge composition contained a high concentration of un-saturated zone soluble material. At 8 days after the storm event discharge composition had become more evolved, returning to base-flow composition. During summer storm events quick subsurface flow dominates the discharge chemistry, leading to dilution. After storm events high concentrations flushed during infiltration flow along slower hydrological paths make a high contribution to discharge. Recovery of the system after the storm event leads to the discharge of water that has either travelled along even slower hydrological paths, or more likely, is less diluted by subsurface quick flow.

Prolonged rainfall for 14 days after a dry summer period, and the ensuing rise in water table, led to a decrease in discharge concentration but little change in the evolved nature. Discharge collected 14 days after the initial storm events either consisted of diluted base flow or slow infiltrating flow. Given the rise in water table and the close grouping of samples over a period of 7 days it is probable that dilution of base-flow by infiltrating rainfall has occurred. As these were the last samples collected from the discharge, further evolution of the discharge chemistry is difficult to predict. Depending on subsequent rainfall volume and longevity the discharge base-flow component may have remained diluted or returned to summer base-flow composition.

Evolved state of water source versus acid-base characteristic.

Comparison of the acid-base nature of discharge chemistry and the evolved state of flushed water depends upon the prior saturation of material and the size of precipitation event (Figure 7.23). Summer storm events and the first rainfall of winter, after a dry, cold January, flush large volumes of relatively new dilute water through quick subsurface flow paths. The contribution of reacted old water is high compared to later in the year when the spoil is more saturated. Storm events later in the wet season

mostly contribute new water through quick subsurface flow to the discharge. The difference in water sources between saturated and unsaturated conditions indicate the retarding of slow infiltration flow by a high water table. Conversely the group of summer post peak flow sample have a greater proportion of new water and acidic character compared to summer base-flow. Contribution from a new water source with acid characteristics still occurs at 14 days after an initial period of high rainfall and relatively continuous low rainfall. Continued rainfall, albeit at a low level (~ 1mm per day after the initial three day event) appears to have raised the water table, leading to supply to discharge along rapid sub-surface flow-paths. The acid character of this group of samples can be attributed to flushing of pyrite oxidation products from the originally unsaturated heap.

Summary of PCA

Composition and mixing of winter and summer base-flow water sources in spoil material prior to discharge are all controlled by meteoric precipitation. High flushing in the winter and spring periods led to a removal of a high volume of soluble salts from the heap. Variation in discharge in both summer and winter is caused by dilution of base-flow by storm events, and increased concentration due to flushing of the unsaturated zone. During winter flushing the dominant dissolved material is derived from ion exchange and clay weathering. Pyrite oxidation products dominate the summer base flow and peak discharge compositions. Elevation of the summer water table leads to dilution of base flow and therefore of discharge composition for long periods of time.

7.5.3. Implications for discharge characterisation

Two seasonally controlled end-member compositions of spoil pore water mix with rainfall to provide the discharge chemistry at Bowden Close. The two end-members are temporally and spatially controlled by precipitation volume, i.e. the extent of heap flushing, saturation and dry period available for the build up of oxidation products. Precipitation volume and the availability of soluble material, control the formation of AMD at this site.

In this study, summer and winter base flow are defined as chemically distinct sources of pore water. However, for hydrograph separation the base-flow contribution was defined as one conservative chemical source. Christopherson and Hooper (1990) indicate that in hydrograph separation the use of pre-defined end-members may lead to errors in the final calculation of ground water contribution. PCA suggests that for AMD data at least, separate summer and winter base flow compositions should be used

in chemical hydrograph separation rather than maximum and minimum conservative tracer values.

Most characterisation of spoil heap AMD discharge tends to occur during summer months when base-flow is little diluted by heavy precipitation. Typically base-flow characteristics are used to monitor pyrite oxidation rates from dissolved sulphate, which is less diluted during dry periods. However, care should be taken to ensure that base flow is collected rather than post storm event run-off. As previously mentioned the difference between summer base and peak flow may also provide a good estimation of pyrite oxidation rates within the un-saturated zone.

As the temperate UK climate usually provides relatively dry winters with little snowfall, a build up in pyrite oxidation product may occur during this period. Heavy late-winter to early-spring flushing may therefore also provide a high proportion dissolved metal species at a high volume of flow. Combined high flow-rate and formation of colloidal metal species will lead to an increase in the distance travelled by AMD pollutants such as Al (Pffifer et al., 1996). Where the typical summer loading and flow rate are used to design remediation strategy, winter fluctuations may be ignored. Characterisation of seasonal changes in discharge is necessary in order to incorporate such fluctuations into the design of a suitable remediation treatment. Given the recent increase in regularity of major 100 year flooding ev ents (Environment Agency UK) changes in the chemical characteristics of UK spoil heap discharges can be expected. As such remediation schemes need to be designed to cope with large differences in flow regime and chemical content.

7.6 Summary and Conclusions

Two chemically discrete water sources, summer and winter base flow, have been identified from the variation in chemistry of the Bowden Close discharge. Each water source is dependent on flushing volume (including prior flushing) and the extent of pyrite oxidation and soluble salt precipitation during dry periods. Summer base flow evolves into winter base flow by extensive dilution and addition of ion exchange products. The reverse process occurs due to lack of rainfall allowing a build up of pyrite oxidation products and a fall in water table. Periodic flushing of soluble salts into the lowered saturated zone increases dissolved concentration and acidity, producing summer base flow. Hydrological flow-paths are controlled by the extent of heap saturation and determine the extent of contribution from base flow and rapid subsurface flow to the discharge. Raised summer water table after prolonged rainfall leads to

dilution of summer base flow and perhaps the start of the summer to winter transformation.

Changes in base flow characteristics with time indicate that a remediation strategy account for such seasonal changes where possible. High contributions of evolved water occur in winter as well as in summer, yet the characteristics of winter discharge are relatively alkaline. Discharge volume at this particular site was constant during base-flow, yet the winter to summer change in flow rate was large.

Interpretation of chemical hydrograph separation and scatter plot matrix presentation allowed preliminary interpretation of potential end-members and seasonally dependent discharge chemistry. However use of PCA has allowed further delineation of data and identification of the amount of control over discharge chemistry each end-member has. Although specific end-member compositions are not identified the general direction of composition and processes contributing to stream chemistry have been identified.

Chapter 8

Comparison of static, cyclic and flow leaching with a field example.

8.1 Introduction

In this final chapter the work presented in this thesis is brought together in a comparative fashion.

- A comparison of water-rock regimes mimicked in Chapters 5 and 6 is made using both direct observations of chemical evolution and total flux and statistical analysis of total flux. Interpretation of the controls on leachate chemistry for each water-rock regime is made using the results of this comparison.

- The findings of water-rock regime simulation are compared to seasonal changes identified in the chemistry of an AMD discharge in Chapter 7.

- The fulfilment of objectives laid out in chapter 1 is reviewed and implications for AMD modelling considered.

- Recommendations for research following on from the presented work are made.

8.2 Comparison of water-rock regimes

The water-rock regime within a rock body, whether intact strata or waste heap, controls weathering processes and most importantly the transport of dissolved products. In Chapters 5 and 6 experiments designed to mimic the water-rock regimes in rock bodies have been described. Here, the chemical evolution of leachate and formation of pyrite oxidation fronts from different water-rock regimes are evaluated. A comparison of the total flux of material from each water-rock regime is also made to show which style of water-rock interaction potentially produces the greatest volume of pollutant. Combined interpretation and statistical analysis of total flux is used to determine the importance of processes controlling embedded mineral weathering at the waste particle scale.

8.2.1 Comparison of total flux from different water-rock regimes

Leachate evolution patterns in dissolved output from mimicked water-rock regimes suggest that increased dissolved content was a result of longer exposure to water. To quantify contributions to discharge from each mimicked zone, total flux of dissolved matter from each zone over the period of leaching may be compared. Before any comparison is made, corrections are required for the effects of dilution and exposure time to water. As static and cyclic leaching experiments were over three times the

length of flushing experiments some adjustment for different exposure times is required
prior to comparison (Table 8.1). Similarly, the volume of water used differed between
water-rock regimes, and therefore correction to total flux is required. The total flux of
dissolved matter was corrected for total volume of water used in leaching and estimated
total time of exposure to water (Table 8.1). Flux rate values are reported in mg of
dissolved element, per g of the original waste rock, per day of exposure ($mgg^{-1}day^{-1}$).
Exposure time for flushed samples was estimated at half the total number of days of the
experiment, due to pump tubing inefficiency. Elemental flux rates were also calculated
in order to determine the dissolution of different mineral phases with changing water-
rock regime (Figures 8.1-8.6, Table 8.A., Appendix II Results).

Treatment	Time of exposure (days)	Volume of water (mL)	Style of exposure
Cyclically leached	191	1470	Static
Statically leached	383	70	Static
Upper daily flushed	3.33	4000	Kinetic
Lower daily flushed	1.67	2000	Kinetic
Upper weekly flushed	1.25	1050	Kinetic
Lower weekly flushed	0.63	525	Kinetic

Table 8.1. Treatment parameters for all water-rock regimes.

Treatment	UWC	UWS	WC	WS
Cyclically leached	0.003 ± 0.001	0.015 ± 0.005	0.0016 ± 0.0002	0.0031 ± 0.0007
Statically leached	0.00009 ± 0.00003	0.00022 ± 0.00003	0.00014 ± 0.00007	0.00012 ± 0.00002
Upper daily flushed	0.085 ± 0.002	0.152 ± 0.007	0.8 ± 0.5	0.9 ± 0.7
Lower daily flushed	0.052 ± 0.005	0.57 ± 0.02	1.9 ± 0.4	3 ± 2
Upper weekly flushed	0.013 ± 0.002	1.55 ± 0.06	0.54 ± 0.09	0.8 ± 0.2
Lower weekly flushed	0.014 ± 0.002	0.07 ± 0.05	2 ± 1	2.1 ± 0.8

Table 8.2. Total flux for individual treatments of each lithology in mg of dissolved
material, per g of original sample, per day of leaching ($mgg^{-1}day^{-1}$).
Values are the sum of mean values calculated from replicates of each
treatment and therefore differ from direct calculation using values in
Table 6.4. Errors shown are 1σ, n=4 for cyclically leached, 3 for
statically leached and 2 for all other treatments.

Mean total element flux per day was greatest from the shale rock-types under
flushing water-rock regimes (Table 8.2). Stagnantly and cyclically leached fluxes were
lower than that calculated for the flushed samples. Samples leached with purified rather
than mineralised water also tended to release lower fluxes, especially from the

weathered rock types (Table 8.2). Extended drying time for the flushed samples only made a noticeable difference for the un-weathered rock-types. For the weathered rock types, flushing with mineralised water produces a higher flux. For the UWS, weekly flushing with mineralised water lead to the greatest flux, suggesting that prolonged drying lead to a build up of material more rapidly removed by Milli-RO water.

Individual element flux

Breakdown of the total flux into individual element flux allows interpretation of the key minerals phases and reactions producing the bulk of leachate content. Gypsum dissolution made up a large proportion of soluble material removed from the UWS (Figure 8.1). The high output from weekly flushing of the UWS with Milli-RO water suggests that neutralisation of pyrite oxidation products during longer drying periods produced more dissolution of carbonate and dolomite.

The UWC released the lowest overall flux of dissolved matter for all water rock regimes. Although the low inorganic mineral content limited the volume of ionic material dissolved, elements released suggested gypsum dissolution, ion exchange and pyrite oxidation (Figure 8.2).

Pyrite oxidation and secondary mineral dissolution both contributed to the high flux of dissolved material from weathered rock-types (Figures 8.3 and 8.4). Prolonged drying increased dissolved flux. With the lower volume of water used in weekly flushing (Table 8.1) the flux at each sampling was greater than from each daily flushing.

Cyclic and stagnant leaching dissolved gypsum in the UWS (Figures 8.5 and 8.6), whilst pyrite oxidation provided material from the weathered rock types. The WS released a lower and higher volume of material during stagnant and cyclic leaching respectively compared to the WC (Table 8.1). Pyrite oxidation fronts in stagnantly leached rock were observed further into samples than during cyclic leaching. The higher pyrite content of the WC would have led to a greater flux of Fe, S and Ca during stagnant leaching (Figure 8.4). During cyclic leaching the influx of oxidant to the rock matrix was limited by pore size distribution, of which the shale had a greater fraction of macro and meso-porosity. During cyclic leaching oxidation was concentrated in the outer regions of rock, with pyrite close to larger pore spaces more vulnerable to oxidation. As the shale has a higher proportion of larger pore spaces more of albeit a smaller pyrite population was oxidised in the WS, compared with the WC by cyclic leaching.
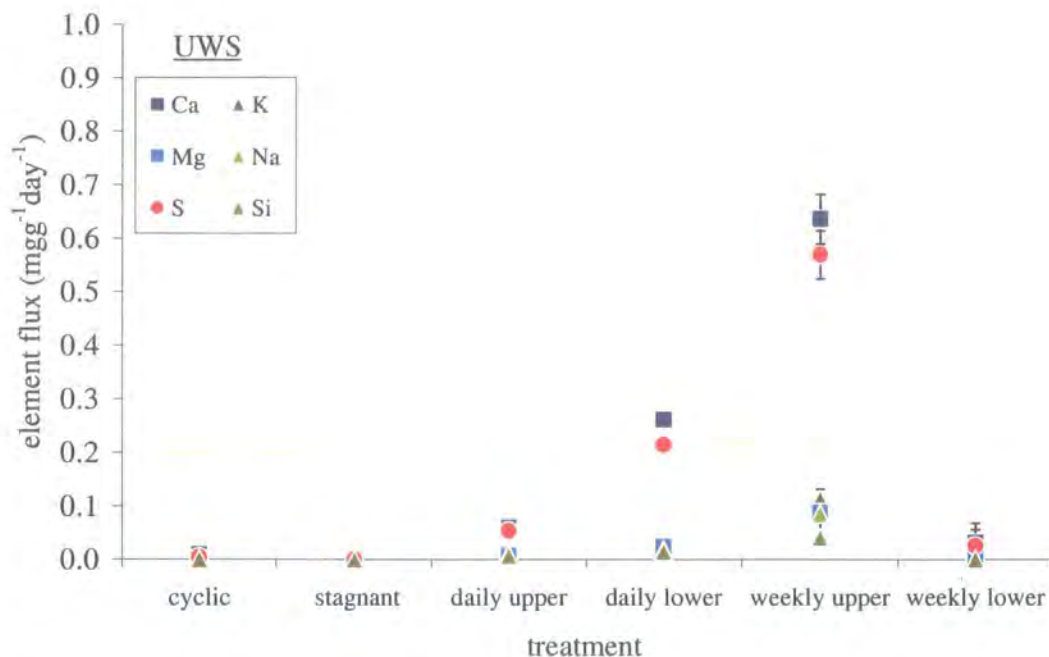
Figure 8.1. UWS leachate element flux (mgg^{-1}day^{-1}) for each water-rock regime.
Errors shown are 1σ, n=4 for cyclic, 3 for stagnant, and 2 to daily and
weekly upper and lower flushed samples.
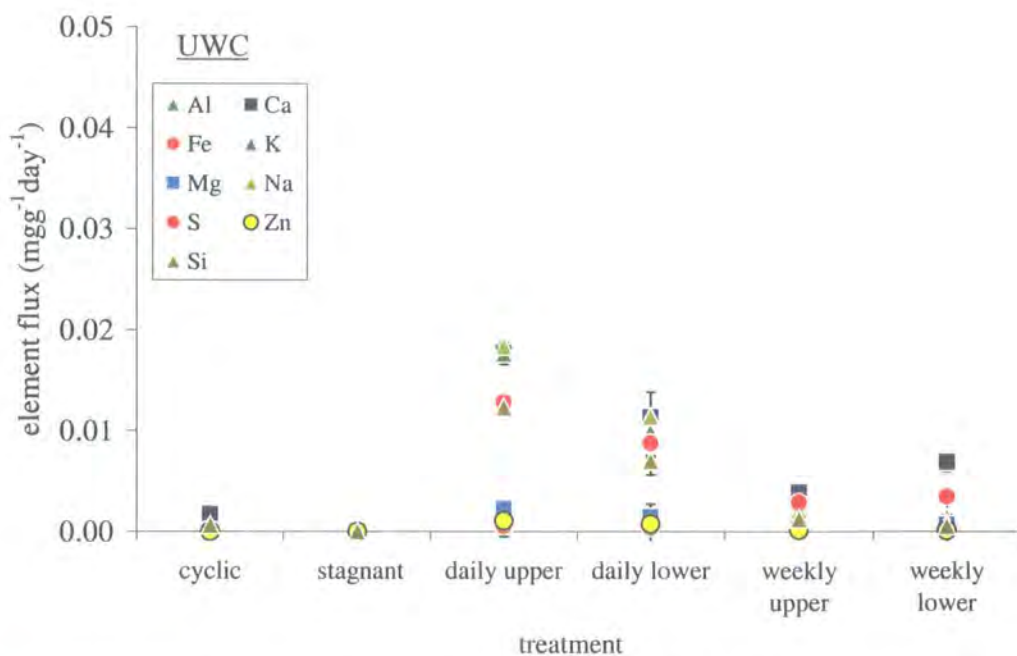
Figure 8.2. UWC leachate element flux (mgg^{-1}day^{-1}) for each water-rock regime.
Errors shown are 1σ, n=4 for cyclic, 3 for stagnant, and 2 to daily and
weekly upper and lower flushed samples..
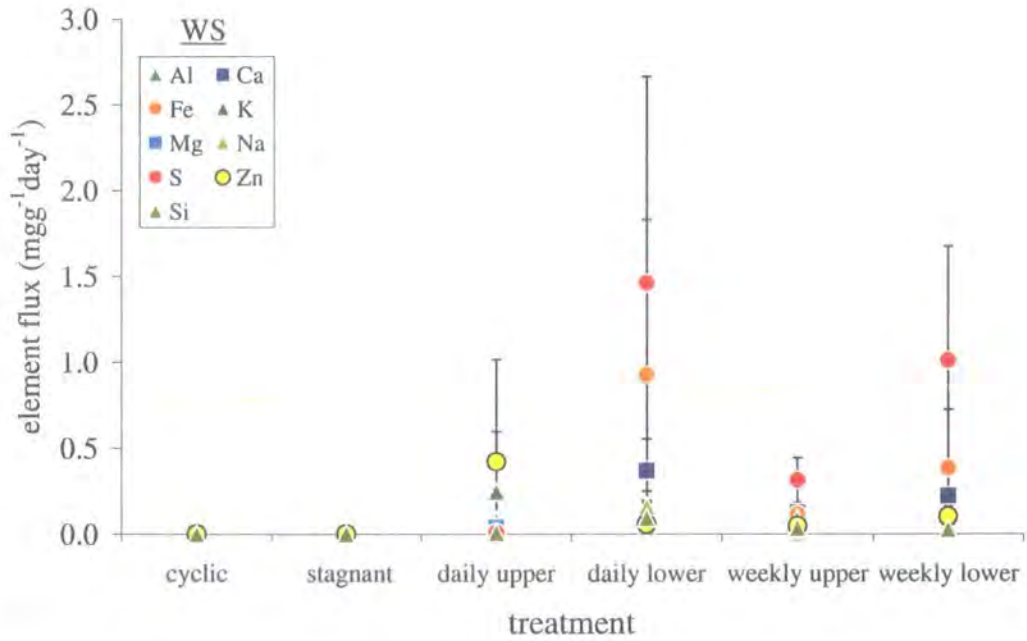
Figure 8.3. WS leachate element flux ($mgg^{-1}day^{-1}$) for each water-rock regime. Errors shown are 1σ, n=4 for cyclic, 3 for stagnant, and 2 to daily and weekly upper and lower flushed samples.
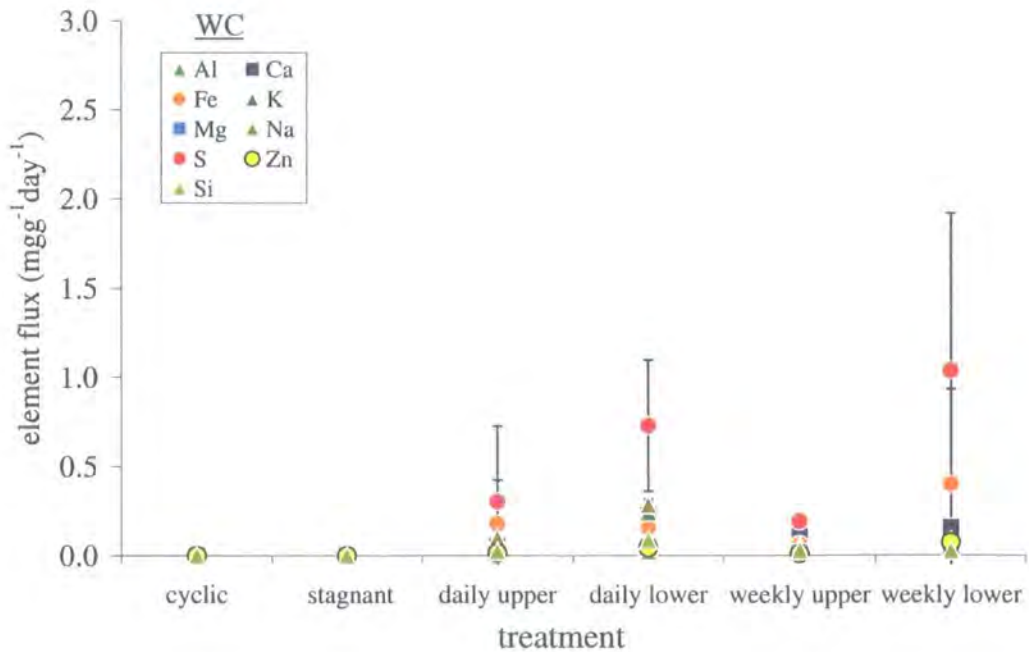
Figure 8.4. WC leachate element flux ($mgg^{-1}day^{-1}$) for each water-rock regime. Errors shown are 1σ, n=4 for cyclic, 3 for stagnant, and 2 to daily and weekly upper and lower flushed samples.
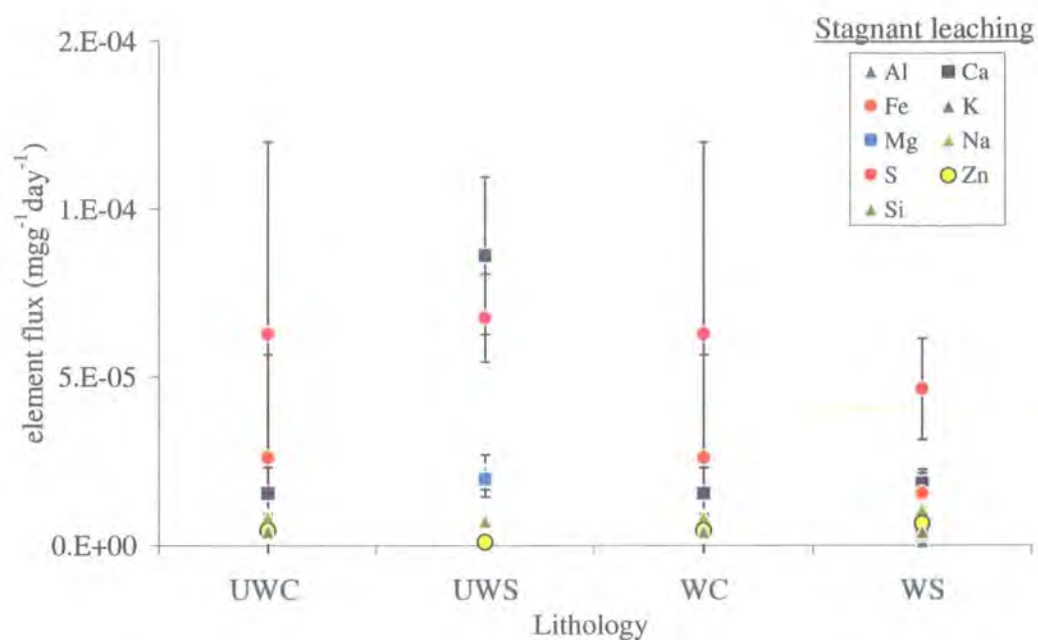
Figure 8.5. Stagnant leaching - element flux ($mgg^{-1}day^{-1}$) for each rock-type. Errors shown are 1σ for the mean maximum concentration analysed during stagnant leaching of each rock type, n=3
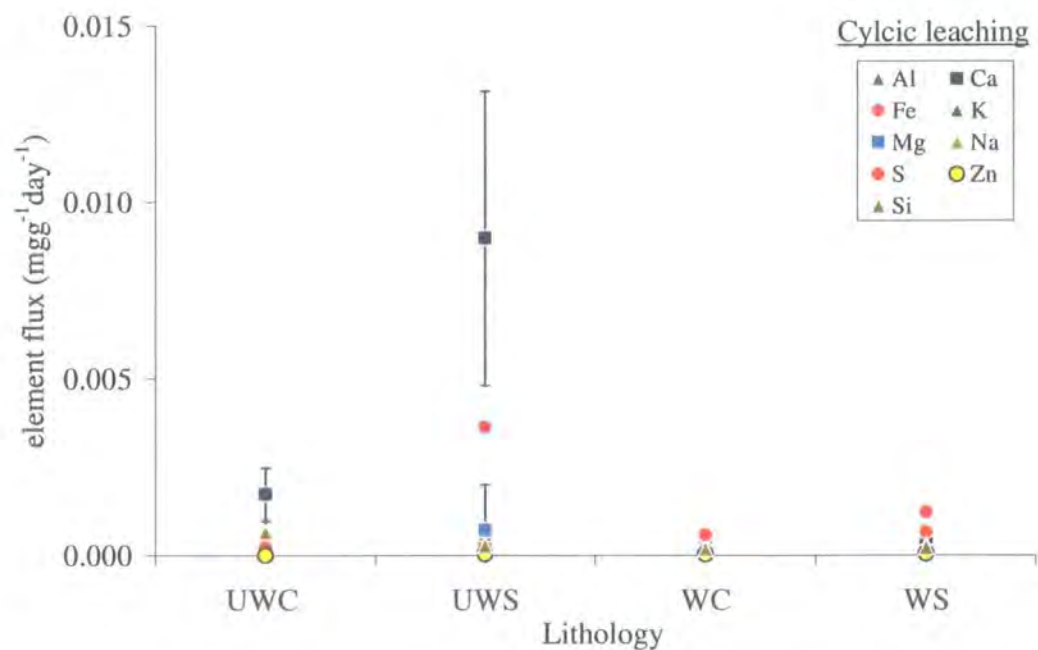
Figure 8.6. Cyclic leaching - element flux ($mgg^{-1}day^{-1}$) for each rock-type. Errors shown are 1σ, n=4.

8.2.2   Statistical analysis of elemental flux

Leachate chemistry dependence on lithology, flushing volume and drying time was identified from elemental and total flux comparison of all water-rock regimes. Here the data set is statistically analysed to identify the significant differences between water-rock regime element flux caused by treatment and rock type. A two-way ANOVA (section 6.3.4.2) is used to test for significant effects of the two factors of lithology and treatment on leachate elemental flux. Within lithology there were four rock types and within treatment there were six styles of water-rock regime i.e. cyclic and stagnant leaching, daily and weekly flushing using Milli-RO water and mineralised leachate. As the number of replicates performed differs between flushing, stagnant and cyclically leached regimes, the power of the ANOVA test is lowered. Loss of power of ANOVA means that the likelihood of not identifying significant differences at the 95 % confidence interval increases, especially when differences are small. Conclusions drawn from the lack of significant difference may be flawed, as a difference may actually exist. These factors are accounted for whilst interpreting the results of ANOVA.

8.2.2.1   Results of two-way ANOVA

Significant differences in Al, Ca, Fe, Mg, Mn, Na and S fluxes were identified for both lithology and treatment (Table 8.3). The flux of Zn was only significantly influenced by lithology. Similarly, treatment alone significantly influenced K and Si flux. The control of K and Si flux by treatment alone suggests that ion exchange or clay weathering were ubiquitous between water-rock regimes. High Zn content in the weathered rock types, especially the WS lead to the significant control, on this element flux, by lithology alone.

Significant interaction of lithology and treatment was identified for Ca, K, Mg, Mn, Na and S but not for Al, Fe, Zn and Si. No significant interaction for elemental flux means that changes in flux from one lithology under each treatment, and vice versa, will be the same for all lithologies. Where significant interaction was identified such proportionality was not shown by element flux from each lithology for all treatments and vice versa. For element fluxes where significant interaction occurs it was usually associated with high removal of material by daily flushing with either mineralised or Milli-RO water from different lithologies. Interaction for Ca flux was caused by the high output from the UWS.

Response flux	Lithology	Treatment	Lithology vs Treatment
Al	✔	✔	✗
Ca	✔	✔	✔
Fe	✔	✔	✗ (0.054)
K	✗	✔	✔
Mg	✔	✔	✔
Mn	✔	✔	✔
Na	✔	✔	✔
S	✔	✔	✔
Zn	✔	✗	✗
Si	✗	✔	✗

Table 8.3. Results of two-way ANOVA of effects of treatment and lithology on total element flux, ✔ = significant difference caused by variable; ✗ = no significant difference caused by variable. Where P value is very close to significant interval value is given in parenthesis

8.2.2.2 Magnitude of effects

Where two or more variables significantly influence a response, the relative magnitude of their effect is of interest. In two-way ANOVA Al, Ca, K, Mg, Mn, Na and S were all significantly influenced by two or more variables. Using the calculation of ω^2_{effect} the proportion of variance explained by each variable can be determined (Section 6.3.4, Howell, 1997).

Source	Lithology	Treatment	Lithology vs Treatment	Error
Al	0.11	0.10	-	0.73
Ca	0.35	0.34	0.13	0.18
Fe	0.11	0.08	-	0.71
K	-	0.27	0.10	0.61
Mg	0.17	0.41	0.07	0.36
Mn	0.12	0.53	0.18	0.17
Na	0.03	0.68	0.11	0.18
S	0.09	0.29	0.06	0.56
Zn	0.06	-	-	0.84
Si	-	0.62	-	0.35

Table 8.4. Magnitude of effect ω^2_{effect} of lithology, treatment and interaction of treatment and lithology on element flux. Blank cells are values for which ANOVA found no significant difference.

Calculation of ω^2_{effect} relies on the number of replicates per sample, which differs between flushing, stagnant and cyclic leaching. A value of 2 was used (flow leaching) rather than 3 or 4 from cyclic and stagnant leaching bringing error into the calculation of ω^2_{effect} for each factor, yet some idea of the proportion is still provided.

For Al and Ca flux the magnitude of effect of treatment and lithology were very close (Table 8.4). Greater influence by lithology was shown for Fe, although interaction of the two factors also had a high influence on the flux of this element. Treatment influence over Na was high, whereas S, Mg, Mn had a lower but still greater influence by this factor. In general there was a greater control by treatment than found from magnitude of effects of flushed samples only (section 6.3.4.). The much lower elemental flux from static and cyclic leached samples relative to flushed samples explains the significant control by treatment. Between a range of water-rock regimes, exposure time, physical and chemical weathering and water volume are more significant than lithology in controlling element flux. Within each water-rock regime, lithology is the main influence over the majority of major element flux.

8.2.2.3 Main effect plots

Effect of lithology

Main effect plots indicate that Na flux was usually greatest from the coal rock-types. All other elements had greater fluxes from the shale rock types, except for K and Si, which tended to increase from the weathered rock types (Figure 8.7). Total element flux from the UWC and WC matrix indicates that K flux correlated with Na suggesting that ion exchange was probably the source of monovalent ions. Higher weathered rock types K and Si flux can be explained by the presence of jarosite, in the weathered rock-types. On dissolution the resulting acidic pore water probably increased the rate of silicate weathering, releasing dissolved Si (Drever, 1997).

Remaining elements had a greater flux from shale rock-types compared to coals. WS flux of Al, Mn and Fe was greatest, being derived from Fe-hydroxides, Fe Mn-oxide and alunite. Mg and S fluxes, derived from gypsum and dolomite, were relatively close between WS and UWS (Figure 8.7). High Ca flux from the UWS from gypsum dissolution has already been identified as a major control in the formation of UWS leachate. The high soluble salt content of the shale rock types combined with the greater macro and meso-porosity lead to greater removal of soluble material from these
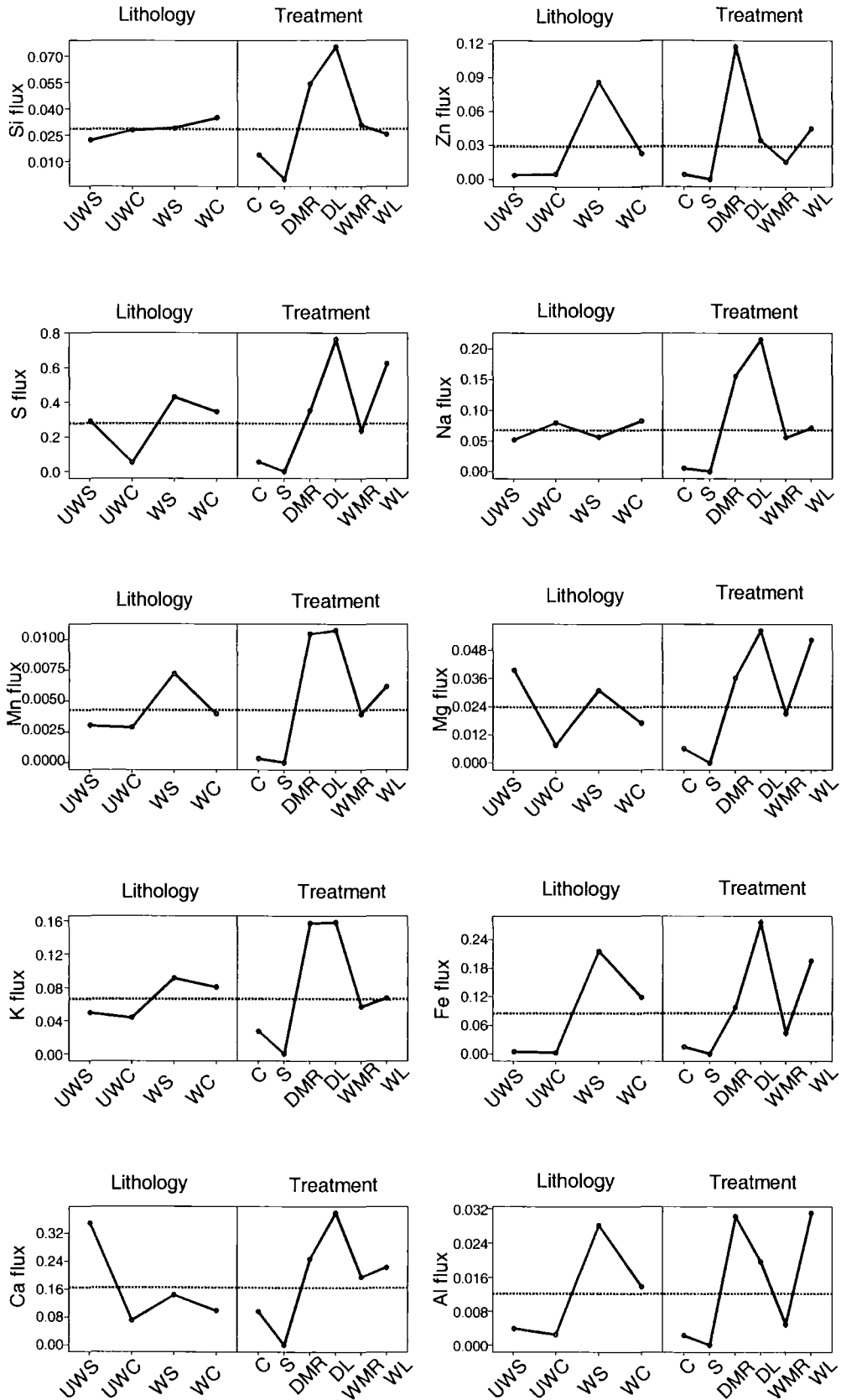
Figure 8.7. Main effect plot for major element flux, showing mean flux (mgg^{-1}day^{-1}) from all treatments of each lithology, and from each treatments regardless of rock-type, (C=cyclic, S=stagnant, DMR=Daily Milli-RO water, DL= Daily Leachate, WMR= Weekly Milli-RO water, WL=Weekly Leachate).

rock matrices. Although the WS and WC are weathered to the same extent, and the WC has the greatest original pyrite content the, yet the WS still releases higher Fe.

Effect of treatment – daily flushing with mineralised water

Treatment influenced the flux of material from all rock regimes in three main ways. In general the flux from daily flushing was always high, although cyclic and weekly flushing with mineralised water also produced relatively high flux of Fe, S and Al (Figure 8.7). A similar effect was also seen for Ca, K, Mn, Mg, Na and Si. The relative of difference in flux between flushing with purified and mineralised water increased through the series Mn, K < Mg, Ca, Na < Fe, S.

The large difference in Fe and S flux was due to the combination of flushed dissolution from two rock samples, plus dissolution of precipitated material from prior flushing with mineralised water. A similar process affected the flux of weekly flushing with mineralised water.

The Lower difference between the flux of Mg, Ca and Na can be attributed to ion exchange and gypsum dissolution occurring during flushing by both water sources. Higher flux from the mineralised water flushed sample was probably caused by the increased ionic strength of the water.

Similar behaviour of Mn and K fluxes from daily flushing suggests that either these elements do not precipitate in secondary minerals, or their release is relatively slow compared to Fe and S. Jarosite becomes unstable at pH higher than 3 (Göttlicher and Gasharova, 2000), hence flushing with Milli-RO water would lead to the release of K. SEM investigation suggests that a high volume of secondary weathering minerals precipitated within mineralised water flushed samples. The slightly higher K (and Mn) flux from daily flushing with mineralised water may be due to the high volume of soluble material present.

Effect of treatment – daily flushing with Milli-RO water

Daily flushing of the WS with Milli-RO water released as higher flux of Al and Zn than from mineralised water (Figure 8.7). A wide range of secondary minerals, including alunite and the oxidation products of sphlalerite or pyrite containing Zn, contributed to leachate solution. Higher flux from leaching with Milli-RO water rather than mineralised water may be attributed to greater dissolution by slightly higher volume of purified water (Table 8.1).

8.2.2.4 *Post-hoc* Tukey test

Although distributions of element flux between the factors of variables have been described in main effect plots above, *post-hoc* testing identifies the significance of described differences. A *post-hoc* Tukey test was performed on all data, with pairwise comparisons of response variance of each factor.

Main effect plots demonstrated five groupings of element flux from different lithologies: high Na from coals, high Mg, S and K from shales, high Mn, Zn, Fe and Al from the WS, high Ca from the UWS and increasing Si from the weathered rock types. *Post-hoc* testing shows the significant differences in those identified by main effect plots. The higher Na flux from coals compared to shales in the main effect plot, is further delineated by *post-hoc* testing which shows that Na flux is significantly different between the UWS and coals and the WS and WC (Table 8.5).

Grouped Responses	Significant differences	Controlling Process
Ca	UWS ≠ all other rock types	Gypsum dissolution
Ca, Mg, Na	UWS ≠ coals	Gypsum / dolomite dissolution and ion exchange
Al, Fe, Mn, Zn	UWS ≠ WS	Fe-hydroxides, Fe-Mn oxides, alunite
S	UWC ≠ all other rock-types	Greater gypsum and pyrite content
Mg, Mn, Na	WS ≠ WC	Ion exchange / connate brine dissolution, Fe-Mn oxides, dolomite dissolution

Table 8.5. Elemental fluxes for which a *post hoc* Tukey test identified significant differences between pairs of lithologies. Probable reasons for differences are given.

The greater release of Mg, K and S from shale rock types was only shown to be significant for Mg between the UWS and coals, and between two weathered rock types. Dolomite dissolution and possible co-precipitation with gypsum controlled the flux of Mg. Main effect plots identified the influence of ion exchange and possibly jarosite precipitation, on K flux. However, post-hoc testing does not identify a significant difference between the K flux from any rock type, indicating that differences in K flux between lithologies are relatively small. Both S main effect plot and *post-hoc* testing show that the S flux is significantly greater from the WC and both shale rock-types compared to the UWC, due to their gypsum and pyrite content. The greater flux of pyrite oxidation products from the WC compared to the UWC was caused by the higher pyrite content of the WC. Significantly greater fluxes of Fe, Zn, Al and Mn from the

WS compared to the UWS can be attributed to the wide range of secondary minerals already present in the WS. High Ca flux from the UWS, compared to all other rock types, indicates the ease of gypsum solubility from this rock-type.

Similarly, pairwise comparison of treatments for each element flux can be used to identify the significance of effects discussed in the previous section (Table 8.6). Main effect plots showed relatively high major element flux from samples flushed daily with Milli-RO water; flushed daily and weekly with mineralised water, and cyclic leaching. Differences were caused by high dissolution from samples previously flushed with mineralised water. Soluble salts precipitated from mineralised leachate were usually products of pyrite oxidation and subsequent neutralisation reactions. A high Al and Zn flux from daily flushing with purified water suggested that the original secondary mineral phase in the WS particularly, was underwent greater dissolution in Milli-RO water.

Cyclic	Cyclic					
Stagnant	Ca	**Stagnant**				
Daily Milli-RO water	Ca, Mn, Na, K, Si, Mg	Ca, Si, K, Mg, Mn, Na	**Daily Milli-RO water**			
Daily mineralised water	Ca, Mn, Na, K, Mg, S, Fe	Si, K, Mg, Mn, Na, S, Ca, Fe	Ca, S, Mn, Na	**Daily mineralised water**		
Weekly Milli-RO water	Ca, Mn, Na	Ca, Si, Mn, Na	K, Mn, Na, Si, Ca	Ca, K, Mg, Mn, Na, Si	**Weekly Milli-RO water**	
Weekly mineralised water	Ca, Mn, Na, S, Mg	Ca, Si, Na, Mn, S	Na, Si, S, Ca	Ca, Na, Mn, Si	Mg, Ca	**Weekly mineralised water**

Table 8.6. Elemental fluxes for which a *post hoc* Tukey test identified significant differences between pairs of treatments.

Post-hoc testing shows that the Ca flux is significantly different between all treatments. Given that the main source of this element is gypsum for all rock types, difference between treatments is expected. Only Ca, S, Mn and Na show significant differences between flux from daily flushing with either Milli-RO water or mineralised

water. The precipitation of these elements in secondary minerals can be assumed to play a large part in their availability to subsequent flushing. Significant difference between daily and weekly flushing with mineralised water and for Ca, Na, Mg, Mn and Si suggests that a prolonged period of drying may have only significantly affected gypsum, ion exchange and clay weathering. Prolonged drying and pyrite oxidation increase clay weathering by acidic attack.

8.2.2.5 Summary of statistical testing of total elemental fluxes

Contrary to the findings of statistical analysis on flow leaching alone (section 6.3.4, chapter 6), treatment was found to strongly control the elemental flux per day from factorial combinations of treatment and lithology.

Original content of weathering products controlled leachate composition. Although the flux of Fe and S from WC was not significantly lower than the WS, there is still agreement with limited oxidant flux in coal micro-porosity. Daily flushing with mineralised water released the highest flux of most elements, apart from Al. Ion exchange or dissolution of connate brines, gypsum dissolution and Fe-Mn oxide dissolution caused differences in daily flushing with mineralised and Milli-RO water.

Differences between flushing daily and weekly with mineralised water suggested that ion exchange, dissolution of Fe-Mn oxides and gypsum dissolution influenced chemistry. Significant difference between Mg and Ca during weekly flushing with mineralised and Milli-RO water implies low pore water pH in samples flushed with the former.

8.2.3 Controls of leachate chemical evolution and total flux of dissolved material

A schematic mass balance equation can be written for the total flux of dissolved material in the leachate from all water-rock regimes:

Leachate chemistry	=	Soluble material	+	Prior leachate content	+	Dissolved pyrite oxidation products	-	Precipitation from solution

For different water-rock regimes the input from each source or sink will change according to variables of flowing and static leaching, drying period and rock leaching with different waters. After the removal of soluble material and prior leachate content, only the dissolution of pyrite oxidation products and the precipitation from solution changes stagnant leachate chemistry. Cyclic leaching introduces fresh leachate to the system, increasing dissolution due to the dilute nature of Milli-RO water. Increased

precipitation from solution with time may be caused by the pH gradient between Milli-RO water and acidic pore water, especially in rock-types with a high pyrite content. Flushing samples increases dissolution, with dry periods allowing an increase in soluble material available for flushing.

Obviously, for each water-rock regime, the leachate chemistry is affected by the variables that define that water-rock regime. The relative influence of each sink or source terms on final discharge quality is of most interest here. In the following sections, controlling processes for each sink and source term are discussed, relative to the influencing variables of each water-rock regime.

8.2.3.1 Leaching with flowing versus stagnant water

Commonly, numerical simulations of AMD formation assume that transport of dissolved oxidation products within porous media is rapid compared to the pyrite oxidation reaction. The time for transport may be ignored, and leachate chemistry is directly linked to pyrite oxidation rate for pyrite throughout the whole rock particle. In the various water-rock regimes mimicked in this study, leaching under stagnant conditions allowed some form of equilibrium between the ambient leaching fluid and the whole of the rock sample. Under stagnant conditions the pyrite oxidation front ingress continued to the centre of samples, yet under cyclic leaching the pyrite oxidation was concentrated in the outer zone of rock. The work carried out in this study does not provide any strong conclusions concerning actual rates of pyrite oxidation under different water rock regimes. However, the strong influence of dissolution of precipitated material on leachate chemistry and that pyrite weathering occurs via a series of steps of oxidation, dissolution and precipitation and re-precipitation have been shown. This style of leachate formation by secondary mineral dissolution and re-precipitation is more important for flow and cyclic leaching than stagnant leaching. Thus between unsaturated conditions and saturated conditions the manner of AMD formation will differ due to control by two mineral systems i.e. pyrite oxidation and secondary mineral dissolution.

8.2.3.2 Drying periods

Dry periods during the weathering of spoil heap material are usually expected to increase the dissolved content of leachate (Morin and Hutt, 1994). The close range of flux from high pyrite wt% samples with day or week-long dry periods, suggests that flushing volume is more important than the volume of soluble material available (Table

8.1). Increased advective transport in unsaturated pores, increased oxidant influx and dissolution due to flushing with dilute leachate, encouraged a greater dissolved flux from cyclic leaching relative to stagnant.

In relation to the overall mass balance for leachate formation increased drying period leads to increased available soluble material, however, the release of this phase depends strongly on the regularity of flushing. The use of preferential flow-paths in flushed samples increased dissolution and transport from certain areas of samples. Increasing the volume of water during intensive sampling led to high initial concentrations derived from the larger volume of sample flushed. Thus increasing the volume of water-rock interaction rather than drying period alone lead influenced leachate chemistry.

8.2.3.3 Leaching with mineralised or Milli-RO (purified) water

Where a sample contains a pyrite phase, flushing with mineralised water containing dissolved Fe^{3+} or Fe^{2+} will eventually lead to acceleration of pyrite oxidation, via the production of further Fe^{3+}. SEM investigation revealed that cyclically leached or flushed samples treated with Milli-RO water contained less precipitated material than rock treated with mineralised water. Treatment with Milli-RO water lead to greater removal of pyrite oxidation products and a 'cleaner' appearance of pyrite grains in the outer regions of examined sections. Flushing of rock with mineralised water lead to Fe-sulphate precipitation, compared to upper samples, and more fracturing. Secondary mineral growth possibly led to fracture expansion, whether from leachate evaporation or *in-situ* pyrite oxidation.

8.2.3.4 Mineralogy

The key aim of this study was to describe the controls on pyrite oxidation in coal-bearing strata as a precursor of AMD generation. Leaching experiments indicate that leachate chemical evolution occurs through a series of indirect contributions from the dissolution and re-precipitation of secondary minerals, formed after pyrite oxidation. Such a cyclical manner of transport of original pyrite material agrees with Blowes and Jambor's (1990) suggestion that secondary mineral dissolution controls AMD chemistry.

Dissolution and reaction rates of carbonates, alumino-silicates, sulphides and prior secondary minerals control AMD chemistry. Mineral dissolution rate typically depends on pH of the leaching solution, surface area, temperature and the presence of organic molecules (Lasaga, 1984). Assuming that the latter two factors were respectively

homogenous and unknown in this study, only the effects of surface area and pH can be commented on. In the described leaching experiments, overall flux of material was limited by availability of soluble material, pyrite weathering rate and the solubility of precipitated material. Rock physical characteristics also played an important role in dissolution of material, with the shale rock types releasing a higher proportion of material due to a greater proportion of effective macro and meso-porosity

8.2.4   Relating small-scale, water-rock interaction to large-scale, leachate formation

Flushed unsaturated zones

Daily flushing of rock samples released the greatest amount of material per day closely followed by weekly flushing. High flux of dissolved material from flushed samples confirms that unsaturated spoil heap material and rock strata strongly control discharge chemical evolution. Paktunc and Davé (2000) found that the removal of pyritic material over a year of intermittent flushing of uranium mine waste columns was greatest in the upper part of columns. Similarly, investigations of spoil heap and mine tailings weathering profiles have shown that usually the unsaturated zone is most weathered (Blowes and Jambor, 1990, Elberling et al., 1994). Elberling and Nicholson (1996) report that the balance between diffusion of oxygen into spoil and coal material with uptake by pyrite oxidation reactions, controls the depth of greatest oxidation. However, Guo et al. (1994) and Kuo and Ritchie (1999) have shown that thermal convection may be more important than diffusion of oxygen due to uptake by oxidation in supplying oxidant. Evidence of hardpan formation and precipitation at the top of the capillary zone between the saturated and unsaturated zone in mine tailings has been found by Blowes et al. (1991). The formation of zones of greatest oxidation indicates that intermittent wetting leads to precipitation of weathering minerals at the wet-dry interface. Similarly our samples of partially wet and dry material showed high precipitation with lower removal rates.

Saturated zones

Total saturation of waste rock material is commonly used as a remediation strategy in preventing further sulphide oxidation (Simms et al., 2000). The slow oxidation under saturated conditions is usually attributed to the much lower dissolved O_2 content of water. The oxidation of pyrite occurs mainly due to Fe^{3+}, with the presence of O_2 required to oxidise Fe^{2+} (Moses and Herman, 1989). Depletion of O_2 and thus Fe^{3+}

when used in pyrite oxidation would eventually decrease the rate of reaction. However, it has been shown that the O atoms attached to the water molecules actually oxidised Fe^{2+} rather than dissolved molecular O_2 (Moses and Herman, 1989). Therefore in saturated tailings oxidation of Fe^{2+} to Fe^{3+} should be possible.

In this study, saturated leaching of coal-bearing strata showed that the rate-limiting step in the formation of chemical leachate was the diffusive transport of dissolved material, from the rock matrix. Pyrite oxidation typically occurred further into rock samples in stagnant leaching, compared to cyclic leaching, yet precipitated oxidation products normally remained *in-situ* (Chapter 5). Saturation of tailings probably leads to the formation of an 'equilibrium' system where pyrite embedded in rock is oxidised, yet as precipitated material is not removed as rapidly as during flushing. Studies of actual mine waste and columns of rock waste material have shown that O_2 depletion does occur at depth (Elberling et al., 1994). In the study performed here O_2 diffusion from atmospheric conditions would have been rapid, relative to conditions in spoil material or rock strata. Perhaps the conditions mimicked would be more akin to those experienced by rock just below the water table surface, or within the upper zone of flooded tailings. Fluctuations in water table would perhaps lead to a large rise in spoil pore water concentrations following a fall then rise in the upper limit of saturated depth.

8.2.5 Comparison of mimicked water-rock regimes with identified water sources contributing to an AMD discharge.

Monitoring of an AMD discharge during summer and winter as described in Chapter 7 can be compared to controlling factors identified in each mimicked water-rock regime. Large scale effects of drying period, leaching with flowing and stagnant water and leaching with a purified or mineralised water source can be identified from analysis of changing AMD chemistry.

In mimicked water-rock regimes, flushing of rock led to the removal of high magnitudes of dissolved matter. In saturated rock the removal of dissolved matter was slow due to diffusive transport. Direct comparison of leachate, before corrections for volume of water and time of exposure are made show a higher leachate concentration from stagnant leaching. Dissolution under flowing water and stagnant water can be related to discharge chemistry during rainfall and dry periods. During and directly after rainfall, discharge chemistry results from the combination of flushed material from the unsaturated zone and base-flow from a relatively saturated zone. Separation of the storm chemical hydrograph suggests that a high contribution of concentrated base-flow is made to the total discharge. PCA indicates that flushing actually removes high

concentrations of dissolved material from the unsaturated spoil material, which adds to the base-flow composition. Thus concentration in discharge is generally higher directly after rainfall events in both summer and winter. During base-flow concentrations are higher, but the volume of flow is lower, therefore the total flux is lower from saturated flow.

Dry periods in water-rock regime mimicking and during monitoring of AMD discharge, led to an increase in concentration at subsequent flushing events. Regular flushing or rainfall led to dilution of base-flow, and rapid removal of soluble material at the AMD site. Spoil material that has been flushed regularly i.e. in winter contains a low proportion of soluble material. Similarly in small-scale rock experiments, a build-up of oxidation products is not allowed in regularly flushed material. However, the difference between the total flux per day of material from regular flushing and flushing after prolonged drying, is relatively small in both experimental leachate and actual discharge chemistry (Table 8.2, Figures 7.19 to 7.20).

Flushing with purified water or mineralised water in experimental regimes can be related to the formation of AMD from high or low intensity rainfall events. During storm events flushing will be carried out mainly by rainwater. During normal intensity rainfall slower hydrological paths will be taken by percolating fluid, leading to greater interaction with spoil material. In mimicking of water-rock regimes, flushing with mineralised water led to some precipitation of secondary minerals along flow-path, a portion of which dissolved to contribute to leachate composition. It is difficult to make a comparison of AMD chemical change with that from experimental leaching as the flow path of water sources contributing to discharge are rather more complex.

It is difficult to compare the leachate from clearly defined small-scale water-rock regimes with a much larger discharge that has probably formed from mixing of at least two, if not more, sources of water. However, the general trend of high concentration derived from water which is allowed to remain in contact with rock for a long period compared to dilution in water which flows over the rock is true of both systems. Although there are basic links between mimicked water-rock regimes and the interpreted pattern of AMD formation, it is difficult to bridge gaps where AMD formation is due to relatively complex mixing of water sources.

8.3 Summary and implications of study

1 Phosphate encapsulation of pyrite

A phosphate tracer solution was developed to investigate pyrite oxidation front ingress. Development of this tracer indicated that when rock is already weathered, the low pH of pore water solution inhibits Fe-phosphate precipitation, apart from at the edge of samples. If Fe-phosphate were to be used as an encapsulation technology, pore water pH would have to be sustained at around 5. The ingress of phosphate coating would also depend on the factors identified here, suggesting that even after several months of treatment, pyrite at the centre of rock particles may not be coated. During this period of time rock pH would have to be sustained above pH 5 to ensure stabilisation of any coating which had already formed.

2 Monitoring the ingress of an abiotic pyrite oxidation front in coal-bearing strata

Ingress of the pyrite oxidation front during the small-scale leaching of coal-bearing strata depends upon transport mechanism, pyrite morphology and pore size distribution.

Dominant transport mechanism of oxidant

Observed pyrite oxidation front ingress suggests that the SCM is a good description of pyrite weathering in coal-bearing strata. However, most dissolved material is removed along cleavage planes. Diffusion of oxidant and therefore ingress of an oxidation front, is more rapid along compared to across cleavage. Dissolved oxidant influx is limited within the period investigated by diffusive transport into micro-pore space rather than the depletion of O_2 by pyrite oxidation.

Pyrite morphology

Two pyrite oxidation fronts were identified for framboidal and more consolidated pyrite indicating that pyrite morphology affected the rate of oxidation front ingress. Framboidal pyrite was relatively rapidly oxidised due to greater porosity compared to consolidated and massive pyrite, which tended to form layers of Fe-sulphate precipitation. These layers were initially partial coatings, supporting the previously noted concentration of reaction at pyrite surface regions of high energy (McKibben and Barnes, 1986).

High pyrite content of a rock-type generally led to a high output of dissolved Fe and S, yet the difference in porosity introduced by clays in the coal and shale rock matrix

produced a lower rate of flux from the coal. Even though the pyrite content in the coal rock type was greater, the shale released greater Fe and S total flux. Oxidation would have also been retarded by slower diffusion of O_2 into the coal.

Rock pore size distribution

Precipitation of oxidation products usually occurred *in-situ* unless pore water pH was low enough to maintain dissolved salts in solution. Where dissolved oxidation products were transported to the sample surface the sharp pH gradient, between the ambient leachate and rock pore-water, encouraged precipitation. The proximity of these secondary minerals to the ambient leachate suggests that their dissolution will contribute to leachate chemistry.

3 Comparison of in-situ *abiotic pyrite oxidation rates with those predicted from pyrite alone*

- Under-estimation of surface area and prior oxidation product introduced a large error in the estimation of *in-situ* oxidation rates. Estimates of the difference in framboid surface area estimated from diameter to that calculated from individual crystals suggest an order of magnitude difference. Corrected *in-situ* pyrite oxidation rates were within range of rates predicted from pyrite oxidation alone using McKibben and Barnes' (1989) rate constants.

- Precipitation and dissolution of secondary Fe^{3+} minerals such as jarosite and gypsum contribute to leachate chemistry as well as direct removal of dissolved pyrite oxidation products. As similar control has been shown in field and column experiments, the oxidation of pyrite by Fe^{3+} in flooded tailings is probably not significant (Blowes and Jambor, 1990, Simms et al., 2000).

- Low oxidation rates reported from saturated rock are partly caused by the precipitation of oxidation products, *in-situ* on pyrite grains, and the slow time for diffusive transport from the rock matrix.

4 Homogeneity of pyrite distribution and other rock characteristics in coal-bearing strata.

- The scale of significant variance for major elements in the analysed coal-bearing strata existed spatially at the 10 m scale within and between each seam and stratigraphically.

- Physical properties and elements associated pervasive phenomena such as connate brines i.e. Na and Mg, only vary stratigraphically, between seams.

- Vertical trends in the distribution of acid producing and neutralising minerals were probably more important than horizontal trends in terms of variance in distribution.

- Significant variance in whole S and pyrite content occurred over a 30 m exposure of the Main Seam of the Durham Coalfield.

- Using mean seam characteristic values when predicting leachate quality may lead to a large error in calculation.

Correlation of other chemical and physical properties of coal-bearing strata provides information about the controlling processes in their distribution. Little variance in pore space characteristics along seam suggests this characteristic's dependence on the seam material compressibility and solubility. The scaling of the effects of these characteristics on leachate water quality will be relatively simple due to lack of significant variance within each seam. A strong correlation between Ti content and effective, meso and macro-porosity suggests that detrital sediment was associated with larger pore spaces. As larger connected pore spaces will lead to faster and more invasive transport of oxidant and dissolved metals, a positive correlation of pyrite and Ti content may be a primary indicator of a highly polluting rock type.

Vertical trends in sediment mineralogy and fluid diffusion probably control the observed heterogeneity in sampled seam characteristics. Although analysis of vertical trends in rock seams may not be useful in ABA, numerical modelling may benefit from such resolution.

5 Investigating seasonal changes in chemistry of an AMD discharge and the controls on discharge chemistry

Monitoring of the Bowden Close AMD discharge in Co. Durham over a period of winter to summer lead to identification of two temporally discrete chemical sources. These sources mixed with influent rainwater in varying proportions depending on spoil heap saturation to provide the observed discharge chemistry. The two chemical sources or types of base-flow occurred in winter and summer. Dominant water-rock reactions included ion exchange, pyrite oxidation product dissolution and carbonate dissolution. These processes controlled the chemical composition of base-flow sources.

The effects of dry periods on discharge chemistry

After prolonged dry periods, when a lack of flushing by rainfall allowed a build up of pyrite oxidation products, storm and rainfall events flushed soluble material into the

discharge and also into base-flow. Summer base flow was characterised by an increase in concentration i.e. TDS and acid character, although the first winter rainfall after a relatively dry December led to increased acidity in the discharge. Prolonged dry periods allowed a build up in acidic pyrite oxidation products however, as winter base flow would have been relatively dilute, the similarity between initial winter flushing and mid summer flushing was only in acidity and not concentration of dissolved material. Prolonged summer rainfall did, however, lead to a dilution of base flow and produced discharge of a similar composition to initial winter discharge suggesting the start of a return to winter base flow composition.

The effect of wet periods on discharge chemistry

In late winter to spring continual flushing of the heap led to removal of a large proportion of soluble salts and the dilution of dissolved pyrite oxidation products. Winter base-flow was characterised by pyrite oxidation products, ion exchange and clay weathering products.

8.4 Recommendations for further work

1- Application to modelling and further statistical analysis

Although certain controlling factors have been identified in the waste particle scale weathering of coal-bearing strata, numerical application has not been attempted. A model of oxidant ingress and products dissolution would need to incorporate the retardation of dissolved oxidant diffusion by available pore space. Precipitation at the water-rock interface due to pH change may be simulated by using a model linked to a geochemical equilibrium package, such as that designed Wunderly et al, (MINTOX, 1996). Differences in transport mechanism between water-rock regime, within partially saturated material would also be important constituents of any numerical simulation. Statistical analysis of data has, at the very least, provided a more robust analysis of chemical data produced during leaching experiments. However, in order to gain a better idea of controls on rock leaching, a more balanced experimental design is required.

2- Investigation of leachate chemistry controls in column leaching

The obvious missing component in this work has been the lack of column experiments, which may have bridged the gap between individual particle scale processes and large-scale AMD formation. Column experiments were deliberately

omitted due to the ubiquity of these tests reported in the literature. Now that small-scale controls on oxidation within rock particles have been identified, the next step in this work would be to investigate how these controls translate to larger scale column leaching.

3- Testing the characterisation of coal

Characterisation of coal-bearing strata at the outcrop scale was performed to show variation in chemical and physical rock properties. For a more robust test of the use of coal seam characteristics in the prediction of overburden weathering, a larger mine scale characterisation based on similar analysis would be useful. Currently trends in rock characteristics have only been analysed at the regional scale (Glick et al., 1987, Turner and Davidson, 2002). Analysis at the mine scale may be more useful to predicting polluting potential. Characterisation of coal-mine strata and the overburden material dumped after rock extraction may be extremely informative. The ability to accurately link extracted rock properties with the AMD emanating from spoil material after the extraction of that coal would be an extremely useful tool. The occurrence of Ti-oxides and pyrite within coal-bearing strata may identify a potential polluting rock type. Further investigation of this potential marker is required.

4- Testing hydrograph separation and PCA identification of AMD end-member contributions

Monitoring of an AMD discharge over seasonal changes and storm events led to a better understanding of the manner in which final discharge is formed. In many studies of AMD formation pore water analysis from tube well or lysimeter data is available for a direct access to the components forming discharge chemistry. Where this is not possible, PCA of changing AMD chemistry and volume may provide a method of identifying potential composition of components. However, to thoroughly test this method, some comparison between the PCA results and actual pore water data is required.

References

Al, T.A. and Blowes, D.W., 1996. Storm-water hydrograph separation of run off from a mine-tailings impoundment formed by thickened tailings discharge at Kidd Creek, Timmins, Ontario. *Journal of Hydrology*, **180**, 55-78.

Alpers, C. N., Blowes, D. W., Nordstrom, D. K., and Jambor, J. L., 1994, Secondary Minerals and Acid Mine-Water Chemistry, in Jambor, J. L., and Blowes, D. W., eds., Environmental Geochemistry of Sulfide Mine-Wastes: Mineralogical Association of Canada Short Course Handbook, vol **22**, p. 247-270

Bain, J.G., Blowes, D.W., Robertson, W.D., and Frind, E.O., 2000. Modelling of sulfide reaction with reactive transport at a mine drainage site. *Journal of Contaminant Hydrology*, **41**, 23-47.

Banks, H.J. and Company Ltd., 1996, The Northwood opencast coal mine, Brandon, County Durham – site report. The Banks Group, Ferryhill, Co.Durham.

Baron, D. and Palmer, C.D., 1996. Solubility of jarosite at 4-35 °C. *Geochimica et Cosmochimica Acta*, **60** (2), 185-195.

Belzile, N., Maki, S., Yu-Wei, C., and Goldsack, D., 1997, Inhibition of pyrite oxidation by surface treatment, *The Science of the Total Environment* **196**, (1997) 177-186.

Bierens de Haan, S., 1991. A review of the rate of pyrite oxidation in aqueous systems at low temperature. *Earth Science Rev.,* **41**, 1-10.

Bigham, J.M., Schewertmann, U., Traina, S.J., Winland, R.L., and Wolf, M., 1996, Schewertmanite and the chemical modelling of iron in acid sulfate waters. *Geochimica et Cosmochimica Acta*, **60**, 2111-2121.

Blowes, D.W. and Jambor, J.L., 1990, The pore water geochemistry and mineralogy of vadose zone of sulphide tailings. *Applied Geochemistry*, **5**, 327-346.

Blowes, D.W., Reardon, E.J., Jambor, J.L., and Cherry, J.A., 1991, The formation and potential importance of cemented layers in inactive sulfide mine tailings. *Geochimica et Cosmochimica Acta*, **55**, 965-978.

Bonnissel-Gissenger, P., Alnot, M., Ehrhardt, J. and Behra, P., 1998, Surface oxidation of pyrite as a function of pH. *Environ. Sci. Tech.* **32** , 2839-2845.

Bou-Raad, M., Hobday, M.D. and Rix, C.J., 2000. Aqueous extraction of oxalate and other anions from coal. *Fuel* **79**, 1185-1193.

Brandvold, L.A. and McLemore, V.T., 1998. A study of the analytical variation of sampling and analysis of stream sediments from areas contaminated by mining and milling. *Journal of Geochemical Exploration* **64**, 185-196.

Brown, J.G., Glynn, P.D. and Bassett. R.L., 1999. Geochemistry and Reactive Transport of metal contaminants in ground water, Pinal Creek Basin, Arizona. In Proc. USGS Toxic substances hydrology program technical meeting, Charleston, South Carolina, March 8-12, vol. 1. Contamination from hard rock mining, water resources investigation Report 99-40 ISA.

Bustin, R.M., 1999, Variation in pore size distribution with coal rank and composition; potential for substantial resources of free gas in matrix porosity in low rank coals. In GSA Annual Meeting Abstracts with Programs, Boulder, CO, **31** (7), pp 384, Source GeoRefS.

Butler, I.B. and Rickard, D., 2000. Framboidal pyrite formation via the oxidation of iron (II) monosulfide by hydrogen sulphide. *Geochimica et Cosmochimica Acta*, **64**, (15), 2665-2672.

Carter, D.L., Mortland, M.M. and Kemper, W.D., 1986, Specific Surface Area. In: Methods of Soil Analysis: part 1 - Physical and Mineralogical Methods. Agronomy Series Number 9, ASA, Madison, WI. pp .413-423.

Casagrande, D.J., 1987. Sulphur in peat and coal. In: Scott, A.C., Editor, Coal and Coal-bearing Strata: Recent Advances. *Geol. Soc. Spec. Publ.* (**32**), Geological Society, London, Oxford, Blackwell Scientific, 87-107.

Chang, S. and Berner, R.A., 1999. Coal weathering and the geochemical carbon cycle. *Geochimica et Cosmochimica Acta*, **63** (19/20), 3301-3310.

Christopherson, N. and Hooper, R.P., 1992. Multivariate analysis of stream water chemical data: the use of principal components analysis for the end-member mixing problem. *Water Research Res.* **28**, 99-107.

Clarkson, C.R. and Bustin, R.M., 1999, The effect of pore structure and gas pressure upon the transport properties of coal: a laboratory and modeling study. 1. Isotherms and pore volume distributions. *Fuel*, **78**, 1333-1344.

Clarkson, C.R. and Bustin, R.M., 1999, The effect of pore structure and gas pressure upon the transport properties of coal: a laboratory and modeling study. 1. Isotherms and pore volume distributions. *Fuel*, **78**, 1333-1344.

Connely, R.J., Harcourt, K.J., Chapman, J. and D.Williams, 1994. Approach to remediation of ferruginous discharges in the South Wales coalfield, In proc: *5ᵗʰ Int. Mine Water Congress, 1994*, 521-531

Crowley, S.S., Ruppert, L.F., Belkin, H.E., Stanton, R.W. and Moore, T.A, 1993, Factors affecting the geochemistry of a thick, sub-bituminous coal bed in the Powder River Basin : volcanic, detrital, and peat-forming processes. *Organic Geochem.* **20** (6), 843-853.

Deissmann, G. and Bolduc, L., 2000. Envionmental aspects of non-acidic mine drainage. In Applied Mineralogy in Reasearch, Economy, Technology, Ecology and Culture, (2), Eds: Rammalair, D., Medere, J., Oberthur, Th., Heinmann, R.B and Pentinghaus, H., proc. of 6ᵗʰ Int. Congress on applied mineralogy, Goettingen, Germany, 17-19 July 2000.

Destouni G., Malmström M., Berglund S., and Lindgren M., MiMi – Predictive Modelling: State-of-the-art report, MiMi Report 98:1, MISTRA Research Programme: Mitigation of the Environmental Impact from Mining Waste, Stockholm, Sweden, 1998, available at http://www.ce.kth.se/aom/AVAT/mining.html, last accessed on 21ˢᵗ October 2002.

Destouni, G., Malstrom, M., Berglund, S. and Lindgren, M., 1998, MiMi – Predictive modelling - state of the art report. pp 1-20

Doolittle, J.J. and Hossner, L.R., 1997. Acid-base properties of a limed pyritic overburden during simulated weathering. *J. Environ. Qual.* **26**, 1665-1662

Drever, J.I., 1997. The Geochemistry of Natural Waters, surface and ground water environments, 3ʳᵈ edition. McConnin, R.A. (Ed) Prentice Hall, New Jersey.

Dulong, F.T. and Blaine, C.C., 2000, Geochemistry of Pennsylvanian coal-bearing strata; prediction of mine drainage water quality in the Appalachian Basin. In GSA Annual Meeting Abstracts with Programs, Boulder, CO, **32** (7), pp 37-38, Source GeoRefS.

Dulong, F.T., Cecil, C.B. and Fedorko, N., 2001, Chemical affinities of iron and manganese in Pennsylvanian coal-bearing strata in the Central Appalachian basin : implications for contaminated mine drainage. In GSA Annual Meeting, Boston, Massachusetts, Nov 5-8, 2001. Available from http://gsa.confex.com/gsa/2001AM/finalprogram/abstract_28052.htm (accessed 20ᵗʰ June 2002).

Durham Mining Museum available at http://www.dmm.org.uk/, last accessed on 01/10/02.

Earle, J. & Callaghan, T. 1999 Impacts of mine drainage on aquatic life, water uses, and man-made structures. Coal Mine Drainage Project, Pennsylvanian D.E.P. 4:1-13.

Einax, J.W., Zwanxiger, H.W. and Geiß, S, 1997. Chemometrics in environmental analysis. Wiley, Weinheim, Germany.

Elberling, B, Nicholson, R.V., and Scharer, J.M., 1994. A combined kinetic and diffusion model for pyrite oxidation in tailings: a change in controls with time. *Journal of Hydrology*, **157**, 47-60.

Elberling, B. and Nicholson, R.V., 1996. Field determination of sulphide oxidation rates in mine tailings. *Water Resources Research*, **32**, (6), 1773-1784.

Elberling, B., and Damgaard, L.R., 2001. Microscale measurements of oxygen diffusion and consumption in subaqueous sulfide tailings. *Geochimica et Cosmochimica Acta.* **65** (12), 1897-1905.

Elberling, B., Nicholson, R.V. and Scharer, J.M., 1994, A combined kinetic and diffusion model for pyrite oxidation in tailings : a change in controls with time. *Journal of Hydrology*, **157**, 47-60.

Eshleman, K.N., Pollard, J.S. and O'Brien, A.K., 1994. Interactions between groundwater and surface water in a Virginia coastal plain watershed. 1. Hydrological flowpaths. *Hydrological Processes*, **8**, 389-410.

Evangelou, V.P, and Zhang, Y.L., 1995, A review of pyrite oxidation mechanisms and acid mine drainage prevention. *Critical reviews in Env. Sci. and Tech.*, **25** (2), 141-199.

Evangelou, V.P., 1995. Potential Microencapsulation of pyrite by artificial inducement of ferric phosphate coatings, *J.Environ. Qual.*, **24**, 535-542.

Evangelou,V.P., 1998, Pyrite chemistry: The key for abatement of Acid Mine Drainage. In Acidic Mining Lakes, Acid Mine drainage, Liminology and reclamation (Monograph), Eds. Geller, W., Klapper, H. and Solomons, W. Springer-verloy Berlin, Heidelberg.

Evans, K.A., Banwart, S.A., Jarvis, P and Younger, P.L. 2001. Laboratory to Field: Relating Unsaturated Column Flow Experiments to Spoil Heap Effluent Concentrations. Available at http://envdiag.ceh.ac.uk/evans_setac.shtm, last accessed 08/08/02.

Fielding, C.R., 1982, Sedimentology and stratigraphy of the Durham coal measures, and comparisons with other British coalfields. PhD thesis. University of Durham.

Fuge, R., Pearce, F.M, Pearce, N.J. and Perkins, W.T., 1994. Acid mine drainage in Wales and influence of ochre precipitation on water chemistry. In Environmental Geochemistry of Sulfide Oxidation, American Chemical Society, 1994, pp 261-274.

Gayer, R.A., Rose, M., Dehmer, J. and Shao, L.-Y., 1999, Impact of sulphur and trace element geochemistry on the utilisation of a marine influenced coal – case study from the South Wales Variacan foreland basin. *Int. J. of Coal Geology*, **40**, 151-174.

Gerke., H.H., Molson, J.W., and Frind, E.O., 1998. Modelling the effect of chemical heterogeneity on acidification and solute leaching in overburden mine spoils. *Journal of Hydrology*, **209**, 166-185.

Glick, D.C. and Davis, A., 1987, Variability in the inorganic element content of U.S. coals including results of cluster analysis. *Org. Geochem.* , **11** (5). 331-342.

Gosiewska, A., Drelich, J., Laskowski, J.S., and Pawlik, M., 2002. Mineral matter distribution on coal surface and its effect on coal wettability. *Journal of Colloid and Interface Science*, **247**, 107-116.

Göttilicher, J. and Gasharova, B., 2000, Interactions of iron and sulfur bearing solid phases with water in surface coal mining pits and acidic mining lakes. In Applied Mineralogy in Reasearch, Economy, Technology, Ecology and Culture, (2), Eds: Rammalair, D., Medere, J., Oberthur, Th., Heinmann, R.B and Pentinghaus, H., proc. of 6th Int. Congress on applied mineralogy, Goettingen, Germany, 17-19 July 2000.

Guo, W., Parizek, R. and Rose, A., 1994. The role of thermal convection in resupplying O_2 to strip coal mine spoil. *Soil Science*, **158** (1), 47-55.

Carboniferous coals from the Zonguldak basin (NW Turkey) and their variations with rank and maceral composition. *Int. J.of Coal Geology*, **48**, 133-144.

Gürdal, G., and Yalçin, M.N., 2001, Pore volume and surface area of the Carboniferous coals from the Zonguldak basin (NW Turkey) and their variations with rank and maceral composition. *Int. J.of Coal Geology*, **48**, 133-144.

Herbert, R.B., 1996. Metal retention by oxide precipitation from ground water in Dalarna, Sweden. *Applied Geochemistry*, **11**, 229-235.

Holz, M. and Kalreuth, W., 2000, Application of sequence stratigraphy to coal research: an example of the Early Permian Rio Bonito Formation of southernmost Brazilian Gondwanaland. In Proc. AAPG Annual Meeting 2000, New Orleans.

Hornberger, R.J. and Brady, K.B.C., 2000, Kinetic (Leaching) Tests for the Prediction of Mine Drainage Quality. In: Brady, K.B.C, Smith, M.W. and Schueck, J. Eds. *Coal Mine Drainage Prediction and Pollution Prevention in Pennsylvania*, Pennsylvania Department of Environmental Protection.

Howell, D.C., 1997, <u>Statistical methods for psychology</u>, 4th Edition, ed Hinrichs, C., Wadsworth, CA.

Jarvis, A.P. and Younger, P.L., 1997. <u>Dominating chemical factors in mine water induced impoverishment of the invertebrate fauna of two streams in the Durham coalfield, UK</u>. *Chemistry and Ecology*, **13**, 249-270.

Johannesson, K.H., Lyons, W.B., Yelken, M.A., Gaudette, H.E., and Setzenbach, K.J., 1996. <u>Geochemistry of the rare earth elements in hypersaline and dilute acidic natural terrestrial waters: complexation behaviour and middle rare earth element enrichments</u>. *Chem. Geol.* **133**, 125-144.

Kania, T., 2000, Laboratory methods for acid-base accounting. <u>In: Brady, K.B.C, Smith, M.W. and Schueck, J. Eds. *Coal Mine Drainage Prediction and Pollution Prevention in Pennsylvania,*</u> Pennsylvania Department of Environmental Protection.

Katsube, T.J and Williamson, M.A., 1994, <u>Effects of diagenesis on shale nano-pore structure and implications for sealing capacity.</u> *Clay Minerals*, **29**, 451-461.

Katsube, T.J, Mudford, B.S. and Best, M.E., 1991, <u>Petrophysical characteristics of shales from the Scotian shelf.</u> *Geophysics*, **56** (10), 1681-1689.

Kerth, M. and Wiggering, H., 1998. The weathering of colliery spoil in the Ruhr – problems and solutions. In <u>Reclamation, Treatment and utilization of coal mining wastes,</u> Rainbow (Ed.). Balkema, Rotterdam, pp 417-424.

Kortenski, J and Kostova, I, 1996, <u>Occurrence and morphology of pyrite in Bulgarian coals.</u> *Int. J. of Coal Geology*, **29**, 273-290.

Kuo, E.Y. and Ritchie, A.I.M, 1999. Enhanced oxygen transport by convection in sulfidic rock piles: the influence of the form of the sulfide oxidation rate. <u>In Proc. International Mine Water Congress, September 1999, Seville, Spain</u>, vol. **2**, pp 445-460.

Lasaga, A.C., 1984. <u>Chemical kinetics of water-rock interactions</u>. *Journal of Geophysical Res.*, **89** (B6), 4009-4025.

Lawrence, D.J.D. and Jackson, I., 1990, <u>Geology and land-planning: Morpeth – Bedlington – Ashington, Parts 1 and 2</u>, Technical Report WA/90/19, BGS.

Leblanc, M., Achard, B., Othman, B., Luck, J.M., Betrand-Sarfati, J. and Ch.Personné, J., 1996. <u>Accumulation of arsenic from acidic mine waters by ferruginous bacterial accretions (stromatolites).</u> *Applied Geochemistry*, **11**, 541-554.

Levenspiel, O, 1972, <u>Chemical Reaction engineering</u>. 2nd edition, New York, Wiley.

Lumsdon, D.G. and L.J. Evans. 1995. Predicting chemical speciation and computer simulation. p. 86-134. In A.M. Ure and C.M. Davidson (ed.) <u>Chemical speciation in the environment</u>. Chapman and Hall, London.

Macklin, M.G., Hudson-Edwards, K.A. and Dawson, E.J., 1997. The significance of pollution from historic metal mining to the Pennine orefields on river sediment contaminant fluxes to the North Sea. *Sci. Tot. Environment*, **194/195**, 391-397.

Macklin, M.G., Hudson-Edwards, K.A., Jamieson, H.E., Brewer, P., Coulthard, T.J., Howard, A.J. and Remenda, V.H., 1999, Physical stability and rehabilitation of sustainable aquatic and riparian ecosystems in the Rio Guadiamar, Spain, following the Aznalcóllar mine tailings dam failure. In proc: Mine, Water and Environment Congress, September 1999, Seville, Spain vol. 1, pp 271-278.

Malmström, M.E., Destouni G., Banwart S.A and Strömberg B.H.E, 2000, Resolving the Scale-Dependence of Mineral Weathering Rates. *Environ. Sci. Tech.* **34**(7), 1375-1378

Martys, N.S. and Ferraris, C.F., 1997. Capillary transport in mortars and concrete. *Cement and Concrete Res.*, **27** (5), 747-760.

McGiness, S. and Johnson, D.B., 1993. Seasonal variations in the microbiology and chemistry of an acid mine drainage stream. *Sci. Tot. Environment*, **132**, 27-41.

McKibben, M.A. and Barnes, H.L., 1986, Oxidation of pyrite in low temperature acidic solutions : Rate laws and surface textures. *Geochimica et Cosmochimica Acta*, **50**, 1509-1520.

Miller, J.C., and Miller, J.N., 1993, Statistics for analytical chemistry, 3rd Edition, Wessex, Ellis Horwood and Prentice Hall.

Morin, K.A. and Hutt, N.M., 1994. An empirical technique for predicting the chemistry of water seeping from mine-rock piles. In Proc. Third International Conference on the Abatement of Acidic Drainage, Pittsburgh, PA,USA, April 24-29, 1994.

Moses, C.O., and Herman, J.S., 1991, Pyrite oxidation at circumneutral pH. *Geochimica et Cosmochimica Acta*, **55**, 471-482.

Moses, C.O., Nordstrom, D.K., Herman, J.S., and Mills, L.A., 1987. Aqueous pyrite oxidation by dissolved oxygen and by ferric iron. *Geochimica et Cosmochimica Acta*, **51**, 1561-1571.

Murkowsky, M-Th, 1968, Mineral matter in coal. In Murchinson, D. and Westoll, T.S. eds., Coal and coal-bearing strata, Edinburgh, Oliver and Boyd, 309-319.

Nicholson, R.V., Gillham, R.W. and Reardon, E.J., 1988, Pyrite Oxidation in carbonate- buffered solution : 1 Experimental kinetics. *Geochimica et Cosmochimica Acta*, **52**, 1077-1085.

Nicholson, R.V., Gillham, R.W. and Reardon, E.J., 1990, Pyrite Oxidation in carbonate- buffered solution : 2. Rate control by oxide coatings. *Geochimica et Cosmochimica Acta*, **54**, 395-402.

Noël, M.M. and Ritchie, A.I.M, 1999. Some physical properties of water transport in waste rock material. In Proc. International Mine Water Congress, September 1999, Seville, Spain, vol. **2**, pp 449-454.

Nordstrom, D.K. 1982. Aqueous pyrite oxidation and the consequent formation of secondary iron minerals. In Acid Sulfate Weathering. J.A. Kittrick, D.S. Fanning, and L.R. Hossner (Eds.), Soil Sci. Soc. America Spec. Pub. 10. pp 37-56

Nordstrom, D.K., Alpers, C.N., Ptacek, C.J. and Blowes, D.W., 2000. Negative pH and extremely acidic mine waters from Iron Mountain, California. *Environ. Sci.Tech.*, **34**, 254-258.

Nordstrom, D.K., and Alpers, C., 1999. Negative pH, efflorescent mineralogy, and consequences for environmental restoration at the Iron Mountain Superfund site, California. In Proc. Natl. Acad. Sci. USA, vol. **96**, pp 3455-3462.

Nyavor, K. and Egiebor, N.O., 1995. Controls of pyrite oxidation by phosphate coating, *The Science of the Total Environment*, **162**, 225-237.

O'Brien, C. and Hendershot, W.H., 1993. Separating streamflow into groundwater, solum and upwelling flow and its implications for hydrochemical modelling. *Journal of Hydrology*, **146**, 1-12.

Oeklers, E.H., 1996, Physical and chemical properties of rocks and fluids for chemical mass transport calculations. In Reactive transport in porous media, eds: Lichtner, P.C., Steefel, C.I., and Oelkers, E.H., Reviews in Mineralogy, (34), Mineralogical Society of America.

OSMRE, (U.S. Office of Surface Mining), 2002, Factors controlling acid mine drainage formation - Acid Mine Drainage Index. Available from http://www.osmre.gov/amdform.htm (accessed 12th June 2002).

Paktunc, A.D. and Davé, N.K., 2000. Mineralogy of pyritic waste rock leached by column experiments and prediction of acid mine drainage. In Applied Mineralogy in Reasearch, Economy, Technology, Ecology and Culture, (2), Eds: Rammalair, D., Medere, J., Oberthur, Th., Heinmann, R.B and Pentinghaus, H., proc. of 6th Int. Congress on applied mineralogy, Goettingen, Germany, 17-19 July 2000.

Peiffer, S., Beierkuhnlein, C., Sandhage-Hofmann, A., Kaupenjohann, M., and Bär, S., 1997. Impact of high aluminium loading on a small catchment area (Thuringia slate

mining area) – geochemical transformations and hydrological transport. *Water, Air and Soil Pollution*, **94**, 401-416.

Pinder, G.F. and Jones, J.F., 1969. Determination of the groundwater component of peak discharge from the chemistry of total runoff. *Water Resources Res.* **5**(2), 439-445.

Prein, A. and Mull, R., 1998. Oxygen as a limiting factor for pyrite weathering in the overburden of open pit lignite areas. In Acidic mining lakes : acid mine drainage, limnology and reclamation ; Walter Geller, Helmut Klapper, Wim Salomons, (Eds.) Springer, 1998 Berlin, London, pp 237-250.

Rose, A.W. & Cravotta, C.A. Geochemistry of coal-mine drainage. In: Brady, K.B.C, Smith, M.W. and Schueck, J. Eds. Coal Mine Drainage Prediction and Pollution Prevention in Pennsylvania, Pennsylvania Department of Environmental Protection, 1: pp 1-26.

Sadler, P., 1999, Predicting groundwater recovery after mine closure. In proc: Mine, Water and Environment Congress, September 1999, Seville, Spain pp 437-444.

Schafer, J.L., White, M.L. and Caenepeel, C.L., 1979. Application of the shrinking core model for copper oxide leaching. *Mining Eng.* 165-171.

Schüring, J., Kölling, M and Schulz, H.D., 1997. The potential formation of acid mine drainage in pyrite-bearing hard-coal tailings under water-saturated conditions: an experimental approach. *Environmental Geology*, **31** (1), 59-65.

Şenel, G., Güruz, G., and Yücel, H., 2001, Characterization of pore structure of Turkish coals. *Energy and Fuels*, **15**, 331-338.

Simms, P.H., Yanful, E.K., St-Arnaud, L., and Aubé, 2000. A laboratory evaluation of metal release and transport in flooded pre-oxidised mine tailings. *Applied Geochemistry*, **15**, 1245-1263.

Singer, P.C. and Stumm, W.V., 1970. Acid min drainage: the rate determining step. *Science*, **167**, 1121-1123.

Skousen, J., Simmons, J., MacDonald, L.M., and Ziemkiewicz, P., 2002, Acid base accounting to predict post-mining drainage quality on surface mines. Submitted to Journal of Environmental Water Quality. Available at http://www.wvu.edu/~agexten/landrec/JEQABA.pdf, (accessed 10th July 2002).

Sobek, A.A., schuller, W.A., Freeman, J.R. and Smith, R.M., 1978, Field and Laboratory methods applicable to overburden and minesoils. U.S. E.P.A., Report EPA-600/2-78-054.

Soulsby, C., Chen, M., Ferrier, R.C., Helliwell, R.C., Jenkins, A. and Harriman, R., 1998. Hydrogeochemistry of shallow groundwater in an upland Scottish catchment. *Hydrological Processes*, **12**, 1111-1127.

Spears, D.A. and Martinez-Tarazona, M.R., 1992. Geochemical and mineralogical characteristics of a power station feed-coal, Eggborough, England. *International Journal of coal Geology*, **22**, 1-20.

Spears, D.A., 1987, Mineral matter in coal, with special reference to the Pennine coalfields. In Scott, A.C., ed., Coal and Coal-bearing strata : Recent advances, Oxford, Blackwell Scientific, 171-187.

Spotts, E. and Dollhopf, D.J., 1992. Evaluation of phosphate materials for control of acid production in pyritic mine overburden. *J. Environ.Qual.* **21**, 627-634

SPWLA, (Society of professional well log analysts), 2002, Glossary. Available at http://www.spwla.org/ (accessed 10th July 2002).

Stefanoff, J.G. and Kim, Y., 1994. Reduction of leachability of heavy metals in acid mine drainage. *J.Environ. Sci. Health* **A29(2)**, 371-388

Stewart, B.R., Daniels, W.L. and Jackson, M.L., 1997. Evaluation of leachate quality from codisposed coal fly ash and coal refuse. *J.Environ. Qual* **26,** 1416-1424

Stiller, A.H., Renton, J.J. and Rymer, T.E., 1989. An experimental evaluation of the use of rock phosphate (apatite) for the amelioration of acid-producing coal mine waste. *Mining Science and Technology* **9**, 283-287

Strauss, H., and Schieber, J., 1989, A sulfur isotope study of pyrite genesis: The Mid-Proterozoic Newland Formation, Belt Supergroup, Montana. *Geochimica et Cosmochimica Acta*, **54**, 197-204.

Strömberg, B., 1997, Weathering kinetics of sulphidic mining waste : An assessment of geochemical processes in the Atik mining waste rock deposits. Doctoral thesis, TRITA-OOK-1043 Dept. Chem., Inorg. Chem., KTH, Stockholm.

Stumm, W. and Morgan, J., 1999. Aquatic Chemistry – Chemical Equilibria and Rates in Natural Waters, 3rd edition, Wiley, New York.

Utzmann, A., Van Cappellen, P., Schmincke, H. and Garbe-Schönberg, D., 2000. Experimental determination of low-temperature dissolution kinetics of silicate glasses. In Proc. Goldschmidt 2000, Oxford, UK, 3-8 September 2000, Journal of Conference abstracts, vol **5** (2), 1028.

Vandiviere, M.M. and Evangelou, V.P., 1998. Comparitive testing between conventional and microencapsulation approaches in controlling pyrite oxidation. *Journal of Geochemical Exploration* **64**, 161-176

Ward, R.C. and Robinson, M., 1990. Principles of hydrology, 3rd edition, McGraw-Hill, Berkshire, England.

Watson, W.D., Ruppert, L.F., Bragg, L.J. and Tewalt, S.J., 2001, A geostatistical approach to predicting sulfur content in the Pittsburgh coal bed. *Int. J.of Coal Geology*, **48**, 1-22.

Webb, J.A. and Sasowsky, I.D., 1994. The interaction of acid mine drainage with a carbonate terrain: evidence from the Obey River, north-central Tennessee. *Journal of Hydrology,* **161**, 327-346

Widler, A.M. and Seward, T.M., 2002, The adsorption of gold (I) hydrosulphide complexes by iron sulphide surfaces. *Geochimica et Cosmochimica Acta*, **54**, 395-402.

Wiggering, H., 1987. Weathering of clay minerals in waste dumps of upper carboniferous coal-bearing strata, the Ruhr area, West Germany, *Applied Clay Science* **2**, 353-361

Wiggering, H., 1993. Sulphide oxidation – an environmental problem with colliery spoil dumps. *Environmental Geology* **22**, 99-105

Wilkin, R.T., Barnes, H.L. and Brantley, S.L., 1996. The size distribution of framboidal pyrite in modern sediments: An indicator of redox conditions. *Geochimica et Cosmochimica Acta*, **60**, (20), 3897-3912.

Williams, E.G. and Keith, M.L., 1963, Relationship between sulfur in coals and the occurrence of marine roof beds. *Economic Geology*, **58**, 720-729.

Worrall, F., and Pearson, D.G., 2000, The development of acidic groundwaters in coal-bearing strata: part 1. Rare earth element fingerprinting. *App. Geochem.*, **16**, 1465-1480.

Wunderly, M.D., Blowes, D.W., Frind, E.O. and Ptacek, C.J., 1996, Sulfide mineral oxidation and subsequent reactive transport of oxidation products in mine tailings impoundments : A numerical model. *Water Resources Research*, **32**, 3173-3187.

WVGES, 2001, West Virginia Geological & Economic Survey, Glossary, West Virginia, US. - Available at http://www.wvgs.wvnet.edu/www/datastat/te/Glossary.htm last accessed on the 21st October 2002.

Yanful, E.K., Orlandea, M.P. and Eliasziw, M, 2000. Controlling acid drainage in a pyritic mine waste rock. Part 1: statistical analysis of drainage data. *Water, Air, and Soil Pollution*, **122**, 369-388.

Younger, P.L. and Adams, R., 1999. Predicting Mine Water Rebound, Technical Report W179, Environment Agency, Bristol, UK, pp 1-109.

Younger, P.L., 1995a, Polluted groundwater in abandoned coalfields: some hydrogeological and geochemical idiosyncrasies. In Proc. 4th Annual Conference on Groundwater Pollution, 15th-16th March 1995, London.

Younger, P.L., 1995b. Hydrogeochemistry of minewaters flowing from abandoned coal workings in County Durham. *Quarterly J. Eng. Geol.,* **28**, 101-113.

Younger, P.L., 1998. Coalfield abandonment: geochemical processes and hydrochemical products. In Nicholson, K. (Ed). Energy and the environment: Geochemistry of fossil, nuclear and renewable resources, MacGregor Science, pp1-29.

Younger, P.L., 2000, Predicting temporal changes in total iron concentrations in groundwaters flowing from abandoned deep mines: a first approximation. *Journal of Contaminant Hydrology,* **44**, (1), 47-69.

Younger, P.L., 2000. Pilot-scale passive treatment of acidic mine drainage using a downward-flow reducing and alkalinity producing system (RAPS) at Bowden Close, County Durham, UK. In Final report to CDENT and Durham County Council, September, 2000.

Zgarlyike, C.J. and Steadman, E.N., 1990. Advanced SEM techniques to characterize coal minerals. *Scanning Microscopy,* **4** (3), 579-590.

Zhang, Y.L., and Evangelou, V.P., 1997. Formation of ferric hydroxide-silica coatings on pyrite and its oxidation behaviour, **163**, 53-62.
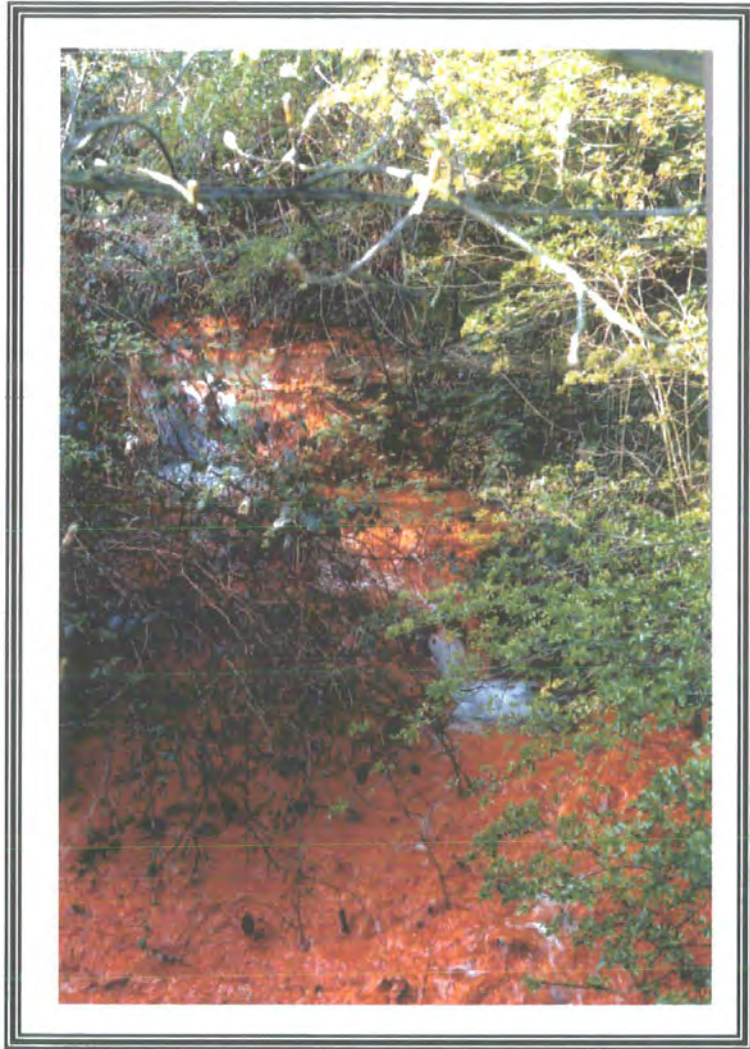
Endispiece - Stoney Heap uncontrolled acid mine discharge, County Durham, UK.

Appendix I Methods

Sample preparation for major element analysis by Inductively Coupled Plasma - Optical Emission Spectrometry (ICP-OES)

To prepare each sample for major element analysis by ICP-OES:

1. Aqueous samples were vacuum filtered through a 45 μm cellulose nitrate filter paper.
2. 10 mL of the filtrate was placed in a plastic auto-sampler tube and acidified with 50μL of concentrated HNO_3 and agitated to mix.
3. An internal spike was added to all samples to check for calibration drift during analysis. 100μL of a 100mgL^{-1} Y solution made from a 1000 mgL^{-1} Y standard was used.
4. The sample was agitated to mix the solutions thoroughly.
5. Samples were either analysed immediately or stored at 5°C until analysis was possible, usually within a week. Once acidified and stored at low temperature little change in solution concentration occurred.

Prior to analysis combined calibration standards for Al, Ca, Cu, Fe, K, Mg, Mn, Na, P, S, Si and Zn were made up at 0, 0.5, 1, 5, 10 and 20 mgL^{-1}. An internal spike of 100 mgL^{-1} was added to the sample concentration as in samples, i.e. 100μL of 100mgL^{-1} Y per 10 mL of standard. When the samples were known to be highly concentrated, 100 and 200 mgL^{-1} standards were also used in the calibration.

All analyses were performed on a Perkin Elmer Optima 3300 RL ICP-OES machine, with plasma torch view height at 7mm. The machine was calibrated with combined standards prior to analysis and the 0, 1 and 10 mgL^{-1} standards were re-analysed every 30 samples, and all standards were analysed at the end of a sample run to check for drift.

At least two wavelengths were collected for each element to cover high and low intensity, and collected spectra were reprocessed using ICP WinLab software. Where drift was identified by variation in Y internal spike, this was automatically corrected for by the software.

Sobek's (1978) method for oxidizable sulphur extraction.

Method 1 Back titration with NaOH

1. To remove acid leachable phases a paste was made with 2 g of powdered rock and 1 mL 1% BRIJ35 solution. To this paste 200 mLs of 10% HCl solution was added and the samples left over-night. After filtering through Whatman no.1 filter paper, the residue was washed with Milli-Q water.
2. The residue was dried at 105°C, re-weighed, then mixed with 1 mL of 1% BRIJ35 solution in a 500mL glass beaker. The resultant paste was mixed with 20 mL of 30% H_2O_2, and covered with parafilm then heated to 40°C. When the solution stopped bubbling a further 10 mL of 30 % H_2O_2 was added to the beaker which was resealed and left to react overnight at room temperature.
3. The samples were subsequently heated to 90°C until reaction ceased. If, however the samples continued to react, on heating to 90°C, no further addition of H_2O_2 was made until the reaction ceased.

4. Samples were allowed to cool then were filtered through a Whatman no.1 filter paper and the filtrate titrated against 0.1 M NaOH solution to pH 7.

Method 2 Sequential Extraction

1. Two grams of powdered rock was mixed to a paste with 1 mL of a 1% BRIJ35 solution then mixed with 200 mL of 10% HCl solution and left over-night. The subsequent leachate was filtered using a Whatman no.1 filter paper, and the residue washed with up to 100 mL of Milli-Q water. The filtrate was made up to 300 mL and a 50 mL aliquot was acidified 250 µL concentrated HNO_3 for ICP-OES analysis.
2. The residue was dried at 105°C, re-weighed, then mixed with 1 mL of 1% BRIJ35 solution in a 500mL glass beaker. The resultant paste was mixed with 20 mL of 30% H_2O_2, and covered with parafilm then heated to 40°C. When the solution stopped bubbling a further 10 mL of 30 % H_2O_2 was added to the beaker which was resealed and left to react overnight at room temperature.
3. Samples were subsequently heated to 90°C, and if no bubbling appeared a further 5mL of 30 % H_2O_2 was added and heating continued. If, however the samples continued to react, on heating to 90°C, no further addition of H_2O_2 was made until the reaction ceased. Thus, the addition of 5 mL aliquots of H_2O_2 was used to gauge the extent of removal of the oxidizable phase.
4. Once reaction had ceased (usually within another 10 hours), the samples were allowed to cool, then were filtered and the residue washed with up to 200 mL Milli-Q water. The filtrate was made up to 300 mL and a 50 mL aliquot was removed and acidfied with concentrated HNO_3 for major element analysis by ICP-OES.

Preparation of polished resin blocks for SEM examination

1. Prior to cutting each sample was coated in cold setting epoxy resin (Epo-Thin, Buehler Krautkramer) to provide a cohesive cutting surface.
2. Each sample was cut with a diamond-impregnated cutting disc (without lubricant) to give a flat, orientated surface.
3. After thorough drying in a warm (40°C) oven for 24 hours, all samples were embedded in a cold setting epoxy resin (Epo-Thin, Buehler Krautkramer), initially under vacuum for 15 minutes then left for 48 hours at room temperature to cure.
4. Each sample was ground again on the coarse diamond disc to remove the thin layer of resin from the surface of the specimen. This was followed by further grinding on a 1200 grit silicon carbide disc to prepare the sample for polishing.
5. Polishing was carried out on a rotary polisher (Buehler Metaserv) using a Texmet 1000 cloth and Buehler Mastermet 2 (0.02 µm non-crystallising colloidal silica polishing suspension). The cloth was charged with Mastermet 2 and the specimen polished for one minute without lubricant and then for a further 2 minutes with a water drip-feed. .
6. The specimen was examined under a reflected light microscope to check the level of polish. If necessary, step 4 was repeated until the majority of scratches and pits were removed.
7. Prior to examination, blocks were electrostatically carbon-coated to prevent surface charging.

Chapter 3 Results

Tables of results of experiment described in Chapter 3. Treatment solutions combination of P and H_2O_2 are shown are in first two columns. All mean values displayed are given to the first uncertain decimal place - 1σ, n=3 unless otherwise shown, or 0.01 $mgL^{-1}g^{-1}$ pyrite for ICP-OES analyses, or 2 decimal places for pH meter depending on which value is lowest.

Initial treatment concentrations		Treatment leachate concentration		Test leachate concentration		
H_2O_2 (%)	P (mgL^{-1})	Fe $mgL^{-1}g^{-1}$ (n=3)	S $mgL^{-1}g^{-1}$ (n=3)	Fe $mgL^{-1}g^{-1}$ (n=2)	S $mgL^{-1}g^{-1}$ (n=2)	P $mgL^{-1}g^{-1}$ (n=2)
0.03	1240	0.2 ± 0.1	30 ± 9	706 ± 50	1469 ± 173	8 ± 2
0.03	124	0.07 ± 0.07	35 ± 4	899 ± 234	1630 ± 364	9 ± 3
0.03	12.4	3 ± 3	133 ± 5	728 ± 101	1500 ± 80	6.5 ± 0.4
0.03	0	64 ± 4	139 ± 6	686 ± 144	1450 ± 201	5.6 ± 0.9
0.01	1240	0.09 ± 0.05	23 ± 2	991 ± 247	1894 ± 506	10 ± 2
0.01	124	0.11 ± 0.03	21 ± 2	801 ± 250	1576 ± 321	7 ± 2
0.01	12.4	0.40 ± 0.00	78 ± 1	599 ± 222	1412 ± 117	6.0 ± 0.9
0.01	0	26.83 ± 0.09	66 ± 1	478 ± 282	1785 ± 568	4.6 ± 0.4
0.0	1240	0.07 ± 0.01	10 ± 4	791 ± 160	1511 ± 207	7 ± 2
0.0	124	0.02 ± 0.01	10 ± 4	770 ± 260	1597 ± 282	8 ± 2
0.0	12.4	1.0 ± 0.3	29 ± 7	641 ± 147	1286 ± 216	5 ± 2
0.0	0	11 ± 9	30 ± 14	596 ± 72	1207 ± 101	4.6 ± 0.8

Table 3.A. 1st Optimisation treatment and test leachate Fe, S and P concentration.

Initial treatment concentrations		Treatment leachate concentration		Test leachate concentration		
H_2O_2 (%)	P (mgL^{-1})	Fe $mgL^{-1}g^{-1}$ (n=3)	S $mgL^{-1}g^{-1}$ (n=3)	Fe $mgL^{-1}g^{-1}$ (n=3)	S $mgL^{-1}g^{-1}$ (n=3)	P $mgL^{-1}g^{-1}$ (n=3)
0.01	800	85 ± 20	433 ± 0.86	37 ± 8	95 ± 17	2.6 ± 0.6
0.01	550	5.8 ± 0.8	420 ± 57	32 ± 5	90 ± 17	2.2 ± 0.5
0.01	300	7.4 ± 0.3	476 ± 15	47 ± 20	121 ± 37	2.4 ± 0.2
0.01	80	9.3 ± 0.7	451 ± 43	45 ± 2	116 ± 2	2.6 ± 0.3
0.005	800	2.6 ± 0.4	184 ± 12	44 ± 9	101 ± 8	2.8 ± 0.6
0.005	550	2.5 ± 0.1	191 ± 14	52 ± 29	112 ± 30	2.2 ± 1
0.005	300	22 ± 3	259 ± 8.4	69 ± 19	146 ± 24	3 ± 2
0.005	80	19 ± 8	270 ± 24	65 ± 2	165 ± 3	1.9 ± 0.2
0.00	800	2 ± 2	8.0 ± 1	60 ± 27	129 ± 17	2 ± 1
0.00	550	3.4 ± 0.1	9.0 ± 0.4	66 ± 2	142 ± 15	2.0 ± 0.9
0.00	300	2.9 ± 0.5	7.4 ± 1	64 ± 31	129 ± 33	1.9 ± 0.8
0.00	80	3.4 ± 0.7	8.8 ± 0.5	54 ± 6	137 ± 28	1.5 ± 0.1

Table 3.B. Treatment and test leachate Fe, S and P concentrations per gram of pyrite, calculated from leachate concentration from 0.1g pyrite.

Time (min)	Fe mgL^{-1}g^{-1} (n=2)	S mgL^{-1}g^{-1} (n=2)	P mgL^{-1}g^{-1} (n=2)	pH (n=2)	Blank pH (n=1)
5	0.22 ± 0.02	9 ± 4	60 ± 43	5.12 ± 0.08	5.38
10	0.11 ± 0.02	10 ± 2	110 ± 52	5.23 ± 0.02	5.35
20	0.12 ± 0.06	10 ± 3	71 ± 110	5.30 ± 0.01	5.34
30	0.13 ± 0.02	12.8 ± 0.9	32 ± 26	5.37 ± 0.02	5.26
45	0.10 ± 0.03	14.6 ± 0.8	71 ± 10	5.43 ± 0.01	5.28
60	0.04 ± 0.05	9 ± 12	74 ± 53	5.50 ± 0.02	5.32
120	0.15 ± 0.01	16 ± 1	58 ± 24	5.58 ± 0.06	5.38
240	0.08 ± 0.02	18 ± 1	111 ± 32	5.62 ± 0.03	5.27
360	0.08 ± 0.00	21.92 ± 0.01	99 ± 44	5.58 ± 0.06	5.34
600	0.17 ± 0.08	26 ± 2	45 ± 24		
1440	0.38 ± 0.04	53 ± 1	84 ± 11	5.1 ± 0.1	5.35
2880	0.53 ± 0.01	75 ± 3	113 ± 24	4.3 ± 0.1	5.35

Table 3.C. Fe, S, P concentration and pH of leachate of pyrite treated with 60 mgl-1g-1 P and 0.005% H_2O_2 over a period of 2880 minutes. pH value at 420 minutes replaces 360 and 600 minute values.

Time (min)	Fe mgL^{-1}g^{-1}	S mgL^{-1}g^{-1}	P mgL^{-1}g^{-1}
5	7.3	66.3	0.02
10	16 ± 8	85 ± 31	0.2 ± 0.1
20	2 ± 7	60 ± 8	0.4 ± 0.1
45	15.1	79.9	0.2
60	8.9	96.3	2.6
120	19.5	77.2	0.2
240	2.6	50.8	0.1
360	8.9	55.1	0.1
600	5.0	41.4	0.1
1440	11.5	47.9	0.1
2880	4.6	42.9	0.1

Table 3.D. Fe, S and P concentration in test leachate of pyrite pre-treated with 60 mgL^{-1} P and 0.005% H_2O_2 over a period of 2880 minutes. Where mean value is shown (n=2) the standard error of the mean represents uncertainty in this value.

Chapter 4 Results

Seam	Sample	Sub-sample	Pyrite	SiO$_2$	Al$_2$O$_3$	Fe$_2$O$_3$	MgO	CaO	Na$_2$O	K$_2$O	TiO$_2$	MnO	P$_2$O$_5$	S	Total
			wt %	wt %	wt %	wt %	wt %	wt %	wt %	wt %	wt %	wt %	wt %	wt %	wt %
MSUL	2	A	1.42	1.65	1.12	1.37	0.01	0.00	0.00	0.02	0.06	0.00	0.02	1.84	6.09
		B	1.33	1.89	1.30	1.73	0.00	0.03	0.03	0.01	0.06	0.00	0.01	1.83	6.89
		C	0.42	1.39	0.89	0.98	0.01	0.04	0.00	0.01	0.04	0.00	0.03	1.39	4.78
	3	A	8.76	8.47	4.58	0.42	0.06	0.00	0.00	0.37	0.31	0.00	0.01	0.83	15.06
		B	1.90	6.39	3.32	0.74	0.04	0.02	0.00	0.73	0.19	0.00	0.04	1.32	12.80
		C	3.28	2.27	1.42	0.58	0.03	0.01	0.00	0.03	0.10	0.00	0.05	1.43	5.92
	4	A	1.48	2.99	2.10	4.48	0.03	0.04	0.01	0.15	0.10	0.00	0.03	3.90	13.84
		B	3.94	2.19	1.28	0.07	0.00	0.01	0.00	0.01	0.06	0.00	0.02	1.06	4.70
		C	2.91	1.89	1.22	0.79	0.00	0.00	0.02	0.01	0.07	0.00	0.02	1.39	5.41
MSBL	1	A	1.17	0.41	0.39	9.35	0.02	0.03	0.01	0.00	0.01	0.00	0.01	7.13	17.36
		B	1.44	0.78	0.57	0.87	0.00	0.00	0.00	0.00	0.05	0.00	0.01	1.30	3.58
		C	0.96	0.87	0.58	1.24	0.00	0.00	0.00	0.00	0.09	0.00	0.01	1.66	4.45
	2	A	2.41	0.68	0.41	0.44	0.00	0.01	0.00	0.01	0.08	0.00	0.01	1.21	2.84
		B	1.42	1.37	0.87	0.81	0.00	0.01	0.00	0.03	0.09	0.00	0.03	1.34	4.54
		C	1.57	1.49	1.03	1.18	0.01	0.01	0.00	0.00	0.04	0.00	0.01	1.49	5.26
	3	A	0.81	0.42	0.38	1.34	0.01	0.01	0.00	0.00	0.04	0.00	0.01	1.69	3.89
		B	1.63	1.07	0.67	0.62	0.01	0.00	0.00	0.00	0.16	0.00	0.01	1.38	3.92
		C	1.26	0.03	0.10	1.36	0.00	0.00	0.00	0.00	0.01	0.00	0.01	1.82	3.33
MSP	1	A	7.80	25.00	13.91	2.17	0.37	0.02	0.06	1.69	0.55	0.00	0.04	0.79	44.61
		B	4.05	24.88	13.87	2.18	0.39	0.02	0.09	1.88	0.48	0.00	0.03	0.80	44.62
		C		39.75	21.25	2.29	1.02	0.00	0.23	4.97	0.55	0.00	0.04	0.42	70.53
	2	A	1.50	41.55	29.34	1.60	0.56	0.00	0.15	0.97	0.94	0.00	0.03	0.10	75.24
		B	2.10	39.59	25.86	1.58	0.55	0.00	0.09	1.12	0.84	0.00	0.02	0.13	69.79
		C	2.70	38.06	25.34	1.42	0.48	0.00	0.13	0.95	0.96	0.00	0.03	0.18	67.55
	3	A	4.50	32.93	21.46	4.56	0.49	0.27	0.13	1.58	0.72	0.01	0.22	1.53	63.89
		B		9.57	8.75	33.51	0.14	0.48	0.08	0.09	0.16	0.01	0.39	29.46	82.64
		C	11.70	16.09	12.06	17.14	0.20	0.18	0.05	0.55	0.37	0.01	0.12	12.60	59.36
MSSE	1	A	0.21	56.15	24.37	0.91	0.49	0.00	0.16	1.63	1.05	0.00	0.02	0.00	84.78
		B	0.18	54.42	25.10	0.96	0.52	0.00	0.16	1.76	1.07	0.00	0.02	0.00	83.97
		C	0.35	53.61	26.27	0.87	0.51	0.00	0.15	1.66	1.04	0.00	0.02	0.00	84.13
	2	A	0.39	44.87	32.07	1.66	0.54	0.01	0.15	1.37	0.96	0.00	0.13	0.03	81.80
		B	0.29	44.19	30.35	1.49	0.54	0.00	0.16	1.36	1.03	0.00	0.07	0.02	79.20
		C	0.39	45.15	29.14	1.60	0.54	0.00	0.16	1.38	1.03	0.00	0.06	0.02	79.08
	3	A	0.37	48.37	28.79	1.33	0.66	0.02	0.14	1.69	0.99	0.01	0.02	0.01	82.02
		B	0.67	49.89	27.35	1.00	0.65	0.01	0.13	1.70	1.03	0.00	0.01	0.00	81.77
		C	0.43	43.06	31.60	1.45	0.66	0.03	0.16	1.54	1.00	0.00	0.07	0.00	79.56

Table 4.A. Northwood Main seam lower (MSBL) and upper leaf (MSUL), parting (MSP) and seat-earth (MSSE) pyrite wt %, whole S and element oxide wt % calculated from XRF. Both ferrous and ferric forms of Fe are calculated from the same Fe$_2$O$_3$ content, although most Fe is assumed to be ferrous (Fe (II)) in statistical analysis.

Seam	Sample	Sub-sample	Density	Total Porosity	Pore Size Distribution			Effective Porosity	Specific surface area
					Micro	Meso	Macro		
			gcm^{-3}	cm^3g^{-1}	%	%	%	%	cm^2g^{-1}
MSUL	2	A	1.26	0.51	96.38	2.51	1.12	-	20.62
		B	1.27	0.50	94.73	3.77	1.50	3.40	27.79
		C	1.26	0.50	92.80	4.69	2.51	3.76	22.89
	3	A	1.24	0.52	94.72	2.83	2.45	4.71	49.30
		B	1.32	0.48	93.99	5.01	1.00	5.63	23.57
		C	1.26	0.51	95.43	3.69	0.88	6.51	28.16
	4	A	1.27	0.51	96.87	2.41	0.72	2.71	40.47
		B	1.25	0.52	-	-	-	2.78	23.55
		C	1.23	0.52	95.92	3.45	0.63	3.13	25.31
MSBL	1	A	1.25	0.50	94.96	4.04	1.00	3.41	22.31
		B	1.25	0.52	96.40	2.60	1.00	2.34	32.98
		C	1.25	0.51	94.18	4.63	1.19	5.14	34.63
	2	A	1.24	0.50	94.75	4.31	0.95	5.23	29.80
		B	1.25	0.51	94.02	4.75	1.23	4.06	36.43
		C	1.26	0.51	94.64	4.27	1.08	4.16	36.17
	3	A	1.25	0.51	95.62	3.49	0.89	1.33	24.39
		B	0.94	0.63	98.02	1.58	0.41	3.97	25.16
		C	1.25	0.52	96.09	2.59	1.32	4.84	24.97
MSP	1	A		0.30	-	-	-	15.26	76.14
		B	1.71	0.32	83.99	10.05	5.96	3.87	88.78
		C	1.79	0.30	85.88	9.84	4.27	14.86	18.79
	2	A	2.24	0.13	-	-	-	8.01	107.38
		B	2.09	0.18	84.49	12.33	3.17	53.93	98.30
		C	2.11	0.16	85.64	11.68	2.68	13.39	81.85
	3	A	1.87	0.27	93.63	4.93	1.45	-	99.82
		B	2.04	0.19	83.55	5.99	10.46	9.38	95.51
		C	1.67	0.36	95.34	2.48	2.19	8.37	30.35
MSSE	1	A	2.47	0.05	37.26	49.93	12.80	-	-
		B	2.48	0.04	-	80.22	19.78	-	-
		C	2.47	0.04	-	-	-	-	-
	2	A	2.39	0.08	84.58	11.24	4.18	-	-
		B	2.41	0.04	16.03	73.30	10.66	-	-
		C	2.36	0.08	58.69	31.42	9.89	-	-
	3	A	2.27	0.09	64.08	28.05	7.87	-	-
		B	2.42	0.03	-	65.70	34.30	-	-
		C	2.50	0.05	68.08	31.92	0.00	-	-

Table 4.B. Northwood strata, Main seam upper (MSUL) and lower leaf (MSBL), parting (MSP) and seat-earth (MSSE), physical characteristics including total porosity, density, effective porosity, specific surface area and pore size distribution. Spaces are lost samples, seat-earth (MSSE) samples were not analysed for specific surface area.

Figures 4.A to K. XRD scan plots of cps vs 2θ for one named sub-sample per sample of each Northwood seam. Identified mineral 2θ are marked on figures, with explanation in legend.
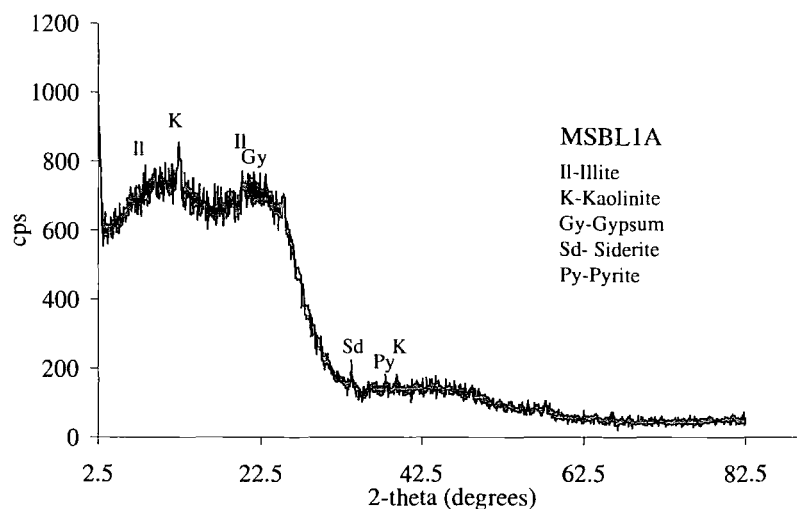
Figure 4.A. MSBL1A XRD scan data – 2 theta (2θ°) vs counts per second (cps)
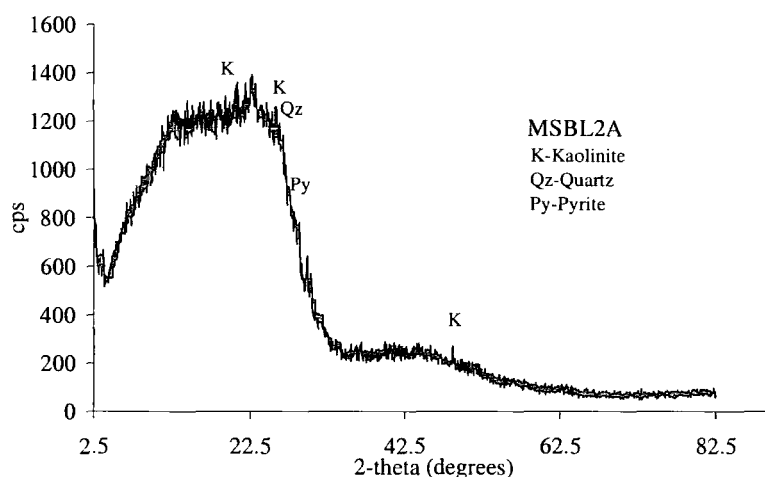
Figure 4.B. MSBL2A XRD scan data – 2 theta (2θ°) vs counts per second (cps)
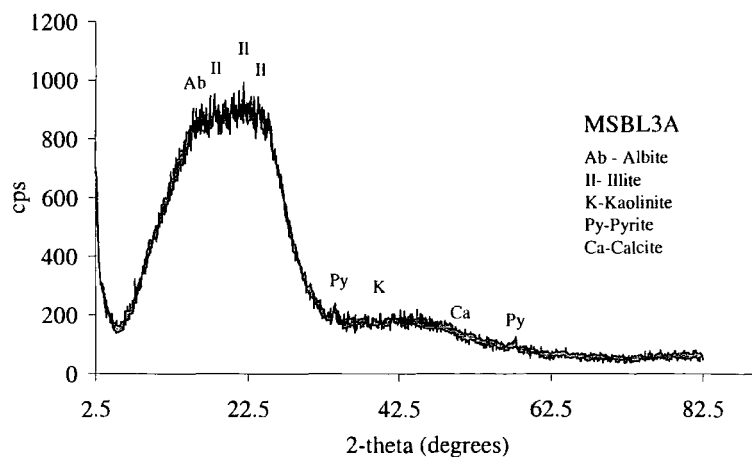
Figure 4.C. MSBL3A XRD scan data – 2 theta (2θ°) vs counts per second (cps)
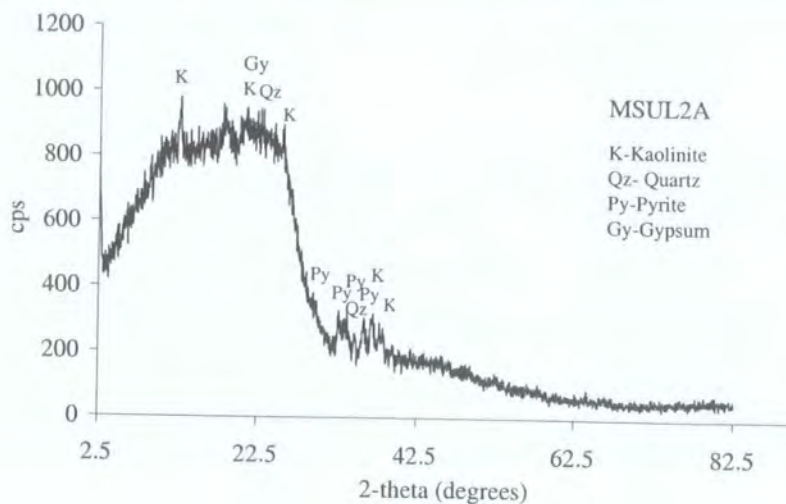
Figure 4.D. MSUL2A XRD scan data – 2 theta ($2\theta°$) vs counts per second (cps)
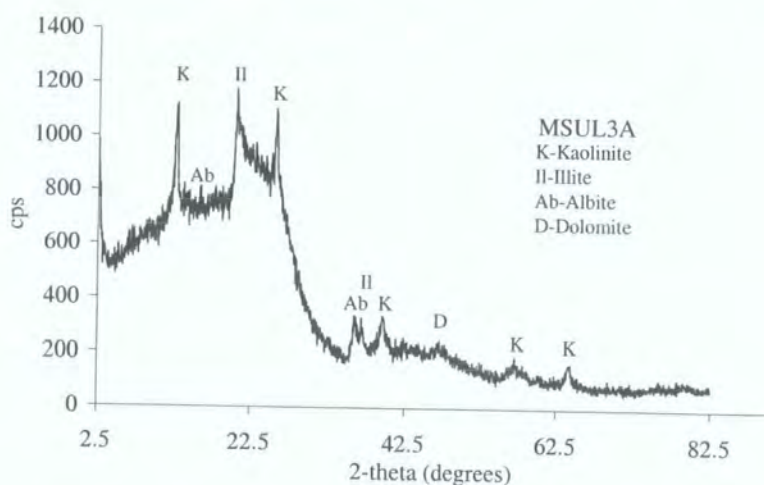
Figure 4.E. MSUL3A XRD scan data – 2 theta ($2\theta°$) vs counts per second (cps)
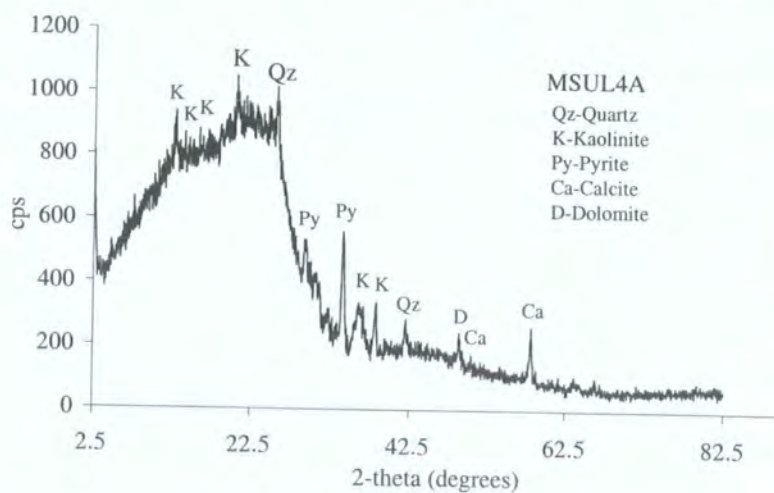
Figure 4.F. MSUL4A XRD scan data – 2 theta ($2\theta°$) vs counts per second (cps)
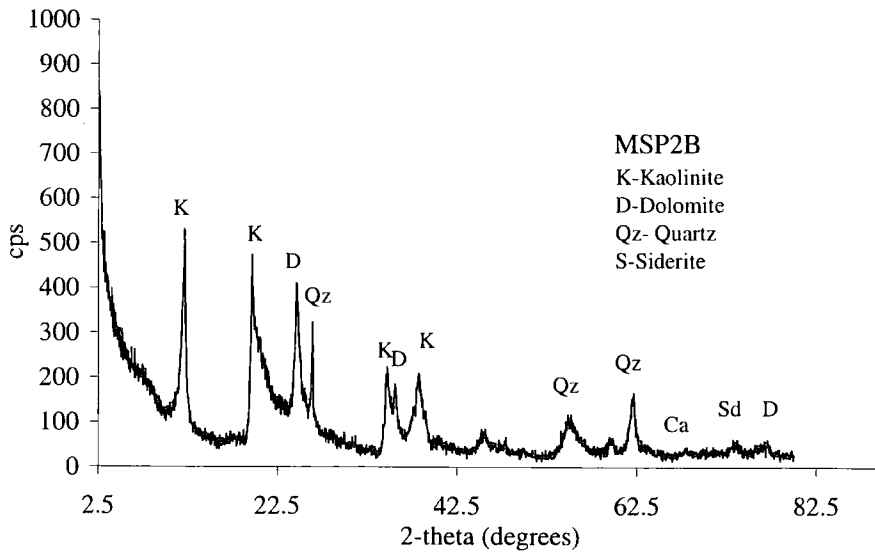
Figure 4.G. MSP2B XRD scan data – 2 theta (2θ°) vs counts per second (cps)
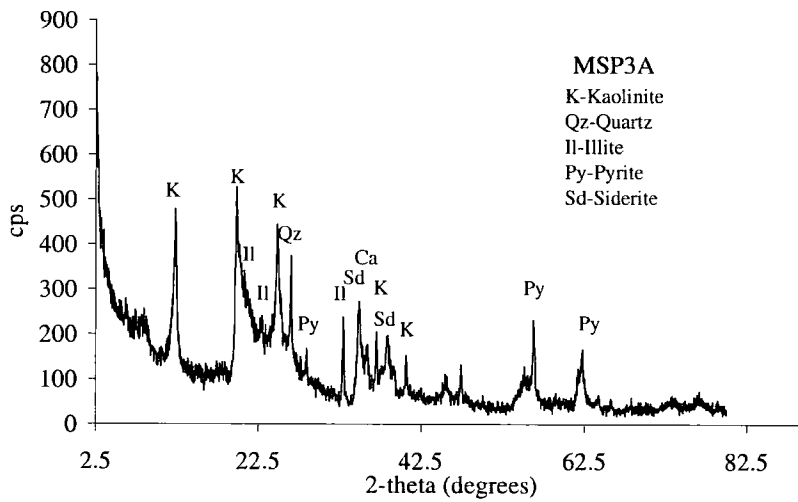
Figure 4.H. MSP3A XRD scan data – 2 theta (2θ°) vs counts per second (cps)
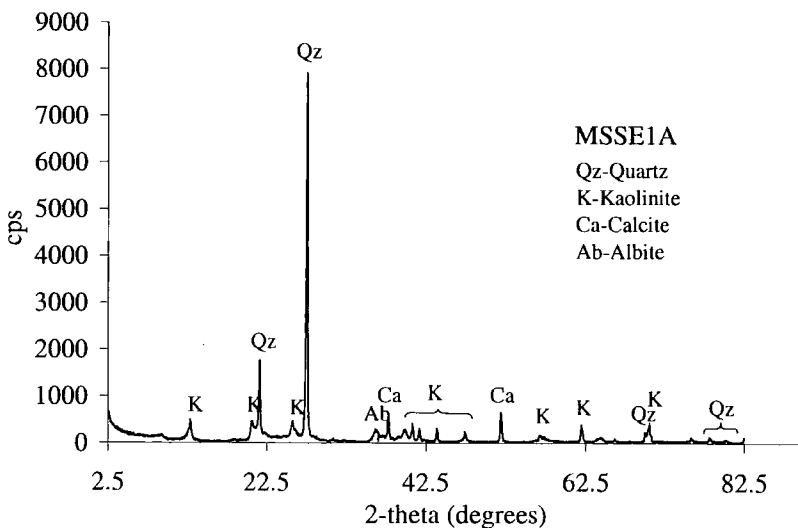
Figure 4.I. MSSE1A XRD scan data – 2 theta (2θ°) vs counts per second (cps)
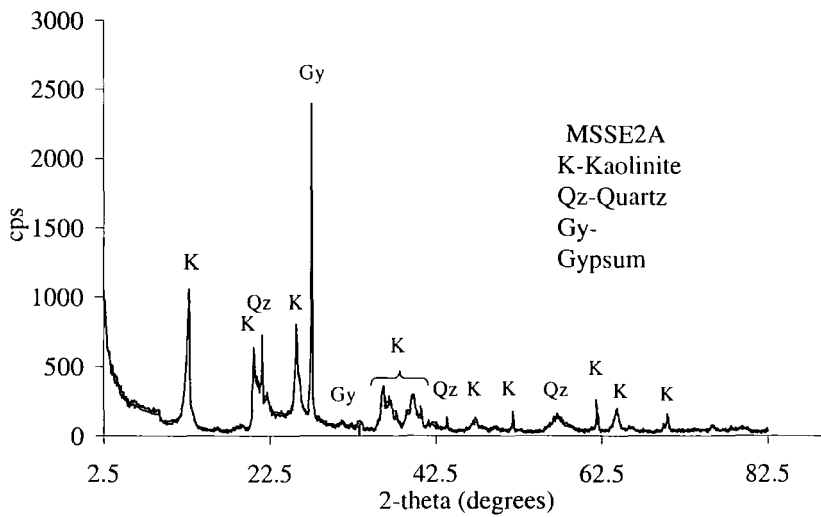
Figure 4.J. MSSE2A XRD scan data – 2 theta (2θ°) vs counts per second (cps)
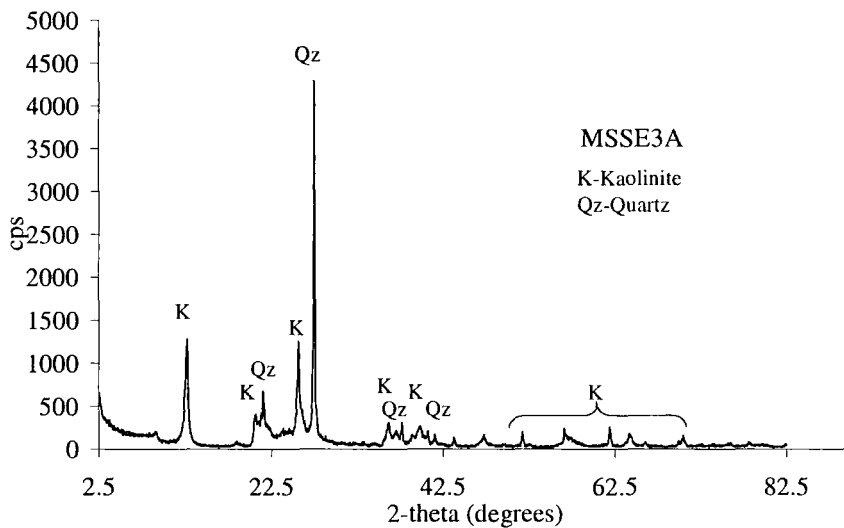
Figure 4.K. MSSE3A XRD scan data – 2 theta (2θ°) vs counts per second (cps)

Porosity	MSUL	MSBL	MSP	MSSE
MSUL	-	✗	✗	✔
MSBL	✗	-	✗	✔
MSP	✗	✗	-	✔
MSSE	✔	✔	✔	-

Micro-porosity	MSUL	MSBL	MSP	MSSE
MSUL	-	✗	✔	✔
MSBL	✗	-	✔	✔
MSP	✔	✔	-	✔
MSSE	✔	✔	✔	-

Macro-porosity	MSUL	MSBL	MSP	MSSE
MSUL	-	✗	✗	✔
MSBL	✗	-	✗	✔
MSP	✗	✗	-	✔
MSSE	✔	✔	✔	-

Meso-porosity	MSUL	MSBL	MSP	MSSE
MSUL	-	✗	✗	✔
MSBL	✗	-	✗	✔
MSP	✗	✗	-	✔
MSSE	✔	✔	✔	-

Effective Porosity	MSUL	MSBL	MSP
MSUL	-	✗	✗
MSBL	✗	-	✗
MSP	✗	✗	-

Specific Surface area	MSUL	MSBL	MSP
MSUL	-	✗	✔
MSBL	✗	-	✔
MSP	✔	✔	-

Table 4.C. Results of *post-hoc* pair-wise comparisons of seam variance for each physical characteristic (Tukey test). ✗ = Compared seams are not significantly different, ✔ = Compared seams are significantly different for a specified characteristic. Main seam lower (MSBL) and upper leaf (MSUL), parting (MSP) and seat-earth (MSSE).

Pyrite	MSUL	MSBL	MSP	MSSE
MSUL	-	✗	✔	✔
MSBL	✗	-	✔	✗
MSP	✔	✔	-	✔
MSSE	✔	✗	✔	-

TiO_2	MSUL	MSBL	MSP	MSSE
MSUL	-	✗	✔	✔
MSBL	✗	-	✔	✗
MSP	✔	✔	-	✔
MSSE	✔	✗	✔	-

SiO_2	MSUL	MSBL	MSP	MSSE
MSUL	-	✗	✔	✔
MSBL	✗	-	✔	✔
MSP	✔	✔	-	✔
MSSE	✔	✔	✔	-

CaO	MSUL	MSBL	MSP	MSSE
MSUL	-	✗	✔	✗
MSBL	✗	-	✔	✗
MSP	✔	✔	-	✔
MSSE	✗	✗	✔	-

Al_2O_3	MSUL	MSBL	MSP	MSSE
MSUL	-	✗	✔	✔
MSBL	✗	-	✔	✔
MSP	✔	✔	-	✔
MSSE	✔	✔	✔	-

Na_2O	MSUL	MSBL	MSP	MSSE
MSUL	-	✗	✔	✔
MSBL	✗	-	✔	✔
MSP	✔	✔	-	✗
MSSE	✔	✔	✗	-

Fe_2O_3	MSUL	MSBL	MSP	MSSE
MSUL	-	✗	✔	✗
MSBL	✗	-	✗	✗
MSP	✔	✗	-	✔
MSSE	✗	✗	✔	-

K_2O	MSUL	MSBL	MSP	MSSE
MSUL	-	✗	✔	✔
MSBL	✗	-	✔	✔
MSP	✔	✔	-	✗
MSSE	✔	✔	✗	-

MgO	MSUL	MSBL	MSP	MSSE
MSUL	-	✗	✔	✔
MSBL	✗	-	✔	✔
MSP	✔	✔	-	✗
MSSE	✔	✔	✗	-

S	MSUL	MSBL	MSP	MSSE
MSUL	-	✗	✗	✗
MSBL	✗	-	✗	✗
MSP	✗	✗	-	✗
MSSE	✗	✗	✗	-

Table 4.D cont. Results of *post-hoc* pair-wise comparisons of seam variance for each physical characteristic (Tukey test). ✗ = Compared seams are not significantly different, ✔ = Compared seams are significantly different for a specified characteristic. Main seam lower (MSBL) and upper leaf (MSUL), parting (MSP) and seat-earth (MSSE).

Chapter 5 Results

Time (mins)	Fe (mgl⁻¹)cleavage perpendicular		Fe (mgl⁻¹)cleavage parallel		blank Fe
	Milli-RO	1% H_2O_2	Milli-RO	1% H_2O_2	
5	0.00	0.00	0.00	0.00	0.00
10	0.00	0.00	0.00	0.00	0.00
20	0.00	0.00	0.00	0.00	0.00
30	0.00	0.00	0.00	0.00	0.00
40	0.00	0.01	0.04	0.00	0.00
50	0.00	0.00	0.00	0.00	0.00
60	0.00	0.00	0.00	0.00	0.00
120	0.00	0.00	0.00	0.00	0.00
240	0.00	0.00	0.00	0.00	0.00
360	0.00	0.00	0.00	0.00	0.00
480	0.00	0.00	0.00	0.00	0.00
960	0.00	0.00	0.00	0.00	0.00
1440	0.00	0.00	0.00	0.00	0.04
2880	0.00	0.02	0.00	0.00	0.00
4320	0.00	0.21	0.00	0.01	0.00
5760	0.00	0.17	0.00	0.02	0.00
10080	0.00	0.69	0.00	0.01	0.00
14400	0.00	0.25	0.00	0.02	0.00
15840	0.00	0.32	0.00	0.07	0.00
17280	0.01	0.47	0.00	0.07	0.00
18720	0.00	0.28	0.00	0.05	0.00
20160	0.00	0.84	0.00	0.06	0.00
21600	0.00	0.45	0.00	0.05	0.00
25900	0.00	0.62	0.00	0.06	0.00

Table 5.A. Fe concentration within coal leachate from samples treated with 1% H_2O_2 and Milli-RO. Samples were orientated with cleavage parallel or perpendicular to the treatment fluid.

Time (mins)	S (mgl^{-1}) cleavage perpendicular		S (mgl^{-1}) cleavage parallel		blank S
	Milli-RO	1% H_2O_2	Milli-RO	1% H_2O_2	
0	0.76	0.86	0.82	0.79	0.76
5	0.80	0.81	0.82	1.00	0.73
10	0.82	0.89	0.75	0.78	0.88
20	0.87	0.79	0.81	0.83	0.83
30	0.89	0.82	0.86	0.83	0.90
40	0.87	0.65	0.80	0.91	0.73
50	0.75	0.92	1.23	0.91	0.85
60	0.85	0.83	0.76	0.71	0.76
120	0.76	0.82	0.85	0.65	0.78
240	1.05	0.98	1.52	0.95	0.91
360	0.93	1.39	0.85	1.03	0.98
480	0.96	1.09	0.97	1.04	0.84
960	0.97	1.19	1.06	1.18	0.83
1440	1.08	1.36	0.98	1.16	1.06
2880	0.86	1.59	0.75	1.22	0.97
4320	0.88	1.84	0.96	1.15	0.88
5760	1.36	2.73	1.17	1.47	1.12
10080	0.59	1.58	0.63	0.97	0.66
14400	0.69	1.96	0.64	1.11	0.75
15840	0.86	2.49	0.89	1.32	0.81
17280	0.33	1.89	0.31	0.69	0.20
18720	0.45	0.98	0.39	0.65	0.14
20160	0.40	1.35	0.34	0.71	0.11
21600	0.30	1.55	0.34	0.77	0.17
25900	0.34	1.81	0.33	0.74	0.23

Table 5.B.   S concentration within coal leachate from samples treated with 1% H_2O_2 and Milli-RO. Samples were orientated with cleavage parallel or perpendicular to the treatment fluid.
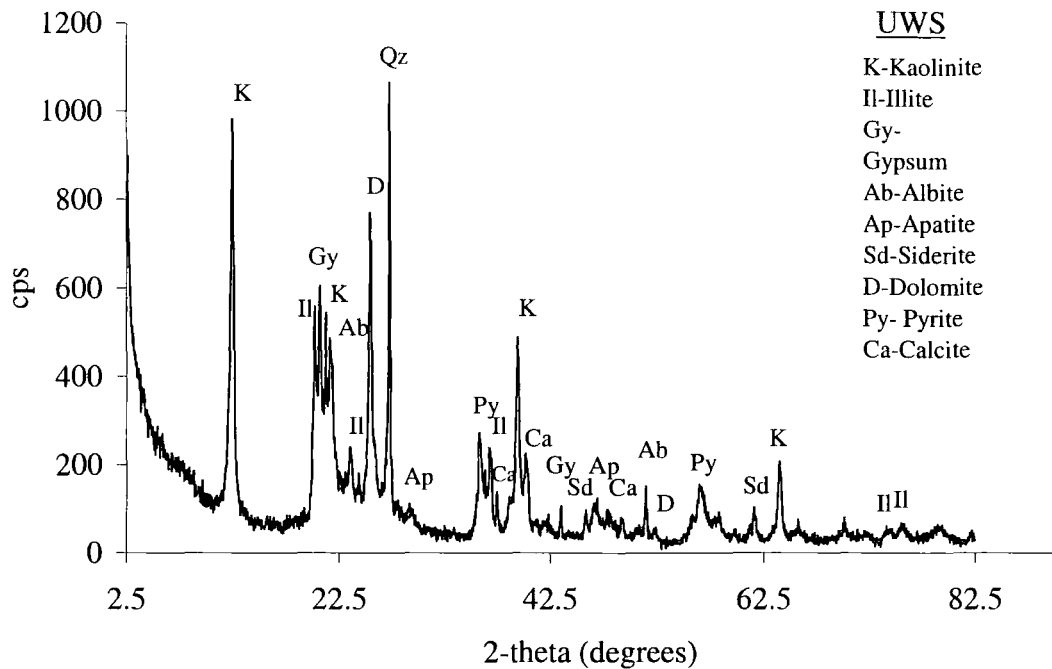
Figure 5.A. XRD analysis of UWS, 2θ (°) plotted against cps for raw powder.
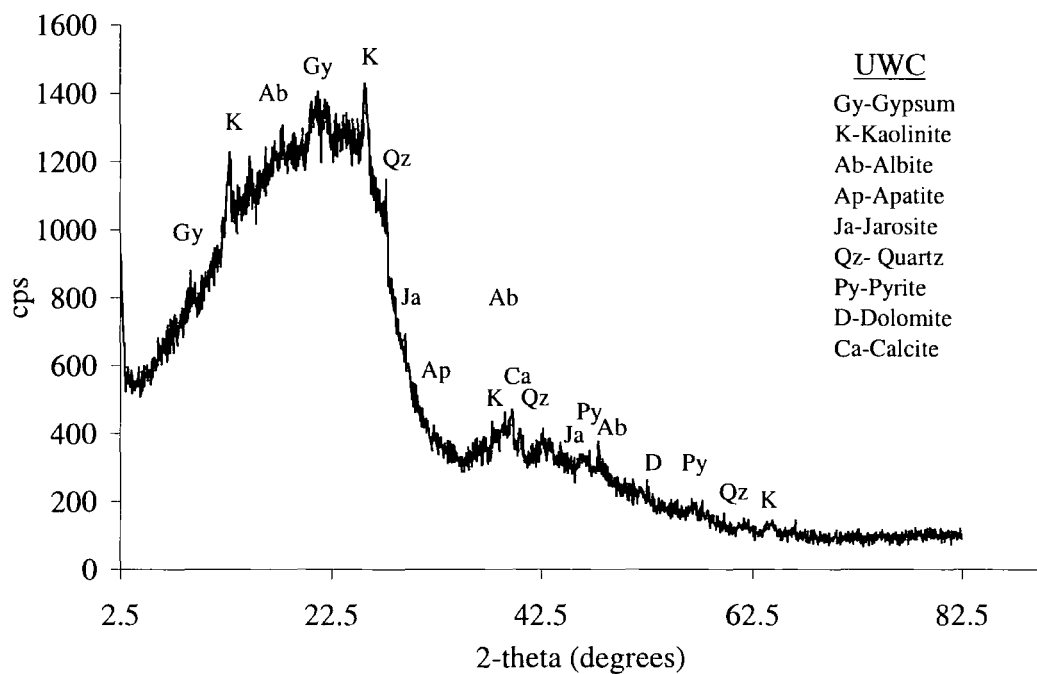
Figure 5.B. XRD analysis of UWC, 2θ (°) plotted against cps for raw powder.
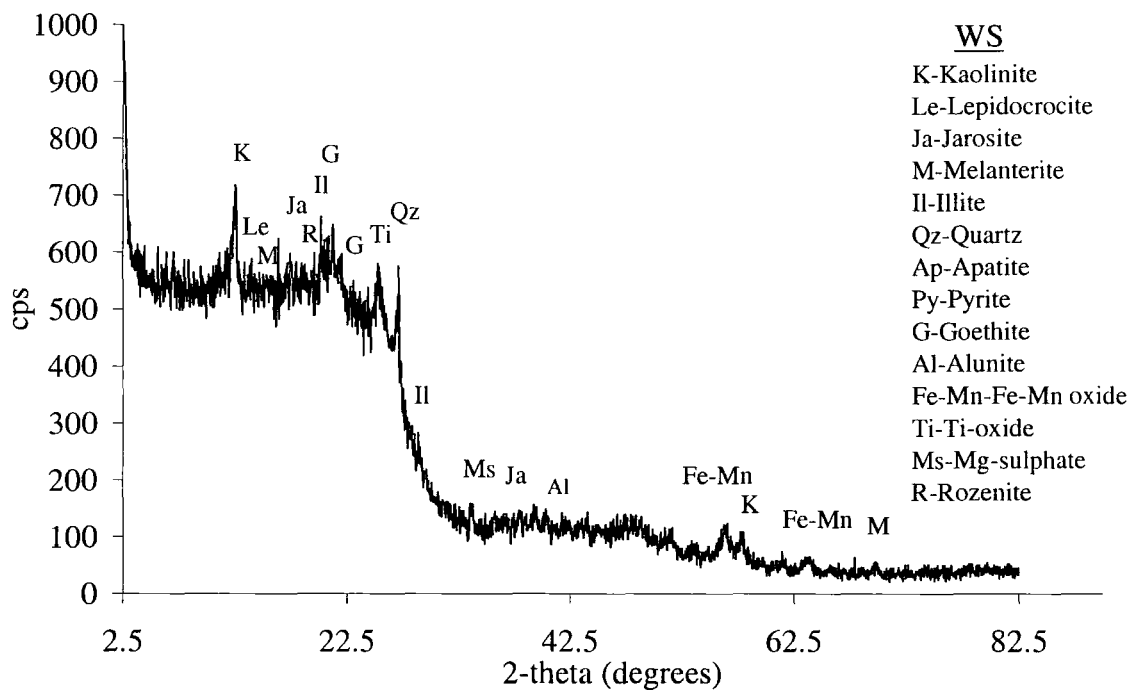
Figure 5.C. XRD analysis of WS, 2θ (°) plotted against cps for raw powder.
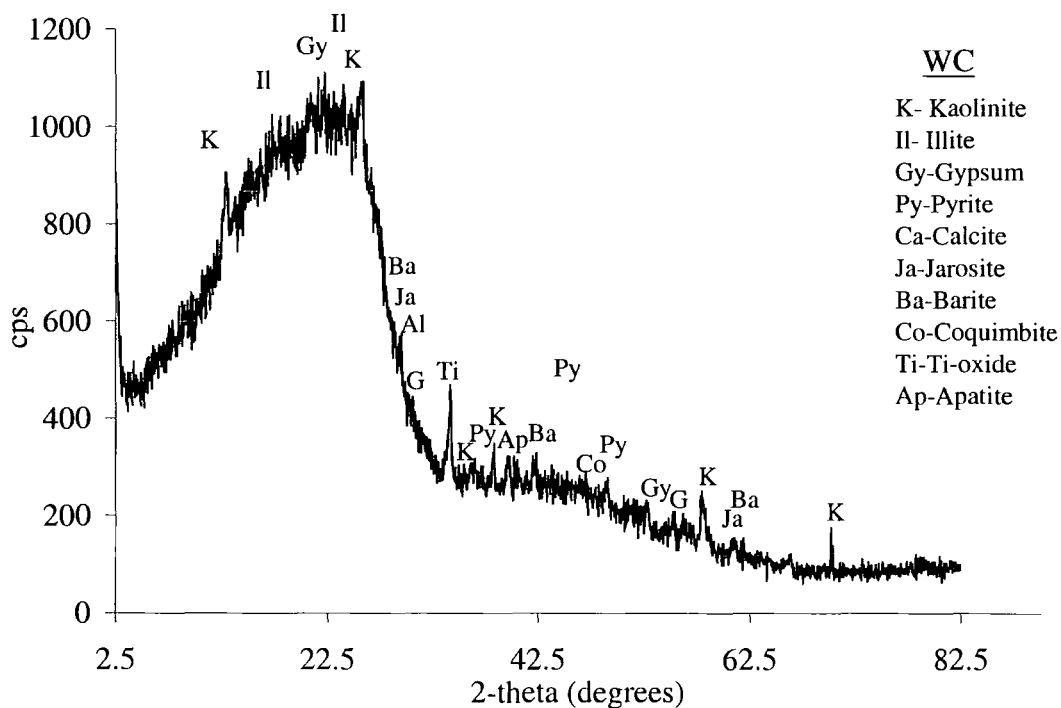
Figure 5.D. XRD analysis of WC, 2θ (°) plotted against cps for raw powder.

	UWC		UWS		WS		WC	
	XRF	**ICP-OES**	**XRF**	**ICP-OES**	**XRF**	**ICP-OES**	**XRF**	**ICP-OES**
Al	7.9 ± 0.2	3 ± 1	0.34 ± 0.02	0.2 ± 0.1	0.35 ± 0.02	0.24 ± 0.06	0.24 ± 0.01	0.4 ± 0.2
Ca	0.18 ± 0.00	1.6 ± 0.1	0.07 ± 0.00	0.6 ± 0.2	0.04 ± 0.00	0.42 ± 0.1	0.12 ± 0.01	0.6 ± 0.2
Fe (II)	2.10 ± 0.06	1.8 ± 0.3	0.18 ± 0.02	0.19 ± 0.08	1.0 ± 0.1	6 ± 4	1.9 ± 0.6	5 ± 7
K	0.57 ± 0.01	0.2 ± 0.1	0.01 ± 0.00	0.11 ± 0.05	0.02 ± 0.00	0.12 ± 0.07	0.01 ± 0.00	0.12 ± 0.06
Mg	0.11 ± 0.01	0.53 ± 0.06	0.01 ± 0.00	0.07 ± 0.02	0.01 ± 0.00	0.06 ± 0.02	0.03 ± 0.00	0.11 ± 0.05
Mn	0.00 ± 0.00	0.27 ± 0.00	0.00 ± 0.00	0.04 ± 0.06	0.00 ± 0.00	0.03 ± 0.07	0.00 ± 0.00	0.02 ± 0.06
Na	0.01 ± 0.00	0	0.00 ± 0.00	0.02 ± 0.4	0.00 ± 0.00	0	0.00 ± 0.00	0.6 ± 0.6
P	0.09 ± 0.00	0.17 ± 0.03	0.01 ± 0.00	1.2 ± 0.6	0.00 ± 0.00	0.9 ± 0.2	0.00 ± 0.00	1.4 ± 0.8
Si	20.7 ± 0.4	2 ± 1	0.83 ± 0.07	0.05 ± 0.03	1.23 ± 0.03	0.17 ± 0.07	0.54 ± 0.03	0.4 ± 0.3
Ti	0.68 ± 0.01	–	0.02 ± 0.00	–	0.05 ± 0.00	–	0.02 ± 0.00	–

Table 5.C. Calculated wt % of major elements after XRF analysis for major oxide content of un-weathered coal, (UWC) un-weathered shale (UWS), weathered coal (WC) and weathered shale (WS).

	UWS - HCl	UWS - H₂O₂	UWC – HCl	UWC - H₂O₂
Al	1.4 ± 0.2	1.5 ± 0.1	0.10 ± 0.08	0.10 ± 0.03
Ca	1.4 ± 0.1	0.15 ± 0.00	0.2 ± 0.1	0.41 ± 0.08
Cu	0	0	0	0
Fe	1.5 ± 0.1	0.4 ± 0.1	0.09 ± 0.04	0.11 ± 0.03
K	0.20 ± 0.08	0.02 ± 0.04	0.04 ± 0.03	0.07 ± 0.02
Mg	0.44 ± 0.04	0.10 ± 0.02	0.01 ± 0.03	0.04 ± 0.01
Mn	0.14 ± 0.00	0.13 ± 0.00	0.04± 0.06	0
Na	0	0	0.00 ± 0.00	0.014 ± 0.03
P	0.13 ± 0.01	0.04 ± 0.02	0.34 ± 0.02	1.0 ± 0.3
S	0.18 ± 0.02	0.4 ± 0.01	0.4 ± 0.2	0.9 ± 0.3
Zn	0	0.12 ± 0.02	0.02 ± 0.04	0.002 ± 0.003
Si	0.94 ± 0.09	1.5 ± 1.1	0.02 ± 0.01	0.03 ± 0.01

	WS – HCl	WS - H₂O₂	WC – HCl	WC - H₂O₂
Al	0.14 ± 0.04	0.10±0.02	0.18 ± 0.08	0.2 ± 0.1
Ca	0.17 ± 0.02	0.25 ± 0.07	0.27 ± 0.08	0.3 ± 0.2
Cu	0	0.00 ± 0.00	0.00 ± 0.00	0.01 ± 0.01
Fe	1.61 ± 0.8	4.5 ± 3.4	0.24 ± 0.08	5.1 ± 6.4
K	0.05 ± 0.03	0.07 ± 0.04	0.09 ± 0.02	0.03 ± 0.03
Mg	0.03 ± 0.01	0.03 ± 0.01	0.07 ± 0.03	0.04 ± 0.02
Mn	0.03 ± 0.07	0	0.002 ± 0.003	0.02 ± 0.05
Na	0	0	0.05 ± 0.06	0.5 ± 0.5
P	0.02 ± 0.00	0.8 ± 0.2	0.03 ± 0.005	1.4 ± 0.8
S	1.3 ± 0.6	4.7 ± 2.6	0.2 ± 0.1	5.9 ± 5.5
Zn	0.05 ± 0.04	0.00 ± 0.00	0.02 ± 0.03	0.1 ± 0.3
Si	0.07 ± 0.04	0.11 ± 0.03	0.15 ± 0.07	0.2 ± 0.2

Table 5.D. Major element wt % of acid leachable (HCl) and oxidizable (H₂O₂) extracts for un-weathered coal (UWC), un-weathered shale (UWS), weathered shale (WS) and weathered coal (WC).

Chapter 5 Leachate chemistry detailed descriptions and figures

Leachate chemical evolution for all lithologies under cyclic and stagnant conditions is described in the following sections. For cyclic and stagnant leaching, treatment of whole and cleavage edge samples is followed by a comparison of leachate evolution and total flux from each rock type. Where the dissolved concentration of an element fell below or close to detection after mass correction i.e. <0.01 $mgL^{-1}g^{-1}$ it is not discussed.

Cyclic leaching of UWS

Whole samples

Within the initial 58 days of UWS cyclical leaching Ca release to solution rose to a maximum of 13 ± 2 mg L^{-1} g^{-1} at 58 day (Table 5G). Subsequently Ca concentration fell to between 0.06 ± 0.01 mg L^{-1} g^{-1} and 0.09 ± 0.01 mg L^{-1} g^{-1} until day 200, then varied between 0.04 ± 0.01 and 0.01 ± 0.00 mg L^{-1} g^{-1} for the remainder of the experiment. The behaviour of K, Mg, Na, S and Si was similar with maximum

concentrations at 58 days, followed by a drop to pseudo steady-state dissolution with time. Solution pH throughout the experiment remains between 7.5 and 6.5, decreasing within the final 67 days of leaching to 6.3.

Leaching of these elements to solution suggests that dissolution of gypsum and dolomite produced S, Ca and Mg. Ion exchange may have removed K and Na from the clay phase of the UWS. Influx of dilute Milli-RO water at the start of each cycle would have encouraged the removal of mono-valent cations (Stumm and Morgan, 1990).Falling pH towards the end of cyclic leaching suggests that pyrite oxidation may have occurred (Table 5G). However, leachate pH > 5 suggests that any Fe produced during the oxidation of pyrite would have precipitated.

Cleavage edge samples

Cyclic leaching of the cleavage edge of UWS released maximum dissolved concentrations of Al, Fe, Mg, Mn, S and Si in the day 29 leachate. Maximum concentrations of Ca, K and Na were released in the day 58 (Table 5H). After this peak output dissolved concentrations decreased to below 0.2 $mgL^{-1}g^{-1}$. Both Ca and S were released throughout the leaching experiment, with maximum concentrations of 17 ± 8 $mgL^{-1}g^{-1}$ of Ca and 7 ± 6 $mgL^{-1}g^{-1}$ of S. Similarly K, Mg, Na and Si are released at relatively constant concentrations in cyclic leachate for the remainder of leaching.

Leachate pH from the cleavage edge of the UWS remained between 5.2 ± 0.7 on day 150 and 7.0 ± 0.2 on day 268 (Table 5H). Minimum pH occurs prior to a small peak in S concentration at day 170 and maximum pH at day 268. Following the maximum, leachate pH falls until the end of the experiment. Generally, decreases in pH occur prior to a rise in dissolved S, suggesting acidity was produced by pyrite oxidation. Concurrent increase in Ca and pH indicates that neutralisation by carbonate phase minerals also occurred.

Dissolved concentrations released from the cleavage edge and whole samples of UWS during cyclic leaching were within the same range (Table 5E). However the rate of removal of material from the cleavage edge samples was initially higher than from the whole samples. Within cleavage edge samples fluid circulation is restricted, and perhaps even channelled in one direction. The lack of circulation and concentration of fluid diffusion in the higher porosity of the cleavage plane led to increased dissolution of material, especially S, Mg and Ca. Leachate pH of the cleavage edge sample was also slightly lower than the whole sample leachate. In conjunction with the higher dissolved S output, lower pH suggests that greater removal of pyrite oxidation products occurred along cleavage. Given the association of pyrite with organic material along cleavage planes, the faster oxidation along this plane is expected.

Cyclic leaching of UWC

Whole samples

Cyclic leachate from the UWC produced maximum dissolved Ca of 3.2 ± 0.4 mg L^{-1} g^{-1} at 58 days (Table 5I). Subsequently, dissolved Ca decreased to vary from 0.04 to 0.01, then fell to below detection at day 287. Other dissolved elements included K, Mg, Na, Si and S which all had peak concentrations of less than 1 mg L^{-1} g^{-1} at 58 days of cyclic leaching. Concentration of K, Mg and Si fell below detection by 225 days. After 225 days low concentrations (< 0.1 $mgL^{-1}g^{-1}$) of Na and S were still being dissolved. During the wetting and drying cycles of the UWC the pH in the leachate falls from 7.2 to around 5.3 (± 1.13).

Leachate content during cyclic leaching of the UWC suggests that weathering of gypsum, dolomite, calcite and pyrite took place. Lowering in leachate pH towards the end of the experiment also suggests the occurrence of pyrite oxidation. Again at the

range of solution pH measured any Fe^{3+} produced would precipitate as Fe hydroxides or sulphates. Cation exchange would also explain the presence of Na and K in solution. However, the presence of jarosite, as identified in the UWC by XRD, would also provide a soluble source of Fe^{3+}, K^+ and metal acidity (Bigham et al., 1996). As dissolution of K fell below detection after 225 days, it is probable that a limited jarosite source supplied this element rather than cation exchange. Most Si dissolution occurred within the initial period of wash-out from the UWC suggesting that prior oxidation or processing provided most of this phase. Organic acids may weather silicate minerals, although Al is usually the primary product of this reaction (Drever, 1997).

Cleavage edge samples

As for leaching of whole UWC samples, concentrations released from the UWC cleavage edge samples during cyclic leaching were relatively low (Table 5J). Maximum Ca and S occurred over days 29 and 58 of leaching at 2 ± 1 mgL^{-1}g^{-1} of Ca and 0.2 ± 0.2 and 0.10 ± 0.04 mgL^{-1}g^{-1} of S. Subsequently, low S concentrations of less than 0.02 mgL^{-1}g^{-1} were released to solution for the remainder of leaching. A small peak of 0.06 ± 0.01 mgL^{-1}g^{-1} of S at day 205 of leaching was the only change from the low S output after day 58. All other major elements detected in solution i.e. Mg, Na and Si peaked at below 0.2 mgL^{-1}g^{-1} during the 29 to 58 day leaching apart from K. A small peak in K release of up to 0.04 mgL^{-1}g^{-1} over days 133 to 205 followed the maximum concentration of 0.35 ± 0.00 mgL^{-1}g^{-1} of K on day 58.

Leachate pH from the cleavage edge of the UWC remained between 4.7 ± 0.2 at day 382 and 6.59 ± 0.09 at day 268 (Table 5J). The association of low leachate pH either prior to or concurrent with increased S and K concentrations suggests that dissolution of the jarosite as identified by XRD occurred. Carbonate phase neutralisation of produced acidity would have lead to the precipitation of phases such as gypsum, explaining the lack of Ca dissolution during the main part of leaching. At the leachate pH range experienced in this experiment most dissolved products such as ferrous and ferric Fe and SO_4^{2-} would tend to precipitate.

Overall the total flux of material from the cleavage edge and whole samples was within the same range (Table 5E). However Mg and S from the cleavage edge samples were both released at two times the concentration from whole samples. Increased pyrite oxidation along the greater porosity of the cleavage plane coupled with dolomite dissolution can account for the increase in Mg and S.

Cyclic leaching of the WS

Whole samples

High concentrations of Fe, S and Ca were present in the WS leachate during the initial 58 days of cyclic leaching (Table 5K). After peaking at 12 ± 6 mg L^{-1} g^{-1} dissolved S fluctuated between 0.7 and 0.45 mgL^{-1}g^{-1} until the end of the experiment. Similarly maximum Fe concentration of 7 ± 4 mgL^{-1}g^{-1} occurred at 58 days, and then varied between 0.5 and 0.02 mg L^{-1} g^{-1}. Maximum Al, Ca, Mg and Zn concentrations also occurred at day 58, subsequently falling below detection by 120 days of cyclic leaching. Concentrations of dissolved K, Na and Si were either below detection or at 0.1 mg L^{-1} g^{-1} after an initial peak at 58 days.

Leachate pH was initially low at 2.8, but rose to a maximum of 5.8 at day 133. Subsequently leachate pH varied between 3.3 and 3.7, with one drop to 0.95 at 225 days. The release of Al, Ca and Mg can be attributed to the dissolution of alunite, gypsum and Mg-sulphate formed during prior pyrite oxidation. Dissolution of Fe, S and Zn during the initial 100 days of cyclic leaching was mainly due to prior weathering

of pyrite and possibly sphalerite. Subsequent low concentrations of dissolved Fe and S in the final 282 days of leaching are derived from active pyrite oxidation.

Cation exchange, jarosite and acidic clay weathering may have lead to the continued presence of Na, K and Si respectively. Dissolved K decreased to below detection with time suggesting that jarosite precipitation, with concurrent H^+ release, was the most likely sink process. Cation exchange would explain the continued release of Na but not Si. As the dissolution of Na and Si tended to follow the same trend it is probable that they were derived from the same source. Connate pore waters may contain high Na due to the presence of brines (Spears, 1980). Similarly pore water will also be associated with dissolved organic acids that may have weathered the silicate phase (Drever, 1997). However, the presence of very low pH pore water due to inorganic acidity (e.g. H_2SO_4) is the most likely cause of continued Na and Si release from clay weathering.

Cleavage edge samples

During the cyclic leaching of the WS cleavage edge the release of most detected dissolved major elements reached a maximum at day 58 (Table 5L). Both Ca and S had relatively high maximum concentrations at 13 ± 6 mgL^{-1}g^{-1} of Ca and 6 ± 4 mgL^{-1}g^{-1} of S. Subsequently the dissolved leachate concentration of Ca fell to below 0.1 mgL^{-1}g^{-1} whilst both dissolved Fe and S were removed at over 0.1 mgL^{-1}g^{-1}. Concentration of K, Na, Mg, Al, Mn, Zn and Si all remained below 0.6 mgL^{-1}g^{-1} for the duration of leaching.

Leachate pH ranged between 4 ± 3 and 5.9 ± 0.5 during cyclic leaching of the WS cleavage edge. Low values in leachate pH tended to follow or be associated with peaks in Fe, S, K, Na, Ca, Zn and Si dissolved concentration at days 205, 268 and 339. Pyrite oxidation and subsequent buffering of acidity by clay minerals and remnants of carbonate minerals would produce such peaks. The presence of Zn suggests that sphalerite or pyrite with Zn impurities was also oxidised. The cyclical nature of the peaks in leachate concentration suggests that initiated pyrite oxidation is alternately accelerated then decelerated. A possible mechanism for such a cycle would be the alternate increase in pore water neutralisation by clay weathering and subsequent acidification of pore water by pyrite oxidation. Dissolution of Fe^{3+} from jarosite at pore water pH < 3.5 would increase rates of oxidation. However, increased clay buffering of acidic pore water would increase pH, precipitating Fe^{3+} decreasing oxidation rates. If jarosite was the main precipitant on drying, its dissolution after wetting will increase pore water Fe^{3+}, increasing pyrite oxidation rates again. However, the slow rate of dissolution of this mineral will limit the rate of Fe^{3+} release (Bigham et al., 1996)

In comparison with whole leached samples the total flux from the cleavage edge samples contained twice the amount of Ca and Mg (Table 5E). Concentrations of K, Fe, S and Zn were all reduced by up to 6 times in the total flux from the cleavage edge of the WS. Leachate pH from the cleavage edge samples was also around 4 whereas leachate pH of whole samples was closer to 3. Higher pH and leachate Ca and Mg suggests a greater weathering of the dolomite phase in the cleavage edge samples leading to greatly reduced release of dissolved Fe. Restricted movement of pore water along the cleavage plane, with oxidant introduced from one face only may have also reduced oxidation in these WS samples. Pulses in pyrite oxidation were also identified from the dissolved content of the whole WS samples, yet these were not as strongly defined. Here the effect of restricting fluid influx to one cleavage edge of WS samples has led to greater reaction between pore water and the carbonate phase of the rock.

Cyclic leaching of WC

Whole samples

Similar to the previously described WS leaching, Fe, S and Ca concentrations were highest during cyclic leaching of the WC, reaching maximum values within the initial 58 days (Table 5M). After peaking at 17 ± 8 mgL^{-1}g^{-1} the S concentration fell to vary between 0.2 ± 0.2 and 0.6 ± 0.2 mgL^{-1}g^{-1} for the remainder of the experiment. Maximum Fe concentration of 10 ± 6 mgL^{-1}g^{-1} coincided with that of S at 58 days. Subsequently dissolved Fe dropped to 0.07 ± 0.06 mgL^{-1}g^{-1}. The maximum leachate concentration of 5.7 ± 0.7 mg L^{-1} g^{-1} of Ca also occurred at day 58. Following this peak dissolved Ca rapidly dropped to below detection by 100 days, with rare occurrences in solution at 133 and 188 days. Other elements present in solution were Zn, Na, Al, Mg and K. Concentrations of Zn and Na reached a maximum of close to 2 mg L^{-1} g^{-1} within 58 days. Remaining dissolved elements Al, Mg and K, stayed below 1

mg L^{-1} g^{-1} during the initial 58 days then typically fall below detection by day 150.

Leachate pH for the cyclically leached WC usually remained between 3.5 and 4.3. However, there was a trough in pH of 1.91 and below measurement at 183 and 205 days respectively, followed by a rise to 4.2 at 225 days.

After the initial period of high concentrations of elements leached to solution from the WC, continued removal of Fe and S was derived from active pyrite oxidation. Again the dissolution of K, Na and Si may have been caused by either of jarosite dissolution, pore water interaction or ion exchange. Given the late stage peaks in Na, K and Si dissolution concurrent with peaks in Fe and S output at days 268 and 339 it is possible that natro-jarosite formation occurred during dry periods. The coincident dissolution of Si was due to clay weathering by the very low pH pore water suggested from leachate solution pH.

Cleavage samples

Again Ca, S and Fe had the highest maximum dissolved concentrations, at 1.6 ± 0.1 mgL^{-1}g^{-1} of Ca, 1.1 ± 0.8 mgL^{-1}g^{-1} of S and 0.8 ± 0.7 mgL^{-1}g^{-1} of Fe on day 29 of leaching (Table 5N). Other detected major element concentration including Al, Mg, Na, Zn and Si also reached a maximum at day 29, apart from K and P which peaked at day 133. Concentrations in solution remained below 0.5 mgL^{-1}g^{-1} after day 85 of cyclic leaching.

Peaks in dissolved output of Al, Ca, Fe, Mg, Na, S, Zn and Si occurred within leachate between 133 and 382 days of leaching. Such fluctuations suggest that oxidation of pyrite associated with Zn lead to clay and dolomite weathering.

Leachate pH range of 2 to 4 indicates silicate buffering of acidity produced by pyrite oxidation. Low leachate pH tended to coincide with peaks in leachate content. However leachate with the lowest pH of 2 has a relatively low total dissolved content. If jarosite precipitation was occurring within this sample, the consequent release of H$^+$ may account for the large drop in measured pH.

Total flux of dissolved material leached from the WC cleavage edge was lower for all analytes compared to the whole sample leaching (Table 5E). Only P dissolution was greater from the cleavage edge sample, suggesting the acid dissolution of apatite. Both dissolved Fe and S were up to ten times lower from the cleavage edge samples. As both WS and WC samples contain similar amounts of carbonate the slower release of dissolved material from the coal can be attributed to the different pore size distributions of these rock-types. Higher proportion of macro and meso-porosity within the shale allowed the rapid diffusion of dissolved Ca and Mg from the rock. However the coal

has a greater proportion of micro-porosity, limiting even cleavage interaction with the leaching fluid.

UWS	Al	Ca	Fe	K	Mg	Na	S	Zn	Si
Whole	0.01 ± 0.00	20 ± 2	0.00 ± 0.00	1.5 ± 0.2	0.65 ± 0.06	0.29 ± 0.02	3.1 ± 0.3	0.04 ± 0.02	0.82 ± 0.08
Cleavage edge	0.5 ± 0.5	26 ± 14	0.9 ± 0.8	1.8 ± 0.4	2 ± 1	0.4 ± 0.1	11 ± 6	0.1 ± 0.03	0.8 ± 0.2

UWC	Al	Ca	Fe	K	Mg	Na	S	Zn	Si
Whole	0.01 ± 0.00	4.90 ± 0.06	0.01 ± 0.00	0.34 ± 0.00	0.15 ± 0.00	0.38 ± 0.00	0.22 ± 0.00	0.01 ± 0.00	0.18 ± 0.00
Cleavage	0.01 ± 0.01	5 ± 2	0.01 ± 0.01	0.6 ± 0.1	0.11 ± 0.03	0.22 ± 0.07	0.6 ± 0.2	0.00 ± 0.02	0.13 ± 0.03

WS	Al	Ca	Fe	K	Mg	Na	S	Zn	Si
whole	0.3 ± 0.1	7 ± 2	16 ± 5	0.9 ± 0.4	0.25 ± 0.08	0.8 ± 0.2	28 ± 7	0.9 ± 0.3	0.35 ± 0.09
Cleavage	0.08 ± 0.03	15 ± 6	1.8 ± 0.8	0.33 ± 0.18	0.7 ± 0.3	0.7 ± 0.2	11 ± 4	0.4 ± 0.3	0.39 ± 0.05

WC	Al	Ca	Fe	K	Mg	Na	S	Zn	Si
Whole	0.9 ± 0.3	9 ± 1	21 ± 9	0.6 ± 0.3	0.6 ± 0.2	4 ± 3	36 ± 11	6 ± 5	0.64 ± 0.09
Cleavage	0.16 ± 0.08	2.0 ± 0.2	1.3 ± 0.7	0.6 ± 0.6	0.17 ± 0.02	0.5 ± 0.3	4 ± 1	0.6 ± 0.4	0.18 ± 0.07

Table 5.E. Whole and cleavage edge total dissolved element flux during cyclic leaching. Values given in $mgL^{-1}g^{-1}$, errors shown are random and propagated from 1σ of each summed term (n=4).

Stagnant Leaching

Three samples from the group eighteen samples of each rock type leached continuously over the period of a year, (316 to 380 days), were sacrificially removed from solution every 2 months. Resultant leachate was analysed for major element chemistry and the concentration corrected for the mass of the sample giving a value in $mg\ L^{-1}\ g^{-1}$. After removal of samples from stagnant leaching at 205 days and 316 days, remaining samples had lost a substantial volume of solution by evaporation. To counteract drying 60 mL of fresh Milli-RO water was added to all remaining stagnant samples at 205 days and 316 days. The effect of the addition of Milli-RO water is interpreted in the following descriptions of leachate chemistry.

Compared to the cyclic leaching, stagnant leaching is a closed system where the only loses from solution are due to precipitation or dilution. The described values represent the cumulative dissolution of the leached sample.

Stagnant leaching of UWS

Whole samples

Dissolved S content in the UWS leachate increased to a peak of 3.3 ± 0.9 mg L^{-1} g^{-1} at 268. At 316 and 382 days dissolved S dropped to 1.6 ± 0.6 mg L^{-1} g^{-1} then increased 3 ± 2 mg L^{-1} g^{-1} respectively (Table 5O). Only Ca had comparative concentrations to S (>2 mg L^{-1} g^{-1}) with Si, Na, Mg concentrations remaining below 0.1 mg L^{-1} g^{-1}. Dissolved Ca, Si, Na and Mg concentrations increased within 150 days of stagnant leaching only to decrease towards the end of the experiment.

Leachate pH derived from stagnant leaching of the UWS decreased with time from 6.5 ± 0.3 to 4.0 ± 0.6 at day 268, then rose to 5 ± 1 by the end of leaching.

Dissolution of Ca, S and Mg from the UWS indicates the weathering of gypsum and perhaps dolomite. The pyrite content of this rock type is relatively low at 0.7 ± 0.2 wt %. However the decrease in pH to <5 suggests that pyrite oxidation did occur. The drop in concentration within 316 days follows an increase in Ca and S concentration, caused by the addition of Milli-RO water to all samples at 205 days. Lowered pH at day 268 suggests that pyrite oxidation was also encouraged by the addition of dissolved O_2 in the Milli-RO water. Dissolution of carbonate phases between the 268 and 316 day samples and dilution during the latter sampling led to increased pH and precipitation from solution. Continued pyrite oxidation between days 316 and 382 led to lower pH and greater dissolved content.

Cleavage edge samples

Release of dissolved major elements from stagnant leaching of the UWS cleavage edge followed the same pattern as that of whole samples (Table 5P). Both dissolved Ca and S concentrations were highest in solution with maximum values of 2 ± 2 $mgL^{-1}g^{-1}$ of Ca and S at day 382. Leachate concentrations of Mg, Na, and Si remained below 0.3 $mgL^{-1}g^{-1}$ for the duration of the experiment. Initially leachate content increased to a peak in the 268 day sample. Subsequently dissolved content decreased then increased at 382 days. Leachate pH remained between 7.4 ± 0.7 and 8.0 ± 0.6, with a decrease in pH at 316 days associated with low dissolved leachate content. A similar dip in dissolved content with pH in the whole sample leachates was explained by increased pyrite oxidation leading to precipitation of Ca and S in oxidation products such as gypsum. In the cleavage sample's case dilution with Milli-RO water at days 205 and 316 led to dips in the leachate content.

Comparison of cleavage edge and whole sample UWS peak flux shows the lower release of dissolved matter from the cleavage edge due to lower exposed surface area (Table 5F).

Stagnant leaching of UWC

Whole samples

Dissolved concentrations of Ca, S and Mg within the UWC leachate were relatively high (>0.1 mg L^{-1} g^{-1}) and K, Mn, Si are relatively low (< 0.1 mg L^{-1} g^{-1}) (Table 5Q). The Ca content increased throughout the initial 205 days of leaching, reaching a plateau at around 1.1 mg L^{-1} g^{-1}, then falling to 0.2 ± 0.2 mg L^{-1} g^{-1} in the 316 day leachate. Most other detectable elements reached maximum concentration at 205 days except S which decreased at this point then rose to 0.6 ± 6 mg L^{-1} g^{-1} at 268 days. At 316 days all dissolved element concentrations had significantly decreased. Stagnant leachate pH in the UWC samples remained between 7.5 and 6.8 throughout the experiment.

Relatively high Ca, S and Mg leachate content for the UWC suggests that pyrite oxidation, acidic dissolution of calcite and the dissolution of gypsum were key processes. Dilution with Milli-RO water at day 205 only leads to a slight fall in leachate pH for day 268. Again the influx of Milli-RO water containing dissolved oxygen increases pyrite oxidation. The large drop in element concentration in the final leachate of day 316 corresponds to a drop in the UWS leachate. Lowered dissolved content can be attributed to increased pH. Carbonate mineral dissolution in response to pyrite oxidation between days 268 and 316 led to the increased pH.

Cleavage edge samples

Leaching of the cleavage edge of UWC samples produced peak concentrations for most analytes at the end of the experimental period (Table 5R). However instead of a general increase from the start to the end of stagnant leaching, leachate concentration dropped at day 205 due to dilution of the sample with Milli-RO water.

Overall dissolved concentrations of Ca, Mg, K, Si and S were greatest with a maximum of 0.4 ± 0.1 mgL^{-1}g^{-1} Ca at 316 days. Initial release of S was very low, yet reached a maximum value at 316 days of 0.19 ± 0.04 mgL^{-1}g^{-1}.

Leachate pH remained between 6.68 and 7.80, with a rise in pH at 205 days due to dilution by Milli-RO water, added to increase the volume of evaporated solution to at least 10 mL. Compared to whole UWC sample leachate, the total flux from stagnant leaching of the cleavage edge released a lower total flux of all analyses (Table 5F). Again the difference in surface area is probably the main cause of this difference. Compared with the UWS cleavage edge leaching of the UWC released lower total flux, due to differences in matrix and soluble mineral content.

Stagnant leaching of WS

Whole samples

Constant leaching of the WS provided high dissolved S and Fe concentrations (Table 5S). Both Fe and S behaved similarly throughout stagnant leaching with maximum values of 13 ± 4 mg L^{-1} g^{-1} and 9 ± 7 mg L^{-1} g^{-1} respectively, on day 150. Peak concentrations were followed by decrease to 4 ± 1 mg L^{-1} g^{-1} of S and 2 ± 2 mg L^{-1} g^{-1} of Fe at day 316. In the final leachate at day 382, S and Fe concentrations rose to almost twice the previous values. The Ca concentration behaved in a similar manner to Fe and S, peaking at 150 days at 1.3 ± 0.9 mgL^{-1}g^{-1}. Leachate concentrations of Al, Mg, Na, Zn and Si all had maximum values of < 1 mgL^{-1}g^{-1} at day 150, then decreased towards the final sampling at day 382.

WS leachate pH remained between 2.7 to 2.2, being punctuated by two consecutive below measurement values, at days 205 and 268. The very low leachate pH followed maximum leachate element concentrations. Evaporation of the WS leachate required the addition of 10 mL of Milli-RO water to make an analysable water sample. Dilution of the sample led to the lowered concentrations of S and Fe. After evaporation in the WS caused precipitation at day 205, addition of Milli-RO water to all remaining samples did not seem to increase pyrite oxidation. Instead lower dissolved Fe and S concentrations were present at days 268 to 382. However the very low pH was indicative of the complete lack of carbonate phase in the WS. Increased dissolved Na, Si, Mg and Ca suggested buffering of pH towards the end of the experiment by alumino-silicate mineral weathering.

Cleavage edge samples

Leachate concentrations during stagnant leaching of the WS generally increased throughout the period of experiment, decreasing in the final sample at 316 days (Table

5T). Dissolved S content reached the greatest magnitude at 3.3 ± 0.4 mgL^{-1}g^{-1} on day 205 of leaching. Similarly Fe, Al and Mg reached peak concentrations of below 1.3 mgL^{-1}g^{-1} in the 205 day leachate. Maximum concentrations of Ca, Na, Zn and Si of up to 2 ± 3 mgL^{-1}g^{-1} (of Zn) all occurred at day 268 of leaching. Stagnant leaching of the WS cleavage edge released a leachate between values below detection and 4.43.

The increase in leachate concentration between 85 and 205 days can be attributed to sample dissolution and leachate evaporation. Addition of fresh Milli-RO water on day 205 led to slight dilution of the day 268 leachate and very low pH. Low pH in the day 268 leachate was probably caused by increased pyrite oxidation by Fe^{3+}. The final rise in pH was probably due to buffering of previous acidity by clay weathering accompanied by precipitation of dissolved salts.

In comparison with whole stagnantly leached WS samples edge leaching released similar concentrations of most elements except for Fe and S (Table 5F). The peak flux of Fe and S was several times lower from cleavage edge leaching. Obviously restriction of dissolved O_2 transport into the WS matrix decreased the rate of pyrite oxidation. Dissolution and removal of soluble material during leaching of cleavage edge and whole samples was not affected by the restriction of fluid circulation. The total flux of Al and Si was also up to four times lower from leaching WS cleavage edge. The reduction in pyrite oxidation, and therefore pore water acidity lead to a decrease in clay weathering and a decrease in dissolved Al and Si.

Stagnant leaching of WC

Whole samples

Relatively high (> 2 mg L^{-1} g^{-1}) concentrations of S and Fe varied concurrently in the stagnant leachate of the WC (Table 5U). Initial S concentration of 9.3 ± 0.3 mg L^{-1} g^{-1}, fell to 3.3 ± 0.9 mg L^{-1} g^{-1} before rising to a peak of 16 ± 3 mg L^{-1} g^{-1} at 205 days. After this point the concentration decreased again to 7 ± 6 mg L^{-1} g^{-1} for the final sampling at day 316. The dissolved Fe content was usually about 2 mg L^{-1} g^{-1} lower than S over the period of stagnant leaching. Dissolved Ca, Al, Mg, Na, Zn and Si followed the same pattern at concentrations below 1 mg L^{-1} g^{-1}.

Stagnantly leached WC produced solution pH between 3.15 and 2.5, with a drop to below measurement range on sampling day 205. The very low pH coincided with the maximum dissolved leachate concentration for all analytes.

High concentrations of Fe and S in solution throughout the period of stagnant WC leaching are derived from the prior and initiated weathering of pyrite. Low concentrations of Ca, Al, Mg, Na and Si suggest that alunite, gypsum, and perhaps natro-jarosite were slowly being dissolved. The decrease in leachate content towards the end of the experiment and the step increase in pH at 268 days were due to the addition of Milli-RO water at day 205. Dilution of pore water with fresh Milli-RO water seemed to halt rather than increase oxidation. Within the pH range of the stagant WC leachate, Fe^{3+} would be the dominant oxidant. At the pH range of Milli-RO water, Fe^{3+} would precipitate as Fe-hydroxide. Although leachate pH did not rise out of the range pyrite oxidation buffering, pyrite oxidation rate is suppressed enough that precipitation of dissolved material is still observed as decreasing leachate concentration.

Cleavage edge samples

The release of S from leaching of the WC cleavage edge was consistently above 1 mgL^{-1}g^{-1} (Table 5V). All other dissolved analytes remained below 1 mgL^{-1}g^{-1} except for Na and Zn. Concentrations of S reached a maximum at days 205 and 150 of 6 mgL^{-1}g^{-1}, falling to 3 then finally 2 mgL^{-1}g^{-1} in the 316 day leachate. Other analytes including Fe,

Ca, Al, Mg, K, Na, Zn, and Si increased to a peak in either the 205 or 268 day leachates, then decreased towards the end of stagnant leaching.

Stagnant leaching of the WC cleavage edge produced a leachate with pH between 4.7 ± 0.8 and 7 ± 2. The two extremes of pH occurred on days 150 and 205, with the final low pH probably caused by leachate evaporation. The previous high pH may have been caused by dolomite weathering as indicated by increased dissolved Ca and Mg. After day 268 of stagnant leaching the solution pH remained relatively constant at 5, suggesting carbonate weathering was buffering pyrite oxidation.

Whole WC stagnant leaching again released similar quantities of most analytes apart from Al, S, Fe and Si (Table 5F). Reduction of pyrite oxidation due to restricted oxidant and consequent reduced weathering of clays lead to lower dissolution of these analytes.

UWS	Al	Ca	Fe	K	Mg	Mn	Na	S	Zn	Si
Whole at day 268	0.00 ± 0.00	3.1 ± 0.9	0.00 ± 0.00	0.4 ± 0.1	0.7 ± 0.2	0.01 ± 0.00	0.13 ± 0.03	3 ± 1	0.00 ± 0.00	0.23 ± 0.09
Cleavage at day 268	0.00 ± 0.00	1.5 ± 0.6	0.00 ± 0.00	0.25 ± 0.07	0.34 ± 0.07	0.00 ± 0.00	0.11 ± 0.03	1.7 ± 0.3	0.00 ± 0.00	0.05 ± 0.03

UWC	Al	Ca	Fe	K	Mg	Mn	Na	S	Zn	Si
Whole at day 205	0.00 ± 0.00	1.1 ± 0.4	0.00 ± 0.00	0.1 ± 0.1	0.3 ± 0.1	0.01 ± 0.00	0.01 ± 0.00	0.3 ± 0.2	0.00 ± 0.00	0.07 ± 0.04
Cleavage at day 316	0.01 ± 0.00	0.4 ± 0.1	0.01 ± 0.00	0.04 ± 0.05	0.13 ± 0.03	0.02 ± 0.00	0.03 ± 0.01	0.19 ± 0.04	0.01 ± 0.00	0.10 ± 0.09

WS	Al	Ca	Fe	K	Mg	Mn	Na	S	Zn	Si
Whole at day 150	0.5 ± 0.4	1.3 ± 0.9	9 ± 7	0.01 ± 0.04	0.7 ± 0.6	0.03 ± 0.03	0.8 ± 0.5	13 ± 4	1 ± 0.6	0.4 ± 0.4
Cleavage at day 205	0.09 ± 0.07	0.7 ± 0.1	1.3 ± 0.9	0.02 ± 0.00	0.5 ± 0.2	0.01 ± 0.00	0.3 ± 0.2	3.3 ± 0.4	0.5 ± 0.3	0.13 ± 0.03

WC	Al	Ca	Fe	K	Mg	Mn	Na	S	Zn	Si
Whole at day 205	0.5 ± 0.1	0.6 ± 0.3	10 ± 3	0.01 ± 0.02	0.29 ± 0.06	0.01 ± 0.00	0.6 ± 0.5	16 ± 3	0.8 ± 0.7	0.3 ± 0.7
Cleavage at day 268	0.07 ± 0.07	0.5 ± 0.3	0.9 ± 0.7	0.04 ± 0.03	0.3 ± 0.1	0.00 ± 0.00	0.3 ± 0.1	6 ± 5	0.4 ± 0.2	0.07 ± 0.00

Table 5.F. Whole and cleavage edge peak dissolved element flux during stagnant leaching. Values given in $mgL^{-1}g^{-1}$, errors shown are 1 σ (n=3).

Cyclic leaching major element dissolved concentrations for the UWS, UWC, WS and WC whole and cleavage edge samples.

UWS (whole sample)

Day	Al	Ca	Fe	K	Mg	Na	S	Zn	Si	pH
14	0.00 ± 0.00	4.2 ± 0.9	0.00 ± 0.00	0.13 ± 0.02	0.09 ± 0.02	0.04 ± 0.01	0.51 ± 0.07	0.00 ± 0.00	0.05 ± 0.01	
29	0.00 ± 0.00	1.2 ± 0.9	0.00 ± 0.00	0.03 ± 0.03	0.02 ± 0.02	0.02 ± 0.01	0.1 ± 0.1	0.00 ± 0.00	0.03 ± 0.02	7.42
58	0.00 ± 0.00	13 ± 2	0.00 ± 0.00	0.9 ± 0.2	0.31 ± 0.05	0.17 ± 0.02	1.6 ± 0.3	0.00 ± 0.00	0.38 ± 0.07	7.41
85	0.00 ± 0.00	0.12 ± 0.02	0.00 ± 0.00	0.06 ± 0.01	0.03 ± 0.00	0.01 ± 0.00	0.10 ± 0.02	0.00 ± 0.00	0.04 ± 0.01	6.84
100	0.00 ± 0.00	0.00 ± 0.00	0.00 ± 0.00	0.00 ± 0.00	0.03 ± 0.01	0.00 ± 0.00	0.00 ± 0.00	0.04 ± 0.02	0.00 ± 0.00	6.9 ± 0.2
120	0.00 ± 0.00	0.06 ± 0.00	0.00 ± 0.00	0.02 ± 0.00	0.00 ± 0.00	0.00 ± 0.00	0.02 ± 0.01	0.00 ± 0.00	0.03 ± 0.01	6.83 ± 0.07
133	0.00 ± 0.00	0.09 ± 0.01	0.00 ± 0.00	0.03 ± 0.00	0.02 ± 0.00	0.01 ± 0.00	0.02 ± 0.01	0.00 ± 0.00	0.04 ± 0.01	6.6 ± 0.1
150	0.00 ± 0.00	0.06 ± 0.01	0.00 ± 0.00	0.04 ± 0.00	0.01 ± 0.00	0.00 ± 0.00	0.04 ± 0.02	0.00 ± 0.00	0.02 ± 0.01	7.14 ± 0.05
170	0.00 ± 0.00	0.09 ± 0.02	0.00 ± 0.00	0.04 ± 0.01	0.02 ± 0.00	0.01 ± 0.00	0.10 ± 0.03	0.00 ± 0.00	0.03 ± 0.00	6.5 ± 0.4
183	0.00 ± 0.00	0.06 ± 0.01	0.00 ± 0.00	0.04 ± 0.00	0.01 ± 0.00	0.02 ± 0.01	0.05 ± 0.02	0.00 ± 0.00	0.04 ± 0.00	6.2 ± 0.1
205	0.00 ± 0.00	0.06 ± 0.01	0.00 ± 0.00	0.04 ± 0.01	0.02 ± 0.00	0.00 ± 0.00	0.10 ± 0.02	0.00 ± 0.00	0.03 ± 0.01	6.4 ± 0.1
225	0.00 ± 0.00	0.04 ± 0.01	0.00 ± 0.00	0.02 ± 0.00	0.01 ± 0.00	0.00 ± 0.00	0.05 ± 0.01	0.00 ± 0.00	0.02 ± 0.00	6.76 ± 0.07
239	0.00 ± 0.00	0.02 ± 0.00	0.00 ± 0.00	0.01 ± 0.00	0.01 ± 0.00	0.00 ± 0.00	0.03 ± 0.00	0.00 ± 0.00	0.01 ± 0.00	6.66 ± 0.00
254	0.00 ± 0.00	0.04 ± 0.01	0.00 ± 0.00	0.01 ± 0.00	0.01 ± 0.00	0.01 ± 0.00	0.05 ± 0.01	0.00 ± 0.00	0.02 ± 0.00	6.63 ± 0.06
268	0.00 ± 0.00	0.03 ± 0.01	0.00 ± 0.00	0.03 ± 0.1	0.01 ± 0.00	0.00 ± 0.00	0.03 ± 0.01	0.00 ± 0.00	0.03 ± 0.00	6.0 ± 0.5
287	0.00 ± 0.00	0.03 ± 0.00	0.00 ± 0.00	0.01 ± 0.00	0.01 ± 0.00	0.00 ± 0.00	0.05 ± 0.01	0.00 ± 0.00	0.02 ± 0.00	6.67 ± 0.05
307	0.00 ± 0.00	0.02 ± 0.00	0.00 ± 0.00	0.01 ± 0.00	0.01 ±0.00	0.00 ± 0.00	0.05 ± 0.01	0.00 ± 0.00	0.01 ± 0.00	6.75 ± 0.08
316	0.00 ± 0.00	0.01 ± 0.00	0.00 ± 0.00	0.01 ± 0.00	0.00 ± 0.00	0.00 ± 0.00	0.01 ± 0.00	0.00 ± 0.00	0.01 ± 0.00	6.7 ± 0.1
339	0.00 ± 0.00	0.03 ± 0.01	0.00 ± 0.00	0.00 ± 0.00	0.01 ± 0.00	0.01 ± 0.00	0.06 ± 0.01	0.00 ± 0.00	0.02 ±0.00	6.5 ± 0.1
361	0.00 ± 0.00	0.03 ± 0.02	0.00 ± 0.00	0.01 ± 0.00	0.01 ± 0.00	0.00 ± 0.00	0.05 ± 0.01	0.00 ± 0.00	0.01 ± 0.00	6.1 ± 0.3
382	0.00 ± 0.00	0.04 ± 0.01	0.00 ± 0.00	0.02 ± 0.00	0.01 ± 0.00	0.00 ± 0.00	0.05 ± 0.01	0.00 ± 0.00	0.02 ± 0.00	6.3 ± 0.3
Total Flux	0.01 ± 0.00	20 ± 2	0.00 ± 0.00	1.5 ± 0.2	0.65 ± 0.06	0.29 ± 0.02	3.1 ± 0.3	0.04 ± 0.02	0.82 ± 0.08	

Table 5.G. Major element dissolved concentration in UWS cyclic leachate removed over a period of 382 days, and total flux given in mgL^{-1}g^{-1}. Error shown is 1σ, n=4, 0.00 + 0.00 indicates concentration below detection.

Day	Al	Ca	Fe	K	Mg	Mn	Na	S	Zn	Si	pH
14	0.00 ± 0.0	1.14 ± 0.78	0.00 ± 0.00	0.05 ± 0.04	0.02 ± 0.01	0.00 ± 0.00	0.01 ± 0.01	0.11 ± 0.07	0.00 ± 0.00	0.01 ± 0.01	
29	0.46 ± 0.52	6.33 ± 11.89	0.88 ± 0.78	0.16 ± 0.07	1.40 ± 1.21	0.12 ± 0.11	0.14 ± 0.10	7.16 ± 5.87	0.02 ± 0.02	0.35 ± 0.23	
58	0.00 ± 0.00	17.39 ± 8.05	0.00 ± 0.00	1.12 ± 0.36	0.38 ± 0.18	0.00 ± 0.00	0.20 ± 0.07	2.31 ± 1.14	0.00 ± 0.00	0.18 ± 0.06	
85	0.00 ± 0.00	0.19 ± 0.06	0.00 ± 0.00	0.07 ± 0.02	0.04 ± 0.01	0.00 ± 0.00	0.02 ± 0.01	0.18 ± 0.06	0.00 ± 0.00	0.02 ± 0.01	
100	0.00 ± 0.02	0.00 ± 0.00	0.00 ± 0.00	0.00 ± 0.00	0.04 ± 0.01	0.00 ± 0.00	0.00 ± 0.00	0.00 ± 0.00	0.07 ± 0.01	0.00 ± 0.00	6.54 ± 0.24
120	0.00 ± 0.00	0.06 ± 0.02	0.00 ± 0.02	0.03 ± 0.02	0.00 ± 0.02	0.00 ± 0.02	0.00 ± 0.02	0.00 ± 0.03	0.00 ± 0.02	0.00 ± 0.02	6.54 ± 0.24
133	0.00 ± 0.00	0.11 ± 0.01	0.00 ± 0.02	0.04 ± 0.01	0.02 ± 0.00	0.00 ± 0.00	0.01 ± 0.00	0.02 ± 0.03	0.00 ± 0.00	0.02 ± 0.01	6.36 ± 0.21
150	0.00 ± 0.00	0.05 ± 0.05	0.00 ± 0.00	0.04 ± 0.02	0.01 ±0.01	0.00 ± 0.00	0.00 ± 0.00	0.03 ± 0.04	0.00 ± 0.00	0.00 ± 0.01	5.21 ± 0.66
170	0.00 ± 0.00	0.11 ± 0.03	0.00 ± 0.00	0.05 ± 0.01	0.02 ± 0.01	0.00 ± 0.00	0.01 ± 0.01	0.13 ± 0.03	0.00 ± 0.00	0.01 ± 0.01	6.15 ± 0.73
183	0.00 ± 0.00	0.08 ± 0.01	0.00 ± 0.00	0.04 ± 0.01	0.02 ± 0.00	0.00 ± 0.00	0.01 ± 0.01	0.07 ± 0.01	0.00 ± 0.00	0.03 ± 0.01	6.26 ± 0.44
205	0.00 ± 0.00	0.09 ± 0.02	0.00 ± 0.00	0.04 ± 0.01	0.02 ± 0.00	0.00 ± 0.00	0.00 ± 0.00	0.14 ± 0.02	0.00 ± 0.00	0.02 ± 0.01	6.52 ± 0.07
225	0.00 ± 0.00	0.06 ± 0.01	0.00 ± 0.00	0.02 ± 0.00	0.01 ± 0.00	0.00 ± 0.00	0.00 ± 0.00	0.07 ± 0.02	0.00 ± 0.00	0.01 ± 0.01	6.50 ± 0.13
239	0.00 ± 0.00	0.03 ± 0.01	0.00 ± 0.00	0.01 ± 0.00	0.01 ± 0.00	0.00 ± 0.00	0.00 ± 0.00	0.04 ± 0.01	0.00 ± 0.00	0.00 ± 0.00	5.79 ± 0.28
254	0.00 ± 0.00	0.06 ± 0.01	0.00 ± 0.00	0.01 ± 0.01	0.01 ± 0.00	0.00 ± 0.00	0.01 ± 0.02	0.07 ± 0.01	0.00 ± 0.00	0.01 ± 0.01	6.54 ± 0.07
268	0.00 ± 0.00	0.05 ± 0.01	0.00 ± 0.00	0.02 ± 0.00	0.01 ± 0.00	0.00 ± 0.00	0.00 ± 0.02	0.02 ± 0.01	0.00 ± 0.00	0.02 ± 0.01	6.95 ± 0.20
287	0.00 ± 0.00	0.04 ± 0.01	0.00 ± 0.00	0.02 ± 0.00	0.01 ± 0.00	0.00 ± 0.00	0.00 ± 0.00	0.05 ± 0.01	0.00 ± 0.00	0.01 ± 0.01	6.62 ± 0.08
307	0.00 ± 0.00	0.02 ± 0.00	0.00 ± 0.00	0.01 ± 0.00	0.01 ± 0.00	0.00 ± 0.00	0.00 ± 0.00	0.01 ± 0.01	0.00 ± 0.00	0.01 ± 0.00	6.50 ± 0.14
316	0.00 ± 0.00	0.01 ± 0.02	0.00 ± 0.00	0.01 ± 0.01	0.00 ± 0.00	0.00 ± 0.00	0.00 ± 0.02	0.02 ± 0.01	0.00 ± 0.00	0.00 ± 0.00	6.57 ± 0.42
339	0.00 ± 0.00	0.04 ± 0.01	0.00 ± 0.00	0.00 ± 0.00	0.01 ± 0.00	0.00 ± 0.00	0.00 ± 0.03	0.06 ± 0.02	0.00 ± 0.00	0.02 ± 0.01	6.48 ± 0.08
361	0.00 ± 0.00	0.03 ± 0.02	0.00 ± 0.00	0.01 ± 0.01	0.01 ± 0.00	0.00 ± 0.00	0.00 ± 0.00	0.04 ± 0.01	0.00 ± 0.00	0.01 ± 0.00	6.18 ± 0.11
382	0.00 ± 0.00	0.06 ± 0.02	0.00 ± 0.00	0.02 ± 0.01	0.02 ± 0.01	0.00 ± 0.00	0.00 ± 0.00	0.06 ± 0.02	0.00 ± 0.00	0.01 ± 0.01	5.81 ± 0.38
Total flux	0.5 ± 0.5	26 ± 14	0.9 ± 0.8	1.8 ± 0.4	2 ± 1	0.1 ± 0.1	0.4 ± 0.1	11 ± 6	0.10 ± 0.03	0.8 ± 0.2	

Table 5.H. Blank and mass corrected major element concentrations and total flux from cyclically leached partially coated UWS over the period of 382 days (mgL^{-1}g^{-1}). Errors shown are 1σ, n=4.

Day	Al	Ca	Fe	K	Mg	Na	S	Zn	Si	pH
14	0.00 ± 0.00	0.41 ± 0.07	0.00 ± 0.00	0.01 ± 0.01	0.01 ± 0.00	0.00 ± 0.00	0.01 ± 0.00	0.00 ± 0.00	0.01 ± 0.01	7.10
29	0.00 ± 0.00	1.1 ± 0.8	0.00 ± 0.00	0.02 ± 0.01	0.03 ± 0.01	0.02 ± 0.01	0.00 ± 0.00	0.00 ± 0.00	0.02 ± 0.01	7.17
58	0.00 ± 0.00	3.2 ± 0.4	0.00 ± 0.00	0.14 ± 0.06	0.07 ± 0.06	0.22 ± 0.06	0.09 ± 0.05	0.00 ± 0.00	0.11 ± 0.03	6.89
85	0.00 ± 0.00	0.05 ± 0.03	0.00 ± 0.00	0.04 ± 0.01	0.02 ± 0.01	0.02 ± 0.01	0.00 ± 0.00	0.00 ± 0.00	0.00 ± 0.00	6.84
100	0.00 ± 0.00	0.00± 0.00	0.00 ± 0.00	0.00 ± 0.00	0.00 ± 0.00	0.00 ± 0.00	0.00 ± 0.00	0.00 ± 0.00	0.00 ± 0.00	6.7 ± 0.1
120	0.00 ± 0.00	0.02 ± 0.02	0.00 ± 0.00	0.00 ± 0.00	0.00 ± 0.00	0.00 ± 0.00	0.00 ± 0.00	0.00 ± 0.00	0.00 ± 0.00	6.1 ± 0.1
133	0.00 ± 0.00	0.02 ± 0.03	0.00 ± 0.00	0.01 ± 0.00	0.01 ± 0.01	0.02 ± 0.01	0.00 ± 0.00	0.00 ± 0.00	0.00 ± 0.00	6.25 ± 0.04
150	0.00 ± 0.00	0.00 ± 0.01	0.00 ± 0.00	0.03 ± 0.01	0.00 ± 0.00	0.00 ± 0.00	0.00 ± 0.00	0.00 ± 0.00	0.00 ± 0.00	5.8 ± 0.2
170	0.00 ± 0.00	0.01 ± 0.02	0.00 ± 0.00	0.03 ± 0.01	0.00 ± 0.01	0.02 ± 0.01	0.01 ± 0.01	0.00 ± 0.00	0.00 ± 0.00	6.44 ± 0.05
183	0.00 ± 0.00	0.04 ± 0.01	0.00 ± 0.00	0.04 ± 0.01	0.01 ± 0.02	0.03 ± 0.02	0.01 ± 0.00	0.00 ± 0.00	0.03 ± 0.01	6.49 ± 0.06
205	0.00 ± 0.00	0.01 ± 0.01	0.00 ± 0.00	0.03 ± 0.01	0.00 ± 0.00	0.00 ± 0.00	0.06 ± 0.02	0.00 ± 0.00	0.00 ± 0.00	6.7 ± 0.2
225	0.00 ± 0.00	0.00 ± 0.00	0.00 ± 0.00	0.00 ± 0.00	0.00 ± 0.00	0.00 ± 0.00	0.01 ± 0.00	0.00 ± 0.00	0.00 ± 0.00	6.77 ± 0.04
239	0.00 ± 0.00	0.00 ± 0.00	0.00 ± 0.00	0.00 ± 0.00	0.00 ± 0.00	0.00 ± 0.00	0.00 ± 0.00	0.00 ± 0.00	0.00 ± 0.00	6.64 ± 0.02
254	0.00 ± 0.00	0.01 ± 0.01	0.00 ± 0.00	0.00 ± 0.00	0.00 ± 0.00	0.01 ± 0.00	0.01 ± 0.00	0.00 ± 0.00	0.00 ± 0.00	6.65 ± 0.07
268	0.00 ± 0.00	0.00 ± 0.01	0.00 ± 0.00	0.00 ± 0.00	0.00 ± 0.01	0.01 ± 0.01	0.01 ± 0.00	0.00 ± 0.00	0.00 ± 0.01	6.5 ± 0.1
287	0.00 ± 0.00	0.00 ± 0.00	0.00 ± 0.00	0.00 ± 0.00	0.00 ± 0.00	0.00 ± 0.00	0.01 ± 0.01	0.00 ± 0.00	0.00 ± 0.00	6.6 ± 0.1
307	0.00 ± 0.00	0.00 ± 0.00	0.00 ± 0.00	0.00 ± 0.00	0.00 ± 0.00	0.00 ± 0.00	0.00 ± 0.00	0.00 ± 0.00	0.00 ± 0.00	6.0 ± 0.2
316	0.00 ± 0.00	0.00 ± 0.00	0.00 ± 0.00	0.00 ± 0.00	0.00 ± 0.00	0.00 ± 0.00	0.00 ± 0.00	0.00 ± 0.00	0.00 ± 0.00	6.63 ± 0.09
339	0.00 ± 0.00	0.00 ± 0.00	0.00 ± 0.00	0.00 ± 0.00	0.00 ± 0.02	0.01 ± 0.02	0.01 ± 0.01	0.00 ± 0.00	0.00 ± 0.00	6.6 ± 0.4
361	0.00 ± 0.00	0.00 ± 0.00	0.00 ± 0.00	0.00 ± 0.00	0.00 ± 0.00	0.00 ± 0.00	0.01 ± 0.00	0.00 ± 0.00	0.00 ± 0.00	5.74 ± 0.03
382	0.00 ± 0.00	0.00 ± 0.00	0.00 ± 0.00	0.00 ± 0.00	0.00 ± 0.00	0.00 ± 0.00	0.00 ± 0.00	0.00 ± 0.00	0.00 ± 0.00	5 ± 1
Total Flux	0.01 ± 0.00	4.90 ± 0.06	0.01 ± 0.00	0.34 ± 0.00	0.15 ± 0.00	0.38 ± 0.00	0.22 ± 0.00	0.01 ± 0.00	0.18 ± 0.00	

Table 5.I. Major element dissolved concentration in UWC cyclic leachate removed over a period of 382 days, and total flux given in $mgL^{-1}g^{-1}$. Error shown is 1σ, n=4, 0.00 + 0.00 indicates concentration below detection.

UWC (cleavage edge)

Day	Al	Ca	Fe	K	Mg	Mn	Na	S	Zn	Si	pH
14	0.00 ± 0.01	0.10 ± 0.05	0.00 ± 0.00	0.01 ± 0.04	0.00 ± 0.00	0.00 ± 0.00	0.00 ± 0.01	0.00 ± 0.00	0.00 ± 0.00	0.00 ± 0.00	
29	0.00 ± 0.00	2.27 ± 1.41	0.00 ± 0.00	0.06 ± 0.11	0.04 ± 0.03	0.00 ± 0.00	0.03 ± 0.01	0.24 ± 0.21	0.00 ± 0.00	0.02 ± 0.01	
58	0.00 ± 0.00	2.24 ± 0.76	0.00 ± 0.00	0.35 ± 0.00	0.04 ± 0.02	0.00 ± 0.00	0.13 ± 0.07	0.10 ± 0.04	0.00 ± 0.00	0.07 ± 0.03	
85	0.00 ± 0.00	0.03 ± 0.01	0.00 ± 0.00	0.03 ± 0.00	0.01 ± 0.00	0.00 ± 0.00	0.01 ± 0.00	0.00 ± 0.02	0.00 ± 0.00	0.00 ± 0.00	
100	0.00 ± 0.00	0.00 ± 0.00	0.00 ± 0.00	0.00 ± 0.00	0.00 ± 0.00	0.00 ± 0.00	0.00 ± 0.00	0.00 ± 0.00	0.00 ± 0.02	0.00 ± 0.00	6.42 ± 0.16
120	0.00 ± 0.00	0.00 ± 0.00	0.00 ± 0.00	0.00 ± 0.00	0.00 ± 0.00	0.00 ± 0.00	0.00 ± 0.00	0.00 ± 0.01	0.00 ± 0.00	0.00 ± 0.00	6.39 ± 0.16
133	0.00 ± 0.00	0.00 ± 0.00	0.00 ± 0.00	0.01 ± 0.02	0.00 ± 0.00	0.00 ± 0.00	0.00 ± 0.00	0.00 ± 0.01	0.00 ± 0.00	0.00 ± 0.00	6.50 ± 0.12
150	0.00 ± 0.00	0.00 ± 0.00	0.00 ± 0.00	0.04 ± 0.00	0.00 ± 0.00	0.00 ± 0.00	0.00 ± 0.01	0.00 ± 0.01	0.00 ± 0.00	0.00 ± 0.00	6.29 ± 0.11
170	0.00 ± 0.00	0.00 ± 0.00	0.00 ± 0.00	0.03 ± 0.00	0.00 ± 0.00	0.00 ± 0.00	0.01 ± 0.01	0.01 ± 0.01	0.00 ± 0.00	0.00 ± 0.00	6.08 ± 0.34
183	0.00 ± 0.00	0.00 ± 0.00	0.00 ± 0.00	0.03 ± 0.00	0.00 ± 0.00	0.00 ± 0.00	0.03 ± 0.00	0.02 ± 0.01	0.00 ± 0.00	0.02 ± 0.01	6.43 ± 0.06
205	0.00 ± 0.00	0.00 ± 0.00	0.00 ± 0.00	0.02 ± 0.00	0.00 ± 0.00	0.00 ± 0.00	0.00 ± 0.01	0.06 ± 0.01	0.00 ± 0.00	0.00 ± 0.00	6.44 ± 0.07
225	0.00 ± 0.00	0.00 ± 0.00	0.00 ± 0.00	0.00 ± 0.00	0.00 ± 0.00	0.00 ± 0.00	0.00 ± 0.00	0.02 ± 0.01	0.00 ± 0.00	0.00 ± 0.00	6.57 ± 0.09
239	0.00 ± 0.00	0.00 ± 0.00	0.00 ± 0.00	0.00 ± 0.00	0.00 ± 0.00	0.00 ± 0.00	0.00 ± 0.00	0.01 ± 0.01	0.00 ± 0.00	0.00 ± 0.00	6.05 ± 0.20
254	0.00 ± 0.00	0.00 ± 0.00	0.00 ± 0.00	0.00 ± 0.03	0.00 ± 0.00	0.00 ± 0.00	0.01 ± 0.00	0.02 ± 0.01	0.00 ± 0.00	0.00 ± 0.00	6.42 ± 0.07
268	0.00 ± 0.00	0.00 ± 0.00	0.00 ± 0.00	0.00 ± 0.00	0.00 ± 0.00	0.00 ± 0.00	0.00 ± 0.01	0.01 ± 0.01	0.00 ± 0.00	0.01 ± 0.00	6.59 ± 0.09
287	0.00 ± 0.00	0.00 ± 0.00	0.00 ± 0.00	0.00 ± 0.00	0.00 ± 0.00	0.00 ± 0.00	0.00 ± 0.01	0.02 ± 0.01	0.00 ± 0.00	0.00 ± 0.00	6.49 ± 0.20
307	0.00 ± 0.00	0.00 ± 0.00	0.00 ± 0.00	0.00 ± 0.00	0.00 ± 0.00	0.00 ± 0.00	0.00 ± 0.00	0.00 ± 0.00	0.00 ± 0.00	0.00 ± 0.00	6.41 ± 0.07
316	0.00 ± 0.00	0.00 ± 0.00	0.00 ± 0.00	0.00 ± 0.01	0.00 ± 0.00	0.00 ± 0.00	0.00 ± 0.00	0.01 ± 0.01	0.00 ± 0.00	0.00 ± 0.00	6.26 ±0 .03
339	0.00 ± 0.00	0.00 ± 0.01	0.00 ± 0.00	0.01 ± 0.01	0.00 ± 0.00	0.00 ± 0.00	0.00 ± 0.02	0.00 ± 0.02	0.00 ± 0.00	0.00 ± 0.00	6.04 ± 0.20
361	0.00 ± 0.00	0.00 ± 0.00	0.00 ± 0.00	0.00 ± 0.00	0.00 ± 0.00	0.00 ± 0.00	0.00 ± 0.01	0.02 ± 0.01	0.00 ± 0.00	0.00 ± 0.00	6.55 ± 0.12
382	0.00 ± 0.00	0.00 ± 0.00	0.00 ± 0.00	0.01 ± 0.00	0.00 ± 0.00	0.00 ± 0.00	0.00 ± 0.00	0.01 ± 0.01	0.00 ± 0.00	0.00 ± 0.00	4.67 ± 0.16
Total flux	0.01 ± 0.01	5 ± 2	0.01 ± 0.01	0.6 ± 0.1	0.11 ± 0.03	0.01 ± 0.00	0.22 ± 0.07	0.6 ± 0.2	0.00 ± 0.02	0.13 ± 0.03	

Table 5.J. Blank and mass corrected major element concentrations and total flux from cyclically leached partially coated UWC over the period of 382 days in mgL^{-1}g^{-1}. Errors shown are 1σ, n=4.

day	Al	Ca	Fe	K	Mg	Na	S	Zn	Si	pH
14	0.07± 0.06	1.3± 0.4	3 ± 2	0.02 ± 0.02	0.07 ± 0.06	0.11 ± 0.1	4 ± 3	0.2 ± 0.2	0.00 ± 0.00	2.80
29	0.06± 0.04	1.4± 0.7	3 ± 1	0.01 ± 0.00	0.06 ± 0.03	0.13 ± 0.06	4 ± 2	0.12 ± 0.07	0.04 ± 0.01	3.12
58	0.12± 0.07	4 ± 2	7 ± 4	0.3 ± 0.2	0.11 ± 0.06	0.4 ± 0.2	12± 6	0.2 ± 0.1	0.19 ± 0.09	3.29
85	0.01± 0.01	0.01± 0.02	0.6 ± 0.6	0.00 ± 0.00	0.00 ± 0.00	0.00 ± 0.00	0.9 ± 0.7	0.00 ± 0.0	0.00 ± 0.01	3.45
100	0.00± 0.00	0.00 ± 0.00	0.00 ± 0.00	0.00 ± 0.00	0.00 ± 0.00	0.00 ± 0.00	0.00 ± 0.00	0.4 ± 0.2	0.00 ± 0.00	3.4 ± 0.1
120	0.01± 0.01	0.00 ± 0.00	0.3 ± 0.3	0.00 ± 0.00	0.00 ± 0.00	0.00 ± 0.00	0.4 ± 0.2	0.00 ± 0.00	0.00 ± 0.00	3.3 ± 0.1
133	0.00 ± 0.00	0.00 ± 0.00	0.2 ± 0.2	0.00 ± 0.00	0.00 ± 0.00	0.00 ± 0.00	0.5 ± 0.4	0.00 ± 0.00	0.00 ± 0.00	6 ± 2
150	0.00 ± 0.00	0.00 ± 0.00	0.3 ± 0.3	0.04 ± 0.00	0.00 ± 0.00	0.00 ± 0.00	0.5 ± 0.3	0.00 ± 0.00	0.00 ± 0.00	4 ± 1
170	0.00 ± 0.00	0.00 ± 0.00	0.4 ± 0.4	0.03 ± 0.01	0.00 ± 0.00	0.03 ± 0.01	0.7 ± 0.4	0.00 ± 0.00	0.00 ± 0.00	6 ± 0.2
183	0.00 ± 0.00	0.03± 0.01	0.3 ± 0.3	0.05 ± 0.01	0.00 ± 0.00	0.04 ±0.01	0.6 ± 0.3	0.00 ± 0.00	0.03 ± 0.01	3.5 ± 0.2
205	0.00 ± 0.00	0.03± 0.01	0.3 ± 0.3	0.05 ± 0.01	0.00 ± 0.00	0.04 ± 0.01	0.6 ± 0.3	0.00 ± 0.00	0.03 ± 0.01	3.5 ± 0.2
225	0.00 ± 0.00	0.00 ± 0.00	0.5 ± 0.4	0.02 ± 0.01	0.00 ± 0.00	0.00 ± 0.00	1.1 ± 0.5	0.00 ± 0.00	0.01 ± 0.01	0.95
239	0.00 ± 0.00	0.00 ± 0.00	0.06 ± 0.05	0.00 ± 0.01	0.00 ± 0.00	0.01 ± 0.00	0.3 ± 0.2	0.00 ± 0.00	0.00 ± 0.00	3.7 ± 0.2
254	0.00 ± 0.00	0.00 ± 0.00	0.1 ± 0.1	0.00 ± 0.01	0.00 ± 0.00	0.01 ± 0.01	0.5 ± 0.3	0.00 ± 0.00	0.00 ± 0.00	3.3± 0.3
268	0.00 ± 0.00	0.00 ± 0.00	0.1 ± 0.1	0.02 ± 0.00	0.00 ± 0.00	0.00 ± 0.00	0.5 ± 0.2	0.00 ± 0.00	0.01 ± 0.01	3.5 ± 0.2
287	0.00 ± 0.00	0.00 ± 0.00	0.08 ± 0.07	0.00 ± 0.00	0.00 ± 0.00	0.01 ± 0.01	0.5 ± 0.3	0.00 ± 0.00	0.00 ± 0.01	3.4 ± 0.2
307	0.00 ± 0.00	0.00 ± 0.00	0.04 ± 0.03	0.00 ± 0.00	0.00 ± 0.00	0.00 ± 0.00	0.5 ± 0.3	0.00 ± 0.00	0.00 ± 0.00	3.5 ± 0.3
316	0.00 ± 0.00	0.00 ± 0.00	0.02 ± 0.02	0.00 ± 0.00	0.00 ± 0.00	0.00 ± 0.00	0.14 ± 0.08	0.00 ± 0.00	0.00 ± 0.00	3.7 ± 0.3
339	0.00 ± 0.00	0.00 ± 0.00	0.12 ± 0.08	0.00 ± 0.00	0.00 ± 0.00	0.03 ± 0.02	0.5 ± 0.2	0.00 ± 0.00	0.00 ± 0.01	3.3 ± 0.1
361	0.00 ± 0.00	0.00 ± 0.00	0.09 ± 0.08	0.00 ± 0.00	0.00 ± 0.00	0.00 ± 0.00	0.4 ± 0.2	0.00 ± 0.00	0.00 ± 0.00	3.7 ± 0.2
Total Flux	0.3 ± 0.1	7 ± 2	16 ± 5	0.9 ± 0.4	0.25 ± 0.08	0.8 ± 0.2	28 ± 7	0.9 ± 0.3	0.35 ± 0.09	

Table 5.K. Blank and mass corrected major element concentrations and total flux from cyclically leached whole WS over the period of 361 days in mgL^{-1}g^{-1}. Errors shown are 1σ, n=4.

xxx

WS (cleavage edge)

Day	Al	Ca	Fe	K	Mg	Mn	Na	S	Zn	Si	pH
14	0.00 ± 0.00	0.62 ± 0.19	0.00 ± 0.00	0.00 ± 0.01	0.02 ± 0.01	0.00 ± 0.00	0.00 ± 0.02	0.74 ± 0.55	0.01 ± 0.01	0.03 ± 0.02	
29	0.00 ± 0.00	1.56 ± 0.90	0.11 ± 0.09	0.01 ± 0.00	0.07 ± 0.05	0.00 ± 0.02	0.05 ± 0.14	0.81 ± 4.09	0.03 ± 0.03	0.02 ± 0.01	
58	0.03 ± 0.02	12.97 ± 5.77	0.63 ± 0.54	0.01 ± 0.02	0.52 ± 0.32	0.03 ± 0.02	0.54 ± 0.14	6.43 ± 4.09	0.27 ± 0.2	0.26 ± 0.04	
85	0.01 ± 0.01	0.03 ± 0.01	0.12 ± 0.23	0.04 ± 0.01	0.02 ± 0.02	0.00 ± 0.00	0.00 ± 0.02	0.22 ± 0.18	0.00 ± 0.01	0.00 ± 0.01	
100	0.00 ± 0.00	0.00 ± 0.01	0.00 ± 0.00	0.09 ± 0.17	0.00 ± 0.00	0.00 ± 0.00	0.00 ± 0.00	0.00 ± 0.00	0.00 ± 0.2	0.00 ± 0.00	5.29 ± 1
120	0.00 ± 0.01	0.02 ± 0.01	0.08 ± 0.15	0.00 ± 0.00	0.00 ± 0.01	0.00 ± 0.00	0.00 ± 0.00	0.10 ± 0.10	0.00 ± 0.00	0.00 ± 0.01	5.85 ± 0.5
133	0.00 ± 0.00	0.01 ± 0.03	0.00 ± 0.02	0.01 ± 0.00	0.01 ± 0.01	0.00 ± 0.00	0.00 ± 0.00	0.00 ± 0.16	0.00 ± 0.00	0.00 ± 0.00	5.31 ± 1
150	0.00 ± 0.01	0.01 ± 0.02	0.04 ± 0.09	0.03 ± 0.00	0.01 ± 0.01	0.00 ± 0.00	0.00 ± 0.00	0.13 ± 0.13	0.00 ± 0.00	0.00 ± 0.00	4.94 ± 1
170	0.00 ± 0.01	0.02 ± 0.02	0.07 ± 0.15	0.03 ± 0.01	0.01 ± 0.01	0.00 ± 0.00	0.02 ± 0.02	0.19 ± 0.2	0.00 ± 0.01	0.00 ± 0.01	4.63 ± 1
183	0.00 ± 0.01	0.05 ± 0.02	0.07 ± 0.10	0.05 ± 0.01	0.01 ± 0.01	0.00 ± 0.00	0.03 ± 0.01	0.22 ± 0.08	0.01 ± 0.01	0.03 ± 0.01	
205	0.01 ± 0.01	0.03 ± 0.03	0.16 ± 0.29	0.03 ± 0.01	0.01 ± 0.02	0.00 ± 0.00	0.01 ± 0.02	0.38 ± 0.05	0.02 ± 0.02	0.01 ± 0.01	4.76 ± 1
225	0.00 ± 0.00	0.01 ± 0.01	0.03 ± 0.05	0.00 ± 0.0	0.00 ± 0.00	0.00 ± 0.00	0.00 ± 0.00	0.14 ± 0.1	0.00 ± 0.00	0.00 ± 0.00	3.78 ± 3
239	0.00 ± 0.00	0.01 ± 0.01	0.01 ± 0.02	0.00 ± 0.00	0.00 ± 0.00	0.00 ± 0.00	0.01 ± 0.01	0.11 ± 0.2	0.00 ± 0.00	0.00 ± 0.00	4.78 ± 0.7
254	0.00 ± 0.01	0.01 ± 0 .01	0.08 ± 0.14	0.00 ± 0.00	0.01 ± 0.01	0.00 ± 0.00	0.02 ± 0.01	0.18 ± 0.1	0.00 ± 0.00	0.00 ± 0.00	4.47 ± 0.8
268	0.00 ± 0.01	0.02 ± 0.02	0.11 ± 0.19	0.03 ± 0.02	0.01 ± 0.01	0.00 ± 0.00	0.00 ± 0.02	0.20 ± 0.03	0.01 ± 0.01	0.01 ± 0.01	4.35 ± 0.9
287	0.00 ± 0.00	0.01 ± 0.01	0.07 ± 0.13	0.00 ± 0.00	0.00 ± 0.00	0.00 ± 0.00	0.00 ± 0.01	0.22 ± 0.03	0.00 ± 0.01	0.00 ± 0.00	4.83 ± 0.9
307	0.00 ± 0.00	0.01 ± 0.01	0.02 ± 0.04	0.00 ± 0.00	0.00 ± 0.00	0.00 ± 0.00	0.00 ± 0.00	0.05 ± 0.2	0.00 ± 0.00	0.00 ± 0.00	4.60 ± 0.8
316	0.00 ± 0.00	0.00 ± 0.00	0.01 ± 0.02	0.00 ± 0.00	0.00 ± 0.00	0.00 ± 0.00	0.00 ± 0.00	0.06 ± 0.06	0.00 ± 0.00	0.00 ± 0.00	4.77 ± 0.7
339	0.00 ± 0.01	0.02 ± 0.02	0.13 ± 0.24	0.00 ± 0.01	0.01 ± 0.01	0.00 ± 0.00	0.01 ± 0.06	0.25	0.00 ± 0.00	0.01 ± 0.01	4.73 ± 1
361	0.00 ± 0.00	0.01 ± 0.00	0.03 ± 0.05	0.00 ± 0.01	0.00 ± 0.00	0.00 ± 0.00	0.00 ± 0.03	0.17	0.00 ± 0.00	0.00 ± 0.00	4.82 ± 0.8
Total Flux	0.08 ± 0.03	15 ± 6	1.8 ± 0.8	0.33 ± 0.18	0.7 ± 0.3	0.04 ± 0.02	0.7 ± 0.2	11 ± 4	0.4 ± 0.3	0.39 ± 0.05	

Table 5.L. Blank and mass corrected major element concentrations and total flux from cyclically leached partially coated WS over the period of 361 days in $mgL^{-1}g^{-1}$. Errors shown are 1σ, n=4.

IXXX

Day	Al	Ca	Fe	K	Mg	Na	S	Zn	Si	pH
14	0.2 ± 0.1	2 ± 1	6 ± 5	0.00 ± 0.01	0.16 ± 0.09	2 ± 3	9 ± 8	3 ± 4	0.02 ± 0.01	4.15
29	0.13 ± 0.06	1.3 ± 0.3	3 ± 2	0.01 ± 0.00	0.08 ± 0.02	1 ± 1	4 ± 3	1 ± 1	0.05 ± 0.01	4.15
58	0.4 ± 0.2	5.7 ± 0.7	10 ± 7	0.04 ± 0.08	0.23 ± 0.07	2 ± 2	17 ± 8	2 ± 3	0.38 ± 0.08	4.21
85	0.06 ± 0.08	0.05 ± 0.08	1 ± 1	0.04 ± 0.01	0.1 ± 0.1	0.1 ± 0.2	2 ± 1	0.2 ± 0.3	0.02 ± 0.02	4.39
100	0.00 ± 0.00	0.00 ± 0.00	0.00 ± 0.00	0.3 ± 0.3	0.00 ± 0.00	0.00 ± 0.00	0.00 ± 0.00	0.3 ± 0.3	0.00 ± 0.01	3.5 ± 0.2
120	0.00 ± 0.00	0.00 ± 0.00	0.2 ± 0.2	0.00 ± 0.00	0.00 ± 0.00	0.00 ± 0.00	0.2 ± 0.2	0.00 ± 0.00	0.01 ± 0.00	3.6 ± 0.2
133	0.01 ± 0.01	0.04 ± 0.03	0.2 ± 0.4	0.01 ± 0.01	0.02 ± 0.01	0.03 ± 0.05	0.4 ± 0.50	0.04 ± 0.06	0.01 ± 0.01	3.8 ± 0.2
150	0.00 ± 0.00	0.00 ± 0.00	0.1 ± 0.2	0.04 ± 0.00	0.00 ± 0.00	0.00 ± 0.00	0.3 ± 0.2	0.00 ± 0.00	0.00 ± 0.00	3.8 ± 0.2
170	0.00 ± 0.00	0.00 ± 0.00	0.2 ± 0.2	0.04 ± 0.00	0.00 ± 0.00	0.03 ± 0.01	0.5 ± 0.3	0.00 ± 0.00	0.00 ± 0.00	3.8 ± 0.2
183	0.00 ± 0.00	0.00 ± 0.00	0.1 ± 0.1	0.05 ± 0.00	0.00 ± 0.00	0.05 ± 0.02	0.4 ± 0.2	0.00 ± 0.00	0.04 ± 0.00	3.8 ± 0.2
205	0.00 ± 0.00	0.00 ± 0.00	0.2 ± 0.2	0.02 ± 0.00	0.00 ± 0.00	0.00 ± 0.01	0.6 ± 0.3	0.01 ± 0.01	0.01 ± 0.01	1.9 ± 0.9
225	0.00 ± 0.00	0.00 ± 0.00	0.04 ± 0.01	0.00 ± 0.00	0.00 ± 0.00	0.01 ± 0.01	0.21 ± 0.09	0.00 ± 0.00	0.01 ± 0.00	Out of range
239	0.00 ± 0.00	0.00 ± 0.00	0.04 ± 0.06	0.00 ± 0.00	0.00 ± 0.00	0.00 ± 0.00	0.15 ± 0.07	0.00 ± 0.00	0.00 ± 0.00	4.2 ± 0.2
254	0.00 ± 0.00	0.00 ± 0.00	0.03 ± 0.01	0.00 ± 0.00	0.00 ± 0.00	0.02± 0.01	0.3 ± 0.1	0.00 ± 0.00	0.01 ± 0.00	3.7 ± 0.3
268	0.00 ± 0.00	0.00 ± 0.00	0.03 ± 0.01	0.05 ± 0.01	0.00 ± 0.00	0.00 ± 0.00	0.3 ± 0.1	0.00 ± 0.00	0.02 ± 0.01	3.7 ± 0.3
287	0.00 ± 0.00	0.00 ± 0.00	0.05 ± 0.04	0.00 ± 0.00	0.00 ± 0.00	0.01 ± 0.01	0.4 ± 0.2	0.00 ± 0.00	0.01 ± 0.01	3.7 ± 0.3
307	0.00 ± 0.00	0.00 ± 0.00	0.03 ± 0.03	0.00 ± 0.00	0.00 ± 0.00	0.00 ± 0.00	0.3 ± 0.2	0.00 ± 0.00	0.01 ± 0.00	3.7 ± 0.3
316	0.00 ± 0.00	0.00 ± 0.00	0.01 ± 0.01	0.00 ± 0.00	0.00 ± 0.00	0.00 ± 0.00	0.2 ± 0.1	0.00 ± 0.00	0.00 ± 0.00	4.0 ± 0.3
339	0.01 ± 0.00	0.00 ± 0.00	0.08 ± 0.05	0.01 ± 0.02	0.00 ± 0.00	0.00 ± 0.00	0.3 ± 0.2	0.00 ± 0.00	0.01 ± 0.01	3.5 ± 0.3
361	0.00 ± 0.00	0.00 ± 0.00	0.05 ± 0.04	0.00 ± 0.01	0.00 ± 0.00	0.00 ± 0.00	0.25 ± 0.09	0.00 ± 0.00	0.01 ± 0.01	4.3 ± 0.3
382	0.00 ± 0.00	0.00 ± 0.00	0.07 ± 0.06	0.00 ± 0.00	0.00 ± 0.00	0.00 ± 0.00	0.26 ± 0.20	0.00 ± 0.00	0.01 ± 0.00	3.5 ± 0.3
Total Flux	0.9 ± 0.3	9 ± 1	21 ± 9	0.6 ± 0.3	0.6 ± 0.2	4 ± 3	36 ± 11	6 ± 5	0.64 ± 0.09	

Table 5.M. Blank and mass corrected major element concentrations and total flux from cyclically leached whole WC over the period of 382 days in mgL^{-1}g^{-1}. Errors shown are 1σ, n=4.

Day	Al	Ca	Fe	K	Mg	Mn	Na	S	Zn	Si	pH
14	0.00 ± 0.00	0.17 ± 0.16	0.02 ± 0.03	0.01 ± 0.01	0.01 ± 0.01	0.00 ± 0.00	0.00 ± 0.00	0.14 ± 0.12	0.00	0.00 ± 0.00	
29	0.07 ± 0.07	1.57 ± 0.14	0.79 ± 0.65	0.01 ± 0.00	0.06 ± 0.01	0.00 ± 0.00	0.18 ± 0.23	1.13 ± 0.79	0.21 ± 0.01	0.02 ± 0.00	
85	0.03 ± 0.03	0.09 ± 0.06	0.18 ± 0.21	0.03 ± 0.01	0.04 ± 0.02	0.00 ± 0.00	0.08 ± 0.09	0.44 ± 0.45	0.08 ± 0.29	0.01 ± 0.00	
100	0.00 ± 0.00	0.01 ± 0.02	0.00 ± 0.00	0.07 ± 0.08	0.00 ± 0.01	0.00 ± 0.00	0.00 ± 0.00	0.00 ± 0.00	0.04 ± 0.13	0.02 ± 0.07	4.12 ± 0.4
120	0.00 ± 0.01	0.02 ± 0.01	0.04 ± 0.06	0.00 ± 0.01	0.00 ± 0.00	0.00 ± 0.00	0.00 ± 0.03	0.06 ± 0.14	0.02 ± 0.21	0.00 ± 0.00	4.10 ± 0.4
133	0.00 ± 0.00	0.02 ± 0.02	0.00 ± 0.05	0.31 ± 0.61	0.01 ± 0.00	0.00 ± 0.00	0.01 ± 0.01	0.00 ± 0.19	0.01 ± 0.04	0.01 ± 0.00	4.11 ± 0.3
150	0.01 ± 0.01	0.01 ± 0.01	0.01 ± 0.02	0.03 ± 0.00	0.00 ± 0.00	0.00 ± 0.00	0.00 ± 0.02	0.16 ± 0.16	0.00 ± 0.02	0.00 ± 0.00	4.19 ± 0.3
170	0.00 ± 0.01	0.01 ± 0.02	0.03 ± 0.05	0.03 ± 0.01	0.00 ± 0.00	0.00 ± 0.00	0.06 ± 0.05	0.23 ± 0.16	0.04 ± 0.03	0.00 ± 0.00	4.01 ± 0.2
183	0.01 ± 0.01	0.05 ± 0.02	0.03 ± 0.03	0.03 ± 0.01	0.01 ± 0.00	0.00 ± 0.00	0.06 ± 0.05	0.21 ± 0.14	0.04 ± 0.08	0.03 ± 0.01	4.10 ± 0.3
205	0.01 ± 0.01	0.05 ± 0.02	0.03 ± 0.03	0.03 ± 0.01	0.01 ± 0.00	0.00 ± 0.00	0.06 ± 0.05	0.21 ± 0.14	0.04 ± 0.06	0.03 ± 0.01	4.10 ± 0.3
225	0.00 ± 0.00	0.01 ± 0.00	0.02 ± 0.01	0.00 ± 0.00	0.00 ± 0.00	0.00 ± 0.00	0.01 ± 0.03	0.14 ± 0.08	0.02 ± 0.06	0.00 ± 0.00	1.73 ± 2
239	0.00 ± 0.00	0.00 ± 0.00	0.01 ± 0.01	0.00 ± 0.00	0.00 ± 0.00	0.00 ± 0.00	0.00 ± 0.01	0.11 ± 0.05	0.01 ± 0.03	0.00 ± 0.00	4.42 ± 0.4
254	0.00 ± 0.00	0.01 ± 0.01	0.02 ± 0.02	0.00 ± 0.00	0.00 ± 0.00	0.00 ± 0.00	0.02 ± 0.02	0.15 ± 0.08	0.02 ± 0.01	0.01 ± 0.00	3.99 ± 0.2
268	0.01 ± 0.00	0.01 ± 0.00	0.03 ± 0.02	0.00 ± 0.00	0.01 ± 0.00	0.00 ± 0.00	0.00 ± 0.03	0.15 ± 0.08	0.03 ± 0.03	0.02 ± 0.01	4.17 ± 0.3
287	0.00 ± 0.00	0.00 ± 0.00	0.02 ± 0.01	0.00 ± 0.00	0.00 ± 0.00	0.00 ± 0.00	0.01 ± 0.02	0.16 ± 0.07	0.02 ±0 .03	0.00 ± 0.00	4.18 ± 0.3
307	0.00 ± 0.00	0.00 ± 0.00	0.00 ± 0.01	0.00 ± 0.00	0.00 ± 0.00	0.00 ± 0.00	0.00 ± 0.00	0.04 ± 0.02	0.00 ± 0.03	0.00 ± 0.00	4.21 ± 0.3
316	0.00 ± 0.00	0.00 ± 0.00	0.01 ± 0.01	0.00 ± 0.00	0.00 ± 0.00	0.00 ± 0.00	0.00 ± 0.00	0.10 ± 0.04	0.00 ± 0.00	0.00 ± 0.00	6.01 ± 1
339	0.00 ± 0.00	0.01 ± 0.01	0.03 ± 0.03	0.00 ± 0.02	0.00 ± 0.00	0.00 ± 0.00	0.03 ± 0.02	0.16 ± 0.08	0.02 ± 0.03	0.01 ± 0.00	4.33 ± 0.3
361	0.00 ± 0.00	0.00 ± 0.00	0.02 ± 0.02	0.01 ± 0.01	0.00 ± 0.00	0.00 ± 0.00	0.00 ± 0.03	0.08 ± 0.10	0.00 ± 0.01	0.00 ± 0.00	4.25 ± 0.2
382	0.00 ± 0.00	0.00 ± 0.00	0.02 ± 0.03	0.01 ± 0.00	0.00 ± 0.00	0.00 ± 0.00	0.00 ± 0.01	0.12 ± 0.05	0.00 ± 0.01	0.00 ± 0.00	4.13 ± 0.3
Total Flux	0.16 ± 0.08	2.0 ± 0.2	1.3 ± 0.7	0.6 ± 0.6	0.17 ± 0.02	0.01 ± 0.01	0.5 ± 0.3	4 ± 1	0.6 ± 0.4	0.18 ± 0.07	

Table 5.N. Blank and mass corrected major element concentrations and total flux from cyclically leached partially coated WC over the period of 382 days in mgL^{-1}g^{-1}. Errors shown are 1σ, n=4.

Blank and mass corrected major element concentrations and total flux from stagnantly leached whole and cleavage edge UWS, UWC, WS and WC over a period of 382 days in $mgL^{-1}g^{-1}$. Errors shown are 1σ, n=4.

day	Al	Ca	Fe	K	Mg	Mn	Na	S	Zn	Si	pH
85	0.00 ± 0.00	0.12 ± 0.02	0.00 ± 0.00	0.06 ± 0.01	0.03 ± 0.00	0.00 ± 0.00	0.02 ± 0.02	0.06 ± 0.01	0.00 ± 0.00	0.05 ± 0.02	
150	0.00 ± 0.00	1.8 ± 0.3	0.00 ± 0.00	0.02 ± 0.03	0.39 ± 0.05	0.00 ± 0.00	0.06 ± 0.01	2.2 ± 0.4	0.00 ± 0.00	0.12 ± 0.06	6.5 ± 0.3
205	0.00 ± 0.39	1.69 ± 0.00	0.00 ± 0.02	0.21 ± 0.08	0.38 ± 0.00	0.00 ± 0.02	0.10 ± 0.00	2.44 ± 0.00	0.00 ± 0.04	0.2 ± 0.1	7.14
268	0.00 ± 0.00	3.1 ± 0.9	0.00 ± 0.00	0.4 ± 0.1	0.7 ± 0.2	0.01 ± 0.00	0.13 ± 0.03	3 ± 1	0.00 ± 0.00	0.23 ± 0.09	4.0 ± 0.6
316	0.01 ± 0.00	1.3 ± 0.4	0.01 ± 0.00	0.21 ± 0.05	0.3 ± 0.1	0.01 ± 0.00	0.06 ± 0.01	1.6 ± 0.6	0.01 ± 0.00	0.09 ± 0.03	5.3 ± 0.6
382	0.00 ± 0.00	3 ± 2	0.00 ± 0.00	0.4 ± 0.2	0.7 ± 0.4	0.01 ± 0.01	0.07 ± 0.03	3 ± 2	0.01 ± 0.01	0.15 ± 0.09	5 ± 1
Total Flux	0.02 ± 0.4	11 ± 2	0.01 ± 0.02	1.2 ± 0.2	2.5 ± 0.5	0.03 ± 0.02	0.44 ± 0.05	13 ± 3	0.02 ± 0.04	0.8 ± 0.2	

Table 5.O. UWS stagnant leachate chemistry from whole samples at two month stages over the period of 382 days.

day	Al	Ca	Fe	K	Mg	Mn	Na	S	Zn	Si	pH
85	0.00 ± 0.00	0.65 ± 0.09	0.00 ± 0.00	0.15 ± 0.03	0.14 ± 0.01	0.00 ± 0.00	0.04 ± 0.01	0.7 ± 0.2	0.00 ± 0.00	0.04 ± 0.01	7.48
150	0.00 ± 0.00	1.8 ± 0.6	0.00 ± 0.00	0.21 ± 0.07	0.34 ± 0.08	0.00 ± 0.00	0.07 ± 0.02	1.6 ± 0.4	0.00 ± 0.00	0.08 ± 0.04	7.4 ± 0.7
205	0.00 ± 0.00	1.6 ± 0.4	0.00 ± 0.00	0.22 ± 0.05	0.32 ± 0.09	0.00 ± 0.00	0.10 ± 0.04	1.8 ± 0.6	0.00 ± 0.00	0.08 ± 0.04	7.9 ± 0.4
268	0.00 ± 0.00	1.5 ± 0.6	0.00 ± 0.00	0.25 ± 0.07	0.34 ± 0.07	0.00 ± 0.00	0.11 ± 0.03	1.7 ± 0.3	0.00 ± 0.00	0.05 ± 0.03	8.0 ± 0.6
316	0.01 ± 0.00	0.5 ± 0.1	0.01 ± 0.00	0.12 ± 0.03	0.11 ± 0.03	0.01 ± 0.00	0.04 ± 0.01	0.37 ± 0.07	0.01 ± 0.00	0.04 ± 0.01	6.9 ± 0.1
382	0.00 ± 0.00	2 ± 2	0.00 ± 0.00	0.2 ± 0.1	0.4 ± 0.3	0.00 ± 0.00	0.05 ± 0.04	2 ± 2	0.00 ± 0.00	0.08 ± 0.04	6.8 ± 0.3
Total Flux	0.01 ± 0.01	8 ± 2	0.01 ± 0.00	1.2 ± 0.2	1.7 ± 0.4	0.02 ± 0.00	0.42 ± 0.06	8 ± 2	0.01 ± 0.00	0.37 ± 0.08	

Table 5.P. UWS stagnant leachate chemistry from cleavage edge samples at two month stages over the period of 382 days.

day	Al	Ca	Fe	K	Mg	Mn	Na	S	Zn	Si	pH
85	0.00 ± 0.00	0.20 ± 0.09	0.00 ± 0.00	0.04 ± 0.00	0.06 ± 0.03	0.00 ± 0.00	0.01 ± 0.00	0.08 ± 0.03	0.00 ± 0.00	0.00 ± 0.01	
150	0.00 ± 0.00	0.9 ± 0.6	0.00 ± 0.00	0.00 ± 0.01	0.3 ± 0.2	0.01 ± 0.01	0.00 ± 0.01	0.6 ± 0.4	0.00 ± 0.00	0.04 ± 0.02	7.6 ± 0.1
205	0.00 ± 0.00	1.1 ± 0.4	0.00 ± 0.00	0.1 ± 0.1	0.3 ± 0.1	0.01 ± 0.00	0.01 ± 0.00	0.3 ± 0.2	0.00 ± 0.00	0.07 ± 0.04	7.5 ± 0.2
268	0.00 ± 0.00	1.1 ± 0.7	0.00 ± 0.00	0.05 ± 0.01	0.3 ± 0.2	0.01 ± 0.01	0.00 ± 0.01	0.6 ± 0.6	0.00 ± 0.00	0.05 ± 0.01	6.9 ± 0.3
316	0.01 ± 0.00	0.2 ± 0.2	0.01 ± 0.00	0.06 ± 0.04	0.05 ± 0.04	0.02 ± 0.00	0.04 ± 0.00	0.04 ± 0.02	0.01 ± 0.00	0.06 ± 0.02	6.9 ± 0.9
Total Flux	0.03 ± 0.00	7 ± 1	0.01 ± 0.00	0.5 ± 0.1	2.0 ± 0.3	0.07 ± 0.01	0.09 ± 0.02	3.0 ± 0.7	0.02 ± 0.00	0.37 ± 0.05	

Table 5.Q. UWC stagnant leachate chemistry from whole samples at two month stages over the period of 316 days.

day	Al	Ca	Fe	K	Mg	Mn	Na	S	Zn	Si	pH
85	0.01 ± 0.00	0.09 ± 0.01	0.00 ± 0.00	0.04 ± 0.02	0.03 ± 0.01	0.00 ± 0.00	0.00 ± 0.00	0.00 ± 0.03	0.00 ± 0.00	0.00 ± 0.01	6.68
150	0.00 ± 0.00	0.16 ± 0.09	0.00 ± 0.00	0.00 ± 0.00	0.04 ± 0.03	0.00 ± 0.00	0.00 ± 0.00	0.10 ± 0.07	0.00 ± 0.00	0.01 ± 0.00	7.17 ± 0.00
205	0.00	0.00	0.00	0.03	0.00	0.00	0.02	0.00	0.00	0.00	7.80
268	0.00 ± 0.00	0.12 ± 0.07	0.00 ± 0.00	0.05 ± 0.01	0.03 ± 0.02	0.00 ± 0.00	0.00 ± 0.01	0.03 ± 0.02	0.00 ± 0.00	0.02 ± 0.01	6.8 ± 0.2
316	0.01 ± 0.00	0.4 ± 0.1	0.01 ± 0.00	0.04 ± 0.05	0.13 ± 0.03	0.02 ± 0.00	0.03 ± 0.01	0.19 ± 0.04	0.01 ± 0.00	0.10 ± 0.09	6.97 ± 0.02
Total Flux	0.02 ± 0.00	0.7 ± 0.2	0.01 ± 0.00	0.16 ± 0.06	0.23 ± 0.04	0.02 ± 0.00	0.06 ± 0.01	0.31 ± 0.09	0.01 ± 0.00	0.14 ± 0.09	

Table 5.R. UWC stagnant leachate chemistry from cleavage edge samples at two month stages over the period of 316 days.

day	Al	Ca	Fe	K	Mg	Mn	Na	S	Zn	Si	pH
85	0.3 ± 0.3	0.3 ± 0.3	6 ± 4	0.04 ± 0.01	0.2 ± 0.3	0.02 ± 0.03	0.2 ± 0.3	8 ± 3	0.3 ± 0.4	0.1 ± 0.2	
150	0.5 ± 0.4	1.3 ± 0.9	9 ± 7	0.01 ± 0.04	0.7 ± 0.6	0.03 ± 0.03	0.8 ± 0.5	13 ± 4	1 ± 0.6	0.4 ± 0.4	2.7 ± 0.2
205	0.26 ± 0.00	0.48 ± 0.00	2.74 ± 0.00	0.06 ± 0.00	0.28 ± 0.00	0.02 ± 0.00	0.29 ± 0.00	5.03 ± 0.00	0.4 ± 0.00	0.23 ± 0.00	Out of range
268	0.15 ± 0.05	0.24 ± 0.02	2.6 ± 0.7	0.01 ± 0.01	0.11 ± 0.05	0.01 ± 0.00	0.04 ± 0.07	7 ± 2	0.2 ± 0.2	0.13 ± 0.03	0.00 ± 0.00
316	0.16 ± 0.05	0.25 ± 0.09	2 ± 2	0.02 ± 0.02	0.12 ± 0.07	0.02 ± 0.01	0.3 ± 0.2	4 ± 1	0.4 ± 0.3	0.2 ± 0.1	2.6 ± 0.3
382	0.27 ± 0.08	0.2 ± 0.1	4 ± 3	0.01 ± 0.02	0.18 ± 0.04	0.01 ± 0.00	0.3 ± 0.2	8 ± 3	0.3 ± 0.2	0.3 ± 0.1	2.3 ± 0.1
Total Flux	2.0 ± 0.5	2 ± 1	35 ± 9	0.10 ± 0.05	1.3 ± 0.6	0.06 ± 0.04	1.7 ± 0.6	49 ± 6	2.6 ± 0.8	1.3 ± 0.5	

Table 5.S. WS stagnant leachate chemistry from whole samples at two month stages over the period of 316 days.

day	Al	Ca	Fe	K	Mg	Mn	Na	S	Zn	Si	pH
85	0.01 ± 0.01	0.09 ± 0.03	0.05 ± 0.07	0.03 ± 0.00	0.04 ± 0.02	0.00 ± 0.00	0.01 ± 0.00	0.3 ± 0.1	0.00 ± 0.00	0.01 ± 0.01	4.43
150	0.02 ± 0.01	0.7 ± 0.6	0.5 ± 0.3	0.00 ± 0.02	0.3 ± 0.2	0.02 ± 0.01	0.2 ± 0.2	1.9 ± 0.8	0.3 ± 0.3	0.09 ± 0.04	4.38
205	0.09 ± 0.07	0.7 ± 0.1	1.3 ± 0.9	0.02 ± 0.00	0.5 ± 0.2	0.01 ± 0.00	0.3 ± 0.2	3.3 ± 0.4	0.5 ± 0.3	0.13 ± 0.03	3.5 ± 0.4
268	0.03 ± 0.04	0.8 ± 0.6	0.3 ± 0.3	0.02 ± 0.02	0.4 ± 0.3	0.01 ± 0.01	1 ± 2	3 ± 2	2 ± 3	0.15 ± 0.08	0.00 ± 0.00
316	0.02 ± 0.00	0.21 ± 0.03	0.1 ± 0.1	0.02 ± 0.00	0.11 ± 0.03	0.01 ± 0.00	0.15 ± 0.04	0.84 ± 0.24	0.20 ± 0.06	0.07 ± 0.01	4.1 ± 0.7
Total Flux	0.17 ± 0.08	2.5 ± 0.9	2 ± 1	0.09 ± 0.03	1.3 ± 0.4	0.06 ± 0.02	2 ± 2	9 ± 3	3 ± 3	0.46 ± 0.09	

Table 5.T. WS stagnant leachate chemistry from cleavage edge samples at two month stages over the period of 316 days.

day	Al	Ca	Fe	K	Mg	Mn	Na	P	S	Zn	Si	pH
85	0.5 ± 0.1	0.52 ± 0.08	8.4 ± 0.6	0.03 ± 0.02	0.4 ± 0.2	0.03 ± 0.04	0.24 ± 0.03	0.03 ± 0.01	9.3 ± 0.3	0.37 ± 0.05	0.3 ± 0.2	
150	0.17 ± 0.07	0.20 ± 0.03	2.3 ± 1.6	0.00 ± 0.00	0.12 ± 0.04	0.00 ± 0.00	0.05 ± 0.01	0.00 ± 0.00	3.3 ± 0.9	0.10 ± 0.02	0.2 ± 0.10	3.15 ± 0.06
205	0.5 ± 0.1	0.6 ± 0.3	10 ± 3	0.01 ± 0.02	0.29 ± 0.06	0.01 ± 0.00	0.6 ± 0.5	0.00 ± 0.01	16 ± 3	0.8 ± 0.7	0.3 ± 0.7	0
268	0.5 ± 0.2	0.43 ± 0.06	10 ± 4	0.06 ± 0.02	0.24 ± 0.07	0.01 ± 0.00	0.30 ± 0.07	0.00 ± 0.03	13 ± 6	0.5 ± 0.1	0.4 ± 0.1	2.5 ± 0.2
316	0.4 ± 0.1	0.4 ± 0.2	4 ± 4	0	0.26 ± 0.04	0.02 ± 0.00	0.6 ± 0.4	0.01 ± 0.01	7 ± 6	0.8 ± 0.5	0.3 ± 0.5	2.5 ± 0.3
Total Flux	2.0 ± 0.3	2.2 ± 0.31	35 ± 7	0.10 ± 0.04	1.3 ± 0.2	0.06 ± 0.04	1.7 ± 0.6	0.04 ± 0.03	49 ± 9	2.6 ± 0.9	1.3 ± 0.3	

Table 5.U. WC stagnant leachate chemistry from whole samples at two month stages over the period of 316 days.

day	Al	Ca	Fe	K	Mg	Mn	Na	S	Zn	Si	PH
85	0.01 ± 0.00	0.2 ± 0.1	0.2 ± 0.2	0.04 ± 0.01	0.11 ± 0.07	0.00 ± 0.00	0.03 ± 0.02	2 ± 2	0.03 ± 0.02	0.01 ± 0.02	5 ± 1
150	0.01 ± 0.02	0.4 ± 0.4	0.1 ± 0.2	0.00 ± 0.02	0.3 ± 0.3	0.01 ± 0.01	0.2 ± 0.3	6 ± 3	0.2 ± 0.4	0.1 ± 0.2	7 ± 2
205	0.07 ± 0.07	0.5 ± 0.3	0.9 ± 0.7	0.04 ± 0.03	0.3 ± 0.1	0.00 ± 0.00	0.3 ± 0.1	6 ± 5	0.4 ± 0.2	0.07 ± 0.00	4.7 ± 0.8
268	0.10 ± 0.1	0.3 ± 0.2	0.6 ± 0.5	0.05 ± 0.03	0.3 ± 0.2	0.01 ± 0.00	1 ± 2	3 ± 3	2 ± 4	0.08 ± 0.04	5 ± 1
316	0.1 ± 0.1	0.3 ± 0.1	0.6 ± 0.9	0.02 ± 0.01	0.2 ± 0.1	0.02 ± 0.01	0.5 ± 0.8	3 ± 3	0.7 ± 1	0.10 ± 0.07	5 ± 2
382	0.02 ± 0.02	0.4 ± 0.2	0.2 ± 0.2	0.05 ± 0.03	0.20 ± 0.07	0.00 ± 0.00	0.2 ±0.3	2 ± 1	0.2 ± 0.3	0.2 ± 0.1	5 ± 2
Total Flux	0.3 ± 0.2	2.0 ± 0.5	3 ± 1	0.19 ± 0.05	1.3 ± 0.4	0.04 ± 0.01	3 ± 2	21 ± 7	4 ± 4	0.3 ± 0.2	

Table 5.V. WC stagnant leachate chemistry from cleavage edge samples at two month stages over the period of 316 days.

Chapter 6 Results

1st week Daily	Al	Ca	Fe	K	Mg	Na	S	Zn	Si	pH
WS initial	0.00 ± 0.00	0.02 ± 0.02	0.05 ± 0.05	0.00 ± 0.00	0.01 ± 0.00	0.00 ± 0.00	0.10 ± 0.06	0.00 ± 0.00	0.00 ± 0.00	6.25 ± 0.14
WS final	0.00 ± 0.00	0.00 ± 0.00	0.01 ± 0.00	0.00 ± 0.00	0.00 ± 0.00	0.00 ± 0.00	0.02 ± 0.01	0.00 ± 0.00	0.00 ± 0.00	6.56 ± 0.00
WC initial	0.00 ± 0.00	0.02 ± 0.01	0.02 ± 0.02	0.09 ± 0.13	0.01 ± 0.01	0.00 ± 0.00	0.07 ± 0.02	0.00 ± 0.00	0.00 ± 0.00	6.53 ± 0.11
WC final	0.00 ± 0.00	0.00 ± 0.00	0.00 ± 0.00	0.00 ± 0.00	0.00 ± 0.00	0.00 ± 0.00	0.01 ± 0.01	0.00 ± 0.00	0.00 ± 0.00	6.59 ± 0.02
UWS initial	0.00 ± 0.00	0.08 ± 0.03	0.00 ± 0.00	0.00 ± 0.00	0.01 ± 0.00	0.00 ± 0.00	0.08 ± 0.03	0.00 ± 0.00	0.00 ± 0.00	6.37 ± 0.06
UWS final	0.00 ± 0.00	0.01 ± 0.00	0.00 ± 0.00	0.00 ± 0.00	0.00 ± 0.00	0.00 ± 0.00	0.01 ± 0.00	0.00 ± 0.00	0.00 ± 0.00	6.56 ± 0.04
UWC initial	0.00 ± 0.00	0.02 ± 0.02	0.00 ± 0.00	0.00 ± 0.00	0.00 ± 0.00	0.01 ± 0.01	0.00 ± 0.00	0.00 ± 0.00	0.00 ± 0.00	6.29 ± 0.17
UWC final	0.00 ± 0.00	0.00 ± 0.00	0.00 ± 0.01	0.00 ± 0.00	0.00 ± 0.00	0.01 ± 0.01	0.00 ± 0.00	0.00 ± 0.00	0.00 ± 0.00	6.60 ± 0.04

Table 6.Ai. Initial and final lower outflow solute concentrations (mgL^{-1} ± 1σ, n=2) for all daily flushed samples, in the first week of flushing.

2nd week Daily	Al	Ca	Fe	K	Mg	Na	S	Zn	Si	pH
WS start	0.00 ± 0.00	0.01 ± 0.00	0.01 ± 0.00	0.00 ± 0.00	0.00 ± 0.00	0.00 ± 0.00	0.02 ± 0.02	0.00 ± 0.00	0.00 ± 0.00	6.48 ± 0.24
WS end	0.00 ± 0.00	0.00 ± 0.00	0.01 ± 0.00	0.00 ± 0.00	0.00 ± 0.00	0.00 ± 0.00	0.01 ± 0.00	0.00 ± 0.00	0.00 ± 0.00	6.74 ± 0.13
WC start	0.00 ± 0.00	0.01 ± 0.00	0.00 ± 0.01	0.00 ± 0.00	0.00 ± 0.00	0.00 ± 0.00	0.02 ± 0.02	0.00 ± 0.00	0.00 ± 0.00	6.51 ± 0.30
WC end	0.00 ± 0.00	0.01 ± 0.00	0.00 ± 0.01	0.00 ± 0.00	0.00 ± 0.00	0.00 ± 0.00	0.01 ± 0.02	0.00 ± 0.00	0.00 ± 0.00	6.67 ± 0.03
UWS start	0.00 ± 0.00	0.02 ± 0.01	0.00 ± 0.00	0.00 ± 0.00	0.00 ± 0.00	0.00 ± 0.00	0.02 ± 0.01	0.00 ± 0.00	0.00 ± 0.00	6.45 ± 0.05
UWS end	0.00 ± 0.00	0.02 ± 0.01	0.00 ± 0.00	0.00 ± 0.00	0.00 ± 0.00	0.00 ± 0.00	0.02 ± 0.00	0.00 ± 0.00	0.00 ± 0.00	6.74 ± 0.09
UWC start	0.00 ± 0.00	0.02 ± 0.02	0.00 ± 0.01	0.00 ± 0.00	0.00 ± 0.00	0.00 ± 0.00	0.01 ± 0.01	0.00 ± 0.00	0.00 ± 0.00	6.59
UWC end	0.00 ± 0.00	0.00 ± 0.00	0.00 ± 0.00	0.00 ± 0.00	0.00 ± 0.00	0.00 ± 0.00	0.00 ± 0.00	0.00 ± 0.00	0.00 ± 0.00	6.73 ± 0.04

Table 6.Aii. Initial and final lower outflow solute concentrations (mgL^{-1} ± 1σ, n=2) for all daily flushed samples, in the second week of flushing.

Results of flushing experiments

Major elements are described in terms of the mineral phase groups of clays (Na, K and Si), carbonates and sulphates (Ca, Mg and S) and sulphides (S, Fe and Zn). Using these divisions, the minerals undergoing dissolution can be tentatively identified. To limit the volume of data for interpretation, elements whose concentrations remained close to detection limits ($0.01 mgL^{-1}$) are ignored. In keeping with the previous chapter, values are described to two decimal places or to 1σ, depending on which is greater.

A peak in Na, K, Ca and Si leachate content occurs for all combinations of flow regimes and rock types at 47 day of the experiment. The ubiquity of this peak suggests contamination of the in-flowing Milli-RO water. Blanks were samples of Milli-RO water taken from the tubing network, i.e. the same source used on samples. Any contamination from within the supply vessel and tubing would have been removed during correction. The remaining presence of this peak suggests contamination may have occurred during sample preparation for ICP-OES analysis. Since the presence of this peak in Na, K, Ca and Si does not affect the overall pattern of elemental dissolution from samples it is described but not discussed further. An isolated peak in blank corrected Na concentration also occurs in the 120 day outflows for daily flushed upper and lower UWS, UWC and WC. The isolated nature of this peak and its appearance in daily flushed samples only suggests its origin in sample preparation for ICP-OES. This peak is also included in the description of leachate chemistry but not discussed further.

UWS

Daily Flushing – UWS

Upper UWS flushing

Daily flushing of the upper UWS with 25 mL of Milli-RO water released less than 5 $mgL^{-1}g^{-1}$ of Ca, K, S, Mg, Na and Si. Concentrations of Ca and S varied together, showing the greatest range in leachate content between $0 - 0.2 \pm 0.2$ $mgL^{-1}g^{-1}$ and $0 - 0.15 \pm 0.14$ $mgL^{-1}g^{-1}$ respectively (Table Bi). Daily flushing of the UWS produced the same trend in Ca and S dissolution. Ca and S dissolution increased to above or close to 0.07 $mgL^{-1}g^{-1}$ on days 14 to 47, reaching their maximum peak at the 70 day sampling. Concentrations for the 70 day leachate were 0.29 $mgL^{-1}g^{-1}$ of Ca with 0.25 $mgL^{-1}g^{-1}$ of S from one replicate and 0.05 $mgL^{-1}g^{-1}$ of Ca with 0.05 $mgL^{-1}g^{-1}$ of S from the second replicate. The large error associated with the 70 day Ca and S peak is therefore due to this difference. However examination of previous data indicates peak concentration from both replicate outflows (Table 6Bi). Subsequently, Ca and S concentrations fluctuated between 0.00 and 0.02 $mgL^{-1}g^{-1}$.

Concentrations of Na, Mg, K and Si all remained between 0 and 0.02 $mgL^{-1}g^{-1}$ over the period of the experiment, apart from a Na peak 0.06 ± 0.01 $mgL^{-1}g^{-1}$ at day 120. Leaching of Mg followed the same trend as Ca and S, suggesting gypsum and dolomite dissolution (Table 6Bi).

Outflow pH of the daily flushed UWS remained between 7 ± 0.15 and 6.0 ± 0.06 (Table 6Bi). The rise and fall of pH between these two extremes occurred over days 117 to 118. The pH rise coincided with a drop in S concentration and was followed by the Na peak at 200 days of daily flushing. At days 69 to 70 a pH drop of 6.49 to 6.13 coincided with the maximum peak in Ca, S and Mg concentration. Although the reason for lowered pH is not clear the consequence is increased leachate dissolved content.

Lower UWS flushing

Similar trends in outflow chemistry were shown by both upper and lower daily flushed UWS sample outflows (Table 6Bii). As the upper outflow was the leaching

media for the lower samples this is a not surprising. However yet closer inspection reveals the individual characteristics of the lower outflow.

Again, Ca and S followed similar trends during flushing, with the greatest concentration ranges of 0 - 0.12 ± 0.15 mgL^{-1}g^{-1} Ca and 0 - 0.11 ± 0.13 mgL^{-1}g^{-1} S (Table 6Bii). At day 5 an isolated peak in both Ca and S of 0.08 ± 0.03 mgL^{-1}g^{-1}, was followed by increasing release to solution up to a maximum at day 63. Between days 63 and 78 both Ca and S release dropped from 0.12 to 0.01 mgL^{-1}g^{-1} and subsequently remained below 0.02 mgL^{-1}g^{-1}. In general the decrease in Ca and S post-peak concentrations was slower than for upper sample outflow. Leaching with mineralised water may therefore encourage dissolution in the lower sample.

Lower sample K, Mg, Na and Si leachate concentrations remained between 0 - 0.02 mgL^{-1}g^{-1}, apart from a peak in Na peak of 0.04 ± 0.05 mgL^{-1}g^{-1} on day 120. Again Mg release followed the same trend as Ca and S suggesting that dolomite dissolution occurred in both upper and lower samples. Lower UWS outflow pH varied between 5.89 ± 0.11 and 6.74 ± 0.09 during daily flushing following a similar trend to that of the upper sample.

Minimum daily flushed UWS lower sample dissolution.

Although similar trends in element output are shown by both upper and lower UWS daily flushed samples, the lower leachate has its own characteristics. Over the initial 69 day flushing period, lower leachate Ca and S content was occasionally higher than the upper leachate content (Tables 6Bi-ii). Maximum concentrations also occurred at different times, with Ca and S peaks in upper and lower leachate occurring on days 70 and 63 respectively. Differences in peak occurrence indicate the control of lower leachate composition by lower sample dissolution and upper outflow leachate composition. The most obvious difference between upper and lower leachate trends in the relative smoothness of lower leachate chemical evolution.

Weekly flushing – UWS

Upper UWS weekly flushing

Weekly flushing of the upper UWS sample with Milli-RO water produced a leachate dominated by Ca and S behaviour. Leachate concentrations varied between 0 to 0.15 ± 0.13 mgL^{-1}g^{-1} Ca and 0 to 0.14 ± 0.11 mgL^{-1}g^{-1} S (Table 6Biii). During the initial days of flushing Ca and S dissolution increased then fell to a minimum at day 26. Both Ca and S rose again to their maximum concentrations at day 70, subsequently remaining below 0.05 mgL^{-1}g^{-1}. Although Si, Mg, Na and K followed the trend of Ca and S dissolution, all remained below 0.02 mgL^{-1}g^{-1} in the upper UWS weekly flushed leachate. Solution pH of the varied between 5.98 ± 0.04 and 6.72 ± 0.11, with the minimum value coinciding with peak Ca and S.

Lower UWS weekly flushing

Lower UWS outflow was derived from weekly sample flushing with the upper outflow. Leachate chemistry evolved in a pattern close to that of the upper outflow (Table 6 Biv). Again dissolved Ca and S concentrations were greatest ranging between 0.01 ± 0.02 to 0.14 ± 0.17 mgL^{-1}g^{-1} for Ca and 0 to 0.12 ± 0.18 mgL^{-1}g^{-1} for S. Dissolution of Na, Si, K and Mg remained below 0.02 mgL^{-1}g^{-1}.

Lower sample leachate pH ranged between 5.97 ± 0.06 and 6.76 ± 0.31. Two pH drops occurred at day 63 and day 117. An apparent peak in lower leachate solution content at day 70 followed the pH drop at day 63. However a pH drop and dissolved content increase in the upper outflow on day 70 probably caused the increase in dissolved content of the lower leachate. Although the second drop in lower outflow pH

coincided with a drop in upper outflow pH on day 117, dissolved content peaked in the previous week (day 108) for both outflows. Out of phase pH and dissolved content in the lower sample was therefore caused by peaks in upper outflow dissolved content.

Minimum weekly flushed UWS lower sample dissolution.

Although the upper and lower leachate for weekly flushing of the UWS showed similar patterns, the lower outflow did evolve independently (Table 6Biii-iv). Peak Ca and S in the upper outflow on day 70 of flushing also appeared in the lower outflow. However the lower outflow maximum Ca and S content occurred on day 47, with a minimum lower sample output of 0.1 $mgL^{-1}g^{-1}$ for both analyses. In general the lower sample output is higher and more consistent than the upper sample. Upper sample outflow chemistry does affect the outflow chemistry of the lower sample, probably causing the smoothing of lower outflow chemical evolution.

UWC flushing

Daily Flushing UWC

Daily Flushing of Upper UWC

Daily flushing of UWC samples with Milli-RO water removed Ca, S, K, Na and Si (Table 6Ci). Of these, Ca and S were present in the greatest quantity ranging between 0 - 0.03 ± 0.00 $mgL^{-1}g^{-1}$ of Ca and 0 - 0.01 ± 0.01 $mgL^{-1}g^{-1}$ of S. However unlike their behaviour in the UWS leachate, Ca and S release did not follow the same trends. Over the 8 to 47 day flushing period a small peak leachate content occurred with a maximum of 0.04 ± 0.00 $mgL^{-1}g^{-1}$ of K. For the remainder of leaching Ca and S fluctuated between of 0 – 0.01 ± 0.00 $mgL^{-1}g^{-1}$ concurrent with anomalous releases of K and Na. Outflow pH varied between 5.98 ± 0.04 and 6.70 ± 0.04 with no obvious correlation with leachate chemistry.

Daily Flushing of Lower UWC with upper sample outflow

Daily flushing of lower UWC with the upper outflow produced a leachate with a similar chemical evolution to its predecessor. Concentrations of Ca and S were usually between 0 and 0.03 ± 0.00 $mgL^{-1}g^{-1}$ Ca and 0 and 0.04 ± 0.03 $mgL^{-1}g^{-1}$ S (Table 6Cii). Maximum Ca concentration occurred in the 47 day flushing and the peak S concentration was in the 141 day leachate. Other dissolved elements at concentrations higher than 0.01 $mgL^{-1}g^{-1}$ during the experimental period were Na, K and Si. Their release coincided with that of S and Ca during the initial 47 days. An isolated Na peak of 0.12 ± 0.04 $mgL^{-1}g^{-1}$ occurred at day 120.

Outflow pH of the lower UWC leachate varied between 5.17 ± 1.20 and 6.84 ± 0.01. During the first 91 days of flushing pH remained relatively stable (6.28 - 6.58). Subsequent leachate pH fluctuated between 6.82 and 5.17, with minimum values followed by increased S dissolution. Pyrite oxidation may explain the large drops in pH and increased S. Any Fe released during reaction would precipitate as Fe- hydroxide as pH was greater than 4 (Stumm and Morgan 1986).

Minimum dissolution of daily flushed lower UWC

The difference between upper and lower discharges suggests little dissolution in the lower sample occurred (Table 6Ci-ii). A 0.01 - 0.02 $mgL^{-1}g^{-1}$ difference in S between days 128 to 141 represents the late stage rise in S dissolution from the lower sample.

Weekly flushing UWC

Upper UWC weekly flushing

Weekly flushing of the upper UWC with Milli-RO water produced low dissolved concentrations of Ca, K, Na, S and Si (Table 6Ciii). Increasing dissolution peaked at 0.02 - 0.03 mgL^{-1}g^{-1} for Ca, K, Na, S and Si on day 47. During the remaining period of leaching Ca, K, Na and Si content rarely rose above 0 mgL^{-1}g^{-1}. A peak in dissolved S of 0.03 ± 0.00 mgL^{-1}g^{-1} occurred over the final two sampling points.

The fall in solution pH fell from 6.75 ± 0.05 to 6.18 ± 0.14 from day 14 to 63 may have been connected to a rise in dissolved S, Na and Ca at day 63. Subsequently pH remained between 6.14 ± 0.04 and 6.51 ± 0.01, before dropping to 5.45 ± 1.90 at the same time as S dissolution increased.

Lower UWC weekly flushing

Weekly flushing of the lower UWC with upper sample outflow released concentrations of Na, Ca, Si and Mg below 0.03 mgL^{-1}g^{-1} (Table 6Civ). Peaks in Ca and S concentration of 0.03 ± 0.04 mgL^{-1}g^{-1} Ca and 0.02 ± 0.00 mgL^{-1}g^{-1} S occurred on days 128 and 141 of flushing respectively. Outflow pH for the weekly flushed, lower UWC sample, remained between 6.05 ± 0.06 and 6.69 ± 0.01 for the duration of leaching.

Difference between upper and lower weekly flushed UWC

There was little difference between the dissolution of lower and upper UWC samples (Table 6 Ciii-iv). From day 128 to 163 of flushing the lower sample release of Ca and S was greater than the upper by a maximum of 0.03 mgL^{-1}g^{-1}.

WS flushing

Unlike the UWC, flushing of WS samples with Milli-RO water and upper outflow leachate lead to dissolution of most of the major elements analysed for (Tables 6Di-iv). Output concentrations from the lower weekly flushed WS reached up to 0.25 mgL^{-1}g^{-1}, comparable with the UWS leachate. Here WS leachate for all water-rock regimes are described followed by a summary and interpretation of findings.

WS Daily flushing

Upper daily flushed WS

Daily flushed WS outflow consistently contained Fe, S and Ca (Table 6Di). Concentrations of Fe varied between 0 and 0.05 ± 0.05 mgL^{-1}g^{-1}, whilst S varied between 0 and 0.07 ± 0.07 mgL^{-1}g^{-1} throughout flushing. An initial period of Fe and S dissolution peaked at 26 days, then dropped to rise again at day 69 and the start of an intensive sampling period. Over this five day period Fe and S concentrations dropped off swiftly from a peak of 0.05 ± 0.05 mgL^{-1}g^{-1} of Fe and 0.06 ± 0.05 mgL^{-1}g^{-1} of S. Subsequently S concentrations rose to 0.04 mgL^{-1}g^{-1} whilst Fe remained at 0.01 ± 0.01 mgL^{-1}g^{-1}, up to the second intensive sampling period of 117-120 days. Here S and Fe concentrations dropped slightly, only to increase again at day 133.

Fluctuations in Fe and S dissolution can be related to Ca dissolution in some cases. Leachate Ca concentration ranged between 0 and 0.05 ± 0.01 mgL^{-1}g^{-1}, with the maximum value occurring during a drop in Fe and S at day 128. During the initial 69 days of flushing Ca tended to follow Fe and S trends. After this point Ca dissolution behaved in the opposite fashion to Fe and S. Initially prior oxidation product

dissolution, including gypsum, dominate leachate behaviour. The onset of pyrite oxidation initiated localised acidic weathering of carbonates after 69 days of flushing.

Concentrations of K, Na and Si remained below 0.04 $mgL^{-1}g^{-1}$ with peaks at day 47 for all three analytes. In the latter half of the flushing period a peak in K of 0.02 ± 0.03 occurred from day 119 to 128, possibly associated with the dissolution of jarosite $(KFe_3(SO_4)_2(OH)_6)$. A peak in Si of 0.02 ± 0.01 $mgL^{-1}g^{-1}$ was also present on day 128 concurrent with the maximum Ca concentration. This suggests that acidic weathering may have led to clay dissolution at day 128.

WS daily outflow pH ranged between 6.62 ± 0.02 and 4.93 ± 0.68. In the later half of the experiment minimum pH values coincided with peaks in Fe and S release. The relatively high pH values for leachate on days 78 to 108 were associated with carbonate dissolution, demonstrated by dissolved Ca concentrations over this period.

Lower daily flushed WS

Flushing of the lower WS sample with outflow from the upper sample produced a leachate with a similar chemical trend to that of the upper outflow (Table 6Dii).

Dissolved Fe and S varied between 0 to 0.10 ± 0.13 $mgL^{-1}g^{-1}$ and 0.01 ± 0.01 to 0.13 ± 0.17 $mgL^{-1}g^{-1}$ respectively. Outside of peak concentrations, Fe and S release remained between 0.01 to 0.04 $mgL^{-1}g^{-1}$. Concurrent peaks in Fe and S concentration occurred at days 55, 70 and 117 to 133. Leachate Ca content varied between 0 to 0.04 ± 0.05 $mgL^{-1}g^{-1}$ with peaks at days 1, 55 and 128. Dissolved concentrations of Na, K, Mg, Si and Zn were below 0.03 $mgL^{-1}g^{-1}$ during leaching. For Na, K and Si release was associated with the 55 day peak in Fe and S and the 117-133 day period. Correlation between K and the release of Fe and S was particularly strong over the 117-133 period suggesting the dissolution of jarosite.

Daily flushed lower WS outflow pH fluctuated between 4.79 and 6.62 ± 0.08. Changes in pH can be linked to the total dissolved content of leachate. During the initial peak in Fe, S and Ca concentration up to day 55 of flushing, solution pH decreased. From day 55 to 117 pH varied between 6.44 and 5.76. Subsequently pH fell to 5.25 during the second intensive sampling period (day 118). Combined Ca release and pH rise to 6.36 ± 0.13 in the day 128 leachate may have been a result of carbonate leaching. However a release of 0.05 ± 0.01 $mgL^{-1}g^{-1}$ from the upper sample is probably the main source of the lower leachate Ca.

Minimum output of daily flushed lower WS

Differences in upper and lower outflow contents suggest that both samples released similar concentrations of Fe, S and Ca (Table 6Di-ii). Lower sample minimum input ranged between 0.01and 0.12 $mgL^{-1}g^{-1}$ and lower outflow chemistry was strongly controlled by lower sample dissolution. During the initial 63 days of flushing, the lower sample constantly released a minimum of below 0.03 $mgL^{-1}g^{-1}$ of Ca and S. Leachate of pH >5 during the initial 63 days encouraged Fe–hydroxide precipitation and lowered dissolved Fe. Subsequent rises in lower sample Fe and S output usually coincided with large pH drops. After the 63 day flushing point dissolved Ca fell until the start of the second intensive sampling period at day 118. The similarity in upper and lower leachate Ca content during this period suggests that the lower leachate peak is a remnant of upper leachate Ca. The low difference between upper and lower outflow K suggests jarosite dissolution only occurred in the upper sample at 118 to 128 days. WS Weekly flushing

Upper WS weekly flushing

Predominant dissolved species in the weekly flushed WS upper outflow were Fe, S and Ca (Table 6Diii). Concentrations of Fe and S ranged between 0 to 0.03 ± 0.03

$mgL^{-1}g^{-1}$ and 0 to 0.05 ± 0.04 $mgL^{-1}g^{-1}$ respectively for the duration of the experiment. Dissolved Fe and S concentrations peaked on days 8 and 70.

Release of Ca followed Fe and S trends, varying between 0 - 0.03 ± 0.00 $mgL^{-1}g^{-1}$. However the maximum dissolved Ca occurred at day 47. This Ca peak concurred with those of K, Mg, Na and Si. Release of up to 0.01 $mgL^{-1}g^{-1}$ of Zn coincided with peaks in S concentration. The late stage correlation of Fe, S, Na and Ca on days 70 to 108 may be due to the dissolution of calcite and natro-jarosite ($NaFe_3(SO_4)_2(OH)_6$).

Drops in outflow pH usually followed peaks in Fe and S dissolution, with pH fluctuating between 5.43 ± 0.86 and 6.79 ± 0.03. The large error in the minimum pH value is due to differences in pyrite content and therefore leachate pH, between the two replicate WS samples. Unlike daily flushed WS leachate, pH for weekly Milli-RO water flushed WS increased at the end of the experiment.

Lower WS weekly flushing

Exposure of WS to the upper sample outflow described above lead to increased dissolved content following the same trends (Table 6Div). Concentrations of Fe ranged between 0 – 0.11 ± 0.13 $mgL^{-1}g^{-1}$ and S between 0 – 0.25 ± 0.29 $mgL^{-1}g^{-1}$ throughout flushing, with peak concentrations at day 78.

Leachate Ca content evolved in a similar pattern as S and Fe, although the day 1 sample contained 0.13 $mgL^{-1}g^{-1}$ Ca compared to 0 $mgL^{-1}g^{-1}$ Fe. Except for the day 1 and a 78 day peak of 0.05 ± 0.06 $mgL^{-1}g^{-1}$, dissolved Ca remained between 0 and 0.03 ± 0.01 $mgL^{-1}g^{-1}$.

Most other analytes including Al, K, Mg, Na, Zn and Si reached maximum concentrations at or below 0.03 $mgL^{-1}g^{-1}$ in the 78 day outflow. Aside from this peak Zn dissolution coincided with S release, as did Mg with Ca release and Al was detected in almost all leachates after 70 days of the experiment. Outflow pH varied between 4.66 ± 0.88 and 6.29 ± 0.34, correlating well with dissolved content. Minimum pH at day 78 corresponded to the maximum concentration for most analytes. Similarly drops in pH between days 108 to 117 and 141 to 163 relate to high dissolved leachate contents. Between days 128 to 133 a rise in pH to 6.29 coincided with Mg and Ca dissolution, suggesting dolomite leaching.

Minimum output of weekly flushed lower WS

The difference in the lower and upper outflow contents indicates that the lower sample was releasing S, Fe and Ca at values below 0.1 $mgL^{-1}g^{-1}$ throughout leaching (Tables 6Diii-iv). The peak in the day 78 sample contained peaks for all element analysed for. A rise in lower sample pH and drop in dissolved content followed this peak. The rapid removal of the day 78 peak in element washout suggests that some slaking may have occurred for the WS sample.

WC

WC Daily flushing

Upper daily flushed WC

Upper WC outflow most consistently contained S usually accompanied by Ca, Fe and Na. Leachate S varied between 0 and 0.07 ± 0.05 $mgL^{-1}g^{-1}$ and Fe from 0 to 0.05 ± 0.06 $mgL^{-1}g^{-1}$ (Table 6Ei). Maximum values for Fe and S coincided on day 70 of leaching.

Solution Ca content was relatively low at 0 to 0.03 ± 0.00 mgL^{-1}g^{-1}, reaching its maximum at day 47. High Na, K and Si concentrations occurred at day 47 followed by a peak in Na alone of 0.06 ± 0.05 mgL^{-1}g^{-1} at day 120.

Daily flushed WC outflow pH remained between 5.48 ± 0.95 and 6.69 ± 0.41 with drops in pH occurring over or at the start of intensive sampling (Figure 6.22). Increased flushing of prior oxidation products caused falling pH over the first intensive sampling period (69 to 78 days). At the start of the second intensive flushing period (117-120 days) pH fell then rose over the remaining days. Flushing of weathering products formed during experimental leaching occurred on day 117. The following rise in pH may have been due to dilution or neutralisation. Release of low of Ca 0.01 ± 0.01 mgL^{-1}g^{-1} on days 118 to 119 suggests that dilution of dissolved species caused solution pH to rise.

Lower daily flushed WC

Lower WC out-flow usually contained Ca, Fe, S and Na, however Na, K Si and Zn were released intermittently (Table 6Eii). An initial peak in Ca, Fe, K, Mg and S concentrations occurred at the 5 day flushing with an upper limit of 0.09 ± 0.13 mgL^{-1}g^{-1} of K. During the initial period dissolution of easily soluble prior weathering products such as jarosite occurred in the weathered rock-type. A subsequent of 0.04 ± 0.03 mgL^{-1}g^{-1} of S and 0.01 ± 0.01 mgL^{-1}g^{-1} of Fe occurred on day 26. For the remainder of the experiment dissolved S content ranged between 0 to 0.05 ± 0.03 mgL^{-1}g^{-1} with Fe at the lower range of 0 to 0.01 mgL^{-1}g^{-1}.

Dissolved Ca, K, Na and Si of less than 0.06 ± 0.00 mgL^{-1}g^{-1} formed a peak in leachate concentration on day 47.

Lower WC outflow pH ranged between 5.34 ± 0.30 and 6.74. Similarity in pH trends of lower and upper WC leachates suggests that strong patterns in the upper leachate can be identified in lower leachate chemistry.

Minimum dissolution of lower flushed WC

Differences between lower and upper WC leachate confirm Fe, Ca, K, Na and S as the most consistently released analytes from lower WC daily flushing (Tables 6Ei-ii). Calculated concentrations reached by all dissolved analytes in solution were of the same order as those in the upper outflow, i.e. above 0.01 mgL^{-1}g^{-1}.

WC Weekly Flushing

Upper weekly flushed WC

Weekly flushing of the WC sample with Milli-RO water released low concentrations of Ca, Fe, Na, Si and S, with none released at concentrations greater than 0.04 mgL^{-1}g^{-1} (Table 6Eiii). Leachate Fe and S rose to a peak within 14 days of weekly flushing, with the actual S maximum concentration occurring in the samples at day 141.

At day 47 there was an initial peak in Ca, K, Na and Si concentrations of close to 0.03 mgL^{-1}g^{-1}. Maximum Ca release of 0.04 ± 0.06 mgL^{-1}g^{-1} coincided with the S peak in the day 141 leachate.

Outflow pH for the WC weekly flushed sample varied little between 5.53 ± 0.25 to 6.58 ± 0.11. Minimum pH occurred at day 120 and was followed by a slow rise until day 141. Carbonate dissolution and the release of Ca into the day 141 outflow caused the observed rising pH.

Lower weekly flushed WC

Weekly flushing of WC with upper sample outflow dissolved greater concentrations of all analyses than in the original upper outflow (Table 6Eiv). Dissolved S

concentration showed no isolated peaks. Concentrations of S varied from 0.01 ± 0.01 mgL^{-1}g^{-1} to 0.13 ± 0.13 mgL^{-1}g^{-1} yet usually remained greater than 0.06 mgL^{-1}g^{-1}. Outflow Fe content ranged between 0 and 0.05 ± 0.07 mgL^{-1}g^{-1}, also with no isolated peaks.

Peaks in Na, Mg, K, Al and Ca concentration were concurrent at day 47, days 70 - 78, days 108 - 117 and day 141. These pulses in leachate concentration usually did not rise above 0.02 mgL^{-1}g^{-1}. However an isolated Ca peak of 0.05 ± 0.07 mgL^{-1}g^{-1} coincided with elevated K and S concentrations in the day 141 leachate.

Dissolution of Zn of up to 0.02 ± 0.02 mgL^{-1}g^{-1} followed that of S suggesting that either during or prior to the experiment, sphalerite had been oxidised.

Lower outflow pH varied between 4.97 ± 1.22 and 6.50 ± 0.12. Overall pH remained below 6 except at the maximum value of 6.50 ± 0.12 on day 14 of flushing. Changes in pH tended to be slightly out of step with dissolved content variation. Low pH values were recorded in leachate following samples with low dissolved S and Fe concentration. However pH variation was also mirrored by changes in upper outflow values. Flushing media chemistry may have controlled the lower leachate final pH.

Minimum output of lower weekly flushed WC

The difference between upper and lower sample outflows suggests that the lower sample released Fe, S, Ca, Al, Mg, K, Na, Zn and Si (Tables 6Eiii and iv). Concentrations of Fe and S remained between 0.01 and 0.06 mgL^{-1}g^{-1} of Fe and 0.01 and 0.13 mgL^{-1}g^{-1} of S. Other elements were released at concentration below 0.01 mgL^{-1}g^{-1}. The peak in Ca concentration at day 141 of upper sample leaching is also found in the lower sample leachate. As with pH, the concentration of some analytes is controlled by the upper sample chemistry.

Tables of mean pH and major element concentration ($mgL^{-1}g^{-1}$) in outflow water from flow experiment over 163 days. Flow regime, rock type and sample position (i.e. upper sample - 50 mL of purifed water, lower sample - 25 mL of outflow from upper sample per flushing). Errors shown are 1σ (n=2), where no error is shown n=1, where calculated 1σ = 0.00 value is below detection.

day	Ca	K	Mg	Na	S	Si	pH
1	0.00 ± 0.00	0.00 ± 0.00	0.00 ± 0.00	0.00 ± 0.00	0.00 ± 0.00	0.00 ± 0.00	-
5	0.00 ± 0.00	0.00 ± 0.00	0.00 ± 0.00	0.00 ± 0.00	0.00 ± 0.00	0.00 ± 0.00	6.32
8	0.01 ± 0.00	0.00 ± 0.00	0.00 ± 0.00	0.00 ± 0.00	0.00 ± 0.00	0.00 ± 0.00	6.33 ± 0.04
14	0.05 ± 0.02	0.00 ± 0.00	0.00 ± 0.00	0.00 ± 0.00	0.04 ± 0.02	0.00 ± 0.00	6.42 ± 0.08
26	0.08 ± 0.05	0.00 ± 0.00	0.01 ± 0.00	0.01 ± 0.00	0.07 ± 0.04	0.01 ± 0.00	6.26 ± 0.08
47	0.04 ± 0.00	0.02 ± 0.01	0.01 ± 0.00	0.01 ± 0.00	0.02 ± 0.00	0.02 ± 0.00	6.26 ± 0.01
55	0.00 ± 0.00	0.00 ± 0.00	0.00 ± 0.00	0.00 ± 0.00	0.00 ± 0.00	0.00 ± 0.00	± 0.00
63	0.01 ± 0.00	0.00 ± 0.00	0.00 ± 0.00	0.01 ± 0.00	0.01 ± 0.00	0.00 ± 0.00	6.32 ± 0.02
69	0.01 ± 0.01	0.00 ± 0.00	0.00 ± 0.00	0.00 ± 0.00	0.02 ± 0.00	0.00 ± 0.00	6.49 ± 0.06
70	0.2 ± 0.2	0.00 ± 0.00	0.01 ± 0.01	0.01 ± 0.00	0.15 ± 0.14	0.00 ± 0.00	6.13 ± 0.02
72	0.01 ± 0.00	0.00 ± 0.00	0.00 ± 0.00	0.01 ± 0.01	0.01 ± 0.00	0.00 ± 0.00	6.27 ± 0.04
73	0.01 ± 0.01	0.00 ± 0.00	0.00 ± 0.00	0.01 ± 0.01	0.01 ± 0.01	0.00 ± 0.00	6.26 ± 0.05
78	0.00 ± 0.01	0.00 ± 0.00	0.00 ± 0.00	0.01 ± 0.00	0.00 ± 0.01	0.00 ± 0.00	6.1 ± 0.3
91	0.01 ± 0.00	0.00 ± 0.00	0.00 ± 0.00	0.00 ± 0.00	0.00 ± 0.00	0.00 ± 0.00	6.5 ± 0.2
108	0.00 ± 0.00	0.00 ± 0.00	0.00 ± 0.00	0.01 ± 0.00	0.01 ± 0.00	0.00 ± 0.00	6.62 ± 0.01
117	0.00 ± 0.00	0.00 ± 0.00	0.00 ± 0.00	0.00 ± 0.00	0.01 ± 0.00	0.00 ± 0.00	6.00 ± 0.06
118	0.00 ± 0.00	0.01 ± 0.01	0.00 ± 0.00	0.00 ± 0.00	0.00 ± 0.00	0.00 ± 0.00	7.3 ± 0.2
119	0.00 ± 0.00	0.00 ± 0.00	0.00 ± 0.00	0.00 ± 0.00	0.00 ± 0.00	0.00 ± 0.00	6.6 ± 0.
120	0.00 ± 0.00	0.00 ± 0.00	0.00 ± 0.00	0.06 ± 0.01	0.02 ± 0.00	0.00 ± 0.00	6.51 ± 0.02
128	0.02 ± 0.01	0.00 ± 0.00	0.00 ± 0.00	0.00 ± 0.00	0.00 ± 0.00	0.00 ± 0.00	6.3 ± 0.2
133	0.02 ± 0.02	0.00 ± 0.00	0.00 ± 0.00	0.00 ± 0.00	0.01 ± 0.01	0.00 ± 0.00	6.43 ± 0.04
141	0.00 ± 0.00	0.00 ± 0.00	0.00 ± 0.00	0.00 ± 0.00	0.00 ± 0.00	0.00 ± 0.00	6.6 ± 0.3
163	0.01 ± 0.00	0.01 ± 0.01	0.00 ± 0.00	0.00 ± 0.00	0.01 ± 0.01	0.00 ± 0.00	6.74 ± 0.02
Total Flux	0.47 ± 0.18	0.06 ± 0.02	0.05 ± 0.01	0.14 ± 0.02	0.43 ± 0.15	0.04 ± 0.01	

Table 6Bi. Mean daily outflow chemistry from upper UWS duplicate samples.

Day	Ca	K	Mg	Na	S	Si	pH
1	0.01 ± 0.01	0.00 ± 0.00	0.00 ± 0.00	0.00 ± 0.00	0.01 ± 0.01	0.00 ± 0.00	6.33 ± 0.04
5	0.08 ± 0.03	0.00 ± 0.00	0.01 ± 0.00	0.00 ± 0.00	0.08 ± 0.03	0.00 ± 0.00	6.37 ± 0.06
8	0.01 ± 0.00	0.00 ± 0.00	0.00 ± 0.00	0.00 ± 0.00	0.00 ± 0.00	0.00 ± 0.00	6.17 ± 0.02
14	0.02 ± 0.01	0.00 ± 0.00	0.00 ± 0.00	0.00 ± 0.00	0.02 ± 0.01	0.00 ± 0.00	6.45 ± 0.05
26	0.04 ± 0.01	0.01 ± 0.00	0.01 ± 0.00	0.00 ± 0.00	0.03 ± 0.01	0.01 ± 0.00	6.30 ± 0.04
47	0.06 ± 0.00	0.01 ± 0.02	0.01 ± 0.00	0.01 ± 0.01	0.06 ± 0.02	0.01 ± 0.02	6.20 ± 0.00
55	0.01 ± 0.01	0.01 ± 0.00	0.00 ± 0.00	0.00 ± 0.00	0.01 ± 0.01	0.00 ± 0.00	
63	0.12 ± 0.15	0.01 ± 0.01	0.01 ± 0.01	0.01 ± 0.01	0.11 ± 0.13	0.00 ± 0.00	6.32 ± 0.10
69	0.08 ± 0.09	0.01 ± 0.00	0.01 ± 0.01	0.01 ± 0.00	0.06 ± 0.01	0.00 ± 0.00	6.31 ± 0.24
70	0.07 ± 0.05	0.01 ± 0.01	0.01 ± 0.01	0.01 ± 0.01	0.07 ± 0.06	0.00 ± 0.00	6.33 ± 0.06
72	0.01 ± 0.01	0.00 ± 0.00	0.00 ± 0.00	0.00 ± 0.00	0.01 ± 0.01	0.00 ± 0.00	6.33 ± 0.16
73	0.03 ± 0.02	0.01 ± 0.00	0.00 ± 0.00	0.00 ± 0.00	0.03 ± 0.02	0.01 ± 0.01	6.24 ± 0.12
78	0.02 ± 0.01	0.02 ± 0.01	0.01 ± 0.00	0.00 ± 0.01	0.01 ± 0.00	0.01 ± 0.00	6.15 ± 0.04
91	0.00 ± 0.00	0.00 ± 0.00	0.00 ± 0.00	0.00 ± 0.00	0.00 ± 0.01	0.00 ± 0.00	6.47
108	0.01 ± 0.00	0.00 ± 0.00	0.00 ± 0.00	0.00 ± 0.00	0.01 ± 0.00	0.00 ± 0.00	6.64 ± 0.06
117	0.01 ± 0.01	0.00 ± 0.00	0.00 ± 0.00	0.00 ± 0.00	0.01 ± 0.01	0.00 ± 0.00	5.89 ± 0.11
118	0.01 ± 0.01	0.01 ± 0.00	0.00 ± 0.00	0.00 ± 0.00	0.01 ± 0.01	0.00 ± 0.00	6.72 ± 0.00
119	0.01 ± 0.01	0.01 ± 0.00	0.00 ± 0.00	0.00 ± 0.00	0.01 ± 0.01	0.00 ± 0.00	6.69 ± 0.05
120	0.00 ± 0.00	0.00 ± 0.00	0.00 ± 0.00	0.04 ± 0.05	0.01 ± 0.00	0.00 ± 0.00	6.51 ± 0.05
128	0.02 ± 0.00	0.00 ± 0.00	0.00 ± 0.00	0.00 ± 0.00	0.00 ± 0.00	0.00 ± 0.00	6.21 ± 0.10
133	0.01 ± 0.00	0.00 ± 0.00	0.00 ± 0.00	0.00 ± 0.00	0.01 ± 0.00	0.00 ± 0.00	6.31 ± 0.40
141	0.01 ± 0.01	0.00 ± 0.00	0.00 ± 0.00	0.00 ± 0.00	0.00 ± 0.00	0.00 ± 0.00	6.73 ± 0.02
163	0.02 ± 0.00	0.01 ± 0.01	0.00 ± 0.00	0.00 ± 0.00	0.01 ± 0.00	0.00 ± 0.00	6.70
Total Flux	0.63 ± 0.19	0.10 ± 0.03	0.08 ± 0.02	0.09 ± 0.06	0.6 ± 0.2	0.05 ± 0.02	

Table 6Bii. Mean daily outflow chemistry from lower UWS duplicate samples.

Day	Ca	K	Mg	Na	S	Si	pH
1	0.00 ± 0.00	0.00 ± 0.00	0.00 ± 0.00	0.00 ± 0.00	0.00 ± 0.00	0.00 ± 0.00	-
8	0.07 ± 0.03	0.00 ± 0.00	0.01 ± 0.00	0.00 ± 0.00	0.05 ± 0.03	0.00 ± 0.00	-
14	0.05 ± 0.01	0.00 ± 0.00	0.00 ± 0.00	0.00 ± 0.00	0.03 ± 0.01	0.00 ± 0.00	6.41 ± 0.08
26	0.04 ± 0.04	0.00 ± 0.00	0.00 ± 0.00	0.00 ± 0.00	0.04 ± 0.03	0.01 ± 0.00	6.55 ± 0.06
47	0.02 ± 0.01	0.02 ± 0.00	0.00 ± 0.00	0.01 ± 0.01	0.01 ± 0.01	0.02 ± 0.00	6.31 ± 0.07
55	0.01 ± 0.01	0.01 ± 0.01	0.00 ± 0.00	0.00 ± 0.00	0.00 ± 0.01	0.00 ± 0.00	-
63	0.01 ± 0.00	0.00 ± 0.00	0.00 ± 0.00	0.00 ± 0.00	0.02 ± 0.01	0.00 ± 0.00	6.09 ± 0.08
70	0.15 ± 0.13	0.00 ± 0.00	0.01 ± 0.01	0.01 ± 0.00	0.14 ± 0.11	0.00 ± 0.00	5.98 ± 0.04
78	0.02 ± 0.01	0.01 ± 0.00	0.00 ± 0.00	0.00 ± 0.00	0.02 ± 0.01	0.00 ± 0.00	6.62 ± 0.01
91	0.04 ± 0.02	0.00 ± 0.00	0.00 ± 0.00	0.00 ± 0.00	0.02 ± 0.03	0.00 ± 0.00	6.72 ± 0.11
108	0.05 ± 0.04	0.00 ± 0.00	0.00 ± 0.00	0.01 ± 0.00	0.05 ± 0.04	0.00 ± 0.00	6.58 ± 0.06
117	0.01 ± 0.00	0.00 ± 0.00	0.00 ± 0.00	0.00 ± 0.00	0.03 ± 0.00	0.00 ± 0.00	5.99 ± 0.01
128	0.03 ± 0.01	0.00 ± 0.00	0.00 ± 0.00	0.00 ± 0.00	0.00 ± 0.00	0.00 ± 0.00	6.52 ± 0.02
133	0.02 ± 0.00	0.00 ± 0.00	0.00 ± 0.00	0.00 ± 0.00	0.01 ± 0.00	0.00 ± 0.00	6.06 ± 0.40
141	0.01 ± 0.01	0.01 ± 0.01	0.00 ± 0.00	0.00 ± 0.00	0.00 ± 0.00	0.00 ± 0.00	6.49 ± 0.16
163	0.03 ± 0.03	0.01 ± 0.00	0.00 ± 0.00	0.00 ± 0.00	0.02 ± 0.02	0.00 ± 0.00	6.80 ± 0.08
Total Flux	0.6 ± 0.2	0.07 ± 0.01	0.05 ± 0.01	0.03 ± 0.01	0.5 ± 0.1	0.03 ± 0.00	

Table 6Biii. Mean weekly outflow chemistry from upper UWS duplicate samples.

day	Ca	K	Mg	Na	S	Si	pH
1	0.03 ± 0.04	0.00 ± 0.00	0.00 ± 0.00	0.00 ± 0.00	0.03 ± 0.03	0.00 ± 0.00	6.31 ± 0.08
14	0.05 ± 0.03	0.00 ± 0.00	0.00 ± 0.00	0.00 ± 0.00	0.04 ± 0.03	0.00 ± 0.00	6.10 ± 0.07
26	0.04 ± 0.01	0.01 ± 0.00	0.01 ± 0.00	0.00 ± 0.00	0.03 ± 0.01	0.01 ± 0.00	6.56 ± 0.08
47	0.14 ± 0.17	0.04 ± 0.02	0.02 ± 0.02	0.02 ± 0.00	0.12 ± 0.18	0.02 ± 0.01	6.28 ± 0.02
55	0.01 ± 0.02	0.01 ± 0.01	0.00 ± 0.00	0.00 ± 0.00	0.01 ± 0.02	0.00 ± 0.00	-
63	0.04 ± 0.02	0.00 ± 0.00	0.01 ± 0.00	0.02 ± 0.01	0.05 ± 0.02	0.00 ± 0.00	6.01 ± 0.00
70	0.07 ± 0.06	0.01 ± 0.00	0.01 ± 0.01	0.01 ± 0.00	0.07 ± 0.06	0.00 ± 0.00	6.10 ± 0.10
78	0.03 ± 0.01	0.01 ± 0.00	0.01 ± 0.00	0.00 ± 0.00	0.03 ± 0.01	0.00 ± 0.00	6.54 ± 0.04
91	0.06 ± 0.01	0.00 ± 0.00	0.01 ± 0.00	0.01 ± 0.01	0.05 ± 0.00	0.00 ± 0.00	6.56 ± 0.17
108	0.06 ± 0.03	0.00 ± 0.00	0.01 ± 0.00	0.02 ± 0.00	0.07 ± 0.04	0.00 ± 0.00	6.62 ± 0.01
117	0.04 ± 0.01	0.00 ± 0.01	0.00 ± 0.00	0.00 ± 0.00	0.06 ± 0.02	0.00 ± 0.00	5.97 ± 0.06
128	0.02 ± 0.01	0.00 ± 0.00	0.00 ± 0.00	0.00 ± 0.00	0.00 ± 0.00	0.00 ± 0.00	6.23 ± 0.12
133	0.05 ± 0.04	0.00 ± 0.00	0.01 ± 0.00	0.00 ± 0.00	0.04 ± 0.03	0.00 ± 0.00	6.76 ± 0.31
141	0.08 ± 0.11	0.01 ± 0.00	0.01 ± 0.01	0.00 ± 0.00	0.00 ± 0.00	0.00 ± 0.00	6.60 ± 0.08
163	0.07 ± 0.04	0.02 ± 0.01	0.01 ± 0.01	0.00 ± 0.00	0.06 ± 0.04	0.00 ± 0.00	6.70 ± 0.00
Total Flux	0.47 ± 0.00	0.10 ± 0.00	0.08 ± 0.00	0.08 ± 0.00	0.45 ± 0.00	0.03 ± 0.00	

Table 6Biv. Mean weekly outflow chemistry from lower UWS duplicate samples.

day	Ca	K	Na	S	Si	pH
1	0.00 ± 0.00	0.00 ± 0.00	0.00 ± 0.00	0.00 ± 0.00	0.00 ± 0.00	-
5	0.00 ± 0.00	0.00 ± 0.00	0.00 ± 0.00	0.00 ± 0.00	0.00 ± 0.00	6.56 ± 0.31
8	0.01 ± 0.00	0.00 ± 0.00	0.00 ± 0.00	0.00 ± 0.00	0.00 ± 0.00	6.36 ± 0.01
14	0.01 ± 0.00	0.00 ± 0.00	0.00 ± 0.01	0.00 ± 0.00	0.00 ± 0.00	6.02 ± 0.02
26	0.01 ± 0.00	0.01 ± 0.00	0.01 ± 0.01	0.01 ± 0.00	0.01 ± 0.00	6.51 ± 0.01
47	0.03 ± 0.00	0.04 ± 0.00	0.03 ± 0.00	0.00 ± 0.00	0.03 ± 0.00	6.37 ± 0.02
55	0.00 ± 0.00	0.00 ± 0.00	0.00 ± 0.00	0.00 ± 0.00	0.00 ± 0.00	0.00 ± 0.00
63	0.00 ± 0.00	0.00 ± 0.00	0.00 ± 0.00	0.00 ± 0.00	0.00 ± 0.00	6.44 ± 0.01
69	0.00 ± 0.00	0.00 ± 0.00	0.00 ± 0.01	0.01 ± 0.00	0.00 ± 0.00	6.63 ± 0.04
70	0.01 ± 0.00	0.00 ± 0.00	0.00 ± 0.00	0.01 ± 0.00	0.00 ± 0.00	6.52 ± 0.06
72	0.00 ± 0.00	0.00 ± 0.01	0.00 ± 0.00	0.01 ± 0.00	0.00 ± 0.00	6.40 ± 0.08
73	0.00 ± 0.00	0.00 ± 0.00	0.01 ± 0.01	0.00 ± 0.00	0.00 ± 0.01	6.52 ± 0.01
78	0.01 ± 0.00	0.00 ± 0.00	0.00 ± 0.00	0.01 ± 0.00	0.00 ± 0.00	6.22 ± 0.12
91	0.01 ± 0.00	0.00 ± 0.00	0.01 ± 0.02	0.00 ± 0.00	0.00 ± 0.00	6.49 ± 0.11
108	0.00 ± 0.00	0.00 ± 0.00	0.00 ± 0.00	0.00 ± 0.00	0.00 ± 0.00	6.66 ± 0.00
117	0.00 ± 0.00	0.00 ± 0.00	0.00 ± 0.00	0.00 ± 0.00	0.00 ± 0.00	5.98 ± 0.04
118	0.00 ± 0.00	0.02 ± 0.00	0.00 ± 0.00	0.00 ± 0.00	0.00 ± 0.00	6.92 ± 0.25
119	0.00 ± 0.00	0.00 ± 0.00	0.01 ± 0.01	0.00 ± 0.00	0.00 ± 0.00	6.70 ± 0.04
120	0.00 ± 0.00	0.00 ± 0.00	0.07 ± 0.04	0.00 ± 0.00	0.00 ± 0.00	6.46 ± 0.33
128	0.01 ± 0.00	0.00 ± 0.00	0.00 ± 0.00	0.00 ± 0.00	0.00 ± 0.00	6.53 ± 0.00
133	0.00 ± 0.00	0.00 ± 0.00	0.00 ± 0.00	0.00 ± 0.00	0.00 ± 0.00	6.27 ± 0.27
141	0.00 ± 0.00	0.01 ± 0.02	0.00 ± 0.00	0.01 ± 0.01	0.00 ± 0.00	6.67 ± 0.11
163	0.00 ± 0.00	0.01 ± 0.01	0.00 ± 0.00	0.01 ± 0.00	0.00 ± 0.00	6.74
Total Flux	0.11 ± 0.01	0.10 ± 0.02	0.17 ± 0.05	0.08 ± 0.01	0.05 ± 0.01	

Table 6Ci. Mean daily outflow chemistry from upper UWC duplicate samples.

day	Ca	K	Na	S	Si	pH
1	0.00 ± 0.00	0.00 ± 0.00	0.00 ± 0.00	0.01 ± 0.02	0.00 ± 0.00	6.28 ± 0.18
5	0.00 ± 0.00	0.00 ± 0.00	0.01 ± 0.01	0.00 ± 0.00	0.00 ± 0.00	6.29 ± 0.17
8	0.01 ± 0.00	0.00 ± 0.00	0.00 ± 0.00	0.00 ± 0.00	0.00 ± 0.00	6.54 ± 0.05
14	0.02 ± 0.02	0.00 ± 0.00	0.00 ± 0.00	0.01 ± 0.01	0.00 ± 0.00	6.59
26	0.01 ± 0.00	0.01 ± 0.00	0.01 ± 0.00	0.01 ± 0.00	0.01 ± 0.00	6.44
47	0.03 ± 0.00	0.03 ± 0.00	0.03 ± 0.01	0.00 ± 0.00	0.03 ± 0.00	6.37 ± 0.01
55	0.00 ± 0.00	0.00 ± 0.00	0.00 ± 0.00	0.00 ± 0.00	0.00 ± 0.00	-
63	0.01 ± 0.00	0.00 ± 0.00	0.00 ± 0.00	0.00 ± 0.00	0.00 ± 0.00	6.45
69	0.00 ± 0.00	0.00 ± 0.00	0.01 ± 0.01	0.01 ± 0.00	0.00 ± 0.00	6.54 ±0 .03
70	0.00 ± 0.00	0.00 ± 0.00	0.01 ± 0.01	0.01 ± 0.00	0.00 ± 0.00	6.56 ±0 .08
72	0.00 ± 0.00	0.00 ± 0.00	0.00 ± 0.00	0.01 ± 0.00	0.00 ± 0.00	6.40 ± 0.04
73	0.01 ± 0.00	0.00 ± 0.00	0.01 ± 0.00	0.00 ± 0.00	0.01 ± 0.00	6.58
78	0.01 ± 0.00	0.01 ± 0.00	0.01 ± 0.00	0.01 ± 0.00	0.00 ± 0.00	6.37 ± 0.03
91	0.01 ± 0.00	0.00 ± 0.00	0.02 ± 0.00	0.00 ± 0.00	0.00 ± 0.00	6.56 ± 0.06
108	0.00 ± 0.00	0.00 ± 0.00	0.00 ± 0.00	0.00 ± 0.00	0.00 ± 0.00	6.65 ± 0.01
117	0.00 ± 0.00	0.00 ± 0.00	0.00 ± 0.00	0.00 ± 0.00	0.00 ± 0.00	6.05 ± 0.01
118	0.00 ± 0.00	0.00 ± 0.00	0.00 ± 0.00	0.00 ± 0.00	0.00 ± 0.00	6.82 ± 0.01
119	0.00 ± 0.00	0.01 ± 0.00	0.02 ± 0.02	0.00 ± 0.00	0.00 ± 0.00	6.71 ± 0.02
120	0.00 ± 0.00	0.00 ± 0.00	0.12 ± 0.04	0.01 ± 0.00	0.00 ± 0.00	6.84 ± 0.01
128	0.01 ± 0.00	0.00 ± 0.00	0.00 ± 0.00	0.00 ± 0.00	0.00 ± 0.00	5.17 ± 1.20
133	0.01 ± 0.00	0.00 ± 0.00	0.00 ± 0.00	0.00 ± 0.00	0.00 ± 0.00	5.72 ± 1.07
141	0.00 ± 0.00	0.01 ± 0.01	0.01 ± 0.01	0.04 ± 0.03	0.00 ± 0.00	6.69 ± 0.03
163	0.00 ± 0.00	0.01 ± 0.01	0.00 ± 0.00	0.01 ± 0.00	0.00 ± 0.00	-
Total Flux	0.13 ± 0.02	0.09 ± 0.02	0.26 ± 0.05	0.13 ± 0.04	0.05 ± 0.00	

Table 6Cii. Mean daily outflow chemistry from lower UWC duplicate samples.

Day	Ca	K	Na	S	Si	pH
1	0.01	0.00	0.00	0.00	0.00	0.00
8	0.00 ± 0.00	0.00 ± 0.00	0.00 ± 0.00	0.00 ± 0.00	0.00 ± 0.00	-
14	0.01 ± 0.01	0.00 ± 0.00	0.00 ± 0.00	0.00 ± 0.00	0.00 ± 0.00	6.75 ± 0.05
26	0.01	0.00	0.02	0.01	0.01 ± 0.01	6.59 ± 0.05
47	0.02 ± 0.00	0.03 ± 0.00	0.02 ± 0.01	0.00 ± 0.00	0.02 ± 0.01	6.51 ± 0.05
55	0.00 ± 0.00	0.02 ± 0.01	0.00 ± 0.01	0.00 ± 0.00	0.00 ± 0.00	0.00 ± 0.00
63	0.01 ± 0.00	0.00 ± 0.01	0.02 ± 0.00	0.01 ± 0.00	0.00 ± 0.00	6.18 ± 0.14
70	0.00 ± 0.00	0.00 ± 0.00	0.00 ± 0.01	0.00 ± 0.00	0.00 ± 0.00	6.41 ± 0.04
78	0.01 ± 0.00	0.00 ± 0.00	0.00 ± 0.00	0.01 ± 0.00	0.00 ± 0.00	6.64 ± 0.03
91	0.00 ± 0.00	0.00 ± 0.00	0.00 ± 0.00	0.00 ± 0.00	0.00 ± 0.00	6.58 ± 0.08
108	0.00 ± 0.00	0.00 ± 0.00	0.01 ± 0.00	0.00 ± 0.00	0.00 ± 0.00	6.62 ± 0.04
117	0.00 ± 0.00	0.00 ± 0.00	0.00 ± 0.01	0.00 ± 0.00	0.00 ± 0.00	6.14 ± 0.01
128	0.00 ± 0.00	0.00 ± 0.00	0.00 ± 0.00	0.00 ± 0.00	0.00 ± 0.00	6.53 ± 0.06
133	0.00 ± 0.00	0.00 ± 0.00	0.00 ± 0.00	0.00 ± 0.00	0.00 ± 0.00	6.51 ± 0.01
141	0.00 ± 0.00	0.00 ± 0.00	0.00 ± 0.00	0.03 ± 0.00	0.00 ± 0.00	5.45 ± 1.90
163	0.00 ± 0.00	0.01 ± 0.00	0.00 ± 0.00	0.01 ± 0.04	0.00 ± 0.00	6.80
Total Flux	0.09 ± 0.01	0.01 ± 0.03	0.07 ± 0.02	0.07 ± 0.04	0.01 ± 0.01	

Table 6Ciii. Mean weekly outflow chemistry from upper UWC duplicate samples.

Day	Ca	K	Na	S	Si	pH
1	0.00	0.00	0.00	0.00	0.00	6.40
14	0.01 ± 0.00	0.00 ± 0.00	0.00 ± 0.00	0.00 ± 0.00	0.00 ± 0.00	6.29 ± 0.01
47	0.03	0.03	0.01 ± 0.00	0.00	0.03	6.35
55	0.00 ± 0.00	0.01 ± 0.01	0.00 ± 0.00	0.00 ± 0.00	0.00 ± 0.00	0.00 ± 0.00
63	0.01 ± 0.00	0.00 ± 0.00	0.01 ± 0.00	0.01 ± 0.00	0.00 ± 0.00	6.17 ± 0.19
70	0.00 ± 0.00	0.00 ± 0.00	0.00 ± 0.00	0.01 ± 0.00	0.00 ± 0.00	6.39 ± 0.01
78	0.01 ± 0.00	0.00 ± 0.00	0.01 ± 0.01	0.01 ± 0.00	0.00 ± 0.00	6.63 ± 0.01
91	0.01 ± 0.00	0.00 ± 0.00	0.00 ± 0.00	0.00 ± 0.00	0.00 ± 0.00	6.52 ± 0.01
108	0.00 ± 0.00	0.00 ± 0.00	0.00 ± 0.00	0.00 ± 0.00	0.00 ± 0.00	6.59 ± 0.06
117	0.00 ± 0.00	0.00 ± 0.00	0.00 ± 0.00	0.00 ± 0.00	0.00 ± 0.00	6.05 ± 0.06
128	0.03 ± 0.04	0.00 ± 0.00	0.00 ± 0.00	0.01 ± 0.01	0.00 ± 0.00	6.08 ± 0.30
133	0.01 ± 0.00	0.00 ± 0.00	0.00 ± 0.00	0.00 ± 0.00	0.00 ± 0.00	6.69 ± 0.01
141	0.02 ± 0.00	0.01 ± 0.00	0.00 ± 0.00	0.02 ± 0.00	0.00 ± 0.00	6.55 ± 0.23
163	0.00 ± 0.00	0.02 ± 0.01	0.01 ± 0.01	0.01 ± 0.00	0.00 ± 0.00	6.64 ± 0.16
Total Flux	0.13 ± 0.04	0.07 ± 0.01	0.04 ± 0.01	0.08 ± 0.01	0.03 ± 0.00	

Table 6Civ. Mean weekly outflow chemistry from lower UWC duplicate samples.

Day	Al	Ca	Fe	K	Na	S	Si	pH
1	0.00 ± 0.00	0.01 ± 0.01	0.00 ± 0.00	0.00 ± 0.00	0.00 ± 0.00	0.01 ± 0.00	0.00 ± 0.00	-
5	0.00 ± 0.00	0.00 ± 0.00	0.00 ± 0.00	0.00 ± 0.00	0.00 ± 0.00	0.00 ± 0.00	0.00 ± 0.00	6.27 ± 0.00
8	0.00 ± 0.00	0.01 ± 0.01	0.00 ± 0.00	0.00 ± 0.00	0.00 ± 0.00	0.01 ± 0.00	0.00 ± 0.00	6.31 ± 0.03
14	0.00 ± 0.00	0.01 ± 0.00	0.01 ± 0.00	0.00 ± 0.00	0.00 ± 0.00	0.02 ± 0.00	0.00 ± 0.00	6.31 ± 0.03
26	0.00 ± 0.00	0.02 ± 0.02	0.04 ± 0.05	0.01 ± 0.00	0.02 ± 0.00	0.07 ± 0.07	0.01 ± 0.00	6.20 ± 0.10
47	0.00 ± 0.00	0.03 ± 0.01	0.02 ± 0.01	0.03 ± 0.00	0.04 ± 0.03	0.03 ± 0.01	0.04 ± 0.01	6.10 ± 0.08
55	0.00 ± 0.00	0.00 ± 0.00	0.01 ± 0.00	0.00 ± 0.00	0.00 ± 0.00	0.00 ± 0.00	0.00 ± 0.00	-
63	0.00 ± 0.00	0.00 ± 0.00	0.00 ± 0.00	0.00 ± 0.00	0.00 ± 0.00	0.00 ± 0.00	0.00 ± 0.00	6.29 ± 0.3
69	0.00 ± 0.00	0.01 ± 0.00	0.05 ± 0.05	0.00 ± 0.00	0.01 ± 0.01	0.06 ± 0.05	0.00 ± 0.00	6.23 ± 0.39
70	0.00 ± 0.00	0.00 ± 0.00	0.02 ±0 .02	0.00 ± 0.00	0.00 ± 0.01	0.04 ± 0.03	0.00 ± 0.00	6.33 ± 0.55
72	0.00 ± 0.00	0.00 ± 0.00	0.01 ± 0.00	0.00 ± 0.00	0.00 ± 0.00	0.02 ± 0.00	0.00 ± 0.00	6.30 ± 0.13
73	0.00 ± 0.00	0.01 ± 0.00	0.01 ± 0.00	0.00 ± 0.00	0.01 ± 0.00	0.02 ± 0.00	0.00 ± 0.01	5.03 ± 0.48
78	0.00 ± 0.00	0.01 ± 0.00	0.01 ± 0.01	0.00 ± 0.00	0.01 ± 0.01	0.03 ± 0.01	0.00 ± 0.00	6.09 ± 0.1
91	0.02 ± 0.03	0.01 ± 0.00	0.00 ± 0.00	0.00 ± 0.00	0.00 ± 0.00	0.02 ± 0.01	0.00 ± 0.00	6.61
108	0.03 ± 0.04	0.00 ± 0.00	0.02 ± 0.01	0.00 ± 0.00	0.00 ± 0.01	0.04 ± 0.01	0.00 ± 0.00	6.21 ± 0.06
117	0.00 ± 0.00	0.00 ± 0.00	0.04 ± 0.05	0.00 ± 0.00	0.00 ± 0.00	0.04 ± 0.05	0.00 ± 0.00	4.93 ± 0.68
118	0.00 ± 0.00	0.00 ± 0.00	0.01 ± 0.00	0.01 ± 0.01	0.01 ± 0.02	0.02 ± 0.01	0.00 ± 0.00	6.62 ± 0.02
119	0.00 ± 0.00	0.01 ± 0.01	0.01 ± 0.01	0.02 ± 0.03	0.00 ± 0.00	0.03 ± 0.01	0.00 ± 0.00	6.37 ± 0.06
120	0.00 ± 0.00	0.01 ± 0.01	0.01 ± 0.01	0.02 ± 0.03	0.00 ± 0.00	0.03 ± 0.01	0.00 ± 0.00	6.01 ± 0.59
128	0.00 ± 0.01	0.05 ± 0.01	0.00 ± 0.00	0.02 ± 0.01	0.00 ± 0.00	0.00 ± 0.00	0.02 ± 0.01	5.67 ± 0.93
133	0.00 ± 0.00	0.02 ± 0.01	0.02 ± 0.03	0.00 ± 0.00	0.00 ± 0.00	0.05 ± 0.06	0.00 ± 0.00	5.21 ± 1.48
141	0.03 ± 0.03	0.00 ± 0.01	0.02 ± 0.03	0.00 ± 0.00	0.01 ± 0.00	0.01 ± 0.00	0.00 ± 0.00	5.65
163	0.03 ± 0.04	0.00 ± 0.00	0.01 ± 0.01	0.01 ± 0.02	0.01 ± 0.01	0.04 ± 0.00	0.00 ± 0.00	6.84
Total Flux	0.08 ± 0.08	0.14 ± 0.06	0.12 ± 0.06	0.30 ± 0.10	0.06 ± 0.04	0.25 ± 0.11	0.05 ± 0.04	

Table 6Di. Mean daily outflow chemistry from upper WS duplicate samples.

day	Ca	Fe	K	Mg	Na	S	Zn	Si	pH
1	0.04 ± 0.05	0.02 ± 0.02	0.00 ± 0.00	0.00 ± 0.01	0.00 ± 0.00	0.07 ± 0.06	0.01 ± 0.01	0.00 ± 0.00	-
5	0.01 ± 0.00	0.03 ± 0.01	0.00 ± 0.00	0.00 ± 0.00	0.00 ± 0.00	0.05 ± 0.00	0.00 ± 0.00	0.00 ± 0.00	5.15
8	0.01 ± 0.01	0.01 ± 0.01	0.00 ± 0.00	0.00 ± 0.00	0.00 ±0 .00	0.03 ± 0.01	0.00 ± 0.00	0.00 ± 0.00	6.62 ± 0.08
14	0.01 ± 0.00	0.00 ± 0.00	0.00 ± 0.00	0.00 ± 0.00	0.01 ± 0.01	0.01 ± 0.00	0.00 ± 0.00	0.00 ± 0.00	5.96 ± 0.49
26	0.02 ± 0.01	0.01 ± 0.01	0.00 ± 0.00	0.00 ± 0.00	0.01 ± 0.01	0.04 ± 0.05	0.00 ± 0.00	0.01 ± 0.01	6.34 ± 0.42
47	0.02 ± 0.02	0.01 ± 0.00	0.02 ± 0.03	0.00 ± 0.00	0.02 ± 0.03	0.02 ± 0.01	0.00 ± 0.00	0.02 ± 0.03	5.60 ± 0.47
55	0.04 ± 0.05	0.03 ± 0.04	0.00 ± 0.01	0.00 ± 0.01	0.00 ± 0.01	0.08 ± 0.12	0.00 ± 0.00	0.01 ± 0.01	5.10
63	0.02 ± 0.02	0.01 ± 0.01	0.02 ± 0.03	0.00 ± 0.00	0.03 ±0.04	0.02 ± 0.01	0.00 ± 0.00	0.02 ± 0.02	6.41
69	0.00 ± 0.00	0.02 ± 0.03	0.00 ± 0.00	0.00 ± 0.00	0.00 ± 0.00	0.03 ± 0.01	0.00 ± 0.00	0.00 ± 0.00	6.06 ± 0.83
70	0.01 ± 0.01	0.08 ± 0.11	0.00 ± 0.00	0.00 ± 0.00	0.01 ± 0.02	0.09 ± 0.10	0.00 ± 0.00	0.00 ± 0.00	6.49 ± 0.21
72	0.00 ± 0.00	0.01 ± 0.01	0.00 ± 0.00	0.00 ± 0.00	0.01 ± 0.01	0.02 ± 0.01	0.00 ± 0.00	0.00 ± 0.00	6.44 ± 0.13
73	0.01 ± 0.00	0.01 ± 0.01	0.00 ± 0.00	0.00 ± 0.00	0.02 ± 0.01	0.03 ± 0.01	0.01 ± 0.01	0.01 ± 0.01	5.79 ± 0.64
78	0.01 ± 0.01	0.01 ± 0.00	0.00 ± 0.00	0.00 ± 0.00	0.00 ± 0.00	0.02 ± 0.00	0.00 ± 0.00	0.00 ± 0.00	5.76 ± 0.50
91	0.01 ± 0.01	0.02 ± 0.03	0.00 ± 0.01	0.00 ± 0.00	0.00 ± 0.02	0.04 ± 0.04	0.00 ± 0.00	0.00 ± 0.01	6.22 ± 0.35
108	0.01 ± 0.01	0.01 ± 0.00	0.00 ± 0.00	0.00 ± 0.00	0.00 ± 0.01	0.03 ± 0.01	0.00 ± 0.00	0.00 ± 0.00	6.54 ± 0.15
117	0.00 ± 0.00	0.01 ± 0.00	0.00 ± 0.00	0.00 ± 0.00	0.01 ± 0.01	0.02 ± 0.01	0.00 ± 0.00	0.00 ± 0.00	5.44 ± 0.17
118	0.02 ± 0.0	0.08 ± 0.09	0.01 ± 0.00	0.00 ± 0.00	0.00 ± 0.00	0.11 ± 0.10	0.00 ± 0.00	0.00 ± 0.00	5.25 ± 1.70
119	0.00 ± 0.00	0.10 ± 0.13	0.01 ± 0.00	0.00 ± 0.00	0.00 ± 0.00	0.11 ± 0.12	0.00 ± 0.00	0.00 ± 0.00	5.88 ± 1.04
120	0.01 ± 0.01	0.06 ± 0.07	0.01 ± 0.00	0.00 ± 0.00	0.00 ± 0.00	0.08 ± 0.08	0.00 ± 0.00	0.00 ± 0.00	5.45 ± 1.58
128	0.04 ± 0.02	0.10 ± 0.14	0.02 ± 0.02	0.01 ± 0.00	0.00 ± 0.00	0.13 ± 0.17	0.01 ± 0.00	0.01 ± 0.01	6.36 ± 0.13
133	0.01 ± 0.01	0.10 ± 0.14	0.00 ± 0.00	0.00 ± 0.00	0.00 ± 0.00	0.13 ± 0.17	0.00 ± 0.00	0.00 ± 0.00	5.97 ± 0.27
141	0.02 ± 0.03	0.04 ± 0.05	0.02 ± 0.02	0.00 ± 0.00	0.00 ± 0.00	0.01 ± 0.01	0.00 ± 0.00	0.01 ± 0.01	6.11 ± 0.62
163	0.00 ± 0.00	0.00 ± 0.01	0.00 ± 0.00	0.00 ± 0.00	0.01 ± 0.02	0.03 ± 0.00	0.00 ± 0.00	0.00 ± 0.00	4.79
Total Flux	0.31 ± 0.07	0.77 ± 0.29	0.13 ± 0.02	0.05 ± 0.01	0.13 ± 0.03	1.22 ± 0.33	0.05 ± 0.01	0.08 ± 0.01	

Table 6Dii. Mean daily outflow chemistry from lower WS duplicate samples.

day	Ca	Fe	K	Mg	Na	S	Zn	Si	pH
1	0.00 ± 0.00	0.01 ± 0.01	0.00 ± 0.00	0.00 ± 0.00	0.00 ± 0.01	0.02 ± 0.01	0.00 ± 0.00	0.00 ± 0.00	0.00
8	0.02 ± 0.01	0.03 ± 0.00	0.00 ± 0.00	0.00 ± 0.00	0.00 ± 0.01	0.07 ± 0.00	0.00 ± 0.00	0.00 ± 0.00	0.00 ± 0.00
14	0.02 ± 0.01	0.01 ± 0.01	0.00 ± 0.00	0.00 ± 0.00	0.00 ± 0.00	0.02 ± 0.01	0.01 ± 0.01	0.00 ± 0.00	6.14
26	0.02 ± 0.00	0.01 ± 0.00	0.01 ± 0.00	0.00 ± 0.00	0.00 ± 0.00	0.02 ± 0.01	0.00 ± 0.00	0.01 ± 0.00	6.31 ± 0.13
47	0.03 ± 0.00	0.01 ± 0.01	0.03 ± 0.00	0.01 ± 0.00	0.03 ± 0.02	0.03 ± 0.02	0.01 ± 0.01	0.03 ± 0.00	6.08 ± 0.34
55	0.00 ± 0.00	0.01 ± 0.01	0.00 ± 0.00	0.00 ± 0.00	0.00 ± 0.00	0.01 ± 0.01	0.01 ± 0.01	0.00 ± 0.00	0.00
63	0.00 ± 0.00	0.00 ± 0.00	0.00 ± 0.00	0.00 ± 0.00	0.00 ± 0.00	0.02 ± 0.01	0.00 ± 0.00	0.00 ± 0.00	5.90 ± 0.06
70	0.02 ± 0.00	0.03 ± 0.03	0.00 ± 0.00	0.00 ± 0.00	0.01 ± 0.01	0.05 ± 0.04	0.01 ± 0.01	0.00 ± 0.00	6.35 ± 0.12
78	0.01 ± 0.00	0.01 ± 0.01	0.00 ± 0.00	0.00 ± 0.00	0.02 ± 0.01	0.02 ± 0.02	0.00 ± 0.00	0.00 ± 0.00	5.61 ± 0.62
91	0.01 ± 0.00	0.01 ± 0.00	0.00 ± 0.00	0.00 ± 0.00	0.02 ± 0.01	0.03 ±0 .02	0.00 ± 0.00	0.00 ± 0.00	6.28 ± 0.16
108	0.01 ± 0.02	0.01 ± 0.01	0.01 ± 0.01	0.00 ± 0.00	0.01 ± 0.00	0.04 ± 0.04	0.01 ± 0.01	0.00 ± 0.00	6.46 ± 0.22
117	0.00 ± 0.00	0.01 ± 0.01	0.00 ± 0.00	0.00 ± 0.00	0.00 ± 0.00	0.02 ± 0.03	0.00 ± 0.01	0.00 ± 0.00	5.43 ± 0.86
128	0.01 ± 0.00	0.00 ± 0.00	0.00 ± 0.00	0.00 ± 0.00	0.00 ± 0.00	0.00 ± 0.00	0.00 ± 0.00	0.00 ± 0.00	6.37 ± 0.18
133	0.01 ± 0.00	0.00 ± 0.00	0.00 ± 0.00	0.00 ± 0.00	0.00 ± 0.00	0.01 ± 0.00	0.00 ± 0.00	0.00 ± 0.00	6.35 ± 0.09
141	0.00 ± 0.00	0.00 ± 0.00	0.01 ± 0.02	0.00 ± 0.00	0.00 ± 0.00	0.00 ± 0.00	0.00 ± 0.00	0.00 ± 0.00	6.59 ± 0.07
163	0.00 ± 0.00	0.00 ± 0.00	0.02 ± 0.00	0.00 ± 0.00	0.00 ± 0.00	0.00 ± 0.00	0.00 ± 0.00	0.00 ± 0.00	6.79 ± 0.03
Total Flux	0.15 ± 0.03	0.14 ± 0.05	0.09 ± 0.03	0.03 ± 0.00	0.10 ± 0.05	0.37 ± 0.11	0.06 ± 0.03	0.04 ± 0.01	

Table 6Diii. Mean weekly outflow chemistry from upper WS duplicate samples.

day	Al	Ca	Fe	K	Mg	Na	S	Zn	Si	pH
1	0.00	0.13	0.00	0.00	0.01	0.01	0.11	0.00	0.00	6.17
8	0	0	0	0	0	0	0	0	0	0.00
14	0.00 ± 0.00	0.02 ± 0.01	0.03 ± 0.01	0.00 ± 0.00	0.01 ± 0.00	0.00 ± 0.01	0.09 ± 0.05	0.01 ± 0.00	0.00 ± 0.00	5.40 ± 0.72
26	0.00 ± 0.00	0.01 ± 0.01	0.01 ± 0.01	0.00 ± 0.00	0.00 ± 0.00	0.01 ± 0.01	0.05 ± 0.05	0.00 ± 0.00	0.01 ± 0.01	5.84 ± 1.06
47	0.00 ± 0.00	0.03 ± 0.01	0.02 ± 0.01	0.02 ± 0.02	0.01 ± 0.00	0.02 ± 0.01	0.07 ± 0.02	0.01 ± 0.00	0.02 ± 0.01	5.55 ± 0.75
55	0.00 ± 0.00	0.00 ± 0.00	0.02 ± 0.00	0.01 ± 0.00	0.00 ± 0.00	0.00 ± 0.00	0.03 ± 0.03	0.01 ± 0.00	0.00 ± 0.00	0.00
63	0.00 ± 0.00	0.01 ± 0.00	0.04 ± 0.00	0.00 ± 0.00	0.01 ± 0.00	0.00 ± 0.00	0.11 ± 0.01	0.01 ± 0.00	0.00 ± 0.00	5.92 ± 0.18
70	0.00 ± 0.01	0.01 ± 0.01	0.03 ± 0.03	0.00 ± 0.00	0.00 ± 0.00	0.03 ± 0.01	0.08 ± 0.07	0.01 ± 0.00	0.00 ± 0.00	5.48 ± 1.12
78	0.02 ± 0.02	0.05 ± 0.06	0.11 ± 0.13	0.00 ± 0.00	0.02 ± 0.03	0.03 ± 0.01	0.25 ± 0.29	0.03 ± 0.03	0.00 ± 0.00	4.66 ± 0.88
91	0.00 ± 0.00	0.01 ± 0.01	0.00 ± 0.00	0.00 ± 0.00	0.00 ± 0.00	0.00 ± 0.00	0.03 ± 0.02	0.00 ± 0.00	0.00 ± 0.00	6.22
108	0.01 ± 0.01	0.02 ± 0.02	0.05 ± 0.05	0.00 ± 0.00	0.01 ± 0.01	0.01 ± 0.02	0.14 ± 0.13	0.01 ± 0.01	0.00 ± 0.00	5.48 ± 1.19
117	0.01 ± 0.01	0.00 ± 0.00	0.04 ± 0.04	0.00 ± 0.00	0.00 ± 0.00	0.00 ± 0.00	0.09 ± 0.08	0.01 ± 0.00	0.00 ± 0.00	5.23 ± 0.81
128	0.01 ± 0.01	0.01 ± 0.01	0.01 ± 0.02	0.00 ± 0.00	0.01 ± 0.01	0.00 ± 0.00	0.02 ± 0.03	0.00 ± 0.01	0.00 ± 0.00	6.29 ± 0.34
133	0.01 ± 0.01	0.01 ± 0.00	0.02 ± 0.03	0.00 ± 0.00	0.01 ± 0.01	0.00 ± 0.00	0.06 ± 0.06	0.00 ± 0.00	0.00 ± 0.00	5.27 ± 1.34
141	0.01 ± 0.00	0.00 ± 0.00	0.04 ± 0.02	0.01 ± 0.01	0.00 ± 0.00	0.00 ± 0.00	0.04 ± 0.05	0.00 ± 0.00	0.00 ± 0.00	4.71 ± 0.29
163	0.01 ± 0.02	0.00 ± 0.00	0.05 ± 0.07	0.05 ± 0.07	0.01 ± 0.01	0.00 ± 0.00	0.10 ± 0.12	0.01 ± 0.01	0.00 ± 0.00	5.49 ± 1.57
Total Flux	0.08 ± 0.03	0.33 ± 0.07	0.46 ± 0.17	0.10 ± 0.07	0.10 ± 0.03	0.12 ± 0.03	1.25 ± 0.37	0.12 ± 0.04	0.03 ± 0.00	

Table 6Div. Mean weekly outflow chemistry from lower WS duplicate samples.

day	Ca	Fe	K	Na	S	Si	pH
1	0.00 ± 0.00	0.00 ± 0.00	0.00 ± 0.00	0.00 ± 0.00	0.01 ± 0.01	0.00 ± 0.00	-
5	0.00 ± 0.00	0.00 ± 0.00	0.00 ± 0.00	0.00 ± 0.00	0.00 ± 0.00	0.00 ± 0.00	6.35 ± 0.04
8	0.01 ± 0.00	0.00 ± 0.00	0.00 ± 0.00	0.00 ± 0.00	0.01 ± 0.00	0.00 ± 0.00	6.69 ± 0.41
14	0.01 ± 0.00	0.01 ± 0.01	0.00 ± 0.00	0.01 ± 0.02	0.01 ± 0.00	0.00 ± 0.00	6.69 ± 0.41
26	0.01 ± 0.00	0.00 ± 0.00	0.00 ± 0.00	0.01 ± 0.00	0.02 ± 0.00	0.01 ± 0.00	6.21 ± 0.09
47	0.03 ± 0.00	0.00 ± 0.00	0.03 ± 0.00	0.02 ± 0.01	0.00 ± 0.00	0.03 ± 0.00	6.22 ± 0.06
55	0.00 ± 0.00	0.00 ± 0.00	0.00 ± 0.00	0.00 ± 0.00	0.00 ± 0.00	0.00 ± 0.00	0.00 ± 0.00
63	0.00 ± 0.00	0.00 ± 0.00	0.00 ± 0.00	0.00 ± 0.01	0.01 ± 0.00	0.00 ± 0.00	6.29 ± 0.21
69	0.00 ± 0.00	0.00 ± 0.00	0.00 ± 0.00	0.00 ± 0.00	0.01 ± 0.00	0.00 ± 0.00	6.49 ± 0.04
70	0.01 ± 0.00	0.05 ± 0.06	0.00 ± 0.00	0.01 ± 0.00	0.07 ± 0.05	0.00 ± 0.00	6.20 ± 0.57
72	0.00 ± 0.00	0.02 ± 0.01	0.00 ± 0.00	0.01 ± 0.00	0.03 ± 0.01	0.00 ± 0.00	6.15 ± 0.14
73	0.00 ± 0.00	0.01 ± 0.01	0.00 ± 0.00	0.01 ± 0.01	0.02 ± 0.01	0.00 ± 0.00	6.05 ± 0.21
78	0.01 ± 0.00	0.01 ± 0.00	0.00 ± 0.00	0.01 ± 0.00	0.03 ± 0.00	0.00 ± 0.00	5.70 ± 0.64
91	0.00 ± 0.00	0.00 ± 0.00	0.00 ± 0.00	0.00 ± 0.00	0.01 ± 0.01	0.00 ± 0.00	6.44 ± 0.06
108	0.00 ± 0.00	0.01 ± 0.01	0.00 ± 0.00	0.00 ± 0.00	0.03 ± 0.01	0.00 ± 0.00	6.43 ± 0.11
117	0.00 ± 0.00	0.01 ± 0.02	0.00 ± 0.00	0.00 ± 0.00	0.03 ± 0.00	0.00 ± 0.00	5.48 ± 0.95
118	0.00 ± 0.00	0.02 ± 0.01	0.02 ± 0.00	0.00 ± 0.00	0.03 ± 0.01	0.00 ± 0.00	6.43 ± 0.25
119	0.00 ± 0.00	0.01 ± 0.01	0.00 ± 0.00	0.01 ± 0.00	0.02 ± 0.01	0.00 ± 0.00	6.40 ± 0.15
120	0.00 ± 0.00	0.00 ± 0.00	0.00 ± 0.00	0.06 ± 0.05	0.03 ± 0.00	0.00 ± 0.00	6.46 ± 0.10
128	0.00 ± 0.00	0.00 ± 0.00	0.00 ± 0.00	0.00 ± 0.00	0.00 ± 0.00	0.00 ± 0.00	6.28 ± 0.13
133	0.00 ± 0.00	0.01 ± 0.01	0.00 ± 0.00	0.00 ± 0.00	0.02 ± 0.01	0.00 ± 0.00	6.11 ± 0.32
141	0.00 ± 0.00	0.00 ± 0.00	0.00 ± 0.00	0.00 ± 0.00	0.00 ± 0.00	0.00 ± 0.00	6.48 ± 0.30
163	0.00 ± 0.00	0.00 ± 0.00	0.00 ± 0.00	0.00 ± 0.00	0.03 ± 0.00	0.00 ± 0.00	6.64 ± 0.04
Total Flux	0.10 ± 0.01	0.19 ± 0.07	0.06 ± 0.01	0.15 ± 0.05	0.42 ± 0.06	0.04 ± 0.00	

Table 6Ei. Mean daily outflow chemistry from upper WC duplicate samples.

Day	Ca	Fe	K	Mg	Na	S	Zn	Si	pH
1	0.01 ± 0.00	0.00 ± 0.00	0.00 ± 0.00	0.00 ± 0.00	0.00 ± 0.00	0.01 ± 0.00	0.00 ± 0.00	0.00 ± 0.00	6.19 ± 0.00
5	0.02 ± 0.01	0.02 ± 0.02	0.09 ± 0.13	0.01 ± 0.01	0.00 ± 0.00	0.07 ± 0.02	0.00 ± 0.00	0.00 ± 0.00	6.53 ± 0.11
8	0.01 ± 0.01	0.00 ± 0.00	0.00 ± 0.00	0.00 ± 0.00	0.00 ± 0.00	0.01 ± 0.00	0.00 ± 0.00	0.00 ± 0.00	6.23 ± 0.56
14	0.01 ± 0.00	0.00 ± 0.00	0.00 ± 0.00	0.00 ± 0.00	0.00 ± 0.00	0.02 ± 0.02	0.00 ± 0.00	0.00 ± 0.00	6.51 ± 0.30
26	0.02 ± 0.00	0.01 ± 0.01	0.00 ± 0.00	0.01 ± 0.00	0.01 ± 0.00	0.04 ± 0.03	0.00 ± 0.00	0.01 ± 0.00	6.23 ± 0.18
47	0.04 ± 0.00	0.00 ± 0.00	0.06 ± 0.00	0.01 ± 0.00	0.03 ± 0.00	0.01 ± 0.00	0.00 ± 0.00	0.04 ± 0.00	6.24 ± 0.08
55	0.00 ± 0.00	0.00 ± 0.00	0.00 ± 0.00	0.00 ± 0.00	0.00 ± 0.00	0.00 ± 0.00	0.00 ± 0.00	0.00 ± 0.00	0.00 ± 0.00
63	0.01 ± 0.00	0.00 ± 0.00	0.00 ± 0.01	0.00 ± 0.00	0.01 ± 0.01	0.02 ± 0.00	0.00 ± 0.00	0.00 ± 0.00	6.44 ± 0.08
69	0.00 ± 0.00	0.01 ± 0.01	0.00 ± 0.00	0.00 ± 0.00	0.00 ± 0.00	0.02 ± 0.01	0.00 ± 0.00	0.00 ± 0.00	6.42 ± 0.18
70	0.01 ± 0.00	0.01 ± 0.01	0.00 ± 0.00	0.00 ± 0.00	0.04 ± 0.02	0.04 ± 0.02	0.02 ± 0.00	0.00 ± 0.00	6.49 ± 0.26
72	0.00 ± 0.00	0.01 ± 0.01	0.00 ± 0.00	0.00 ± 0.00	0.02 ± 0.00	0.04 ± 0.02	0.00 ± 0.00	0.00 ± 0.00	6.19 ± 0.11
73	0.01 ± 0.00	0.01 ± 0.01	0.01 ± 0.01	0.00 ± 0.00	0.01 ± 0.02	0.03 ± 0.02	0.00 ± 0.00	0.01 ± 0.00	5.93 ± 0.01
78	0.02 ± 0.01	0.01 ± 0.01	0.01 ± 0.01	0.00 ± 0.00	0.02 ± 0.02	0.04 ± 0.02	0.00 ± 0.00	0.00 ± 0.00	6.02 ± 0.35
91	0.00 ± 0.00	0.00 ± 0.01	0.01 ± 0.02	0.00 ± 0.00	0.00 ± 0.00	0.00 ± 0.00	0.00 ± 0.00	0.00 ± 0.00	6.54 ± 0.05
108	0.00 ± 0.00	0.01 ± 0.02	0.00 ± 0.00	0.00 ± 0.00	0.00 ± 0.00	0.04 ± 0.03	0.00 ± 0.00	0.00 ± 0.00	6.48 ± 0.11
117	0.00 ± 0.00	0.01 ± 0.00	0.00 ± 0.00	0.00 ± 0.00	0.00 ± 0.00	0.02 ± 0.02	0.00 ± 0.00	0.00 ± 0.00	5.34 ± 0.30
118	0.01 ± 0.01	0.01 ± 0.00	0.01 ± 0.00	0.00 ± 0.00	0.01 ± 0.02	0.04 ± 0.04	0.00 ± 0.00	0.00 ± 0.00	6.52 ± 0.12
119	0.01 ± 0.00	0.01 ± 0.00	0.01 ± 0.00	0.00 ± 0.00	0.00 ± 0.00	0.03 ± 0.02	0.00 ± 0.00	0.00 ± 0.00	6.61 ± 0.02
120	0.00 ± 0.00	0.00 ± 0.00	0.00 ± 0.00	0.00 ± 0.00	0.09 ± 0.05	0.05 ± 0.03	0.00 ± 0.00	0.00 ± 0.00	6.46 ± 0.11
128	0.00 ± 0.00	0.00 ± 0.00	0.00 ± 0.00	0.00 ± 0.00	0.00 ± 0.00	0.00 ± 0.00	0.00 ± 0.00	0.00 ± 0.00	6.13 ± 0.10
133	0.00 ± 0.00	0.00 ± 0.00	0.00 ± 0.00	0.00 ± 0.00	0.00 ± 0.00	0.02 ± 0.03	0.00 ± 0.00	0.00 ± 0.00	6.15 ± 0.34
141	0.00 ± 0.00	0.00 ± 0.00	0.00 ± 0.00	0.00 ± 0.00	0.00 ± 0.00	0.00 ± 0.00	0.00 ± 0.00	0.00 ± 0.00	6.47 ± 0.15
163	0.00 ± 0.00	0.00 ± 0.00	0.00 ± 0.00	0.00 ± 0.00	0.00 ± 0.00	0.06 ± 0.02	0.00 ± 0.00	0.00 ± 0.00	6.74
Total Flux	0.19 ± 0.02	0.13 ± 0.04	0.20 ± 0.13	0.04 ± 0.01	0.24 ± 0.06	0.61 ± 0.09	0.04 ± 0.00	0.07 ± 0.00	

Table 6Eii. Mean daily outflow chemistry from lower WC duplicate samples.

Day	Ca	Fe	K	Na	S	Si	pH
1	0.00 ± 0.00	0.00 ± 0.00	0.00 ± 0.00	0.00 ± 0.00	0.00 ± 0.01	0.00 ± 0.00	-
8	0.01 ± 0.00	0.01 ± 0.02	0.00 ± 0.00	0.00 ± 0.00	0.03 ± 0.02	0.00 ± 0.00	0.00
14	0.01 ± 0.01	0.02 ± 0.03	0.00 ± 0.00	0.00 ± 0.00	0.02 ± 0.03	0.00 ± 0.00	6.22 ± 0.15
26	0.01 ± 0.00	0.01 ± 0.01	0.00 ± 0.00	0.01 ± 0.00	0.02 ± 0.01	0.01 ± 0.00	5.95 ± 0.08
47	0.02 ± 0.00	0.01 ± 0.01	0.03 ± 0.00	0.03 ± 0.01	0.02 ± 0.01	0.02 ± 0.00	6.13 ± 0.01
55	0.00 ± 0.00	0.00 ± 0.01	0.02 ± 0.02	0.00 ± 0.00	0.00 ± 0.00	0.00 ± 0.00	0.00 ± 0.00
63	0.00 ± 0.00	0.00 ± 0.00	0.00 ± 0.00	0.00 ± 0.00	0.01 ± 0.00	0.00 ± 0.00	5.87 ± 0.30
70	0.01 ± 0.00	0.01 ± 0.01	0.00 ± 0.00	0.01 ± 0.01	0.02 ± 0.00	0.00 ± 0.00	5.97 ± 0.13
78	0.01 ± 0.00	0.00 ± 0.00	0.00 ± 0.00	0.01 ± 0.00	0.01 ± 0.00	0.00 ± 0.00	6.42 ± 0.37
91	0.00 ± 0.00	0.00 ± 0.00	0.00 ± 0.00	0.00 ± 0.00	0.00 ± 0.00	0.00 ± 0.00	6.50 ± 0.01
108	0.00 ± 0.00	0.00 ± 0.00	0.00 ± 0.00	0.00 ± 0.00	0.01 ± 0.00	0.00 ± 0.00	6.42 ± 0.03
117	0.00 ± 0.00	0.00 ± 0.00	0.00 ± 0.00	0.00 ± 0.00	0.01 ± 0.01	0.00 ± 0.00	5.53 ± 0.25
128	0.00 ± 0.00	0.00 ± 0.00	0.00 ± 0.00	0.00 ± 0.00	0.00 ± 0.00	0.00 ± 0.00	6.05 ± 0.52
133	0.00 ± 0.00	0.00 ± 0.00	0.00 ± 0.00	0.00 ± 0.00	0.00 ± 0.00	0.00 ± 0.00	6.42 ± 0.03
141	0.04 ± 0.06	0.00 ± 0.00	0.01 ± 0.00	0.00 ± 0.00	0.04 ± 0.05	0.00 ± 0.00	6.58 ± 0.07
163	0.00 ± 0.00	0.00 ± 0.00	0.00 ± 0.00	0.00 ± 0.00	0.02 ± 0.00	0.00 ± 0.00	6.58 ± 0.11
Total Flux	0.13 ± 0.09	0.07 ± 0.05	0.06 ± 0.02	0.06 ± 0.02	0.23 ± 0.09	0.03 ± 0.00	

Table 6Eiii. Mean weekly outflow chemistry from upper WC duplicate samples.

Day	Al	Ca	Fe	K	Mg	Na	S	Zn	Si	pH
1	0.00 ± 0.00	0.01 ± 0.01	0.01 ± 0.01	0.00 ± 0.00	0.00 ± 0.00	0.00 ± 0.00	0.02 ± 0.02	0.00 ± 0.00	0.00 ± 0.00	5.79 ± 0.95
8	0.00 ± 0.01	0.02 ± 0.02	0.03 ± 0.04	0.00 ± 0.00	0.01 ± 0.01	0.00 ± 0.00	0.08 ± 0.10	0.01 ± 0.02	0.00 ± 0.00	5.49 ± 0.76
14	0.00 ± 0.00	0.01 ± 0.00	0.00 ± 0.00	0.01 ± 0.02	0.00 ± 0.00	0.00 ± 0.00	0.01 ± 0.01	0.00 ± 0.00	0.00 ± 0.00	6.50 ± 0.12
26	0.01 ± 0.01	0.02 ± 0.01	0.02 ± 0.02	0.01 ± 0.01	0.01 ± 0.01	0.02 ± 0.01	0.08 ± 0.06	0.01 ± 0.01	0.01 ± 0.00	5.88 ± 1.17
47	0.01 ± 0.01	0.02 ± 0.03	0.02 ± 0.03	0.02 ± 0.02	0.01 ± 0.01	0.02 ± 0.03	0.07 ± 0.11	0.01 ± 0.01	0.02 ± 0.02	5.70
55	0.00 ± 0.00	0.00 ± 0.00	0.01 ± 0.01	0.01 ± 0.00	0.00 ± 0.00	0.00 ± 0.00	0.01 ± 0.01	0.00 ± 0.00	0.00 ± 0.00	0.00 ± 0.00
63	0.01 ± 0.01	0.01 ± 0.01	0.04 ± 0.06	0.00 ± 0.00	0.01 ± 0.01	0.02 ± 0.01	0.10 ± 0.12	0.01 ± 0.01	0.00 ± 0.00	5.09 ± 1.46
70	0.01 ± 0.01	0.02 ± 0.01	0.05 ± 0.07	0.00 ± 0.00	0.01 ± 0.01	0.02 ± 0.02	0.12 ± 0.12	0.02 ± 0.02	0.00 ± 0.00	5.30 ± 1.05
78	0.01 ± 0.01	0.02 ± 0.01	0.05 ± 0.07	0.00 ± 0.00	0.01 ± 0.01	0.02 ± 0.00	0.12 ± 0.10	0.01 ± 0.01	0.00 ± 0.00	5.56 ± 1.61
91	0.00 ± 0.00	0.00 ± 0.00	0.04 ± 0.06	0.00 ± 0.00	0.00 ± 0.00	0.00 ± 0.00	0.08 ± 0.07	0.00 ± 0.00	0.00 ± 0.00	5.94 ± 1.00
108	0.01 ± 0.01	0.00 ± 0.00	0.05 ± 0.07	0.00 ± 0.00	0.00 ± 0.01	0.00 ± 0.00	0.13 ± 0.13	0.01 ± 0.01	0.00 ± 0.00	5.61 ± 1.38
117	0.01 ± 0.01	0.00 ± 0.00	0.04 ± 0.05	0.00 ± 0.00	0.00 ± 0.00	0.00 ± 0.00	0.09 ± 0.08	0.01 ± 0.00	0.00 ± 0.00	4.97 ± 1.22
128	0.00 ± 0.00	0.00 ± 0.00	0.01 ± 0.01	0.00 ± 0.00	0.00 ± 0.00	0.00 ± 0.00	0.01 ± 0.01	0.00 ± 0.00	0.00 ± 0.00	5.34 ± 1.33
133	0.00 ± 0.00	0.00 ± 0.00	0.04 ± 0.05	0.00 ± 0.00	0.00 ± 0.00	0.00 ± 0.00	0.07 ± 0.08	0.00 ± 0.00	0.00 ± 0.00	5.33 ± 1.67
141	0.00 ± 0.00	0.05 ± 0.07	0.00 ± 0.00	0.01 ± 0.00	0.00 ± 0.00	0.00 ± 0.00	0.10 ± 0.03	0.00 ± 0.00	0.00 ± 0.00	5.50 ± 1.39
163	0.01 ± 0.01	0.00 ± 0.00	0.06 ± 0.08	0.00 ± 0.00	0.00 ± 0.00	0.00 ± 0.00	0.12 ± 0.06	0.00 ± 0.00	0.00 ± 0.00	5.71 ± 1.67
Total Flux	0.06 ± 0.02	0.19 ± 0.08	0.5 ± 0.2	0.06 ± 0.02	0.06 ± 0.01	0.10 ± 0.03	1.2 ± 0.3	0.09 ± 0.03	0.03 ± 0.00	

Table 6Eiv. Mean weekly outflow chemistry from lower WC duplicate samples.

Lithology	Flush media	Al	Ca	Fe	K	Mg	Mn	Na	S	Zn	Si
WS	Milli-RO	0.0087	0.1089	0.1122	0.0731	0.0191	0.0073	0.0844	0.2456	0.0070	0.0664
	water	0.0084	0.0721	0.1435	0.0394	0.0113	0.0046	0.0486	0.2633	0.0050	0.0440
	Mineralised	0.0033	0.0443	0.0377	0.0412	0.0085	0.0031	0.0364	0.0926	0.0066	0.0278
	water	0.0074	0.0771	0.2065	0.0328	0.0115	0.0030	0.0384	0.3219	0.0070	0.0233
UWS	Milli-RO	0.0023	0.1679	0.0040	0.0526	0.0164	0.0023	0.0408	0.1411	0.0026	0.0299
	water	0.0020	0.1565	0.0008	0.0242	0.0189	0.0021	0.0410	0.1351	0.0016	0.0251
	Mineralised	0.0020	0.1273	0.0016	0.0191	0.0119	0.0019	0.0083	0.1259	0.0020	0.0049
	water	0.0013	0.1066	0.0006	0.0243	0.0166	0.0013	0.0132	0.0932	0.0018	0.0157
WC	Milli-RO	0.0043	0.0490	0.0226	0.0434	0.0049	0.0049	0.0500	0.1085	0.0035	0.0429
	water	0.0055	0.0395	0.0666	0.0338	0.0063	0.0040	0.0311	0.1362	0.0053	0.0375
	Mineralised	0.0026	0.0345	0.0069	0.0322	0.0048	0.0031	0.0254	0.0806	0.0032	0.0291
	water	0.0044	0.0400	0.0317	0.0602	0.0092	0.0031	0.0289	0.1227	0.0043	0.0256
UWC	Milli-RO	0.0021	0.0517	0.0018	0.0567	0.0065	0.0030	0.0555	0.0345	0.0022	0.0417
	water	0.0022	0.0555	0.0009	0.0617	0.0071	0.0031	0.0558	0.0380	0.0029	0.0414
	Mineralised	0.0012	0.0319	0.0014	0.0264	0.0039	0.0015	0.0362	0.0209	0.0016	0.0208
	water	0.0013	0.0323	0.0008	0.0319	0.0044	0.0015	0.0304	0.0284	0.0030	0.0198

Table 6.F. Daily flushed total flux corrected for partial collection of leachate, used for ANOVA.

Lithology	Flush media	Al	Ca	Fe	K	Mg	Mn	Na	S	Zn	Si
WS	Milli-RO	0.00031	0.00667	0.00434	0.00429	0.00116	0.00027	0.00367	0.01315	0.00141	0.00180
	water	0.00058	0.00836	0.00909	0.00446	0.00135	0.00029	0.00682	0.02420	0.00423	0.00225
	Mineralised	0.00051	0.00598	0.00418	0.00378	0.00112	0.00017	0.00173	0.01593	0.00180	0.00050
	water	0.00333	0.00725	0.01862	0.00115	0.00355	0.00038	0.00392	0.04406	0.00433	0.00113
UWS	Milli-RO	0.00403	0.52495	0.00700	0.06475	0.04769	0.00316	0.02644	0.41301	0.00198	0.02647
	water	0.00335	0.60689	0.00563	0.06070	0.05051	0.00361	0.04009	0.49212	0.00295	0.02970
	Mineralised	0.00372	0.51142	0.00114	0.10943	0.08495	0.00362	0.08983	0.48484	0.00166	0.03747
	water	0.00372	0.51142	0.00114	0.10943	0.08495	0.00362	0.08983	0.48484	0.00166	0.03747
WC	Milli-RO	0.00038	0.00366	0.00048	0.00276	0.00058	0.00026	0.00268	0.01113	0.00041	0.00179
	water	0.00030	0.00923	0.00637	0.00351	0.00095	0.00023	0.00315	0.01160	0.00080	0.00167
	Mineralised	0.00286	0.00486	0.02303	0.00140	0.00255	0.00033	0.00387	0.04934	0.00386	0.00127
	water	0.00023	0.00443	0.00061	0.00161	0.00032	0.00016	0.00119	0.01213	0.00040	0.00035
UWC	Milli-RO	0.00019	0.00383	0.00007	0.00230	0.00045	0.00022	0.00295	0.00236	0.00016	0.00181
	water	0.00020	0.00472	0.00015	0.00329	0.00062	0.00026	0.00403	0.00450	0.00017	0.00259
	Mineralised	0.00015	0.00315	0.00006	0.00074	0.00031	0.00014	0.00125	0.00212	0.00014	0.00016
	water	0.00011	0.00235	0.00005	0.00208	0.00039	0.00012	0.00055	0.00164	0.00010	0.00088

Table 6.G. Weekly flushed total flux used for ANOVA

Chapter 7 Results

date	pH	mV	Ms	T	TDS	depth	velocity	flow rate	rainfall
18.01.00	4.85	223.25	1174.75	8.60		14	40	1817	4
23.01.01	5.60	176.33	724.33	7.20	470.00	17	33	1593	5
24.01.01	5.63	56.02	676.80	6.92	473.20	19	33	1633	25
25.01.01	5.36	73.06	867.40	7.28	607.60	17	25	1140	0
26.01.01	5.27	86.44	997.60	7.50	697.60	15	33	1533	1
28.01.01	5.38	80.50	1219.80	7.82	800.00	14	17	747	1
29.01.01	4.97	104.98	1403.40	8.48	877.00	12	25	1070	0
9.02.01	6.23	35.63	867.00	6.57	605.67	17	50	2280	0
15.02.01	5.00	92.74	1178.00	8.18	811.20	15	25	1165	0
21.02.01	4.57	114.90	1.64	8.75	1119.50	15	14	640	0
23.03.01	4.81	108.30	1303.00	8.30	920.00	13	12	532	0
29.03.01	4.92	102.20	1265.00	8.10	802.00	15	17	776	15
10.04.01	5.45	70.00	889.00	7.80	631.33	14	24	1082	47
18.04.01	4.83	105.10	1285.33	8.57	898.00	12	19	790	15
19.04.01	4.86	104.33	1445.00	9.70	1015.33	12	15	635	1
24.04.01	4.87	103.67	1381.67	9.83	965.33	12	13	550	11
25.04.01	4.84	105.03	1378.33	9.37	1157.33	11	10	386	3
26.04.01	4.89	102.30	1389.00	8.80	976.67	12	11	466	0
27.04.01	4.99	95.60	1253.00	8.70	924.00	11	13	529	0
05.05.01	4.38	127.80	1600.00	9.20	1130.00	11	5	99	0
06.05.01	4.74	110.50	1930.00	9.20	1317.00	11	13	248	11
14.05.01	4.62	117.80	2170.00	9.30	1315.00	10	13	242	0
15.05.01	4.74	110.92	921.80	9.20	965.00	10	13	242	0
26.05.01	4.67	129.40	2650.00	10.50	1100.00	9	13	233	0
29.05.01	4.47	119.30	2400.00	9.70	1660.00	10	13	236	0
30.05.01	4.39	123.90	2380.00	9.70	1640.00	10	8	157	3
31.05.01	4.45	120.60	2400.00	9.80	1237.00	10	8	161	4
01.06.01	4.45	120.50	2400.00	10.10	1690.00	10	8	360	0
04.06.01	4.66	129.30	2650.00	9.30	1253.00	9	2	225	0
08.06.01	4.46	127.40	2650.00	17.80	1250.00	9	3	372	0
09.06.01									
16.06.01	6.22	34.10	2000.00	10.00	1213.00	10	4	696	25
17.06.01	4.33	246.80	1940.00	10.00	1210.00	10	4	600	0
25.06.01	4.65	129.90	2350.00	10.50	1670.00	10	2	240	0
26.06.01	4.67	129.40	2650.00	10.50	1830.00	9	2	240	0
27.06.01	4.63	130.80	2520.00	10.50	1098.00	9	1	240	0
28.06.01	4.64	133.00	2550.00	9.00	1107.00	9	2	350	0
29.06.01	4.55	135.60	2570.00	9.00	1800.00	9	3	460	0
12.07.01	4.57	134.20	2640.00	10.20	1790.00	9	2	225	7
13.07.01	4.45	133.70	2850.00	10.00	1255.00	9	4	300	1
26.07.01	4.25	129.80		9.70		9	2	300	0
27.07.01	4.46	130.50		10.10		9	2	230	0
28.07.01	4.56	124.50		9.50		9	2	230	0
29.07.01	4.54	125.70		9.60		9	2	235	0
30.07.01	4.53	126.20		9.30		9	2	240	0
31.07.01	4.20	134.00		9.40		9	2	222	1

Table 7.A. Bowden Close discharge chemical and physical characteristics from January to July, 2001.

date	Al	Ca	Fe	K	Mg	Mn	Na	S	Zn	Si
18.01.00	2.67	47.41	5.12	5.16	19.44	0.82	7.21	56.20	0.00	7.69
23.01.01	1.05	50.39	2.65	4.34	17.82	0.77	6.86	51.85	0.00	6.39
24.01.01	21.24	138.71	50.48	6.21	56.84	4.95	3.86	271.15	0.78	13.83
25.01.01	28.29	168.50	70.71	6.90	70.01	6.86	4.20	355.20	1.10	16.43
26.01.01	14.11	123.99	37.29	6.45	50.46	3.54	4.17	199.77	0.51	13.91
28.01.01	6.66	67.16	17.53	5.13	27.89	1.62	2.35	96.41	0.14	8.60
29.01.01	8.77	80.19	22.98	5.45	32.78	2.18	2.56	126.59	0.25	9.29
9.02.01	17.01	137.13	42.57	7.45	56.12	4.17	4.44	236.49	0.64	15.05
15.02.01	6.42	76.55	15.78	5.75	29.08	1.52	2.35	100.62	0.14	8.77
21.02.01	23.72	148.51	56.80	6.90	60.96	5.45	5.33	267.61	0.70	13.48
23.03.01	23.14	134.47	49.74	5.08	55.78	4.71	7.37	245.52	1.70	12.52
29.03.01	24.07	147.15	57.08	6.52	60.70	5.46	4.85	266.04	0.67	13.36
10.04.01	8.54	79.70	22.22	5.28	31.83	1.98	5.72	118.93	0.85	8.42
18.04.01	10.81	91.13	26.61	5.56	36.72	2.43	6.90	147.58	1.03	9.25
19.04.01	19.22	121.57	46.55	6.09	54.40	4.46	8.11	243.87	1.78	11.70
24.04.01	20.83	128.73	50.60	6.20	57.80	4.84	8.36	265.60	1.92	12.17
25.04.01	21.81	139.23	52.54	5.85	60.47	5.10	7.41	246.46	2.02	12.74
26.04.01	19.26	129.50	47.73	5.62	55.49	4.60	7.28	224.86	1.86	11.83
27.04.01	18.23	125.16	46.24	5.49	54.29	4.41	6.93	217.08	1.72	11.64
05.05.01	25.42	150.42	62.25	5.99	65.46	5.96	7.95	289.82	2.33	13.33
06.05.01	26.91	157.48	66.35	6.19	68.59	6.32	8.17	302.86	2.45	13.91
14.05.01	31.22	173.41	76.51	6.23	75.96	7.33	9.19	352.59	2.83	15.19
15.05.01	30.93	171.24	76.19	6.50	76.57	7.25	9.08	346.88	2.80	14.98
26.05.01	29.64	144.88	65.09	5.78	71.51	6.80	10.66	287.34	2.74	12.24
29.05.01	30.17	149.34	67.68	6.12	73.94	7.06	10.37	299.79	2.79	12.53
30.05.01	13.00	152.33	69.78	6.08	75.45	7.27	10.87	306.86	2.89	12.76
31.05.01	31.47	155.81	70.55	6.12	77.88	7.56	10.07	316.18	2.96	12.84
01.06.01	43.08	215.60	98.18	7.85	99.11	10.33	18.51	423.46	3.75	18.09
04.06.01	48.89	222.40	102.38	8.12	111.08	11.82	19.69	472.18	4.12	18.57
08.06.01	37.93	194.60	84.31	7.29	90.14	9.29	15.31	390.08	3.26	15.71
08.06.02	9.26	86.35	23.17	5.12	33.96	2.06	9.23	114.78	0.87	9.18
16.06.01	27.35	153.20	63.11	6.97	73.21	6.83	14.28	285.08	2.37	13.49
17.06.01	32.03	180.69	74.20	6.85	84.54	7.90	17.32	339.58	2.79	16.41
25.06.01	38.53	183.61	82.97	7.56	85.58	9.17	15.69	372.54	3.31	16.23
26.06.01	36.46	171.66	78.04	6.97	82.50	8.67	14.07	352.77	3.15	14.95
27.06.01	38.20	175.44	79.85	6.76	85.44	9.00	15.26	365.14	3.25	15.33
28.06.01	39.51	182.52	83.39	7.06	88.37	9.40	16.74	380.86	3.66	15.83
29.06.01	39.51	174.61	83.39	7.06	88.37	9.40	16.74	380.86	3.66	15.83
12.07.01	45.21	206.36	97.22	8.06	112.19	11.19	15.29	514.72	4.09	16.67
13.07.01	46.02	209.74	98.46	8.24	114.38	11.45	14.23	515.47	4.08	16.90
26.07.01	22.03	97.08	44.24	3.75	48.74	5.39	2.74	212.38	1.18	8.20
27.07.01	22.21	96.70	43.55	3.74	48.61	5.41	2.67	217.21	1.14	8.17
28.07.01	24.37	106.25	47.88	4.13	53.63	6.01	2.94	240.35	1.18	8.91
29.07.01	20.58	91.64	41.02	3.59	46.36	5.11	2.60	209.25	1.01	7.66
30.07.01	21.18	94.59	41.58	4.11	47.60	5.31	2.84	219.82	1.06	7.95
31.07.01	23.09	99.79	45.01	3.82	0.00	5.64	2.76	236.27	1.14	8.49

Table 7.B. Bowden Close discharge dissolved major element chemistry from January to July 2001.

Chapter 8 Results

UWS

Treatment	Al	Ca	Fe	K	Mg	Mn	Na	S	Zn	Si
Cyclic	8.13E-05	1.44E-02	1.71E-04	5.19E-04	4.80E-04	1.95E-05	1.20E-04	2.68E-03	3.16E-05	2.87E-04
	1.58E-04	4.29E-03	4.89E-04	6.11E-04	1.05E-03	7.65E-05	1.60E-04	5.11E-03	3.84E-05	3.30E-04
	2.36E-06	8.84E-03	0.00E+00	5.94E-04	2.78E-04	2.89E-06	1.17E-04	1.51E-03	3.12E-05	1.40E-04
	3.66E-04	8.39E-03	5.24E-04	7.14E-04	1.04E-03	7.08E-05	1.90E-04	5.26E-03	3.64E-05	3.22E-04
Stagnant	1.31E-06	6.92E-05	8.92E-07	1.64E-05	1.52E-05	1.52E-06	6.35E-06	6.19E-05	9.09E-07	5.45E-06
	1.47E-06	1.13E-04	1.04E-06	2.80E-05	2.53E-05	1.77E-06	8.37E-06	8.24E-05	1.03E-06	8.85E-06
	1.50E-06	7.60E-05	1.03E-06	2.09E-05	1.84E-05	1.74E-06	6.17E-06	5.82E-05	1.03E-06	7.65E-06
Daily MR	6.91E-04	5.04E-02	1.20E-03	1.58E-02	4.92E-03	6.84E-04	1.22E-02	4.23E-02	7.77E-04	8.97E-03
	6.03E-04	4.69E-02	2.31E-04	7.26E-03	5.68E-03	6.17E-04	1.23E-02	4.05E-02	4.78E-04	7.54E-03
Daily Min	1.20E-03	7.64E-02	9.90E-04	1.15E-02	7.15E-03	1.14E-03	5.00E-03	7.56E-02	1.22E-03	2.96E-03
	8.01E-04	6.40E-02	3.86E-04	1.46E-02	9.99E-03	7.84E-04	7.90E-03	5.59E-02	1.06E-03	9.42E-03
Weekly MR	3.22E-03	4.20E-01	5.60E-03	5.18E-02	3.82E-02	2.53E-03	2.12E-02	3.30E-01	1.58E-03	2.12E-02
	2.68E-03	4.86E-01	4.50E-03	4.86E-02	4.04E-02	2.89E-03	3.21E-02	3.94E-01	2.36E-03	2.38E-02
Weekly Min	3.31E-04	8.79E-02	1.08E-04	1.79E-02	1.16E-02	1.66E-04	0.00E+00	7.21E-02	4.47E-04	4.56E-04
	2.49E-04	3.49E-02	7.67E-05	9.19E-03	5.23E-03	7.82E-05	0.00E+00	2.82E-02	2.62E-04	0.00E+00

UWC

Treatment	Al	Ca	Fe	K	Mg	Mn	Na	S	Zn	Si
Cyclic	3.19-06	2.32E-03	3.80E-06	2.55E-04	5.54E-05	1.91E-06	8.61E-05	3.55E-04	2.25E-06	5.19E-05
	2.96E-06	6.46E-04	1.55E-06	2.35E-04	1.56E-05	1.82E-06	5.39E-05	1.26E-04	1.59E-06	3.34E-05
	3.80E-06	2.11E-03	2.08E-06	1.86E-04	4.72E-05	2.39E-06	1.34E-04	1.52E-04	2.50E-06	7.61E-05
	7.79E-06	1.85E-03	2.74E-06	2.49E-04	4.10E-05	2.06E-06	7.49E-05	2.31E-04	3.70E-06	2.47E-03
Stagnant	2.00E-06	6.74E-05	1.57E-06	1.67E-05	1.58E-05	2.27E-06	8.28E-06	1.27E-05	1.40E-06	1.48E-05
	2.78E-06	1.82E-05	1.99E-06	3.59E-06	4.66E-06	3.19E-06	7.49E-06	5.10E-06	1.95E-06	8.47E-06
	2.56E-06	1.61E-05	1.77E-06	1.02E-05	4.40E-06	2.92E-06	7.17E-06	5.92E-06	1.84E-06	8.47E-06
Daily MR	6.39E-04	1.55E-02	5.50E-04	1.70E-02	1.96E-03	8.94E-04	1.67E-02	1.03E-02	6.45E-04	1.25E-02
	6.61E-04	1.67E-02	2.70E-04	1.85E-02	2.12E-03	9.27E-04	1.67E-02	1.14E-02	8.82E-04	1.24E-02
Daily Min	6.91E-04	1.92E-02	8.64E-04	1.58E-02	2.34E-03	8.99E-04	2.17E-02	1.26E-02	9.50E-04	1.25E-02
	8.08E-04	1.94E-02	4.69E-04	1.92E-02	2.62E-03	8.98E-04	1.83E-02	1.70E-02	1.81E-03	1.19E-02
Weekly MR	1.53E-04	3.06E-03	6.00E-05	1.84E-03	3.62E-04	1.74E-04	2.36E-03	1.89E-03	1.27E-04	1.44E-03
	1.60E-04	3.77E-03	1.18E-04	2.63E-03	4.95E-04	2.09E-04	3.22E-03	3.60E-03	1.37E-04	2.08E-03
Weekly Min	2.44E-04	5.05E-03	9.94E-05	1.19E-03	5.02E-04	2.21E-04	2.00E-03	3.39E-03	2.21E-04	2.48E-04
	1.76E-04	3.76E-03	7.73E-05	3.32E-03	6.29E-04	1.88E-04	8.87E-04	2.62E-03	1.52E-04	1.41E-03

WS

Treatment	Al	Ca	Fe	K	Mg	Mn	Na	S	Zn	Si
Cyclic	4.54E-05	5.70E-04	5.88E-04	3.83E-04	1.00E-04	3.84E-05	4.42E-04	1.29E-03	3.65E-05	3.48E-04
	4.39E-05	3.78E-04	7.52E-04	2.06E-04	5.91E-05	2.40E-05	2.54E-04	1.38E-03	2.59E-05	2.30E-04
	1.72E-05	2.32E-04	1.98E-04	2.16E-04	4.44E-05	1.61E-05	1.91E-04	4.85E-04	3.48E-05	1.45E-04
	3.86E-05	4.04E-04	1.08E-03	1.72E-04	6.03E-05	1.57E-05	2.01E-04	1.69E-03	3.66E-05	1.22E-04
Stagnant	8.00E-07	1.74E-05	1.13E-05	1.12E-05	3.04E-06	6.95E-07	9.58E-06	3.43E-05	3.69E-06	4.71E-06
	1.52E-06	2.18E-05	2.37E-05	1.16E-05	3.53E-06	7.64E-07	1.78E-05	6.32E-05	1.10E-05	5.88E-06
	1.34E-06	1.56E-05	1.09E-05	9.86E-06	2.92E-06	4.40E-07	4.53E-06	4.16E-05	4.69E-06	1.31E-06
Daily MR	9.99E-04	2.18E-03	5.58E-03	3.45E-04	1.07E-03	1.15E-04	1.18E-03	1.32E-02	1.30E-03	3.39E-04
	1.62E-01	3.25E-02	1.31E-02	4.94E-01	7.26E-02	2.94E-02	1.11E-02	2.63E-03	8.41E-01	1.54E-02
Daily Min	1.80E-02	2.37E-01	2.82E-01	1.85E-01	4.34E-02	1.58E-02	1.57E-01	6.06E-01	4.76E-02	9.78E-02
	6.39E-02	5.00E-01	1.57E+00	1.35E-01	8.05E-02	1.66E-02	1.63E-01	2.31E+00	6.62E-02	8.94E-02
Weekly MR	5.15E-03	1.12E-01	7.29E-02	7.20E-02	1.96E-02	4.47E-03	6.16E-02	2.21E-01	2.38E-02	3.03E-02
	9.76E-03	1.40E-01	1.53E-01	7.49E-02	2.27E-02	4.92E-03	1.15E-01	4.07E-01	7.10E-02	3.78E-02
Weekly Min	1.72E-02	2.01E-01	1.40E-01	1.27E-01	3.76E-02	5.66E-03	5.83E-02	5.35E-01	6.04E-02	1.68E-02
	1.12E-01	2.44E-01	6.25E-01	3.86E-02	1.19E-01	1.29E-02	1.32E-01	1.48E+00	1.45E-01	3.80E-02

Table 8.A. Flux per g of sample, per day (calculated from the total dissolved flux from partially coated samples in mgg⁻¹day⁻¹) as tested by ANOVA for variance between various water-rock regimes. 'E-' represents 'x 10'.

WC

Treatment	Al	Ca	Fe	K	Mg	Mn	Na	S	Zn	Si
Cyclic	2.24E-05	2.57E-04	1.18E-04	2.27E-04	2.57E-05	2.58E-05	2.62E-04	5.68E-04	1.86E-05	2.25E-04
	2.87E-05	2.07E-04	3.49E-04	1.77E-04	3.32E-05	2.09E-05	1.63E-04	7.13E-04	2.75E-05	1.96E-04
	1.36E-05	1.81E-04	3.60E-05	1.68E-04	2.49E-05	1.60E-05	1.33E-04	4.22E-04	1.67E-05	1.52E-04
	2.32E-05	2.09E-04	1.66E-04	3.15E-04	4.80E-05	1.62E-05	1.52E-04	6.42E-04	2.25E-05	1.34E-04
Stagnant	9.89E-07	9.55E-06	1.25E-06	7.19E-06	1.51E-06	6.83E-07	7.01E-06	2.91E-05	1.08E-06	4.68E-06
	7.71E-07	2.41E-05	1.66E-05	9.16E-06	2.48E-06	6.12E-07	8.22E-06	3.03E-05	2.08E-06	4.37E-06
	7.46E-06	1.27E-05	6.01E-05	3.66E-06	6.65E-06	8.63E-07	1.01E-05	1.29E-04	1.01E-05	3.31E-06
Daily MR	6.76E-05	1.33E-03	1.83E-04	4.83E-04	9.73E-05	4.92E-05	3.56E-04	3.64E-03	1.20E-04	1.04E-04
	2.49E-02	1.05E-01	3.51E-01	6.40E-02	1.94E-02	6.24E-03	1.97E-01	6.03E-01	2.67E-02	4.93E-02
Daily Min	1.14E-02	2.03E-01	4.21E-02	1.17E-01	2.79E-02	1.01E-02	3.14E-01	4.66E-01	3.95E-02	9.09E-02
	2.79E-02	2.52E-01	2.66E-01	3.67E-01	6.46E-02	1.02E-02	2.51E-01	9.88E-01	4.64E-02	8.23E-02
Weekly MR	6.36E-03	6.15E-02	8.02E-03	4.63E-02	9.74E-03	4.39E-03	4.51E-02	1.87E-01	6.96E-03	3.01E-02
	4.96E-03	1.55E-01	1.07E-01	5.89E-02	1.59E-02	3.94E-03	5.29E-02	1.95E-01	1.34E-02	2.81E-02
Weekly Min	9.60E-02	1.63E-01	7.74E-01	4.70E-02	8.56E-02	1.11E-02	1.30E-01	1.66E+00	1.30E-01	4.26E-02
	7.57E-03	1.49E-01	2.05E-02	5.41E-02	1.09E-02	5.51E-03	3.98E-02	4.08E-01	1.34E-02	1.16E-02

Table 8.A.continued. Flux per g of sample, per day (calculated from the total dissolved flux from partially coated samples in $mgg^{-1}day^{-1}$) as tested by ANOVA for variance between various water-rock regimes. 'E-' represents 'x 10'